

---

---

# BOUNDARY LAYER RESPONSE

## TO ARBITRARY ACCELERATING FLOW

---

---

By

MADELEINE LELON COMBRINCK



Department of Mechanical and Aeronautical Engineering  
Faculty of Engineering, Built Environment and IT  
University of Pretoria

A dissertation submitted to the University of Pretoria  
in accordance with the requirements of the degree of  
DOCTOR OF PHILOSOPHY  
in the Faculty of Engineering, Built Environment and IT.

August 2016



UNIVERSITEIT VAN PRETORIA  
UNIVERSITY OF PRETORIA  
YUNIBESITHI YA PRETORIA



## Abstract

This thesis was aimed developing a fundamental understanding of the boundary layer response to arbitrary motion. In this context arbitrary motion was defined as the unsteady translation and rotation of an object.

Research objectives were developed from the gaps in knowledge as defined during the literature survey. The objectives were divided into three main activities; mathematical formulations for non-inertial bulk flow and boundary layer equations, implementation of said formulations in a numerical solver and simulations for various applications in arbitrary motion.

Mathematical formulations were developed for the bulk flow and boundary layer equations in arbitrary motion. It was shown that the conservation of momentum and energy equations remains invariant in the non-inertial forms. The conservations of momentum equation can at most have six fictitious terms for unsteady arbitrary motion. The origin of the terms were found to be from transformation of the material derivative to the non-inertial frame. All fictitious terms were found to be present in the boundary layer equations, none could be eliminated during an order of magnitude analysis.

The vector form of the non-inertial equations were implemented in a novel OpenFOAM solver. The non-inertial solver requires prescribed motion input and operate on a stationary mesh. Validation of the solver was done using analytical solutions of a steady, laminar flat plate and rotating disk respectively.

Numerical simulation were done for laminar flow on a translating plate, rotating disk and rotating cone in axial flow. A test matrix was executed to investigated various cases of acceleration and deceleration over a range of 70 g to 700 000g. The boundary layer profiles, boundary layer parameters and skin friction coefficients were reported.

Three types of boundary layer responses to arbitrary motion were defined. Response Type I is viscous dominant and mimics the steady state velocity profile. In Response Type II certain regions of the boundary layer are dominated by viscosity and others by momentum. Response Type III is dominated by momentum. In acceleration the near-wall velocity gradient increases with increasing acceleration. In deceleration separation occurs at a result of momentum changes in the flow.

The mechanism that causes these responses have been identified using the developed boundary layer equations. In acceleration the relative frame fictitious terms become a momentum source which results in an increase in velocity gradient at the wall. In deceleration the relative frame fictitious terms become a momentum sink that induced an adverse pressure gradient and subsequently laminar separation.

### Keywords

Non-Inertial Reference Frames, Fictitious Forces, Boundary Layer Equations, OpenFOAM, Laminar Flat Plate, Laminar Rotating Disk, Rotating Cone in Axial Flow.



UNIVERSITEIT VAN PRETORIA  
UNIVERSITY OF PRETORIA  
YUNIBESITHI YA PRETORIA

## Abstrak

Hierdie tesis is gerig op die ontwikkeling van 'n fundamentele begrip aangaande die grenslaag reaksie op arbitrêre beweging. In hierdie konteks word arbitrêre beweging gedefinieer as die ongestadigde translasië en rotasie van 'n voorwerp.

Navorsingsdoelwitte is ontwikkel uit die gapings soos omskryf in die literatuuroorsig. Die doelwitte is verdeel in drie hoof aktiwiteite; wiskundige formulerings vir ongestadigde vloei en grenslaag vergelykings, implementering van hierdie formulerings in 'n numeriese kode en simulaties vir verskeie gevalle van arbitrêre beweging.

Wiskundige formulerings is ontwikkel vir die vloei en grenslaag vergelykings in arbitrêre beweging. Daar is bewys dat die behoud van massa en energie vergelykings onveranderd in die nie-inertiële vorms bly. Die behoud van momentum vergelyking kan hoogstens ses fiktiewe terme vir ongestadigde, arbitrêre beweging hê. Die oorsprong van die terme is vanuit die transformasie van die ongestadigde en adveksie terme (aan die linker kant van die momentum vergelyking) na die nie-inertiële raam. Alle fiktiewe terme is teenwoordig in die grenslaag vergelykings.

Die vektor vorm van die nie-inertiële vergelykings is in 'n nuwe OpenFOAM oplosser geïmplementeer. Die nie-inertiële oplosser vereis voorgeskrewe beweging insette en werk op 'n stilstaande rooster. Die oplosser is getoets teen analitiese oplossings van 'n gestadigde, laminêre plaat plaat en 'n roterende skyf, onderskeidelik.

Numeriese simulaties is gedoen vir laminêre vloei op 'n translêrende plaat, roterende skyf en roterende konus in aksiale vloei. 'n Toets matriks is gebruik om ondersoek in te stel na gevalle van versnelling en vertraging oor 'n verskeidenheid van 70 g tot 700 000 g. Die grenslaag profiele, grenslaag parameters en oppervlak wrywingskoëffisiënte is aangemeld nie.

Drie tipes grenslaag reaksies op arbitrêre beweging is gedefinieer. Reaksie Tipe I is viskeus dominant en boots die bestendige snelheidsprofiel na. In reaksie Tipe II sekere dele van die grenslaag is oorheers deur viskositeit en ander deur momentum. Reaksie Tipe III word in totaliteit oorheers deur momentum. In versnelling die snelheid helling teen die objek neem toe met toenemende versnelling. In vertraging is 'n negatiewe snelheidsprofiel waargeneem as gevolg van momentum veranderinge in die vloei.

Die meganisme wat hierdie reaksies veroorsaak is geïdentifiseer deur die grenslaag vergelykings. In versnelling word die fiktiewe terme 'n bron van momentum. Dit lei tot 'n toename in snelheid helling op die objek. In vertraging word die fiktiewe terme 'n momentum gebruiker wat 'n negatiewe drukgradiënt veroorsaak en gevolglik laminêre vloei wegbreking veroorsaak.



UNIVERSITEIT VAN PRETORIA  
UNIVERSITY OF PRETORIA  
YUNIBESITHI YA PRETORIA

## Résumé

Cette thèse avait pour but de développer une compréhension fondamentale de la réponse de la couche limite au mouvement arbitraire. Dans ce contexte, le mouvement arbitraire a été défini comme la traduction instationnaire d'un objet.

Les objectifs ont été divisés en trois parties principales; formulations mathématiques pour l'écoulement dans un repère non-inertiel, mise en œuvre desdites formulations dans un solveur numérique et diverses applications en mouvement arbitraire.

Les formulations mathématiques ont été développées pour le flux de masse et les équations de la couche limite en mouvement arbitraire. Il a été montré que la conservation de masse et d'énergie restent invariantes sous les formes non inertielles. La conservation de l'équation met en exergue six termes inertiels en mouvement arbitraire instable.

La forme vectorielle des équations non-inertielles ont été mis en œuvre dans le code OpenFOAM. Ce code nécessite des conditions initiales de quantité de mouvement prescrites et un maillage fixe. La validation du code a été effectuée à l'aide de solutions analytiques pour une plaque plane laminaire stable et un disque en rotation.

Les simulations numériques ont été réalisées pour un écoulement laminaire sur une plaque en translation, un disque en rotation et un cône en rotation-translation. Les effets d'un écoulement en accélération et décélération ont été étudiés entre 70 g et 700000 g. Les paramètres de la couche limite et des coefficients de frottement de paroi ont été déterminés.

Trois types de réponse pour la couche limite dans un mouvement arbitraire ont été définis.

La réponse de type 1 : la viscosité est dominante et le profil de vitesse est similaire à celui de l'état d'équilibre. La réponse de type 2 : Certaines régions de la couche limite sont dominées par les effets de viscosité et d'autres par la quantité de mouvement. La réponse type 3 est dominée par la quantité de mouvement. Avec l'augmentation de l'accélération de l'écoulement, le gradient de vitesse proche de la paroi augmente. Dans le cas de la décélération, une séparation de la couche limite se produit à la suite des changements des quantités de mouvement dans l'écoulement.

Le mécanisme qui provoque ces phénomènes a été identifié en analysant la couche limite. Les termes de l'accélération deviennent une source d'impulsion qui se traduit par une augmentation du gradient de vitesse sur la paroi. Les termes dus à la décélération deviennent un puits d'énergie de quantité de mouvement induisant un gradient de pression négative et par la suite une séparation.



UNIVERSITEIT VAN PRETORIA  
UNIVERSITY OF PRETORIA  
YUNIBESITHI YA PRETORIA

## Абстрактные

Этот тезис был направлен на разработку фундаментального понимания реакции пограничного слоя на произвольные движения. В этом контексте произвольное движение было определено как неустановившееся сдвига и вращения объекта.

Цели исследования были разработаны на основе пробелов в знаниях, как это определено в ходе исследования литературы. Цели были разделены на три основных направлений деятельности; математические формулировки для неинерциальной объемного потока и уравнений пограничного слоя, реализация указанных композиций в численном решателе и моделирования для различных применений в произвольном движении.

Математические препараты были разработаны для потока сыпучих и уравнений пограничного слоя в произвольном движении. Было показано, что сохранение импульса и энергии уравнений остается неизменной в неинерциальных формах. В консервирования уравнения импульса можно самое большее шесть фиктивных условия для произвольного неустановившегося движения. были найдены происхождение терминов, чтобы быть от превращения производного материала к неинерциальной. Все они были признаны фиктивными термины присутствовать в уравнениях пограничного слоя, ни одна не может быть устранена в течение порядка анализа величины.

Вектор форма неинерциальных уравнений были реализованы в новой OpenFOAM решателя. Неинерциальную решатель требует предписанного входного движения и действуют на стационарной сеткой. Проверка решателя было сделано с использованием аналитических решений устойчивой, ламинарного плоской пластины и вращающегося диска соответственно.

Численное моделирование проводились для ламинарного потока на переводческой пластине, вращающийся диск и вращающийся конус в осевом потоке. Тест матрица была выполнена для исследованных различных случаев ускорения и замедления в диапазоне от 70 г до 700 000 г. Профили пограничного слоя, были представлены параметры пограничного слоя и коэффициенты трения кожи.

Были определены три типа ответов пограничного слоя произвольного движения. Ответ Тип I вязкая доминирующими и мимику установившийся профиль скорости. В типе реагирования II определенные области пограничного слоя преобладают вязкости и другие по инерции. Ответ типа III преобладают импульса. При ускорении пристенных градиента скорости возрастает с увеличением ускорения. При замедлении разделение происходит в результате изменения импульса в потоке.

Механизм, который вызывает эти реакции были идентифицированы с использованием разработанных уравнений пограничного слоя. При ускорении Относительный каркасные фиктивные термины становятся источником импульса, который приводит к увеличению градиента скорости у стенки. В замедлении Относительный кадра фиктивные члены становятся стоком импульс, который индуцируется неблагоприятный градиент давления, а затем ламинарный разделение.



UNIVERSITEIT VAN PRETORIA  
UNIVERSITY OF PRETORIA  
YUNIBESITHI YA PRETORIA



## Publications

### Conference Articles

**ID 2014\_0577.**

M.L. Combrinck and L.N. Dala.

*Eulerian Derivation of Non-Inertial Navier Stokes Equations.*

29<sup>th</sup> Congress of the International Council of the Aeronautical Sciences.

St. Petersburg, Russia, 7-12 September 2014.

**ID 2014\_AS005.**

M.L. Combrinck, L.N. Dala and I.I. Lipatov.

*Eulerian Derivation of Non-Inertial Navier Stokes Equations.*

International Aerospace Symposium of South Africa.

Pretoria, South Africa, 23-25 November 2014.

**ID 1570075653.**

M.L. Combrinck, L.N. Dala and I.I. Lipatov.

*Eulerian Derivation of Non-Inertial Navier Stokes Equations for Compressible Flow in Constant, Pure Rotation.*

11<sup>th</sup> International Conference of Heat Transfer, Fluid Mechanics and Thermodynamics.

Skukuza, South Africa, 20-23 July 2015.

**ID 1570235498.**

M.L. Combrinck, L.N. Dala and I.I. Lipatov.

*Boudnary Layer Response to Arbitrary Acceleration.*

12<sup>th</sup> International Conference of Heat Transfer, Fluid Mechanics and Thermodynamics.

Malaga, Spain, 10-13 July 2016.

## Journal Articles

### **ID EJMFLU\_2015\_157.**

M.L. Combrinck, L.N. Dala and I.I. Lipatov.

Eulerian Derivation of Non-Inertial Navier Stokes Equations for Incompressible Flow in Constant, Pure Rotation.

*European Journal of Mechanics /B Fluids.*

Submitted: May 2015 First Revision: November 2015 Second Revision: August 2016 Status: Under review.

### **ID AeroJ\_2015\_4466.**

M.L. Combrinck, L.N. Dala and I.I. Lipatov.

Eulerian Derivation of Non-Inertial Navier-Stokes Equations in Arbitrary Acceleration for Aero-Ballistic Applications.

*The Aeronautical Journal.*

Submitted: September 2015 Status: Under review.

### **ID R&D\_2015\_13.**

M.L. Combrinck, L.N. Dala and I.I. Lipatov.

Eulerian Derivation of the Non-Inertial Navier-Stokes Equations in Arbitrary Rotation.

*The R&D Journal.*

Submitted: September 2015 Status: Under review.

### **ID ASENG\_1536.**

M.L. Combrinck, L.N. Dala and I.I. Lipatov.

Boundary Response To Acceleration and Deceleration on a Flat Plate.

*Journal of Aerospace Engineering.*

Submitted: November 2015 Status: Under review.

## Dedication and Acknowledgements



### **Werner Heisenberg (1901-1976)**

*When I meet God, I am going to ask him two questions:  
"Why relativity? And why turbulence?"*

I would like to dedicate this work in its entirety to God.

Immortal Beloved, You are my Light and my Salvation. You have never left me and never forsaken me. Thank you for this life and this opportunity, I will literally forever be grateful. The dance with You is a beautiful one and I am looking forward to our adventures to come.

As during a study like this there are so many people to thank for their support and guidance. You each have my gratitude for your role in enhancing my life.

Prof. Laurent Dala. I don't even know how to begin to thank you for all that you have done for me. All the doors you have opened, all the motivational discussions and telling me to dress like a lady at all times. From the bottom of my heart, thank you. And it now takes me an hour to get dressed in the morning.

Prof. Igor Ivanovich Lipatov. Thank you for all the arrangements that allowed me to spend time at the FALT. I am looking forward to working with you more in the future!

Mrs. Valerie Dala. Mon amie, there are very few true friends in this world and I am fortunate to call you mine. Thank you for allowing me to disrupt your Sundays and letting me sleep in your guest room from time to time. You are a blessing in my life.

Thank you to my long-suffering parents for all their support, love and understanding. Mom, thank you for teaching me to be practical and always be gracious. Dad, thank you for teaching me to dream and telling me to "do it like a lady".

Thank you to my sister, Dr. Estie Cloete and her husband Dr. Flip Cloete. You are the sun as I am the moon. You rule by day as I rule by night. Yet we meet each other at dawn and at dusk for the perfect end and the perfect start to each day.

Marius-Corne Meijer. You are the baby brother I always wanted and a good partner in dark humour. Thank you for teaching me Russian, without the basics I would have gotten tea instead of vodka.

Adriaan Steenkamp. Thank you for teaching me many valuable lessons both in engineering and in life. Thank you most of all for giving me the opportunity to grow, to learn and to succeed. You are probably the only person who understands that I frequently wonder about things like *What is the colour of unicorn blood?*, *What would I look like if I had a tail like Avatar* and other important life questions. (I still maintain that I would be an awesome dictator once my quest for world domination is fulfilled. I will make a note to leave a position for you on my council of advisers.)

Elia Gule. Thank you for sharing your insight into coding. I appreciate your help.

Dr. Johan Heyns. Thank you for many, many motivational discussions. You taught me many lessons, but the one thing that stands out is: "If I had more time, I would have written you a shorter letter".

Dr Oliver Oxtoby. Thank you for your patience, kindness and willingness to teach. You are a true English gentlemen.

Dr. Rocos El Khouri. Thank you for believing in my work and talking with me through some concepts.

Prof. Akira Kageyama. Thank you for your correspondence and patience in explaining your work. Someday, some place on this small planet I hope that we can have a discussion in person.

The Moscow Institute of Physics and Technology, Department of Aeromechanics and Flight Engineering. Prof. Sergey Serokhvostov and Dr. Michael Lipatov for all the arrangements and welcoming me to the Russian Federation. Ivan Veronich and Vlad for allowing me to invade their office.

Vasja and Anton. Thank you for welcoming me in Russia and making my stay memorable. It was such a honour to be invited to your parents Dacha for tea. I will wave to you from across the channel.

Ansie Stegen and Marlene Snyman. You are the best neighbours and friends ever! Thank you that we can share a passion for good wine and cheese. And for understanding that I sometimes "zone out and go to my happy place" when in company of others.

Camille and Francoise Dala. Thank you for welcoming me into your hearts and home in the South of France. I came to you as a stranger and I left your house as a daughter. Thank you for the wonderful time and fond memories.

Prof. Mostapha Tarfaoui. Thank you for always enquiring if I am finished yet and reminding me that there is life after a PhD.

Philip van der Merwe aka "the life coach". Thank you for all that you have taught me in our sessions. Your techniques really helped me to stay motivated through the most difficult parts of this study.

and J. My trust in you started on a narrow gravel road without a railing high up in the mountains of Lesotho. It continued to selecting the perfect bottle of wine for a meal and it lives on to this day. You have changed my world in ways I could never have imagined. A tram ride in St. Petersburg, slamming a hotel door in someone's face and looking at a zebra will never quite be the same again.

Wij zullen altijd Botlierskop!

## Author's Declaration

I declare that the work in this dissertation was carried out in accordance with the requirements of the University's Regulations and Code of Practice for Research Degree Programmes and that it has not been submitted for any other academic award. Except where indicated by specific reference in the text, the work is the candidate's own work. Work done in collaboration with, or with the assistance of, others, is indicated as such. Any views expressed in the dissertation are those of the author.

SIGNED: ..... DATE: .....



M.L. Combrinck (left) with a family friend, Tanya Roode (right) in Moscow, September 2015



UNIVERSITEIT VAN PRETORIA  
UNIVERSITY OF PRETORIA  
YUNIBESITHI YA PRETORIA

## Table of Contents

	Page
<b>List of Tables</b>	<b>xix</b>
<b>List of Figures</b>	<b>xxi</b>
<b>CHAPTERS</b>	
<hr/>	
<b>1 Introduction</b>	<b>1</b>
1.1 Background . . . . .	1
1.2 Research Approach . . . . .	5
1.3 Thesis Overview . . . . .	7
<b>2 Literature Survey</b>	<b>9</b>
2.1 Accelerating Flow Implementation . . . . .	9
2.2 Derivation of Non-Inertial Navier-Stokes Equations . . . . .	12
2.3 Boundary Layers in Unsteady Flow . . . . .	12
2.4 Boundary Layers in Rotating Flow . . . . .	16
<b>3 Non-Inertial Equations in Vector Form</b>	<b>19</b>
3.1 Non-inertial Navier-Stokes Equations for Constant, Pure Rotation . . . . .	20
3.1.1 Frame Transformations . . . . .	20
3.1.2 Incompressible Flow Conditions . . . . .	24
3.1.3 Compressible Flow Conditions . . . . .	32
3.1.4 Incompressible Equations as a Special Case of the Compressible Equations . . .	35
3.2 Non-inertial Navier-Stokes Equations for Variable, Pure Rotation . . . . .	38
3.2.1 Frame Transformations . . . . .	38
3.2.2 Incompressible Flow Conditions . . . . .	40
3.2.3 Compressible Flow Conditions . . . . .	49
3.2.4 Constant Rotation Equations as a Special Case of the Variable Rotation Equations	50
3.3 Non-Inertial Navier-Stokes Equation for Arbitrary Motion . . . . .	51
3.3.1 Frame Transformations . . . . .	51

TABLE OF CONTENTS

---

3.3.2	Compressible Flow Conditions . . . . .	54
3.3.3	Special Cases of the Arbitrary Acceleration Flow for Compressible Conditions . . . . .	62
3.4	Closure . . . . .	66
<b>4</b>	<b>Non-Inertial Equations in Component Form</b>	<b>71</b>
4.1	Non-Inertial Equations in Cartesian Coordinates . . . . .	72
4.1.1	Incompressible Flow Conditions . . . . .	72
4.1.2	Compressible Flow Conditions . . . . .	73
4.2	Inertial Navier-Stokes Equations in Cylindrical Coordinates . . . . .	75
4.2.1	Transformation for Cartesian to Cylindrical Coordinates . . . . .	75
4.2.2	Incompressible Flow Conditions . . . . .	76
4.2.3	Compressible Flow Conditions . . . . .	78
4.3	Non-Inertial Navier-Stokes Equations in Cylindrical Coordinates . . . . .	82
4.3.1	Incompressible Flow Conditions . . . . .	82
4.3.2	Compressible Flow Conditions . . . . .	87
4.4	Non-Inertial Equations in Curvilinear Coordinates . . . . .	92
4.4.1	Vector Operation in Curvilinear Systems . . . . .	92
4.4.2	Incompressible Flow Conditions . . . . .	95
4.4.3	Compressible Flow Conditions . . . . .	98
4.5	Closure . . . . .	102
<b>5</b>	<b>Non-Inertial Boundary Layer Equations</b>	<b>105</b>
5.1	Non-Inertial Boundary Layer Equations for a Flat Plate - Cartesian Formulation . . . . .	107
5.1.1	NON-DIMENSIONAL ANALYSIS . . . . .	109
5.1.2	Continuity Equation for Boundary Layer Flows . . . . .	110
5.1.3	Conservation of Momentum Equation for Boundary Layer Flows . . . . .	111
5.1.4	Validation of Equations . . . . .	117
5.1.5	Non-Inertial Boundary Layer Equations for Variable Rotation . . . . .	119
5.1.6	Non-Inertial Boundary Layer Equations for Arbitrary Acceleration . . . . .	120
5.2	Non-Inertial Boundary Layer Equations for a Flat Plate - Cylindrical Formulation . . . . .	122
5.2.1	Non-Dimensional Analysis . . . . .	122
5.2.2	Continuity Equation for Boundary Layer Flows . . . . .	123
5.2.3	Conservation of Momentum Equation for Boundary Layer Flows . . . . .	124
5.2.4	Validation of Equations . . . . .	130
5.2.5	Non-Inertial Boundary Layer Equations for Variable Rotation . . . . .	134
5.2.6	Non-Inertial Boundary Layer Equations for Arbitrary Acceleration . . . . .	135
5.3	Non-Inertial Boundary Layer Equations for a Flat Plate - Curvilinear Formulation . . . . .	137
5.3.1	Continuity Equation . . . . .	137
5.3.2	Conservation of Momentum Equation for Boundary Layer Flows . . . . .	137



5.3.3	Validation of Equations . . . . .	140
5.4	Closure . . . . .	143
<b>6</b>	<b>Non-Inertial Solver Implementation and Validation</b>	<b>147</b>
6.1	Code Implementation . . . . .	150
6.1.1	Open Source Field Operation And Manipulation - OPENFOAM® . . . . .	150
6.1.2	Code Architecture . . . . .	150
6.2	Theoretical Formulation . . . . .	153
6.2.1	Assumptions . . . . .	153
6.2.2	Governing Equations . . . . .	154
6.2.3	Closure Models . . . . .	155
6.3	Case Set-up . . . . .	156
6.3.1	Computational Domains . . . . .	156
6.3.2	Boundary Conditions . . . . .	160
6.3.3	Numerical Method . . . . .	165
6.4	Validation Results . . . . .	166
6.4.1	Laminar Flat Plate . . . . .	166
6.4.2	Laminar Rotating Disk . . . . .	172
6.5	Closure . . . . .	182
<b>7</b>	<b>Boundary Layer Response in Pure Rotation - Flat Plate Flow</b>	<b>183</b>
7.1	Case Description . . . . .	184
7.2	Results and Discussion - Acceleration . . . . .	187
7.2.1	Velocity Profiles . . . . .	187
7.2.2	Boundary Layer Parameters . . . . .	195
7.2.3	Skin Friction Coefficients . . . . .	204
7.3	Results and Discussion - Deceleration . . . . .	206
7.3.1	Velocity Profiles . . . . .	206
7.3.2	Boundary Layer Parameters . . . . .	213
7.3.3	Skin Friction Coefficients . . . . .	220
7.4	Closure . . . . .	222
<b>8</b>	<b>Boundary Layer Response in Pure Rotation - Rotating Disk Flow</b>	<b>227</b>
8.1	Case Description . . . . .	228
8.2	Results and Discussion - Acceleration . . . . .	231
8.2.1	Velocity Profiles . . . . .	231
8.2.2	Boundary Layer Parameters . . . . .	240
8.2.3	Skin Friction Coefficients . . . . .	251
8.3	Results and Discussion - Deceleration . . . . .	253

TABLE OF CONTENTS

---

8.3.1	Velocity Profiles . . . . .	253
8.3.2	Boundary Layer Parameters . . . . .	262
8.3.3	Skin Friction Coefficients . . . . .	272
8.4	Closure . . . . .	274
<b>9</b>	<b>Boundary Layer Response in Combined Translation and Rotation - Arbitrary Cone Flow</b>	<b>281</b>
9.1	Case Description . . . . .	283
9.2	Results and Discussion - Acceleration . . . . .	285
9.2.1	Velocity Profiles . . . . .	285
9.2.2	Boundary Layer Parameters . . . . .	301
9.2.3	Skin Friction Coefficients . . . . .	304
9.3	Results and Discussion - Deceleration . . . . .	307
9.3.1	Velocity Profiles . . . . .	307
9.3.2	Boundary Layer Parameters . . . . .	321
9.3.3	Skin Friction Coefficients . . . . .	323
9.4	Results and Discussion - Arbitrary Motion . . . . .	325
9.4.1	Velocity Profiles . . . . .	325
9.4.2	Boundary Layer Parameters . . . . .	333
9.4.3	Skin Friction Coefficients . . . . .	337
9.5	Closure . . . . .	339
<b>10</b>	<b>Conclusion</b>	<b>343</b>
10.1	Contributions . . . . .	344
10.2	Suggested Further Work . . . . .	351
10.2.1	Mathematical Research . . . . .	351
10.2.2	Improvements to the Code . . . . .	352
10.2.3	Numerical Research . . . . .	352
10.3	Alternative Applications . . . . .	353
	<b>Bibliography</b>	<b>355</b>
	<b>APPENDICES</b>	
<b>A</b>	<b>Proof of Identities</b>	<b>367</b>
<b>B</b>	<b>Code Formulations for the Accelerating Reference Frame Solving Utility</b>	<b>371</b>
B.1	ARFrhoPimpleFoam Code Formulation . . . . .	371
B.2	ARFModel Code Formulation . . . . .	378
B.3	ARFFreeStreamVelocity Boundary Implementation . . . . .	389
B.4	Case Structure . . . . .	393

## List of Tables

<b>Table</b>	<b>Page</b>
4.1 Relations between the Curvilinear Coordinate System and Other Systems . . . . .	92
5.1 Relations between the Curvilinear Coordinate System and Other Systems . . . . .	138
6.1 Boundary Conditions of the Translating Plate . . . . .	162
6.2 Minimum and Maximum Reynolds Numbers of the Translating Plate . . . . .	162
6.3 Boundary Conditions of the Rotating Disk . . . . .	163
6.4 Minimum and Maximum Reynolds Numbers of the Rotating Disk . . . . .	163
6.5 Boundary Conditions of the Translating, Rotating Cone . . . . .	164
6.6 Maximum Reynolds Numbers of the Translating, Rotating Cone . . . . .	164
6.7 Boundary Layer Properties of the Translating Plate 0.2 m . . . . .	171
6.8 Tangential Boundary Layer Properties of the Rotating Disk at 0.14 m radius . . . . .	176
6.9 Radial Boundary Layer Properties of the Rotating Disk at 0.14 m radius . . . . .	176
7.1 Examples of Accelerating Objects . . . . .	183
7.2 Flat Plate Test Matrix . . . . .	184
8.1 Rotating Disk Test Matrix . . . . .	227
9.1 Translating, Rotating Cone Test Matrix Group II and Group III . . . . .	282
9.2 Translating, Rotating Cone Test Matrix Group IV and Group V . . . . .	283
9.3 Translating, Rotating Cone Test Matrix Group VI . . . . .	283
9.4 Cone Arbitrary Motion Results Matrix . . . . .	328



UNIVERSITEIT VAN PRETORIA  
UNIVERSITY OF PRETORIA  
YUNIBESITHI YA PRETORIA

## List of Figures

<b>Figure</b>	<b>Page</b>
1.1 Rotating Reference Frame Depicting the Motion of the Moving Earth . . . . .	2
1.2 Relation between the Inertial and Non-Inertial Reference Frames . . . . .	3
1.3 Flow Diagram Depicting the Research Approach . . . . .	6
2.1 The Fixed and Relative Frame as Described by Forsberg [25] . . . . .	10
2.2 Reference Frames of an Aircraft Flying in Arbitrary Motion (Limache [3]) . . . . .	11
2.3 Surface Cooling Effect on the Boundary Layer Profile (Back [28]) . . . . .	14
2.4 Flow Speed Effect on the Boundary Layer Profile (Back [28]) . . . . .	15
2.5 Visualization of the Boundary Layer Profiles (Ram [45] left) and Transition (Kobayashi [46] right) on a Rotating Disk . . . . .	17
2.6 Hot-Wire Measurement of the Mean Velocity Profile in the Radial (left) and Azimuthal (right) Directions (Zoueshtiagh [48]) . . . . .	17
2.7 Disturbance Propagation and Boundary Layer Transition on Spinning Objects in Axial Flow (Kohama [40], Kobayashi [55]) . . . . .	18
3.1 Frames of Observation (O, O' and $\hat{O}$ ) for Point P . . . . .	20
3.2 Galilean Transformation between Frames . . . . .	21
3.3 Local Galilean Transformation between Frames . . . . .	22
3.4 Relation between Frame O' and Frame $\hat{O}$ . . . . .	23
3.5 Local Galilean Transformation between Frames . . . . .	38
3.6 Relation between Frame O' and Frame $\hat{O}$ . . . . .	40
3.7 Frames of Observation (O, O' and $\hat{O}$ ) for Point P . . . . .	51
3.8 Point Description between Frames . . . . .	52
3.9 Relation between Rotational and Orientation Preserving Frames . . . . .	54
3.10 Deflections of a Particle Travelling in the Northern and Southern Hemispheres (left) and the Corresponding Directions of the Velocity Vector (right) . . . . .	68
3.11 Two Components of the Coriolis force: Outward Component due to Eötvös effect (left) and Deflection on the Earth's Surface in Northern and Southern Hemisphere (right) . . . . .	68
3.12 Deflection due to the Magnus Effect in the Inertial Frame (left) and the Non-Inertial Frame (right) . . . . .	69

List of Figures

---

4.1	Depiction of Various Coordinates Systems . . . . .	71
4.2	Description of a Point in the Cartesian and Cylindrical Coordinates System . . . . .	75
4.3	Cartesian and Cylindrical descriptions of point P . . . . .	75
4.4	Cartesian (left) and Cylindrical (right) Control Volumes . . . . .	80
4.5	Co-ordinate Surfaces and Intersection Coordinate Curve Lines at Point P . . . . .	92
4.6	Curvilinear Finite Control Volume . . . . .	93
5.1	Regions Associated with the Laminar Boundary Layer . . . . .	105
5.2	Graphical Representation of the Displacement Thickness Parameter . . . . .	106
5.3	Graphical Representation of the Momentum Thickness Parameter . . . . .	107
5.4	Boundary Layer Parameters . . . . .	107
5.5	Boundary Layer Scaling Parameters . . . . .	108
5.6	Perturbation Parameter $\varepsilon$ on a Flat Surface . . . . .	108
5.7	Flow over a Rotation Flat Surface (Mager [81]) . . . . .	109
5.8	Flat Plate in Cylindrical Co-ordinates . . . . .	122
5.9	Visualization of Physical Meaning of Fictitious Forces . . . . .	134
5.10	Visualization of the Fictitious Forces in Cylindrical and Cartesian Co-ordinates . . . . .	145
6.1	Physical Interpretation of the Boundary Layer Parameters . . . . .	147
6.2	Comparison between the Boundary Layer, Displacement and Momentum Thicknesses . . . . .	148
6.3	Boundary Layer Parameters on a Flat Plate . . . . .	148
6.4	Correlation of Critical Reynolds Number, Transition Reynolds Number versus Shape Factor from Wazzan et al. [78] . . . . .	149
6.5	Accelerating Reference Frame (ARF) Model Code Architecture . . . . .	151
6.6	Graphical Representation of Test Cases; Translating Plate, Rotating Disk and Translating, Rotating Cone . . . . .	153
6.7	Orientating Image of the Boundary Layer . . . . .	156
6.8	Computational Domain for Translating Plate Case . . . . .	157
6.9	Computational Domain for Rotating Disk Case . . . . .	157
6.10	Computational Domain for Translating, Rotating Cone Case . . . . .	158
6.11	Grid independence of the laminar flat plate . . . . .	158
6.12	Grid independence of the laminar rotating disk . . . . .	159
6.13	Grid independence of the translating, rotating cone . . . . .	159
6.14	Boundary Condition Definition for <i>fixedValue</i> , <i>zeroGradient</i> and <i>inletOutlet</i> . . . . .	160
6.15	Boundary Condition Definition for <i>empty</i> , <i>symmetryPlane</i> and <i>cyclic</i> . . . . .	160
6.16	Boundary Condition Definition for <i>waveTransmissive</i> and <i>ARFFreeStreamVelocity</i> . . . . .	161
6.17	Graphical Representation of Translating Plate Boundary Condition . . . . .	162
6.18	Graphical Representation of Rotating Disk Boundary Condition . . . . .	163
6.19	Graphical Representation of Translating, Rotating Cone Boundary Condition . . . . .	164

6.20	Pressure Implicit with Splitting of Operator (PISO) Solution Algorithm . . . . .	165
6.21	Graphical Representation of the Boundary Layer on a Flat Plate . . . . .	166
6.22	Steady State Solution for a Laminar Flat Plate at 10 m/s . . . . .	167
6.23	Steady State Solution for a Laminar Flat Plate at 45 m/s . . . . .	168
6.24	Steady State Solution for a Laminar Flat Plate at 80 m/s . . . . .	168
6.25	Comparison of Boundary Layer Parameters at 10 m/s . . . . .	169
6.26	Comparison of Boundary Layer Parameters at 45 m/s . . . . .	170
6.27	Comparison of Boundary Layer Parameters at 80 m/s . . . . .	170
6.28	Skin Friction Coefficients and Wall Shear Stress . . . . .	171
6.29	Graphical Representation of the Boundary Layer on a Rotating Disk . . . . .	172
6.30	Non-Inertial Tangential Velocity Profiles . . . . .	173
6.31	Comparison between Numerical and Analytical Tangential Velocity Results . . . . .	173
6.32	Non-Inertial Radial Velocity Profiles . . . . .	174
6.33	Comparison between Numerical and Analytical Radial Velocity Results . . . . .	174
6.34	Comparison of Tangential Boundary Layer Characteristic Profiles for 10 rad/s . . . . .	177
6.35	Comparison of Radial Boundary Layer Characteristic Profiles for 10 rad/s . . . . .	177
6.36	Comparison of Tangential Boundary Layer Characteristic Profiles for 45 rad/s . . . . .	178
6.37	Comparison of Radial Boundary Layer Characteristic Profiles for 45 rad/s . . . . .	178
6.38	Comparison of Tangential Boundary Layer Characteristic Profiles for 80 rad/s . . . . .	179
6.39	Comparison of Radial Boundary Layer Characteristic Profiles for 80 rad/s . . . . .	179
6.40	Wall Shear Stress in the Tangential (left) and Radial (right) Directions . . . . .	180
6.41	Skin Friction Coefficients for Steady State Conditions . . . . .	181
7.1	Graphical Representation of the Boundary Layer on a Flat Plate . . . . .	184
7.2	Wall Shear Stress as a Function of Velocity Gradient . . . . .	185
7.3	Frame Definitions for Non-Inertial Flow . . . . .	186
7.4	Non-Dimensional Velocity Profiles: Translating Flat Plate - Acceleration Grouping I . . . . .	187
7.5	Non-Dimensional Velocity Profiles: Translating Flat Plate - Acceleration Grouping II . . . . .	188
7.6	Non-Dimensional Velocity Profiles: Translating Flat Plate - Acceleration Grouping III . . . . .	188
7.7	Sample Results and Observations for the Lower Acceleration Cases . . . . .	189
7.8	Sample Results and Observations for the Higher Acceleration Cases . . . . .	190
7.9	Boundary Layer Profiles for Steady and Accelerating Conditions . . . . .	191
7.10	Increased Wall Velocity Gradient for Accelerating Conditions . . . . .	193
7.11	Acceleration Response Regions by Type in Simulation Results . . . . .	194
7.12	Physical Interpretation of the Boundary Layer Parameters . . . . .	195
7.13	Boundary Layer Parameters on a Flat Plate . . . . .	195
7.14	Displacement Thickness Comparison for the Accelerating Flat Plate . . . . .	196
7.15	Displacement Thickness Derivatives Comparison for the Accelerating Flat Plate . . . . .	196
7.16	Displacement Thickness Comparison at $x = 0.05$ m in Accelerating Conditions . . . . .	197

List of Figures

---

7.17 Displacement Thickness Comparison at $x = 0.2$ m in Accelerating Conditions . . . . .	197
7.18 Momentum Thickness Comparison for the Accelerating Flat Plate . . . . .	199
7.19 Momentum Thickness Derivatives Comparison for the Accelerating Flat Plate . . . . .	199
7.20 Momentum Thickness Comparison at $x = 0.05$ m in Accelerating Conditions . . . . .	200
7.21 Momentum Thickness Comparison at $x = 0.2$ m in Accelerating Conditions . . . . .	200
7.22 Shape Factor Comparison for the Accelerating Flat Plate . . . . .	202
7.23 Shape Factor Derivative Comparison for the Accelerating Flat Plate . . . . .	202
7.24 Shape Factor Comparison at Various Plate Positions for the Accelerating Plate . . . . .	203
7.25 Comparison between Skin Friction Coefficients at Various Free-Stream Reynolds Numbers for Accelerating Conditions . . . . .	204
7.26 Comparison between Skin Friction Coefficients at Various Plate Positions for Accelerating Conditions . . . . .	205
7.27 First and Second Derivatives of the Skin Friction Coefficients in Accelerating Conditions . . . . .	205
7.28 Non-Dimensional Velocity Profiles: Translating Flat Plate - Deceleration Grouping I . . . . .	206
7.29 Non-Dimensional Velocity Profiles: Translating Flat Plate - Deceleration Grouping II . . . . .	207
7.30 Non-Dimensional Velocity Profiles: Translating Flat Plate - Deceleration Grouping III . . . . .	207
7.31 Sample Results and Observations for the Lower Deceleration Cases . . . . .	208
7.32 Sample Results and Observations for the Higher Deceleration Cases . . . . .	209
7.33 Boundary Layer Profiles for Steady and Deceleration Conditions . . . . .	210
7.34 Adverse Pressure Gradient for Decelerating Conditions . . . . .	211
7.35 Acceleration Response Regions by Type in Simulation Results . . . . .	212
7.36 Displacement Thickness Comparison for the Decelerating Flat Plate . . . . .	213
7.37 Displacement Thickness Comparison for the Decelerating Flat Plate . . . . .	213
7.38 Displacement Thickness Comparison at $x = 0.05$ m in Decelerating Conditions . . . . .	214
7.39 Displacement Thickness Comparison at $x = 0.2$ m in Decelerating Conditions . . . . .	214
7.40 Momentum Thickness Comparison for the Decelerating Flat Plate . . . . .	215
7.41 Momentum Thickness Comparison for the Decelerating Flat Plate . . . . .	216
7.42 Momentum Thickness Comparison at $x = 0.05$ m in Decelerating Conditions . . . . .	216
7.43 Momentum Thickness Comparison at $x = 0.2$ m in Decelerating Conditions . . . . .	217
7.44 Shape Factor Comparison for the Decelerating Flat Plate . . . . .	218
7.45 Comparison of Shape Factor Discontinuities and Momentum Thickness for the Decelerat- ing Flat Plate . . . . .	218
7.46 Shape Factor Comparison at Various Plate Positions in Decelerating Conditions . . . . .	219
7.47 Comparison between Skin Friction Coefficients at Various Free-Stream Reynolds Numbers for Decelerating Conditions . . . . .	220
7.48 Comparison between Skin Friction Coefficients at Various Plate Positions for Decelerating Conditions . . . . .	221
7.49 First and Second Derivatives of the Skin Friction Coefficients in Decelerating Conditions . . . . .	221



7.50	Response Types for Accelerating and Decelerating Conditions on a Flat Plate . . . . .	222
7.51	Boundary Layer Profiles for Steady, Acceleration and Deceleration Conditions on a Flat Plate	223
7.52	Accelerating and Decelerating Mechanisms of Boundary Layer Response on a Flat Plate . .	223
7.53	Variability in Boundary Layer Profiles for Different Starting and Acceleration Conditions on a Flat Plate . . . . .	224
7.54	Shape Factor Changes for Accelerating and Decelerating Flow Mapped on the Graph of Wazzan et al. [78] . . . . .	225
7.55	Results of the Shape Factor Response for Acceleration (left) and Deceleration (Right) Events on a Flat Plate . . . . .	226
7.56	Result of the Skin Friction Coefficient Response to Arbitrary Translation on a Flat Plate . .	226
8.1	Graphical Representation of the Boundary Layer on a Rotating Disk . . . . .	228
8.2	Depiction of the laminar boundary layer on the flat plate (left) and in the tangential direction on a rotating disk (right) . . . . .	228
8.3	Depiction of the laminar boundary layer on a rotating disk in the radial direction . . . . .	229
8.4	Frame definitions for non-inertial flow . . . . .	230
8.5	Non-Dimensional Tangential Velocity Profiles: Rotating Disk - Acceleration Grouping I . .	231
8.6	Non-Dimensional Tangential Velocity Profiles: Rotating Disk - Acceleration Grouping II . .	232
8.7	Non-Dimensional Tangential Velocity Profiles: Rotating Disk - Acceleration Grouping III .	232
8.8	Non-Dimensional Radial Velocity Profiles: Rotating Disk - Acceleration Grouping I . . . .	233
8.9	Non-Dimensional Radial Velocity Profiles: Rotating Disk - Acceleration Grouping II . . . .	234
8.10	Non-Dimensional Radial Velocity Profiles: Rotating Disk - Acceleration Grouping III . . .	234
8.11	Sample results and observations for tangential flow in acceleration . . . . .	235
8.12	Boundary layer profile for steady angular acceleration . . . . .	236
8.13	Acceleration Response Types of the Rotating Disk . . . . .	238
8.14	Sample Results of the Radial Velocity Profiles in Acceleration . . . . .	239
8.15	Tangential Boundary Layer on a Rotating Disk . . . . .	240
8.16	Tangential Displacement Thickness Comparison for the Accelerating Rotating Disk . . . .	241
8.17	Tangential Displacement Thickness Derivatives Comparison for the Accelerating Rotating Disk . . . . .	242
8.18	Tangential Displacement Thickness Comparison at $r = 0.14$ m in Accelerating Conditions .	242
8.19	Tangential Momentum Thickness Comparison for the Accelerating Rotating Disk . . . . .	243
8.20	Tangential Momentum Thickness Derivative Comparison for the Accelerating Rotating Disk	243
8.21	Tangential Momentum Thickness Comparison at $r = 0.14$ m in Accelerating Conditions . .	244
8.22	Tangential Shape Factor Comparison for the Accelerating Rotating Disk . . . . .	245
8.23	Tangential Shape Factor Derivative Comparison for the Accelerating Rotating Disk . . . .	245
8.24	Radial Displacement Thickness Comparison for the Accelerating Rotating Disk . . . . .	246
8.25	Radial Displacement Thickness Derivatives Comparison for the Accelerating Rotating Disk	246
8.26	Radial Displacement Thickness Comparison at $r = 0.14$ m in Accelerating Conditions . . . .	247

List of Figures

---

8.27 Radial Momentum Thickness Comparison for the Accelerating Rotating Disk . . . . .	248
8.28 Radial Momentum Thickness Derivative Comparison for the Accelerating Rotating Disk . . . . .	248
8.29 Radial Momentum Thickness Comparison at $r = 0.14$ m in Accelerating Conditions . . . . .	249
8.30 Radial Shape Factor Comparison for the Accelerating Rotating Disk . . . . .	249
8.31 Comparison between Skin Friction Coefficients at Various Free-Stream Rotational Reynolds Numbers for Accelerating Conditions . . . . .	251
8.32 Comparison between Skin Friction Coefficients at Various Disk Positions for Accelerating Conditions . . . . .	252
8.33 Derivatives of Skin Friction Coefficient for Accelerating Conditions . . . . .	252
8.34 Non-Dimensional Tangential Velocity Profiles: Rotating Disk - Deceleration Grouping I . . . . .	253
8.35 Non-Dimensional Tangential Velocity Profiles: Rotating Disk - Deceleration Grouping II . . . . .	254
8.36 Non-Dimensional Tangential Velocity Profiles: Rotating Disk - Deceleration Grouping III . . . . .	254
8.37 Non-Dimensional Radial Velocity Profiles: Rotating Disk - Deceleration Grouping I . . . . .	255
8.38 Non-Dimensional Radial Velocity Profiles: Rotating Disk - Deceleration Grouping II . . . . .	256
8.39 Non-Dimensional Radial Velocity Profiles: Rotating Disk - Deceleration Grouping III . . . . .	256
8.40 Sample results and observations for tangential flow in deceleration . . . . .	257
8.41 Boundary layer profile for steady angular deceleration . . . . .	258
8.42 Deceleration Response Types of the Rotating Disk . . . . .	260
8.43 Sample Results of the Radial Velocity Profiles in Deceleration . . . . .	261
8.44 Tangential Displacement Thickness Comparison for the Decelerating Rotating Disk . . . . .	262
8.45 Tangential Displacement Thickness Derivative Comparison for the Decelerating Rotating Disk . . . . .	262
8.46 Tangential Displacement Thickness Comparison at $r = 0.14$ m in Decelerating Conditions . . . . .	263
8.47 Tangential Momentum Thickness Comparison for the Decelerating Rotating Disk . . . . .	264
8.48 Tangential Momentum Thickness Derivative Comparison for the Decelerating Rotating Disk . . . . .	264
8.49 Tangential Momentum Thickness Comparison at $r = 0.14$ m in Decelerating Conditions . . . . .	265
8.50 Tangential Shape Factor Derivative Comparison for the Decelerating Rotating Disk . . . . .	265
8.51 Comparison of Tangential Shape Factor Discontinuities and Momentum Thickness for the Decelerating Disk . . . . .	266
8.52 Tangential Shape Factor Comparison at Various Radial Positions for the Decelerating Disk . . . . .	266
8.53 Radial Displacement Thickness Comparison for the Decelerating Rotating Disk . . . . .	267
8.54 Radial Displacement Thickness Derivative Comparison for the Decelerating Rotating Disk . . . . .	267
8.55 Radial Displacement Thickness Comparison at $r = 0.14$ m in Decelerating Conditions . . . . .	268
8.56 Radial Momentum Thickness Comparison for the Decelerating Rotating Disk . . . . .	269
8.57 Radial Momentum Thickness Derivative Comparison for the Decelerating Rotating Disk . . . . .	269
8.58 Radial Momentum Thickness Comparison at $r = 0.14$ m in Decelerating Conditions . . . . .	270
8.59 Radial Shape Factor Comparison for the Decelerating Rotating Disk . . . . .	271

8.60 Comparison of Radial Shape Factor Values and Momentum Thickness for the Decelerating Disk . . . . .	271
8.61 Comparison between Skin Friction Coefficients at Various Free-Stream Rotational Reynolds Numbers for Decelerating Conditions . . . . .	272
8.62 Comparison between Skin Friction Coefficients at Various Disk Positions for Decelerating Condition . . . . .	273
8.63 Derivatives of Skin Friction Coefficient for Decelerating Conditions . . . . .	273
8.64 Response types for accelerating (left) and decelerating (right) conditions on a rotating disk in the tangential direction . . . . .	274
8.65 Response to accelerating (left) and decelerating (right) conditions on a rotating disk in the radial direction . . . . .	275
8.66 Boundary layer profiles for steady, acceleration and deceleration conditions on a rotating disk	275
8.67 Accelerating and decelerating mechanisms of boundary layer response on a rotating disk . .	276
8.68 Variability in boundary layer profiles for different starting and acceleration conditions on a rotating disk . . . . .	277
8.69 Results of the tangential shape factor response for acceleration (left) and deceleration (right) events on a rotating disk . . . . .	278
8.70 Results of the radial shape factor response for acceleration (left) and deceleration (right) events on a rotating disk . . . . .	279
8.71 Result of the skin friction coefficient response to arbitrary rotation on a rotating disk . . . .	279
9.1 Orientating Image of the Rotating Cone in Axial Flow . . . . .	281
9.2 Graphical Representation of the Boundary Layer on a Rotating Cone in Axial Flow . . . . .	284
9.3 Comparison between Group 2 and Group 3 Simulation Results for Acceleration . . . . .	285
9.4 Non-Dimensional $s$ -Direction Velocity Profiles: Group 2 Accelerating Cone . . . . .	286
9.5 Non-Dimensional $s$ -Direction Velocity Profiles: Group 3 Accelerating Cone . . . . .	287
9.6 Non-Dimensional $z$ -Direction Velocity Profiles: Group 2 Accelerating Cone . . . . .	288
9.7 Non-Dimensional $z$ -Direction Velocity Profiles: Group 3 Accelerating Cone . . . . .	289
9.8 Responses of the Boundary Layer on the Cone to Acceleration in Translation . . . . .	290
9.9 Accelerating Velocity Profile in the $s$ -Direction on the Cone . . . . .	290
9.10 Non-inertial Force Acting on a Cone in Arbitrary Motion . . . . .	292
9.11 Strained Element . . . . .	292
9.12 Comparison between Group 4 and Group 5 Simulation Results for Acceleration . . . . .	294
9.13 Non-Dimensional $s$ -Direction Velocity Profiles: Group 4 Accelerating Cone . . . . .	295
9.14 Non-Dimensional $s$ -Direction Velocity Profiles: Group 5 Accelerating Cone . . . . .	296
9.15 Non-Dimensional $z$ -Direction Velocity Profiles: Group 4 Accelerating Cone . . . . .	297
9.16 Non-Dimensional $z$ -Direction Velocity Profiles: Group 5 Accelerating Cone . . . . .	298
9.17 Responses of the Boundary Layer on the Cone to Acceleration in Rotation . . . . .	299
9.18 Accelerating Velocity Profile in the $z$ -Direction on the Cone . . . . .	299

List of Figures

---

9.19	Comparison of Shape Factor for the Group 2 (left) and Group 4 (right) Cases . . . . .	301
9.20	Shape Factor in $s$ -Direction for Translational Acceleration . . . . .	302
9.21	Derivatives of Shape Factor in $s$ -Direction for Translational Acceleration . . . . .	302
9.22	Shape Factor in $z$ -Direction for Rotational Acceleration . . . . .	303
9.23	Derivatives of Shape Factor in $z$ -Direction for Rotational Acceleration . . . . .	303
9.24	Comparison of Skin Friction Coefficient for the Group 2 (left) and Group 4 (right) Cases . .	304
9.25	Skin Friction Coefficient in $s$ -Direction for Translational Acceleration . . . . .	305
9.26	Derivatives of Skin Friction Coefficient in $s$ -Direction for Translational Acceleration . . . .	305
9.27	Skin Friction Coefficient in $z$ -Direction for Rotational Acceleration . . . . .	306
9.28	Derivatives of Skin Friction Coefficient in $z$ -Direction for Rotational Acceleration . . . . .	306
9.29	Comparison between Group 2 and Group 3 Simulation Results for Deceleration . . . . .	307
9.30	Non-Dimensional $s$ -Direction Velocity Profiles: Group 2 Decelerating Cone . . . . .	308
9.31	Non-Dimensional $s$ -Direction Velocity Profiles: Group 3 Decelerating Cone . . . . .	309
9.32	Non-Dimensional $z$ -Direction Velocity Profiles: Group 2 Decelerating Cone . . . . .	310
9.33	Non-Dimensional $z$ -Direction Velocity Profiles: Group 3 Decelerating Cone . . . . .	311
9.34	Responses of the Boundary Layer on the Cone to Deceleration in Translation . . . . .	312
9.35	Decelerating Velocity Profile in the $s$ -Direction on the Cone . . . . .	312
9.36	Comparison between Group 4 and Group 5 Simulation Results for Deceleration . . . . .	314
9.37	Non-Dimensional $s$ -Direction Velocity Profiles: Group 4 Decelerating Cone . . . . .	315
9.38	Non-Dimensional $s$ -Direction Velocity Profiles: Group 5 Decelerating Cone . . . . .	316
9.39	Non-Dimensional $z$ -Direction Velocity Profiles: Group 4 Decelerating Cone . . . . .	317
9.40	Non-Dimensional $z$ -Direction Velocity Profiles: Group 5 Decelerating Cone . . . . .	318
9.41	Responses of the Boundary Layer on the Cone to Deceleration in Rotation . . . . .	319
9.42	Decelerating Velocity Profile in the $z$ -Direction on the Cone . . . . .	319
9.43	Shape Factor in $s$ -Direction for Translational Deceleration . . . . .	321
9.44	Shape Factor in $z$ -Direction for Rotational Deceleration . . . . .	322
9.45	Skin Friction Coefficient in $s$ -Direction for Translational Deceleration . . . . .	323
9.46	Derivatives of Skin Friction Coefficient in $s$ -Direction for Translational Deceleration . . . .	324
9.47	Skin Friction Coefficient in $z$ -Direction for Rotational Deceleration . . . . .	324
9.48	Comparison between Group 6a,b,c and d at a Condition 2.5 m/s 7 rad/s . . . . .	325
9.49	Comparison between Group 6a and Group 6c . . . . .	326
9.50	Comparison between Group 6b and Group 6d . . . . .	327
9.51	Mechanisms Associated with Case 6a of the Cone . . . . .	329
9.52	Mechanisms Associated with Case 6a of the Cone . . . . .	330
9.53	Mechanisms Associated with Case 6a of the Cone . . . . .	331
9.54	Mechanisms Associated with Case 6a of the Cone . . . . .	332
9.55	Group 6a Shape Factor in the $s$ -Direction . . . . .	333
9.56	Group 6b Shape Factor in the $s$ -Direction . . . . .	333

9.57	Group 6a Shape Factor in the z-Direction . . . . .	334
9.58	Group 6d Shape Factor in the z-Direction . . . . .	334
9.59	Group 6b Shape Factor in the z-Direction . . . . .	335
9.60	Group 6c Shape Factor in the z-Direction . . . . .	335
9.61	Group 6c Shape Factor in the s-Direction . . . . .	336
9.62	Group 6d Shape Factor in the s-Direction . . . . .	336
9.63	Group 6a Skin Friction Coefficient . . . . .	337
9.64	Group 6b Skin Friction Coefficient . . . . .	337
9.65	Group 6c Skin Friction Coefficient . . . . .	338
9.66	Group 6d Skin Friction Coefficient . . . . .	338
9.67	Comparison of Various Profile at a Free-Stream of 2 m/s 7.5 rad/s . . . . .	339
9.68	Flow Mechanisms for Translation . . . . .	340
9.69	Flow Mechanisms for Rotation . . . . .	340
9.70	Skin Friction Coefficient Comparisons with respect to Arbitrary Motion in Translation . . .	341
9.71	Skin Friction Coefficient Comparisons for Arbitrary Motion . . . . .	341
10.1	Response Types for Accelerating and Decelerating Conditions on a Flat Plate . . . . .	347
10.2	Comparison between the Arbitrary Flow Mechanisms for the Translating Plate (left) and the Longitudinal Velocity Component of the Rotating Cone in Axial Flow (right) . . . . .	348
10.3	Comparison between the Arbitrary Flow Mechanisms for the Rotating Disk (left) and the Tangential Velocity Component of the Rotating Cone in Axial Flow (right) . . . . .	348
10.4	Results of the tangential shape factor response for acceleration (left) and deceleration (right) events on a rotating disk . . . . .	350
10.5	Skin Friction Coefficient Comparisons for Arbitrary Motion on the Cone . . . . .	351
B.1	ARFrhoPimpleFoam Solver Root Folder . . . . .	371
B.2	ARFrhoPimpleFoam Solver Make Folder . . . . .	372
B.3	ARFrhoPimpleFoam Solver Installation Location . . . . .	372
B.4	ARFrhoPimpleFoam Solver Dependent Utilities . . . . .	372
B.5	ARFrhoPimpleFoam C++ Main Code . . . . .	373
B.6	ARFrhoPimpleFoam C++ Create Fields Header File . . . . .	374
B.7	ARFrhoPimpleFoam C++ rhoEqn.H Code . . . . .	375
B.8	ARFrhoPimpleFoam C++ EEqn.H Code . . . . .	376
B.9	ARFrhoPimpleFoam C++ UEqn.H Code . . . . .	377
B.10	ARF Library Root Folder . . . . .	378
B.11	ARFModel Library Root Folder . . . . .	378
B.12	ARFModel Library Sources . . . . .	378
B.13	ARFModel C++ Source Code ARFProperties Constructors . . . . .	379
B.14	ARFModel C++ Source Code Vector Definitions . . . . .	380

List of Figures

---

B.15 ARFModel C++ Source Code - Coriolis and Centrifugal Source Calculation . . . . .	381
B.16 ARFModel C++ Source Code - Euler and Rotation-Translation Interaction Source Calculation	382
B.17 ARFModel C++ Source Code - Frame Acceleration and Source Summation Calculations . .	383
B.18 ARFModel C++ Source Code Velocity Calculation . . . . .	384
B.19 ARFModel C++ Source Code Internal Field and Boundary Layer Correction . . . . .	385
B.20 ARFModel Header File Returned Parameters . . . . .	386
B.21 tabulatedAcceleration Library Root Folder . . . . .	387
B.22 tabulatedAcceleration C++ Source Constructors . . . . .	387
B.23 tabulatedAcceleration C++ Source Member Functions . . . . .	388
B.24 ARF derivedFvPatchFields Root Folder . . . . .	389
B.25 ARFVelocity Boundary Condition Description . . . . .	389
B.26 ARFVelocity Boundary Condition Source Code . . . . .	390
B.27 ARFFreestreamVelocity Boundary Condition Description . . . . .	391
B.28 ARFFreestreamVelocity Boundary Condition Source Code . . . . .	392
B.29 OpenFOAM Case Initial Set-up . . . . .	393
B.30 OpenFOAM Root Case Folder . . . . .	394
B.31 OpenFOAM Mesh Description Files . . . . .	394
B.32 OpenFOAM Case System Folder . . . . .	394
B.33 OpenFOAM Case Initial Conditions Folder . . . . .	395
B.34 OpenFOAM Case Constant Folder . . . . .	395
B.35 Acceleration Reference Frame Properties File . . . . .	396
B.36 Tabulated Frame Velocity at Specified Time . . . . .	397
B.37 Turbulence Model Description . . . . .	397
B.38 Thermo-Physical Property Specification . . . . .	398



## Nomenclature

### OPERATORS

$\wedge$	Cross Product
$\otimes$	Dyadic Cross Product
$\cdot$	Dot Product
$\nabla$	Nabla or Del Operator
$\nabla \cdot$	Divergence
$\nabla \wedge$	Curl
$\nabla^2$	Laplacian
$\mathbf{G}$	Galilean Operator
$R$	Rotational Transform Operator

### SUPER SCRIPTS AND SUB SCRIPTS

$\cdot$	First Derivative of Time
$'$	Orientation Preserving Frame
$\wedge$	Non-Inertial Frame
$\star$	Non-Dimensional Quantity
$\infty$	Far-Field Values
1	Projection on First Principal Direction
2	Projection on Second Principal Direction
3	Projection on Third Principal Direction
$r$	Projection on r-axis
$rel$	Relative Conditions
$t$	Time
$\Delta t$	Change in Time
$x$	Projection on x-axis
$y$	Projection on y-axis
$z$	Projection on z-axis
$I$	Incompressible Form
$T$	Transpose of Matrix
$\theta$	Projection on $\theta$ -axis





List of Figures

---

**ALPHABET**

<b>a</b>	Acceleration Vector	$[m/s^2]$
<b>b</b>	Arbitrary Vector	$[m/s]$
<i>e</i>	Inertial Energy	$[kgm^2/s^2]$
<i>h</i>	Geometry Scaling Factor	$[nondimensional]$
<b>i</b>	Unit Vector	$(\mathbf{i}, \mathbf{j}, \mathbf{k}), (\mathbf{e}_r, \mathbf{e}_\theta, \mathbf{e}_z)$
<i>k</i>	Heat Transfer Coefficient	$[kg/s^3K]$
<i>p</i>	Pressure	$[kg/ms^2]$
<i>r</i>	Displacement in r-direction	$[m]$
<b>r</b>	Distance from Axis of Rotation	$[m]$
<i>t</i>	Time	$[s]$
<b>u</b>	Velocity Vector	$[m/s]$
<i>u</i>	Velocity in x-direction	$[m/s]$
<i>v</i>	Velocity in y-direction	$[m/s]$
<i>w</i>	Velocity in z-direction	$[m/s]$
<i>x</i>	Displacement in x-direction	$[m]$
<b>x</b>	Position Vector	$[m]$
<i>y</i>	Displacement in y-direction	$[m]$
<i>z</i>	Displacement in z-direction	$[m]$
<i>H</i>	Shape Factor	$[nondimensional]$
<b>I</b>	Identity Matrix	$[nondimensional]$
<i>L</i>	Characteristic Length	$[m]$
<i>O</i>	Frame Designation	$[nondimensional]$
<i>Re</i>	Reynolds Number	$[nondimensional]$
<i>T</i>	Temperature	$[K]$
<i>U</i>	Characteristic Velocity	$[m/s]$
<b>V</b>	Frame Velocity Vector	$[m/s]$
<b>X</b>	Position vector	$[m]$

**GREEK LETTERS**

$\delta$	Boundary Layer Thickness	$[m]$
$\delta^*$	Displacement Thickness	$[m]$
$\epsilon$	Element of	$[nondimensional]$
$\epsilon$	Perturbation Parameter	$[nondimensional]$
$\eta$	Nondimensional distance	$[nondimensional]$
$\theta$	Displacement in $\theta$ -direction	$[rad]$
$\theta$	Momentum Thickness (boundary layer )	$[m]$
$\lambda$	Second Viscosity	$[kg/ms]$
$\mu$	Dynamic Viscosity	$[kg/ms]$
$\nu$	Kinematic Viscosity	$[kg/ms]$
$\rho$	Density	$[kg/m^3]$
$\tau$	Stress Tensor	$[kg/ms^2]$
$\varphi$	Dissipation Function	$[kg^2/ms^3]$
$\psi$	Specific Pressure $\frac{p}{\rho}$	$[m^2/s^2]$
$\omega$	Rotational Speed	$[rad/s]$
$\Omega$	Rotational Speed around the z-axis	$[rad/s]$
$\Omega$	Displacement in $\theta$ -direction	$[rad]$



## Introduction

The aim of this research is to investigate the response of the boundary layer on the surface of an aero-ballistic airframe subjected to arbitrary motion. In this context arbitrary motion is defined as unsteady acceleration and deceleration respectively, in both translation and rotation. The research question for this project is defined as:

### ? Research Question

How does the boundary layer on an airframe in arbitrary motion respond the unsteady flow conditions?

## 1.1 Background

There are significant gaps in the body of knowledge with regards to studies in arbitrary motion. The few studies that investigate these effects, rely mostly on steady motion and therefore do not activate the non-inertial effects (Biedron and Thomas [1], Gardi [2], Limache [3]) There are some cases that consider pre-scribed motion and transient effects, however most fail to realise the importance of the boundary layer. It makes use of inviscid formulations of the standard Navier-Stokes equations and slip wall conditions (Inoue et al. [4], Roohani and Skews [5]).

The standard Navier-Stokes equation cannot capture the relative flow properties involved in arbitrary motion. This form of the equations resolves the flow problem in an inertial reference frame (Batchelor [6], Greenspan [7]). In rotational flow problems, the symmetry between the inertial frame and the non-inertial frame is broken. The mathematical model in the inertial frame cannot account for the observed behaviour. This can be accounted for by the inclusion of non-inertial effects that present as fictitious forces on the right hand side of the non-inertial momentum equation (Meriam and Kraige

CHAPTER 1. INTRODUCTION

[8], White [9]). Solving the system from the non-inertial perspective leads to enhanced simulation results that are capable of quantifying the acceleration terms.

In this work two observational reference frames are considered: an inertial and a non-inertial frame of reference. The inertial frame is tied to the stationary state of motion of the observer (Eulerian perspective) where all the laws of physics take the simplest form. In the non-inertial frame (Lagrangian perspective) the simplest form does not prevail; the observer is no longer stationary and fictitious forces must be introduced to account for observer motion. This is illustrated through Newton's Second Law of Motion (Meriam and Kraige [8]). In the case of an inertial frame the equation is:

$$\Sigma F_i = ma_i \tag{1.1}$$

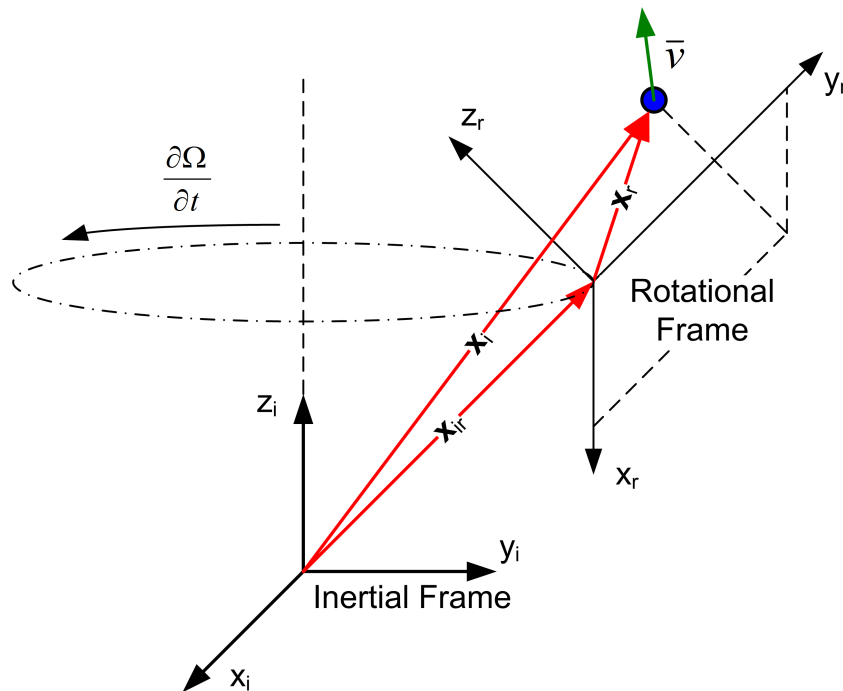
The subscript "i" indicates that the vectors are described in the inertial coordinate system. In the case on a non-inertial frame the equation becomes:

$$\Sigma F_r + \Sigma F_{fictitious} = ma_r \tag{1.2}$$

In this equation the subscript "r" indicates that the vectors are described from the non-inertial coordinate system.

A rotating reference frame is a special case of a non-inertial reference frame. This frame rotates relative to an inertial frame (*Figure 1.1*).

Figure 1.1: Rotating Reference Frame Depicting the Motion of the Moving Earth



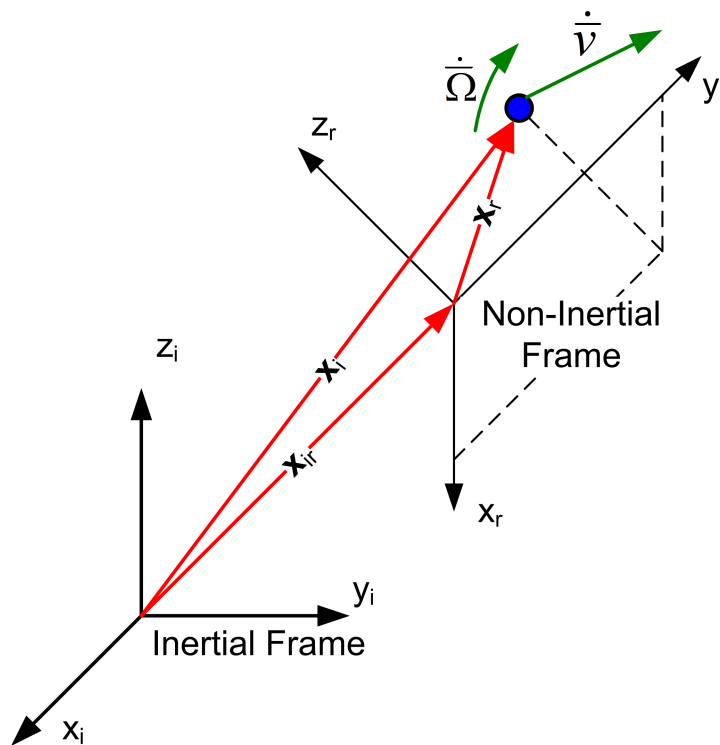
An everyday example is the surface of the earth. The effect of the rotating reference frame can be illustrated by utilizing a Foucault pendulum (Hart et al. [10], Somerville [11]). The rotation of the Earth

causes the pendulum to change its plane of oscillation (fixed in space) with respect to its surroundings (moving with the Earth). The explanation of the apparent change in orientation from an Earth-bound (non-inertial) frame of reference requires the introduction of the fictitious Coriolis force (associated with a rotational reference frame). In an inertial frame outside the Earth, no such fictitious force is necessary. Therefore, fictitious forces do not arise from any physical interaction but rather from the acceleration of the non-inertial frame itself.

The fictitious forces at play here - Coriolis, Euler and Centrifugal forces (Persson [12]) - are proportional to the mass of the fluid element. The Coriolis force acts in a direction perpendicular to the rotational axis and to the velocity of the body in the rotating frame. The centrifugal force acts outward in the radial direction and is proportional to the distance of the body from the axis of the rotating frame. Both these forces are proportional to the angular velocity of the mass in the rotating frame. The Euler force appears when the rotational speed of the frame is not constant. It is therefore proportional to the mass as well as the angular acceleration.

Apart from the fictitious forces that are observed in the non-inertial frame, there are a number of body effects that influences the trajectory of airframes executing arbitrary motion. One such effect, that is high applicable in the aerospace and defence environment, is the Magnus effect (Magnus [13]). This occurs due to the rotation of the object around its own axis while in forward motion (*Figure 1.2*).

Figure 1.2: Relation between the Inertial and Non-Inertial Reference Frames



This rotation is used as a stabilization method since launched airframes are inherently unstable during the initial stages of flight. Positive attitude (a combination of the pitch and yaw angles) must

## CHAPTER 1. INTRODUCTION

---

be maintained either through fin or spin stabilization of the projectile. High rates of change in angular acceleration, along with the changes in airframe attitude, influence the aerodynamic properties of the airframe significantly (Costello and Sahu [14], DeSpirito and Heavy [15]).

Aerodynamic characteristics, such as drag and lift coefficients, are transient parameters required as input to computational performance models. Examples in the defence environment are trajectory codes, missile manoeuvring codes and combustion codes. Most of these applications occur in arbitrary motion. The accuracy of the result of the simulations depends on the confidence of the aerodynamic characteristics (Costello and Sahu [14], Sahu [16, 17], Silton [18]).

Current methods of characterizing aerodynamic coefficients are through empirical methods, wind tunnel measurements, spark range testing and computational models (Davis et al. [19], Pettersson et al. [20], Wernert et al. [21]). In specialized cases, i.e. where accelerating flow is present, neither of these methods (with the exception of spark range testing which is costly and complicated) provides an accurate representation of reality. Conventional wind tunnels are limited by its inability to control the temperature of the airflow. The exact flow conditions, whether it is for internal or external flow, cannot be accurately mimicked. A further drawback that the test piece remains stationary, therefore the rotational effects are not taken into account.

Simulation techniques fail to obtain accurate results since the physics associated with variable rotational and accelerating flow is not fully accounted for. Flow that is in acceleration further requires specialised discretization and meshing techniques that allow for a stable solution.

No case could thus far be found where the simulation was conducted in the relative frame with inclusion of the boundary layer. Some studies accounted for the non-internal effects by the artificial addition of mass (Gledhill et al. [22], Roohani and Skews [5]). Although this method is recommended by certain commercial codes it cannot accurately describe the response of the boundary layer to the arbitrary acceleration in the bulk flow. Other studies do derive the non-inertial terms but makes use a hybrid method in the absolute frame in order to neglect these non-inertial sources terms. This makes the matrices significantly easier to solve (with a reduced stiffness in comparison with matrices containing the source terms) with conventional numerical schemes. Most studies, however, works exclusively from the absolute frame and thus avoid the overhead of resolving the flow in the relative frame.

Investigating the response of boundary layers in arbitrary accelerating flow conditions requires an in-depth understanding of the underlying flow physics. This is be accomplished though the development of a complete mathematical model from first principles. The origin of the fictitious terms, (Coriolis, Euler and centrifugal as well as acceleration of the relative frame with respect to the absolute frame), are seated within the relativity of the non-inertial frame and can be properly evaluated through mathematical derivation (Kageyama and Hyodo [23]). This method can be extended to compressible, viscous derivation of the non-inertial Navier-Stokes equation for arbitrary motion.

In order to clearly define the scope of this research, the following gaps in the literature are addressed within this work:

- Mathematical derivation of non-inertial Navier-Stokes and boundary layer equations. A rigorous and formalized approach are followed and documented.
- Implementation of a non-inertial Navier-Stokes formulation in OpenFOAM. To the best knowledge of the applicant no solver has been written that makes provision for all the acceleration terms.
- Response of the boundary layer to arbitrary motion. Most boundary layer response studies focussed on linear acceleration while aero-ballistic airframes require investigation into arbitrary motion.

## 1.2 Research Approach

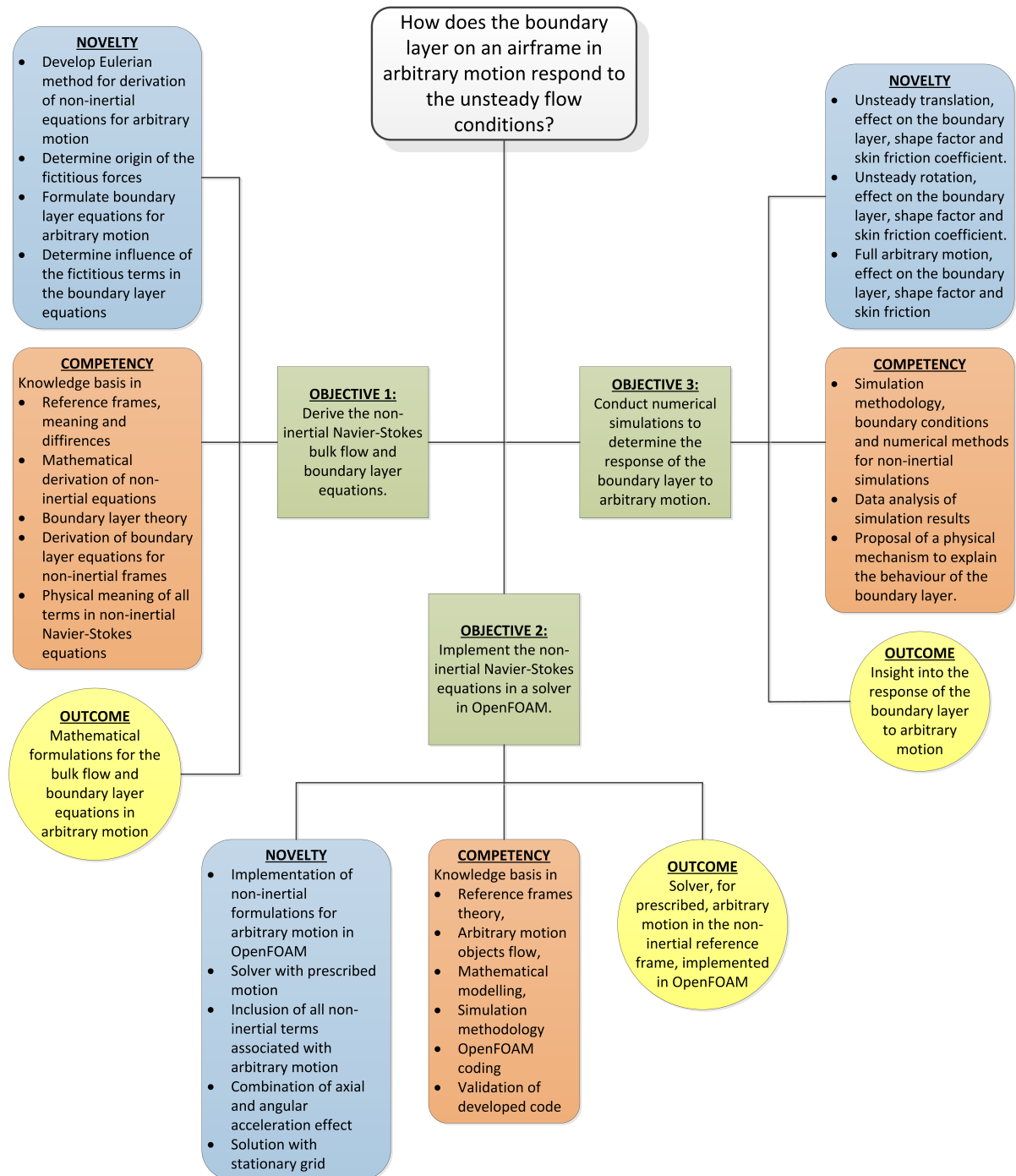
The research question is:

*How does the boundary layer on an airframe in arbitrary motion respond to the unsteady flow conditions?*

The research approach used is depicted in *Figure 1.3*. The phases of the thesis and corresponding objectives are shown. The novelties, competencies built and outcome of each objective is depicted. The objectives address the gaps in knowledge as identified in the literature survey:

- **Objective 1:** *Derive the non-inertial Navier-Stokes bulk flow and boundary layer equations.* The outcome of this phase is the mathematical formulations for the bulk flow and boundary layer in arbitrary motion. This is accomplished by the development of an Eulerian method for non-inertial equation derivation. The boundary layer equations are derived using an order of magnitude analysis.
- **Objective 2:** *Implement the non-inertial Navier-Stokes equations in a solver in OpenFOAM.* The outcome of this phase is the development of a solver for prescribed, arbitrary motion in the non-inertial reference frame, implemented in OpenFOAM.
- **Objective 3:** *Conduct numerical simulations to determine the response of the boundary layer to arbitrary motion.* The outcome of this phase is to provide insight into the response of the boundary layer to arbitrary motion. This is accomplished through analysis of the simulation results.

Figure 1.3: Flow Diagram Depicting the Research Approach



## 1.3 Thesis Overview

The introduction, *Chapter 1*, provides the background to the work conducted in this research. It discusses the research approach that is followed and gives an overview of the thesis. The literature survey is discussed in *Chapter 2*.

In *Chapter 3* the non-inertial equations are derived in the vector form. This is done for pure rotation both in constant and variable rotation. The Eulerian method established is extended to derive the non-inertial equations for full arbitrary motion. The equations established here were implemented in the non-inertial solver in OpenFOAM.

The component form of the equations derived in *Chapter 3* is obtained in *Chapter 4*. Equations are described in the Cartesian, Cylindrical and Curvilinear co-ordinates systems respectively. These formulations are used in *Chapter 5* where the boundary layer equations are derived using a order of magnitude analysis.

The non-inertial boundary layer equations of *Chapter 5* is used in *Chapters 7, 8 and 9* to devise a mechanism for the response of the boundary layer to arbitrary motion.

In *Chapter 6* the non-inertial equations are implemented in a solver. The code implementation, theoretical formulations, case set-up and validation results for this solver is discussed in this chapter.

*Chapters 7, 8 and 9* provides the simulation results for arbitrary motion of a flat plate, rotating disk and rotating cone in axial flow respectively. The response of the boundary layer to arbitrary motion is determined in each case. A mechanism is proposed to explain the response of the velocity profile, shape factor and skin friction coefficient in each case.

This study is concluded with *Chapters 10*. In this chapter the contributions of this work is discussed. Further work and alternative applications of the methods is indicated.

The thesis has two appendixes. In *Appendix A* proof of the identities used in the derivations are given. *Appendix B* depicts the code formulations for the Accelerating Reference Frame solving utility designated **ARFrhoPimpleFoam**.



UNIVERSITEIT VAN PRETORIA  
UNIVERSITY OF PRETORIA  
YUNIBESITHI YA PRETORIA



## Literature Survey

The literature survey focussed on studies that implemented accelerating flow conditions, derivations of the non-inertial Navier-Stokes equations and investigations that resolved the boundary layer for various cases. In this thesis the laminar flat plate, laminar rotating disk and rotating cone in axial flow are used as validation and implementation cases.

### 2.1 Accelerating Flow Implementation

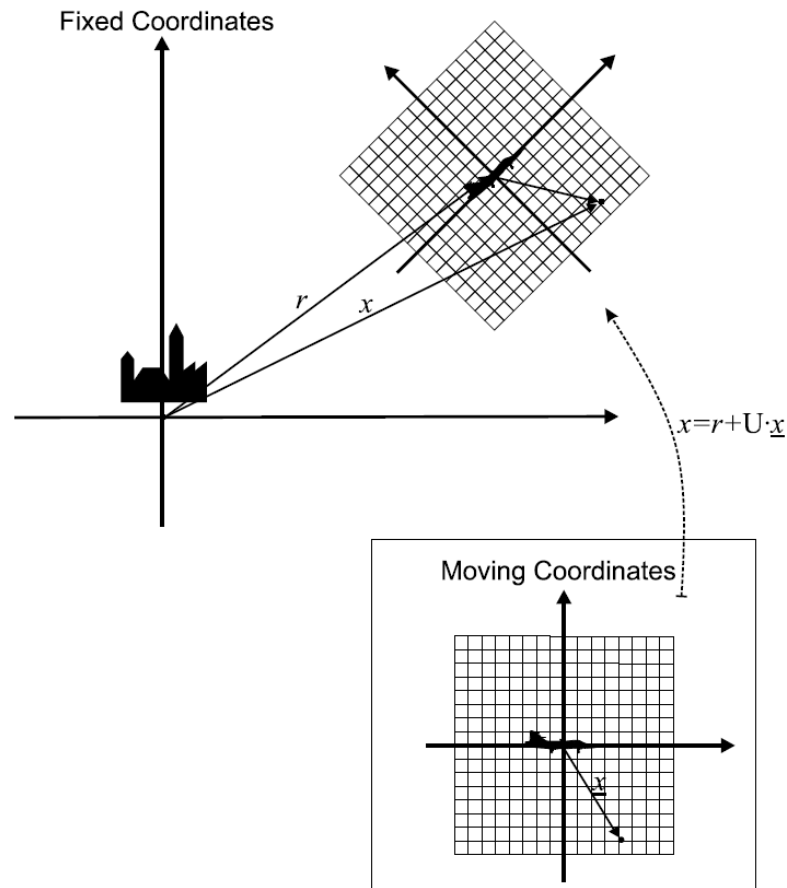
It has only been in recent years that arbitrary acceleration of airframes had been investigated (Roohani and Skews [5], Gledhill et al. [22]). Studies were previously limited to steady state conditions (DeSpirito and Heavy [15], Garibaldi et al. [24]) and in the small number of cases that considered acceleration, constant properties both in translation and rotation was assumed (Limache [3], Biedron and Thomas [1], Gardi [2]). This can be attributed to the difficulty in obtaining experimental results to for validation purposes, the level of difficulty to implement and resolve the formulations of the non-inertial equations and the high expense in computational resources. The recent advances in and availability of computational resources, along with the increased cost of experimentation, has seen to an increase in the requirement and feasibility for high validity Computational Fluid Dynamic (CFD) studies of a more advanced nature. This literature survey has shown that, although the mathematical models that describe arbitrary acceleration have been developed in the 19th century, there are still gaps in published literature concerning this topic.

The derivation of the Navier-Stokes equation in a non-inertial frame (Batchelor [6], Greenspan [7]) has been the foundation for the finite volume formulation. The implementation and application of these equations has been done in various manners in the literature (Biedron and Thomas [1], Gardi [2], Gledhill et al. [22], Inoue et al. [4], Limache [3], Roohani and Skews [5]).

CHAPTER 2. LITERATURE SURVEY

Gledhill et al. [22] made use of the formulation of Forsberg [25], where a hybrid method is developed from the perspective of the absolute frame utilizing co-rotating velocities. This method negates the detrimental effect of the source terms where the properties of the numerical scheme are affected and the conservative character is lost (2.1).

Figure 2.1: The Fixed and Relative Frame as Described by Forsberg [25]



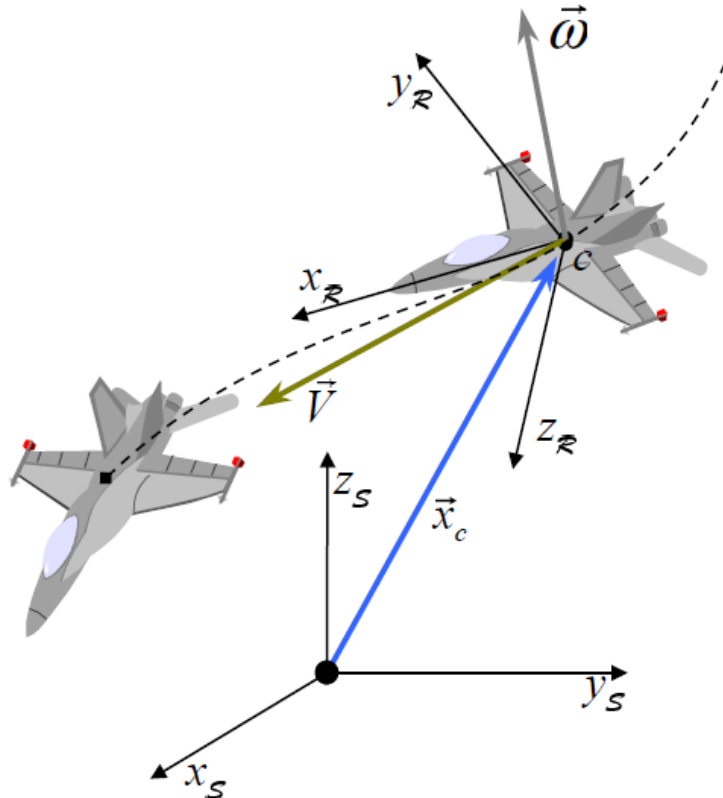
Although the use of the relative velocities serves to reduce the inaccuracies arising from the truncation error in the solution, the matrix increases in stiffness with the addition of the non-inertial source terms. The hybrid method is further significantly easier to implement into a moving grid. This study investigated acceleration effects on missiles at sharp turns, but the hybrid method does not allow for variable rotational velocities.

Roohani and Skews [5] made use of the standard Navier-Stokes formulation (without the acceleration terms in the non-inertial frame) and accounted for the acceleration effects through time-dependant boundary conditions and user-defined functions for mass addition. This methodology artificially introduces the lumped effect of acceleration without quantifying the terms involved. Comparisons were made between the steady state values, acceleration and retardation effects on aerofoils and it was found that there is a significant change in the position of the shock wave location (and hence the aerodynamic

performance) at the same Mach number for steady state and transient acceleration with the greatest effects occurring in the transient regime.

Limache [3] investigated the implementation of non-inertial frame for the purpose of aerodynamic modelling (*Figure 2.2*).

Figure 2.2: Reference Frames of an Aircraft Flying in Arbitrary Motion (Limache [3])



He briefly describes the formulations of the non-inertial Navier-Stokes equations with arbitrary acceleration, but implements the equations in its steady form (aerodynamic steady motion) for inviscid applications (Euler equations).

Biedron and Thomas [1] also describe the formulation of the non-inertial Navier-Stokes Equation, but implement the equations in a manner similar than Gledhill et al. [22] in the absolute frame for steady aerodynamic motions. It is noted in this work that using the absolute-velocity formulation allows for more accurate evaluation of the fluxes in a finite-volume scheme. It is described in this paper as a conservative manner of handling the equations. The energy equation in Biedron and Thomas [1] in the relative frame is implemented without the source terms associated with the acceleration effects. This is in contrast with the formulations of Gardi [2] and Limache [3].

Gardi [2] investigated the differences between the Moving Reference Frame and Arbitrary Lagrangian Eulerian approaches to the study of moving domains. He very briefly touches on the derivation of the material acceleration in a non-inertial reference frame using a Lagrangian approach. But, as is

the case with this approach, it is more intuitive (utilizing Newton's second law) than rigorously mathematical. In this study all the non-inertial acceleration terms were implemented and partially validated against theoretical results. In the last validation case that concerned the flutter on a NACA0012 aerofoil, preference was given to an inviscid solution with slip wall boundaries.

Inoue et al. [4] investigates the focusing of shock waves generated by the linear acceleration of projectiles. The main contribution of the paper is through the simulation of an unsteady flow field past a projectile in parabolic motion and linear acceleration. The acceleration terms are not included in the formulation of the momentum equations and the viscous (diffusion) terms are neglected. In supersonic flow conditions the tendency of most studies is to neglect the viscous terms from the Navier-Stokes equations.

Studies such as Garibaldi et al. [24] and DeSpirito and Heavy [15] investigate spinning bodies in the absolute frame. The non-inertial acceleration effects is not taken into account, inclusion thereof enhance the understanding of the observed effects during flight and result in more accurate prediction of aerodynamic coefficients.

## 2.2 Derivation of Non-Inertial Navier-Stokes Equations

It is apparent from the literature that very few studies derived the equations from first principles. Instead the equation is just implemented in the form it is obtained in from the citations listed in the references. A proper understanding of the meaning of terms can be obtained through derivation of the equations. In some instances it is difficult to differentiate between the terms in the absolute frame and the relative frame, understanding the origin of the terms negates such confusions. The studies that do derive the equations (Forsberg [25]) generally make use of the Lagrangian fluid parcel concept. As an alternative method, adopting an Eulerian approach to the derivation of the non-inertial Navier-Stokes equations Kageyama and Hyodo [23] has the following advantages:

- This approach is general and can be used for any vector field even in cases where the fluid parcel concept is not relevant.
- The physical meaning of this type of derivation is clear as it makes use of local Galilean and rotational transformations.
- This approach is mathematically rigorous.

## 2.3 Boundary Layers in Unsteady Flow

Studies (Brinich and Neumann [26]), Yuan and Piomelli [27], Back [28], Escudier et al. [29], Webster and Eaton [30]) have shown that in favourable pressure gradients (associated with accelerating flow) the structure of the turbulent boundary layer undergo significant changes and resembles the characteristics of a laminar boundary layer. This is referred to re-laminarization of the turbulent boundary layer. The

physics of the boundary layer can be adequately described by laminar boundary layer theory if the acceleration parameter exceeds  $3 \times 10^{-6}$  (Escudier et al. [29], Yuan and Piomelli [27], Webster and Eaton [30]). In the low velocity, laminar near-wall region the viscous components of the flow are orders larger than the momentum components. The flow in the near wall region can therefore not be approximated with either slip wall conditions or Euler equations. Proper resolution of the laminar boundary layer is required both for studies that investigate far-field shock structures and wall-bounded shock interactions (Pirozzoli et al. [31]).

There are a few studies that investigated acceleration effects within the boundary layer (Moore [32], Brinich and Neumann [26], Vleggaar [33], Back [28], Back and Cuffel [34], Bogolepov and Lipatov [35], Dala and Lipatov [36], Samad & Garret (2010)). The majority of the studies took place in the seventies and made use of analytical approaches, mainly the asymptotic methods. This was before computational power was developed at a level that allowed for flow to be solved by means of computational fluid dynamics. There is a gap in the literature with regards to asymptotic methods in acceleration that extends from the late 70's to the late 90's. During this period boundary layers in accelerating flow was either neglected or approximated with wall functions. In recent years, the analytical methods were reintroduced as studies have shown that wall functions cannot adequately describe the response of boundary layers to acceleration effects. The asymptotic methods are a useful tool that enhances understanding of the flow physics.

Moore [32] stated that unsteady laminar boundary layer flow in bodies starting from rest was used by Blasius [37] to investigate the onset of separation and transient effects of impulsive start. He pointed out that those studies only accounted for the earliest phase of motion and that studies were required to investigate unsteady boundary layer flow for longer times elapsed since start and higher at speeds. His applications related to rocket-driven missiles where the boundary layer effects such as skin friction and heat transfer are unsteady for entire ballistic trajectory. Moore further discussed the assumption (Kay [38]) that at high speeds the boundary layer responds with no time lag to changes in stream velocity. The boundary layer would therefore be given the same properties at any instance as it would be in a steady simulation. The question that arises from this: is there a delay in the response of the boundary layer to external stimulus and how does the temporal changes in the bulk flow propagate into the boundary layer? From Roohani and Skews [5] it can be seen that there is a delay in the response of the terminal shock to external flow changes. If the boundary layer in this case were to respond immediately, while the terminal shock is delayed, it will result in interactions between the boundary layer and the shock system. This can not be ignored as it not only influence the aerodynamic performance of the airframe, but it also have an impact on the bulk flow.

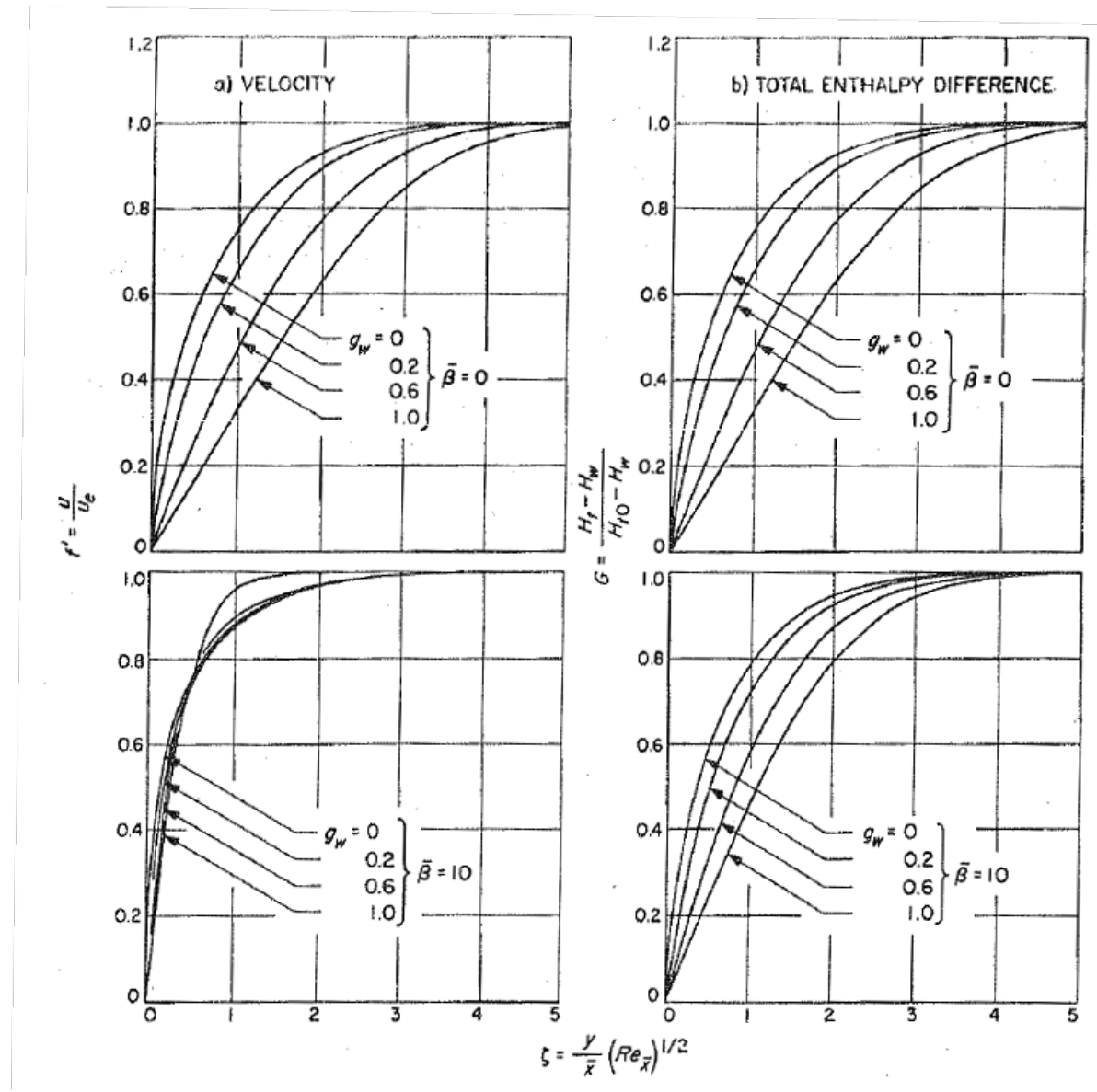
In Moore [32] a compressible, laminar flow over semi-infinite flat plate in rectilinear accelerated flight through still air – which is an idealization of missile flight – investigated through asymptotic methods. His work concluded that in comparison with a quasi-steady state the constant acceleration case results in a thinner boundary layer with greater skin friction coefficient and lower wall temperature. The results indicate that boundary layers in arbitrarily accelerating flow do not respond in the same

CHAPTER 2. LITERATURE SURVEY

manner as a steady state boundary layer. Therefore there is a temporal effect in the response that must be considered. It cannot be assumed without investigation that the response of the boundary layer and the shock system are within the same temporal phase. It is possible that there is some differences in the mechanisms of temporal transportation of information from the bulk flow to the boundary layer and across a terminal shock respectively. Interactions between the boundary layer and the shock wave will then appear.

Back [28] investigated the structure of laminar boundary layer analytically over a large range of flow acceleration, surface cooling (*Figure 2.3*) and flow speeds (*Figure 2.4*).

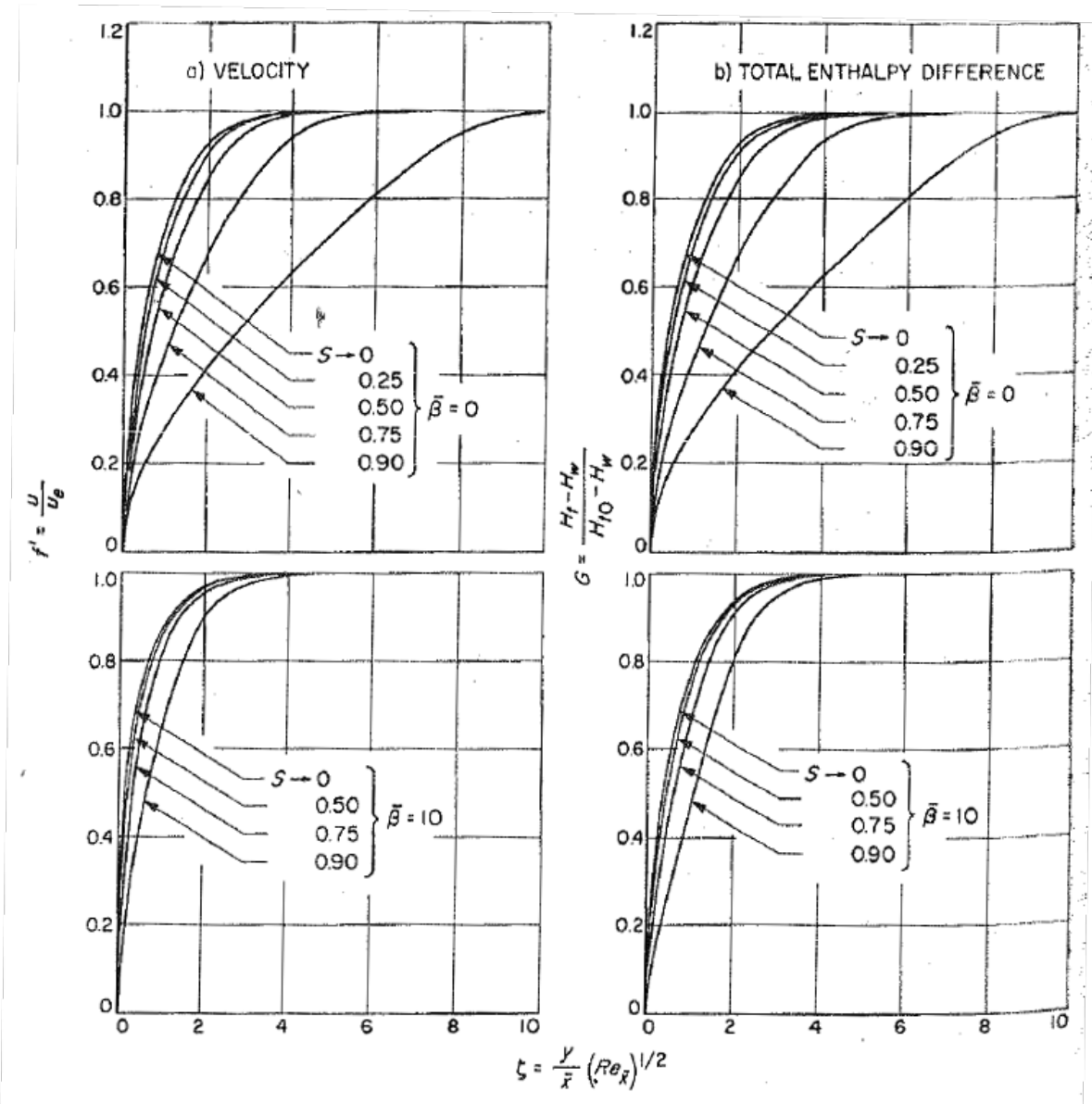
Figure 2.3: Surface Cooling Effect on the Boundary Layer Profile (Back [28])



The focus was on the influence of the variable parameters on skin friction and heat transfer para-

2.3. BOUNDARY LAYERS IN UNSTEADY FLOW

Figure 2.4: Flow Speed Effect on the Boundary Layer Profile (Back [28])



meters as well as boundary layer thickness. The effects of acceleration, cooling and flow speed were found to be significant in aero-ballistic applications. Back [28] noted that due to surface cooling, acceleration and lower Reynolds numbers associated with higher altitude flights or higher internal flow temperatures, laminar boundary layer pockets are found over increasingly larger portions of the surface. Even turbulent boundary layers have been found to revert towards laminar boundary layers in regions of flow acceleration under certain conditions. He further noted that studies on the effects of acceleration and cooling on the structure of laminar boundary layers were becoming more important at the time. In his work it was found that velocity and total enthalpy profiles are steepened near the surface due to acceleration and cooling, while flow speed (compressibility) effects react opposite to this. Boundary



layer thicknesses are strongly dependent on acceleration, cooling and flow speed while friction and heat transfer increased with acceleration and decreased with cooling. This study was extended to include the compressibility effects (Back and Cuffel [34]), in laminar boundary layers with large acceleration and cooling with application on a supersonic nozzle.

Vleggaar [33] investigated the heat transfer and momentum transfer to accelerating surfaces. He followed a systematic approach of formulating the conservation equation for the asymptotic method both in rectangular co-ordinates as well as cylindrical. Three types of cases were considered: acceleration on finite surfaces and continuous surface with and without acceleration and rotation. Vleggaar [33] concentrated on the method to the extent that almost no comments were made with regards to the results obtained. His results on a continuous flat surface have the same tendency as the results from Back [28]; with acceleration shear stress and heat flux increase, while displacement, momentum and boundary layer thicknesses decrease. On the continuous cylindrical surfaces a rotation component is added, yet all accelerations are constant. Momentum transfer increase with acceleration and rotation. It is however curious that the heat transfer decrease with acceleration, but show increase when adding the rotation component. Momentum and displacement thicknesses decrease with acceleration and rotation and the boundary layer reacts in a similar manner.

The most recent study that was found is from Samad and Garrett [39] who investigated the laminar boundary-layer flow over rotating spheroids. The numerical solution and an asymptotic method for determining the laminar boundary was compared with one another. They noted very few studies have been done at that point on laminar flow over spheroids.

## 2.4 Boundary Layers in Rotating Flow

Two cases in this study have been selected for analysing unsteady rotational flow. The first is the laminar, rotating disk and the second is the rotating cone in axial flow. These cases are of interest not only for their fundamental interest, but for the practical applications as well. Applications of interest in the turbo-machinery and aeronautical where flow control relies on accurate prediction of boundary layer disturbance propagation and transitions (Kohama [40]).

An analytical solution for the laminar, rotating disk were derived by von Karman [41] and discussed in detail by Schlichting [42]. The limit for laminar flow were determined by Imayama [43] and Schmid and Henningson [44]. The flow can generally be assumed laminar on a smooth disk for a Reynolds number below 500.

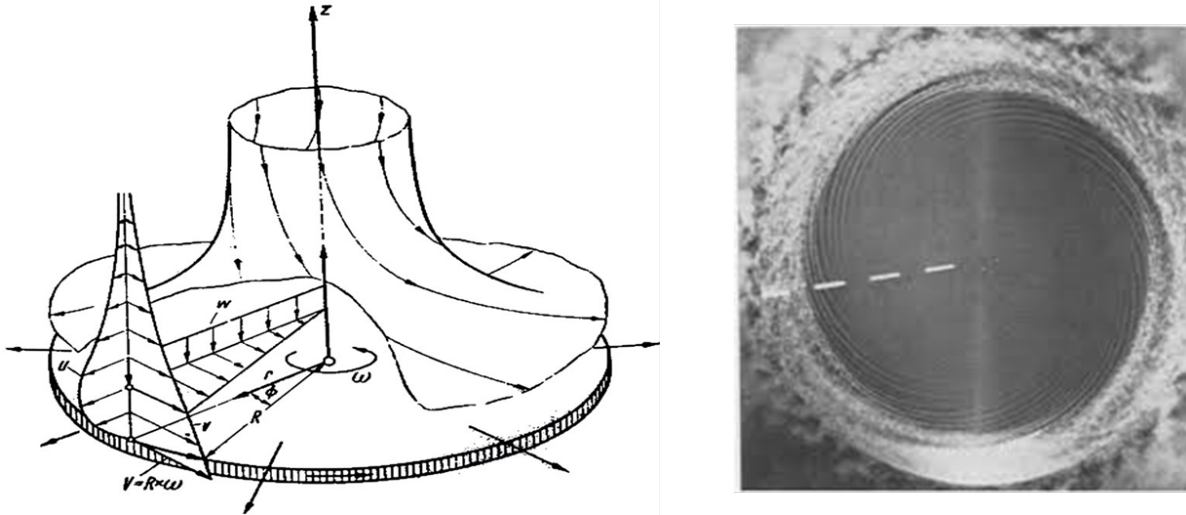
The velocity profiles (Ram [45]) and spiral vortex visualization (Kobayashi et al. [46]) is shown in *Figure 2.5* below. The tangential velocity component of the rotating disk assume the velocity of the disk in the near-wall region and approaches zero velocity further away from the disk. This is as observed from the absolute frame where the flow in the far-field is stationary and the disk is in motion. The flow has a radial component due to the Coriolis and Centrifugal forces acting in the radial direction. Spiral vortices are observed in the transition region (Kobayashi et al. [46]) at a rotational Reynolds number of



2.4. BOUNDARY LAYERS IN ROTATING FLOW

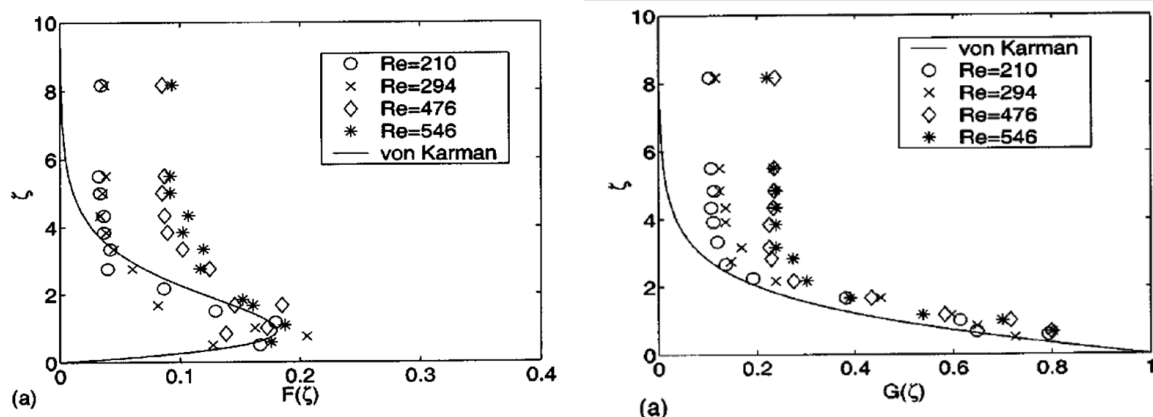
approximately 500.

Figure 2.5: Visualization of the Boundary Layer Profiles (Ram [45] left) and Transition (Kobayashi [46] right) on a Rotating Disk



A cyclonic vortex is present at the centre of the disk (Moulin and Flór [47]). This vortex becomes smaller with increasing disk rotational velocity. The von Karman solution of the rotating disk do not account for the effect of this vortex on the boundary layer. Zoueshtiagh et al. [48] conducted hot-wire experiments on smooth rotating disks. His results indicates that there are differences in the far-field profile values between the von Karman results and the experimental results (Figure 2.6). However, the von Karman solution provides a good estimate of the velocity profile in the near-wall region.

Figure 2.6: Hot-Wire Measurement of the Mean Velocity Profile in the Radial (left) and Azimuthal (right) Directions (Zoueshtiagh [48])



Various studies have been conducted in recent years to investigate transition, stability, heat transfer and surface suction on rotating disks (Attia [49], Harris et al. [50], Siddiqui [51], Zoueshtiagh et al. [48]). The studies are aimed at obtaining a better understanding of the mechanisms in the boundary layer for

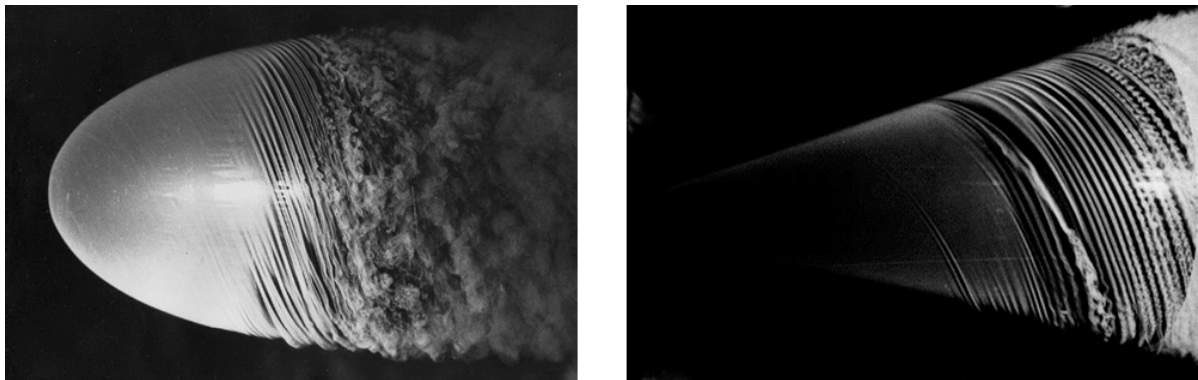
## CHAPTER 2. LITERATURE SURVEY

---

flow control purposes.

The rotating disk provide results that are analogous with rotating machines such as turbine blades. In the aeronautical field flying objects, such a projectiles and aircraft nose cones, resemble rotating cone. A vast number of studies are available that investigates transition on rotating cones in axial flow (Garret and Peake [52], Hussain et al. [53], Kargar and Mansour [54], Kobayashi et al. [55], Kohama [40], Towers and Garrett [56]).

Figure 2.7: Disturbance Propagation and Boundary Layer Transition on Spinning Objects in Axial Flow (Kohama [40], Kobayashi [55])



A rotating cone in axial flow can be considered laminar below a Reynolds number of 249.64 (Mansour and Kargar [57]). Significant work has been done by Garret and Peake [52] to investigate the effect of cone angle and axial flow on transition. It has been found that a larger cone angle delays separation. Furthermore, axial flow stabilizes the boundary layer on a cone and further delays separation.

## Non-Inertial Equations in Vector Form

Arbitrary flow conditions, which segregate inertial from non-inertial reference frames, are widely applicable to the motion of aero-ballistic airframes such as missiles, projectiles, grenades and mortars. A missile can be accelerated by an on-board engine that generates thrust to counter the effect of drag. Spin stabilized projectiles are subjected to high rates of change in the spin axis over the ballistic trajectory. Grenades and mortars experience unsteady deceleration as the target is approached. All of these are examples of arbitrary motion in non-inertial reference frames. The flow field surrounding the airframes can be expressed using the non-inertial Navier-Stokes equations.

Developing a fundamental understanding of the non-inertial equations is pertinent to the development of a computational code that is capable of solving such flows accurately. Firstly the correct formulations of the equations are not intuitive and must be rigorously derived. Secondly, once the equations are implemented, the correct boundary and initial conditions must be utilized to obtain a stable and realistic solution. Deriving the non-inertial equations enhance understanding of the flow physics. This in turn assists in formulating the numerical methods required for computations.

Deriving the equations in the vector form is general. This allows for direct implementation of the governing equations in the computational code, OpenFOAM as described in *Chapter 6*. In this chapter the non-inertial Navier-Stokes Equations for constant rotation, variable rotation and arbitrary motion (both in rotation and translation) are derived. The mathematical identities related to this chapter are located in *Appendix A*.

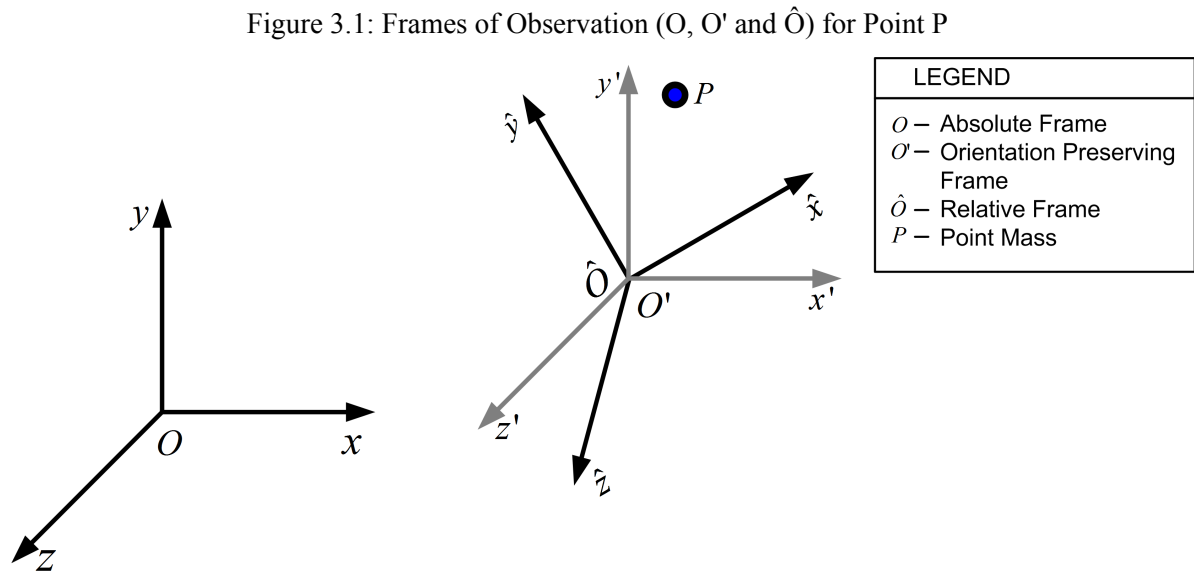
### 3.1 Non-inertial Navier-Stokes Equations for Constant, Pure Rotation

The non-inertial Navier-Stokes equations for constant rotation is derived here using a method based on the work of Kageyama and Hyodo [23]. They established an Eulerian method for deriving the Coriolis force in the momentum equation. This was done for constant, pure rotation in incompressible flow. The method is expanded upon to derive the full set of non-inertial Navier-Stokes equations for compressible flow. In subsequent sections, *Sections 3.2 and 3.3* respectively, the equation sets are derived for variable rotation and full arbitrary motion.

#### 3.1.1 Frame Transformations

The first step in the derivation is to define the relation of the inertial and non-inertial frames with respect to each other. These relations are mathematically described in terms of transformation operators, i.e. local Galilean transform and rotational transform, and is used to change the perspective of the observer.

Assume that three (3) frames exist;  $O$ ,  $O'$  and  $\hat{O}$  as indicated in *Figure 3.1*.



Frame  $O$  is the stationary, inertial frame. This is also referred to as the absolute frame. Frame  $O'$  is an orientation preserving frame ( $\mathbf{i}$  and  $\mathbf{i}'$  has the same orientation), which can be either inertial or non-inertial depending on the cases analysed. This frame shares an origin with the rotational Frame  $\hat{O}$ . Frame  $\hat{O}$  is the non-inertial, rotational frame and is therefore not orientation preserving. This frame is also referred to as the relative frame.

Now consider a point  $P$  which can be observed, and therefore described, from all the frames; Frame  $O$ , Frame  $O'$  and Frame  $\hat{O}$ . Point  $P$  is rotating around the origin of Frame  $O$ , but it is stationary in Frames  $O'$  and  $\hat{O}$ .

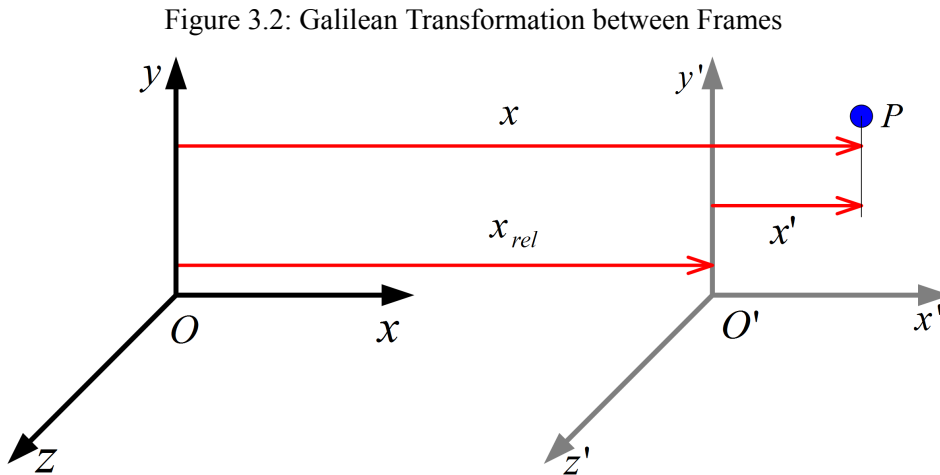
### 3.1. NON-INERTIAL NAVIER-STOKES EQUATIONS FOR CONSTANT, PURE ROTATION

A set of equations are developed to describe the motion of point P in the rotational Frame  $\hat{O}$ . This development results in the non-inertial Navier-Stokes equations for constant, pure rotation. Point P is described below in Frame O from where a local Galilean transformation (defined in *Section 3.1.1.1*),  $G^{\mathbf{M}}$ , is used to transform it to Frame O'. The rotational transform (defined in *Section 3.1.1.2*),  $R^{\Omega t}$ , is then used to transform the resulting equations (as described in Frame O') to the rotational Frame  $\hat{O}$ .

#### 3.1.1.1 Local Galilean Transformation

The standard Galilean transform is limited in its application to constant translation cases. In *Figure 3.2* such a motion is depicted between Frames O and O'. The Galilean transform is used to transform vectors between two reference frames that only differ by a constant vector of motion.

A visual example of this is a train going through a station at constant velocity on a straight train track. If the station platform is considered to be Frame O (which is stationary), then the train is in Frame O' and the displacement between the station and the train can be described as shown in the figure below.



Assume that the origins of the two frames above intersect at time  $t = 0$  (the train drives through the station at time  $t = 0$ ) and that Frame O' is moving at a constant velocity  $V$  in the x-direction (the train is moving at constant speed on a straight track). At time  $t = \Delta t$ , the Frames O and O' are then distance  $x_{rel}$  from each other (the train is distance  $x_{rel}$  from the station).

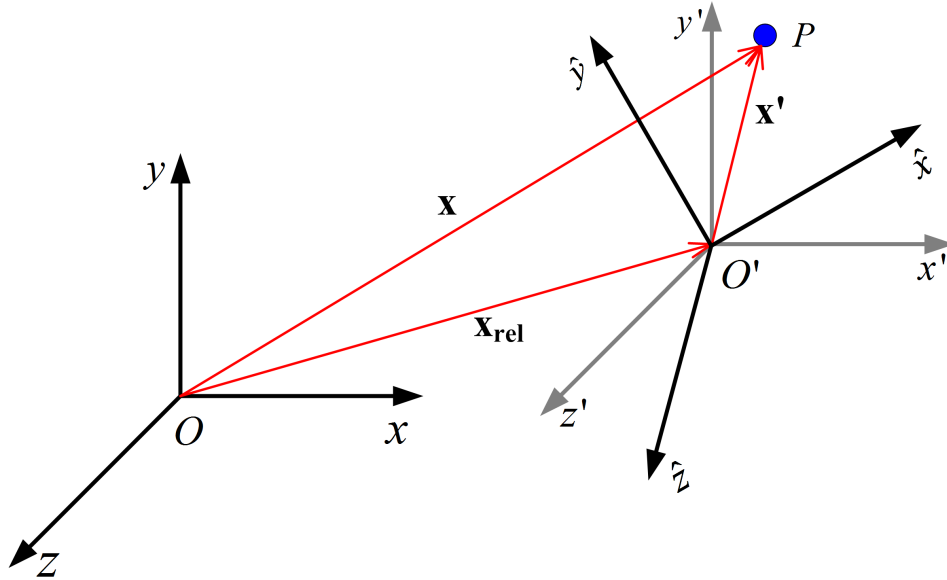
The relationship between the coordinates points for this single event between Frames O and O' is described by *Equation 3.1*. This is known as a standard form of the Galilean transform.

$$\begin{aligned}
 x' &= x - V \Delta t \\
 y' &= y \\
 z' &= z \\
 t' &= t
 \end{aligned}
 \tag{3.1}$$

CHAPTER 3. NON-INERTIAL EQUATIONS IN VECTOR FORM

If it is assumed that the constant motion need not be exclusively in the x-direction (or in translation for that matter) and that it can be presented as a vector of motion as shown in *Figure 3.3*. The motion between the frames is then described by the vector  $\mathbf{x}_{\text{rel}}$  as it was done in Kageyama and Hyodo [23].

Figure 3.3: Local Galilean Transformation between Frames



Let all the Frames ( $O, O'$  and  $\hat{O}$ ) share the same origin where the point  $P$  is stationary in the rotational Frame  $\hat{O}$ . If the rotation is around the  $z$ -axis of Frame  $O$ , the angular acceleration vector  $\boldsymbol{\Omega}$  is described by  $\boldsymbol{\Omega} = (0, 0, \Omega)$ . Therefore point  $P$  is rotating with a constant angular velocity,  $\mathbf{v}_{\text{rel}}$ , around the origin or the inertial Frame  $O$ . The  $\mathbf{x}_{\text{rel}}$  component is described as:

$$\mathbf{x}_{\text{rel}} = \mathbf{V}_{\text{rel}} \Delta t \quad (3.2)$$

where

$$\mathbf{V}_{\text{rel}} = \boldsymbol{\Omega} \wedge \mathbf{x} \quad (3.3)$$

The local Galilean transform operator,  $\mathbf{G}^{\mathbf{M}}$ , is introduced. Any vector defined in the inertial Frame  $O$  can be related to the vector as observed from the orientation preserving Frame  $O'$  by:

$$\mathbf{u}'(\mathbf{x}', t) = \mathbf{G}^{\mathbf{M}} \mathbf{u}(\mathbf{x}, t) \quad (3.4)$$

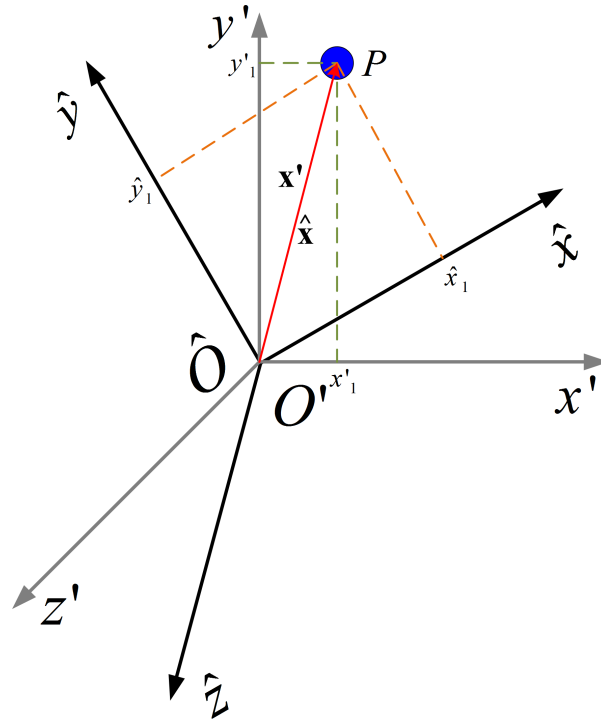
This definition leads to a mathematical description that directly relates the vector fields in the inertial Frame  $O$ , to the vector fields in the orientation preserving Frame  $O'$ :

$$\begin{aligned}
 \mathbf{u}'(\mathbf{x}', t) &= \mathbf{G}^{\mathbf{M}} \mathbf{u}(\mathbf{x}, t) \\
 &= \mathbf{G}^{\boldsymbol{\Omega} \wedge \mathbf{x}} \mathbf{u}(\mathbf{x}, t) \\
 &= \mathbf{u}(\mathbf{x}, t) - \boldsymbol{\Omega} \wedge \mathbf{x} \\
 \mathbf{u}'(\mathbf{x}', t) &= \mathbf{u}(\mathbf{x}, t) + \mathbf{x} \wedge \boldsymbol{\Omega}
 \end{aligned} \quad (3.5)$$

### 3.1.1.2 Rotational Transformation

Frame  $\hat{O}$  shares an origin with the Frame  $O'$ , therefore the vector components in  $\hat{O}$  is related to  $O'$  through a rotational transform (Figure 3.4).

Figure 3.4: Relation between Frame  $O'$  and Frame  $\hat{O}$



The rotation, in this case, is around the  $z$ -axis of Frame  $O$  (that shares an origin with Frame  $O'$ ) with a constant angular velocity of  $\boldsymbol{\Omega} = (0, 0, \Omega)$ . The rotational transform,  $R^{\boldsymbol{\Omega}t}$ , that relates the vectors in Frame  $O'$  to the vectors in Frame  $\hat{O}$  is described by,

$$R^{\boldsymbol{\Omega}t} = \begin{bmatrix} \cos \Omega t & \sin \Omega t & 0 \\ -\sin \Omega t & \cos \Omega t & 0 \\ 0 & 0 & 1 \end{bmatrix} \quad (3.6)$$

such that:

$$\begin{bmatrix} \hat{x} \\ \hat{y} \\ \hat{z} \end{bmatrix} = R^{\boldsymbol{\Omega}t} \begin{bmatrix} x' \\ y' \\ z' \end{bmatrix} \quad (3.7)$$

The first column of the  $R^{\boldsymbol{\Omega}t}$  tensor represents the projection of the  $x'$  vector component (defined in the  $O'$  Frame) on the  $\hat{x}, \hat{y}$  and  $\hat{z}$  axis (defined in the  $\hat{O}$  Frame). In the same manner is the second and third columns the projection of  $y'$  and  $z'$  respectively on the rotational axes,  $\hat{y}$  and  $\hat{z}$ .

From the above, a description follows that relates the vectors in Frame  $O'$  to the vectors in Frame  $\hat{O}$ :

$$\hat{\mathbf{u}}(\hat{\mathbf{x}}, t) = R^{\Omega t} \mathbf{u}'(\mathbf{x}', t) \quad (3.8)$$

*Equations 3.8* and *3.5* can further be used to describe a vector as seen from Frame  $\hat{O}$  in relation to a vector in Frame  $O$ .

$$\hat{\mathbf{u}}(\hat{\mathbf{x}}, t) = R^{\Omega t} G^{\Omega \wedge \mathbf{x}} \mathbf{u}(\mathbf{x}, t) \quad (3.9)$$

$R^{\Omega t}$  is therefore the rotational transform that operates on  $\mathbf{x}'$  to obtain the  $\hat{\mathbf{x}}$  coordinates in the rotational frame. From *Equations 3.5* and *3.9* it is shown that for the velocity vector the following relation holds:

$$\hat{\mathbf{u}}(\hat{\mathbf{x}}, t) = R^{\Omega t} [\mathbf{u}(\mathbf{x}, t) + \mathbf{x} \wedge \boldsymbol{\Omega}] \quad (3.10)$$

### 3.1.2 Incompressible Flow Conditions

The local Galilean invariance,  $G^{\Omega \wedge \mathbf{x}}$ , and the rotational transform,  $R^{\Omega t}$ , have been described for constant rotational conditions. Both the operators are required to derive the non-inertial Navier-Stokes equations for constant rotation. The Galilean invariance is required to account for the relative motion between the frames, whilst maintaining the orientation of the unit vectors. The rotational transform is required to account of the change in orientation of the unit vectors due rotational motion of the relative frame.

In this section the non-inertial Navier-Stokes equations for conservation of mass, momentum and energy for constant rotation in incompressible flow are derived using an Eulerian approach adapted from Kageyama and Hyodo [23]. The derivation commences from the perspective of the absolute observer (Eulerian approach) instead of using the conventional Lagrangian method where the derivation is done directly from the relative observation point.

#### 3.1.2.1 Continuity Equation

The conservation of mass equation, referred to as the continuity equation, in the inertial frame takes the form (White [9]):

$$\frac{\partial \rho}{\partial t} + (\nabla \cdot \rho \mathbf{u}) = 0 \quad (3.11)$$

The first term represents the temporal change in density due to compressibility of the flow. In compressible fluids the density is a non-constant function of pressure and temperature (Anderson [58]). Any fluid particle that interacts with a adjacent fluid particle as a result of a bulk pressure force undergoes compression where the specific volume of the flow is decreased. Specific volume is the inverse of density and results in temporal variation of the density field. When the bulk compressibility of the flow is small in comparison to pressure variations in the free stream, variations in pressure cause only small changes in specific volume and hence density. The flow is then assumed to be incompressible when changes in pressure and temperature causes very small temporal variations in density. This assumption is used in low Mach number flows, typically below Mach 0.3. This case is assumed to be incompressible



### 3.1. NON-INERTIAL NAVIER-STOKES EQUATIONS FOR CONSTANT, PURE ROTATION

and the temporal density term can be neglected (Anderson [58], White [9]), but for the purposes of the derivation it remains in the equation until the last step.

The second term is the divergence of density and velocity which represents the residual mass flux of a given control volume.

The non-inertial form of the unsteady density term can be described as:

$$\frac{\partial \hat{\rho}}{\partial t}(\hat{\mathbf{x}}_t, t) = \lim_{\Delta t \rightarrow 0} \frac{\hat{\rho}(\hat{\mathbf{x}}_{t+\Delta t}, t + \Delta t) - \hat{\rho}(\hat{\mathbf{x}}_t, t)}{\Delta t} \quad (3.12)$$

A Taylor series expansion of the term  $\hat{\rho}(\hat{\mathbf{x}}_{t+\Delta t}, t + \Delta t)$  provides:

$$\hat{\rho}(\hat{\mathbf{x}}_{t+\Delta t}, t + \Delta t) = \hat{\rho}(\mathbf{x}_t, t) + [\Delta t(\boldsymbol{\Omega} \wedge \mathbf{x}_t) \cdot \nabla] \hat{\rho}(\mathbf{x}_t, t) + (\Delta t \frac{\partial}{\partial t}) \hat{\rho}(\mathbf{x}_t, t) + \dots \quad (3.13)$$

Substitution of this expansion in the *Equation 3.12* and manipulation result in an expression that relates the non-inertial, unsteady density to the inertial frame.

$$\frac{\partial \hat{\rho}}{\partial t} = R^{\Omega t} \left[ \frac{\partial \rho}{\partial t} + (\boldsymbol{\Omega} \wedge \mathbf{x}_t) \cdot \nabla \rho \right] \quad (3.14)$$

The second term of the continuity equation is affected by both frame transformations since it contains the velocity vector:

$$\begin{aligned} (\hat{\nabla} \cdot \hat{\rho} \hat{\mathbf{u}}) &= R^{\Omega t} G^{\Omega \wedge \mathbf{x}} (\nabla \cdot \rho \mathbf{u}) \\ &= R^{\Omega t} [\nabla \cdot \rho (G^{\Omega \wedge \mathbf{x}} \mathbf{u})] \end{aligned} \quad (3.15)$$

*Equation 3.10* is used to complete the local Galilean transformation, and the equation becomes:

$$\begin{aligned} (\hat{\nabla} \cdot \hat{\rho} \hat{\mathbf{u}}) &= R^{\Omega t} [\nabla \cdot \rho (\mathbf{u} + \mathbf{x} \wedge \boldsymbol{\Omega})] \\ &= R^{\Omega t} [\nabla \cdot (\rho \mathbf{u}) + \nabla \cdot \rho (\mathbf{x} \wedge \boldsymbol{\Omega})] \end{aligned}$$

The equation can be manipulated to the convenient form where the second term is of equal size and opposite sign on the second term in *Equation 3.14*.

$$\hat{\nabla} \cdot \hat{\rho} \hat{\mathbf{u}} = R^{\Omega t} [\nabla \cdot (\rho \mathbf{u}) - (\boldsymbol{\Omega} \wedge \mathbf{x}) \cdot \nabla \rho] \quad (3.16)$$

The addition of *Equations 3.14* and *3.16* lead to a relation between the continuity equation in the inertial and rotational frames:

$$\frac{\partial \hat{\rho}}{\partial t} + \hat{\nabla} \cdot \hat{\rho} \hat{\mathbf{u}} = R^{\Omega t} \left[ \frac{\partial \rho}{\partial t} + \nabla \cdot (\rho \mathbf{u}) \right] \quad (3.17)$$

The right hand side of the equation is equal to zero since this represents the continuity equation in the inertial frame (*Equation 3.11*):

$$\frac{\partial \hat{\rho}}{\partial t} + \hat{\nabla} \cdot \hat{\rho} \hat{\mathbf{u}} = 0 \quad (3.18)$$

CHAPTER 3. NON-INERTIAL EQUATIONS IN VECTOR FORM

---

Since this is the incompressible case, the temporal term is equal to zero. The continuity equation for the rotational frame therefore takes the form:

$$\hat{\nabla} \cdot \hat{\rho} \hat{\mathbf{u}} = 0 \quad (3.19)$$

The physical meaning of this equation describes the very nature of incompressible flow assumption; the residual mass flux in a specific control volume is zero (Anderson [58]). This means that there are no compressible effects in the flow because the same amount of mass flux that enters a domain exits it. The transient density term causes a change in the residual mass flux in the domain that manifests itself in the form of compressibility.

### 3.1.2.2 Momentum Equation

The inertial equation for incompressible momentum conservation is describe by the equation below (White [9]):

$$\frac{\partial \mathbf{u}}{\partial t} + (\mathbf{u} \cdot \nabla) \mathbf{u} = -\nabla \psi + \nu \nabla^2 \mathbf{u} \quad (3.20)$$

where  $\psi$  is the pressure per unit mass where the pressure is divided by the density. The density was divided into all the terms of the equation since the flow is assumed to be incompressible:

$$\psi = \frac{p}{\rho} \quad (3.21)$$

The transformation of the equation above to the rotational frame is done in a similar manner as in *Section 3.1.2.1* - the terms are transformed separately and then summed to find the final expression.

The first term that is transformed, to obtain an expression that relates the inertial Frame O to the rotational Frame  $\hat{O}$ , is the time dependant term. It is expressed here through the definition of the derivative at a point (Tannehill et al. [59]):

$$\frac{\partial \hat{\mathbf{u}}}{\partial t}(\hat{\mathbf{x}}_t, t) = \lim_{\Delta t \rightarrow 0} \frac{\hat{\mathbf{u}}(\hat{\mathbf{x}}_{t+\Delta t}, t + \Delta t) - \hat{\mathbf{u}}(\hat{\mathbf{x}}_t, t)}{\Delta t} \quad (3.22)$$

The expression above, which is in the non-inertial Frame  $\hat{O}$ , can be related to the inertial Frame O by finding an inertial expression for  $\hat{\mathbf{u}}(\hat{\mathbf{x}}_{t+\Delta t}, t + \Delta t)$  in the form of *Equation 3.9*:

$$\hat{\mathbf{u}}(\hat{\mathbf{x}}_{t+\Delta t}, t + \Delta t) = R^{\Omega(t+\Delta t)} G^{\Omega \wedge \mathbf{x}_{t+\Delta t}} [\mathbf{u}(\mathbf{x}_{t+\Delta t}, t + \Delta t)] \quad (3.23)$$

The method that is used to expand the relation above, in the inertial frame, is described in the paragraph below.

Perform a Taylor series expansion for  $\mathbf{x}_{t+\Delta t}$ :

$$\mathbf{x}_{t+\Delta t} = \mathbf{x}_t + \mathbf{V}_{\text{rel}} \Delta t + O(\Delta t^2) \quad (3.24)$$

### 3.1. NON-INERTIAL NAVIER-STOKES EQUATIONS FOR CONSTANT, PURE ROTATION

The resulting series is truncated at the second order term since this case involves constant motion and the higher order terms represents the arbitrary motion. The derivative term is substituted with *Equation 3.3*. Re-arrangement of the terms lead to an expression for displacement over the specific time interval:

$$\mathbf{x}_{t+\Delta t} - \mathbf{x}_t = \mathbf{x}_{\Delta t} = (\boldsymbol{\Omega} \wedge \mathbf{x}_t)\Delta t \quad (3.25)$$

A Fourier series expansion is done for  $\mathbf{u}(\mathbf{x}_{t+\Delta t}, t + \Delta t)$ , and with substitution of *Equation 3.25* it results in:

$$\mathbf{u}(\mathbf{x}_{t+\Delta t}, t + \Delta t) = \mathbf{u}(\mathbf{x}_t, t) + [\Delta t(\boldsymbol{\Omega} \wedge \mathbf{x}_t) \cdot \nabla] \mathbf{u}(\mathbf{x}_t, t) + \left(\Delta t \frac{\partial}{\partial t}\right) \mathbf{u}(\mathbf{x}_t, t) \quad (3.26)$$

*Equation 3.26* is substituted into *Equation 3.23* to get the expression:

$$\hat{\mathbf{u}}(\hat{\mathbf{x}}_{t+\Delta t}, t + \Delta t) = R^{\boldsymbol{\Omega}(t+\Delta t)} G^{\boldsymbol{\Omega} \wedge \mathbf{x}_{t+\Delta t}} \{ \mathbf{u}(\mathbf{x}_t, t) + [\Delta t(\boldsymbol{\Omega} \wedge \mathbf{x}_t) \cdot \nabla] \mathbf{u}(\mathbf{x}_t, t) + \left(\Delta t \frac{\partial}{\partial t}\right) \mathbf{u}(\mathbf{x}_t, t) \} \quad (3.27)$$

$G^{\boldsymbol{\Omega} \wedge \mathbf{x}_{t+\Delta t}}$  can be simplified as shown below. *Equation 3.24* is substituted in the operator and truncated at the first order. The error made with this simplification is of order  $\Delta t$ . It is shown further on in this section that  $\Delta t$  approximates a very small number,  $\varepsilon$ . Therefore the error approximates a very small number  $\varepsilon$ , when

$$\begin{aligned} \Delta t &\rightarrow \varepsilon \\ \varepsilon &\rightarrow 0 \end{aligned} \quad (3.28)$$

Subsequently, it can be shown that:

$$\begin{aligned} G^{\boldsymbol{\Omega} \wedge \mathbf{x}_{t+\Delta t}} &= G^{\boldsymbol{\Omega} \wedge \{ \mathbf{x}_t + \Delta t(\boldsymbol{\Omega} \wedge \mathbf{x}_t + O[\Delta t^2]) \}} \\ &= G^{\boldsymbol{\Omega} \wedge \{ \mathbf{x}_t(1 + O[\Delta t]) \}} \approx G^{\boldsymbol{\Omega} \wedge \mathbf{x}_t} \end{aligned} \quad (3.29)$$

The expression for  $\hat{\mathbf{u}}(\hat{\mathbf{x}}_{t+\Delta t}, t + \Delta t)$ , then becomes:

$$\hat{\mathbf{u}}(\hat{\mathbf{x}}_{t+\Delta t}, t + \Delta t) = R^{\boldsymbol{\Omega}(t+\Delta t)} G^{\boldsymbol{\Omega} \wedge \mathbf{x}_t} \{ \mathbf{u}(\mathbf{x}_t, t) + [\Delta t(\boldsymbol{\Omega} \wedge \mathbf{x}_t) \cdot \nabla] \mathbf{u}(\mathbf{x}_t, t) + \left(\Delta t \frac{\partial}{\partial t}\right) \mathbf{u}(\mathbf{x}_t, t) \} \quad (3.30)$$

The assumption was made that point P is fixed in the rotating frame and the rotation is around the shared origin of the Frames O, O' and  $\hat{O}$ , with this in mind an expression can be derived for  $\mathbf{x}_t$ :

$$\begin{aligned} \hat{\mathbf{x}} &= R^{\boldsymbol{\Omega}(t+\Delta t)} \mathbf{x}_{t+\Delta t} = R^{\boldsymbol{\Omega}t} \mathbf{x}_t \\ \mathbf{x}_t &= R^{\boldsymbol{\Omega}\Delta t} \mathbf{x}_{t+\Delta t} \end{aligned} \quad (3.31)$$

This relation is substituted in the Taylor series expansion for  $\mathbf{x}_{t+\Delta t}$ :

$$\begin{aligned} \mathbf{x}_{t+\Delta t} &= \mathbf{x}_t + \Delta t \mathbf{V} + O[\Delta t^2] \\ &= R^{\boldsymbol{\Omega}\Delta t} \mathbf{x}_{t+\Delta t} + \Delta t(\boldsymbol{\Omega} \wedge \mathbf{x}_t) + O[\Delta t^2] \end{aligned} \quad (3.32)$$

Re-arrange this equation and consider in the limit as  $\Delta t$  approaches  $\varepsilon$  as  $\varepsilon$  tends to 0:

$$\lim_{\Delta t \rightarrow 0} \frac{R^{\boldsymbol{\Omega}\Delta t} \mathbf{x}_{t+\Delta t} - \mathbf{x}_{t+\Delta t}}{\Delta t} = \lim_{\Delta t \rightarrow 0} (\mathbf{x}_t \wedge \boldsymbol{\Omega}) \quad (3.33)$$

CHAPTER 3. NON-INERTIAL EQUATIONS IN VECTOR FORM

Considering this relation for any vector  $\mathbf{b}$  (where in the case  $\mathbf{b} \rightarrow \mathbf{x}_t$ ), and take into account that  $\mathbf{x}_{t+\Delta t} \rightarrow \mathbf{x}_t$  as  $\Delta t \rightarrow 0$ , the following equation is arrived at:

$$\lim_{\Delta t \rightarrow 0} \frac{R^{\Omega \Delta t} \mathbf{b} - \mathbf{b}}{\Delta t} = \mathbf{b} \wedge \boldsymbol{\Omega} \quad (3.34)$$

By applying the same analogies as in *Equation 3.31* to the velocity field, it can be shown that *Equation 3.34* is valid when  $\mathbf{b} \rightarrow \mathbf{u}_t$ .

Substitute *Equation 3.30* into *Equation 3.22* to obtain the equation:

$$\frac{\partial \hat{\mathbf{u}}}{\partial t}(\hat{\mathbf{x}}_t, t) = \lim_{\Delta t \rightarrow 0} \frac{R^{\Omega(t+\Delta t)} G^{\Omega \wedge \mathbf{x}_t} \{ [1 - \frac{1}{R^{\Omega \Delta t}} + (\Delta t (\boldsymbol{\Omega} \wedge \mathbf{x}_t) \cdot \nabla)] \mathbf{u}(\mathbf{x}_t, t) + (\Delta t \frac{\partial}{\partial t}) \mathbf{u}(\mathbf{x}_t, t) \}}{\Delta t} \quad (3.35)$$

By using *Equation 3.34*, and after re-arrangement of the terms the following expression is arrived at:

$$\frac{\partial \hat{\mathbf{u}}}{\partial t}(\hat{\mathbf{x}}_t, t) = R^{\Omega t} \left[ \frac{\partial}{\partial t} + (\boldsymbol{\Omega} \wedge \mathbf{x}_t) \cdot \nabla - \boldsymbol{\Omega} \wedge \right] [G^{\Omega \wedge \mathbf{x}} \mathbf{u}(\mathbf{x}_t, t)] \quad (3.36)$$

Substitution of *Equation 3.10* into the equation above results in:

$$\begin{aligned} \frac{\partial \hat{\mathbf{u}}}{\partial t}(\hat{\mathbf{x}}_t, t) &= R^{\Omega t} \left[ \frac{\partial}{\partial t} + (\boldsymbol{\Omega} \wedge \mathbf{x}_t) \cdot \nabla - \boldsymbol{\Omega} \wedge \right] (\mathbf{u}(\mathbf{x}_t, t)) \\ &+ R^{\Omega t} \left[ \frac{\partial}{\partial t} + (\boldsymbol{\Omega} \wedge \mathbf{x}_t) \cdot \nabla - \boldsymbol{\Omega} \wedge \right] (\mathbf{x}_t \wedge \boldsymbol{\Omega}) \end{aligned} \quad (3.37)$$

In the equation above the transient component of  $[\frac{\partial}{\partial t} + (\boldsymbol{\Omega} \wedge \mathbf{x}_t) \cdot \nabla - \boldsymbol{\Omega} \wedge](\mathbf{x}_t \wedge \boldsymbol{\Omega})$  is equal to zero. This is shown piecewise in the paragraphs below. Consider the transient components of the term first:

$$\frac{\partial}{\partial t}(\mathbf{x}_t \wedge \boldsymbol{\Omega}) = \frac{\partial \mathbf{x}_t}{\partial t} \wedge \boldsymbol{\Omega} + \mathbf{x}_t \wedge \frac{\partial \boldsymbol{\Omega}}{\partial t} = 0 \quad (3.38)$$

The first term is zero because the magnitude of  $\mathbf{x}_t$  is constant over the time domain; its magnitude does not change with respect to the origin since this case involves pure rotation. The second term is zero due to constant rotation of the point P. In the case where the rotation is not constant, this term plays a role as seen in *Section 3.2*.

By introduction of the identity below (see *Appendix A*), the terms  $[(\boldsymbol{\Omega} \wedge \mathbf{x}_t) \cdot \nabla - \boldsymbol{\Omega} \wedge](\mathbf{x}_t \wedge \boldsymbol{\Omega})$  can be simplified. In this case  $\mathbf{a}$  represents a vector.

$$(\mathbf{a} \cdot \nabla)(\mathbf{x}_t \wedge \boldsymbol{\Omega}) = \mathbf{a} \wedge \boldsymbol{\Omega} \quad (3.39)$$

The entire term is hence cancelled out:

$$\begin{aligned} [(\boldsymbol{\Omega} \wedge \mathbf{x}_t) \cdot \nabla - \boldsymbol{\Omega} \wedge](\mathbf{x}_t \wedge \boldsymbol{\Omega}) &= [(\boldsymbol{\Omega} \wedge \mathbf{x}_t) \cdot \nabla](\mathbf{x}_t \wedge \boldsymbol{\Omega}) - \boldsymbol{\Omega} \wedge (\mathbf{x}_t \wedge \boldsymbol{\Omega}) \\ &= \boldsymbol{\Omega} \wedge (\mathbf{x}_t \wedge \boldsymbol{\Omega}) - \boldsymbol{\Omega} \wedge (\mathbf{x}_t \wedge \boldsymbol{\Omega}) \\ &= 0 \end{aligned} \quad (3.40)$$

### 3.1. NON-INERTIAL NAVIER-STOKES EQUATIONS FOR CONSTANT, PURE ROTATION

This leads to the final description of the unsteady terms in the momentum equation. Note the appearance of one part of the Coriolis effect manifesting in the relation below.

$$\frac{\partial \hat{\mathbf{u}}}{\partial t}(\hat{\mathbf{x}}_t, t) = R^{\Omega t} \left[ \frac{\partial}{\partial t} + (\boldsymbol{\Omega} \wedge \mathbf{x}_t) \cdot \nabla - \underbrace{\boldsymbol{\Omega} \wedge}_{\text{Coriolis}} \right] (\mathbf{u}(\mathbf{x}_t, t)) \quad (3.41)$$

The relation of the inertial to the rotational advection term is described in the following manner:

$$\begin{aligned} (\hat{\mathbf{u}} \cdot \hat{\nabla}) \hat{\mathbf{u}} &= R^{\Omega t} G^{\Omega \wedge \mathbf{x}} (\mathbf{u} \cdot \nabla) \mathbf{u} \\ &= R^{\Omega t} (G^{\Omega \wedge \mathbf{x}} \mathbf{u} \cdot \nabla) G^{\Omega \wedge \mathbf{x}} \mathbf{u} \end{aligned} \quad (3.42)$$

Substitution of *Equation 3.10* into the equation above results in:

$$\begin{aligned} (\hat{\mathbf{u}} \cdot \hat{\nabla}) \hat{\mathbf{u}} &= R^{\Omega t} [(\mathbf{u} + \mathbf{x} \wedge \boldsymbol{\Omega}) \cdot \nabla] (\mathbf{u} + \mathbf{x} \wedge \boldsymbol{\Omega}) \\ &= R^{\Omega t} [(\mathbf{u} + \mathbf{x} \wedge \boldsymbol{\Omega}) \cdot \nabla] \mathbf{u} + R^{\Omega t} [(\mathbf{u} + \mathbf{x} \wedge \boldsymbol{\Omega}) \cdot \nabla] (\mathbf{x} \wedge \boldsymbol{\Omega}) \end{aligned} \quad (3.43)$$

Dividing out all the terms gives the final relation of the advection term between the frames. Note the appearance of the centrifugal effect and the other part of the Coriolis effect from the transformation of the advection term.

$$(\hat{\mathbf{u}} \cdot \hat{\nabla}) \hat{\mathbf{u}} = R^{\Omega t} \left[ (\mathbf{u} \cdot \nabla) \mathbf{u} + ((\mathbf{x} \wedge \boldsymbol{\Omega}) \cdot \nabla) \mathbf{u} + \underbrace{(\mathbf{u} \wedge \boldsymbol{\Omega})}_{\text{Coriolis}} + \underbrace{(\mathbf{x} \wedge \boldsymbol{\Omega}) \wedge \boldsymbol{\Omega}}_{\text{Centrifugal}} \right] \quad (3.44)$$

The gradient of the specific pressure term in the momentum equation is described between Frames  $\hat{O}$  and  $O$  in the following manner:

$$\hat{\nabla} \hat{\psi} = R^{\Omega t} G^{\Omega \wedge \mathbf{x}} \nabla \psi \quad (3.45)$$

Scalars are invariant under Galilean transformation (Kleppner and Kolenkow [60], McCauley [61]). Scalars are not invariant under the rotational transform if spatial operations is performed on it since the axis along which the discretization is performed, changes between all the frames. The relation between the gradient of specific pressure in the inertial and rotational frames is therefore described by:

$$\hat{\nabla} \hat{\psi} = R^{\Omega t} \nabla \psi \quad (3.46)$$

The diffusion term in the inertial Frame  $O$  can be related to the rotational Frame  $\hat{O}$  in the following manner:

$$\begin{aligned} \nu \hat{\nabla}^2 \hat{\mathbf{u}} &= R^{\Omega t} G^{\Omega \wedge \mathbf{x}} \nu \nabla^2 \mathbf{u} \\ &= R^{\Omega t} \nu \nabla^2 G^{\Omega \wedge \mathbf{x}} \mathbf{u} \\ &= R^{\Omega t} \nu \nabla^2 (\mathbf{u} + \mathbf{x} \wedge \boldsymbol{\Omega}) \\ &= R^{\Omega t} \nu [\nabla^2 \mathbf{u} + \nabla^2 (\mathbf{x} \wedge \boldsymbol{\Omega})] \end{aligned} \quad (3.47)$$

CHAPTER 3. NON-INERTIAL EQUATIONS IN VECTOR FORM

---

If it is considered that, as shown in *Appendix A*,

$$\nabla^2(\mathbf{x} \wedge \boldsymbol{\Omega}) = 0 \quad (3.48)$$

the diffusion term is invariant under Galilean transformation:

$$\nu \hat{\nabla}^2 \hat{\mathbf{u}} = R^{\Omega t} \nu \nabla^2 \mathbf{u} \quad (3.49)$$

Note that the pressure and viscous terms are Galilean invariant in this instance and combine the two components in a vector  $\mathbf{f}(\mathbf{x}, t)$ :

$$\mathbf{f}(\mathbf{x}, t) = -\nabla\psi + \nu \nabla^2 \mathbf{u} \quad (3.50)$$

The new, combined parameter in the inertial and rotational frames is related in the following manner due to the invariance:

$$\hat{\mathbf{f}}(\hat{\mathbf{x}}, t) = R^{\Omega t} \mathbf{f}(\mathbf{x}, t) \quad (3.51)$$

The transformation of the momentum is completed through the summation of the unsteady and advection terms in the rotational and inertial frames as determined in *Equations 3.41* and *3.44*:

$$\begin{aligned} \frac{\partial \hat{\mathbf{u}}}{\partial t} + (\hat{\mathbf{u}} \cdot \hat{\nabla}) \hat{\mathbf{u}} &= R^{\Omega t} \left[ \frac{\partial \mathbf{u}}{\partial t} + (\mathbf{u} \cdot \nabla) \mathbf{u} + 2\mathbf{u} \wedge \boldsymbol{\Omega} + \mathbf{x} \wedge \boldsymbol{\Omega} \wedge \boldsymbol{\Omega} \right] \\ &= R^{\Omega t} \left[ \frac{\partial \mathbf{u}}{\partial t} + (\mathbf{u} \cdot \nabla) \mathbf{u} \right] + R^{\Omega t} [2\mathbf{u} \wedge \boldsymbol{\Omega} + \mathbf{x} \wedge \boldsymbol{\Omega} \wedge \boldsymbol{\Omega}] \end{aligned} \quad (3.52)$$

The first term grouping of the equation above is simplified as shown in the equations below. This was done using *Equations 3.20*, *3.50* and *3.51*.

$$\begin{aligned} R^{\Omega t} \left[ \frac{\partial \mathbf{u}}{\partial t} + (\mathbf{u} \cdot \nabla) \mathbf{u} \right] &= R^{\Omega t} (-\Delta\psi + \nu \nabla^2 \mathbf{u}) \\ &= R^{\Omega t} \mathbf{f}(\mathbf{x}, t) \\ &= \hat{\mathbf{f}}(\hat{\mathbf{x}}, t) \end{aligned} \quad (3.53)$$

The second term grouping, with the insertion of *Equation 3.10*, becomes:

$$\begin{aligned} R^{\Omega t} [2\mathbf{u} \wedge \boldsymbol{\Omega} + \mathbf{x} \wedge \boldsymbol{\Omega} \wedge \boldsymbol{\Omega}] &= 2(R^{\Omega t} \mathbf{u}) \wedge \boldsymbol{\Omega} + (R^{\Omega t} \mathbf{x}) \wedge \boldsymbol{\Omega} \wedge \boldsymbol{\Omega} \\ &= 2[\hat{\mathbf{u}} - R^{\Omega t}(\mathbf{x} \wedge \boldsymbol{\Omega})] \wedge \boldsymbol{\Omega} + (R^{\Omega t} \mathbf{x}) \wedge \boldsymbol{\Omega} \wedge \boldsymbol{\Omega} \\ &= 2\hat{\mathbf{u}} \wedge \boldsymbol{\Omega} - \hat{\mathbf{x}} \wedge \boldsymbol{\Omega} \wedge \boldsymbol{\Omega} \end{aligned} \quad (3.54)$$

The two simplifications above are filled back into *Equation 3.52* and results in the non-inertial momentum equation for constant rotation.

$$\frac{\partial \hat{\mathbf{u}}}{\partial t} + (\hat{\mathbf{u}} \cdot \hat{\nabla}) \hat{\mathbf{u}} = -\hat{\nabla}\hat{\psi} + \nu \hat{\nabla}^2 \hat{\mathbf{u}} + \underbrace{2\hat{\mathbf{u}} \wedge \boldsymbol{\Omega}}_{\text{Coriolis}} - \underbrace{\hat{\mathbf{x}} \wedge \boldsymbol{\Omega} \wedge \boldsymbol{\Omega}}_{\text{Centrifugal}} \quad (3.55)$$

It can be seen from the equation above that the fictitious forces associated with constant rotation is the centrifugal and the Coriolis effects. The centrifugal effect originates from the transformation of the advection terms while the Coriolis effect is from both the transient and advection terms.

### 3.1.2.3 Energy Equation

The general energy equation in the inertial Frame O takes the following form (White [9]):

$$\frac{\partial \rho e}{\partial t} + (\nabla \cdot \rho e \mathbf{u}) = -p(\nabla \cdot \mathbf{u}) + \nabla \cdot (k \nabla T) + \varphi \quad (3.56)$$

The time dependant term is transformed in a similar manner as shown in *Section 3.1.2.1* where the continuity equation was derived. The first term is therefore transformed and the non-inertial component becomes:

$$\frac{\partial \hat{\rho} \hat{e}}{\partial t} = R^{\Omega t} \left[ \frac{\partial \rho e}{\partial t} + (\boldsymbol{\Omega} \wedge \mathbf{x}) \cdot \nabla (\rho e) \right] \quad (3.57)$$

The convective term is transformed between Frames O and  $\hat{O}$  with the use of the rotational transform, local Galilean transform and by substitution of *Equation 3.10*:

$$\begin{aligned} (\hat{\nabla} \cdot \hat{\rho} \hat{e} \hat{\mathbf{u}}) &= R^{\Omega t} G^{\boldsymbol{\Omega} \wedge \mathbf{x}} (\nabla \cdot \rho e \mathbf{u}) \\ &= R^{\Omega t} [\nabla \cdot \rho e (\mathbf{u} + \mathbf{x} \wedge \boldsymbol{\Omega})] \\ &= R^{\Omega t} [\nabla \cdot \rho e \mathbf{u} + \nabla \cdot \rho e (\mathbf{x} \wedge \boldsymbol{\Omega})] \end{aligned} \quad (3.58)$$

The terms that represents the rate of work done by the normal pressure forces is transform between the Frames O and  $\hat{O}$  and *Equation 3.10* is inserted:

$$\begin{aligned} -\hat{p}(\hat{\nabla} \cdot \hat{\mathbf{u}}) &= R^{\Omega t} G^{\boldsymbol{\Omega} \wedge \mathbf{x}} [-p(\nabla \cdot \mathbf{u})] \\ &= R^{\Omega t} [-p \nabla \cdot (\mathbf{u} + \mathbf{x} \wedge \boldsymbol{\Omega})] \\ &= R^{\Omega t} [-p \nabla \cdot \mathbf{u} - p \nabla \cdot (\mathbf{x} \wedge \boldsymbol{\Omega})] \end{aligned} \quad (3.59)$$

It can be shown that this terms is also invariant under transformation by the insertion of *Identity 1* in *Appendix A* :

$$-\hat{p}(\hat{\nabla} \cdot \hat{\mathbf{u}}) = R^{\Omega t} (-p \nabla \cdot \mathbf{u}) \quad (3.60)$$

The diffusion is invariant under Galilean transformation since the heat transfer coefficient (k) and temperature (T) are scalars. The transformation between the frames O and  $\hat{O}$  then becomes:

$$\begin{aligned} \hat{\nabla} \cdot (\hat{k} \hat{\nabla} \hat{T}) &= R^{\Omega t} G^{\boldsymbol{\Omega} \wedge \mathbf{x}} [\nabla \cdot (k \nabla T)] \\ &= R^{\Omega t} [\nabla \cdot (k \nabla T)] \end{aligned} \quad (3.61)$$

The dissipation function,  $\varphi$ , is a scalar value that represents the rate at which mechanical energy is expended in the process of deformation of the fluid due to viscosity (Anderson [58]). This property, in component form, can be described by:

$$\tau : \nabla \mathbf{u} = 2\mu \left[ \left( \frac{\partial u}{\partial x} \right)^2 + \left( \frac{\partial v}{\partial y} \right)^2 + \left( \frac{\partial w}{\partial z} \right)^2 - \frac{1}{3} (\nabla \cdot \mathbf{u})^2 \right] + \mu \left[ \left( \frac{\partial v}{\partial x} + \frac{\partial u}{\partial y} \right)^2 + \left( \frac{\partial w}{\partial y} + \frac{\partial v}{\partial z} \right)^2 + \left( \frac{\partial u}{\partial z} + \frac{\partial w}{\partial x} \right)^2 \right] \quad (3.62)$$

## CHAPTER 3. NON-INERTIAL EQUATIONS IN VECTOR FORM

---

The above equation indicates that the dissipation function is a scalar and therefore invariant under Galilean transformation:

$$\begin{aligned}\hat{\varphi} &= R^{\Omega t} G^{\Omega \wedge \mathbf{x}} \varphi \\ &= R^{\Omega t} \varphi\end{aligned}\quad (3.63)$$

All the transformed terms of the energy equation is summed to obtain the equation below.

$$\frac{\partial \hat{\rho} \hat{e}}{\partial t} + (\hat{\nabla} \cdot \hat{\rho} \hat{e} \hat{\mathbf{u}}) + \hat{p}(\hat{\nabla} \cdot \hat{\mathbf{u}}) - \hat{\nabla} \cdot (\hat{k} \hat{\nabla} \hat{T}) + \hat{\varphi} = R^{\Omega t} \left[ \frac{\partial \rho e}{\partial t} + (\nabla \cdot \rho e \mathbf{u}) + p(\nabla \cdot \mathbf{u}) - \nabla \cdot (k \nabla T) + \varphi \right] \quad (3.64)$$

The right hand side of the equation is equal to zero, as shown in *Equation 3.56*. The energy equation in the non-inertial frame for constant rotation is invariant under transformation in this specific case:

$$\frac{\partial \hat{\rho} \hat{e}}{\partial t} + (\hat{\nabla} \cdot \hat{\rho} \hat{e} \hat{\mathbf{u}}) = -\hat{p}(\hat{\nabla} \cdot \hat{\mathbf{u}}) + \hat{\nabla} \cdot (\hat{k} \hat{\nabla} \hat{T}) + \hat{\varphi} \quad (3.65)$$

This equation can be further simplified with the assumption of incompressibility and using *Equation 3.19*:

$$\frac{\partial \hat{\rho} \hat{e}}{\partial t} + (\hat{\nabla} \cdot \hat{\rho} \hat{e} \hat{\mathbf{u}}) = \hat{\nabla} \cdot (\hat{k} \hat{\nabla} \hat{T}) + \hat{\varphi}_I \quad (3.66)$$

Note that the energy equation is invariant under transformation. This is in agreement with the work of Diaz et al. [62] who determined that there are no fictitious effects in the non-inertial energy equation using a point mass method.

### 3.1.3 Compressible Flow Conditions

The effect of compressibility in the boundary layer of an object in arbitrary motion cannot be assumed negligible. The boundary layer equations for this type of flow must first be determined. This investigates the presence of compressible terms in the non-inertial boundary layer for arbitrary rates of change in translation and rotation. This is further explored in *Chapter 5*.

The full compressible formulations for non-inertial Navier-Stokes equations for conservation of mass, momentum and energy for constant rotation in compressible flow are derived using the same Eulerian approach (Kageyama and Hyodo [23]) as in *Section 3.1.2*.

#### 3.1.3.1 Continuity Equation

The general continuity equation in the rotational Frame  $\hat{O}$  was derived in *Equation 3.18*. This has shown that the equation is invariant under transformation. The compressible, non-inertial equation thus remains:

$$\frac{\partial \hat{\rho}}{\partial t} + \hat{\nabla} \cdot \hat{\rho} \hat{\mathbf{u}} = 0 \quad (3.67)$$



### 3.1.3.2 Momentum Equation

The incompressible form of the momentum equation as shown in *Equation 3.20*, made the assumption that the temporal change in density is negligible (Anderson [58]). Therefore, the equation could be simplified by dividing density into all the terms as there are no temporal change in density. The diffusion term in particular could be simplified in a manner that would facilitate easy transformation for incompressible conditions. In this case the divergence of the velocity gradient yields the same results as taking the laplacian of the velocity vector.

$$\overbrace{\frac{\partial \mathbf{u}}{\partial t} + (\mathbf{u} \cdot \nabla) \mathbf{u} = -\nabla \psi + \underbrace{\nu \nabla^2 \mathbf{u}}_{\text{Laplacian}}}_{\text{Incompressible Momentum Equation}} \quad (3.68)$$

This is not the case when compressibility has to be accounted for. The compressible Navier-Stokes Equation in the inertial frame takes the form (White [9], Anderson [58], Tannehill et al. [59]):

$$\overbrace{\frac{\partial}{\partial t} \rho \mathbf{u} + \nabla \cdot (\rho \mathbf{u} \otimes \mathbf{u})}_{\text{Material Derivative}} = -\nabla p + \underbrace{\nabla \cdot [\mu(\nabla \mathbf{u} + \nabla \mathbf{u}^T) + \lambda(\nabla \cdot \mathbf{u}) \mathbf{I}]}_{\text{Compressible Stress Tensor}} \quad (3.69)$$

Density,  $\rho$ , remains part of the momentum material derivative. Pressure gradients are represented by  $\nabla p$ , instead of pressure gradient per unit mass,  $\nabla \psi$ .

The full compressible stress tensor is used to represent momentum diffusion in the flow:

$$\boldsymbol{\tau}(x, y, z) = \begin{bmatrix} 2\mu \frac{\partial u}{\partial x} + \lambda \nabla \cdot \mathbf{u} & \mu \left( \frac{\partial u}{\partial y} + \frac{\partial v}{\partial x} \right) & \mu \left( \frac{\partial u}{\partial z} + \frac{\partial w}{\partial x} \right) \\ \mu \left( \frac{\partial u}{\partial y} + \frac{\partial v}{\partial x} \right) & 2\mu \frac{\partial v}{\partial y} + \lambda \nabla \cdot \mathbf{u} & \mu \left( \frac{\partial v}{\partial z} + \frac{\partial w}{\partial y} \right) \\ \mu \left( \frac{\partial u}{\partial z} + \frac{\partial w}{\partial x} \right) & \mu \left( \frac{\partial v}{\partial z} + \frac{\partial w}{\partial y} \right) & 2\mu \frac{\partial w}{\partial z} + \lambda \nabla \cdot \mathbf{u} \end{bmatrix} \quad (3.70)$$

The same methodology that was used in *Section 3.1.2* is used here to derive the non-inertial form of the momentum equation. Inertial terms are transformed to the non-inertial frame using the local Galilean transformation for pure rotation (*Equation 3.5*), and the Rotational transform matrix (*Equation 3.10*).

First consider the unsteady term in the rotational Frame  $\hat{O}$  and apply the product rule for partial derivatives. This operation results in two terms that were not considered during the incompressible case:

$$\frac{\partial}{\partial t} (\hat{\rho} \hat{\mathbf{u}}) = \hat{\rho} \frac{\partial \hat{\mathbf{u}}}{\partial t} + \hat{\mathbf{u}} \frac{\partial \hat{\rho}}{\partial t} \quad (3.71)$$

With the aid of *Equation 3.9* (which describe a vector as seen from Frame  $\hat{O}$  in relation to a vector in Frame  $O$ ) and *Equation 3.36* (which expressed the non-inertial velocity derivative in terms of inertial parameters) the above becomes:

$$\frac{\partial}{\partial t} (\hat{\rho} \hat{\mathbf{u}}) = R^{\Omega t} G^{\Omega \wedge \mathbf{x}} \left[ \rho \frac{\partial \mathbf{u}}{\partial t} + \rho (\boldsymbol{\Omega} \wedge \mathbf{x}) \cdot \nabla \mathbf{u} - \rho \boldsymbol{\Omega} \wedge \mathbf{u} + \mathbf{u} \frac{\partial \rho}{\partial t} \right] \quad (3.72)$$

CHAPTER 3. NON-INERTIAL EQUATIONS IN VECTOR FORM

The product rule is then used to combine the terms  $\rho \frac{\partial \mathbf{u}}{\partial t}$  and  $\mathbf{u} \frac{\partial \rho}{\partial t}$  so that the equation above simplifies to:

$$\frac{\partial}{\partial t}(\hat{\rho} \hat{\mathbf{u}}) = R^{\Omega t} \left[ \frac{\partial}{\partial t}(\rho) + \rho(\boldsymbol{\Omega} \wedge \mathbf{x}) \cdot \nabla - \rho \boldsymbol{\Omega} \wedge \right] G^{\Omega \wedge \mathbf{x}} \mathbf{u} \quad (3.73)$$

The equation is of the same form as *Equation 3.36*. It is therefore shown that the final form of the equation is similar to *Equation 3.41*, but with the inclusion of the density scalar:

$$\frac{\partial}{\partial t}(\hat{\rho} \hat{\mathbf{u}}) = R^{\Omega t} \left[ \frac{\partial}{\partial t}(\rho) + \rho(\boldsymbol{\Omega} \wedge \mathbf{x}) \cdot \nabla - \underbrace{\rho \boldsymbol{\Omega} \wedge}_{\text{Coriolis}} \right] \mathbf{u} \quad (3.74)$$

The relation between the non-inertial and inertial frames for the advection term in the compressible Navier-Stokes momentum equation is:

$$\hat{\nabla} \cdot (\hat{\rho} \hat{\mathbf{u}} \otimes \hat{\mathbf{u}}) = R^{\Omega t} G^{\Omega \wedge \mathbf{x}} [\nabla \cdot (\rho \mathbf{u} \otimes \mathbf{u})] \quad (3.75)$$

By using *Equation 3.5* the equation above is expanded into:

$$\begin{aligned} \hat{\nabla} \cdot (\hat{\rho} \hat{\mathbf{u}} \otimes \hat{\mathbf{u}}) &= R^{\Omega t} \{ \nabla \cdot \rho [(\mathbf{u} + \mathbf{x} \wedge \boldsymbol{\Omega}) \otimes (\mathbf{u} + \mathbf{x} \wedge \boldsymbol{\Omega})] \} \\ &= R^{\Omega t} \{ (\nabla \cdot \rho \mathbf{u}) \otimes \mathbf{u} + (\nabla \cdot \rho \mathbf{u}) \otimes (\mathbf{x} \wedge \boldsymbol{\Omega}) + [\nabla \cdot \rho (\mathbf{x} \wedge \boldsymbol{\Omega})] \otimes \mathbf{u} + [\nabla \cdot \rho (\mathbf{x} \wedge \boldsymbol{\Omega})] \otimes (\mathbf{x} \wedge \boldsymbol{\Omega}) \} \end{aligned} \quad (3.76)$$

As shown in *Section 3.1.2.2* and *Appendix A*, the identity below can be used to simplify the equation.

$$(\nabla \cdot \mathbf{a}) \otimes (\mathbf{x} \wedge \boldsymbol{\Omega}) = \mathbf{a} \wedge \boldsymbol{\Omega} \quad (3.77)$$

This leads to the following expression for relating the diffusion term in the rotational Frame  $\hat{O}$  to the terms in the inertial Frame  $O$ :

$$\hat{\nabla} \cdot (\hat{\rho} \hat{\mathbf{u}} \otimes \hat{\mathbf{u}}) = R^{\Omega t} \left[ \nabla \cdot \rho \mathbf{u} \otimes \mathbf{u} + \underbrace{\rho \mathbf{u} \wedge \boldsymbol{\Omega}}_{\text{Coriolis}} + \nabla \cdot \rho (\mathbf{x} \wedge \boldsymbol{\Omega}) \otimes \mathbf{u} + \underbrace{(\rho \mathbf{x} \wedge \boldsymbol{\Omega}) \wedge \boldsymbol{\Omega}}_{\text{Centrifugal}} \right] \quad (3.78)$$

The pressure gradient term in the momentum equation is transformed in a similar manner than shown in *Section 3.1.2.2*. This part of the equation remains Galilean invariant since it is a scalar (Kleppner and Kolenkow [60], McCauley [61]).

$$\begin{aligned} \hat{\nabla} \hat{p} &= R^{\Omega t} G^{\Omega \wedge \mathbf{x}} \nabla p \\ \hat{\nabla} \hat{p} &= R^{\Omega t} \nabla p \end{aligned} \quad (3.79)$$

In the transformation of the diffusion term the difference between the compressible and incompressible cases must be noted. Divergence of the velocity vector is not equal to zero, therefore the completed diffusion term must be accounted for. The expression for relating the diffusion term between Frame  $\hat{O}$  and Frame  $O$  hence becomes:

$$\hat{\nabla} \cdot [\hat{\mu}(\hat{\nabla} \hat{\mathbf{u}} + \hat{\nabla} \hat{\mathbf{u}}^T) + \hat{\lambda}(\hat{\nabla} \cdot \hat{\mathbf{u}})\hat{\mathbf{I}}] = R^{\Omega t} G^{\Omega \wedge \mathbf{x}} \nabla \cdot [\mu(\nabla \mathbf{u} + \nabla \mathbf{u}^T) + \lambda(\nabla \cdot \mathbf{u})\mathbf{I}] \quad (3.80)$$

With implementation of *Equation 3.10*, the right hand side of the equation above becomes:

$$R^{\Omega t} \nabla \cdot \{ \mu [\nabla(\mathbf{u} + \mathbf{x} \wedge \boldsymbol{\Omega}) + \nabla(\mathbf{u} + \mathbf{x} \wedge \boldsymbol{\Omega})^T] + \lambda(\nabla \cdot (\mathbf{u} + \mathbf{x} \wedge \boldsymbol{\Omega}))\mathbf{I} \} \quad (3.81)$$

### 3.1. NON-INERTIAL NAVIER-STOKES EQUATIONS FOR CONSTANT, PURE ROTATION

If it is considered (as derived in *Appendix A*) that,

$$\nabla(\mathbf{x} \wedge \boldsymbol{\Omega}) + \nabla(\mathbf{x} \wedge \boldsymbol{\Omega})^T = 0 \quad (3.82)$$

and

$$\nabla \cdot (\mathbf{x} \wedge \boldsymbol{\Omega}) = 0 \quad (3.83)$$

it can be shown that, as in the case of incompressible flow, the diffusion component of the momentum equation is invariant for constant rotation conditions:

$$\hat{\nabla} \cdot [\hat{\mu}(\hat{\nabla}\hat{\mathbf{u}} + \hat{\nabla}\hat{\mathbf{u}}^T) + \hat{\lambda}(\hat{\nabla} \cdot \hat{\mathbf{u}})\hat{\mathbf{I}}] = R^{\boldsymbol{\Omega}t} \nabla \cdot [\mu(\nabla\mathbf{u} + \nabla\mathbf{u}^T) + \lambda(\nabla \cdot \mathbf{u})\mathbf{I}] \quad (3.84)$$

The same principle of summation of the parts, as used in *Section 3.1.2.2*, is used to obtain the final form of the non-inertial momentum equation:

$$\frac{\partial \hat{\rho}\hat{\mathbf{u}}}{\partial t} + \hat{\nabla} \cdot (\hat{\rho}\hat{\mathbf{u}} \otimes \hat{\mathbf{u}}) = -\hat{\nabla}\hat{p} + \hat{\nabla} \cdot [\hat{\mu}(\hat{\nabla}\hat{\mathbf{u}} + \hat{\nabla}\hat{\mathbf{u}}^T) + \hat{\lambda}(\hat{\nabla} \cdot \hat{\mathbf{u}})\hat{\mathbf{I}}] + \underbrace{2\rho\hat{\mathbf{u}} \wedge \boldsymbol{\Omega}}_{\text{Coriolis}} - \underbrace{\rho\hat{\mathbf{x}} \wedge \boldsymbol{\Omega} \wedge \boldsymbol{\Omega}}_{\text{Centrifugal}} \quad (3.85)$$

#### 3.1.3.3 Energy Equation

The general energy equation remains the same as described in the previous section:

$$\frac{\partial \rho e}{\partial t} + (\nabla \cdot \rho e \mathbf{u}) = -p(\nabla \cdot \mathbf{u}) + \nabla \cdot (k \nabla T) + \varphi \quad (3.86)$$

This equation remains invariant in the non-inertial frame as shown in *Equation 3.65*

$$\frac{\partial \hat{\rho}\hat{e}}{\partial t} + (\hat{\nabla} \cdot \hat{\rho}\hat{e}\hat{\mathbf{u}}) = -\hat{p}(\hat{\nabla} \cdot \hat{\mathbf{u}}) + \hat{\nabla} \cdot (\hat{k}\hat{\nabla}\hat{T}) + \hat{\varphi} \quad (3.87)$$

Take again note that there are not fictitious effects present in the energy equation.

#### 3.1.4 Incompressible Equations as a Special Case of the Compressible Equations

The incompressible momentum equation is a special case of the compressible momentum equation. The latter assumes that the velocity of the flow is low enough (below Mach 0.3) that the compressible effects does not have a significant effect on the flow properties. The difference between the incompressible flow (*Equation 3.55*) and the compressible flow (*Equation 3.85*) is seen in the diffusion terms and the presence of the density parameter in all terms. The fictitious forces, Coriolis and Centrifugal, are again presents and has the same origins, from the material derivative, as in the incompressible case.

If the flow is assumed to be incompressible, the mass flux is close to zero. This is a special case of compressible flow that assumes that no temporal changes in density occurs.

The compressible continuity equation in the rotational frame was determined in *Equation 3.18* :

$$\frac{\partial \hat{\rho}}{\partial t} + \hat{\nabla} \cdot \hat{\rho}\hat{\mathbf{u}} = 0 \quad (3.88)$$

CHAPTER 3. NON-INERTIAL EQUATIONS IN VECTOR FORM

The applied assumption of incompressibility results in the transient change in density being zero:

$$\begin{aligned}\frac{\partial \hat{\rho}}{\partial t} &\rightarrow \varepsilon \\ \varepsilon &\rightarrow 0\end{aligned}\quad (3.89)$$

The equation therefore becomes:

$$\hat{\nabla} \cdot \hat{\rho} \hat{\mathbf{u}} = 0 \quad (3.90)$$

This provides the same result *Equation 3.19* which is the derived, incompressible continuity equation in the rotational frame.

The derived, compressible momentum equation in the rotational frame (*Equation 3.85*) is:

$$\frac{\partial \hat{\rho} \hat{\mathbf{u}}}{\partial t} + \hat{\nabla} \cdot (\hat{\rho} \hat{\mathbf{u}} \otimes \hat{\mathbf{u}}) = -\hat{\nabla} \hat{p} + \hat{\nabla} \cdot [\hat{\mu}(\hat{\nabla} \hat{\mathbf{u}} + \hat{\nabla} \hat{\mathbf{u}}^T) + \hat{\lambda}(\hat{\nabla} \cdot \hat{\mathbf{u}}) \hat{\mathbf{I}}] + 2\rho \hat{\mathbf{u}} \wedge \boldsymbol{\Omega} - \rho \hat{\mathbf{x}} \wedge \boldsymbol{\Omega} \wedge \boldsymbol{\Omega} \quad (3.91)$$

The first term that must be simplified to account from incompressibility is the diffusion term:

$$\hat{\nabla} \cdot [\hat{\mu}(\hat{\nabla} \hat{\mathbf{u}} + \hat{\nabla} \hat{\mathbf{u}}^T) + \hat{\lambda}(\hat{\nabla} \cdot \hat{\mathbf{u}}) \hat{\mathbf{I}}] \quad (3.92)$$

Let's consider the x-momentum components of the divergence of the deviatoric stress tensor (*Equation 3.70*). Assume in this instance that the dynamic viscosity  $\mu$  is a constant. Viscosity is a function of temperature which in turn is a function of pressure and density. Therefore, since density is constant in incompressible flow, viscosity is as well. Simplify the relation to obtain the form as shown below:

$$\begin{aligned}\frac{\partial}{\partial x} (2\mu \frac{\partial u}{\partial x} + \lambda \nabla \cdot \mathbf{u}) + \frac{\partial}{\partial y} (\mu (\frac{\partial u}{\partial y} + \frac{\partial v}{\partial x})) + \frac{\partial}{\partial z} (\mu (\frac{\partial u}{\partial z} + \frac{\partial w}{\partial x})) \\ = \mu (2 \frac{\partial^2 u}{\partial x^2} + \frac{\partial^2 u}{\partial y^2} + \frac{\partial^2 u}{\partial z^2} + \frac{\partial^2 v}{\partial y \partial x} + \frac{\partial^2 w}{\partial z \partial x}) + \frac{\partial}{\partial x} (\lambda \nabla \cdot \mathbf{u}) \\ = \mu \nabla^2 u + \mu \frac{\partial}{\partial x} (\nabla \cdot \mathbf{u}) + \frac{\partial}{\partial x} (\lambda \nabla \cdot \mathbf{u})\end{aligned}\quad (3.93)$$

This relation can be written in the vector form to account for all the components of the diffusive momentum if it is assumed that the second viscosity,  $\lambda$ , is constant according to Stokes Hypothesis (White [9]):

$$\hat{\nabla} \cdot \hat{\mu} \hat{\nabla} \hat{\mathbf{u}} + \hat{\nabla} \cdot [(\hat{\mu} + \hat{\lambda})(\hat{\nabla} \cdot \hat{\mathbf{u}})] \quad (3.94)$$

The second term in the expression above is equal to zero if the incompressible continuity equation is substituted into the relation. This result in the following equation:

$$\frac{\partial \hat{\rho} \hat{\mathbf{u}}}{\partial t} + \hat{\nabla} \cdot (\hat{\rho} \hat{\mathbf{u}} \otimes \hat{\mathbf{u}}) = -\hat{\nabla} \hat{p} + \hat{\nabla} \cdot \hat{\mu} \hat{\nabla} \hat{\mathbf{u}} + 2\rho \hat{\mathbf{u}} \wedge \boldsymbol{\Omega} - \rho \hat{\mathbf{x}} \wedge \boldsymbol{\Omega} \wedge \boldsymbol{\Omega} \quad (3.95)$$

Since density is constant in the equation above, it can be divided into the equation. This leads to the non-inertial momentum equation:

$$\frac{\partial \hat{\mathbf{u}}}{\partial t} + (\hat{\mathbf{u}} \cdot \hat{\nabla}) \hat{\mathbf{u}} = -\hat{\nabla} \hat{p} + \nu \hat{\nabla}^2 \hat{\mathbf{u}} + 2\hat{\mathbf{u}} \wedge \boldsymbol{\Omega} - \hat{\mathbf{x}} \wedge \boldsymbol{\Omega} \wedge \boldsymbol{\Omega} \quad (3.96)$$

### 3.1. NON-INERTIAL NAVIER-STOKES EQUATIONS FOR CONSTANT, PURE ROTATION

---

This equation above it the same as *Equation 3.55* which was derived from first principles.

The conservation of energy equation in the rotational frame for compressible flow is described by (*Equation 3.237*):

$$\frac{\partial \hat{\rho} \hat{e}}{\partial t} + (\hat{\nabla} \cdot \hat{\rho} \hat{e} \hat{\mathbf{u}}) = -\hat{p}(\hat{\nabla} \cdot \hat{\mathbf{u}}) + \hat{\nabla} \cdot (\hat{k} \hat{\nabla} \hat{T}) + \varphi \quad (3.97)$$

When the continuity equation (*Equation 3.19*) is applied to this equation it results in:

$$\frac{\partial \hat{\rho} \hat{e}}{\partial t} + (\hat{\nabla} \cdot \hat{\rho} \hat{e} \hat{\mathbf{u}}) = \hat{\nabla} \cdot (\hat{k} \hat{\nabla} \hat{T}) + \hat{\varphi}_I \quad (3.98)$$

This is the same as *Equation 3.66* where the incompressible energy equation in the rotational frame was derived.

The derived incompressible equation provided the same results as the compressible equations with incompressibility conditions. This section therefore indicates that there are no observed discrepancies between the derived equations for the compressible and incompressible cases in the rotational frame.

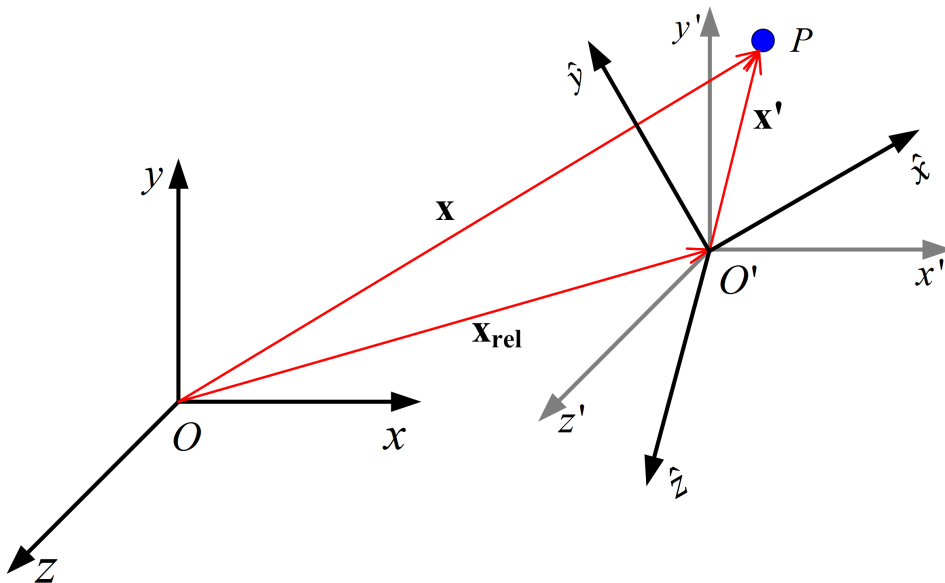
## 3.2 Non-inertial Navier-Stokes Equations for Variable, Pure Rotation

In *Section 3.1* the non-inertial Navier-Stokes Equations for constant, pure rotation were derived. In reality there are very few rotational flow applications where a constant rotational speed is maintained. Even if such a speed is desirable to maintain a specific performance region, the rotation is not constant over the entire duration of the event. Start-up and shut-down conditions involve variable rotational velocities. Examples include helicopter blades, turbine rotors and ship propellers. Additional non-inertial terms manifest when the rotation is about a moving axis of variable nature. In this section these terms are derived and isolated to obtain a better understanding of non-inertial terms for unsteady rotational flow.

### 3.2.1 Frame Transformations

Assume that the same three frame exists as described in *Section 3.1.1*;  $O$ ,  $O'$  and  $\hat{O}$  (*Figure 3.5*).  $O$  is again the stationary frame,  $O'$  is the orientation preserving frame and  $\hat{O}$  is the rotational frame. In *Section 3.1.1*  $\hat{O}$  was rotating at a constant velocity around the shared origin. Here  $\hat{O}$  is rotating around the shared origin with a constant rotational acceleration.

Figure 3.5: Local Galilean Transformation between Frames



#### 3.2.1.1 Local Galilean Transformation

The local Galilean transform, as described in *Section 3.1.1.1*, is here expanded to account for rotational acceleration.

Assume that the frame origins intersect at time  $t = 0$  and that Frame  $O'$  is moving at unsteady velocity,  $\mathbf{v}_{\text{rel}}$ , with acceleration  $\mathbf{a}_{\text{rel}}$  in three dimensional space. At time  $t = \Delta t$  Frame  $O$  and Frame  $O'$

### 3.2. NON-INERTIAL NAVIER-STOKES EQUATIONS FOR VARIABLE, PURE ROTATION

are distance  $\mathbf{x}_{\text{rel}}$  from each other. In *Equation 3.2* there was not an accelerating component, but in this case it is incorporated in the expression to account for the distance travelled by the particle:

$$\mathbf{x}_{\text{rel}} = \mathbf{V}_{\text{rel}}\Delta t + \frac{1}{2}\mathbf{a}_{\text{rel}}\Delta t^2 \quad (3.99)$$

In the equation above the velocity is again described as in *Equation 3.3* :

$$\mathbf{V}_{\text{rel}} = \boldsymbol{\Omega} \wedge \mathbf{x} \quad (3.100)$$

The acceleration is the time derivative of the velocity:

$$\frac{\partial \mathbf{V}_{\text{rel}}}{\partial t} = \frac{\partial}{\partial t} [\boldsymbol{\Omega} \wedge \mathbf{x}] = \frac{\partial \boldsymbol{\Omega}}{\partial t} \wedge \mathbf{x} + \boldsymbol{\Omega} \wedge \frac{\partial \mathbf{x}}{\partial t} \quad (3.101)$$

The second term is equal to zero since this case involves pure rotation. The accelerating component for the rotational case is therefore expressed as:

$$\mathbf{a}_{\text{rel}} = \dot{\boldsymbol{\Omega}} \wedge \mathbf{x} \quad (3.102)$$

*Equation 3.99* is a Taylor series expansion that was truncated after the second order term since constant acceleration was assumed. Had the acceleration not been constant, the additional terms are accounted for by the inclusion of further derivative terms:

$$\mathbf{x}_{\text{rel}} = \mathbf{V}_{\text{rel}}\Delta t + \frac{1}{2!}\mathbf{a}_{\text{rel}}\Delta t^2 + \frac{1}{3!}\dot{\mathbf{a}}_{\text{rel}}\Delta t^3 + \dots \quad (3.103)$$

In this equation it can already be seen that the effect of further derivatives on  $\mathbf{x}_{\text{rel}}$  becomes negligible. This is due to the coefficient  $\Delta t^n$  that becomes smaller and smaller. Subsequently, the effects of the higher order terms are diminished.

In the same manner as in *Equation 3.5*, the relation between the order preserving Frame  $O'$  and the inertial Frame  $O$  is defined with the inclusion of the accelerating components:

$$\begin{aligned} \mathbf{u}'(\mathbf{x}', t) &= G^{\mathbf{M}}\mathbf{u}(\mathbf{x}, t) \\ &= G^{\boldsymbol{\Omega} \wedge \mathbf{x} + (\dot{\boldsymbol{\Omega}} \wedge \mathbf{x})\Delta t}\mathbf{u}(\mathbf{x}, t) \\ &= \mathbf{u}(\mathbf{x}, t) + \mathbf{x} \wedge \boldsymbol{\Omega} + (\mathbf{x} \wedge \dot{\boldsymbol{\Omega}})\Delta t \end{aligned} \quad (3.104)$$

#### 3.2.1.2 Rotational Transformation

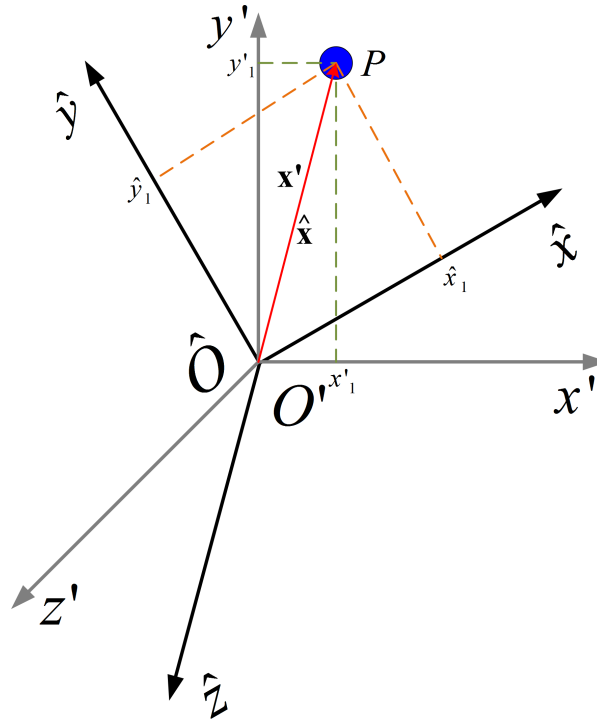
The rotational transform for this case can be defined in the same manner as *Equation 3.9*. The vector components in Frame  $\hat{O}$  is related to Frame  $O'$  by defining a rotational transform and substituting *Equation 3.104* to relate Frame  $\hat{O}$  to Frame  $O$ :

$$\begin{aligned} \hat{\mathbf{u}}(\hat{\mathbf{x}}, t) &= R^{\boldsymbol{\Omega}t + \dot{\boldsymbol{\Omega}}t^2}\mathbf{u}'(\mathbf{x}', t) \\ &= R^{\boldsymbol{\Omega}t + \dot{\boldsymbol{\Omega}}t^2}G^{\boldsymbol{\Omega} \wedge \mathbf{x} + (\dot{\boldsymbol{\Omega}} \wedge \mathbf{x})\Delta t}\mathbf{u}(\mathbf{x}, t) \end{aligned} \quad (3.105)$$

CHAPTER 3. NON-INERTIAL EQUATIONS IN VECTOR FORM

$R^{\Omega t + \dot{\Omega} t^2}$  is the rotational transform that operates on the vector  $\mathbf{x}'$ , defined in Frame  $O'$ , to obtain the  $\hat{\mathbf{x}}$  coordinates in the unsteady rotational Frame  $\hat{O}$  (Figure 3.6).

Figure 3.6: Relation between Frame  $O'$  and Frame  $\hat{O}$



Let's assume that the rotation is around the z-axis. The vector  $\boldsymbol{\Omega}$  is described as  $\boldsymbol{\Omega} = (0, 0, \Omega)$  and vector  $\dot{\boldsymbol{\Omega}}$  is described as  $\dot{\boldsymbol{\Omega}} = (0, 0, \dot{\Omega})$ . The rotational transform in this case is described by:

$$R^{\Omega t + \dot{\Omega} t^2} = \begin{bmatrix} \cos(\Omega t + \dot{\Omega} t^2) & \sin(\Omega t + \dot{\Omega} t^2) & 0 \\ -\sin(\Omega t + \dot{\Omega} t^2) & \cos(\Omega t + \dot{\Omega} t^2) & 0 \\ 0 & 0 & 1 \end{bmatrix} \quad (3.106)$$

From Equations 3.104 and 3.105 it is derived that the following relation holds:

$$\hat{\mathbf{u}}(\hat{\mathbf{x}}, t) = R^{\Omega t + \dot{\Omega} t^2} [\mathbf{u}(\mathbf{x}, t) + \mathbf{x} \wedge \boldsymbol{\Omega} + (\mathbf{x} \wedge \dot{\boldsymbol{\Omega}}) \Delta t] \quad (3.107)$$

## 3.2.2 Incompressible Flow Conditions

### 3.2.2.1 Continuity Equation

Consider the continuity equation in the inertial reference Frame  $O$  (White [9]):

$$\frac{\partial \rho}{\partial t} + (\nabla \cdot \rho \mathbf{u}) = 0 \quad (3.108)$$



### 3.2. NON-INERTIAL NAVIER-STOKES EQUATIONS FOR VARIABLE, PURE ROTATION

The non-inertial form of the unsteady density term can be described as, the same as in *Section 3.1.2.1*

:

$$\frac{\partial \hat{\rho}}{\partial t}(\hat{\mathbf{x}}_t, t) = \lim_{\Delta t \rightarrow 0} \frac{\hat{\rho}(\hat{\mathbf{x}}_{t+\Delta t}, t + \Delta t) - \hat{\rho}(\hat{\mathbf{x}}_t, t)}{\Delta t} \quad (3.109)$$

A Taylor series expansion of the term  $\hat{\rho}(\hat{\mathbf{x}}_{t+\Delta t}, t + \Delta t)$  provides an expression similar to *Equation 3.13* but with the inclusion of the rotational acceleration:

$$\hat{\rho}(\hat{\mathbf{x}}_{t+\Delta t}, t + \Delta t) = \hat{\rho}(\mathbf{x}_t, t) + \{[\Delta t(\boldsymbol{\Omega} \wedge \mathbf{x}_t) + \frac{1}{2}\Delta t^2(\dot{\boldsymbol{\Omega}} \wedge \mathbf{x}_t)] \cdot \nabla\} \hat{\rho}(\mathbf{x}_t, t) + (\Delta t \frac{\partial}{\partial t}) \hat{\rho}(\mathbf{x}_t, t) \quad (3.110)$$

Substitution of this expansion in the *Equation 3.109* and manipulation result in an expression that relates the non-inertial, unsteady density to the inertial frame. This is exactly the same as *Equation 3.14*.

$$\frac{\partial \hat{\rho}}{\partial t} = R^{\boldsymbol{\Omega}t + \dot{\boldsymbol{\Omega}}t^2} \left[ \frac{\partial \rho}{\partial t} + (\boldsymbol{\Omega} \wedge \mathbf{x}_t) \cdot \nabla \rho \right] \quad (3.111)$$

*Equation 3.105* is used to obtain an expression that relates the inertial form of the second term in *Equation 3.108* to the non-inertial Frame  $\hat{\mathcal{O}}$ :

$$\begin{aligned} (\hat{\nabla} \cdot \hat{\rho} \hat{\mathbf{u}}) &= R^{\boldsymbol{\Omega}t + \dot{\boldsymbol{\Omega}}t^2} G^{\boldsymbol{\Omega} \wedge \mathbf{x} + (\dot{\boldsymbol{\Omega}} \wedge \mathbf{x}) \Delta t} (\nabla \cdot \rho \mathbf{u}) \\ &= R^{\boldsymbol{\Omega}t + \dot{\boldsymbol{\Omega}}t^2} \nabla \cdot \rho (G^{\boldsymbol{\Omega} \wedge \mathbf{x} + (\dot{\boldsymbol{\Omega}} \wedge \mathbf{x}) \Delta t} \mathbf{u}) \end{aligned} \quad (3.112)$$

Substituting *Equation 3.107* into the expression above simplifies it to:

$$(\hat{\nabla} \cdot \hat{\rho} \hat{\mathbf{u}}) = R^{\boldsymbol{\Omega}t + \dot{\boldsymbol{\Omega}}t^2} \nabla \cdot \rho [\mathbf{u} + \mathbf{x} \wedge \boldsymbol{\Omega} + (\mathbf{x} \wedge \dot{\boldsymbol{\Omega}}) \Delta t] \quad (3.113)$$

The third term in the relation above is equal to zero as shown in *Appendix A* :

$$\nabla \cdot (\mathbf{x} \wedge \dot{\boldsymbol{\Omega}}) = 0 \quad (3.114)$$

The relation is hence simplified to the following relation, that is the same as *Equation 3.16*:

$$\hat{\nabla} \cdot \hat{\rho} \hat{\mathbf{u}} = R^{\boldsymbol{\Omega}t + \dot{\boldsymbol{\Omega}}t^2} (\nabla \cdot (\rho \mathbf{u}) - (\boldsymbol{\Omega} \wedge \mathbf{x}) \cdot \nabla \rho) \quad (3.115)$$

The addition of *Equation 3.111* and *Equation 3.115* gives a relation for continuity in the rotational Frame  $\hat{\mathcal{O}}$ :

$$\frac{\partial \hat{\rho}}{\partial t} + \hat{\nabla} \cdot \hat{\rho} \hat{\mathbf{u}} = R^{\boldsymbol{\Omega}t + \dot{\boldsymbol{\Omega}}t^2} \left( \frac{\partial \rho}{\partial t} + \nabla \cdot \rho \mathbf{u} \right) \quad (3.116)$$

Implementing *Equation 3.108* and invoking the assumption that the flow is incompressible leads to the final equation for mass conservation in the non-inertial Frame  $\hat{\mathcal{O}}$  :

$$\hat{\nabla} \cdot \hat{\rho} \hat{\mathbf{u}} = 0 \quad (3.117)$$

Consider the term  $(\mathbf{x} \wedge \dot{\boldsymbol{\Omega}}) \Delta t$  in *Equation 3.113*. This term originates from the Taylor series expansion in *Equation 3.103* and contains a  $\Delta t$  component. Any further expansions, due to changes in acceleration

CHAPTER 3. NON-INERTIAL EQUATIONS IN VECTOR FORM

in rotation, contain a  $\Delta t^n$  component. These acceleration terms become negligible in the limit as  $\Delta t^n$  approaches zero:

$$\lim_{\Delta t \rightarrow 0} (\mathbf{x} \wedge \dot{\mathbf{\Omega}}) \Delta t = 0 \quad (3.118)$$

Divergence of the cross product further ensure that these terms, and any higher order terms, becomes zero in accordance to *Equation 3.114*. In the light of this, the derivations for the continuity equation in the rotational Frame  $\hat{O}$  had been proven Galilean invariant whether the rate of rotation it is zero, constant or variable. In any rotational frame *Equation 3.117* holds for incompressible conditions.

### 3.2.2.2 Momentum Equation

The conservation of momentum equation in the inertial Frame O is expressed by (White [9]):

$$\frac{\partial \mathbf{u}}{\partial t} + (\mathbf{u} \cdot \nabla) \mathbf{u} = -\nabla \psi + \nu \nabla^2 \mathbf{u} \quad (3.119)$$

The terms are again, as in *Section 3.1.2.2*, treated separately and then combined to obtain the final transformed equation.

The first transformation concerns the unsteady term where the limit at a point equation is used:

$$\frac{\partial \hat{\mathbf{u}}}{\partial t}(\hat{\mathbf{x}}_t, t) = \lim_{\Delta t \rightarrow 0} \frac{\hat{\mathbf{u}}(\hat{\mathbf{x}}_{t+\Delta t}, t + \Delta t) - \hat{\mathbf{u}}(\hat{\mathbf{x}}_t, t)}{\Delta t} \quad (3.120)$$

The first task is to find an expression for the term  $\hat{\mathbf{u}}(\hat{\mathbf{x}}_{t+\Delta t}, t + \Delta t)$  as a function of the terms in the inertial frame. It follows from *Equation 3.105* that it can be expressed as:

$$\hat{\mathbf{u}}(\hat{\mathbf{x}}_{t+\Delta t}, t + \Delta t) = R^{\mathbf{\Omega}(t+\Delta t) + \dot{\mathbf{\Omega}}(t^2 + \Delta t^2)} [G^{\mathbf{\Omega} \wedge \mathbf{x}_{t+\Delta t} + (\dot{\mathbf{\Omega}} \wedge \mathbf{x}_{t+\Delta t}) \Delta t} \mathbf{u}(\mathbf{x}_{t+\Delta t}, t + \Delta t)] \quad (3.121)$$

For simplification purposes the rotational and local Galilean transforms in this case are shown in the following manner (*Equation 3.29*):

$$\begin{aligned} R^{\mathbf{\Omega}(t+\Delta t) + \dot{\mathbf{\Omega}}(t^2 + \Delta t^2)} &= R^{\mathbf{M}^{t+\Delta t}} \\ G^{\mathbf{\Omega} \wedge \mathbf{x}_{t+\Delta t} + (\dot{\mathbf{\Omega}} \wedge \mathbf{x}_{t+\Delta t}) \Delta t} &= G^{\mathbf{M}^{t+\Delta t}} \end{aligned} \quad (3.122)$$

The Taylor series expansion for  $\mathbf{x}_{t+\Delta t}$  is expressed as:

$$\mathbf{x}_{t+\Delta t} = \mathbf{x}_t + \mathbf{V}_{\text{rel}} \Delta t + \frac{1}{2} \mathbf{a}_{\text{rel}} \Delta t^2 + O(\Delta t^3) \quad (3.123)$$

The equation above is truncated at the second order since the change in acceleration in the case is considered zero. With the substitution of *Equations 3.100* and *3.102* the equation above becomes:

$$\mathbf{x}_{t+\Delta t} - \mathbf{x}_t = \mathbf{x}_{\Delta t} = (\mathbf{\Omega} \wedge \mathbf{x}_t) \Delta t + \frac{1}{2} (\dot{\mathbf{\Omega}} \wedge \mathbf{x}_t) \Delta t^2 \quad (3.124)$$

The Fourier series expansion is obtained for  $\mathbf{u}(\mathbf{x}_{t+\Delta t}, t + \Delta t)$ . Substitute *Equation 3.124* into the expression to obtain:

$$\mathbf{u}(\mathbf{x}_{t+\Delta t}, t + \Delta t) = \mathbf{u}(\mathbf{x}_t, t) + \left\{ \left[ \Delta t (\mathbf{\Omega} \wedge \mathbf{x}_t) + \frac{1}{2} \Delta t^2 (\dot{\mathbf{\Omega}} \wedge \mathbf{x}_t) \right] \cdot \nabla \right\} \mathbf{u}(\mathbf{x}_t, t) + \left( \Delta t \frac{\partial}{\partial t} \right) \mathbf{u}(\mathbf{x}_t, t) \quad (3.125)$$

### 3.2. NON-INERTIAL NAVIER-STOKES EQUATIONS FOR VARIABLE, PURE ROTATION

The equation above is substituted into *Equation 3.121* to get an expression for the non-inertial terms as a function of the inertial terms:

$$\hat{\mathbf{u}}(\hat{\mathbf{x}}_{t+\Delta t}, t + \Delta t) = R^{\mathbf{M}^{t+\Delta t}} G^{\mathbf{M}^{t+\Delta t}} \left\{ \mathbf{u}(\mathbf{x}_t, t) + [\Delta t(\boldsymbol{\Omega} \wedge \mathbf{x}_t) + \frac{1}{2} \Delta t^2 (\dot{\boldsymbol{\Omega}} \wedge \mathbf{x}_t)] \cdot \nabla \right\} \mathbf{u}(\mathbf{x}_t, t) + \left( \Delta t \frac{\partial}{\partial t} \right) \mathbf{u}(\mathbf{x}_t, t) \quad (3.126)$$

In *Section 3.1.2.2 Equation 3.29* it was shown that the following simplification can be made to the local Galilean transformation parameter:

$$G^{\mathbf{M}^{t+\Delta t}} \approx G^{\mathbf{M}^t} \quad (3.127)$$

The above leads to a simplified form:

$$\hat{\mathbf{u}}(\hat{\mathbf{x}}_{t+\Delta t}, t + \Delta t) = R^{\mathbf{M}^{t+\Delta t}} G^{\mathbf{M}^t} \left\{ \mathbf{u}(\mathbf{x}_t, t) + [\Delta t(\boldsymbol{\Omega} \wedge \mathbf{x}_t) + \frac{1}{2} \Delta t^2 (\dot{\boldsymbol{\Omega}} \wedge \mathbf{x}_t)] \cdot \nabla \right\} \mathbf{u}(\mathbf{x}_t, t) + \left( \Delta t \frac{\partial}{\partial t} \right) \mathbf{u}(\mathbf{x}_t, t) \quad (3.128)$$

In order to complete the substitution for *Equation 3.120* further expressions must be defined. Assume that the point P is fixed in the rotating frame, and the rotation is around the origin (meaning that O and O' share an origin), then:

$$\begin{aligned} \hat{\mathbf{x}} &= R^{\mathbf{M}^{t+\Delta t}} \mathbf{x}_{t+\Delta t} = R^{\mathbf{M}^t} \mathbf{x}_t \\ \mathbf{x}_t &= R^{\mathbf{M}^{\Delta t}} \mathbf{x}_{t+\Delta t} \end{aligned} \quad (3.129)$$

Use the expression above and conduct a Taylor series expansion for  $\mathbf{x}_{t+\Delta t}$ :

$$\begin{aligned} \mathbf{x}_{t+\Delta t} &= \mathbf{x}_t + \mathbf{V} \Delta t + \frac{1}{2} \mathbf{a} \Delta t^2 + O[\Delta t^3] \\ &= R^{\mathbf{M}^{\Delta t}} \mathbf{x}_{t+\Delta t} + (\boldsymbol{\Omega} \wedge \mathbf{x}_t) \Delta t + \frac{1}{2} (\dot{\boldsymbol{\Omega}} \wedge \mathbf{x}_t) + O[\Delta t^3] \end{aligned} \quad (3.130)$$

Re-arrange the expression above and consider it in the limit:

$$\lim_{\Delta t \rightarrow 0} \frac{R^{\mathbf{M}^{\Delta t}} \mathbf{x}_{t+\Delta t} - \mathbf{x}_{t+\Delta t}}{\Delta t} = \lim_{\Delta t \rightarrow 0} \left( (\mathbf{x}_t \wedge \boldsymbol{\Omega}) - \frac{1}{2} \Delta t (\dot{\boldsymbol{\Omega}} \wedge \mathbf{x}_t) - O[\Delta t^3] \right) \quad (3.131)$$

If the above is considered for any vector  $\mathbf{b}$ , and if it is taken into account that  $\mathbf{x}_{t+\Delta t} \rightarrow \mathbf{x}_t$  as  $\Delta t \rightarrow 0$ , the following equation related to rotation is obtained:

$$\lim_{\Delta t \rightarrow 0} \frac{R^{\mathbf{M}^{\Delta t}} \mathbf{b} - \mathbf{b}}{\Delta t} = \mathbf{b} \wedge \boldsymbol{\Omega} \quad (3.132)$$

This is the same as *Equation 3.34* and is valid for displacement and velocity vectors as shown in *Section 3.1.2.2*.

With all the required expressions in place *Equation 3.120* can now be completed:

$$\frac{\partial \hat{\mathbf{u}}}{\partial t}(\hat{\mathbf{x}}_t, t) = \lim_{\Delta t \rightarrow 0} \frac{R^{\mathbf{M}^{t+\Delta t}} G^{\mathbf{M}^t} \left\{ \left[ 1 - \frac{1}{R^{\boldsymbol{\Omega} \Delta t}} + \Delta t(\boldsymbol{\Omega} \wedge \mathbf{x}_t) \cdot \nabla + \frac{1}{2} \Delta t^2 (\dot{\boldsymbol{\Omega}} \wedge \mathbf{x}_t) \cdot \nabla \right] \mathbf{u}(\mathbf{x}_t, t) + \left( \Delta t \frac{\partial}{\partial t} \right) \mathbf{u}(\mathbf{x}_t, t) \right\}}{\Delta t} \quad (3.133)$$

CHAPTER 3. NON-INERTIAL EQUATIONS IN VECTOR FORM

---

*Equation 3.132* is used to simplify the expression above and with some re-arrangement of terms the following expression is obtained:

$$\frac{\partial \hat{\mathbf{u}}}{\partial t}(\hat{\mathbf{x}}_t, t) = R^{\mathbf{M}^t} \left[ \frac{\partial}{\partial t} + (\boldsymbol{\Omega} \wedge \mathbf{x}_t) \cdot \nabla - \boldsymbol{\Omega} \wedge \right] [G^{\mathbf{M}^t} \mathbf{u}(\mathbf{x}_t, t)] \quad (3.134)$$

This equation above is the same as *Equation 3.36* for constant rotation. It retains its current form irrespective of any further changes in unsteady rotational motion. All higher order terms, accounting for unsteady rates of change, become negligible when the expression is considered in the limit.

*Equation 3.107* is substituted in the equation above to remove the local Galilean operator from the equation:

$$\begin{aligned} \frac{\partial \hat{\mathbf{u}}}{\partial t}(\hat{\mathbf{x}}_t, t) &= R^{\mathbf{M}^t} \left[ \frac{\partial}{\partial t} + (\boldsymbol{\Omega} \wedge \mathbf{x}_t) \cdot \nabla - \boldsymbol{\Omega} \wedge \right] (\mathbf{u}(\mathbf{x}_t, t)) \\ &+ R^{\mathbf{M}^t} \left[ \frac{\partial}{\partial t} + (\boldsymbol{\Omega} \wedge \mathbf{x}_t) \cdot \nabla - \boldsymbol{\Omega} \wedge \right] (\mathbf{x}_t \wedge \boldsymbol{\Omega}) \\ &+ R^{\mathbf{M}^t} \left[ \frac{\partial}{\partial t} + (\boldsymbol{\Omega} \wedge \mathbf{x}_t) \cdot \nabla - \boldsymbol{\Omega} \wedge \right] (\mathbf{x}_t \wedge \dot{\boldsymbol{\Omega}}) \Delta t \end{aligned} \quad (3.135)$$

The different parts of  $\left[ \frac{\partial}{\partial t} + (\boldsymbol{\Omega} \wedge \mathbf{x}_t) \cdot \nabla - \boldsymbol{\Omega} \wedge \right] (\mathbf{x}_t \wedge \boldsymbol{\Omega})$ , which is the second combination of terms in *Equation 3.135*, are considered here.

The transient term in the equation above can be expanded on with the use of the product rule for partial differential equations:

$$\frac{\partial}{\partial t} (\mathbf{x}_t \wedge \boldsymbol{\Omega}) = \frac{\partial \mathbf{x}_t}{\partial t} \wedge \boldsymbol{\Omega} + \mathbf{x}_t \wedge \frac{\partial \boldsymbol{\Omega}}{\partial t} \quad (3.136)$$

In the equation above the first term on the right hand side is zero because the magnitude of  $\mathbf{x}_t$  is constant, it does not change its magnitude with respect to the origin. The second term is not equal to zero in this case and has to be taken into account since it represents the unsteady rotation, this is called the Euler fictitious force.

The terms  $\left[ (\boldsymbol{\Omega} \wedge \mathbf{x}_t) \cdot \nabla - \boldsymbol{\Omega} \wedge \right] (\mathbf{x}_t \wedge \boldsymbol{\Omega})$  has already been shown in *Section 3.1.2.2* to be equal to zero:

$$\left[ (\boldsymbol{\Omega} \wedge \mathbf{x}_t) \cdot \nabla - \boldsymbol{\Omega} \wedge \right] (\mathbf{x}_t \wedge \boldsymbol{\Omega}) = 0 \quad (3.137)$$

Therefore, the relation  $\left[ \frac{\partial}{\partial t} + (\boldsymbol{\Omega} \wedge \mathbf{x}_t) \cdot \nabla - \boldsymbol{\Omega} \wedge \right] (\mathbf{x}_t \wedge \boldsymbol{\Omega})$ , for this case, simplifies to:

$$\left[ \frac{\partial}{\partial t} + (\boldsymbol{\Omega} \wedge \mathbf{x}_t) \cdot \nabla - \boldsymbol{\Omega} \wedge \right] (\mathbf{x}_t \wedge \boldsymbol{\Omega}) = \mathbf{x}_t \wedge \dot{\boldsymbol{\Omega}} \quad (3.138)$$

The different parts of  $\left[ \frac{\partial}{\partial t} + (\boldsymbol{\Omega} \wedge \mathbf{x}_t) \cdot \nabla - \boldsymbol{\Omega} \wedge \right] (\mathbf{x}_t \wedge \dot{\boldsymbol{\Omega}}) \Delta t$ , which is the third combination of terms in *Equation 3.135*, are considered below.

### 3.2. NON-INERTIAL NAVIER-STOKES EQUATIONS FOR VARIABLE, PURE ROTATION

The transient component of the terms can be expanded again using the product rule. In this case the terms are all equal to zero:

$$\frac{\partial}{\partial t}(\mathbf{x}_t \wedge \dot{\mathbf{\Omega}}) = \frac{\partial \mathbf{x}_t}{\partial t} \wedge \dot{\mathbf{\Omega}} + \mathbf{x}_t \wedge \frac{\partial \dot{\mathbf{\Omega}}}{\partial t} = 0 \quad (3.139)$$

The first term in the equation above is equal to zero because the magnitude of  $\mathbf{x}_t$  is constant due to the pure rotation. The second term in the equation is equal to zero because constant acceleration is considered in this case.

Now consider the term  $[(\mathbf{\Omega} \wedge \mathbf{x}_t) \cdot \nabla - \mathbf{\Omega} \wedge](\mathbf{x}_t \wedge \dot{\mathbf{\Omega}})\Delta t$ . If the identity *Appendix A*:

$$(\mathbf{a} \cdot \nabla)(\mathbf{x}_t \wedge \dot{\mathbf{\Omega}}) = \mathbf{a} \wedge \dot{\mathbf{\Omega}} \quad (3.140)$$

is considered, it can be shown that the entire term is equal to zero:

$$\begin{aligned} [(\mathbf{\Omega} \wedge \mathbf{x}_t) \cdot \nabla - \mathbf{\Omega} \wedge](\mathbf{x}_t \wedge \dot{\mathbf{\Omega}}) &= (\mathbf{\Omega} \wedge \mathbf{x}_t) \wedge \dot{\mathbf{\Omega}} - \mathbf{\Omega} \wedge (\mathbf{x}_t \wedge \dot{\mathbf{\Omega}}) \\ &= 0 \end{aligned} \quad (3.141)$$

The entire third combination of terms in *Equation 3.135* therefore becomes zero:

$$\left[ \frac{\partial}{\partial t} + (\mathbf{\Omega} \wedge \mathbf{x}_t) \cdot \nabla - \mathbf{\Omega} \wedge \right](\mathbf{x}_t \wedge \dot{\mathbf{\Omega}})\Delta t = 0 \quad (3.142)$$

The expressions above leads to the final description of the unsteady terms in the momentum equation for constant rotation:

$$\frac{\partial \hat{\mathbf{u}}}{\partial t}(\hat{\mathbf{x}}_t, t) = R^{\mathbf{M}^t} \left[ \frac{\partial}{\partial t} + (\mathbf{\Omega} \wedge \mathbf{x}_t) \cdot \nabla - \underbrace{\mathbf{\Omega} \wedge}_{\text{Coriolis}} \right](\mathbf{u}(\mathbf{x}_t, t)) + R^{\mathbf{M}^t} \underbrace{(\mathbf{x}_t \wedge \dot{\mathbf{\Omega}})}_{\text{Euler}} \quad (3.143)$$

At this stage it must noted that in any pure rotation, this is the form the unsteady component of the equation takes. Higher order terms that appear in rotation as a result of unsteady behaviour becomes negligible as demonstrated in this section.

Take note in this equation of the appearance of a part of the Coriolis effect and the Euler effect. The Euler term account for the variability in the rotational velocity and is not seen in *Equation 3.20* since that equation is for constant conditions.

The advection term in the non-inertial Navier-Stokes equation for constant rotation is transformed in the following paragraphs. The relation between the inertial and rotational frames can be described by the equation below:

$$\begin{aligned} (\hat{\mathbf{u}} \cdot \hat{\nabla})\hat{\mathbf{u}} &= R^{\mathbf{M}^t} G^{\mathbf{M}^t} (\mathbf{u} \cdot \nabla)\mathbf{u} \\ &= R^{\mathbf{M}^t} (G^{\mathbf{M}^t} \mathbf{u} \cdot \nabla) G^{\mathbf{M}^t} \mathbf{u} \end{aligned} \quad (3.144)$$

With the use of *Equation 3.107*, the equation above is expanded into:

$$\begin{aligned} (\hat{\mathbf{u}} \cdot \hat{\nabla})\hat{\mathbf{u}} &= R^{\mathbf{M}^t} [(\mathbf{u} + \mathbf{x} \wedge \mathbf{\Omega} + (\mathbf{x} \wedge \dot{\mathbf{\Omega}})\Delta t) \cdot \nabla] \mathbf{u} \\ &+ R^{\mathbf{M}^t} [(\mathbf{u} + \mathbf{x} \wedge \mathbf{\Omega} + (\mathbf{x} \wedge \dot{\mathbf{\Omega}})\Delta t) \cdot \nabla](\mathbf{x} \wedge \mathbf{\Omega}) \\ &+ R^{\mathbf{M}^t} [(\mathbf{u} + \mathbf{x} \wedge \mathbf{\Omega} + (\mathbf{x} \wedge \dot{\mathbf{\Omega}})\Delta t) \cdot \nabla](\mathbf{x} \wedge \dot{\mathbf{\Omega}})\Delta t \end{aligned} \quad (3.145)$$

CHAPTER 3. NON-INERTIAL EQUATIONS IN VECTOR FORM

---

The equation above can be simplified by considering it in the limit of  $\Delta t$  as it approaches zero and using the identity in *Equation 3.39* . This leads to the equation:

$$(\hat{\mathbf{u}} \cdot \hat{\nabla})\hat{\mathbf{u}} = R^{\mathbf{M}^t} \left[ (\mathbf{u} \cdot \nabla)\mathbf{u} + ((\mathbf{x} \wedge \boldsymbol{\Omega}) \cdot \nabla)\mathbf{u} + \underbrace{(\mathbf{u} \wedge \boldsymbol{\Omega})}_{\text{Coriolis}} + \underbrace{(\mathbf{x} \wedge \boldsymbol{\Omega}) \wedge \boldsymbol{\Omega}}_{\text{Centrifugal}} \right] \quad (3.146)$$

This is the form the advection terms of the momentum equation take in rotation, irrespective of any unsteady rates of change. In this equation the appearance of the second part of the Coriolis effect and the Centrifugal effect is shown.

The pressure gradient term is considered next. The relation between the inertial and rotational frame for the pressure gradient can be expressed in the manner below:

$$\hat{\nabla}\hat{\psi} = R^{\mathbf{M}^t} G^{\mathbf{M}^t} \nabla\psi \quad (3.147)$$

Since scalars are Galilean invariant under transformation, the equation simplifies to:

$$\hat{\nabla}\hat{\psi} = R^{\mathbf{M}^t} \nabla\psi \quad (3.148)$$

The last term in the momentum equation that must be transformed is the diffusion term. The relation between the inertial and non-inertial frames is described below and *Equation 3.107* is used to expand on the relation:

$$\begin{aligned} \nu \hat{\nabla}^2 \hat{\mathbf{u}} &= R^{\mathbf{M}^t} G^{\mathbf{M}^t} \nu \nabla^2 \mathbf{u} \\ &= R^{\mathbf{M}^t} \nu \nabla^2 G^{\mathbf{M}^t} \mathbf{u} \\ &= R^{\mathbf{M}^t} \nu \nabla^2 [\mathbf{u} + \mathbf{x} \wedge \boldsymbol{\Omega} + (\mathbf{x} \wedge \dot{\boldsymbol{\Omega}})\Delta t] \end{aligned} \quad (3.149)$$

If the following identities, as proofed in *Appendix A* , is substituted in the equation above,

$$\begin{aligned} \nabla^2(\mathbf{x} \wedge \boldsymbol{\Omega}) &= 0 \\ \nabla^2[(\mathbf{x} \wedge \dot{\boldsymbol{\Omega}})\Delta t] &= 0 \end{aligned} \quad (3.150)$$

the advection terms of the momentum equation becomes:

$$\nu \hat{\nabla}^2 \hat{\mathbf{u}} = R^{\mathbf{M}^t} \nu \nabla^2 \mathbf{u} \quad (3.151)$$

Note that the pressure and viscous term is Galilean invariant in this instance and the two components can be combined into a single variable  $\mathbf{f}$ :

$$\mathbf{f}(\mathbf{x}, t) = -\nabla\psi + \nu \nabla^2 \mathbf{u} \quad (3.152)$$

The relation for  $\mathbf{f}$  between the inertial and rotational frames can therefore be described by:

$$\hat{\mathbf{f}}(\hat{\mathbf{x}}, t) = R^{\mathbf{M}^t} \mathbf{f}(\mathbf{x}, t) \quad (3.153)$$

### 3.2. NON-INERTIAL NAVIER-STOKES EQUATIONS FOR VARIABLE, PURE ROTATION

Expressions have been obtained for all the parts of the momentum equation that relates the inertial Frame O to the rotational Frame  $\hat{O}$ . The transformed equation is obtained by the summation of the transient and advection components as derived in *Equations 3.143* and *3.146* :

$$\begin{aligned}\frac{\partial \hat{\mathbf{u}}}{\partial t} + (\hat{\mathbf{u}} \cdot \hat{\nabla}) \hat{\mathbf{u}} &= R^{\mathbf{M}^t} \left[ \frac{\partial \mathbf{u}}{\partial t} + (\mathbf{u} \cdot \nabla) \mathbf{u} + 2\mathbf{u} \wedge \boldsymbol{\Omega} + \mathbf{x} \wedge \boldsymbol{\Omega} \wedge \boldsymbol{\Omega} + \mathbf{x} \wedge \dot{\boldsymbol{\Omega}} \right] \\ &= R^{\mathbf{M}^t} \left[ \frac{\partial \mathbf{u}}{\partial t} + (\mathbf{u} \cdot \nabla) \mathbf{u} \right] + R^{\mathbf{M}^t} \left[ 2\mathbf{u} \wedge \boldsymbol{\Omega} + \mathbf{x} \wedge \boldsymbol{\Omega} \wedge \boldsymbol{\Omega} + \mathbf{x} \wedge \dot{\boldsymbol{\Omega}} \right]\end{aligned}\quad (3.154)$$

First grouping of terms on the right hand side of the equation above can be simplified using *Equations 3.119, 3.152* and *3.153* :

$$\begin{aligned}R^{\mathbf{M}^t} \left[ \frac{\partial \mathbf{u}}{\partial t} + (\mathbf{u} \cdot \nabla) \mathbf{u} \right] &= R^{\mathbf{M}^t} (-\nabla \psi + \nu \nabla^2 \mathbf{u}) \\ &= R^{\mathbf{M}^t} \mathbf{f}(\mathbf{x}, t) \\ &= \hat{\mathbf{f}}(\hat{\mathbf{x}}, t)\end{aligned}\quad (3.155)$$

Second grouping of terms in the transformed equation can be simplified using *Equation 3.107* and become:

$$R^{\mathbf{M}^t} (2\mathbf{u} \wedge \boldsymbol{\Omega} + \mathbf{x} \wedge \boldsymbol{\Omega} \wedge \boldsymbol{\Omega} + \mathbf{x} \wedge \dot{\boldsymbol{\Omega}}) = 2\hat{\mathbf{u}} \wedge \boldsymbol{\Omega} - \hat{\mathbf{x}} \wedge \boldsymbol{\Omega} \wedge \boldsymbol{\Omega} + \hat{\mathbf{x}} \wedge \dot{\boldsymbol{\Omega}} \quad (3.156)$$

The above simplifications can be substituted into *Equation 3.154* and result in the non-inertial momentum equation in a rotational frame:

$$\frac{\partial \hat{\mathbf{u}}}{\partial t} + (\hat{\mathbf{u}} \cdot \hat{\nabla}) \hat{\mathbf{u}} = -\hat{\nabla} \hat{\psi} + \nu \hat{\nabla}^2 \hat{\mathbf{u}} + \underbrace{2\hat{\mathbf{u}} \wedge \boldsymbol{\Omega}}_{\text{Coriolis}} - \underbrace{\hat{\mathbf{x}} \wedge \boldsymbol{\Omega} \wedge \boldsymbol{\Omega}}_{\text{Centrifugal}} + \underbrace{\hat{\mathbf{x}} \wedge \dot{\boldsymbol{\Omega}}}_{\text{Euler}} \quad (3.157)$$

The only difference between the momentum equation in constant rotation, *Equation 3.55*, and variable rotation, *Equation 3.157*, is the appearance of the Euler term.

The Euler term  $\hat{\mathbf{x}} \wedge \dot{\boldsymbol{\Omega}}$  represents the unsteady rotational acceleration of the point P around the axis of rotation which in this case is the origin of Frame O. It has also been shown that the equation above always take this form whether the acceleration in rotation is constant or variable.

#### 3.2.2.3 Energy Equation

Consider the energy equation in the inertial frame (White [9]):

$$\frac{\partial \rho e}{\partial t} + (\nabla \cdot \rho e \mathbf{u}) = -p(\nabla \cdot \mathbf{u}) + \nabla \cdot (k \nabla T) + \varphi \quad (3.158)$$

The various terms can be transformed to the rotational frame separately and then combined to obtain the energy equation in the rotational frame, the same method as was followed in *Section 3.1.2.3* .

The time dependant term can be related between Frame  $\hat{O}$  and Frame O by using the equation below. This is the same equation as in *Section 3.1.2.3* and it is valid in this case as well.

$$\frac{\partial \hat{\rho} \hat{e}}{\partial t} = R^{\boldsymbol{\Omega} t + \dot{\boldsymbol{\Omega}} t^2} \left[ \frac{\partial \rho e}{\partial t} + (\boldsymbol{\Omega} \wedge \mathbf{x}) \cdot \nabla (\rho e) \right] \quad (3.159)$$

CHAPTER 3. NON-INERTIAL EQUATIONS IN VECTOR FORM

---

The relation for the convective term between the inertial and rotational frame is shown below. This equation can be expanded upon with the used of *Equation 3.107* :

$$\begin{aligned}
 (\hat{\nabla} \cdot \hat{\rho} \hat{\mathbf{e}} \hat{\mathbf{u}}) &= R^{\mathbf{M}^t} G^{\mathbf{M}^t} (\nabla \cdot \rho \mathbf{e} \mathbf{u}) \\
 &= R^{\mathbf{M}^t} [\nabla \cdot \rho \mathbf{e} (\mathbf{u} + \mathbf{x} \wedge \boldsymbol{\Omega} + (\mathbf{x} \wedge \dot{\boldsymbol{\Omega}}) \Delta t)] \\
 &= R^{\mathbf{M}^t} [\nabla \cdot \rho \mathbf{e} \mathbf{u} + \nabla \cdot \rho \mathbf{e} (\mathbf{x} \wedge \boldsymbol{\Omega}) + \nabla \cdot \rho \mathbf{e} (\mathbf{x} \wedge \dot{\boldsymbol{\Omega}}) \Delta t]
 \end{aligned} \tag{3.160}$$

The third term on the right hand side of the equation above was shown in *Equation 3.114* to be equal to zero. The convective term therefore becomes Galilean invariant under transformation:

$$(\hat{\nabla} \cdot \hat{\rho} \hat{\mathbf{e}} \hat{\mathbf{u}}) = R^{\mathbf{M}^t} (\nabla \cdot \rho \mathbf{e} \mathbf{u} + \nabla \cdot \rho \mathbf{e} (\mathbf{x} \wedge \boldsymbol{\Omega})) \tag{3.161}$$

The term that represents the rate of work done by the normal force can be related in the inertial and rotational frames as shown below. This term can be expanded upon using *Equation 3.107* .

$$\begin{aligned}
 -\hat{p}(\hat{\nabla} \cdot \hat{\mathbf{u}}) &= R^{\mathbf{M}^t} G^{\mathbf{M}^t} [-p(\nabla \cdot \mathbf{u})] \\
 &= R^{\mathbf{M}^t} [-p \nabla \cdot (\mathbf{u} + \mathbf{x} \wedge \boldsymbol{\Omega} + (\mathbf{x} \wedge \dot{\boldsymbol{\Omega}}) \Delta t)] \\
 &= R^{\mathbf{M}^t} [-p \nabla \cdot \mathbf{u} - p \nabla \cdot (\mathbf{x} \wedge \boldsymbol{\Omega}) - p \nabla \cdot (\mathbf{x} \wedge \dot{\boldsymbol{\Omega}}) \Delta t]
 \end{aligned} \tag{3.162}$$

Showing that the second and third terms is again equal to zero, the same as above and indicated in *Equation 3.114* , this transformation is also invariant.

$$-\hat{p}(\hat{\nabla} \cdot \hat{\mathbf{u}}) = R^{\mathbf{M}^t} (-p \nabla \cdot \mathbf{u}) \tag{3.163}$$

The diffusive term in the rotational frame can be expressed in the inertial frame with the following relation:

$$\hat{\nabla} \cdot (\hat{k} \hat{\nabla} \hat{T}) = R^{\mathbf{M}^t} G^{\mathbf{M}^t} [\nabla \cdot (k \nabla T)] \tag{3.164}$$

Since k and T are scalars the relation is invariant under transformation:

$$\hat{\nabla} \cdot (\hat{k} \hat{\nabla} \hat{T}) = R^{\mathbf{M}^t} [\nabla \cdot (k \nabla T)] \tag{3.165}$$

The full relation between the rotational and inertial frames for the energy equation can be obtained by summation of the components obtained above. This leads to the equation:

$$\frac{\partial \hat{\rho} \hat{\mathbf{e}}}{\partial t} + (\hat{\nabla} \cdot \hat{\rho} \hat{\mathbf{e}} \hat{\mathbf{u}}) + \hat{p}(\hat{\nabla} \cdot \hat{\mathbf{u}}) - \hat{\nabla} \cdot (\hat{k} \hat{\nabla} \hat{T}) + \hat{\varphi} = R^{\mathbf{M}^t} \left[ \frac{\partial \rho \mathbf{e}}{\partial t} + (\nabla \cdot \rho \mathbf{e} \mathbf{u}) + p(\nabla \cdot \mathbf{u}) - \nabla \cdot (k \nabla T) \right] + \varphi \tag{3.166}$$

The right hand side of the equation is equal to zero, this can be seen from re-arrangement of the terms in *Equation 3.158* . The non-inertial energy equation is invariant under transformation in this specific case for constant acceleration in rotation, but it can be seen that this equation remains in this form even if the acceleration is not constant. *Equation 3.117* is further used to arrive at:

$$\frac{\partial \hat{\rho} \hat{\mathbf{e}}}{\partial t} + (\hat{\nabla} \cdot \hat{\rho} \hat{\mathbf{e}} \hat{\mathbf{u}}) = \hat{\nabla} \cdot (\hat{k} \hat{\nabla} \hat{T}) + \hat{\varphi}_I \tag{3.167}$$



### 3.2.3 Compressible Flow Conditions

#### 3.2.3.1 Continuity Equation

The continuity equation was shown to be invariant under the local Galilean transformation for constant rotational acceleration in *Equation 3.116* . Since the compressible case is considered here, the transformed equation becomes:

$$\frac{\partial \hat{\rho}}{\partial t} + \hat{\nabla} \cdot \hat{\rho} \hat{\mathbf{u}} = 0 \quad (3.168)$$

The continuity equation was proven invariant in all instances of unsteady rotation.

#### 3.2.3.2 Momentum Equation

The difference between the compressible and incompressible momentum equation was discussed in *Section 3.1*. It was shown in Section 3.1.3 that the difference between the incompressible and compressible case only manifests in the diffusion term. The equation for variable rotation takes a form similar to *Equation 3.85*, but with the inclusion in this case of the Euler term as seen in *Equation 3.157*:

$$\frac{\partial \hat{\rho} \hat{\mathbf{u}}}{\partial t} + \hat{\nabla} \cdot (\hat{\rho} \hat{\mathbf{u}} \otimes \hat{\mathbf{u}}) = -\hat{\nabla} \hat{p} + \hat{\nabla} \cdot [\hat{\mu}(\hat{\nabla} \hat{\mathbf{u}} + \hat{\nabla} \hat{\mathbf{u}}^T) + \hat{\lambda}(\hat{\nabla} \cdot \hat{\mathbf{u}}) \hat{\mathbf{I}}] + \underbrace{2\rho \hat{\mathbf{u}} \wedge \hat{\boldsymbol{\Omega}}}_{\text{Coriolis}} - \underbrace{\rho \hat{\mathbf{x}} \wedge \hat{\boldsymbol{\Omega}} \wedge \hat{\boldsymbol{\Omega}}}_{\text{Centrifugal}} + \underbrace{\rho \hat{\mathbf{x}} \wedge \dot{\hat{\boldsymbol{\Omega}}}}_{\text{Euler}} \quad (3.169)$$

In the case only pure rotations were considered. If the rotation was about a moving axis, an additional fictitious term would have been present in the momentum equation. This term has its origin from the transient term as shown in *Equation 3.136* . The resulting momentum equation would be:

$$\frac{\partial \hat{\rho} \hat{\mathbf{u}}}{\partial t} + \hat{\nabla} \cdot (\hat{\rho} \hat{\mathbf{u}} \otimes \hat{\mathbf{u}}) = -\hat{\nabla} \hat{p} + \hat{\nabla} \cdot [\hat{\mu}(\hat{\nabla} \hat{\mathbf{u}} + \hat{\nabla} \hat{\mathbf{u}}^T) + \hat{\lambda}(\hat{\nabla} \cdot \hat{\mathbf{u}}) \hat{\mathbf{I}}] + \underbrace{2\rho \hat{\mathbf{u}} \wedge \hat{\boldsymbol{\Omega}}}_{\text{Coriolis}} - \underbrace{\rho \hat{\mathbf{x}} \wedge \hat{\boldsymbol{\Omega}} \wedge \hat{\boldsymbol{\Omega}}}_{\text{Centrifugal}} + \underbrace{\rho \hat{\mathbf{x}} \wedge \dot{\hat{\boldsymbol{\Omega}}}}_{\text{Euler}} + \underbrace{\rho \hat{\mathbf{x}} \wedge \dot{\hat{\boldsymbol{\Omega}}}}_{\text{Moving Axis}} \quad (3.170)$$

This equation applies to all bodies in unsteady rotation. It has been shown that no additional terms are added to the non-inertial formulation even if the rotational rate of change is unsteady (*Equation 3.143*).

#### 3.2.3.3 Energy Equation

The energy equation remains invariant in the non-inertial frame as shown in *Equation 3.167*, only here the incompressibility assumption is not made. The non-inertial energy equation in compressible flow therefore becomes:

$$\frac{\partial \hat{\rho} \hat{e}}{\partial t} + (\hat{\nabla} \cdot \hat{\rho} \hat{e} \hat{\mathbf{u}}) = -\hat{p}(\hat{\nabla} \cdot \hat{\mathbf{u}}) + \hat{\nabla} \cdot (\hat{k} \hat{\nabla} \hat{T}) + \hat{\phi} \quad (3.171)$$

It was shown in *Section 3.2.2.3* that the energy equation is invariant under transformation in all cases of rotation.

### 3.2.4 Constant Rotation Equations as a Special Case of the Variable Rotation Equations

In *Sections 3.1.2 and 3.2.2* it was shown that the continuity and conservation of energy equations are invariant under Galilean transformation for all cases of rotation. This is an important result to show. Even though mass and energy are scalar values which is invariant under Galilean transformation (Kleppner and Kolenkow [60], McCauley [61]), it is not obvious that there are no fictitious effects when deriving the equations using the a Lagrangian approach. The derivation of the momentum equation for the various cases not only provided the appropriate fictitious forces for each case, but it also showed from which transformations the forces originated (see *Equations 3.55, 3.85, 3.157 and 3.169*).

The derivations are based on a Taylor series expansion of the relative motion between the origin of Frame O and the combined origin of Frames O' and  $\hat{O}$ . The constant rotation case is a special case of the variable rotation case since the order at which the Taylor series was truncated, determines the fictitious force involved (see *Equations 3.2 and 3.99*). The variable rotation formulation lead directly to the constant rotation formulation if constant rotation conditions is applies to it. Since the conservation of mass and energy equations is invariant no changes occur in those formulation. This is demonstrated using the momentum equations below.

Consider the momentum equation for variable, pure rotation in the rotational frame in incompressible flow (*Equation 3.157*):

$$\frac{\partial \hat{\mathbf{u}}}{\partial t} + (\hat{\mathbf{u}} \cdot \hat{\nabla}) \hat{\mathbf{u}} = -\hat{\nabla} \hat{\psi} + \nu \hat{\nabla}^2 \hat{\mathbf{u}} + \underbrace{2\hat{\mathbf{u}} \wedge \hat{\boldsymbol{\Omega}}}_{\text{Coriolis}} - \underbrace{\hat{\mathbf{x}} \wedge \hat{\boldsymbol{\Omega}} \wedge \hat{\boldsymbol{\Omega}}}_{\text{Centrifugal}} + \underbrace{\hat{\mathbf{x}} \wedge \dot{\hat{\boldsymbol{\Omega}}}}_{\text{Euler}} \quad (3.172)$$

The fictitious forces involved are the Coriolis force, Centrifugal force and Euler force. In the case where the rotational is constant,  $\dot{\hat{\boldsymbol{\Omega}}} = 0$ , the Euler force becomes zero,  $\hat{\mathbf{x}} \wedge \dot{\hat{\boldsymbol{\Omega}}} = 0$ . The equation then becomes:

$$\frac{\partial \hat{\mathbf{u}}}{\partial t} + (\hat{\mathbf{u}} \cdot \hat{\nabla}) \hat{\mathbf{u}} = -\hat{\nabla} \hat{\psi} + \nu \hat{\nabla}^2 \hat{\mathbf{u}} + \underbrace{2\hat{\mathbf{u}} \wedge \hat{\boldsymbol{\Omega}}}_{\text{Coriolis}} - \underbrace{\hat{\mathbf{x}} \wedge \hat{\boldsymbol{\Omega}} \wedge \hat{\boldsymbol{\Omega}}}_{\text{Centrifugal}} \quad (3.173)$$

This is the same as *Equation 3.55* which describes the momentum equation for constant rotation as seen from the rotational frame. This indicates consistency in the derivations.

### 3.3 Non-Inertial Navier-Stokes Equation for Arbitrary Motion

Rotational cases, as discussed in the previous sections, are very specific. The formulations only applies in applications such as wind turbines and other stationary machinery.

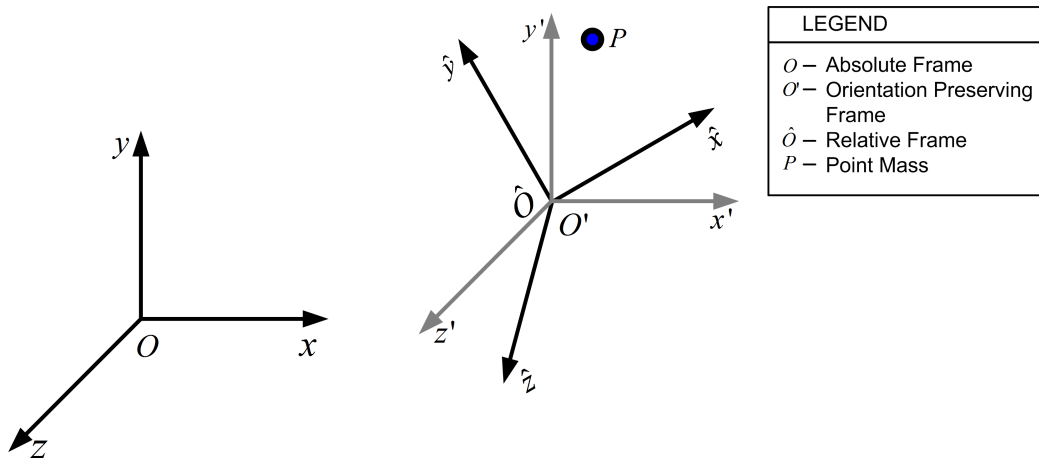
Applications that display fully arbitrary non-inertial behaviour can be found in the aeronautical and aero-ballistic fields. Military aircraft that executes high acceleration manoeuvres and artillery projectiles with air-breathing engines are some examples where arbitrary motion in six degrees of freedom is observed.

The non-inertial mathematical formulations for airframes executing arbitrary motion (both in translation and rotation) are derived here.

#### 3.3.1 Frame Transformations

In this derivation three reference frames (the same as used in *Sections 3.1* and *3.2*) are made use of to transform the inertial Navier-Stokes equations to the non-inertial form (*Figure 3.7*).

Figure 3.7: Frames of Observation ( $O$ ,  $O'$  and  $\hat{O}$ ) for Point  $P$



These frames comprise of:

- Frame  $O$ , which is an inertial frame. This frame is stationary.
- Frame  $O'$ , which is a non-inertial frame. This frame is orientation preserving with respect to Frame  $O$ . It therefore has three degrees of freedom and is free to translate. This frame accounts for the relative translation motion between the inertial and non-inertial frames.
- Frame  $\hat{O}$ , which is a non-inertial, rotating frame. This frame does not preserve orientation therefore it has six degrees of freedom. It can translate and rotate as predicted by the unsteady motion imposed on point  $P$ . This frame shares an origin with Frame  $O'$  so that it can account for the relative rotational motion between the inertial and non-inertial frames.

CHAPTER 3. NON-INERTIAL EQUATIONS IN VECTOR FORM

---

Consider the point P. The motion of this point can be described from each of the three frames. This point is in arbitrary motion in translation and rotation. The rotational axis is about the shared origins of Frame  $\hat{O}$  and Frame  $O'$ .

The flow field that surrounds this point can be described from any of the reference frames. The standard Navier-Stokes equations hold in the inertial frame, therefore the objective is to obtain the correct form of the equations in Frame  $\hat{O}$ . It is accomplished by conducting two transformations.

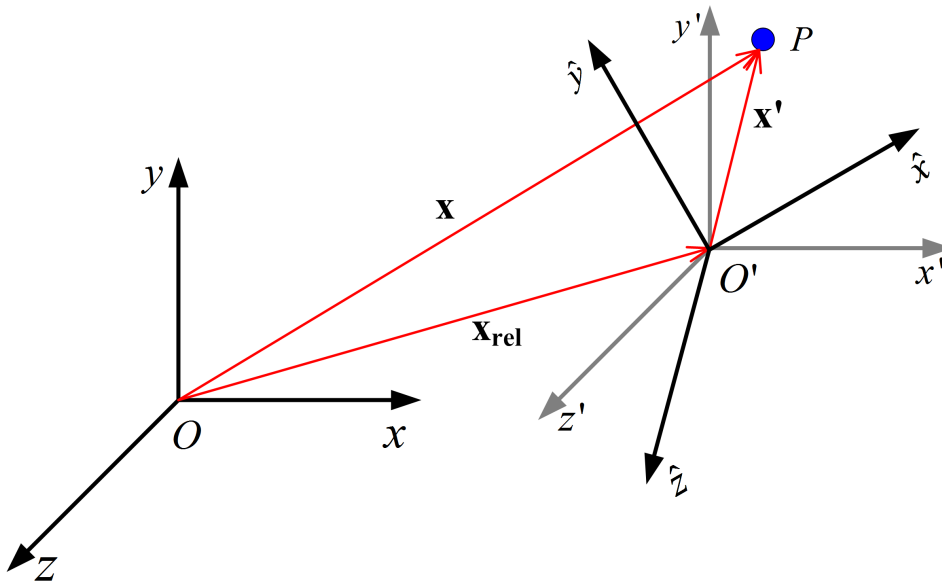
The first transformation accounts for arbitrary motion between the inertial frame and the orientation preserving frame. Since Frame  $O'$  and Frame  $\hat{O}$  shares an origin, this transformation accounts for the translation of Frame  $\hat{O}$  as well. A local Galilean Transformation for unsteady motion is used to this effect.

The second transformation accounts for arbitrary rotation. A transformation from Frame  $O'$  to Frame  $\hat{O}$  is defined. The relation derived during the first transformation is used to describe the flow field in Frame  $\hat{O}$  in terms of the vectors of Frame  $O$ .

### 3.3.1.1 Local Galilean Transformation

For the local Galilean transformation assume that the frame origins intersect at time  $t = 0$  and that frame  $\hat{O}$  is moving at velocity  $\mathbf{v}_{\text{rel}}$  and acceleration  $\mathbf{a}_{\text{rel}}$  in three dimensional space. At time  $t = \Delta t$  Frames  $O$  and  $O'$  are distance  $\mathbf{x}_{\text{rel}}$  from each other. The is depicted in *Figure 3.8*.

Figure 3.8: Point Description between Frames



In *Figure 3.8* the absolute distance can be described in terms of the relative and non-inertial distances:

$$\mathbf{x} = \mathbf{x}_{\text{rel}} + \mathbf{x}' \tag{3.174}$$

### 3.3. NON-INERTIAL NAVIER-STOKES EQUATION FOR ARBITRARY MOTION

The relative distance between the two frames is a summation of the accelerating translation and rotation and is described by:

$$\mathbf{x}_{\text{rel}} = \mathbf{V}_{\text{rel}}\Delta t + \frac{1}{2}\mathbf{a}_{\text{rel}}\Delta t^2 \quad (3.175)$$

The relative velocity component consist of the translating and rotating velocity components so that:

$$\begin{aligned} \mathbf{V}_{\text{rel}} &= \mathbf{V}_{\text{translating}} + \mathbf{V}_{\text{rotating}} \\ &= \mathbf{V}(t) + \boldsymbol{\Omega} \wedge \mathbf{x}' \end{aligned} \quad (3.176)$$

In this equation the translation component is a function of time only as it describes the motion between the origins of Frames O and O'. The rotation is taking place in Frame O' and is therefore defined in this frame.

The acceleration is the time derivative of the velocity:

$$\begin{aligned} \frac{\partial \mathbf{V}_{\text{rel}}}{\partial t} &= \frac{\partial}{\partial t} [\mathbf{V}(t) + \boldsymbol{\Omega} \wedge \mathbf{x}'] \\ &= \mathbf{a}(t) + \frac{\partial \boldsymbol{\Omega}}{\partial t} \wedge \mathbf{x}' + \boldsymbol{\Omega} \wedge \frac{\partial \mathbf{x}'}{\partial t} \end{aligned} \quad (3.177)$$

The first term represents the translational acceleration, while the second and third terms is a result of the rotational velocity. Since both the derivative of  $\mathbf{x}$  and  $\boldsymbol{\Omega}$  is not equal to zero, these terms contribute to the total relative unsteady motion. The accelerating component can therefore be expressed as:

$$\begin{aligned} \mathbf{a}_{\text{rel}} &= \mathbf{a}_{\text{translating}} + \mathbf{a}_{\text{rotating}} \\ &= \underbrace{\mathbf{a}(t)}_{\text{Translating}} + \underbrace{\dot{\boldsymbol{\Omega}} \wedge \mathbf{x}' + \boldsymbol{\Omega} \wedge \dot{\mathbf{x}}'}_{\text{Rotating}} \end{aligned} \quad (3.178)$$

A description for the relative motion can be obtained by substituting *Equations 3.178* and *3.176* into *Equation 3.175*. This results in:

$$\mathbf{x}_{\text{rel}} = [\mathbf{V}(t) + \boldsymbol{\Omega} \wedge \mathbf{x}']\Delta t + \frac{1}{2}[\mathbf{a}(t) + \dot{\boldsymbol{\Omega}} \wedge \mathbf{x}' + \boldsymbol{\Omega} \wedge \dot{\mathbf{x}}']\Delta t^2 \quad (3.179)$$

The relation between the order preserving frame and the inertial frame is defined through a local Galilean transformation:

$$\begin{aligned} \mathbf{u}'(\mathbf{x}', t) &= G^{\mathbf{M}^t} \mathbf{u}(\mathbf{x}, t) \\ &= \mathbf{u}(\mathbf{x}, t) - \mathbf{V}(t) + \mathbf{x}' \wedge \boldsymbol{\Omega} - [\mathbf{a}(t) + \dot{\boldsymbol{\Omega}} \wedge \mathbf{x}' + \boldsymbol{\Omega} \wedge \dot{\mathbf{x}}']\Delta t \end{aligned} \quad (3.180)$$

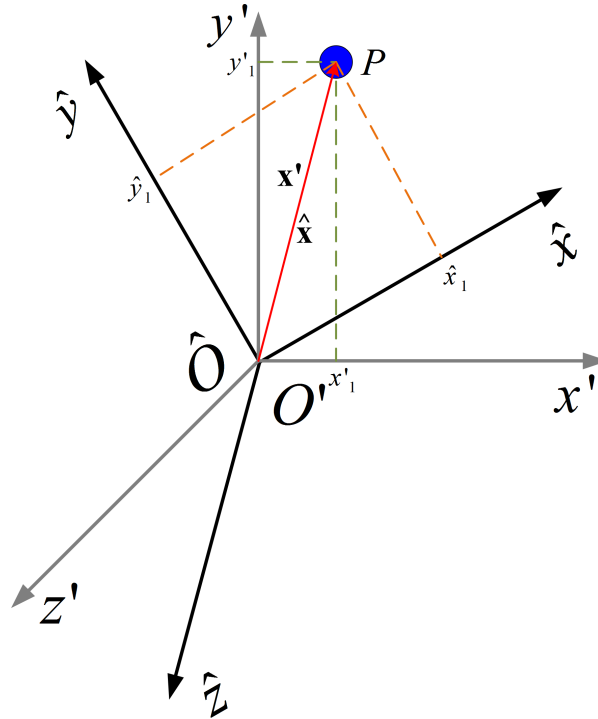
#### 3.3.1.2 Rotational Transform

The rotational transform for this case can be defined as the projection of the vectors in the orientation preserving frame on the rotational frames. This is depicted in *Figure 3.9*.

The vector components in Frame  $\hat{O}$  is related to Frame O' by defining a rotational transform and substituting *Equation 3.180*:

$$\begin{aligned} \hat{\mathbf{u}}(\hat{\mathbf{x}}, t) &= R^{\mathbf{M}^t} \mathbf{u}'(\mathbf{x}', t) \\ &= R^{\mathbf{M}^t} G^{\mathbf{M}^t} \mathbf{u}(\mathbf{x}, t) \end{aligned} \quad (3.181)$$

Figure 3.9: Relation between Rotational and Orientation Preserving Frames



Lets assume that the rotation is around the z-axis, then the vector  $\mathbf{\Omega}$  is described as  $\mathbf{\Omega} = (0, 0, \Omega)$  and vector  $\dot{\mathbf{\Omega}}$  is described as  $\dot{\mathbf{\Omega}} = (0, 0, \dot{\Omega})$ . The rotational transform in this case is described by:

$$R^{\mathbf{M}^t} = \begin{bmatrix} \cos(\Omega t + \dot{\Omega} t^2) & \sin(\Omega t + \dot{\Omega} t^2) & 0 \\ -\sin(\Omega t + \dot{\Omega} t^2) & \cos(\Omega t + \dot{\Omega} t^2) & 0 \\ 0 & 0 & 1 \end{bmatrix} \quad (3.182)$$

From *Equations 3.180 and 3.181* it can be derived that the following relation holds:

$$\hat{\mathbf{u}}(\hat{\mathbf{x}}, t) = R^{\mathbf{M}^t}[\mathbf{u}(\mathbf{x}, t) - \mathbf{V}(t) + \mathbf{x}' \wedge \mathbf{\Omega} - [\mathbf{a}(t) + \dot{\mathbf{\Omega}} \wedge \mathbf{x}' + \mathbf{\Omega} \wedge \dot{\mathbf{x}}'] \Delta t] \quad (3.183)$$

### 3.3.2 Compressible Flow Conditions

#### 3.3.2.1 Continuity Equation

Consider the continuity equation in the inertial reference frame (White [9]):

$$\frac{\partial \rho}{\partial t} + (\nabla \cdot \rho \mathbf{u}) = 0 \quad (3.184)$$

The time dependant term in the inertial and non-inertial frame is related by the same expression in *Sections 3.1.2.1 and 3.2.2.1*. The exception in this case is that the rotation is around the origin of Frame  $O'$ :

$$\frac{\partial \hat{\rho}}{\partial t} = R^{\mathbf{M}^t} \left[ \frac{\partial \rho}{\partial t} + (\mathbf{\Omega} \wedge \mathbf{x}') \cdot \nabla \rho \right] \quad (3.185)$$

### 3.3. NON-INERTIAL NAVIER-STOKES EQUATION FOR ARBITRARY MOTION

The relation between the inertial and non-inertial formulations of the second term in the continuity equation becomes:

$$\begin{aligned} (\hat{\nabla} \cdot \hat{\rho} \hat{\mathbf{u}}) &= R^{\mathbf{M}^t} G^{\mathbf{M}^t} (\nabla \cdot \rho \mathbf{u}) \\ &= R^{\mathbf{M}^t} \nabla \cdot \rho (G^{\mathbf{M}^t} \mathbf{u}) \end{aligned} \quad (3.186)$$

With the implementation of *Equation 3.183* the relation is simplified to:

$$(\hat{\nabla} \cdot \hat{\rho} \hat{\mathbf{u}}) = R^{\mathbf{M}^t} \nabla \cdot \rho [\mathbf{u} - \mathbf{V}(t) + \mathbf{x}' \wedge \boldsymbol{\Omega} - [\mathbf{a}(t) + \dot{\boldsymbol{\Omega}} \wedge \mathbf{x}' + \boldsymbol{\Omega} \wedge \dot{\mathbf{x}}'] \Delta t] \quad (3.187)$$

The divergence of a cross product is equal to zero (see *Appendix A for the proof*), hence a number on the terms in the above relation is cancelled out:

$$\begin{aligned} \nabla \cdot (\dot{\boldsymbol{\Omega}} \wedge \mathbf{x}') &= 0 \\ \nabla \cdot (\boldsymbol{\Omega} \wedge \dot{\mathbf{x}}') &= 0 \end{aligned} \quad (3.188)$$

Furthermore, the divergence of the translational components are equal to zero. This is due to the translation being dependant on the time dimension alone -  $\mathbf{V}(t)$  and  $\mathbf{a}(t)$  are constant throughout the spatial domain at any given time step:

$$\begin{aligned} \nabla \cdot \mathbf{V}(t) &= 0 \\ \nabla \cdot \mathbf{a}(t) &= 0 \end{aligned} \quad (3.189)$$

The relation is hence simplified to an invariant relation as all the additional terms cancels out:

$$\hat{\nabla} \cdot \hat{\rho} \hat{\mathbf{u}} = R^{\mathbf{M}^t} (\nabla \cdot \rho \mathbf{u} + \nabla \cdot \rho \mathbf{x}' \wedge \boldsymbol{\Omega}) \quad (3.190)$$

The addition of *Equations 3.185* and *3.190* give a relation for continuity in the non-inertial frame:

$$\frac{\partial \hat{\rho}}{\partial t} + \hat{\nabla} \cdot \hat{\rho} \hat{\mathbf{u}} = R^{\mathbf{M}^t} \left( \frac{\partial \rho}{\partial t} + \nabla \cdot \rho \mathbf{u} \right) \quad (3.191)$$

By implementing *Equation 3.184*, the final equation for mass conservation in the accelerating frame is obtained:

$$\frac{\partial \hat{\rho}}{\partial t} + \hat{\nabla} \cdot \hat{\rho} \hat{\mathbf{u}} = 0 \quad (3.192)$$

The derivations for the continuity equation, here and in *Sections 3.1.2.1* and *3.2.2.1*, in the non-inertial frame have shown to be invariant to transformation whether the acceleration is zero, constant or variable. In any non-inertial frame *Equation 3.192* holds for compressible conditions.

#### 3.3.2.2 Conservation of Momentum Equation

The compressible Navier-Stokes Equation in the inertial frame takes the form (White [9]):

$$\underbrace{\frac{\partial}{\partial t} \rho \mathbf{u}}_{\text{Unsteady}} + \underbrace{\nabla \cdot (\rho \mathbf{u} \otimes \mathbf{u})}_{\text{Advection}} = - \underbrace{\nabla p}_{\text{Pressure Gradient}} + \underbrace{\nabla \cdot [\mu(\nabla \mathbf{u} + \nabla \mathbf{u}^T) + \lambda(\nabla \cdot \mathbf{u})\mathbf{I}]}_{\text{Compressible Stress Tensor}} \quad (3.193)$$

CHAPTER 3. NON-INERTIAL EQUATIONS IN VECTOR FORM

The non-inertial forms of the separate terms of the equation, are derived from this form to obtain the compressible equations in the acceleration frame.

First consider the unsteady term in the rotational frame and apply the product rule for partial derivatives. This operation results in two terms that was not considered during the incompressible case:

$$\frac{\partial}{\partial t}(\hat{\rho}\hat{\mathbf{u}}) = \hat{\rho} \frac{\partial \hat{\mathbf{u}}}{\partial t} + \hat{\mathbf{u}} \frac{\partial \hat{\rho}}{\partial t} \quad (3.194)$$

The first transformation concerns the unsteady term where an expression is found for:

$$\frac{\partial \hat{\mathbf{u}}}{\partial t}(\hat{\mathbf{x}}_t, t) = \lim_{\Delta t \rightarrow 0} \frac{\hat{\mathbf{u}}(\hat{\mathbf{x}}_{t+\Delta t}, t + \Delta t) - \hat{\mathbf{u}}(\hat{\mathbf{x}}_t, t)}{\Delta t} \quad (3.195)$$

The first task is to find an expression for the term  $\hat{\mathbf{u}}(\hat{\mathbf{x}}_{t+\Delta t}, t + \Delta t)$ . The expression takes a form that is similar to *Equation 3.181*:

$$\hat{\mathbf{u}}(\hat{\mathbf{x}}_{t+\Delta t}, t + \Delta t) = R^{\mathbf{M}^{t+\Delta t}} \mathbf{u}'(\mathbf{x}'_{t+\Delta t}, t + \Delta t) \quad (3.196)$$

The Taylor series expansion for  $\mathbf{x}'_{t+\Delta t}$  is expressed as:

$$\mathbf{x}'_{t+\Delta t} = \mathbf{x}'_t + \mathbf{V}'\Delta t + \frac{1}{2}\mathbf{a}'\Delta t^2 + O(\Delta t^3) \quad (3.197)$$

The expression above is as seen from the orientation preserving frame. Since this frame is free to translate, but not to rotate, only the rotation terms are relevant here. The equation above is truncated at the second order as further changes in acceleration does not have a effect in the non-inertial frame. With the substitution of the rotational components of *Equations 3.176* and *3.178* and further re-arrangement the equation becomes:

$$\mathbf{x}'_{t+\Delta t} - \mathbf{x}'_t = \mathbf{x}'_{\Delta t} = (\boldsymbol{\Omega} \wedge \mathbf{x}'_t)\Delta t + \frac{1}{2}(\dot{\boldsymbol{\Omega}} \wedge \mathbf{x}'_t + \boldsymbol{\Omega} \wedge \dot{\mathbf{x}}'_t)\Delta t^2 \quad (3.198)$$

The Fourier series expansion is obtained for  $\mathbf{u}'(\mathbf{x}'_{t+\Delta t}, t + \Delta t)$ . Substitute *Equation 3.198* into the expression to obtain:

$$\mathbf{u}'(\mathbf{x}'_{t+\Delta t}, t + \Delta t) = \mathbf{u}'(\mathbf{x}'_t, t) + \{[\Delta t(\boldsymbol{\Omega} \wedge \mathbf{x}'_t) + \frac{1}{2}\Delta t^2(\dot{\boldsymbol{\Omega}} \wedge \mathbf{x}'_t + \boldsymbol{\Omega} \wedge \dot{\mathbf{x}}'_t)] \cdot \nabla\} \mathbf{u}'(\mathbf{x}'_t, t) + (\Delta t \frac{\partial}{\partial t}) \mathbf{u}'(\mathbf{x}'_t, t) \quad (3.199)$$

The equation above is substituted into *Equation 3.196* to get the expression:

$$\hat{\mathbf{u}}(\hat{\mathbf{x}}_{t+\Delta t}, t + \Delta t) = R^{\mathbf{M}^{t+\Delta t}} \{ \mathbf{u}'(\mathbf{x}'_t, t) + [[\Delta t(\boldsymbol{\Omega} \wedge \mathbf{x}'_t) + \frac{1}{2}\Delta t^2(\dot{\boldsymbol{\Omega}} \wedge \mathbf{x}'_t + \boldsymbol{\Omega} \wedge \dot{\mathbf{x}}'_t)] \cdot \nabla\} \mathbf{u}'(\mathbf{x}'_t, t) + (\Delta t \frac{\partial}{\partial t}) \mathbf{u}'(\mathbf{x}'_t, t) \} \quad (3.200)$$

The assumption are made that the point P is fixed in the rotating frame, and the rotation is around the origin of Frame O'. The relation of motion between two time steps are:

$$\begin{aligned} \hat{\mathbf{x}} &= R^{\mathbf{M}^{t+\Delta t}} \mathbf{x}'_{t+\Delta t} = R^{\mathbf{M}^t} \mathbf{x}'_t \\ \mathbf{x}'_t &= R^{\mathbf{M}^{\Delta t}} \mathbf{x}'_{t+\Delta t} \end{aligned} \quad (3.201)$$



### 3.3. NON-INERTIAL NAVIER-STOKES EQUATION FOR ARBITRARY MOTION

Next a Taylor series expansion for  $\mathbf{x}'_{t+\Delta t}$  is developed and the equation above is used to arrive at:

$$\begin{aligned}\mathbf{x}'_{t+\Delta t} &= \mathbf{x}'_t + \mathbf{V}'\Delta t + \frac{1}{2}\mathbf{a}'\Delta t^2 + O[\Delta t^3] \\ &= R^{\mathbf{M}^{\Delta t}}\mathbf{x}'_{t+\Delta t} + (\boldsymbol{\Omega} \wedge \mathbf{x}'_t)\Delta t + \frac{1}{2}(\dot{\boldsymbol{\Omega}} \wedge \mathbf{x}'_t + \boldsymbol{\Omega} \wedge \dot{\mathbf{x}}'_t)\Delta t^2 + O[\Delta t^3]\end{aligned}\quad (3.202)$$

Re-arrange the expression above and consider it in the limit yields:

$$\lim_{\Delta t \rightarrow 0} \frac{R^{\mathbf{M}^{\Delta t}}\mathbf{x}'_{t+\Delta t} - \mathbf{x}'_{t+\Delta t}}{\Delta t} = \lim_{\Delta t \rightarrow 0} [-\boldsymbol{\Omega} \wedge \mathbf{x}'_t - \frac{1}{2}\Delta t(\dot{\boldsymbol{\Omega}} \wedge \mathbf{x}'_t + \boldsymbol{\Omega} \wedge \dot{\mathbf{x}}'_t) - O[\Delta t^3]] \quad (3.203)$$

If this expression is considered for any vector  $\mathbf{b}$ , and taken into account that  $\mathbf{x}_{t+\Delta t} \rightarrow \mathbf{x}_t$  as  $\Delta t \rightarrow 0$ , the following equation related to rotation is obtained:

$$\lim_{\Delta t \rightarrow 0} \frac{R^{\mathbf{M}^{\Delta t}}\mathbf{b} - \mathbf{b}}{\Delta t} = \mathbf{b} \wedge \boldsymbol{\Omega} \quad (3.204)$$

With all the required expressions in place *Equation 3.195* can now be completed:

$$\frac{\partial \hat{\mathbf{u}}}{\partial t}(\hat{\mathbf{x}}_t, t) = \lim_{\Delta t \rightarrow 0} \frac{R^{\mathbf{M}^{\Delta t}} \{ [1 - \frac{1}{R^{\mathbf{M}^{\Delta t}}} + \Delta t(\boldsymbol{\Omega} \wedge \mathbf{x}'_t) \cdot \nabla + \frac{1}{2}\Delta t^2(\dot{\boldsymbol{\Omega}} \wedge \mathbf{x}'_t + \boldsymbol{\Omega} \wedge \dot{\mathbf{x}}'_t) \cdot \nabla] \mathbf{u}'(\mathbf{x}'_t, t) + (\Delta t \frac{\partial}{\partial t}) \mathbf{u}'(\mathbf{x}'_t, t) \}}{\Delta t} \quad (3.205)$$

*Equation 3.204* is used to simplify the expression above and with some rearrangement of terms the following expression is obtained:

$$\frac{\partial \hat{\mathbf{u}}}{\partial t}(\hat{\mathbf{x}}_t, t) = R^{\mathbf{M}^t} \left[ \frac{\partial}{\partial t} + (\boldsymbol{\Omega} \wedge \mathbf{x}'_t) \cdot \nabla - \boldsymbol{\Omega} \wedge \right] [G^{\mathbf{M}^t} \mathbf{u}(\mathbf{x}_t, t)] \quad (3.206)$$

This equation above retains its current form irrespective of any further changes in acceleration. All other terms that is inserted to account for variation in acceleration become negligible when the expression is considered in the limit. This equation is similar to *Equations 3.36* and *3.134* indicating that the higher order acceleration terms do not cause any changes in this expression.

Substitute *Equation 3.206* into *Equation 3.194* and with the aid of *Equation 3.181* the above becomes:

$$\frac{\partial}{\partial t}(\hat{\rho} \hat{\mathbf{u}}) = R^{\mathbf{M}^t} G^{\mathbf{M}^t} \left[ \rho \frac{\partial \mathbf{u}}{\partial t} + \rho(\boldsymbol{\Omega} \wedge \mathbf{x}'_t) \cdot \nabla \mathbf{u} - \rho \boldsymbol{\Omega} \wedge \mathbf{u} + \mathbf{u} \frac{\partial \rho}{\partial t} \right] \quad (3.207)$$

The product rule is then used to combine the terms  $\rho \frac{\partial \mathbf{u}}{\partial t}$  and  $\mathbf{u} \frac{\partial \rho}{\partial t}$  so that the equation simplifies to:

$$\frac{\partial}{\partial t}(\hat{\rho} \hat{\mathbf{u}}) = R^{\mathbf{M}^t} \left[ \frac{\partial}{\partial t}(\rho) + \rho(\boldsymbol{\Omega} \wedge \mathbf{x}'_t) \cdot \nabla - \rho \boldsymbol{\Omega} \wedge \right] G^{\mathbf{M}^t} \mathbf{u} \quad (3.208)$$

CHAPTER 3. NON-INERTIAL EQUATIONS IN VECTOR FORM

*Equation 3.183* is substituted in the equation above to remove the local Galilean operator from the equation:

$$\begin{aligned}
\frac{\partial \rho \hat{\mathbf{u}}}{\partial t}(\hat{\mathbf{x}}_t, t) &= R^{\mathbf{M}^t} \left[ \frac{\partial}{\partial t}(\rho) + \rho(\boldsymbol{\Omega} \wedge \mathbf{x}'_t) \cdot \nabla - \rho \boldsymbol{\Omega} \wedge \right] (\mathbf{u}(\mathbf{x}_t, t)) \\
&\quad - R^{\mathbf{M}^t} \left[ \frac{\partial}{\partial t}(\rho) + \rho(\boldsymbol{\Omega} \wedge \mathbf{x}'_t) \cdot \nabla - \rho \boldsymbol{\Omega} \wedge \right] (\mathbf{V}(t)) \\
&\quad + R^{\mathbf{M}^t} \left[ \frac{\partial}{\partial t}(\rho) + \rho(\boldsymbol{\Omega} \wedge \mathbf{x}'_t) \cdot \nabla - \rho \boldsymbol{\Omega} \wedge \right] (\mathbf{x}'_t \wedge \boldsymbol{\Omega}) \\
&\quad + R^{\mathbf{M}^t} \left[ \frac{\partial}{\partial t}(\rho) + \rho(\boldsymbol{\Omega} \wedge \mathbf{x}'_t) \cdot \nabla - \rho \boldsymbol{\Omega} \wedge \right] (\mathbf{a}(t) + \dot{\boldsymbol{\Omega}} \wedge \mathbf{x}'_t + \boldsymbol{\Omega} \wedge \dot{\mathbf{x}}'_t) \Delta t
\end{aligned} \tag{3.209}$$

The different parts of  $[\frac{\partial}{\partial t}(\rho) + \rho(\boldsymbol{\Omega} \wedge \mathbf{x}'_t) \cdot \nabla - \rho \boldsymbol{\Omega} \wedge](\mathbf{x}'_t \wedge \boldsymbol{\Omega})$ , which is the third combination of terms in *Equation 3.209*, are considered here.

The transient term in the equation above can be expanded on with the use of the product rule for partial differential equations:

$$\frac{\partial}{\partial t}(\mathbf{x}'_t \wedge \boldsymbol{\Omega}) = \frac{\partial \mathbf{x}'_t}{\partial t} \wedge \boldsymbol{\Omega} + (\mathbf{x}'_t \wedge \frac{\partial \boldsymbol{\Omega}}{\partial t}) \tag{3.210}$$

In the equation above the first term on the right hand side represents the unsteady motion of point P in the frame O' in cases where the rotation is not purely about the fixed axis. In pure rotation cases this term is equal to zero. The second term represents the unsteady rotation, this is referred to as the Euler fictitious force.

The terms  $[(\boldsymbol{\Omega} \wedge \mathbf{x}'_t) \cdot \nabla - \boldsymbol{\Omega} \wedge](\mathbf{x}'_t \wedge \boldsymbol{\Omega})$  is equal to zero and cancels out:

$$[(\boldsymbol{\Omega} \wedge \mathbf{x}'_t) \cdot \nabla - \boldsymbol{\Omega} \wedge](\mathbf{x}'_t \wedge \boldsymbol{\Omega}) = 0 \tag{3.211}$$

The relation  $[\frac{\partial}{\partial t}(\rho) + \rho(\boldsymbol{\Omega} \wedge \mathbf{x}'_t) \cdot \nabla - \rho \boldsymbol{\Omega} \wedge](\mathbf{x}'_t \wedge \boldsymbol{\Omega})$ , for this case, simplifies to:

$$[\frac{\partial}{\partial t}(\rho) + \rho(\boldsymbol{\Omega} \wedge \mathbf{x}'_t) \cdot \nabla - \rho \boldsymbol{\Omega} \wedge](\mathbf{x}'_t \wedge \boldsymbol{\Omega}) = \rho \dot{\mathbf{x}}'_t \wedge \boldsymbol{\Omega} + \rho \mathbf{x}'_t \wedge \dot{\boldsymbol{\Omega}} \tag{3.212}$$

The entire fourth combination of terms in *Equation 3.209* falls away.

The above leads to the final description of the unsteady terms in the momentum equation for arbitrary acceleration:

$$\frac{\partial \rho \hat{\mathbf{u}}}{\partial t}(\hat{\mathbf{x}}_t, t) = R^{\mathbf{M}^t} \left[ \frac{\partial}{\partial t}(\rho) + \rho(\boldsymbol{\Omega} \wedge \mathbf{x}'_t) \cdot \nabla - \underbrace{\rho \boldsymbol{\Omega} \wedge}_{\text{Coriolis}} \right] (\mathbf{u}(\mathbf{x}_t, t) - \mathbf{V}(t)) + R^{\mathbf{M}^t} \left( \underbrace{\rho \dot{\mathbf{x}}'_t \wedge \boldsymbol{\Omega}}_{\text{Moving Axis}} + \underbrace{\rho \mathbf{x}'_t \wedge \dot{\boldsymbol{\Omega}}}_{\text{Euler}} \right) \tag{3.213}$$

In any arbitrary acceleration case, this is the form the unsteady component of the equation always take. Take note in this equation of the appearance of a part of the Coriolis effect, Euler effect and a term that is related to in frame motion due to rotation that is not purely around a stationary axis.

### 3.3. NON-INERTIAL NAVIER-STOKES EQUATION FOR ARBITRARY MOTION

The relation between the frames for the advection term in the compressible Navier-Stokes momentum equation is:

$$\hat{\nabla} \cdot (\hat{\rho} \hat{\mathbf{u}} \otimes \hat{\mathbf{u}}) = R^{\mathbf{M}^t} G^{\mathbf{M}^t} [\nabla \cdot (\rho \mathbf{u} \otimes \mathbf{u})] \quad (3.214)$$

By using *Equation 3.180* the equation above is expanded into:

$$\begin{aligned} \hat{\nabla} \cdot (\hat{\rho} \hat{\mathbf{u}} \otimes \hat{\mathbf{u}}) &= R^{\mathbf{M}^t} \{ \nabla \cdot \rho [(\mathbf{u} - \mathbf{V}(t) + \mathbf{x}' \wedge \boldsymbol{\Omega} - [\mathbf{a}(t) + \dot{\boldsymbol{\Omega}} \wedge \mathbf{x}' + \boldsymbol{\Omega} \wedge \mathbf{x}'] \Delta t) \\ &\otimes (\mathbf{u} - \mathbf{V}(t) + \mathbf{x}' \wedge \boldsymbol{\Omega} - [\mathbf{a}(t) + \dot{\boldsymbol{\Omega}} \wedge \mathbf{x}' + \boldsymbol{\Omega} \wedge \mathbf{x}'] \Delta t)] \} \\ &= R^{\Omega t} \{ (\nabla \cdot \rho \mathbf{u}) \otimes \mathbf{u} - (\nabla \cdot \rho \mathbf{u}) \otimes (\mathbf{V}(t)) + (\nabla \cdot \rho \mathbf{u}) \otimes (\mathbf{x}' \wedge \boldsymbol{\Omega}) \\ &- [\nabla \cdot \rho (\mathbf{V}(t))] \otimes \mathbf{u} + [\nabla \cdot \rho (\mathbf{V}(t))] \otimes (\mathbf{V}(t)) - [\nabla \cdot \rho (\mathbf{V}(t))] \otimes (\mathbf{x}' \wedge \boldsymbol{\Omega}) \\ &+ [\nabla \cdot \rho (\mathbf{x}' \wedge \boldsymbol{\Omega})] \otimes \mathbf{u} - [\nabla \cdot \rho (\mathbf{x}' \wedge \boldsymbol{\Omega})] \otimes (\mathbf{V}(t)) + [\nabla \cdot \rho (\mathbf{x}' \wedge \boldsymbol{\Omega})] \otimes (\mathbf{x}' \wedge \boldsymbol{\Omega}) \} \end{aligned} \quad (3.215)$$

The identity as derived in *Appendix A* below can be used to simplify the equation.

$$(\nabla \cdot \mathbf{a}) \otimes (\mathbf{x}' \wedge \boldsymbol{\Omega}) = \mathbf{a} \wedge \boldsymbol{\Omega} \quad (3.216)$$

This leads to the following expression for relating the diffusion term in the rotational frame to the terms in the inertial frame:

$$\hat{\nabla} \cdot (\hat{\rho} \hat{\mathbf{u}} \otimes \hat{\mathbf{u}}) = R^{\mathbf{M}^t} [\nabla \cdot \rho \mathbf{u} \otimes \mathbf{u} + \underbrace{\rho \mathbf{u} \wedge \boldsymbol{\Omega}}_{\text{Coriolis}} + \nabla \cdot \rho (\mathbf{x}' \wedge \boldsymbol{\Omega}) \otimes \mathbf{u} + \underbrace{(\rho \mathbf{x}' \wedge \boldsymbol{\Omega}) \wedge \boldsymbol{\Omega}}_{\text{Centrifugal}} + \underbrace{\rho \mathbf{V}(t) \wedge \boldsymbol{\Omega}}_{\text{Magnus}}] \quad (3.217)$$

The original of the second part of the Coriolis and the Centrifugal terms can be seen here. Furthermore, an additional term that represents the change in diffusion due to the interaction between the translating and rotating part of the flow can be seen here. This is referred to as the Magnus force.

The pressure gradient term in the momentum equation is transformed. This part of the equation remain invariant since it is a scalar.

$$\begin{aligned} \hat{\nabla} \hat{p} &= R^{\mathbf{M}^t} G^{\mathbf{M}^t} \nabla p \\ \hat{\nabla} \hat{p} &= R^{\mathbf{M}^t} \nabla p \end{aligned} \quad (3.218)$$

In the transformation of the diffusion term the difference between the compressible and incompressible cases must be noted. The divergence of the velocity vector is not negligible, therefore the completed diffusion term must be accounted for. The expression for relating the diffusion term between the frames hence becomes:

$$\hat{\nabla} \cdot [\hat{\rho} (\hat{\nabla} \hat{\mathbf{u}} + \hat{\nabla} \hat{\mathbf{u}}^T) + \hat{\lambda} (\hat{\nabla} \cdot \hat{\mathbf{u}}) \hat{\mathbf{I}}] = R^{\mathbf{M}^t} G^{\mathbf{M}^t} \nabla \cdot [\mu (\nabla \mathbf{u} + \nabla \mathbf{u}^T) + \lambda (\nabla \cdot \mathbf{u}) \mathbf{I}] \quad (3.219)$$

With the implementation of *Equation 3.183*, the right hand side of the equations becomes:

$$\begin{aligned} R^{\mathbf{M}^t} \nabla \cdot \{ \mu [\nabla (\mathbf{u} - \mathbf{V}(t) + \mathbf{x}' \wedge \boldsymbol{\Omega} - [\mathbf{a}(t) + \dot{\boldsymbol{\Omega}} \wedge \mathbf{x}' + \boldsymbol{\Omega} \wedge \mathbf{x}'] \Delta t) \\ + \nabla (\mathbf{u} - \mathbf{V}(t) + \mathbf{x}' \wedge \boldsymbol{\Omega} - [\mathbf{a}(t) + \dot{\boldsymbol{\Omega}} \wedge \mathbf{x}' + \boldsymbol{\Omega} \wedge \mathbf{x}'] \Delta t)^T] \\ + \lambda (\nabla \cdot (\mathbf{u} - \mathbf{V}(t) + \mathbf{x}' \wedge \boldsymbol{\Omega} - [\mathbf{a}(t) + \dot{\boldsymbol{\Omega}} \wedge \mathbf{x}' + \boldsymbol{\Omega} \wedge \mathbf{x}'] \Delta t)) \mathbf{I} \} \end{aligned} \quad (3.220)$$

CHAPTER 3. NON-INERTIAL EQUATIONS IN VECTOR FORM

If it is considered that, as shown in *Appendix A*,

$$\begin{aligned}\nabla(\mathbf{x}' \wedge \boldsymbol{\Omega}) + \nabla(\mathbf{x}' \wedge \boldsymbol{\Omega})^T &= 0 \\ \nabla \cdot (\mathbf{x}' \wedge \boldsymbol{\Omega}) &= 0\end{aligned}\quad (3.221)$$

It can be shown that the diffusion component of the momentum equation is invariant for constant rotation conditions:

$$\hat{\nabla} \cdot [\hat{\mu}(\hat{\nabla}\hat{\mathbf{u}} + \hat{\nabla}\hat{\mathbf{u}}^T) + \hat{\lambda}(\hat{\nabla} \cdot \hat{\mathbf{u}})\hat{\mathbf{I}}] = R^{\Omega t} \nabla \cdot [\mu(\nabla\mathbf{u} + \nabla\mathbf{u}^T) + \lambda(\nabla \cdot \mathbf{u})\mathbf{I}] \quad (3.222)$$

The final transformation of the momentum equation relies on the summation of the transient and advection terms, as well as further manipulation of the resulting groups of terms.

$$\begin{aligned}\frac{\partial \hat{\rho}\hat{\mathbf{u}}}{\partial t} + \hat{\nabla} \cdot (\hat{\rho}\hat{\mathbf{u}} \otimes \hat{\mathbf{u}}) &= R^{\mathbf{M}^t} \left[ \overbrace{\frac{\partial}{\partial t}(\rho\mathbf{u}) + \nabla \cdot \rho\mathbf{u} \otimes \mathbf{u} - \frac{\partial}{\partial t}(\rho\mathbf{V}(t))}^{\text{Group 1}} \right. \\ &\quad + \overbrace{+\rho\mathbf{x}' \wedge \boldsymbol{\Omega} + \rho\mathbf{x}' \wedge \dot{\boldsymbol{\Omega}} + (\rho\mathbf{x}' \wedge \boldsymbol{\Omega}) \wedge \boldsymbol{\Omega} + 2\rho\mathbf{u} \wedge \boldsymbol{\Omega}}^{\text{Group 2}} \\ &\quad + \overbrace{+\nabla \cdot \rho(\mathbf{x}' \wedge \boldsymbol{\Omega}) \otimes \mathbf{u} + \rho(\boldsymbol{\Omega} \wedge \mathbf{x}') \cdot \nabla\mathbf{u} - \rho(\boldsymbol{\Omega} \wedge \mathbf{x}') \cdot \nabla\mathbf{V}(t)}^{\text{Group 3}} \\ &\quad \left. + \overbrace{+\rho\mathbf{V}(t) \wedge \boldsymbol{\Omega} + \rho\boldsymbol{\Omega} \wedge \mathbf{V}(t)}^{\text{Group 3}} \right] \quad (3.223)\end{aligned}$$

Group 1 is replaced by the equation below, where *Equation 3.193* was used the rotational transform multiplied through the equation. Subsequently the non-inertial form of the terms were obtained:

$$\begin{aligned}R^{\mathbf{M}^t} \left[ \frac{\partial}{\partial t}(\rho\mathbf{u}) + \nabla \cdot \rho\mathbf{u} \otimes \mathbf{u} \right] &= R^{\mathbf{M}^t} [-\nabla p + \nabla \cdot [\mu(\nabla\mathbf{u} + \nabla\mathbf{u}^T) + \lambda(\nabla \cdot \mathbf{u})\mathbf{I}]] \\ &= -\hat{\nabla}\hat{p} + \hat{\nabla} \cdot [\hat{\mu}(\hat{\nabla}\hat{\mathbf{u}} + \hat{\nabla}\hat{\mathbf{u}}^T) + \hat{\lambda}(\hat{\nabla} \cdot \hat{\mathbf{u}})\hat{\mathbf{I}}]\end{aligned}\quad (3.224)$$

The Group 2 terms represent the majority of the fictitious forces. These were manipulated as shown below to determine the non-inertial form:

$$\begin{aligned}R^{\mathbf{M}^t} [\rho\mathbf{x}' \wedge \boldsymbol{\Omega} + \rho\mathbf{x}' \wedge \dot{\boldsymbol{\Omega}} + (\rho\mathbf{x}' \wedge \boldsymbol{\Omega}) \wedge \boldsymbol{\Omega} + 2\rho\mathbf{u} \wedge \boldsymbol{\Omega}] \\ = \rho(R^{\mathbf{M}^t})\mathbf{x}' \wedge \boldsymbol{\Omega} + \rho(R^{\mathbf{M}^t})\mathbf{x}' \wedge \dot{\boldsymbol{\Omega}} + (\rho(R^{\mathbf{M}^t})\mathbf{x}' \wedge \boldsymbol{\Omega}) \wedge \boldsymbol{\Omega} + 2\rho(R^{\mathbf{M}^t})\mathbf{u} \wedge \boldsymbol{\Omega} \\ = \rho\hat{\mathbf{x}} \wedge \boldsymbol{\Omega} + \rho\hat{\mathbf{x}} \wedge \dot{\boldsymbol{\Omega}} + \rho\hat{\mathbf{x}} \wedge \boldsymbol{\Omega} \wedge \boldsymbol{\Omega} + 2\rho[\hat{\mathbf{u}} + \mathbf{V}(t) - \hat{\mathbf{x}} \wedge \boldsymbol{\Omega} + (\mathbf{a}_{\text{relative}})\Delta t] \wedge \boldsymbol{\Omega} \\ = \rho\hat{\mathbf{x}} \wedge \boldsymbol{\Omega} + \rho\hat{\mathbf{x}} \wedge \dot{\boldsymbol{\Omega}} + \rho\hat{\mathbf{x}} \wedge \boldsymbol{\Omega} \wedge \boldsymbol{\Omega} + 2\rho\hat{\mathbf{u}} \wedge \boldsymbol{\Omega} + 2\rho\mathbf{V}(t) \wedge \boldsymbol{\Omega} - 2\rho\hat{\mathbf{x}} \wedge \boldsymbol{\Omega} \wedge \boldsymbol{\Omega} \\ = \rho\hat{\mathbf{x}} \wedge \boldsymbol{\Omega} + \rho\hat{\mathbf{x}} \wedge \dot{\boldsymbol{\Omega}} - \rho\hat{\mathbf{x}} \wedge \boldsymbol{\Omega} \wedge \boldsymbol{\Omega} + 2\rho\hat{\mathbf{u}} \wedge \boldsymbol{\Omega} + 2\rho\mathbf{V}(t) \wedge \boldsymbol{\Omega}\end{aligned}\quad (3.225)$$

The remainder of the terms, Group 3 conveniently cancels each other out.

$$\nabla \cdot \rho(\mathbf{x}' \wedge \boldsymbol{\Omega}) \otimes \mathbf{u} + \rho(\boldsymbol{\Omega} \wedge \mathbf{x}') \cdot \nabla\mathbf{u} - \rho(\boldsymbol{\Omega} \wedge \mathbf{x}') \cdot \nabla\mathbf{V}(t) + \rho\mathbf{V}(t) \wedge \boldsymbol{\Omega} + \rho\boldsymbol{\Omega} \wedge \mathbf{V}(t) = 0 \quad (3.226)$$

Summation of the transformed parts of the momentum equation lead to the final form of the compressible, non-inertial momentum equation for full arbitrary motion:

### 3.3. NON-INERTIAL NAVIER-STOKES EQUATION FOR ARBITRARY MOTION

$$\begin{aligned}
 \frac{\partial \hat{\rho} \hat{\mathbf{u}}}{\partial t} + \hat{\nabla} \cdot (\hat{\rho} \hat{\mathbf{u}} \otimes \hat{\mathbf{u}}) &= -\hat{\nabla} \hat{p} + \hat{\nabla} \cdot [\hat{\mu}(\hat{\nabla} \hat{\mathbf{u}} + \hat{\nabla} \hat{\mathbf{u}}^T) + \hat{\lambda}(\hat{\nabla} \cdot \hat{\mathbf{u}}) \hat{\mathbf{I}}] \\
 &- \underbrace{\frac{\partial}{\partial t}(\rho \mathbf{V}(t))}_{\text{Translation}} + \underbrace{\rho \hat{\mathbf{x}} \wedge \boldsymbol{\Omega} + \rho \hat{\mathbf{x}} \wedge \dot{\boldsymbol{\Omega}}}_{\text{Unsteady motion}} + \underbrace{2\rho \hat{\mathbf{u}} \wedge \boldsymbol{\Omega}}_{\text{Coriolis}} - \underbrace{\rho \hat{\mathbf{x}} \wedge \boldsymbol{\Omega} \wedge \boldsymbol{\Omega}}_{\text{Centrifugal}} + \underbrace{2\rho \mathbf{V}(t) \wedge \boldsymbol{\Omega}}_{\text{Magnus}} \quad (3.227)
 \end{aligned}$$

The equation above indicates that there are six fictitious terms in the non-inertial momentum equation for fully arbitrary motion. These are the only terms that is present during arbitrary acceleration. The higher order terms become negligible or cancel out with other terms during the derivation. A fictitious force that is not present in the rotation cases manifests here. This is the Magnus force that represents the interaction between the translation and rotation of the object. The unsteady translation term, two terms due to unsteady motion and one part of both the Coriolis and the Magnus terms originate in the transformation of the unsteady component of the momentum equation. The remainder inertial terms, second part of the Coriolis and Magnus terms and the Centrifugal term, all has their original in the transformation of the advection term.

#### 3.3.2.3 Energy Equation

Consider the energy equation in the inertial frame (White [9]):

$$\frac{\partial \rho e}{\partial t} + (\nabla \cdot \rho e \mathbf{u}) = -p(\nabla \cdot \mathbf{u}) + \nabla \cdot (k \nabla T) + \varphi \quad (3.228)$$

The various terms can be transformed to the rotational frame separately and then combined to obtained the energy equation in the rotational frame.

The time dependant term can be related between the frames as shown:

$$\frac{\partial \hat{\rho} \hat{e}}{\partial t} = \mathbf{R}^{\mathbf{M}^t} \left[ \frac{\partial \rho e}{\partial t} + (\boldsymbol{\Omega} \wedge \mathbf{x}') \cdot \nabla \rho e \right] \quad (3.229)$$

The relation for the convective term between the inertial and rotational frame is shown below. This equation can be expanded upon with the used of *Equation 3.183*:

$$\begin{aligned}
 &(\hat{\nabla} \cdot \hat{\rho} \hat{e} \hat{\mathbf{u}}) \\
 &= \mathbf{R}^{\mathbf{M}^t} \mathbf{G}^{\mathbf{M}^t} (\nabla \cdot \rho e \mathbf{u}) \\
 &= \mathbf{R}^{\mathbf{M}^t} [\nabla \cdot \rho e (\mathbf{u} - \mathbf{V}(t) + \mathbf{x}' \wedge \boldsymbol{\Omega} - [\mathbf{a}(t) + \dot{\boldsymbol{\Omega}} \wedge \mathbf{x}' + \boldsymbol{\Omega} \wedge \dot{\mathbf{x}}'] \Delta t)]
 \end{aligned} \quad (3.230)$$

The third term grouping on the right hand side of the equation above was shown in *Equation 3.189* to be equal to zero. The convective term therefore becomes Galilean invariant under transformation:

$$(\hat{\nabla} \cdot \hat{\rho} \hat{e} \hat{\mathbf{u}}) = \mathbf{R}^{\mathbf{M}^t} [\nabla \cdot \rho e \mathbf{u} + \nabla \cdot \rho e (\mathbf{x}' \wedge \boldsymbol{\Omega})] \quad (3.231)$$

CHAPTER 3. NON-INERTIAL EQUATIONS IN VECTOR FORM

The term that represents the rate of work done by the normal force can be related in the inertial and rotational frames as shown below. This term can be expanded upon using *Equation 3.183*.

$$\begin{aligned}
 & -\hat{p}(\hat{\nabla} \cdot \hat{\mathbf{u}}) \\
 & = R^{\mathbf{M}^t} G^{\mathbf{M}^t} [-p(\nabla \cdot \mathbf{u})] \\
 & = R^{\mathbf{M}^t} [-p\nabla \cdot (\mathbf{u} - \mathbf{V}(t) + \mathbf{x}' \wedge \boldsymbol{\Omega} - [\mathbf{a}(t) + \dot{\boldsymbol{\Omega}} \wedge \mathbf{x}' + \boldsymbol{\Omega} \wedge \mathbf{x}'] \Delta t)]
 \end{aligned} \tag{3.232}$$

Showing that the second and third terms is again equal to zero, the same as above and indicated in *Equation 3.188*, this transformation is also invariant.

$$-\hat{p}(\hat{\nabla} \cdot \hat{\mathbf{u}}) = R^{\mathbf{M}^t} [-p\nabla \cdot \mathbf{u}] \tag{3.233}$$

The diffusive term in the rotational frame can be expressed in the inertial frame with the following relation:

$$\hat{\nabla} \cdot (\hat{k} \hat{\nabla} \hat{T}) = R^{\mathbf{M}^t} G^{\mathbf{M}^t} [\nabla \cdot (k \nabla T)] \tag{3.234}$$

Since  $k$  and  $T$  are scalars the relation is invariant under transformation:

$$\hat{\nabla} \cdot (\hat{k} \hat{\nabla} \hat{T}) = R^{\mathbf{M}^t} [\nabla \cdot (k \nabla T)] \tag{3.235}$$

The full relation between the rotational and inertial frames for the energy equation can be obtained by summation of the components obtained above. This leads to the equation:

$$\frac{\partial \hat{\rho} \hat{e}}{\partial t} + (\hat{\nabla} \cdot \hat{\rho} \hat{e} \hat{\mathbf{u}}) + \hat{p}(\hat{\nabla} \cdot \hat{\mathbf{u}}) - \hat{\nabla} \cdot (\hat{k} \hat{\nabla} \hat{T}) + \hat{\phi} = R^{\mathbf{M}^t} \left[ \frac{\partial \rho e}{\partial t} + (\nabla \cdot \rho e \mathbf{u}) + p(\nabla \cdot \mathbf{u}) - \nabla \cdot (k \nabla T) + \phi \right] \tag{3.236}$$

The right hand side of the equation is equal to zero, this can be seen from re-arrangement of the terms in *Equation 3.228*. The non-inertial energy equation is invariant under transformation in this specific case for constant acceleration in rotation (Diaz et al. [62]). It can be seen that this equation remains in this form even in the case of unsteady acceleration. *Equation 3.192* is further used to arrive at:

$$\frac{\partial \hat{\rho} \hat{e}}{\partial t} + (\hat{\nabla} \cdot \hat{\rho} \hat{e} \hat{\mathbf{u}}) = -\hat{p}(\hat{\nabla} \cdot \hat{\mathbf{u}}) + \hat{\nabla} \cdot (\hat{k} \hat{\nabla} \hat{T}) + \hat{\phi} \tag{3.237}$$

### 3.3.3 Special Cases of the Arbitrary Acceleration Flow for Compressible Conditions

The non-inertial momentum equation for arbitrary acceleration, both in translation and rotation, was derived in *Equation 3.227*:

$$\begin{aligned}
 \frac{\partial \hat{\rho} \hat{\mathbf{u}}}{\partial t} + \hat{\nabla} \cdot (\hat{\rho} \hat{\mathbf{u}} \otimes \hat{\mathbf{u}}) &= -\hat{\nabla} \hat{p} + \hat{\nabla} \cdot [\hat{\mu}(\hat{\nabla} \hat{\mathbf{u}} + \hat{\nabla} \hat{\mathbf{u}}^T) + \hat{\lambda}(\hat{\nabla} \cdot \hat{\mathbf{u}}) \hat{\mathbf{I}}] \\
 & - \underbrace{\frac{\partial}{\partial t}(\rho \mathbf{V}(t))}_{\text{Translation}} + \underbrace{\rho \hat{\mathbf{x}} \wedge \boldsymbol{\Omega} + \rho \hat{\mathbf{x}} \wedge \dot{\boldsymbol{\Omega}}}_{\text{Euler}} + \underbrace{2\rho \hat{\mathbf{u}} \wedge \boldsymbol{\Omega}}_{\text{Coriolis}} - \underbrace{\rho \hat{\mathbf{x}} \wedge \boldsymbol{\Omega} \wedge \boldsymbol{\Omega}}_{\text{Centrifugal}} + \underbrace{2\rho \mathbf{V}(t) \wedge \boldsymbol{\Omega}}_{\text{Magnus}}
 \end{aligned} \tag{3.238}$$

The equation above contains all the possible fictitious effects that can be present in a fully arbitrary system as well as the full formulation for the compressible stress tensor. This equation can be used to obtain the formulations for special cases such as the incompressible case and various combinations of translational and rotational formulations.

### 3.3. NON-INERTIAL NAVIER-STOKES EQUATION FOR ARBITRARY MOTION

#### 3.3.3.1 Incompressible Flow Conditions

This incompressible form of the non-inertial momentum equation for arbitrary acceleration can be obtained through a combination of the fictitious terms in *Equation 3.227* and the formulation of the diffusive terms as in *Equation 3.157*. This leads to the following equation for the conservation of non-inertial momentum:

$$\frac{\partial \hat{\mathbf{u}}}{\partial t} + (\hat{\mathbf{u}} \cdot \hat{\nabla}) \hat{\mathbf{u}} = -\hat{\nabla} \hat{\psi} + \nu \hat{\nabla}^2 \hat{\mathbf{u}} - \underbrace{\frac{\partial}{\partial t}(\mathbf{V}(t))}_{\text{Translation}} + \underbrace{\hat{\mathbf{x}} \wedge \boldsymbol{\Omega} + \hat{\mathbf{x}} \wedge \dot{\boldsymbol{\Omega}}}_{\text{Unsteady motion}} + \underbrace{2\hat{\mathbf{u}} \wedge \boldsymbol{\Omega}}_{\text{Coriolis}} - \underbrace{\hat{\mathbf{x}} \wedge \boldsymbol{\Omega} \wedge \boldsymbol{\Omega}}_{\text{Centrifugal}} + \underbrace{2\mathbf{V}(t) \wedge \boldsymbol{\Omega}}_{\text{Magnus}} \quad (3.239)$$

As it was shown in all derivations of the non-inertial conservation of mass and energy equations in this chapter, those equations remain unchanged by in its formulations irrespective of the rotations or translations of the associated frames - there are no fictitious effects present (Diaz et al. [62]).

#### 3.3.3.2 Various Translation and Rotation Formulations

*Case I - Pure, Unsteady Rotation*

*Equation 3.227* is used to obtain the non-inertial formulation for the case of pure, unsteady rotation. The limiting conditions for such is flow is where both the translational velocity and subsequently the translational acceleration is zero. There is also be no translational motion within the non-inertial frame:

$$\begin{aligned} \frac{\partial \mathbf{V}(t)}{\partial t} &= 0 \\ \mathbf{V}(t) &= 0 \\ \hat{\mathbf{x}} &= 0 \end{aligned} \quad (3.240)$$

The conditions above is applies to *Equation 3.227* to cancel out the terms that is not relevant to this specific case.

$$\begin{aligned} \frac{\partial \hat{\rho} \hat{\mathbf{u}}}{\partial t} + \hat{\nabla} \cdot (\hat{\rho} \hat{\mathbf{u}} \otimes \hat{\mathbf{u}}) &= -\hat{\nabla} \hat{p} + \hat{\nabla} \cdot [\hat{\mu}(\hat{\nabla} \hat{\mathbf{u}} + \hat{\nabla} \hat{\mathbf{u}}^T) + \hat{\lambda}(\hat{\nabla} \cdot \hat{\mathbf{u}}) \hat{\mathbf{I}}] \\ &\quad - \frac{\partial}{\partial t}(\rho \mathbf{V}(t)) + \rho \hat{\mathbf{x}} \wedge \boldsymbol{\Omega} + \underbrace{\rho \hat{\mathbf{x}} \wedge \dot{\boldsymbol{\Omega}}}_{\text{Euler}} + \underbrace{2\rho \hat{\mathbf{u}} \wedge \boldsymbol{\Omega}}_{\text{Coriolis}} - \underbrace{\rho \hat{\mathbf{x}} \wedge \boldsymbol{\Omega} \wedge \boldsymbol{\Omega}}_{\text{Centrifugal}} + 2\rho \mathbf{V}(t) \wedge \boldsymbol{\Omega} \quad (3.241) \end{aligned}$$

The result is an expressed that corresponds with the expression derived in *Equation 3.169* for the non-inertial momentum equation in unsteady, pure rotation:

$$\frac{\partial \hat{\rho} \hat{\mathbf{u}}}{\partial t} + \hat{\nabla} \cdot (\hat{\rho} \hat{\mathbf{u}} \otimes \hat{\mathbf{u}}) = -\hat{\nabla} \hat{p} + \hat{\nabla} \cdot [\hat{\mu}(\hat{\nabla} \hat{\mathbf{u}} + \hat{\nabla} \hat{\mathbf{u}}^T) + \hat{\lambda}(\hat{\nabla} \cdot \hat{\mathbf{u}}) \hat{\mathbf{I}}] + \underbrace{2\rho \hat{\mathbf{u}} \wedge \boldsymbol{\Omega}}_{\text{Coriolis}} - \underbrace{\rho \hat{\mathbf{x}} \wedge \boldsymbol{\Omega} \wedge \boldsymbol{\Omega}}_{\text{Centrifugal}} + \underbrace{\rho \hat{\mathbf{x}} \wedge \dot{\boldsymbol{\Omega}}}_{\text{Euler}} \quad (3.242)$$

CHAPTER 3. NON-INERTIAL EQUATIONS IN VECTOR FORM

---

*Case II - Pure, Steady Rotation*

The limiting conditions for steady, pure rotation is the same as in the unsteady case with the inclusion of the rotational acceleration being equal to zero:

$$\begin{aligned}\frac{\partial \mathbf{V}(t)}{\partial t} &= 0 \\ \mathbf{V}(t) &= 0 \\ \hat{\mathbf{x}} &= 0 \\ \hat{\mathbf{\Omega}} &= 0\end{aligned}\tag{3.243}$$

This results in an expression for the non-inertial momentum equation in steady, pure rotation that is the same as *Equation 3.85* that was derived using the Eulerian approach.

$$\frac{\partial \hat{\rho} \hat{\mathbf{u}}}{\partial t} + \hat{\nabla} \cdot (\hat{\rho} \hat{\mathbf{u}} \otimes \hat{\mathbf{u}}) = -\hat{\nabla} \hat{p} + \hat{\nabla} \cdot [\hat{\mu}(\hat{\nabla} \hat{\mathbf{u}} + \hat{\nabla} \hat{\mathbf{u}}^T) + \hat{\lambda}(\hat{\nabla} \cdot \hat{\mathbf{u}}) \hat{\mathbf{I}}] + \underbrace{2\hat{\rho} \hat{\mathbf{u}} \wedge \hat{\mathbf{\Omega}}}_{\text{Coriolis}} - \underbrace{\hat{\rho} \hat{\mathbf{x}} \wedge \hat{\mathbf{\Omega}} \wedge \hat{\mathbf{\Omega}}}_{\text{Centrifugal}}\tag{3.244}$$

*Case III - Unsteady Translation*

In the unsteady translation case all the rotation parameters are equal to zero:

$$\begin{aligned}\hat{\mathbf{x}} &= 0 \\ \hat{\mathbf{\Omega}} &= 0 \\ \hat{\mathbf{\Omega}} &= 0\end{aligned}\tag{3.245}$$

This results in the non-inertial momentum equation for unsteady translation:

$$\frac{\partial \hat{\rho} \hat{\mathbf{u}}}{\partial t} + \hat{\nabla} \cdot (\hat{\rho} \hat{\mathbf{u}} \otimes \hat{\mathbf{u}}) = -\hat{\nabla} \hat{p} + \hat{\nabla} \cdot [\hat{\mu}(\hat{\nabla} \hat{\mathbf{u}} + \hat{\nabla} \hat{\mathbf{u}}^T) + \hat{\lambda}(\hat{\nabla} \cdot \hat{\mathbf{u}}) \hat{\mathbf{I}}] - \underbrace{\frac{\partial}{\partial t}(\rho \mathbf{V}(t))}_{\text{Translation}}\tag{3.246}$$

*Case IV - Steady Translation*

The steady translation case is the simplest off all the special cases. All the motion parameters is equal to zero with the exception of the relative frame velocity that is equal to a constant value:

$$\begin{aligned}\frac{\partial \mathbf{V}(t)}{\partial t} &= 0 \\ \hat{\mathbf{x}} &= 0 \\ \hat{\mathbf{\Omega}} &= 0 \\ \hat{\mathbf{\Omega}} &= 0\end{aligned}\tag{3.247}$$

This results in the inertial momentum equation which indicates that constant translation does not cause any fictitious effects in the flow:

$$\frac{\partial \rho \mathbf{u}}{\partial t} + \nabla \cdot (\rho \mathbf{u} \otimes \mathbf{u}) = -\nabla p + \nabla \cdot [\mu(\nabla \mathbf{u} + \nabla \mathbf{u}^T) + \lambda(\nabla \cdot \mathbf{u}) \mathbf{I}]\tag{3.248}$$



### 3.3. NON-INERTIAL NAVIER-STOKES EQUATION FOR ARBITRARY MOTION

---

#### *Case V - Steady Translation, Unsteady Rotation*

In the case where the translation is steady and the rotation is unsteady, the translational acceleration becomes zero and the translational velocity has a constant value:

$$\frac{\partial \mathbf{V}(t)}{\partial t} = 0 \quad (3.249)$$

Applying the above conditions result in an equation where all the rotational terms is preserved as well as the term the represents the interaction between the translation and rotation:

$$\begin{aligned} \frac{\partial \hat{\rho} \hat{\mathbf{u}}}{\partial t} + \hat{\nabla} \cdot (\hat{\rho} \hat{\mathbf{u}} \otimes \hat{\mathbf{u}}) = & -\hat{\nabla} \hat{p} + \hat{\nabla} \cdot [\hat{\mu}(\hat{\nabla} \hat{\mathbf{u}} + \hat{\nabla} \hat{\mathbf{u}}^T) + \hat{\lambda}(\hat{\nabla} \cdot \hat{\mathbf{u}}) \hat{\mathbf{I}}] \\ & + \underbrace{\rho \hat{\mathbf{x}} \wedge \boldsymbol{\Omega}}_{\text{Unsteady motion}} + \underbrace{\rho \hat{\mathbf{x}} \wedge \dot{\boldsymbol{\Omega}}}_{\text{Euler}} + \underbrace{2\rho \hat{\mathbf{u}} \wedge \boldsymbol{\Omega}}_{\text{Coriolis}} - \underbrace{\rho \hat{\mathbf{x}} \wedge \boldsymbol{\Omega} \wedge \boldsymbol{\Omega}}_{\text{Centrifugal}} + \underbrace{2\rho \mathbf{V}(t) \wedge \boldsymbol{\Omega}}_{\text{Magnus}} \end{aligned} \quad (3.250)$$

### 3.4 Closure

This chapter formalized an Eulerian method for the derivation of non-inertial Navier-Stokes equations. The original method was used by Kageyama and Hyodo [23] to derive the Coriolis force for constant rotational flows in incompressible fluids. It was extended here to account for all ranges of motion, from constant pure rotation to full arbitrary accelerating flows, and applied to compressible cases. The main contributions of this chapter can be described as follow:

- It has been shown mathematically that there are no fictitious components in the non-inertial continuity or energy equations. The non-inertial equations takes the same general form as the inertial equations.
- Clarification was obtained on the mathematical origin of the fictitious forces through the derivations. This indicated that the fictitious forces stems from the transformation of the temporal and advection terms. The diffusion terms remain invariant under transformation
- The mathematical sign (positive or negative) of the fictitious forces is dependant on the selection of the positive and negative directions. The signs of the terms that are appropriate in a system conforming to standard sign conventions have been determined.
- The presence of fictitious forces is case dependant. The non-inertial momentum equation for a aero-ballistic case, which involves acceleration in six degrees of freedom, has been derived. It has been shown that the six fictitious forces derived in this chapter is the only additional forces acting on an aero-ballistic system. From this equation the appropriate terms of a specific case can easily be determined.
- The physical meaning of the mathematical fictitious forces can be explored from the equations established in this chapter.

There are a number of misconceptions that have been observed in literature with regards to flow equations in non-inertial reference frames. An example where discrepancies in the literature is seen is in the conservation of energy equation. Some sources add fictitious energy terms to these equations (Limache [3], Gardi [2]). It was shown through derivation that both the continuity and conservation of energy equations remains invariant under transformation - no additional terms are added to these equations:

$$\frac{\partial \hat{\rho}}{\partial t} + \hat{\nabla} \cdot \hat{\rho} \hat{\mathbf{u}} = 0 \quad (3.251)$$

$$\frac{\partial \hat{\rho} \hat{e}}{\partial t} + (\hat{\nabla} \cdot \hat{\rho} \hat{e} \hat{\mathbf{u}}) = -\hat{\rho}(\hat{\nabla} \cdot \hat{\mathbf{u}}) + \hat{\nabla} \cdot (\hat{k} \hat{\nabla} \hat{T}) + \hat{\varphi} \quad (3.252)$$

The equation for full arbitrary acceleration below indicates that there are six fictitious terms in the non-inertial momentum equation. These are the only terms that are present during arbitrary acceleration; the higher order terms become negligible or cancel out with other terms during the derivation. The

equation for fully arbitrary acceleration can be used to explore the appropriate form of the non-inertial momentum equation for steady translation and unsteady rotation.

$$\begin{aligned} \frac{\partial \hat{\rho} \hat{\mathbf{u}}}{\partial t} + \hat{\nabla} \cdot (\hat{\rho} \hat{\mathbf{u}} \otimes \hat{\mathbf{u}}) = & -\hat{\nabla} \hat{p} + \hat{\nabla} \cdot [\hat{\mu}(\hat{\nabla} \hat{\mathbf{u}} + \hat{\nabla} \hat{\mathbf{u}}^T) + \hat{\lambda}(\hat{\nabla} \cdot \hat{\mathbf{u}}) \hat{\mathbf{I}}] \\ & - \underbrace{\frac{\partial}{\partial t}(\rho \mathbf{V}(t))}_{\text{Translation}} + \underbrace{\rho \hat{\mathbf{x}} \wedge \hat{\boldsymbol{\Omega}} + \rho \hat{\mathbf{x}} \wedge \dot{\hat{\boldsymbol{\Omega}}}}_{\text{Unsteady motion}} + \underbrace{2\rho \hat{\mathbf{u}} \wedge \hat{\boldsymbol{\Omega}}}_{\text{Coriolis}} - \underbrace{\rho \hat{\mathbf{x}} \wedge \hat{\boldsymbol{\Omega}} \wedge \hat{\boldsymbol{\Omega}}}_{\text{Centrifugal}} + \underbrace{2\rho \mathbf{V}(t) \wedge \hat{\boldsymbol{\Omega}}}_{\text{Magnus}} \end{aligned} \quad (3.253)$$

The mathematical origin of the fictitious terms can be observed during the derivations. The unsteady translation term, two terms due to unsteady rotational motion and the first parts of the Coriolis and Magnus terms originates in the transformation of the unsteady component of the momentum equation (Equation 3.213).

$$\frac{\partial \rho \hat{\mathbf{u}}}{\partial t}(\hat{\mathbf{x}}_t, t) = R^{\mathbf{M}^t} \left[ \frac{\partial}{\partial t}(\rho) + \rho(\boldsymbol{\Omega} \wedge \mathbf{x}'_t) \cdot \nabla - \underbrace{\rho \boldsymbol{\Omega} \wedge (\mathbf{u}(\mathbf{x}_t, t) - \mathbf{V}(t))}_{\text{Coriolis \& Magnus}} + R^{\mathbf{M}^t} \left( \underbrace{\rho \mathbf{x}'_t \wedge \boldsymbol{\Omega}}_{\text{Moving Axis}} + \underbrace{\rho \mathbf{x}'_t \wedge \dot{\boldsymbol{\Omega}}}_{\text{Euler}} \right) \right] \quad (3.254)$$

The remainder inertial terms, second part of the Coriolis, Centrifugal and the term representing the interaction between the rotation and translation, all has their original in the transformation of the advection term (Equation 3.217).

$$\hat{\nabla} \cdot (\hat{\rho} \hat{\mathbf{u}} \otimes \hat{\mathbf{u}}) = R^{\mathbf{M}^t} \left[ \nabla \cdot \rho \mathbf{u} \otimes \mathbf{u} + \underbrace{\rho \mathbf{u} \wedge \boldsymbol{\Omega}}_{\text{Coriolis}} + \nabla \cdot \rho(\mathbf{x}' \wedge \boldsymbol{\Omega}) \otimes \mathbf{u} + \underbrace{(\rho \mathbf{x}' \wedge \boldsymbol{\Omega}) \wedge \boldsymbol{\Omega}}_{\text{Centrifugal}} + \underbrace{\rho \mathbf{V}(t) \wedge \boldsymbol{\Omega}}_{\text{Magnus}} \right] \quad (3.255)$$

The presence of the majority of the fictitious forces can be intuitively explained as the result of accelerating motion. However, the physical meaning of the Coriolis force has been a subject of many discussions (Dolovich et al. [63], Persson [12], Thornton and Marion [64]). Observation of the effect of both Coriolis and Magnus effects can be explained using a mathematical approach which is seated in an understanding of the cross product operation.

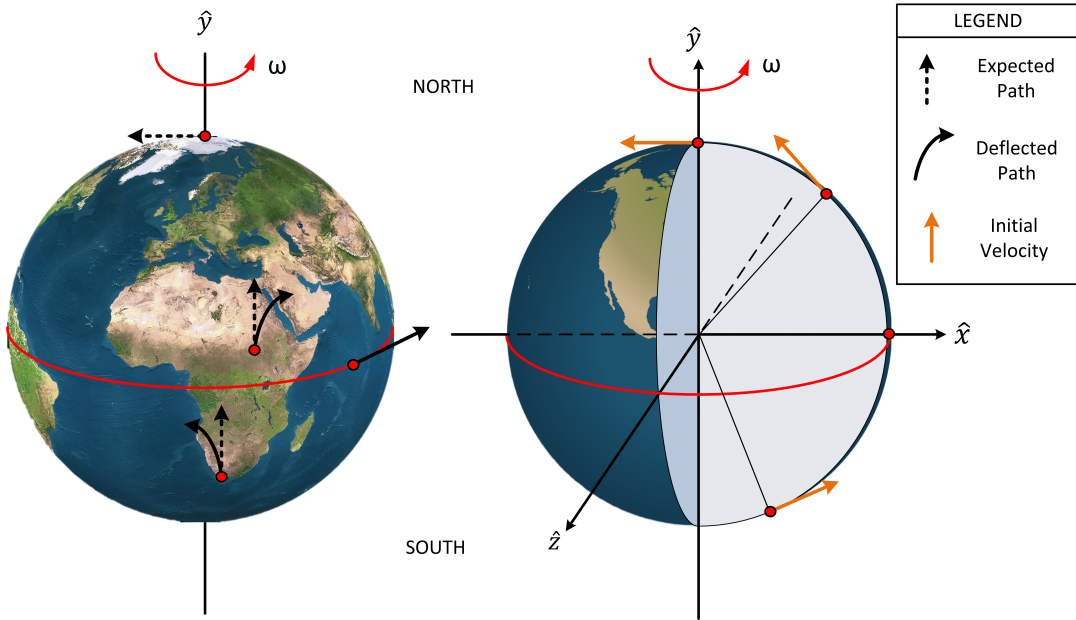
The Coriolis force was first mathematically formulated in 1835 by Gaspard Coriolis, but observations of the effect long preceded the formulation (Persson [12]). Deflections in motion due to the Coriolis effect is three dimensional, but the term Coriolis force is mostly associated with horizontal deflections in the Northern and Southern Hemispheres with respect to the surface of the earth. This has specific application in Meteorology and Geophysics since weather patterns and sea currents are directly influenced by the horizontal component of the Coriolis force.

In Figure 3.10 it is shown that a particle travelling in North on the earth's surface deflects to the right in the North Hemisphere and to the left in the Southern Hemisphere. The difference in deflection is a function of the surface curvature of the earth where a velocity vector in the South has a different orientation than in the North. The result is that the cross product of the velocity and the rotation has a resultant force that is dependant on the hemisphere it operates in.

While the deflection on the surface of the earth has been the most general observation of the Coriolis force, the component vertical to the earth's surface has only been measured in 1908 by Lorand Eötvös

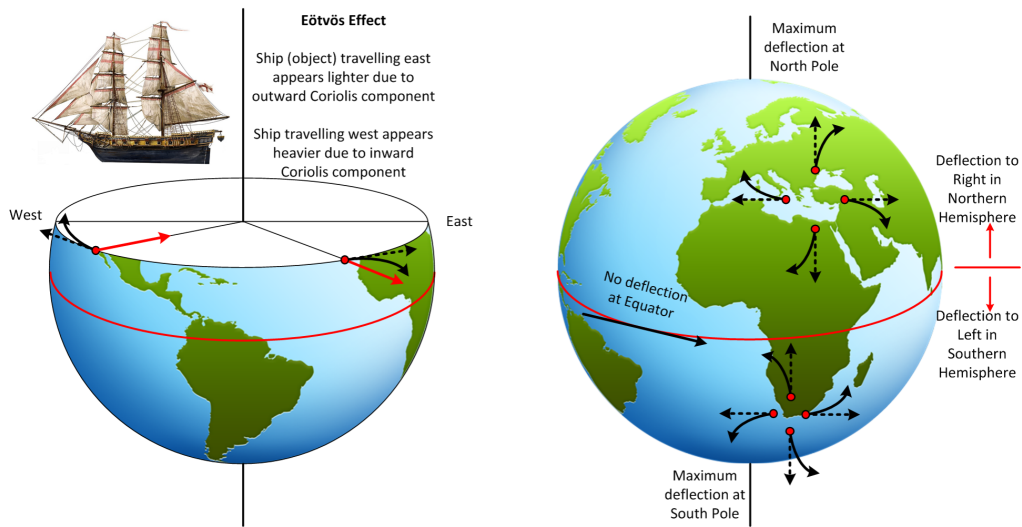
CHAPTER 3. NON-INERTIAL EQUATIONS IN VECTOR FORM

Figure 3.10: Deflections of a Particle Travelling in the Northern and Southern Hemispheres (left) and the Corresponding Directions of the Velocity Vector (right)



(Persson [12]). He observed the effect through gravity readings collected by research ships which indicated that the gravity measurements increased with motion towards the west and decreased when the ships sailed in an easterly direction (Figure 3.11).

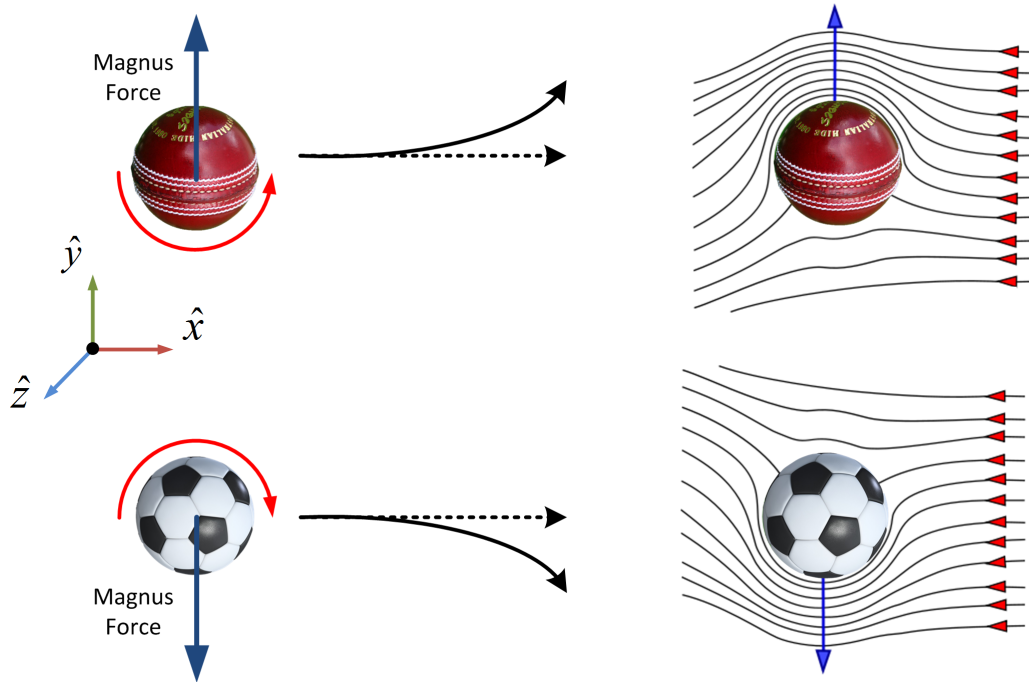
Figure 3.11: Two Components of the Coriolis force: Outward Component due to Eötvös effect (left) and Deflection on the Earth's Surface in Northern and Southern Hemisphere (right)



The Coriolis force is therefore described as a non-inertial force that operates on an object that is in motion relative to a rotational reference frame. The effect of the Coriolis force is to cause deflection of the object in three dimensions in with a magnitude and direction that is determined by the cross product of the object's non-inertial velocity and the rotation of the frame,  $2\rho\hat{\mathbf{u}} \wedge \boldsymbol{\Omega}$ .

The Magnus force has a similar formula to the Coriolis force, but it has a different physical meaning. It is a function of the object's translation and represents the interaction between the rotating and translating motion of the object. It is therefore a non-inertial force that operates on a rotating object that is in motion relative to a inertial reference frame. The effect of the Magnus force is to cause deflection of the object (*Figure 3.12*) in three dimensions with a magnitude and direction that is determined by the cross product of the object's translational velocity and the rotation of the object,  $2\rho\mathbf{V}(t) \wedge \boldsymbol{\Omega}$ .

Figure 3.12: Deflection due to the Magnus Effect in the Inertial Frame (left) and the Non-Inertial Frame (right)



The presence of the Magnus force in the non-inertial momentum equation is not generally seen in literature (Meriam and Kraige [8], White [9]) since non-inertial formulations does not regularly include all the aero-ballistic accelerations and is generally applied to rotating flows. In CFD applications the Magnus force is mostly investigated using a predictive approach (Cayzac et al. [65], Silton [66], Weinacht et al. [67]) instead of with prescribed motion as suggested here.

The work done in this chapter assisted in developing a clear understanding of non-inertial Navier-Stokes equations and provided a baseline with correct formulations for the subsequent chapters.



UNIVERSITEIT VAN PRETORIA  
UNIVERSITY OF PRETORIA  
YUNIBESITHI YA PRETORIA

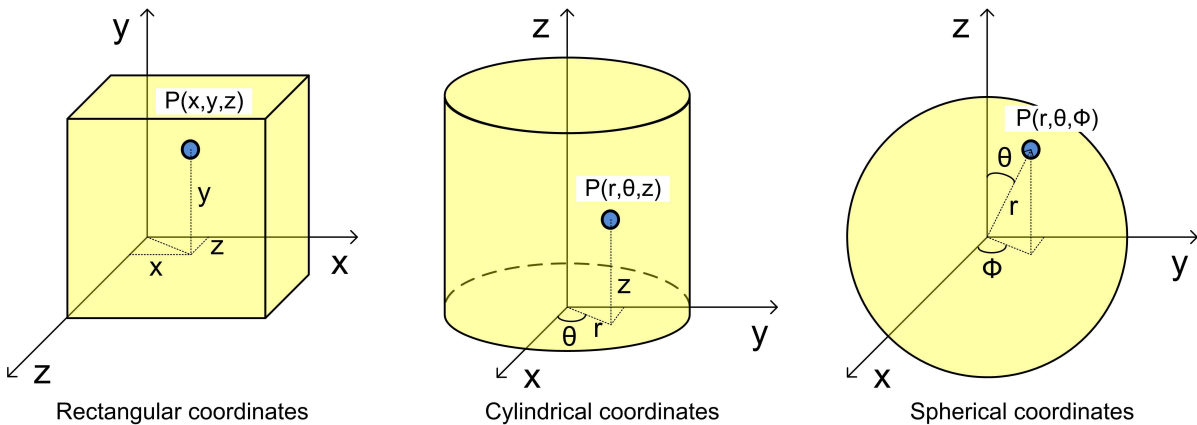
Chapter

4

## Non-Inertial Equations in Component Form

In this chapter the component form of the equations are given in the Cartesian, Cylindrical and Curvilinear systems. The Cartesian coordinates system is the most common system; introductory calculus and mechanics textbooks (Anderson [58], Steward [68], Versteeg and Malalasekera [69]) largely make use of this system and only provides a brief description of other coordinate systems (*Figure 4.1*).

Figure 4.1: Depiction of Various Coordinates Systems



Most aero-ballistic and aeronautical applications lends itself toward analysis in cylindrical or curvilinear coordinates as their geometric features, consisting of cylindrical forms and curves, are better described in such systems. Advanced textbooks that make use of cylindrical systems do provide some formulations for non-inertial Navier-Stokes equations, but those are limited to constant rotation cases (Schlichting [42], White [9]) for turbo-machinery applications. The aim of this chapter is to provide a

frame work for the non-inertial equations for full arbitrary accelerations in component form which are used in a subsequent chapter for boundary layer analysis.

## 4.1 Non-Inertial Equations in Cartesian Coordinates

### 4.1.1 Incompressible Flow Conditions

The incompressible continuity equation is obtained from White [9]:

$$\hat{\nabla} \cdot \hat{\rho} \hat{\mathbf{u}} = 0 \quad (4.1)$$

This equation can be expressed in the Cartesian component form using the Cartesian definition of divergence (Anderson [58], Aris [70]):

$$\frac{\partial \hat{u}}{\partial \hat{x}} + \frac{\partial \hat{v}}{\partial \hat{y}} + \frac{\partial \hat{w}}{\partial \hat{z}} = 0 \quad (4.2)$$

In *Chapter 3, Equation 3.239* the non-inertial momentum equation for arbitrary acceleration in incompressible conditions have been derived:

$$\frac{\partial \hat{\mathbf{u}}}{\partial t} + (\hat{\mathbf{u}} \cdot \hat{\nabla}) \hat{\mathbf{u}} = -\hat{\nabla} \hat{\psi} + \nu \hat{\nabla}^2 \hat{\mathbf{u}} + \underbrace{2\hat{\mathbf{u}} \wedge \hat{\boldsymbol{\Omega}}}_{\text{Coriolis}} - \underbrace{\hat{\mathbf{x}} \wedge \hat{\boldsymbol{\Omega}} \wedge \hat{\boldsymbol{\Omega}}}_{\text{Centrifugal}} + \underbrace{\hat{\mathbf{x}} \wedge \hat{\dot{\boldsymbol{\Omega}}}}_{\text{Euler}} + \underbrace{\hat{\mathbf{x}} \wedge \hat{\boldsymbol{\Omega}}}_{\text{Unsteady motion}} + \underbrace{2\mathbf{V}(t) \wedge \hat{\boldsymbol{\Omega}}}_{\text{Magnus}} - \underbrace{\frac{\partial}{\partial t}(\mathbf{V}(t))}_{\text{Translation}} \quad (4.3)$$

This equation can be expanded into the component form using the Cartesian vector operations, dot and cross products, for divergence, gradient and laplacian operators (Anderson [58], Aris [70]). Each grouping of fictitious terms can be expanded into components in the following manner:

$$2\hat{\mathbf{u}} \wedge \hat{\boldsymbol{\Omega}} = \begin{bmatrix} \hat{\mathbf{i}} & \hat{\mathbf{j}} & \hat{\mathbf{k}} \\ 2\hat{u} & 2\hat{v} & 2\hat{w} \\ \omega_x & \omega_y & \omega_z \end{bmatrix} = (2\hat{v}\omega_z - 2\hat{w}\omega_y)\hat{\mathbf{i}} + (2\hat{w}\omega_x - 2\hat{u}\omega_z)\hat{\mathbf{j}} + (2\hat{u}\omega_y - 2\hat{v}\omega_x)\hat{\mathbf{k}} \quad (4.4)$$

These operations result in the non-inertial component form of the Navier-Stokes equations for full arbitrary acceleration;

#### $\hat{\mathbf{x}}$ -momentum

$$\begin{aligned} \frac{\partial \hat{u}}{\partial t} + \hat{u} \frac{\partial \hat{u}}{\partial \hat{x}} + \hat{v} \frac{\partial \hat{u}}{\partial \hat{y}} + \hat{w} \frac{\partial \hat{u}}{\partial \hat{z}} &= -\frac{\partial \hat{\psi}}{\partial \hat{x}} + \hat{v} \left( \frac{\partial^2 \hat{u}}{\partial \hat{x}^2} + \frac{\partial^2 \hat{u}}{\partial \hat{y}^2} + \frac{\partial^2 \hat{u}}{\partial \hat{z}^2} \right) \\ &+ \underbrace{2\hat{v}\omega_z - 2\hat{w}\omega_y}_{\text{Coriolis}} + \underbrace{\hat{x}(\omega_z^2 + \omega_y^2) - \hat{y}\omega_x\omega_y - \hat{z}\omega_x\omega_z}_{\text{Centrifugal}} \\ &+ \underbrace{\hat{y}\omega_z - \hat{z}\omega_y + \hat{y}\omega_z - \hat{z}\omega_y}_{\text{Euler}} + \underbrace{2V_y\omega_z - 2V_z\omega_y}_{\text{Magnus}} - \underbrace{\frac{\partial V_x}{\partial t}}_{\text{Translation}} \end{aligned} \quad (4.5)$$



#### 4.1. NON-INERTIAL EQUATIONS IN CARTESIAN COORDINATES

##### $\hat{y}$ -momentum

$$\begin{aligned} \frac{\partial \hat{v}}{\partial t} + \hat{u} \frac{\partial \hat{v}}{\partial \hat{x}} + \hat{v} \frac{\partial \hat{v}}{\partial \hat{y}} + \hat{w} \frac{\partial \hat{v}}{\partial \hat{z}} &= -\frac{\partial \hat{\psi}}{\partial \hat{y}} + \hat{v} \left( \frac{\partial^2 \hat{v}}{\partial \hat{x}^2} + \frac{\partial^2 \hat{v}}{\partial \hat{y}^2} + \frac{\partial^2 \hat{v}}{\partial \hat{z}^2} \right) \\ &+ \underbrace{2\hat{w}\omega_x - 2\hat{u}\omega_z}_{\text{Coriolis}} + \underbrace{\hat{y}(\omega_z^2 + \omega_x^2) - \hat{x}\omega_x\omega_y - \hat{z}\omega_y\omega_z}_{\text{Centrifugal}} \\ &+ \underbrace{\hat{z}\omega_x - \hat{x}\omega_z + \hat{z}\omega_x - \hat{x}\omega_z}_{\text{Euler}} + \underbrace{2V_z\omega_x - 2V_x\omega_z}_{\text{Magnus}} - \underbrace{\frac{\partial V_y}{\partial t}}_{\text{Translation}} \end{aligned} \quad (4.6)$$

##### $\hat{z}$ -momentum

$$\begin{aligned} \frac{\partial \hat{w}}{\partial t} + \hat{u} \frac{\partial \hat{w}}{\partial \hat{x}} + \hat{v} \frac{\partial \hat{w}}{\partial \hat{y}} + \hat{w} \frac{\partial \hat{w}}{\partial \hat{z}} &= -\frac{\partial \hat{\psi}}{\partial \hat{z}} + \hat{v} \left( \frac{\partial^2 \hat{w}}{\partial \hat{x}^2} + \frac{\partial^2 \hat{w}}{\partial \hat{y}^2} + \frac{\partial^2 \hat{w}}{\partial \hat{z}^2} \right) \\ &+ \underbrace{2\hat{u}\omega_y - 2\hat{v}\omega_x}_{\text{Coriolis}} + \underbrace{\hat{z}(\omega_y^2 + \omega_x^2) - \hat{x}\omega_x\omega_z - \hat{y}\omega_y\omega_z}_{\text{Centrifugal}} \\ &+ \underbrace{\hat{x}\omega_y - \hat{y}\omega_x + \hat{x}\omega_y - \hat{y}\omega_x}_{\text{Euler}} + \underbrace{2V_x\omega_y - 2V_y\omega_x}_{\text{Magnus}} - \underbrace{\frac{\partial V_z}{\partial t}}_{\text{Translation}} \end{aligned} \quad (4.7)$$

### 4.1.2 Compressible Flow Conditions

The compressible continuity equation is expressed as (White [9]):

$$\frac{\partial \hat{\rho}}{\partial t} + (\hat{\nabla} \cdot \hat{\rho} \hat{\mathbf{u}}) = 0 \quad (4.8)$$

The component form of this equation subsequently becomes (Anderson [58], Aris [70]):

$$\frac{\partial \hat{\rho}}{\partial t} + \frac{\partial \hat{\rho} \hat{u}}{\partial \hat{x}} + \frac{\partial \hat{\rho} \hat{v}}{\partial \hat{y}} + \frac{\partial \hat{\rho} \hat{w}}{\partial \hat{z}} = 0 \quad (4.9)$$

The non-inertial equation for incompressible flow in full arbitrary acceleration conditions were determined in *Chapter 3, Equation 3.227*:

$$\begin{aligned} \frac{\partial \hat{\rho} \hat{\mathbf{u}}}{\partial t} + \hat{\nabla} \cdot (\hat{\rho} \hat{\mathbf{u}} \otimes \hat{\mathbf{u}}) &= -\hat{\nabla} \hat{p} + \hat{\nabla} \cdot \underbrace{[\hat{\mu}(\hat{\nabla} \hat{\mathbf{u}} + \hat{\nabla} \hat{\mathbf{u}}^T) + \hat{\lambda}(\hat{\nabla} \cdot \hat{\mathbf{u}}) \hat{\mathbf{I}}]}_{\text{Deviatoric stress}} \\ &+ \underbrace{2\rho \hat{\mathbf{u}} \wedge \boldsymbol{\Omega}}_{\text{Coriolis}} - \underbrace{\rho \hat{\mathbf{x}} \wedge \boldsymbol{\Omega} \wedge \boldsymbol{\Omega}}_{\text{Centrifugal}} + \underbrace{\rho \hat{\mathbf{x}} \wedge \dot{\boldsymbol{\Omega}} + \rho \hat{\mathbf{x}} \wedge \boldsymbol{\Omega}}_{\text{Euler}} + \underbrace{2\rho \mathbf{V}(t) \wedge \boldsymbol{\Omega}}_{\text{Magnus}} - \underbrace{\frac{\partial}{\partial t}(\rho \mathbf{V}(t))}_{\text{Translation}} \end{aligned} \quad (4.10)$$

The equation can be expressed in the component form using the approach of *Section 4.1.1*. The deviatoric stress tensor components is obtained from Hoffmann and Chiang [71]:

$$\boldsymbol{\tau}(x, y, z) = \begin{bmatrix} 2\mu \frac{\partial u}{\partial x} + \lambda \nabla \cdot \mathbf{u} & \mu \left( \frac{\partial u}{\partial y} + \frac{\partial v}{\partial x} \right) & \mu \left( \frac{\partial u}{\partial z} + \frac{\partial w}{\partial x} \right) \\ \mu \left( \frac{\partial u}{\partial y} + \frac{\partial v}{\partial x} \right) & 2\mu \frac{\partial v}{\partial y} + \lambda \nabla \cdot \mathbf{u} & \mu \left( \frac{\partial v}{\partial z} + \frac{\partial w}{\partial y} \right) \\ \mu \left( \frac{\partial u}{\partial z} + \frac{\partial w}{\partial x} \right) & \mu \left( \frac{\partial v}{\partial z} + \frac{\partial w}{\partial y} \right) & 2\mu \frac{\partial w}{\partial z} + \lambda \nabla \cdot \mathbf{u} \end{bmatrix} \quad (4.11)$$



CHAPTER 4. NON-INERTIAL EQUATIONS IN COMPONENT FORM

The compressible non-inertial momentum equations in the component form is subsequently expressed as;

**$\hat{x}$ -momentum**

$$\begin{aligned}
\frac{\partial \hat{\rho} \hat{u}}{\partial t} + \hat{u} \frac{\partial \hat{\rho} \hat{u}}{\partial \hat{x}} + \hat{v} \frac{\partial \hat{\rho} \hat{u}}{\partial \hat{y}} + \hat{w} \frac{\partial \hat{\rho} \hat{u}}{\partial \hat{z}} &= - \frac{\partial \hat{p}}{\partial \hat{x}} \\
+ \underbrace{\frac{\partial}{\partial \hat{x}} \left[ 2\hat{\mu} \frac{\partial \hat{u}}{\partial \hat{x}} + \hat{\lambda} \left( \frac{\partial \hat{u}}{\partial \hat{x}} + \frac{\partial \hat{v}}{\partial \hat{y}} + \frac{\partial \hat{w}}{\partial \hat{z}} \right) \right] + \frac{\partial}{\partial \hat{y}} \left[ \hat{\mu} \left( \frac{\partial \hat{u}}{\partial \hat{y}} + \frac{\partial \hat{v}}{\partial \hat{x}} \right) \right] + \frac{\partial}{\partial \hat{z}} \left[ \hat{\mu} \left( \frac{\partial \hat{u}}{\partial \hat{z}} + \frac{\partial \hat{w}}{\partial \hat{x}} \right) \right]}_{\text{Compressible diffusion terms}} \\
+ \underbrace{2\hat{\rho} \hat{v} \hat{w}_z - 2\hat{\rho} \hat{w} \hat{w}_y}_{\text{Coriolis}} + \underbrace{\hat{\rho} \hat{x} (\hat{\omega}_z^2 + \hat{\omega}_y^2) - \hat{\rho} \hat{y} \hat{\omega}_x \hat{\omega}_y - \hat{\rho} \hat{z} \hat{\omega}_x \hat{\omega}_z}_{\text{Centrifugal}} \\
+ \underbrace{\hat{\rho} \hat{y} \hat{w}_z - \hat{\rho} \hat{z} \hat{w}_y + \hat{\rho} \hat{y} \hat{\omega}_z - \hat{\rho} \hat{z} \hat{\omega}_y}_{\text{Euler}} + \underbrace{2\hat{\rho} \hat{V}_y \hat{\omega}_z - 2\hat{\rho} \hat{V}_z \hat{\omega}_y}_{\text{Magnus}} - \underbrace{\frac{\partial \hat{\rho} \hat{V}_x}{\partial t}}_{\text{Translation}}
\end{aligned} \tag{4.12}$$

**$\hat{y}$ -momentum**

$$\begin{aligned}
\frac{\partial \hat{\rho} \hat{v}}{\partial t} + \hat{u} \frac{\partial \hat{\rho} \hat{v}}{\partial \hat{x}} + \hat{v} \frac{\partial \hat{\rho} \hat{v}}{\partial \hat{y}} + \hat{w} \frac{\partial \hat{\rho} \hat{v}}{\partial \hat{z}} &= - \frac{\partial \hat{p}}{\partial \hat{y}} \\
+ \underbrace{\frac{\partial}{\partial \hat{x}} \left[ \hat{\mu} \left( \frac{\partial \hat{u}}{\partial \hat{y}} + \frac{\partial \hat{v}}{\partial \hat{x}} \right) \right] + \frac{\partial}{\partial \hat{y}} \left[ 2\hat{\mu} \frac{\partial \hat{v}}{\partial \hat{y}} + \hat{\lambda} \left( \frac{\partial \hat{u}}{\partial \hat{x}} + \frac{\partial \hat{v}}{\partial \hat{y}} + \frac{\partial \hat{w}}{\partial \hat{z}} \right) \right] + \frac{\partial}{\partial \hat{z}} \left[ \hat{\mu} \left( \frac{\partial \hat{v}}{\partial \hat{z}} + \frac{\partial \hat{w}}{\partial \hat{y}} \right) \right]}_{\text{Compressible diffusion terms}} \\
+ \underbrace{2\hat{\rho} \hat{w} \hat{\omega}_x - 2\hat{\rho} \hat{u} \hat{\omega}_z}_{\text{Coriolis}} + \underbrace{\hat{\rho} \hat{y} (\hat{\omega}_z^2 + \hat{\omega}_x^2) - \hat{\rho} \hat{x} \hat{\omega}_x \hat{\omega}_y - \hat{\rho} \hat{z} \hat{\omega}_y \hat{\omega}_z}_{\text{Centrifugal}} \\
+ \underbrace{\hat{\rho} \hat{z} \hat{w}_x - \hat{\rho} \hat{x} \hat{w}_z + \hat{\rho} \hat{z} \hat{\omega}_x - \hat{\rho} \hat{x} \hat{\omega}_z}_{\text{Euler}} + \underbrace{2\hat{\rho} \hat{V}_z \hat{\omega}_x - 2\hat{\rho} \hat{V}_x \hat{\omega}_z}_{\text{Magnus}} - \underbrace{\frac{\partial \hat{\rho} \hat{V}_y}{\partial t}}_{\text{Translation}}
\end{aligned} \tag{4.13}$$

**$\hat{z}$ -momentum**

$$\begin{aligned}
\frac{\partial \hat{\rho} \hat{w}}{\partial t} + \hat{u} \frac{\partial \hat{\rho} \hat{w}}{\partial \hat{x}} + \hat{v} \frac{\partial \hat{\rho} \hat{w}}{\partial \hat{y}} + \hat{w} \frac{\partial \hat{\rho} \hat{w}}{\partial \hat{z}} &= - \frac{\partial \hat{p}}{\partial \hat{z}} \\
+ \underbrace{\frac{\partial}{\partial \hat{x}} \left[ \hat{\mu} \left( \frac{\partial \hat{u}}{\partial \hat{z}} + \frac{\partial \hat{w}}{\partial \hat{x}} \right) \right] + \frac{\partial}{\partial \hat{y}} \left[ \hat{\mu} \left( \frac{\partial \hat{v}}{\partial \hat{z}} + \frac{\partial \hat{w}}{\partial \hat{y}} \right) \right] + \frac{\partial}{\partial \hat{z}} \left[ 2\hat{\mu} \frac{\partial \hat{w}}{\partial \hat{z}} + \hat{\lambda} \left( \frac{\partial \hat{u}}{\partial \hat{x}} + \frac{\partial \hat{v}}{\partial \hat{y}} + \frac{\partial \hat{w}}{\partial \hat{z}} \right) \right]}_{\text{Compressible diffusion terms}} \\
+ \underbrace{2\hat{\rho} \hat{u} \hat{\omega}_y - 2\hat{\rho} \hat{v} \hat{\omega}_x}_{\text{Coriolis}} + \underbrace{\hat{\rho} \hat{z} (\hat{\omega}_y^2 + \hat{\omega}_x^2) - \hat{\rho} \hat{x} \hat{\omega}_x \hat{\omega}_z - \hat{\rho} \hat{y} \hat{\omega}_y \hat{\omega}_z}_{\text{Centrifugal}} \\
+ \underbrace{\hat{\rho} \hat{x} \hat{w}_y - \hat{\rho} \hat{y} \hat{w}_x + \hat{\rho} \hat{x} \hat{\omega}_y - \hat{\rho} \hat{y} \hat{\omega}_x}_{\text{Euler}} + \underbrace{2\hat{\rho} \hat{V}_x \hat{\omega}_y - 2\hat{\rho} \hat{V}_y \hat{\omega}_x}_{\text{Magnus}} - \underbrace{\frac{\partial \hat{\rho} \hat{V}_z}{\partial t}}_{\text{Translation}}
\end{aligned} \tag{4.14}$$

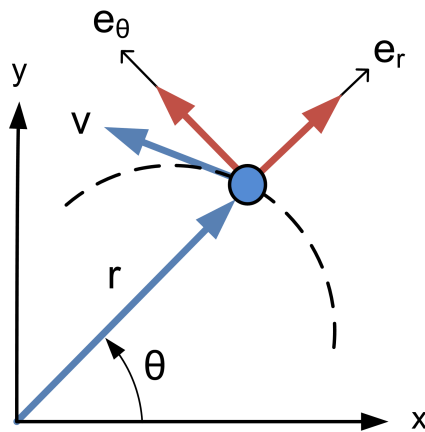
## 4.2 Inertial Navier-Stokes Equations in Cylindrical Coordinates

The component forms of the Cylindrical formulations of the inertial Navier-Stokes equations are first established in this section. The non-inertial equations are explored in the next section, *Section 4.3*.

### 4.2.1 Transformation for Cartesian to Cylindrical Coordinates

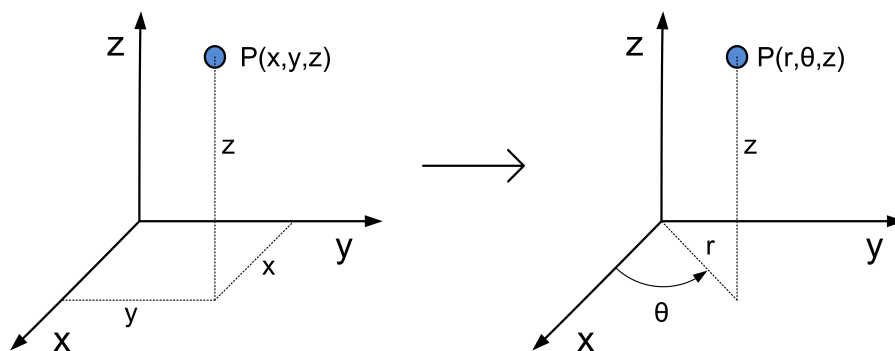
The vector form of the non-inertial Navier-Stokes equations is independent of the coordinates system (White [9]). Therefore the equations that were developed in *Chapter 3* can refer to either the Cartesian, Cylindrical or Curvilinear system. Expression of an inertial equation in the Cylindrical system does not place it in the non-inertial form; the equation remains in the inertial form. The Cylindrical formulation is just a different manner of expressing the same event in an alternative coordinate system (*Figure 4.2*).

Figure 4.2: Description of a Point in the Cartesian and Cylindrical Coordinates System



The Cylindrical form of the Navier-Stokes equations can be obtain either by deriving it from first principles or, the method that is used here, converting it from the Cartesian component form to the Cylindrical (*Figure 4.3*).

Figure 4.3: Cartesian and Cylindrical descriptions of point P



CHAPTER 4. NON-INERTIAL EQUATIONS IN COMPONENT FORM

The conversion is done geometrically. The displacement and velocity components are transformed as indicated in *Equations 4.15* and *4.16* respectively (Anderson [58], Aris [70], Steward [68]).

$$\begin{aligned}x &= r \cos \theta \\y &= r \sin \theta \\z &= z\end{aligned}\tag{4.15}$$

$$\begin{aligned}u &= u_r \cos \theta - u_\theta \sin \theta \\v &= u_r \sin \theta + u_\theta \cos \theta \\w &= u_z\end{aligned}\tag{4.16}$$

The derivatives in the Cartesian and Cylindrical system is related by the following matrix (Anderson [58]):

$$\begin{bmatrix} \frac{\partial \phi}{\partial x} \\ \frac{\partial \phi}{\partial y} \\ \frac{\partial \phi}{\partial z} \end{bmatrix} = \begin{bmatrix} \cos \theta & -\frac{\sin \theta}{r} & 0 \\ \sin \theta & \frac{\cos \theta}{r} & 0 \\ 0 & 0 & 1 \end{bmatrix} \begin{bmatrix} \frac{\partial \phi}{\partial r} \\ \frac{\partial \phi}{\partial \theta} \\ \frac{\partial \phi}{\partial z} \end{bmatrix}\tag{4.17}$$

## 4.2.2 Incompressible Flow Conditions

### 4.2.2.1 Continuity Equation

The incompressible continuity equation in component form was obtained in *Equation 4.2*:

$$\frac{\partial u}{\partial x} + \frac{\partial v}{\partial y} + \frac{\partial w}{\partial z} = 0\tag{4.18}$$

Substitution the conversion equations as described in *Section 4.2.1* results in the following expression:

$$\left( \cos \theta \frac{\partial}{\partial r} - \frac{\sin \theta}{r} \frac{\partial}{\partial \theta} \right) (u_r \cos \theta - u_\theta \sin \theta) + \left( \sin \theta \frac{\partial}{\partial r} + \frac{\cos \theta}{r} \frac{\partial}{\partial \theta} \right) (u_r \sin \theta + u_\theta \cos \theta) + \frac{\partial u_z}{\partial z} = 0\tag{4.19}$$

Re-arrangement of the terms leads to an equation,

$$\frac{\partial u_r}{\partial r} (\cos^2 \theta + \sin^2 \theta) + \frac{u_r}{r} (\cos^2 \theta + \sin^2 \theta) + \frac{1}{r} \frac{\partial u_\theta}{\partial \theta} (\cos^2 \theta + \sin^2 \theta) + \frac{\partial u_z}{\partial z} = 0\tag{4.20}$$

that can be simplified by using the equation:

$$\cos^2 \theta + \sin^2 \theta = 1\tag{4.21}$$

The final equation that represents the Continuity Equation in cylindrical component then becomes:

$$\frac{\partial u_r}{\partial r} + \frac{u_r}{r} + \frac{1}{r} \frac{\partial u_\theta}{\partial \theta} + \frac{\partial u_z}{\partial z} = 0\tag{4.22}$$

This form is in agreement with equations shown in the literature (Anderson [58], Aris [70], Schlichting [42], White [9]).

## 4.2. INERTIAL NAVIER-STOKES EQUATIONS IN CYLINDRICAL COORDINATES

### 4.2.2.2 Conservation of Momentum Equation

The incompressible momentum equation is expressed as White [9]:

$$\frac{\partial \mathbf{u}}{\partial t} + (\mathbf{u} \cdot \nabla) \mathbf{u} = -\nabla \psi + \nu \nabla^2 \mathbf{u} \quad (4.23)$$

Using the definitions for Cartesian gradient and laplacian operations results in the following equation that describes the conservation of momentum in the x-direction (Anderson [58], Aris [70]):

$$\frac{\partial u}{\partial t} + u \frac{\partial u}{\partial x} + v \frac{\partial u}{\partial y} + w \frac{\partial u}{\partial z} = -\frac{\partial \psi}{\partial x} + \nu \left( \frac{\partial^2 u}{\partial x^2} + \frac{\partial^2 u}{\partial y^2} + \frac{\partial^2 u}{\partial z^2} \right) \quad (4.24)$$

This equation can be converted to the Cylindrical system term by term. The Cartesian transient term is transformed to a cylindrical form by using the equations of *Section 4.2.1*:

$$\frac{\partial u}{\partial t} \rightarrow \frac{\partial}{\partial t} (u_r \cos \theta - u_\theta \sin \theta) \quad (4.25)$$

The product rule applies and the expression is expanded to:

$$\frac{\partial}{\partial t} (u_r \cos \theta - u_\theta \sin \theta) = \frac{\partial u_r}{\partial t} \cos \theta + \frac{\partial \cos \theta}{\partial t} u_r - \frac{\partial u_\theta}{\partial t} \sin \theta - \frac{\partial \sin \theta}{\partial t} u_\theta \quad (4.26)$$

The assumptions are made here that,

- the coordinate systems is attached to the body analysed
- the Cartesian and Cylindrical system shares an origin
- the analysis considers small perturbations of the order  $\varepsilon$

The value of  $\theta$  is subsequently very small when,  $\theta \rightarrow \varepsilon$  as  $\varepsilon \rightarrow 0$ . Furthermore,  $\cos \theta \rightarrow 1$ ,  $\sin \theta \rightarrow 0$  and *Equation 4.26* simplifies to:

$$\frac{\partial u}{\partial t} \rightarrow \frac{\partial u_r}{\partial t} \quad (4.27)$$

Using the methodology above the Cylindrical form of the remainder of the Cartesian terms can be obtained.

Convective terms,

$$\begin{aligned} u \frac{\partial u}{\partial x} &\rightarrow u_r \frac{\partial u_r}{\partial r} \\ v \frac{\partial u}{\partial y} &\rightarrow \frac{u_\theta}{r} \frac{\partial u_r}{\partial \theta} - \frac{u_\theta^2}{r} \\ w \frac{\partial u}{\partial z} &\rightarrow u_z \frac{\partial u_r}{\partial z} \end{aligned} \quad (4.28)$$

Pressure term,

$$\frac{\partial \psi}{\partial x} \rightarrow \frac{\partial \psi}{\partial r} \quad (4.29)$$

CHAPTER 4. NON-INERTIAL EQUATIONS IN COMPONENT FORM

Diffusive terms,

$$\begin{aligned}\frac{\partial^2 u}{\partial x^2} &\rightarrow \frac{\partial^2 u_r}{\partial r^2} \\ \frac{\partial^2 u}{\partial y^2} &\rightarrow \frac{1}{r} \frac{\partial u_r}{\partial r} + \frac{1}{r^2} \frac{\partial^2 u_r}{\partial \theta^2} - \frac{2}{r^2} \frac{\partial u_\theta}{\partial \theta} - \frac{u_r}{r^2} \\ \frac{\partial^2 u}{\partial z^2} &\rightarrow \frac{\partial^2 u_r}{\partial z^2}\end{aligned}\quad (4.30)$$

The resulting equation represents the conservation of momentum equation in the **r-direction** of the Cylindrical system which is in agreement with the equation from literature (Anderson [58], Aris [70], Schlichting [42], White [9]):

$$\frac{\partial u_r}{\partial t} + u_r \frac{\partial u_r}{\partial r} + \frac{u_\theta}{r} \frac{\partial u_r}{\partial \theta} - \frac{u_\theta^2}{r} + u_z \frac{\partial u_r}{\partial z} = -\frac{\partial \psi}{\partial r} + \frac{\partial^2 u_r}{\partial r^2} + \frac{1}{r} \frac{\partial u_r}{\partial r} + \frac{1}{r^2} \frac{\partial^2 u_r}{\partial \theta^2} - \frac{2}{r^2} \frac{\partial u_\theta}{\partial \theta} - \frac{u_r}{r^2} + \frac{\partial^2 u_r}{\partial z^2}\quad (4.31)$$

Using the method above it can be shown that for the **y-momentum** and **z-momentum** equations respectively,

$$\frac{\partial v}{\partial t} + u \frac{\partial v}{\partial x} + v \frac{\partial v}{\partial y} + w \frac{\partial v}{\partial z} = -\frac{\partial \psi}{\partial y} + \nu \left( \frac{\partial^2 v}{\partial x^2} + \frac{\partial^2 v}{\partial y^2} + \frac{\partial^2 v}{\partial z^2} \right)\quad (4.32)$$

$$\frac{\partial w}{\partial t} + u \frac{\partial w}{\partial x} + v \frac{\partial w}{\partial y} + w \frac{\partial w}{\partial z} = -\frac{\partial \psi}{\partial z} + \nu \left( \frac{\partial^2 w}{\partial x^2} + \frac{\partial^2 w}{\partial y^2} + \frac{\partial^2 w}{\partial z^2} \right)$$

the equations can be expressed in Cylindrical coordinates for the  **$\theta$ -direction** and  **$z$ -direction** respectively:

$$\frac{\partial u_\theta}{\partial t} + u_r \frac{\partial u_\theta}{\partial r} + \frac{u_\theta}{r} \frac{\partial u_\theta}{\partial \theta} + \frac{u_\theta u_r}{r} + u_z \frac{\partial u_\theta}{\partial z} = -\frac{1}{r} \frac{\partial \psi}{\partial \theta} + \frac{\partial^2 u_\theta}{\partial r^2} + \frac{1}{r} \frac{\partial u_\theta}{\partial r} + \frac{1}{r^2} \frac{\partial^2 u_\theta}{\partial \theta^2} + \frac{2}{r^2} \frac{\partial u_r}{\partial \theta} - \frac{u_\theta}{r^2} + \frac{\partial^2 u_\theta}{\partial z^2}$$

$$\frac{\partial u_z}{\partial t} + u_r \frac{\partial u_z}{\partial r} + \frac{u_\theta}{r} \frac{\partial u_z}{\partial \theta} + u_z \frac{\partial u_z}{\partial z} = -\frac{\partial \psi}{\partial z} + \frac{\partial^2 u_z}{\partial r^2} + \frac{1}{r} \frac{\partial u_z}{\partial r} + \frac{1}{r^2} \frac{\partial^2 u_z}{\partial \theta^2} + \frac{\partial^2 u_z}{\partial z^2}$$

(4.33)

The equations above are in agreement with the literature (Anderson [58], Aris [70], Schlichting [42], White [9]) and indicates consistency in the method used.

## 4.2.3 Compressible Flow Conditions

### 4.2.3.1 Continuity Equation

The component form of the compressible continuity equation in Cartesian coordinates was obtained in Equation 4.8,

$$\frac{\partial \rho}{\partial t} + \frac{\partial \rho u}{\partial x} + \frac{\partial \rho v}{\partial y} + \frac{\partial \rho w}{\partial z} = 0\quad (4.34)$$

## 4.2. INERTIAL NAVIER-STOKES EQUATIONS IN CYLINDRICAL COORDINATES

Using the same method as in *Section 4.2.2.1* the Cylindrical component form is obtained. This equation is similar to the incompressible form but with the inclusion of the transient term.

$$\frac{\partial \rho}{\partial t} + \frac{\partial \rho u_r}{\partial r} + \frac{\rho u_r}{r} + \frac{1}{r} \frac{\partial \rho u_\theta}{\partial \theta} + \frac{\partial \rho u_z}{\partial z} = 0 \quad (4.35)$$

### 4.2.3.2 Conservation of Momentum Equation

The compressible conservation of momentum equation is expressed by White [9]:

$$\frac{\partial}{\partial t} \rho \mathbf{u} + \nabla \cdot (\rho \mathbf{u} \otimes \mathbf{u}) = -\nabla p + \nabla \cdot \underbrace{[\mu(\nabla \mathbf{u} + \nabla \mathbf{u}^T) + \lambda(\nabla \cdot \mathbf{u})\mathbf{I}]}_{\text{deviatoric stress}} \quad (4.36)$$

In *Chapter 3* it was shown that the major difference between the incompressible and compressible formulations of the Navier-Stokes equations lies in the diffusion terms. In *Equation 3.19* it was shown that a number of terms in the deviatoric stress tensor can be neglected in the incompressible case (specifically the terms associated with  $\nabla \cdot \mathbf{u} = 0$ ) and which leads to significant simplifications to the diffusion terms (see *Equation 3.20*). In compressible flow those simplifications are not relevant (since  $\nabla \cdot \mathbf{u} \neq 0$  as shown in *Equation 4.8*) and the full deviatoric stress tensor is considered.

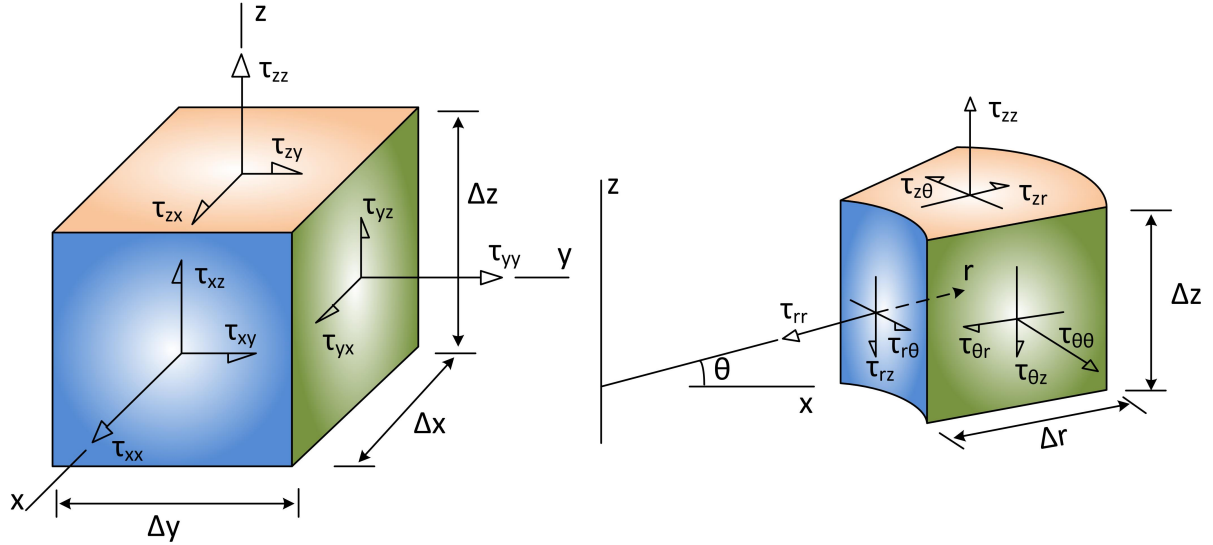
The deviatoric stress tensor takes the following form in the compressible, Cartesian case (Hoffmann and Chiang [71]):

$$\boldsymbol{\tau}(x, y, z) = \begin{bmatrix} \tau_{xx} & \tau_{xy} & \tau_{xz} \\ \tau_{yx} & \tau_{yy} & \tau_{yz} \\ \tau_{zx} & \tau_{zy} & \tau_{zz} \end{bmatrix} \quad (4.37)$$

$$\boldsymbol{\tau}(x, y, z) = \begin{bmatrix} 2\mu \frac{\partial u}{\partial x} + \lambda \nabla \cdot \mathbf{u} & \mu \left( \frac{\partial u}{\partial y} + \frac{\partial v}{\partial x} \right) & \mu \left( \frac{\partial u}{\partial z} + \frac{\partial w}{\partial x} \right) \\ \mu \left( \frac{\partial u}{\partial y} + \frac{\partial v}{\partial x} \right) & 2\mu \frac{\partial v}{\partial y} + \lambda \nabla \cdot \mathbf{u} & \mu \left( \frac{\partial v}{\partial z} + \frac{\partial w}{\partial y} \right) \\ \mu \left( \frac{\partial u}{\partial z} + \frac{\partial w}{\partial x} \right) & \mu \left( \frac{\partial v}{\partial z} + \frac{\partial w}{\partial y} \right) & 2\mu \frac{\partial w}{\partial z} + \lambda \nabla \cdot \mathbf{u} \end{bmatrix} \quad (4.38)$$

The difference between the Cartesian and Cylindrical formulations of the deviatoric stress tensor relies on the geometrical conversions established in *Section 4.2.1*. It is be used here to conduct the conversion with as described by *Figure 4.4*.

Figure 4.4: Cartesian (left) and Cylindrical (right) Control Volumes



The conversions are done separately for each term in the tensor matrix as shown in *Equation 4.38*. The term in first row, first column is designated  $\tau_{xx}$  and is converted as follow:

$$\begin{aligned}
 \tau_{xx} &= 2\mu \frac{\partial u}{\partial x} + \lambda \left( \frac{\partial u}{\partial x} + \frac{\partial v}{\partial y} + \frac{\partial w}{\partial z} \right) \rightarrow \\
 &\left[ 2\mu \left( \cos\theta \frac{\partial}{\partial r} - \frac{\sin\theta}{r} \frac{\partial}{\partial \theta} \right) (u_r \cos\theta - u_\theta \sin\theta) \right. \\
 &+ \lambda \left( \left( \cos\theta \frac{\partial}{\partial r} - \frac{\sin\theta}{r} \frac{\partial}{\partial \theta} \right) (u_r \cos\theta - u_\theta \sin\theta) + \left( \sin\theta \frac{\partial}{\partial r} + \frac{\cos\theta}{r} \frac{\partial}{\partial \theta} \right) (u_r \sin\theta + u_\theta \cos\theta) + \frac{\partial w}{\partial z} \right) \quad (4.39) \\
 &= 2\mu \frac{\partial u_r}{\partial r} + \lambda \left( \frac{\partial u_r}{\partial r} + \frac{u_r}{r} + \frac{1}{r} \frac{\partial u_\theta}{\partial r} + \frac{\partial u_z}{\partial z} \right) \\
 &= 2\mu \frac{\partial u_r}{\partial r} + \lambda \nabla \cdot \mathbf{u} = \tau_{rr}
 \end{aligned}$$

The term in the first row, second column of *Equation 4.38* is designated  $\tau_{xy}$  and is converted as follow:

$$\begin{aligned}
 \tau_{xy} &= \mu \left( \frac{\partial u}{\partial y} + \frac{\partial v}{\partial x} \right) \rightarrow \\
 &\mu \left[ \left( \sin\theta \frac{\partial}{\partial r} + \frac{\cos\theta}{r} \frac{\partial}{\partial \theta} \right) (u_r \cos\theta - u_\theta \sin\theta) + \left( \cos\theta \frac{\partial}{\partial r} - \frac{\sin\theta}{r} \frac{\partial}{\partial \theta} \right) (u_r \sin\theta + u_\theta \cos\theta) \right] \quad (4.40) \\
 &= \mu \left( \frac{1}{r} \frac{\partial u_r}{\partial \theta} - \frac{u_\theta}{r} + \frac{\partial u_\theta}{\partial r} \right) = \tau_{r\theta}
 \end{aligned}$$

The term in the first row, second column is designated  $\tau_{xz}$  and is converted as follow:

$$\begin{aligned}
 \tau_{xz} &= \mu \left( \frac{\partial u}{\partial z} + \frac{\partial w}{\partial x} \right) \rightarrow \\
 &\mu \left[ \frac{\partial}{\partial z} (u_r \cos\theta - u_\theta \sin\theta) + \left( \cos\theta \frac{\partial}{\partial r} - \frac{\sin\theta}{r} \frac{\partial}{\partial \theta} \right) (u_z) \right] \quad (4.41) \\
 &= \mu \left( \frac{\partial u_r}{\partial z} + \frac{\partial u_z}{\partial r} \right) = \tau_{rz}
 \end{aligned}$$



## 4.2. INERTIAL NAVIER-STOKES EQUATIONS IN CYLINDRICAL COORDINATES

By transforming all the terms in the Cartesian deviatoric stress tensor to the Cylindrical system, it can be shown that the Cylindrical stress tensor is expressed as:

$$\boldsymbol{\tau}(x, y, z) = \begin{bmatrix} \tau_{rr} & \tau_{r\theta} & \tau_{rz} \\ \tau_{\theta r} & \tau_{\theta\theta} & \tau_{\theta z} \\ \tau_{zr} & \tau_{z\theta} & \tau_{zz} \end{bmatrix} \quad (4.42)$$

$$\boldsymbol{\tau}(r, \theta, z) = \begin{bmatrix} 2\mu \frac{\partial u_r}{\partial r} + \lambda \nabla \cdot \mathbf{u} & \mu \left( \frac{1}{r} \frac{\partial u_r}{\partial \theta} - \frac{u_\theta}{r} + \frac{\partial u_\theta}{\partial r} \right) & \mu \left( \frac{\partial u_r}{\partial z} + \frac{\partial u_z}{\partial r} \right) \\ \mu \left( \frac{1}{r} \frac{\partial u_r}{\partial \theta} - \frac{u_\theta}{r} + \frac{\partial u_\theta}{\partial r} \right) & 2\mu \left( \frac{1}{r} \frac{\partial u_\theta}{\partial \theta} + \frac{u_r}{r} \right) + \lambda \nabla \cdot \mathbf{u} & \mu \left( \frac{1}{r} \frac{\partial u_z}{\partial \theta} + \frac{\partial u_\theta}{\partial z} \right) \\ \mu \left( \frac{\partial u_r}{\partial z} + \frac{\partial u_z}{\partial r} \right) & \mu \left( \frac{1}{r} \frac{\partial u_z}{\partial \theta} + \frac{\partial u_\theta}{\partial z} \right) & 2\mu \frac{\partial u_z}{\partial z} + \lambda \nabla \cdot \mathbf{u} \end{bmatrix} \quad (4.43)$$

This agrees with the literature as indication in Aris [70].

The x-momentum equation is expressed as:

$$\begin{aligned} \frac{\partial \rho u}{\partial t} + u \frac{\partial \rho u}{\partial x} + v \frac{\partial \rho u}{\partial y} + w \frac{\partial \rho u}{\partial z} = - \frac{\partial p}{\partial x} \\ + \frac{\partial}{\partial x} \left[ 2\mu \frac{\partial u}{\partial x} + (\lambda \nabla \cdot \mathbf{u}) \right] + \frac{\partial}{\partial y} \left[ \mu \left( \frac{\partial u}{\partial y} + \frac{\partial v}{\partial x} \right) \right] + \frac{\partial}{\partial z} \left[ \mu \left( \frac{\partial u}{\partial z} + \frac{\partial w}{\partial x} \right) \right] \end{aligned} \quad (4.44)$$

The r-momentum equation, using the compressible form of Equation 4.31 and the relevant terms of Equation 4.43, can then be expressed as:

$$\begin{aligned} \frac{\partial \rho u_r}{\partial t} + u_r \frac{\partial \rho u_r}{\partial r} + \frac{u_\theta}{r} \frac{\partial \rho u_r}{\partial \theta} - \frac{\rho u_\theta^2}{r} + u_z \frac{\partial \rho u_r}{\partial z} = - \frac{\partial p}{\partial r} \\ + \frac{\partial}{\partial r} \left[ 2\mu \frac{\partial u_r}{\partial r} + \lambda \nabla \cdot \mathbf{u} \right] + \frac{\partial}{\partial \theta} \left[ \mu \left( \frac{1}{r} \frac{\partial u_r}{\partial \theta} - \frac{u_\theta}{r} + \frac{\partial u_\theta}{\partial r} \right) \right] + \frac{\partial}{\partial z} \left[ \mu \left( \frac{\partial u_r}{\partial z} + \frac{\partial u_z}{\partial r} \right) \right] \end{aligned} \quad (4.45)$$

In a similar manner it can be showed that the momentum equations in the  $\theta$ - and  $z$ -direction respectively become:

$$\begin{aligned} \frac{\partial \rho u_\theta}{\partial t} + u_r \frac{\partial \rho u_\theta}{\partial r} + \frac{u_\theta}{r} \frac{\partial \rho u_\theta}{\partial \theta} + \frac{\rho u_\theta u_r}{r} + u_z \frac{\partial \rho u_\theta}{\partial z} = - \frac{1}{r} \frac{\partial p}{\partial \theta} \\ + \frac{\partial}{\partial r} \left[ \mu \left( \frac{1}{r} \frac{\partial u_r}{\partial \theta} - \frac{u_\theta}{r} + \frac{\partial u_\theta}{\partial r} \right) \right] + \frac{\partial}{\partial \theta} \left[ 2\mu \left( \frac{1}{r} \frac{\partial u_\theta}{\partial \theta} + \frac{u_r}{r} \right) + \lambda \nabla \cdot \mathbf{u} \right] + \frac{\partial}{\partial z} \left[ \mu \left( \frac{1}{r} \frac{\partial u_z}{\partial \theta} + \frac{\partial u_\theta}{\partial z} \right) \right] \end{aligned} \quad (4.46)$$

$$\begin{aligned} \frac{\partial \rho u_z}{\partial t} + u_r \frac{\partial \rho u_z}{\partial r} + \frac{u_\theta}{r} \frac{\partial \rho u_z}{\partial \theta} + u_z \frac{\partial \rho u_z}{\partial z} = - \frac{\partial p}{\partial z} \\ + \frac{\partial}{\partial r} \left[ \mu \left( \frac{\partial u_r}{\partial z} + \frac{\partial u_z}{\partial r} \right) \right] + \frac{\partial}{\partial \theta} \left[ \mu \left( \frac{1}{r} \frac{\partial u_z}{\partial \theta} + \frac{\partial u_\theta}{\partial z} \right) \right] + \frac{\partial}{\partial z} \left[ 2\mu \frac{\partial u_z}{\partial z} + \lambda \nabla \cdot \mathbf{u} \right] \end{aligned}$$

### 4.3 Non-Inertial Navier-Stokes Equations in Cylindrical Coordinates

In *Section 4.2* the Cylindrical form of the inertial Navier-Stokes equations were established. This section builds on that work and formulates the non-inertial Navier-Stokes equations in Cylindrical coordinates.

#### 4.3.1 Incompressible Flow Conditions

##### 4.3.1.1 Constant, Pure Rotation

The non-inertial Navier-Stokes equation for incompressible flow in constant, pure rotation was derived in *Chapter 3, Equation 3.55* :

$$\frac{\partial \hat{\mathbf{u}}}{\partial t} + (\hat{\mathbf{u}} \cdot \hat{\nabla}) \hat{\mathbf{u}} = -\hat{\nabla} \hat{\psi} + \hat{\nu} \hat{\nabla}^2 \hat{\mathbf{u}} + \underbrace{2\hat{\mathbf{u}} \wedge \hat{\boldsymbol{\Omega}}}_{\text{Coriolis}} - \underbrace{\hat{\mathbf{x}} \wedge \hat{\boldsymbol{\Omega}} \wedge \hat{\boldsymbol{\Omega}}}_{\text{Centrifugal}} \quad (4.47)$$

The inertial components of this equation were converted to the Cylindrical system in *Section 4.2*, here the cylindrical forms of the fictitious forces are obtained. This can be done in one of two manners; the first is to convert from the Cartesian components using the formulations in *Section 4.1* and the second is to obtain the components directly from the Cylindrical vector operations. Both methods are used for the conversion of the Coriolis force.

##### *Method I - Convert from Cartesian Components*

The component form of the Coriolis force is obtained though the cross product of the non-inertial velocity vector and the rotation vector both in Cartesian coordinates. The conversion equations in *Section 4.1* is used to convert from the Cartesian to the Cylindrical coordinates:

$$2\hat{\mathbf{u}} \wedge \hat{\boldsymbol{\Omega}} = \begin{bmatrix} \hat{\mathbf{i}} & \hat{\mathbf{j}} & \hat{\mathbf{k}} \\ 2\hat{u} & 2\hat{v} & 2\hat{w} \\ \omega_x & \omega_y & \omega_z \end{bmatrix} = (2\hat{v}\omega_z - 2\hat{w}\omega_y)\hat{\mathbf{i}} + (2\hat{w}\omega_x - 2\hat{u}\omega_z)\hat{\mathbf{j}} + (2\hat{u}\omega_y - 2\hat{v}\omega_x)\hat{\mathbf{k}} \quad (4.48)$$

$$\begin{aligned} &\rightarrow [2(\hat{u}_r \sin \hat{\theta} + \hat{u}_\theta \cos \hat{\theta})\omega_z - 2\hat{u}_z(\omega_r \sin \hat{\theta} + \omega_\theta \cos \hat{\theta})]\hat{\mathbf{e}}_r \\ &+ [2\hat{u}_z(\omega_r \cos \hat{\theta} - \omega_\theta \sin \hat{\theta}) - 2(\hat{u}_r \cos \hat{\theta} - \hat{u}_\theta \sin \hat{\theta})\omega_z]\hat{\mathbf{e}}_\theta \\ &+ [2(\hat{u}_r \cos \hat{\theta} - \hat{u}_\theta \sin \hat{\theta})(\omega_r \sin \hat{\theta} + \omega_\theta \cos \hat{\theta}) - 2(\hat{u}_r \sin \hat{\theta} + \hat{u}_\theta \cos \hat{\theta})(\omega_r \cos \hat{\theta} - \omega_\theta \sin \hat{\theta})]\hat{\mathbf{e}}_z \end{aligned} \quad (4.49)$$

Using the same assumptions, as in *Section 4.2*, that  $\theta \rightarrow \varepsilon$  where  $\varepsilon \rightarrow 0$ , then  $\cos \hat{\theta} \rightarrow 1$  and  $\sin \hat{\theta} \rightarrow 0$ . The equation above then simplifies to the Coriolis force components in Cylindrical coordinates:

$$2\hat{\mathbf{u}} \wedge \hat{\boldsymbol{\Omega}} = 2(\hat{u}_\theta \omega_z - \hat{u}_z \omega_\theta)\hat{\mathbf{e}}_r + 2(\hat{u}_z \omega_r - \hat{u}_r \omega_z)\hat{\mathbf{e}}_\theta + 2(\hat{u}_r \omega_\theta - \hat{u}_\theta \omega_r)\hat{\mathbf{e}}_z \quad (4.50)$$

### 4.3. NON-INERTIAL NAVIER-STOKES EQUATIONS IN CYLINDRICAL COORDINATES

#### Method II - Directly from Cylindrical Vector Operation

The second methods obtains the component form of the Coriolis force though the cross product of the non-inertial velocity vector and the rotation vector both in Cylindrical coordinates:

$$2\hat{\mathbf{u}} \wedge \boldsymbol{\Omega} = \begin{bmatrix} \hat{\mathbf{e}}_r & \hat{\mathbf{e}}_\theta & \hat{\mathbf{e}}_z \\ 2\hat{u}_r & 2\hat{u}_\theta & 2\hat{u}_z \\ \omega_r & \omega_\theta & \omega_z \end{bmatrix} = 2(\hat{u}_\theta\omega_z - \hat{u}_z\omega_\theta)\hat{\mathbf{e}}_r + 2(\hat{u}_z\omega_r - \hat{u}_r\omega_z)\hat{\mathbf{e}}_\theta + 2(\hat{u}_r\omega_\theta - \hat{u}_\theta\omega_r)\hat{\mathbf{e}}_z \quad (4.51)$$

The two methods produce exactly the same results. Therefore either of the two can be used. The most direct method is to obtain the fictitious force components directly from the Cylindrical vector operations. This method is used from this point forward.

The centrifugal force components are obtained by in a similar manner as shown above for the Coriolis components:

$$\hat{\mathbf{x}} \wedge \boldsymbol{\Omega} = \begin{bmatrix} \hat{\mathbf{e}}_r & \hat{\mathbf{e}}_\theta & \hat{\mathbf{e}}_z \\ \hat{r} & \hat{r}\hat{\theta} & \hat{z} \\ \omega_r & \omega_\theta & \omega_z \end{bmatrix} = (\hat{r}\hat{\theta}\omega_z - \hat{z}\omega_\theta)\hat{\mathbf{e}}_r + (\hat{z}\omega_r - \hat{r}\omega_z)\hat{\mathbf{e}}_\theta + (\hat{r}\omega_\theta - \hat{r}\hat{\theta}\omega_r)\hat{\mathbf{e}}_z \quad (4.52)$$

$$\hat{\mathbf{x}} \wedge \boldsymbol{\Omega} \wedge \boldsymbol{\Omega} = \begin{bmatrix} \hat{\mathbf{e}}_r & \hat{\mathbf{e}}_\theta & \hat{\mathbf{e}}_z \\ \hat{r}\hat{\theta}\omega_z - \hat{z}\omega_\theta & \hat{z}\omega_x - \hat{r}\omega_z & \hat{r}\omega_y - \hat{r}\hat{\theta}\omega_x \\ \omega_r & \omega_\theta & \omega_z \end{bmatrix} \quad (4.53)$$

$$\begin{aligned} &= [(\hat{z}\omega_r - \hat{r}\omega_z)\omega_z - (\hat{r}\omega_\theta - \hat{r}\hat{\theta}\omega_r)\omega_\theta]\hat{\mathbf{e}}_r + [(\hat{r}\omega_\theta - \hat{r}\hat{\theta}\omega_r)\omega_r - (\hat{r}\hat{\theta}\omega_z - \hat{z}\omega_\theta)\omega_z]\hat{\mathbf{e}}_\theta \\ &+ [(\hat{r}\hat{\theta}\omega_z - \hat{z}\omega_\theta)\omega_\theta - (\hat{z}\omega_r - \hat{r}\omega_z)\omega_r]\hat{\mathbf{e}}_z \\ &\rightarrow (\hat{z}\omega_r\omega_z - \hat{r}\omega_z^2 - \hat{r}\omega_\theta^2)\hat{\mathbf{e}}_r + (\hat{r}\omega_r\omega_\theta + \hat{z}\omega_\theta\omega_z)\hat{\mathbf{e}}_\theta + (\hat{r}\omega_r\omega_z - \hat{z}\omega_r^2 - \hat{z}\omega_\theta^2)\hat{\mathbf{e}}_z \end{aligned} \quad (4.54)$$

The components forms of the Coriolis and Centrifugal fictitious forces have been obtained above, and in addition to *Equations 4.31* and *4.33* the components form of the non-inertial momentum equation for constant, pure rotation are derived:

#### $\hat{r}$ -momentum

$$\begin{aligned} \frac{\partial \hat{u}_r}{\partial t} + \hat{u}_r \frac{\partial \hat{u}_r}{\partial \hat{r}} + \frac{\hat{u}_\theta}{\hat{r}} \frac{\partial \hat{u}_r}{\partial \hat{\theta}} - \frac{\hat{u}_\theta^2}{\hat{r}} + \hat{u}_r \frac{\partial \hat{u}_r}{\partial \hat{z}} &= -\frac{\partial \hat{\psi}}{\partial \hat{r}} + \frac{\partial^2 \hat{u}_r}{\partial \hat{r}^2} + \frac{1}{\hat{r}} \frac{\partial \hat{u}_r}{\partial \hat{r}} + \frac{1}{\hat{r}^2} \frac{\partial^2 \hat{u}_r}{\partial \hat{\theta}^2} - \frac{2}{\hat{r}^2} \frac{\partial \hat{u}_\theta}{\partial \hat{\theta}} - \frac{\hat{u}_r}{\hat{r}^2} + \frac{\partial^2 \hat{u}_r}{\partial \hat{z}^2} \\ &\quad + \underbrace{2\hat{u}_\theta\omega_z - 2\hat{u}_z\omega_\theta}_{\text{Coriolis}} - \underbrace{\hat{z}\omega_r\omega_z + \hat{r}\omega_z^2 + \hat{r}\omega_\theta^2}_{\text{Centrifugal}} \end{aligned} \quad (4.55)$$

#### $\hat{\theta}$ -momentum

$$\begin{aligned} \frac{\partial \hat{u}_\theta}{\partial t} + \hat{u}_r \frac{\partial \hat{u}_\theta}{\partial \hat{r}} + \frac{\hat{u}_\theta}{\hat{r}} \frac{\partial \hat{u}_\theta}{\partial \hat{\theta}} + \frac{\hat{u}_\theta \hat{u}_r}{\hat{r}} + \hat{u}_r \frac{\partial \hat{u}_\theta}{\partial \hat{z}} &= -\frac{1}{\hat{r}} \frac{\partial \hat{\psi}}{\partial \hat{\theta}} + \frac{\partial^2 \hat{u}_\theta}{\partial \hat{r}^2} + \frac{1}{\hat{r}} \frac{\partial \hat{u}_\theta}{\partial \hat{r}} + \frac{1}{\hat{r}^2} \frac{\partial^2 \hat{u}_\theta}{\partial \hat{\theta}^2} + \frac{2}{\hat{r}^2} \frac{\partial \hat{u}_r}{\partial \hat{\theta}} - \frac{\hat{u}_\theta}{\hat{r}^2} + \frac{\partial^2 \hat{u}_\theta}{\partial \hat{z}^2} \\ &\quad + \underbrace{2\hat{u}_z\omega_r - 2\hat{u}_r\omega_z}_{\text{Coriolis}} - \underbrace{\hat{r}\omega_r\omega_\theta - \hat{z}\omega_\theta\omega_z}_{\text{Centrifugal}} \end{aligned} \quad (4.56)$$

**$\hat{z}$ -momentum**

$$\frac{\partial \hat{u}_r}{\partial t} + \hat{u}_r \frac{\partial \hat{u}_r}{\partial \hat{r}} + \frac{\hat{u}_\theta}{\hat{r}} \frac{\partial \hat{u}_r}{\partial \hat{\theta}} + \hat{u}_r \frac{\partial \hat{u}_r}{\partial \hat{z}} = -\frac{\partial \hat{\psi}}{\partial \hat{z}} + \frac{\partial^2 \hat{u}_r}{\partial \hat{r}^2} + \frac{1}{\hat{r}} \frac{\partial \hat{u}_r}{\partial \hat{r}} + \frac{1}{\hat{r}^2} \frac{\partial^2 \hat{u}_r}{\partial \hat{\theta}^2} + \frac{\partial^2 \hat{u}_r}{\partial \hat{z}^2} + \underbrace{2\hat{u}_r \omega_\theta - 2\hat{u}_\theta \omega_r}_{\text{Coriolis}} - \underbrace{\hat{r} \omega_r \omega_z + \hat{z} \omega_r^2 + \hat{z} \omega_\theta^2}_{\text{Centrifugal}} \quad (4.57)$$

**4.3.1.2 Arbitrary Rotation**

The non-inertial momentum equation for variable, pure rotation in incompressible flow was derived in *Chapter 3, Equation 3.157*:

$$\frac{\partial \hat{\mathbf{u}}}{\partial t} + (\hat{\mathbf{u}} \cdot \hat{\nabla}) \hat{\mathbf{u}} = -\hat{\nabla} \hat{\psi} + \hat{\nabla} \hat{\psi}^2 \hat{\mathbf{u}} + \underbrace{2\hat{\mathbf{u}} \wedge \hat{\boldsymbol{\Omega}}}_{\text{Coriolis}} - \underbrace{\hat{\mathbf{x}} \wedge \hat{\boldsymbol{\Omega}} \wedge \hat{\boldsymbol{\Omega}}}_{\text{Centrifugal}} + \underbrace{\hat{\mathbf{x}} \wedge \hat{\dot{\boldsymbol{\Omega}}}}_{\text{Euler}} \quad (4.58)$$

The Cylindrical components of the Euler fictitious force are obtained in a similar manner as the Centrifugal force components in *Section 4.3.1.1*:

$$\hat{\mathbf{x}} \wedge \hat{\dot{\boldsymbol{\Omega}}} = \begin{bmatrix} \hat{\mathbf{e}}_r & \hat{\mathbf{e}}_\theta & \hat{\mathbf{e}}_z \\ \hat{r} & \hat{r}\hat{\theta} & \hat{z} \\ \dot{\omega}_r & \dot{\omega}_\theta & \dot{\omega}_z \end{bmatrix} = (\hat{r}\hat{\theta}\dot{\omega}_z - \hat{z}\dot{\omega}_\theta)\hat{\mathbf{e}}_r + (\hat{z}\dot{\omega}_r - \hat{r}\dot{\omega}_z)\hat{\mathbf{e}}_\theta + (\hat{r}\dot{\omega}_\theta - \hat{r}\hat{\theta}\dot{\omega}_r)\hat{\mathbf{e}}_z \quad (4.59)$$

Following from *Equations 4.55, 4.56 and 4.57* and the description of the Euler components above, the non-inertial momentum equation in cylindrical components is as follow;

**$\hat{r}$ -momentum**

$$\frac{\partial \hat{u}_r}{\partial t} + \hat{u}_r \frac{\partial \hat{u}_r}{\partial \hat{r}} + \frac{\hat{u}_\theta}{\hat{r}} \frac{\partial \hat{u}_r}{\partial \hat{\theta}} - \frac{\hat{u}_\theta^2}{\hat{r}} + \hat{u}_r \frac{\partial \hat{u}_r}{\partial \hat{z}} = -\frac{\partial \hat{\psi}}{\partial \hat{r}} + \frac{\partial^2 \hat{u}_r}{\partial \hat{r}^2} + \frac{1}{\hat{r}} \frac{\partial \hat{u}_r}{\partial \hat{r}} + \frac{1}{\hat{r}^2} \frac{\partial^2 \hat{u}_r}{\partial \hat{\theta}^2} - \frac{2}{\hat{r}^2} \frac{\partial \hat{u}_\theta}{\partial \hat{\theta}} - \frac{\hat{u}_r}{\hat{r}^2} + \frac{\partial^2 \hat{u}_r}{\partial \hat{z}^2} + 2\hat{u}_\theta \omega_z - 2\hat{u}_z \omega_\theta - \hat{z} \omega_r \omega_z + \hat{r} \omega_z^2 + \hat{r} \omega_\theta^2 - \underbrace{\hat{z} \dot{\omega}_\theta}_{\text{Euler}} \quad (4.60)$$

**$\hat{\theta}$ -momentum**

$$\frac{\partial \hat{u}_\theta}{\partial t} + \hat{u}_r \frac{\partial \hat{u}_\theta}{\partial \hat{r}} + \frac{\hat{u}_\theta}{\hat{r}} \frac{\partial \hat{u}_\theta}{\partial \hat{\theta}} + \frac{\hat{u}_\theta \hat{u}_r}{\hat{r}} + \hat{u}_r \frac{\partial \hat{u}_\theta}{\partial \hat{z}} = -\frac{1}{\hat{r}} \frac{\partial \hat{\psi}}{\partial \hat{\theta}} + \frac{\partial^2 \hat{u}_\theta}{\partial \hat{r}^2} + \frac{1}{\hat{r}} \frac{\partial \hat{u}_\theta}{\partial \hat{r}} + \frac{1}{\hat{r}^2} \frac{\partial^2 \hat{u}_\theta}{\partial \hat{\theta}^2} + \frac{2}{\hat{r}^2} \frac{\partial \hat{u}_r}{\partial \hat{\theta}} - \frac{\hat{u}_\theta}{\hat{r}^2} + \frac{\partial^2 \hat{u}_\theta}{\partial \hat{z}^2} + 2\hat{u}_z \omega_r - 2\hat{u}_r \omega_z - \hat{r} \omega_r \omega_\theta - \hat{z} \omega_\theta \omega_z + \underbrace{\hat{z} \dot{\omega}_r - \hat{r} \dot{\omega}_z}_{\text{Euler}} \quad (4.61)$$

**$\hat{z}$ -momentum**

$$\frac{\partial \hat{u}_r}{\partial t} + \hat{u}_r \frac{\partial \hat{u}_r}{\partial \hat{r}} + \frac{\hat{u}_\theta}{\hat{r}} \frac{\partial \hat{u}_r}{\partial \hat{\theta}} + \hat{u}_r \frac{\partial \hat{u}_r}{\partial \hat{z}} = -\frac{\partial \hat{\psi}}{\partial \hat{z}} + \frac{\partial^2 \hat{u}_r}{\partial \hat{r}^2} + \frac{1}{\hat{r}} \frac{\partial \hat{u}_r}{\partial \hat{r}} + \frac{1}{\hat{r}^2} \frac{\partial^2 \hat{u}_r}{\partial \hat{\theta}^2} + \frac{\partial^2 \hat{u}_r}{\partial \hat{z}^2} + 2\hat{u}_r \omega_\theta - 2\hat{u}_\theta \omega_r - \hat{r} \omega_r \omega_z + \hat{z} \omega_r^2 + \hat{z} \omega_\theta^2 + \underbrace{\hat{r} \dot{\omega}_\theta}_{\text{Euler}} \quad (4.62)$$

### 4.3. NON-INERTIAL NAVIER-STOKES EQUATIONS IN CYLINDRICAL COORDINATES

In the case where the rotation is fully arbitrary, in other words the rotation is around of movable axis, *Chapter 3* has indicated that the non-inertial momentum equation takes the form:

$$\frac{\partial \hat{\mathbf{u}}}{\partial t} + (\hat{\mathbf{u}} \cdot \hat{\nabla}) \hat{\mathbf{u}} = -\hat{\nabla} \hat{\psi} + \nu \hat{\nabla}^2 \hat{\mathbf{u}} + \underbrace{2\hat{\mathbf{u}} \wedge \boldsymbol{\Omega}}_{\text{Coriolis}} - \underbrace{\hat{\mathbf{x}} \wedge \boldsymbol{\Omega} \wedge \boldsymbol{\Omega}}_{\text{Centrifugal}} + \underbrace{\hat{\mathbf{x}} \wedge \dot{\boldsymbol{\Omega}}}_{\text{Euler}} + \underbrace{\hat{\mathbf{x}} \wedge \boldsymbol{\Omega}}_{\text{Moving Axis}} \quad (4.63)$$

The Cylindrical components of the arbitrary rotation term (due to the movable axis) is determined in the same manner as for the previous fictitious forces - directly from the Cylindrical vector operation:

$$\hat{\mathbf{x}} \wedge \boldsymbol{\Omega} = \begin{bmatrix} \hat{\mathbf{e}}_r & \hat{\mathbf{e}}_\theta & \hat{\mathbf{e}}_z \\ \hat{u}_r & \hat{u}_\theta & \hat{u}_z \\ \omega_r & \omega_\theta & \omega_z \end{bmatrix} = (\hat{u}_\theta \omega_z - \hat{u}_z \omega_\theta) \hat{\mathbf{e}}_r + (\hat{u}_z \omega_r - \hat{u}_r \omega_z) \hat{\mathbf{e}}_\theta + (\hat{u}_r \omega_\theta - \hat{u}_\theta \omega_r) \hat{\mathbf{e}}_z \quad (4.64)$$

Following from *Equations 4.60, 4.61 and 4.62* and the description of the arbitrary rotation terms above, the non-inertial momentum equations in Cylindrical component form becomes;

#### $\hat{r}$ -momentum

$$\begin{aligned} \frac{\partial \hat{u}_r}{\partial t} + \hat{u}_r \frac{\partial \hat{u}_r}{\partial \hat{r}} + \frac{\hat{u}_\theta}{\hat{r}} \frac{\partial \hat{u}_r}{\partial \hat{\theta}} - \frac{\hat{u}_\theta^2}{\hat{r}} + \hat{u}_r \frac{\partial \hat{u}_r}{\partial \hat{z}} = & -\frac{\partial \hat{\psi}}{\partial \hat{r}} + \frac{\partial^2 \hat{u}_r}{\partial \hat{r}^2} + \frac{1}{\hat{r}} \frac{\partial \hat{u}_r}{\partial \hat{r}} + \frac{1}{\hat{r}^2} \frac{\partial^2 \hat{u}_r}{\partial \hat{\theta}^2} - \frac{2}{\hat{r}^2} \frac{\partial \hat{u}_\theta}{\partial \hat{\theta}} - \frac{\hat{u}_r}{\hat{r}^2} + \frac{\partial^2 \hat{u}_r}{\partial \hat{z}^2} \\ & + 2\hat{u}_\theta \omega_z - 2\hat{u}_z \omega_\theta - \hat{z} \omega_r \omega_z + \hat{r} \omega_z^2 + \hat{r} \omega_\theta^2 - \hat{z} \dot{\omega}_\theta + \underbrace{\hat{u}_\theta \omega_z - \hat{u}_z \omega_\theta}_{\text{Arbitrary Rotation}} \end{aligned} \quad (4.65)$$

#### $\hat{\theta}$ -momentum

$$\begin{aligned} \frac{\partial \hat{u}_\theta}{\partial t} + \hat{u}_r \frac{\partial \hat{u}_\theta}{\partial \hat{r}} + \frac{\hat{u}_\theta}{\hat{r}} \frac{\partial \hat{u}_\theta}{\partial \hat{\theta}} + \frac{\hat{u}_\theta \hat{u}_r}{\hat{r}} + \hat{u}_r \frac{\partial \hat{u}_\theta}{\partial \hat{z}} = & -\frac{1}{\hat{r}} \frac{\partial \hat{\psi}}{\partial \hat{\theta}} + \frac{\partial^2 \hat{u}_\theta}{\partial \hat{r}^2} + \frac{1}{\hat{r}} \frac{\partial \hat{u}_\theta}{\partial \hat{r}} + \frac{1}{\hat{r}^2} \frac{\partial^2 \hat{u}_\theta}{\partial \hat{\theta}^2} + \frac{2}{\hat{r}^2} \frac{\partial \hat{u}_r}{\partial \hat{\theta}} - \frac{\hat{u}_\theta}{\hat{r}^2} + \frac{\partial^2 \hat{u}_\theta}{\partial \hat{z}^2} \\ & + 2\hat{u}_z \omega_r - 2\hat{u}_r \omega_z - \hat{r} \omega_r \omega_\theta - \hat{z} \omega_\theta \omega_z + \hat{z} \dot{\omega}_r - \hat{r} \dot{\omega}_z + \underbrace{\hat{u}_z \omega_r - \hat{u}_r \omega_z}_{\text{Arbitrary Rotation}} \end{aligned} \quad (4.66)$$

#### $\hat{z}$ -momentum

$$\begin{aligned} \frac{\partial \hat{u}_r}{\partial t} + \hat{u}_r \frac{\partial \hat{u}_r}{\partial \hat{r}} + \frac{\hat{u}_\theta}{\hat{r}} \frac{\partial \hat{u}_r}{\partial \hat{\theta}} + \hat{u}_r \frac{\partial \hat{u}_r}{\partial \hat{z}} = & -\frac{\partial \hat{\psi}}{\partial \hat{z}} + \frac{\partial^2 \hat{u}_r}{\partial \hat{r}^2} + \frac{1}{\hat{r}} \frac{\partial \hat{u}_r}{\partial \hat{r}} + \frac{1}{\hat{r}^2} \frac{\partial^2 \hat{u}_r}{\partial \hat{\theta}^2} + \frac{\partial^2 \hat{u}_r}{\partial \hat{z}^2} \\ & + 2\hat{u}_r \omega_\theta - 2\hat{u}_\theta \omega_r - \hat{r} \omega_r \omega_z + \hat{z} \omega_r^2 + \hat{z} \omega_\theta^2 + \hat{r} \dot{\omega}_\theta + \underbrace{\hat{u}_r \omega_\theta - \hat{u}_\theta \omega_r}_{\text{Arbitrary Rotation}} \end{aligned} \quad (4.67)$$

#### 4.3.1.3 Arbitrary Acceleration

In *Chapter 3, Equation 3.239* the non-inertial momentum equation for arbitrary acceleration in incompressible conditions has been derived:

$$\frac{\partial \hat{\mathbf{u}}}{\partial t} + (\hat{\mathbf{u}} \cdot \hat{\nabla}) \hat{\mathbf{u}} = -\hat{\nabla} \hat{\psi} + \nu \hat{\nabla}^2 \hat{\mathbf{u}} + \underbrace{2\hat{\mathbf{u}} \wedge \boldsymbol{\Omega}}_{\text{Coriolis}} - \underbrace{\hat{\mathbf{x}} \wedge \boldsymbol{\Omega} \wedge \boldsymbol{\Omega}}_{\text{Centrifugal}} + \underbrace{\hat{\mathbf{x}} \wedge \dot{\boldsymbol{\Omega}}}_{\text{Euler}} + \underbrace{\hat{\mathbf{x}} \wedge \boldsymbol{\Omega}}_{\text{Unsteady motion}} + \underbrace{2\mathbf{V}(t) \wedge \boldsymbol{\Omega}}_{\text{Magnus}} - \underbrace{\frac{\partial}{\partial t}(\mathbf{V}(t))}_{\text{Translation}} \quad (4.68)$$

CHAPTER 4. NON-INERTIAL EQUATIONS IN COMPONENT FORM

Following from the derivations in *Section 4.3.1* and *Section 4.3.2*, the Cylindrical component form of the equations are determined;

**$\hat{r}$ -momentum**

$$\begin{aligned}
 \frac{\partial \hat{u}_r}{\partial t} + \hat{u}_r \frac{\partial \hat{u}_r}{\partial \hat{r}} + \frac{\hat{u}_\theta}{\hat{r}} \frac{\partial \hat{u}_r}{\partial \hat{\theta}} - \frac{\hat{u}_\theta^2}{\hat{r}} + \hat{u}_r \frac{\partial \hat{u}_r}{\partial \hat{z}} = & -\frac{\partial \hat{\psi}}{\partial \hat{r}} + \frac{\partial^2 \hat{u}_r}{\partial \hat{r}^2} + \frac{1}{\hat{r}} \frac{\partial \hat{u}_r}{\partial \hat{r}} + \frac{1}{\hat{r}^2} \frac{\partial^2 \hat{u}_r}{\partial \hat{\theta}^2} + \frac{2}{\hat{r}^2} \frac{\partial \hat{u}_\theta}{\partial \hat{\theta}} - \frac{\hat{u}_r}{\hat{r}^2} + \frac{\partial^2 \hat{u}_r}{\partial \hat{z}^2} \\
 & + \underbrace{2\hat{u}_\theta \omega_z - 2\hat{u}_z \omega_\theta}_{\text{Coriolis}} - \underbrace{\hat{z} \omega_r \omega_z + \hat{r} \omega_z^2 + \hat{r} \omega_\theta^2}_{\text{Centrifugal}} \\
 & - \underbrace{\hat{z} \dot{\omega}_\theta}_{\text{Euler}} + \underbrace{\hat{u}_\theta \omega_z - \hat{u}_z \omega_\theta}_{\text{Arbitrary Rotation}} \\
 & + \underbrace{2V_\theta \omega_z - 2V_z \omega_\theta}_{\text{Magnus}} - \underbrace{\frac{\partial V_r}{\partial t}}_{\text{Unsteady Translation}}
 \end{aligned} \tag{4.69}$$

**$\hat{\theta}$ -momentum**

$$\begin{aligned}
 \frac{\partial \hat{u}_\theta}{\partial t} + \hat{u}_r \frac{\partial \hat{u}_\theta}{\partial \hat{r}} + \frac{\hat{u}_\theta}{\hat{r}} \frac{\partial \hat{u}_\theta}{\partial \hat{\theta}} + \frac{\hat{u}_\theta \hat{u}_r}{\hat{r}} + \hat{u}_r \frac{\partial \hat{u}_\theta}{\partial \hat{z}} = & -\frac{1}{\hat{r}} \frac{\partial \hat{\psi}}{\partial \hat{\theta}} + \frac{\partial^2 \hat{u}_\theta}{\partial \hat{r}^2} + \frac{1}{\hat{r}} \frac{\partial \hat{u}_\theta}{\partial \hat{r}} + \frac{1}{\hat{r}^2} \frac{\partial^2 \hat{u}_\theta}{\partial \hat{\theta}^2} - \frac{2}{\hat{r}^2} \frac{\partial \hat{u}_r}{\partial \hat{\theta}} - \frac{\hat{u}_\theta}{\hat{r}^2} + \frac{\partial^2 \hat{u}_\theta}{\partial \hat{z}^2} \\
 & + \underbrace{2\hat{u}_z \omega_r - 2\hat{u}_r \omega_z}_{\text{Coriolis}} - \underbrace{\hat{r} \omega_r \omega_\theta - \hat{z} \omega_\theta \omega_z}_{\text{Centrifugal}} \\
 & + \underbrace{\hat{z} \dot{\omega}_r - \hat{r} \dot{\omega}_z}_{\text{Euler}} + \underbrace{\hat{u}_z \omega_r - \hat{u}_r \omega_z}_{\text{Arbitrary Rotation}} \\
 & + \underbrace{2V_z \omega_r - 2V_r \omega_z}_{\text{Magnus}} - \underbrace{\frac{\partial V_\theta}{\partial t}}_{\text{Unsteady Translation}}
 \end{aligned} \tag{4.70}$$

**$\hat{z}$ -momentum**

$$\begin{aligned}
 \frac{\partial \hat{u}_r}{\partial t} + \hat{u}_r \frac{\partial \hat{u}_r}{\partial \hat{r}} + \frac{\hat{u}_\theta}{\hat{r}} \frac{\partial \hat{u}_r}{\partial \hat{\theta}} + \hat{u}_r \frac{\partial \hat{u}_r}{\partial \hat{z}} = & -\frac{\partial \hat{\psi}}{\partial \hat{z}} + \frac{\partial^2 \hat{u}_r}{\partial \hat{r}^2} + \frac{1}{\hat{r}} \frac{\partial \hat{u}_r}{\partial \hat{r}} + \frac{1}{\hat{r}^2} \frac{\partial^2 \hat{u}_r}{\partial \hat{\theta}^2} + \frac{\partial^2 \hat{u}_r}{\partial \hat{z}^2} \\
 & + \underbrace{2\hat{u}_r \omega_\theta - 2\hat{u}_\theta \omega_r}_{\text{Coriolis}} - \underbrace{\hat{r} \omega_r \omega_z + \hat{z} \omega_r^2 + \hat{z} \omega_\theta^2}_{\text{Centrifugal}} \\
 & + \underbrace{\hat{r} \dot{\omega}_\theta}_{\text{Euler}} + \underbrace{\hat{u}_r \omega_\theta - \hat{u}_\theta \omega_r}_{\text{Arbitrary Rotation}} \\
 & + \underbrace{2V_r \omega_\theta - 2V_\theta \omega_r}_{\text{Magnus}} - \underbrace{\frac{\partial V_z}{\partial t}}_{\text{Unsteady Translation}}
 \end{aligned} \tag{4.71}$$

### 4.3.2 Compressible Flow Conditions

#### 4.3.2.1 Constant, Pure Rotation

The non-inertial Navier-Stokes equation for compressible flow in constant, pure rotation was derived in *Chapter 3, Equation 3.85* :

$$\frac{\partial \hat{\rho} \hat{\mathbf{u}}}{\partial t} + \hat{\nabla} \cdot (\hat{\rho} \hat{\mathbf{u}} \otimes \hat{\mathbf{u}}) = -\hat{\nabla} \hat{p} + \hat{\nabla} \cdot [\hat{\mu}(\hat{\nabla} \hat{\mathbf{u}} + \hat{\nabla} \hat{\mathbf{u}}^T) + \hat{\lambda}(\hat{\nabla} \cdot \hat{\mathbf{u}})\hat{\mathbf{I}}] + \underbrace{2\rho \hat{\mathbf{u}} \wedge \boldsymbol{\Omega}}_{\text{Coriolis}} - \underbrace{\rho \hat{\mathbf{x}} \wedge \boldsymbol{\Omega} \wedge \boldsymbol{\Omega}}_{\text{Centrifugal}} \quad (4.72)$$

By using the stress components from the deviatoric stress tensor (*Equation 4.43*) and *Equations 4.55, 4.56* and *4.57* (that provides the formulation for constant, pure rotation in incompressible flow) the component form of the compressible momentum equation in Cylindrical coordinates are determined;

#### $\hat{r}$ -momentum

$$\begin{aligned} \frac{\partial \hat{\rho} \hat{u}_r}{\partial t} + \hat{u}_r \frac{\partial \hat{\rho} \hat{u}_r}{\partial \hat{r}} + \frac{\hat{u}_\theta}{\hat{r}} \frac{\partial \hat{\rho} \hat{u}_r}{\partial \hat{\theta}} - \frac{\hat{\rho} \hat{u}_\theta^2}{\hat{r}} + \hat{u}_z \frac{\partial \hat{\rho} \hat{u}_r}{\partial \hat{z}} = -\frac{\partial \hat{p}}{\partial \hat{r}} \\ + \frac{\partial}{\partial \hat{r}} \left[ 2\hat{\mu} \frac{\partial \hat{u}_r}{\partial \hat{r}} + \hat{\lambda} \hat{\nabla} \cdot \hat{\mathbf{u}} \right] + \frac{\partial}{\partial \hat{\theta}} \left[ \hat{\mu} \left( \frac{1}{\hat{r}} \frac{\partial \hat{u}_r}{\partial \hat{\theta}} - \frac{\hat{u}_\theta}{\hat{r}} + \frac{\partial \hat{u}_\theta}{\partial \hat{r}} \right) \right] + \frac{\partial}{\partial \hat{z}} \left[ \hat{\mu} \left( \frac{\partial \hat{u}_r}{\partial \hat{z}} + \frac{\partial \hat{u}_z}{\partial \hat{r}} \right) \right] \\ \underbrace{+ 2\hat{\rho} \hat{u}_\theta \omega_z - 2\hat{\rho} \hat{u}_z \omega_\theta}_{\text{Coriolis}} - \underbrace{\hat{\rho} \hat{z} \omega_r \omega_z + \hat{\rho} \hat{r} \omega_z^2 + \hat{\rho} \hat{r} \omega_\theta^2}_{\text{Centrifugal}} \end{aligned} \quad (4.73)$$

#### $\hat{\theta}$ -momentum

$$\begin{aligned} \frac{\partial \hat{\rho} \hat{u}_\theta}{\partial t} + \hat{u}_r \frac{\partial \hat{\rho} \hat{u}_\theta}{\partial \hat{r}} + \frac{\hat{u}_\theta}{\hat{r}} \frac{\partial \hat{\rho} \hat{u}_\theta}{\partial \hat{\theta}} + \frac{\hat{\rho} \hat{u}_\theta \hat{u}_r}{\hat{r}} + \hat{u}_z \frac{\partial \hat{\rho} \hat{u}_\theta}{\partial \hat{z}} = -\frac{1}{\hat{r}} \frac{\partial \hat{p}}{\partial \hat{\theta}} \\ + \frac{\partial}{\partial \hat{r}} \left[ \hat{\mu} \left( \frac{1}{\hat{r}} \frac{\partial \hat{u}_r}{\partial \hat{\theta}} - \frac{\hat{u}_\theta}{\hat{r}} + \frac{\partial \hat{u}_\theta}{\partial \hat{r}} \right) \right] + \frac{\partial}{\partial \hat{\theta}} \left[ 2\hat{\mu} \left( \frac{1}{\hat{r}} \frac{\partial \hat{u}_\theta}{\partial \hat{\theta}} + \frac{\hat{u}_r}{\hat{r}} \right) + \hat{\lambda} \hat{\nabla} \cdot \hat{\mathbf{u}} \right] + \frac{\partial}{\partial \hat{z}} \left[ \hat{\mu} \left( \frac{1}{\hat{r}} \frac{\partial \hat{u}_z}{\partial \hat{\theta}} + \frac{\partial \hat{u}_\theta}{\partial \hat{z}} \right) \right] \\ \underbrace{+ 2\hat{\rho} \hat{u}_z \omega_r - 2\hat{\rho} \hat{u}_r \omega_z}_{\text{Coriolis}} - \underbrace{\hat{\rho} \hat{r} \omega_r \omega_\theta - \hat{\rho} \hat{z} \omega_\theta \omega_z}_{\text{Centrifugal}} \end{aligned} \quad (4.74)$$

#### $\hat{z}$ -momentum

$$\begin{aligned} \frac{\partial \hat{\rho} \hat{u}_z}{\partial t} + \hat{u}_r \frac{\partial \hat{\rho} \hat{u}_z}{\partial \hat{r}} + \frac{\hat{u}_\theta}{\hat{r}} \frac{\partial \hat{\rho} \hat{u}_z}{\partial \hat{\theta}} + \hat{u}_z \frac{\partial \hat{\rho} \hat{u}_z}{\partial \hat{z}} = -\frac{\partial \hat{p}}{\partial \hat{z}} \\ + \frac{\partial}{\partial \hat{r}} \left[ \hat{\mu} \left( \frac{\partial \hat{u}_r}{\partial \hat{z}} + \frac{\partial \hat{u}_z}{\partial \hat{r}} \right) \right] + \frac{\partial}{\partial \hat{\theta}} \left[ \hat{\mu} \left( \frac{1}{\hat{r}} \frac{\partial \hat{u}_z}{\partial \hat{\theta}} + \frac{\partial \hat{u}_\theta}{\partial \hat{z}} \right) \right] + \frac{\partial}{\partial \hat{z}} \left[ 2\hat{\mu} \frac{\partial \hat{u}_z}{\partial \hat{z}} + \hat{\lambda} \hat{\nabla} \cdot \hat{\mathbf{u}} \right] \\ \underbrace{+ 2\hat{\rho} \hat{u}_r \omega_\theta - 2\hat{\rho} \hat{u}_\theta \omega_r}_{\text{Coriolis}} - \underbrace{\hat{\rho} \hat{r} \omega_r \omega_z + \hat{\rho} \hat{z} \omega_r^2 + \hat{\rho} \hat{z} \omega_\theta^2}_{\text{Centrifugal}} \end{aligned} \quad (4.75)$$

### 4.3.2.2 Arbitrary Rotation

The non-inertial momentum equation for variable, pure rotation in compressible flow was derived in Chapter 3, Equation 3.169:

$$\frac{\partial \hat{\rho} \hat{\mathbf{u}}}{\partial t} + \hat{\nabla} \cdot (\hat{\rho} \hat{\mathbf{u}} \otimes \hat{\mathbf{u}}) = -\hat{\nabla} \hat{p} + \hat{\nabla} \cdot [\hat{\mu}(\hat{\nabla} \hat{\mathbf{u}} + \hat{\nabla} \hat{\mathbf{u}}^T) + \hat{\lambda}(\hat{\nabla} \cdot \hat{\mathbf{u}})\hat{\mathbf{I}}] + \underbrace{2\rho \hat{\mathbf{u}} \wedge \boldsymbol{\Omega}}_{\text{Coriolis}} - \underbrace{\rho \hat{\mathbf{x}} \wedge \boldsymbol{\Omega} \wedge \boldsymbol{\Omega}}_{\text{Centrifugal}} + \underbrace{\rho \hat{\mathbf{x}} \wedge \dot{\boldsymbol{\Omega}}}_{\text{Euler}} \quad (4.76)$$

Again the stress components are determined by the compressible stress tensor (Equation 4.43) and by also using Equations 4.60, 4.61 and 4.62 (providing the formulation for variable, pure rotation in incompressible flow) the component form of the compressible momentum equation in Cylindrical coordinates are determined;

**r-momentum:**

$$\begin{aligned} \frac{\partial \hat{\rho} \hat{u}_r}{\partial t} + \hat{u}_r \frac{\partial \hat{\rho} \hat{u}_r}{\partial \hat{r}} + \frac{\hat{u}_\theta}{\hat{r}} \frac{\partial \hat{\rho} \hat{u}_r}{\partial \hat{\theta}} - \frac{\hat{\rho} \hat{u}_\theta^2}{\hat{r}} + \hat{u}_z \frac{\partial \hat{\rho} \hat{u}_r}{\partial \hat{z}} = -\frac{\partial \hat{p}}{\partial \hat{r}} \\ + \frac{\partial}{\partial \hat{r}} \left[ 2\hat{\mu} \frac{\partial \hat{u}_r}{\partial \hat{r}} + \hat{\lambda} \hat{\nabla} \cdot \hat{\mathbf{u}} \right] + \frac{\partial}{\partial \hat{\theta}} \left[ \hat{\mu} \left( \frac{1}{\hat{r}} \frac{\partial \hat{u}_r}{\partial \hat{\theta}} - \frac{\hat{u}_\theta}{\hat{r}} + \frac{\partial \hat{u}_\theta}{\partial \hat{r}} \right) \right] + \frac{\partial}{\partial \hat{z}} \left[ \hat{\mu} \left( \frac{\partial \hat{u}_r}{\partial \hat{z}} + \frac{\partial \hat{u}_z}{\partial \hat{r}} \right) \right] \\ + \underbrace{2\hat{\rho} \hat{u}_\theta \omega_z - 2\hat{\rho} \hat{u}_z \omega_\theta}_{\text{Coriolis}} - \underbrace{\hat{\rho} \hat{z} \omega_r \omega_z + \hat{\rho} \hat{r} \omega_z^2 + \hat{\rho} \hat{r} \omega_\theta^2}_{\text{Centrifugal}} - \underbrace{\hat{\rho} \hat{z} \dot{\omega}_\theta}_{\text{Euler}} \end{aligned} \quad (4.77)$$

**$\hat{\theta}$ -momentum**

$$\begin{aligned} \frac{\partial \hat{\rho} \hat{u}_\theta}{\partial t} + \hat{u}_r \frac{\partial \hat{\rho} \hat{u}_\theta}{\partial \hat{r}} + \frac{\hat{u}_\theta}{\hat{r}} \frac{\partial \hat{\rho} \hat{u}_\theta}{\partial \hat{\theta}} + \frac{\hat{\rho} \hat{u}_\theta \hat{u}_r}{\hat{r}} + \hat{u}_z \frac{\partial \hat{\rho} \hat{u}_\theta}{\partial \hat{z}} = -\frac{1}{\hat{r}} \frac{\partial \hat{p}}{\partial \hat{\theta}} \\ + \frac{\partial}{\partial \hat{r}} \left[ \hat{\mu} \left( \frac{1}{\hat{r}} \frac{\partial \hat{u}_r}{\partial \hat{\theta}} - \frac{\hat{u}_\theta}{\hat{r}} + \frac{\partial \hat{u}_\theta}{\partial \hat{r}} \right) \right] + \frac{\partial}{\partial \hat{\theta}} \left[ 2\hat{\mu} \left( \frac{1}{\hat{r}} \frac{\partial \hat{u}_\theta}{\partial \hat{\theta}} + \frac{\hat{u}_r}{\hat{r}} \right) + \hat{\lambda} \hat{\nabla} \cdot \hat{\mathbf{u}} \right] + \frac{\partial}{\partial \hat{z}} \left[ \hat{\mu} \left( \frac{1}{\hat{r}} \frac{\partial \hat{u}_z}{\partial \hat{\theta}} + \frac{\partial \hat{u}_\theta}{\partial \hat{z}} \right) \right] \\ + \underbrace{2\hat{\rho} \hat{u}_z \omega_r - 2\hat{\rho} \hat{u}_r \omega_z}_{\text{Coriolis}} - \underbrace{\hat{\rho} \hat{r} \omega_r \omega_\theta - \hat{\rho} \hat{z} \omega_\theta \omega_z}_{\text{Centrifugal}} + \underbrace{\hat{\rho} \hat{z} \dot{\omega}_r - \hat{\rho} \hat{r} \dot{\omega}_z}_{\text{Euler}} \end{aligned} \quad (4.78)$$

**$\hat{z}$ -momentum**

$$\begin{aligned} \frac{\partial \hat{\rho} \hat{u}_z}{\partial t} + \hat{u}_r \frac{\partial \hat{\rho} \hat{u}_z}{\partial \hat{r}} + \frac{\hat{u}_\theta}{\hat{r}} \frac{\partial \hat{\rho} \hat{u}_z}{\partial \hat{\theta}} + \hat{u}_z \frac{\partial \hat{\rho} \hat{u}_z}{\partial \hat{z}} = -\frac{\partial \hat{p}}{\partial \hat{z}} \\ + \frac{\partial}{\partial \hat{r}} \left[ \hat{\mu} \left( \frac{\partial \hat{u}_r}{\partial \hat{z}} + \frac{\partial \hat{u}_z}{\partial \hat{r}} \right) \right] + \frac{\partial}{\partial \hat{\theta}} \left[ \hat{\mu} \left( \frac{1}{\hat{r}} \frac{\partial \hat{u}_z}{\partial \hat{\theta}} + \frac{\partial \hat{u}_\theta}{\partial \hat{z}} \right) \right] + \frac{\partial}{\partial \hat{z}} \left[ 2\hat{\mu} \frac{\partial \hat{u}_z}{\partial \hat{z}} + \hat{\lambda} \hat{\nabla} \cdot \hat{\mathbf{u}} \right] \\ + \underbrace{2\hat{\rho} \hat{u}_r \omega_\theta - 2\hat{\rho} \hat{u}_\theta \omega_r}_{\text{Coriolis}} - \underbrace{\hat{\rho} \hat{r} \omega_r \omega_z + \hat{\rho} \hat{z} \omega_r^2 + \hat{\rho} \hat{z} \omega_\theta^2}_{\text{Centrifugal}} + \underbrace{\hat{\rho} \hat{r} \dot{\omega}_\theta}_{\text{Euler}} \end{aligned} \quad (4.79)$$



### 4.3. NON-INERTIAL NAVIER-STOKES EQUATIONS IN CYLINDRICAL COORDINATES

In fully arbitrary rotation, *Chapter 3* has established that the non-inertial momentum equation in compressible flow takes the form:

$$\frac{\partial \hat{\rho} \hat{\mathbf{u}}}{\partial t} + \hat{\nabla} \cdot (\hat{\rho} \hat{\mathbf{u}} \otimes \hat{\mathbf{u}}) = -\hat{\nabla} \hat{p} + \hat{\nabla} \cdot [\hat{\mu}(\hat{\nabla} \hat{\mathbf{u}} + \hat{\nabla} \hat{\mathbf{u}}^T) + \hat{\lambda}(\hat{\nabla} \cdot \hat{\mathbf{u}}) \hat{\mathbf{I}}] + \underbrace{2\rho \hat{\mathbf{u}} \wedge \boldsymbol{\Omega}}_{\text{Coriolis}} - \underbrace{\rho \hat{\mathbf{x}} \wedge \boldsymbol{\Omega} \wedge \boldsymbol{\Omega}}_{\text{Centrifugal}} + \underbrace{\rho \hat{\mathbf{x}} \wedge \dot{\boldsymbol{\Omega}}}_{\text{Euler}} + \underbrace{\rho \hat{\mathbf{x}} \wedge \boldsymbol{\Omega}}_{\text{Unpure Rot}} \quad (4.80)$$

As an extension of *Equations 4.77, 4.78 and 4.79* above, as well as the formulation for the fictitious forces in *Section 4.3.1.2*, the Cylindrical formulation for the arbitrary rotation case becomes;

#### $\hat{r}$ -momentum

$$\begin{aligned} \frac{\partial \hat{\rho} \hat{u}_r}{\partial t} + \hat{u}_r \frac{\partial \hat{\rho} \hat{u}_r}{\partial \hat{r}} + \frac{\hat{u}_\theta}{\hat{r}} \frac{\partial \hat{\rho} \hat{u}_r}{\partial \hat{\theta}} - \frac{\hat{\rho} \hat{u}_\theta^2}{\hat{r}} + \hat{u}_z \frac{\partial \hat{\rho} \hat{u}_r}{\partial \hat{z}} = -\frac{\partial \hat{p}}{\partial \hat{r}} \\ + \frac{\partial}{\partial \hat{r}} \left[ 2\hat{\mu} \frac{\partial \hat{u}_r}{\partial \hat{r}} + \hat{\lambda} \hat{\nabla} \cdot \hat{\mathbf{u}} \right] + \frac{\partial}{\partial \hat{\theta}} \left[ \hat{\mu} \left( \frac{1}{\hat{r}} \frac{\partial \hat{u}_r}{\partial \hat{\theta}} - \frac{\hat{u}_\theta}{\hat{r}} + \frac{\partial \hat{u}_\theta}{\partial \hat{r}} \right) \right] + \frac{\partial}{\partial \hat{z}} \left[ \hat{\mu} \left( \frac{\partial \hat{u}_r}{\partial \hat{z}} + \frac{\partial \hat{u}_z}{\partial \hat{r}} \right) \right] \\ + \underbrace{2\hat{\rho} \hat{u}_\theta \omega_z - 2\hat{\rho} \hat{u}_z \omega_\theta}_{\text{Coriolis}} - \underbrace{\hat{\rho} \hat{z} \omega_r \omega_z + \hat{\rho} \hat{r} \omega_z^2 + \hat{\rho} \hat{r} \omega_\theta^2}_{\text{Centrifugal}} \\ - \underbrace{\hat{\rho} \hat{z} \dot{\omega}_\theta}_{\text{Euler}} + \underbrace{\hat{\rho} \hat{u}_\theta \omega_z - \hat{\rho} \hat{u}_z \omega_\theta}_{\text{Arbitrary Rotation}} \end{aligned} \quad (4.81)$$

#### $\hat{\theta}$ -momentum

$$\begin{aligned} \frac{\partial \hat{\rho} \hat{u}_\theta}{\partial t} + \hat{u}_r \frac{\partial \hat{\rho} \hat{u}_\theta}{\partial \hat{r}} + \frac{\hat{u}_\theta}{\hat{r}} \frac{\partial \hat{u}_\theta}{\partial \hat{\theta}} + \frac{\hat{\rho} \hat{u}_\theta \hat{u}_r}{\hat{r}} + \hat{u}_z \frac{\partial \hat{\rho} \hat{u}_\theta}{\partial \hat{z}} = -\frac{1}{\hat{r}} \frac{\partial \hat{p}}{\partial \hat{\theta}} \\ + \frac{\partial}{\partial \hat{r}} \left[ \hat{\mu} \left( \frac{1}{\hat{r}} \frac{\partial \hat{u}_r}{\partial \hat{\theta}} - \frac{\hat{u}_\theta}{\hat{r}} + \frac{\partial \hat{u}_\theta}{\partial \hat{r}} \right) \right] + \frac{\partial}{\partial \hat{\theta}} \left[ 2\hat{\mu} \left( \frac{1}{\hat{r}} \frac{\partial \hat{u}_\theta}{\partial \hat{\theta}} + \frac{\hat{u}_r}{\hat{r}} \right) + \hat{\lambda} \hat{\nabla} \cdot \hat{\mathbf{u}} \right] + \frac{\partial}{\partial \hat{z}} \left[ \hat{\mu} \left( \frac{1}{\hat{r}} \frac{\partial \hat{u}_z}{\partial \hat{\theta}} + \frac{\partial \hat{u}_\theta}{\partial \hat{z}} \right) \right] \\ + \underbrace{2\hat{\rho} \hat{u}_z \omega_r - 2\hat{\rho} \hat{u}_r \omega_z}_{\text{Coriolis}} - \underbrace{\hat{\rho} \hat{r} \omega_r \omega_\theta - \hat{\rho} \hat{z} \omega_\theta \omega_z}_{\text{Centrifugal}} \\ + \underbrace{\hat{\rho} \hat{z} \dot{\omega}_r - \hat{\rho} \hat{r} \dot{\omega}_z}_{\text{Euler}} + \underbrace{\hat{\rho} \hat{u}_z \omega_r - \hat{\rho} \hat{u}_r \omega_z}_{\text{Arbitrary Rotation}} \end{aligned} \quad (4.82)$$

#### $\hat{z}$ -momentum

$$\begin{aligned} \frac{\partial \hat{\rho} \hat{u}_z}{\partial t} + \hat{u}_r \frac{\partial \hat{\rho} \hat{u}_z}{\partial \hat{r}} + \frac{\hat{u}_\theta}{\hat{r}} \frac{\partial \hat{\rho} \hat{u}_z}{\partial \hat{\theta}} + \hat{u}_z \frac{\partial \hat{\rho} \hat{u}_z}{\partial \hat{z}} = -\frac{\partial \hat{p}}{\partial \hat{z}} \\ + \frac{\partial}{\partial \hat{r}} \left[ \hat{\mu} \left( \frac{\partial \hat{u}_r}{\partial \hat{z}} + \frac{\partial \hat{u}_z}{\partial \hat{r}} \right) \right] + \frac{\partial}{\partial \hat{\theta}} \left[ \hat{\mu} \left( \frac{1}{\hat{r}} \frac{\partial \hat{u}_z}{\partial \hat{\theta}} + \frac{\partial \hat{u}_\theta}{\partial \hat{z}} \right) \right] + \frac{\partial}{\partial \hat{z}} \left[ 2\hat{\mu} \frac{\partial \hat{u}_z}{\partial \hat{z}} + \hat{\lambda} \hat{\nabla} \cdot \hat{\mathbf{u}} \right] \\ + \underbrace{2\hat{\rho} \hat{u}_r \omega_\theta - 2\hat{\rho} \hat{u}_\theta \omega_r}_{\text{Coriolis}} - \underbrace{\hat{\rho} \hat{r} \omega_r \omega_z + \hat{\rho} \hat{z} \omega_r^2 + \hat{\rho} \hat{z} \omega_\theta^2}_{\text{Centrifugal}} \\ + \underbrace{\hat{\rho} \hat{r} \dot{\omega}_\theta}_{\text{Euler}} + \underbrace{\hat{\rho} \hat{u}_r \omega_\theta - \hat{\rho} \hat{u}_\theta \omega_r}_{\text{Arbitrary Rotation}} \end{aligned} \quad (4.83)$$

### 4.3.2.3 Arbitrary Acceleration

In *Chapter 3, Equation 3.227* the non-inertial momentum equation for arbitrary acceleration in compressible conditions has been derived:

$$\begin{aligned} \frac{\partial \hat{\rho} \hat{\mathbf{u}}}{\partial t} + \hat{\nabla} \cdot (\hat{\rho} \hat{\mathbf{u}} \otimes \hat{\mathbf{u}}) = & -\hat{\nabla} \hat{p} + \hat{\nabla} \cdot [\hat{\mu}(\hat{\nabla} \hat{\mathbf{u}} + \hat{\nabla} \hat{\mathbf{u}}^T) + \hat{\lambda}(\hat{\nabla} \cdot \hat{\mathbf{u}}) \hat{\mathbf{I}}] \\ & + \underbrace{2\rho \hat{\mathbf{u}} \wedge \boldsymbol{\Omega}}_{\text{Coriolis}} - \underbrace{\rho \hat{\mathbf{x}} \wedge \boldsymbol{\Omega} \wedge \boldsymbol{\Omega}}_{\text{Centrifugal}} + \underbrace{\rho \hat{\mathbf{x}} \wedge \dot{\boldsymbol{\Omega}} + \rho \hat{\mathbf{x}} \wedge \boldsymbol{\Omega}}_{\text{Euler}} + \underbrace{2\rho \mathbf{V}(t) \wedge \boldsymbol{\Omega}}_{\text{Magnus}} - \underbrace{\frac{\partial}{\partial t}(\rho \mathbf{V}(t))}_{\text{Translation}} \end{aligned} \quad (4.84)$$

Unsteady motion

The stress components are determined by the compressible stress tensor in *Equation 4.43* and by also using *Equations 4.69, 4.70* and *4.71* (providing the formulation for arbitrary in incompressible flow) the component form of the compressible momentum equation in Cylindrical coordinates are determined;

#### $\hat{r}$ -momentum

$$\begin{aligned} \frac{\partial \hat{\rho} \hat{u}_r}{\partial t} + \hat{u}_r \frac{\partial \hat{\rho} \hat{u}_r}{\partial \hat{r}} + \frac{\hat{u}_\theta}{\hat{r}} \frac{\partial \hat{\rho} \hat{u}_r}{\partial \hat{\theta}} - \frac{\hat{\rho} \hat{u}_\theta^2}{\hat{r}} + \hat{u}_z \frac{\partial \hat{\rho} \hat{u}_r}{\partial \hat{z}} = & -\frac{\partial \hat{p}}{\partial \hat{r}} \\ & + \frac{\partial}{\partial \hat{r}} \left[ 2\hat{\mu} \frac{\partial \hat{u}_r}{\partial \hat{r}} + \hat{\lambda} \hat{\nabla} \cdot \hat{\mathbf{u}} \right] + \frac{\partial}{\partial \hat{\theta}} \left[ \hat{\mu} \left( \frac{1}{\hat{r}} \frac{\partial \hat{u}_r}{\partial \hat{\theta}} - \frac{\hat{u}_\theta}{\hat{r}} + \frac{\partial \hat{u}_\theta}{\partial \hat{r}} \right) \right] + \frac{\partial}{\partial \hat{z}} \left[ \hat{\mu} \left( \frac{\partial \hat{u}_r}{\partial \hat{z}} + \frac{\partial \hat{u}_z}{\partial \hat{r}} \right) \right] \\ & + \underbrace{2\hat{\rho} \hat{u}_\theta \omega_z - 2\hat{\rho} \hat{u}_z \omega_\theta}_{\text{Coriolis}} - \underbrace{\hat{\rho} \hat{z} \omega_r \omega_z + \hat{\rho} \hat{r} \omega_z^2 + \hat{\rho} \hat{r} \omega_\theta^2}_{\text{Centrifugal}} \\ & - \underbrace{\hat{\rho} \hat{z} \dot{\omega}_\theta}_{\text{Euler}} + \underbrace{\hat{\rho} \hat{u}_\theta \omega_z - \hat{\rho} \hat{u}_z \omega_\theta}_{\text{Arbitrary Rotation}} + \underbrace{2\hat{\rho} V_\theta \omega_z - 2\hat{\rho} V_z \omega_\theta}_{\text{Magnus}} - \underbrace{\frac{\partial \hat{\rho} V_r}{\partial t}}_{\text{Unsteady Translation}} \end{aligned} \quad (4.85)$$

#### $\hat{\theta}$ -momentum

$$\begin{aligned} \frac{\partial \hat{\rho} \hat{u}_\theta}{\partial t} + \hat{u}_r \frac{\partial \hat{\rho} \hat{u}_\theta}{\partial \hat{r}} + \frac{\hat{u}_\theta}{\hat{r}} \frac{\partial \hat{\rho} \hat{u}_\theta}{\partial \hat{\theta}} + \frac{\hat{\rho} \hat{u}_\theta \hat{u}_r}{\hat{r}} + \hat{u}_z \frac{\partial \hat{\rho} \hat{u}_\theta}{\partial \hat{z}} = & -\frac{1}{\hat{r}} \frac{\partial \hat{p}}{\partial \hat{\theta}} \\ & + \frac{\partial}{\partial \hat{r}} \left[ \hat{\mu} \left( \frac{1}{\hat{r}} \frac{\partial \hat{u}_r}{\partial \hat{\theta}} - \frac{\hat{u}_\theta}{\hat{r}} + \frac{\partial \hat{u}_\theta}{\partial \hat{r}} \right) \right] + \frac{\partial}{\partial \hat{\theta}} \left[ 2\hat{\mu} \left( \frac{1}{\hat{r}} \frac{\partial \hat{u}_\theta}{\partial \hat{\theta}} + \frac{\hat{u}_r}{\hat{r}} \right) + \hat{\lambda} \hat{\nabla} \cdot \hat{\mathbf{u}} \right] + \frac{\partial}{\partial \hat{z}} \left[ \hat{\mu} \left( \frac{1}{\hat{r}} \frac{\partial \hat{u}_z}{\partial \hat{\theta}} + \frac{\partial \hat{u}_\theta}{\partial \hat{z}} \right) \right] \\ & + \underbrace{2\hat{\rho} \hat{u}_z \omega_r - 2\hat{\rho} \hat{u}_r \omega_z}_{\text{Coriolis}} - \underbrace{\hat{\rho} \hat{r} \omega_r \omega_\theta - \hat{\rho} \hat{z} \omega_\theta \omega_z}_{\text{Centrifugal}} \\ & + \underbrace{\hat{\rho} \hat{z} \dot{\omega}_r - \hat{\rho} \hat{r} \dot{\omega}_z}_{\text{Euler}} + \underbrace{\hat{\rho} \hat{u}_z \omega_r - \hat{\rho} \hat{u}_r \omega_z}_{\text{Arbitrary Rotation}} + \underbrace{2\hat{\rho} V_z \omega_r - 2\hat{\rho} V_r \omega_z}_{\text{Magnus}} - \underbrace{\frac{\partial \hat{\rho} V_\theta}{\partial t}}_{\text{Unsteady Translation}} \end{aligned} \quad (4.86)$$



4.3. NON-INERTIAL NAVIER-STOKES EQUATIONS IN CYLINDRICAL COORDINATES

**$\hat{z}$ -momentum**

$$\begin{aligned}
\frac{\partial \hat{\rho} \hat{u}_z}{\partial t} + \hat{u}_r \frac{\partial \hat{\rho} \hat{u}_z}{\partial \hat{r}} + \frac{\hat{u}_\theta}{\hat{r}} \frac{\partial \hat{\rho} \hat{u}_z}{\partial \hat{\theta}} + \hat{u}_z \frac{\partial \hat{\rho} \hat{u}_z}{\partial \hat{z}} &= - \frac{\partial \hat{p}}{\partial \hat{z}} \\
+ \frac{\partial}{\partial \hat{r}} \left[ \hat{\mu} \left( \frac{\partial \hat{u}_r}{\partial \hat{z}} + \frac{\partial \hat{u}_z}{\partial \hat{r}} \right) \right] + \frac{\partial}{\partial \hat{\theta}} \left[ \hat{\mu} \left( \frac{1}{\hat{r}} \frac{\partial \hat{u}_z}{\partial \hat{\theta}} + \frac{\partial \hat{u}_\theta}{\partial \hat{z}} \right) \right] + \frac{\partial}{\partial \hat{z}} \left[ 2\hat{\mu} \frac{\partial \hat{\omega}}{\partial \hat{z}} + \hat{\lambda} \hat{\nabla} \cdot \hat{\mathbf{u}} \right] \\
+ \underbrace{2\hat{\rho} \hat{u}_r \omega_\theta - 2\hat{\rho} \hat{u}_\theta \omega_r}_{\text{Coriolis}} - \underbrace{\hat{\rho} \hat{r} \omega_r \omega_z + \hat{\rho} \hat{z} \omega_r^2 + \hat{\rho} \hat{z} \omega_\theta^2}_{\text{Centrifugal}} & \tag{4.87} \\
+ \underbrace{\hat{\rho} \hat{r} \dot{\omega}_\theta}_{\text{Euler}} + \underbrace{\hat{\rho} \hat{u}_r \omega_\theta - \hat{\rho} \hat{u}_\theta \omega_r}_{\text{Arbitrary Rotation}} + \underbrace{2\hat{\rho} V_r \omega_\theta - 2\hat{\rho} V_\theta \omega_r}_{\text{Magnus}} - \underbrace{\frac{\partial \hat{\rho} V_z}{\partial t}}_{\text{Unsteady Translation}}
\end{aligned}$$

## 4.4 Non-Inertial Equations in Curvilinear Coordinates

### 4.4.1 Vector Operation in Curvilinear Systems

An orthogonal curvilinear system is the most general form in which a set of equations can be written. The Cartesian, Cylindrical and Spherical coordinate systems are special cases of the orthogonal curvilinear system. A set of equations in the curvilinear system can be transformed to any of the above mentioned systems by using the table below as shown in Griffiths [72] and Williams [73]:

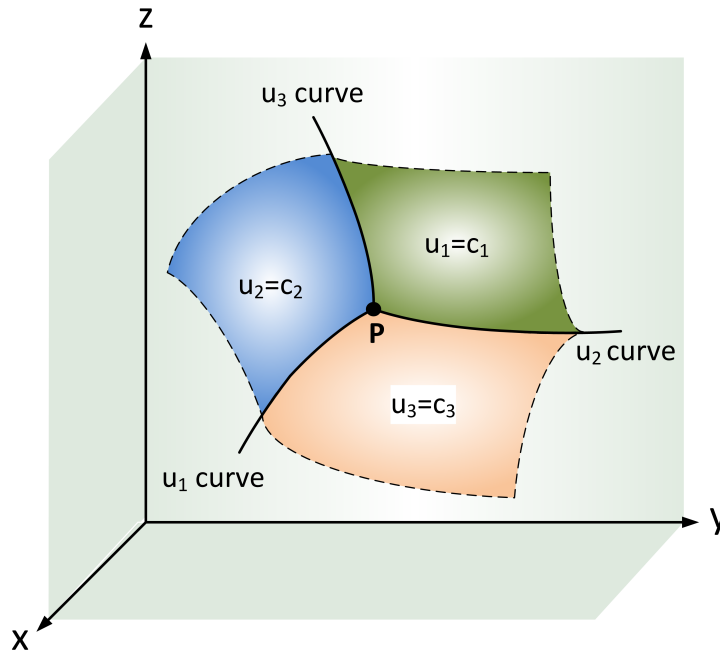
Table 4.1: Relations between the Curvilinear Coordinate System and Other Systems

Curvilinear	$u_1$	$u_2$	$u_3$	$x$	$y$	$z$	$h_1$	$h_2$	$h_3$
Cartesian	$x$	$y$	$z$	$x$	$y$	$z$	1	1	1
Cylindrical	$r$	$\theta$	$z$	$r\cos\theta$	$r\sin\theta$	$z$	1	$r$	1
Spherical	$r$	$\theta$	$\phi$	$r\sin\theta\cos\phi$	$r\sin\theta\sin\phi$	$r\cos\theta$	1	$r$	$r\sin\theta$

Consider a geometry (Figure 4.5) that consists of three surfaces,  $f_1, f_2$  and  $f_3$ . These are defined in the Cartesian system and is related to the coordinates surfaces in the following manner:

$$f_1(x, y, z) = u_1, \quad f_2(x, y, z) = u_2, \quad f_3(x, y, z) = u_3 \quad (4.88)$$

Figure 4.5: Co-ordinate Surfaces and Intersection Coordinate Curve Lines at Point P



The surfaces intersect at a point P. It is from this point that the curvilinear system are described.

4.4. NON-INERTIAL EQUATIONS IN CURVILINEAR COORDINATES

The coordinates surfaces,  $u_1, u_2$  and  $u_3$ , remain constant at a given time step. The surfaces intersect each other at the intersection coordinate curves,  $u_1$  curve,  $u_2$  curve and  $u_3$  curve which form the axes associated with point P.

$$u_1(x, y, z) = c_1, \quad u_2(x, y, z) = c_2, \quad u_3(x, y, z) = c_3 \quad (4.89)$$

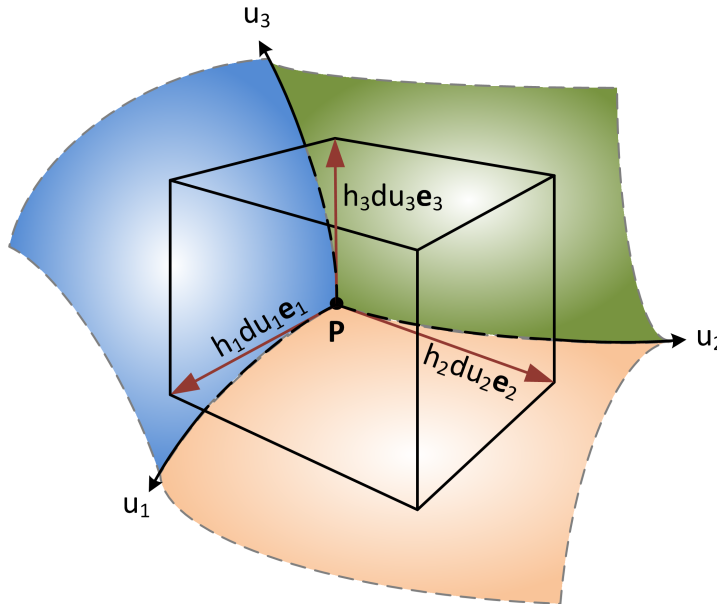
Tangential to the coordinate curves is the unit vectors  $\mathbf{e}_1, \mathbf{e}_2$  and  $\mathbf{e}_3$  that form the axes of the curvilinear system at point P. These are equivalent to the  $\mathbf{i}, \mathbf{j}$  and  $\mathbf{k}$  unit vectors in the Cartesian system. In the curvilinear system the geometry is represented by scaling factors ( $h_1, h_2, h_3$ ) that are used to characterise the surface curvatures. If the arc length between the surfaces  $u_1$  and  $u_1 + du_1$  is defined by  $dl_1$ , then the scaling factor is applied so that  $dl_1 = h_1 du_1$ . The scaling factor accounts for the curvature in the surface of the geometry and is applied in all principle directions:

$$dl_1 = h_1 du_1, \quad dl_2 = h_2 du_2, \quad dl_3 = h_3 du_3 \quad (4.90)$$

These definitions pave the way for establishment of the curvilinear finite control volume from which the equation sets for fluid motion can be derived (Figure 4.6). This leads to the definition:

$$d\mathbf{s} = h_1 du_1 \mathbf{e}_1 + h_2 du_2 \mathbf{e}_2 + h_3 du_3 \mathbf{e}_3 \quad (4.91)$$

Figure 4.6: Curvilinear Finite Control Volume



The finite control volume in the Cartesian and Cylindrical system is well known, and can be related to the Curvilinear system as shown by Griffiths [72] and using Table 4.1.

$$\begin{aligned}
 d\mathbf{s} &= dx \mathbf{i} + dy \mathbf{j} + dz \mathbf{k} \\
 d\mathbf{s} &= dr \mathbf{e}_r + r d\theta \mathbf{e}_\theta + dz \mathbf{e}_z
 \end{aligned} \quad (4.92)$$

CHAPTER 4. NON-INERTIAL EQUATIONS IN COMPONENT FORM

The vector form of the Navier-Stokes equations is independent of the coordinates systems used (White [9]). Therefore the equations can be written from the vector form into the component form of any coordinate system using the appropriate definition of the operators involved. The operator that is most generally used in computational fluid mechanics is the *del-operator* (also referred to as *nabla*) for which the mathematical symbol is  $\nabla$ . In the curvilinear system it is defined as:

$$\nabla_{Curvilinear} = \frac{1}{h_1} \frac{\partial}{\partial u_1} \mathbf{e}_1 + \frac{1}{h_2} \frac{\partial}{\partial u_2} \mathbf{e}_2 + \frac{1}{h_3} \frac{\partial}{\partial u_3} \mathbf{e}_3 \quad (4.93)$$

The relations in *Table 4.1* can be used to obtain the definition of  $\nabla$  in other coordinate systems:

$$\begin{aligned} \nabla_{Cartesian} &= \frac{\partial}{\partial x} \mathbf{i} + \frac{\partial}{\partial y} \mathbf{j} + \frac{\partial}{\partial z} \mathbf{k} \\ \nabla_{Cylindrical} &= \frac{\partial}{\partial r} \mathbf{e}_r + \frac{1}{r} \frac{\partial}{\partial \theta} \mathbf{e}_\theta + \frac{\partial}{\partial z} \mathbf{e}_z \\ \nabla_{Spherical} &= \frac{\partial}{\partial r} \mathbf{e}_r + \frac{1}{r} \frac{\partial}{\partial \theta} \mathbf{e}_\theta + \frac{1}{r \sin \theta} \frac{\partial}{\partial \phi} \mathbf{e}_\phi \end{aligned} \quad (4.94)$$

The definitions of the vector operations required in the curvilinear system are obtained from the literature (Griffiths [72], Marskar [74], Anon [75], Williams [73]). These are used in the section below to expand the vector form of the non-inertial equations into curvilinear components.

Gradient:

$$\nabla f = \frac{1}{h_1} \frac{\partial f}{\partial u_1} \mathbf{e}_1 + \frac{1}{h_2} \frac{\partial f}{\partial u_2} \mathbf{e}_2 + \frac{1}{h_3} \frac{\partial f}{\partial u_3} \mathbf{e}_3 \quad (4.95)$$

Divergence:

$$\nabla \cdot \mathbf{A} = \frac{1}{h_1 h_2 h_3} \left[ \frac{\partial}{\partial u_1} (h_2 h_3 A_1) + \frac{\partial}{\partial u_2} (h_1 h_3 A_2) + \frac{\partial}{\partial u_3} (h_1 h_2 A_3) \right] \quad (4.96)$$

Curl:

$$\nabla \wedge \mathbf{A} = \frac{1}{h_1 h_2 h_3} \begin{bmatrix} h_1 \mathbf{e}_1 & h_2 \mathbf{e}_2 & h_3 \mathbf{e}_3 \\ \frac{\partial}{\partial u_1} & \frac{\partial}{\partial u_2} & \frac{\partial}{\partial u_3} \\ h_1 A_1 & h_2 A_2 & h_3 A_3 \end{bmatrix} \quad (4.97)$$

Laplacian:

$$\nabla^2 f = \frac{1}{h_1 h_2 h_3} \left[ \frac{\partial}{\partial u_1} \left( \frac{h_2 h_3}{h_1} \frac{\partial f}{\partial u_1} \right) + \frac{\partial}{\partial u_2} \left( \frac{h_1 h_3}{h_2} \frac{\partial f}{\partial u_2} \right) + \frac{\partial}{\partial u_3} \left( \frac{h_2 h_1}{h_3} \frac{\partial f}{\partial u_3} \right) \right] \quad (4.98)$$

#### 4.4.2 Incompressible Flow Conditions

The incompressible continuity equation is obtained from Schlichting [42]:

$$\hat{\nabla} \cdot \hat{\rho} \hat{\mathbf{u}} = 0 \quad (4.99)$$

The definitions of the displacement and velocity in the non-inertial frame, using the curvilinear coordinates, are described as:

$$\hat{\mathbf{x}} = \hat{u}_1 \mathbf{e}_1 + \hat{u}_2 \mathbf{e}_2 + \hat{u}_3 \mathbf{e}_3 \quad (4.100)$$

$$\hat{\mathbf{u}} = \hat{V}_1 \mathbf{e}_1 + \hat{V}_2 \mathbf{e}_2 + \hat{V}_3 \mathbf{e}_3 \quad (4.101)$$

Using the definition above for displacement and velocity, along with the definition of the divergence in *Equation 4.96*, the curvilinear continuity equation for incompressible conditions is:

$$\frac{1}{h_1 h_2 h_3} \left[ \frac{\partial}{\partial \hat{u}_1} (h_2 h_3 \hat{V}_1) + \frac{\partial}{\partial \hat{u}_2} (h_1 h_3 \hat{V}_2) + \frac{\partial}{\partial \hat{u}_3} (h_1 h_2 \hat{V}_3) \right] = 0 \quad (4.102)$$

In *Chapter 3, Equation 3.239* the non-inertial momentum equation for arbitrary acceleration in incompressible conditions has been derived:

$$\frac{\partial \hat{\mathbf{u}}}{\partial t} + (\hat{\mathbf{u}} \cdot \hat{\nabla}) \hat{\mathbf{u}} = -\hat{\nabla} \hat{\psi} + v \hat{\nabla}^2 \hat{\mathbf{u}} + \underbrace{2 \hat{\mathbf{u}} \wedge \hat{\boldsymbol{\Omega}}}_{\text{Coriolis}} - \underbrace{\hat{\mathbf{x}} \wedge \hat{\boldsymbol{\Omega}} \wedge \hat{\boldsymbol{\Omega}}}_{\text{Centrifugal}} + \underbrace{\hat{\mathbf{x}} \wedge \dot{\hat{\boldsymbol{\Omega}}}}_{\text{Euler}} + \underbrace{\hat{\mathbf{x}} \wedge \hat{\boldsymbol{\Omega}}}_{\text{Unsteady motion}} + \underbrace{2 \mathbf{V}(t) \wedge \hat{\boldsymbol{\Omega}}}_{\text{Magnus}} - \underbrace{\frac{\partial}{\partial t} (\mathbf{V}(t))}_{\text{Translation}} \quad (4.103)$$

The curvilinear stress tensor is described in Liu et al. [76] and Kee et al. [77] and is used along with *Equation 4.96* to obtain the diffusion terms in component form.

$$\begin{aligned} \hat{\tau}_{11} &= -\hat{p} + 2\hat{\mu} \left( \frac{1}{h_1} \frac{\partial \hat{V}_1}{\partial \hat{u}_1} + \frac{\hat{V}_2}{h_1 h_2} \frac{\partial h_1}{\partial \hat{u}_2} + \frac{\hat{V}_3}{h_1 h_3} \frac{\partial h_1}{\partial \hat{u}_3} \right) + \hat{\lambda} \hat{\nabla} \cdot \hat{\mathbf{u}} \\ \hat{\tau}_{22} &= -\hat{p} + 2\hat{\mu} \left( \frac{1}{h_2} \frac{\partial \hat{V}_2}{\partial \hat{u}_2} + \frac{\hat{V}_3}{h_2 h_3} \frac{\partial h_2}{\partial \hat{u}_3} + \frac{\hat{V}_1}{h_1 h_2} \frac{\partial h_2}{\partial \hat{u}_1} \right) + \hat{\lambda} \hat{\nabla} \cdot \hat{\mathbf{u}} \\ \hat{\tau}_{33} &= -\hat{p} + 2\hat{\mu} \left( \frac{1}{h_3} \frac{\partial \hat{V}_3}{\partial \hat{u}_3} + \frac{\hat{V}_1}{h_1 h_3} \frac{\partial h_3}{\partial \hat{u}_1} + \frac{\hat{V}_2}{h_2 h_3} \frac{\partial h_3}{\partial \hat{u}_2} \right) + \hat{\lambda} \hat{\nabla} \cdot \hat{\mathbf{u}} \\ \hat{\tau}_{12} = \hat{\tau}_{21} &= \hat{\mu} \left[ \frac{h_2}{h_1} \frac{\partial}{\partial \hat{u}_1} \left( \frac{\hat{V}_2}{h_2} \right) + \frac{h_1}{h_2} \frac{\partial}{\partial \hat{u}_2} \left( \frac{\hat{V}_1}{h_1} \right) \right] \\ \hat{\tau}_{23} = \hat{\tau}_{32} &= \hat{\mu} \left[ \frac{h_3}{h_2} \frac{\partial}{\partial \hat{u}_2} \left( \frac{\hat{V}_3}{h_3} \right) + \frac{h_2}{h_3} \frac{\partial}{\partial \hat{u}_3} \left( \frac{\hat{V}_2}{h_2} \right) \right] \\ \hat{\tau}_{31} = \hat{\tau}_{13} &= \hat{\mu} \left[ \frac{h_1}{h_3} \frac{\partial}{\partial \hat{u}_3} \left( \frac{\hat{V}_1}{h_1} \right) + \frac{h_3}{h_1} \frac{\partial}{\partial \hat{u}_1} \left( \frac{\hat{V}_3}{h_3} \right) \right] \end{aligned} \quad (4.104)$$

CHAPTER 4. NON-INERTIAL EQUATIONS IN COMPONENT FORM

The non-inertial momentum equation is expanded into curvilinear components using the vector operations defined in *Section 4.4.1*. The fictitious effect terms are expressed in curvilinear coordinates and expanded as shown in *Equation 4.4*. The relative motion vectors are expressed in curvilinear coordinates:

$$\begin{aligned}\mathbf{V}(\mathbf{t}) &= V_{e_1} \mathbf{e}_1 + V_{e_2} \mathbf{e}_2 + V_{e_3} \mathbf{e}_3 \\ \boldsymbol{\Omega} &= \omega_1 \mathbf{e}_1 + \omega_2 \mathbf{e}_2 + \omega_3 \mathbf{e}_3\end{aligned}\quad (4.105)$$

The non-inertial Navier-Stokes equations for arbitrary acceleration in curvilinear components are shown below. The equations are the same as seen in Kee et al. [77], but with the addition of the fictitious terms.

**$\hat{\mathbf{u}}_1$ -momentum:**

$$\begin{aligned}& \frac{\partial \hat{V}_1}{\partial t} + \frac{\hat{V}_1}{h_1} \frac{\partial \hat{V}_1}{\partial \hat{u}_1} + \frac{\hat{V}_2}{h_2} \frac{\partial \hat{V}_1}{\partial \hat{u}_2} + \frac{\hat{V}_3}{h_3} \frac{\partial \hat{V}_1}{\partial \hat{u}_3} - \hat{V}_2 \left( \frac{\hat{V}_2}{h_1 h_2} \frac{\partial h_2}{\partial \hat{u}_1} - \frac{\hat{V}_1}{h_1 h_2} \frac{\partial h_1}{\partial \hat{u}_2} \right) + \hat{V}_3 \left( \frac{\hat{V}_1}{h_1 h_3} \frac{\partial h_1}{\partial \hat{u}_3} - \frac{\hat{V}_3}{h_1 h_3} \frac{\partial h_3}{\partial \hat{u}_1} \right) \\ &= -\frac{1}{h_1} \frac{\partial \hat{\psi}}{\partial \hat{u}_1} \\ &+ \frac{1}{h_1 h_2 h_3} \left[ \frac{\partial}{\partial \hat{u}_1} \left\{ 2\hat{v} h_2 h_3 \left( \frac{1}{h_1} \frac{\partial \hat{V}_1}{\partial \hat{u}_1} + \frac{\hat{V}_2}{h_1 h_2} \frac{\partial h_1}{\partial \hat{u}_2} + \frac{\hat{V}_3}{h_1 h_3} \frac{\partial h_1}{\partial \hat{u}_3} \right) \right\} \right. \\ &+ \frac{\partial}{\partial \hat{u}_2} \left\{ \hat{v} h_3 h_1 \left[ \frac{h_2}{h_1} \frac{\partial}{\partial \hat{u}_1} \left( \frac{\hat{V}_2}{h_2} \right) + \frac{h_1}{h_2} \frac{\partial}{\partial \hat{u}_2} \left( \frac{\hat{V}_1}{h_1} \right) \right] \right\} \\ &+ \frac{\partial}{\partial \hat{u}_3} \left\{ \hat{v} h_1 h_2 \left[ \frac{h_1}{h_3} \frac{\partial}{\partial \hat{u}_3} \left( \frac{\hat{V}_1}{h_1} \right) + \frac{h_3}{h_1} \frac{\partial}{\partial \hat{u}_1} \left( \frac{\hat{V}_3}{h_3} \right) \right] \right\} \\ &+ \frac{\hat{v}}{h_1 h_2} \left\{ \frac{h_2}{h_1} \frac{\partial}{\partial \hat{u}_1} \left( \frac{\hat{V}_2}{h_2} \right) + \frac{h_1}{h_2} \frac{\partial}{\partial \hat{u}_2} \left( \frac{\hat{V}_1}{h_1} \right) \right\} \frac{\partial h_1}{\partial \hat{u}_2} \\ &+ \frac{\hat{v}}{h_1 h_3} \left\{ \frac{h_1}{h_3} \frac{\partial}{\partial \hat{u}_3} \left( \frac{\hat{V}_1}{h_1} \right) + \frac{h_3}{h_1} \frac{\partial}{\partial \hat{u}_1} \left( \frac{\hat{V}_3}{h_3} \right) \right\} \frac{\partial h_1}{\partial \hat{u}_3} \\ &- \frac{2\hat{v}}{h_1 h_2} \left\{ \frac{1}{h_2} \frac{\partial \hat{V}_2}{\partial \hat{u}_2} + \frac{\hat{V}_3}{h_2 h_3} \frac{\partial h_2}{\partial \hat{u}_3} + \frac{\hat{V}_1}{h_1 h_2} \frac{\partial h_2}{\partial \hat{u}_1} \right\} \frac{\partial h_2}{\partial \hat{u}_1} \\ &- \frac{2\hat{v}}{h_1 h_3} \left\{ \frac{1}{h_3} \frac{\partial \hat{V}_3}{\partial \hat{u}_3} + \frac{\hat{V}_1}{h_1 h_3} \frac{\partial h_3}{\partial \hat{u}_1} + \frac{\hat{V}_2}{h_2 h_3} \frac{\partial h_3}{\partial \hat{u}_2} \right\} \frac{\partial h_3}{\partial \hat{u}_1} \\ &+ \underbrace{2\hat{V}_2 \omega_3 - 2\hat{V}_3 \omega_2}_{\text{Coriolis}} + \underbrace{\hat{u}_1 (\omega_3^2 + \omega_2^2) - \hat{u}_2 \omega_1 \omega_2 - \hat{u}_3 \omega_1 \omega_3}_{\text{Centrifugal}} \\ &+ \underbrace{\hat{u}_2 \dot{\omega}_3 - \hat{u}_3 \dot{\omega}_2 + \hat{u}_2 \omega_3 - \hat{u}_3 \omega_2}_{\text{Euler}} + \underbrace{2V_{e_2} \omega_3 - 2V_{e_3} \omega_2}_{\text{Magnus}} - \underbrace{\frac{\partial V_{e_1}}{\partial t}}_{\text{Translation}}\end{aligned}\quad (4.106)$$





4.4. NON-INERTIAL EQUATIONS IN CURVILINEAR COORDINATES

$\hat{u}_2$ -momentum:

$$\begin{aligned}
& \frac{\partial \hat{V}_2}{\partial t} + \frac{\hat{V}_1}{h_1} \frac{\partial \hat{V}_2}{\partial \hat{u}_1} + \frac{\hat{V}_2}{h_2} \frac{\partial \hat{V}_2}{\partial \hat{u}_2} + \frac{\hat{V}_3}{h_3} \frac{\partial \hat{V}_2}{\partial \hat{u}_3} - \hat{V}_3 \left( \frac{\hat{V}_3}{h_3 h_2} \frac{\partial h_3}{\partial \hat{u}_2} - \frac{\hat{V}_2}{h_2 h_3} \frac{\partial h_2}{\partial \hat{u}_3} \right) + \hat{V}_1 \left( \frac{\hat{V}_2}{h_1 h_2} \frac{\partial h_2}{\partial \hat{u}_1} - \frac{\hat{V}_1}{h_1 h_2} \frac{\partial h_1}{\partial \hat{u}_2} \right) \\
&= - \frac{1}{h_2} \frac{\partial \hat{\psi}}{\partial \hat{u}_2} \\
&+ \frac{1}{h_1 h_2 h_3} \left[ \frac{\partial}{\partial \hat{u}_1} \left\{ \hat{v} h_2 h_3 \left( \frac{h_2}{h_1} \frac{\partial}{\partial \hat{u}_1} \left( \frac{\hat{V}_2}{h_2} \right) + \frac{h_1}{h_2} \frac{\partial}{\partial \hat{u}_2} \left( \frac{\hat{V}_1}{h_1} \right) \right) \right\} \right. \\
&+ \frac{\partial}{\partial \hat{u}_2} \left\{ 2 \hat{v} h_3 h_1 \left[ \frac{1}{h_2} \frac{\partial \hat{V}_2}{\partial \hat{u}_2} + \frac{\hat{V}_3}{h_2 h_3} \frac{\partial h_2}{\partial \hat{u}_3} + \frac{\hat{V}_1}{h_1 h_2} \frac{\partial h_2}{\partial \hat{u}_1} \right] \right\} \\
&+ \left. \frac{\partial}{\partial \hat{u}_3} \left\{ \hat{v} h_1 h_2 \left[ \frac{h_3}{h_2} \frac{\partial}{\partial \hat{u}_2} \left( \frac{\hat{V}_3}{h_3} \right) + \frac{h_2}{h_3} \frac{\partial}{\partial \hat{u}_3} \left( \frac{\hat{V}_2}{h_2} \right) \right] \right\} \right] \\
&+ \frac{\hat{v}}{h_2 h_3} \left\{ \frac{h_3}{h_2} \frac{\partial}{\partial \hat{u}_2} \left( \frac{\hat{V}_3}{h_3} \right) + \frac{h_2}{h_3} \frac{\partial}{\partial \hat{u}_3} \left( \frac{\hat{V}_2}{h_2} \right) \right\} \frac{\partial h_2}{\partial \hat{u}_3} \\
&+ \frac{\hat{v}}{h_2 h_1} \left\{ \frac{h_2}{h_1} \frac{\partial}{\partial \hat{u}_1} \left( \frac{\hat{V}_2}{h_2} \right) + \frac{h_1}{h_2} \frac{\partial}{\partial \hat{u}_2} \left( \frac{\hat{V}_1}{h_1} \right) \right\} \frac{\partial h_2}{\partial \hat{u}_1} \\
&- \frac{2 \hat{v}}{h_2 h_3} \left\{ \frac{1}{h_3} \frac{\partial \hat{V}_3}{\partial \hat{u}_3} + \frac{\hat{V}_1}{h_1 h_3} \frac{\partial h_3}{\partial \hat{u}_1} + \frac{\hat{V}_2}{h_2 h_3} \frac{\partial h_3}{\partial \hat{u}_2} \right\} \frac{\partial h_3}{\partial \hat{u}_2} \\
&- \frac{2 \hat{v}}{h_2 h_1} \left\{ \frac{1}{h_1} \frac{\partial \hat{V}_1}{\partial \hat{u}_1} + \frac{\hat{V}_2}{h_1 h_2} \frac{\partial h_1}{\partial \hat{u}_2} + \frac{\hat{V}_3}{h_1 h_3} \frac{\partial h_1}{\partial \hat{u}_3} \right\} \frac{\partial h_1}{\partial \hat{u}_2} \\
&+ \underbrace{2 \hat{V}_3 \omega_1 - 2 \hat{V}_1 \omega_3}_{\text{Coriolis}} + \underbrace{\hat{u}_2 (\omega_3^2 + \omega_1^2) - \hat{u}_1 \omega_1 \omega_2 - \hat{u}_3 \omega_2 \omega_3}_{\text{Centrifugal}} \\
&+ \underbrace{\hat{u}_3 \dot{\omega}_1 - \hat{u}_1 \dot{\omega}_3 + \hat{u}_3 \omega_1 - \hat{u}_1 \omega_3}_{\text{Euler}} + \underbrace{2 V_{e_3} \omega_1 - 2 V_{e_1} \omega_3}_{\text{Magnus}} - \underbrace{\frac{\partial V_{e_1}}{\partial t}}_{\text{Translation}}
\end{aligned}
\tag{4.107}$$

**$\hat{\mathbf{u}}_3$ -momentum:**

$$\begin{aligned}
& \frac{\partial \hat{V}_3}{\partial t} + \frac{\hat{V}_1}{h_1} \frac{\partial \hat{V}_3}{\partial \hat{u}_1} + \frac{\hat{V}_2}{h_2} \frac{\partial \hat{V}_3}{\partial \hat{u}_2} + \frac{\hat{V}_3}{h_3} \frac{\partial \hat{V}_3}{\partial \hat{u}_3} - \hat{V}_1 \left( \frac{\hat{V}_1}{h_1 h_3} \frac{\partial h_1}{\partial \hat{u}_3} - \frac{\hat{V}_3}{h_1 h_3} \frac{\partial h_3}{\partial \hat{u}_1} \right) + \hat{V}_2 \left( \frac{\hat{V}_3}{h_2 h_3} \frac{\partial h_2}{\partial \hat{u}_1} - \frac{\hat{V}_2}{h_2 h_3} \frac{\partial h_2}{\partial \hat{u}_3} \right) \\
&= -\frac{1}{h_1} \frac{\partial \hat{\psi}}{\partial \hat{u}_3} \\
&+ \frac{1}{h_1 h_2 h_3} \left[ \frac{\partial}{\partial \hat{u}_1} \left\{ \hat{v} h_2 h_3 \left( \frac{h_1}{h_3} \frac{\partial}{\partial \hat{u}_3} \left( \frac{\hat{V}_1}{h_1} \right) + \frac{h_3}{h_1} \frac{\partial}{\partial u_1} \left( \frac{\hat{V}_3}{h_3} \right) \right) \right\} \right. \\
&+ \frac{\partial}{\partial \hat{u}_2} \left\{ \hat{v} h_3 h_1 \left[ \frac{h_3}{h_2} \frac{\partial}{\partial \hat{u}_2} \left( \frac{\hat{V}_3}{h_3} \right) + \frac{h_2}{h_3} \frac{\partial}{\partial \hat{u}_3} \left( \frac{\hat{V}_2}{h_2} \right) \right] \right\} \\
&+ \left. \frac{\partial}{\partial \hat{u}_3} \left\{ 2 \hat{v} h_1 h_2 \left[ \frac{1}{h_3} \frac{\partial \hat{V}_3}{\partial \hat{u}_3} + \frac{\hat{V}_1}{h_1 h_3} \frac{\partial h_3}{\partial \hat{u}_1} + \frac{\hat{V}_2}{h_2 h_3} \frac{\partial h_3}{\partial \hat{u}_2} \right] \right\} \right] \\
&+ \frac{\hat{v}}{h_1 h_3} \left\{ \frac{h_1}{h_3} \frac{\partial}{\partial \hat{u}_3} \left( \frac{\hat{V}_1}{h_1} \right) + \frac{h_3}{h_1} \frac{\partial}{\partial u_1} \left( \frac{\hat{V}_3}{h_3} \right) \right\} \frac{\partial h_3}{\partial \hat{u}_1} \\
&+ \frac{\hat{v}}{h_2 h_3} \left\{ \frac{h_3}{h_2} \frac{\partial}{\partial \hat{u}_2} \left( \frac{\hat{V}_3}{h_3} \right) + \frac{h_2}{h_3} \frac{\partial}{\partial \hat{u}_3} \left( \frac{\hat{V}_2}{h_2} \right) \right\} \frac{\partial h_3}{\partial \hat{u}_2} \\
&- \frac{2 \hat{v}}{h_1 h_3} \left\{ \frac{1}{h_1} \frac{\partial \hat{V}_1}{\partial \hat{u}_1} + \frac{\hat{V}_2}{h_1 h_2} \frac{\partial h_1}{\partial \hat{u}_2} + \frac{\hat{V}_3}{h_1 h_3} \frac{\partial h_1}{\partial \hat{u}_3} \right\} \frac{\partial h_1}{\partial \hat{u}_3} \\
&- \frac{2 \hat{v}}{h_2 h_3} \left\{ \frac{1}{h_2} \frac{\partial \hat{V}_2}{\partial \hat{u}_2} + \frac{\hat{V}_3}{h_2 h_3} \frac{\partial h_2}{\partial \hat{u}_3} + \frac{\hat{V}_1}{h_1 h_2} \frac{\partial h_2}{\partial \hat{u}_1} \right\} \frac{\partial h_2}{\partial \hat{u}_3} \\
&+ \underbrace{2 \hat{V}_1 \omega_2 - 2 \hat{V}_2 \omega_1}_{\text{Coriolis}} + \underbrace{\hat{u}_3 (\omega_2^2 + \omega_1^2) - \hat{u}_1 \omega_1 \omega_3 - \hat{u}_2 \omega_1 \omega_3}_{\text{Centrifugal}} \\
&+ \underbrace{\hat{u}_1 \omega_2 - \hat{u}_2 \omega_1 + \hat{u}_1 \omega_2 - \hat{u}_2 \omega_1}_{\text{Euler}} + \underbrace{2 V_{e_1} \omega_2 - 2 V_{e_2} \omega_1}_{\text{Magnus}} - \underbrace{\frac{\partial V_{e_3}}{\partial t}}_{\text{Translation}}
\end{aligned} \tag{4.108}$$

### 4.4.3 Compressible Flow Conditions

Equation 4.8 defines the compressible continuity equation.

$$\frac{\partial \hat{\rho}}{\partial t} + (\hat{\nabla} \cdot \hat{\rho} \hat{\mathbf{u}}) = 0 \tag{4.109}$$

In a similar manner as shown in the previous section, the curvilinear continuity equation in compressible flow becomes:

$$\frac{\partial \hat{\rho}}{\partial t} + \frac{\hat{V}_1}{h_1} \frac{\partial \hat{\rho}}{\partial \hat{u}_1} + \frac{\hat{V}_2}{h_2} \frac{\partial \hat{\rho}}{\partial \hat{u}_2} + \frac{\hat{V}_3}{h_3} \frac{\partial \hat{\rho}}{\partial \hat{u}_3} + \frac{\hat{\rho}}{h_1 h_2 h_3} \left[ \frac{\partial}{\partial \hat{u}_1} (h_2 h_3 \hat{V}_1) + \frac{\partial}{\partial \hat{u}_2} (h_1 h_3 \hat{V}_2) + \frac{\partial}{\partial \hat{u}_3} (h_1 h_2 \hat{V}_3) \right] = 0 \tag{4.110}$$

4.4. NON-INERTIAL EQUATIONS IN CURVILINEAR COORDINATES

The compressible conservation of momentum equation was determined in *Chapter 3, Equation 3.227* :

$$\begin{aligned} \frac{\partial \hat{\rho} \hat{\mathbf{u}}}{\partial t} + \hat{\nabla} \cdot (\hat{\rho} \hat{\mathbf{u}} \otimes \hat{\mathbf{u}}) = & -\hat{\nabla} \hat{p} + \overbrace{\hat{\nabla} \cdot [\hat{\rho}(\hat{\nabla} \hat{\mathbf{u}} + \hat{\nabla} \hat{\mathbf{u}}^T)] + \hat{\lambda}(\hat{\nabla} \cdot \hat{\mathbf{u}}) \hat{\mathbf{I}}}^{\text{Deviatoric stress}} \\ & + \underbrace{2\rho \hat{\mathbf{u}} \wedge \boldsymbol{\Omega}}_{\text{Coriolis}} - \underbrace{\rho \hat{\mathbf{x}} \wedge \boldsymbol{\Omega} \wedge \boldsymbol{\Omega}}_{\text{Centrifugal}} + \underbrace{\rho \hat{\mathbf{x}} \wedge \dot{\boldsymbol{\Omega}} + \rho \hat{\mathbf{x}} \wedge \boldsymbol{\Omega}}_{\text{Euler}} + \underbrace{2\rho \mathbf{V}(t) \wedge \boldsymbol{\Omega}}_{\text{Magnus}} - \underbrace{\frac{\partial}{\partial t}(\rho \mathbf{V}(t))}_{\text{Translation}} \end{aligned} \quad (4.111)$$

Unsteady motion

Using the methodology of *Section 4.4.2*, the curvilinear component form is obtained. This corresponds with the formulations for Kee et al. [77], with the addition of the fictitious terms.

**$\hat{\mathbf{u}}_1$ -momentum:**

$$\begin{aligned} \hat{\rho} \left[ \frac{\partial \hat{V}_1}{\partial t} + \frac{\hat{V}_1}{h_1} \frac{\partial \hat{V}_1}{\partial \hat{u}_1} + \frac{\hat{V}_2}{h_2} \frac{\partial \hat{V}_1}{\partial \hat{u}_2} + \frac{\hat{V}_3}{h_3} \frac{\partial \hat{V}_1}{\partial \hat{u}_3} - \hat{V}_2 \left( \frac{\hat{V}_2}{h_1 h_2} \frac{\partial h_2}{\partial \hat{u}_1} - \frac{\hat{V}_1}{h_1 h_2} \frac{\partial h_1}{\partial \hat{u}_2} \right) + \hat{V}_3 \left( \frac{\hat{V}_1}{h_1 h_3} \frac{\partial h_1}{\partial \hat{u}_3} - \frac{\hat{V}_3}{h_1 h_3} \frac{\partial h_3}{\partial \hat{u}_1} \right) \right] \\ = -\frac{1}{h_1} \frac{\partial \hat{p}}{\partial \hat{u}_1} + \frac{1}{h_1} \frac{\partial}{\partial \hat{u}_1} (\hat{\lambda} \hat{\nabla} \cdot \hat{\mathbf{u}}) \\ + \frac{1}{h_1 h_2 h_3} \left[ \frac{\partial}{\partial \hat{u}_1} \left\{ 2\hat{\mu} h_2 h_3 \left( \frac{1}{h_1} \frac{\partial \hat{V}_1}{\partial \hat{u}_1} + \frac{\hat{V}_2}{h_1 h_2} \frac{\partial h_1}{\partial \hat{u}_2} + \frac{\hat{V}_3}{h_1 h_3} \frac{\partial h_1}{\partial \hat{u}_3} \right) \right\} \right. \\ + \frac{\partial}{\partial \hat{u}_2} \left\{ \hat{\mu} h_3 h_1 \left[ \frac{h_2}{h_1} \frac{\partial}{\partial \hat{u}_1} \left( \frac{\hat{V}_2}{h_2} \right) + \frac{h_1}{h_2} \frac{\partial}{\partial \hat{u}_2} \left( \frac{\hat{V}_1}{h_1} \right) \right] \right\} \\ + \left. \frac{\partial}{\partial \hat{u}_3} \left\{ \hat{\mu} h_1 h_2 \left[ \frac{h_1}{h_3} \frac{\partial}{\partial \hat{u}_3} \left( \frac{\hat{V}_1}{h_1} \right) + \frac{h_3}{h_1} \frac{\partial}{\partial x_1} \left( \frac{\hat{V}_3}{h_3} \right) \right] \right\} \right] \\ + \frac{\hat{\mu}}{h_1 h_2} \left\{ \frac{h_2}{h_1} \frac{\partial}{\partial \hat{u}_1} \left( \frac{\hat{V}_2}{h_2} \right) + \frac{h_1}{h_2} \frac{\partial}{\partial \hat{u}_2} \left( \frac{\hat{V}_1}{h_1} \right) \right\} \frac{\partial h_1}{\partial \hat{u}_2} \\ + \frac{\hat{\mu}}{h_1 h_3} \left\{ \frac{h_1}{h_3} \frac{\partial}{\partial \hat{u}_3} \left( \frac{\hat{V}_1}{h_1} \right) + \frac{h_3}{h_1} \frac{\partial}{\partial x_1} \left( \frac{\hat{V}_3}{h_3} \right) \right\} \frac{\partial h_1}{\partial \hat{u}_3} \\ - \frac{2\hat{\mu}}{h_1 h_2} \left\{ \frac{1}{h_2} \frac{\partial \hat{V}_2}{\partial \hat{u}_2} + \frac{\hat{V}_3}{h_2 h_3} \frac{\partial h_2}{\partial \hat{u}_3} + \frac{\hat{V}_1}{h_1 h_2} \frac{\partial h_2}{\partial \hat{u}_1} \right\} \frac{\partial h_2}{\partial \hat{u}_1} \\ - \frac{2\hat{\mu}}{h_1 h_3} \left\{ \frac{1}{h_3} \frac{\partial \hat{V}_3}{\partial \hat{u}_3} + \frac{\hat{V}_1}{h_1 h_3} \frac{\partial h_3}{\partial \hat{u}_1} + \frac{\hat{V}_2}{h_2 h_3} \frac{\partial h_3}{\partial \hat{u}_2} \right\} \frac{\partial h_3}{\partial \hat{u}_1} \\ + \hat{\rho} \left[ \underbrace{2\hat{V}_2 \omega_3 - 2\hat{V}_3 \omega_2}_{\text{Coriolis}} + \underbrace{\hat{u}_1(\omega_3^2 + \omega_2^2) - \hat{u}_2 \omega_1 \omega_2 - \hat{u}_3 \omega_1 \omega_3}_{\text{Centrifugal}} \right. \\ \left. + \underbrace{\hat{u}_2 \dot{\omega}_3 - \hat{u}_3 \dot{\omega}_2}_{\text{Euler}} + \hat{u}_2 \omega_3 - \hat{u}_3 \omega_2 + \underbrace{2V_{e_2} \omega_3 - 2V_{e_3} \omega_2}_{\text{Magnus}} - \underbrace{\frac{\partial V_{e_1}}{\partial t}}_{\text{Translation}} \right] \end{aligned} \quad (4.112)$$

Unsteady motion

CHAPTER 4. NON-INERTIAL EQUATIONS IN COMPONENT FORM

**$\hat{\mathbf{u}}_2$ -momentum:**

$$\begin{aligned}
& \hat{\rho} \left[ \frac{\partial \hat{V}_2}{\partial t} + \frac{\hat{V}_1}{h_1} \frac{\partial \hat{V}_2}{\partial \hat{u}_1} + \frac{\hat{V}_2}{h_2} \frac{\partial \hat{V}_2}{\partial \hat{u}_2} + \frac{\hat{V}_3}{h_3} \frac{\partial \hat{V}_2}{\partial \hat{u}_3} - \hat{V}_3 \left( \frac{\hat{V}_3}{h_3 h_2} \frac{\partial h_3}{\partial \hat{u}_2} - \frac{\hat{V}_2}{h_2 h_3} \frac{\partial h_2}{\partial \hat{u}_3} \right) + \hat{V}_1 \left( \frac{\hat{V}_2}{h_1 h_2} \frac{\partial h_2}{\partial \hat{u}_1} - \frac{\hat{V}_1}{h_1 h_2} \frac{\partial h_1}{\partial \hat{u}_2} \right) \right] \\
&= -\frac{1}{h_2} \frac{\partial \hat{p}}{\partial \hat{u}_2} + \frac{1}{h_2} \frac{\partial}{\partial \hat{u}_2} (\hat{\lambda} \hat{\mathbf{v}} \cdot \hat{\mathbf{u}} \\
&+ \frac{1}{h_1 h_2 h_3} \left[ \frac{\partial}{\partial \hat{u}_1} \left\{ \hat{\mu} h_2 h_3 \left( \frac{h_2}{h_1} \frac{\partial}{\partial \hat{u}_1} \left( \frac{\hat{V}_2}{h_2} \right) + \frac{h_1}{h_2} \frac{\partial}{\partial \hat{u}_2} \left( \frac{\hat{V}_1}{h_1} \right) \right\} \right. \\
&+ \frac{\partial}{\partial \hat{u}_2} \left\{ 2 \hat{\mu} h_3 h_1 \left[ \frac{1}{h_2} \frac{\partial \hat{V}_2}{\partial \hat{u}_2} + \frac{\hat{V}_3}{h_2 h_3} \frac{\partial h_2}{\partial \hat{u}_3} + \frac{\hat{V}_1}{h_1 h_2} \frac{\partial h_2}{\partial \hat{u}_1} \right] \right\} \\
&+ \left. \frac{\partial}{\partial \hat{u}_3} \left\{ \hat{\mu} h_1 h_2 \left[ \frac{h_3}{h_2} \frac{\partial}{\partial \hat{u}_2} \left( \frac{\hat{V}_3}{h_3} \right) + \frac{h_2}{h_3} \frac{\partial}{\partial \hat{u}_3} \left( \frac{\hat{V}_2}{h_2} \right) \right] \right\} \right] \\
&+ \frac{\hat{\mu}}{h_2 h_3} \left\{ \frac{h_3}{h_2} \frac{\partial}{\partial \hat{u}_2} \left( \frac{\hat{V}_3}{h_3} \right) + \frac{h_2}{h_3} \frac{\partial}{\partial \hat{u}_3} \left( \frac{\hat{V}_2}{h_2} \right) \right\} \frac{\partial h_2}{\partial \hat{u}_3} \\
&+ \frac{\hat{\mu}}{h_2 h_1} \left\{ \frac{h_2}{h_1} \frac{\partial}{\partial \hat{u}_1} \left( \frac{\hat{V}_2}{h_2} \right) + \frac{h_1}{h_2} \frac{\partial}{\partial \hat{u}_2} \left( \frac{\hat{V}_1}{h_1} \right) \right\} \frac{\partial h_2}{\partial \hat{u}_1} \\
&- \frac{2 \hat{\mu}}{h_2 h_3} \left\{ \frac{1}{h_3} \frac{\partial \hat{V}_3}{\partial \hat{u}_3} + \frac{\hat{V}_1}{h_1 h_3} \frac{\partial h_3}{\partial \hat{u}_1} + \frac{\hat{V}_2}{h_2 h_3} \frac{\partial h_3}{\partial \hat{u}_2} \right\} \frac{\partial h_3}{\partial \hat{u}_2} \\
&- \frac{2 \hat{\mu}}{h_2 h_1} \left\{ \frac{1}{h_1} \frac{\partial \hat{V}_1}{\partial \hat{u}_1} + \frac{\hat{V}_2}{h_1 h_2} \frac{\partial h_1}{\partial \hat{u}_2} + \frac{\hat{V}_3}{h_1 h_3} \frac{\partial h_1}{\partial \hat{u}_3} \right\} \frac{\partial h_1}{\partial \hat{u}_2} \\
&+ \hat{\rho} \left[ \underbrace{2 \hat{V}_3 \omega_1 - 2 \hat{V}_1 \omega_3}_{\text{Coriolis}} + \underbrace{\hat{u}_2 (\omega_3^2 + \omega_1^2) - \hat{u}_1 \omega_1 \omega_2 - \hat{u}_3 \omega_2 \omega_3}_{\text{Centrifugal}} \right. \\
&+ \underbrace{\hat{u}_3 \dot{\omega}_1 - \hat{u}_1 \dot{\omega}_3}_{\text{Euler}} + \hat{u}_3 \omega_1 - \hat{u}_1 \omega_3 + \underbrace{2 V_{e_3} \omega_1 - 2 V_{e_1} \omega_3}_{\text{Magnus}} - \underbrace{\frac{\partial V_{e_1}}{\partial t}}_{\text{Translation}} \left. \right] \\
&\quad \underbrace{\hspace{10em}}_{\text{Unsteady motion}}
\end{aligned} \tag{4.113}$$



4.4. NON-INERTIAL EQUATIONS IN CURVILINEAR COORDINATES

**$\hat{\mathbf{u}}_3$ -momentum:**

$$\begin{aligned}
& \hat{\rho} \left[ \frac{\partial \hat{V}_3}{\partial t} + \frac{\hat{V}_1}{h_1} \frac{\partial \hat{V}_3}{\partial \hat{u}_1} + \frac{\hat{V}_2}{h_2} \frac{\partial \hat{V}_3}{\partial \hat{u}_2} + \frac{\hat{V}_3}{h_3} \frac{\partial \hat{V}_3}{\partial \hat{u}_3} - \hat{V}_1 \left( \frac{\hat{V}_1}{h_1 h_3} \frac{\partial h_1}{\partial \hat{u}_3} - \frac{\hat{V}_3}{h_1 h_3} \frac{\partial h_3}{\partial \hat{u}_1} \right) + \hat{V}_2 \left( \frac{\hat{V}_3}{h_2 h_3} \frac{\partial h_2}{\partial \hat{u}_1} - \frac{\hat{V}_2}{h_2 h_3} \frac{\partial h_2}{\partial \hat{u}_3} \right) \right] \\
&= -\frac{1}{h_1} \frac{\partial \hat{p}}{\partial \hat{u}_3} + \frac{1}{h_3} \frac{\partial}{\partial \hat{u}_3} (\hat{\lambda} \hat{\mathbf{v}} \cdot \hat{\mathbf{u}} \\
&+ \frac{1}{h_1 h_2 h_3} \left[ \frac{\partial}{\partial \hat{u}_1} \left\{ \hat{\mu} h_2 h_3 \left( \frac{h_1}{h_3} \frac{\partial}{\partial \hat{u}_3} \left( \frac{\hat{V}_1}{h_1} \right) + \frac{h_3}{h_1} \frac{\partial}{\partial x_1} \left( \frac{\hat{V}_3}{h_3} \right) \right\} \right. \\
&+ \left. \frac{\partial}{\partial \hat{u}_2} \left\{ \hat{\mu} h_3 h_1 \left[ \frac{h_3}{h_2} \frac{\partial}{\partial \hat{u}_2} \left( \frac{\hat{V}_3}{h_3} \right) + \frac{h_2}{h_3} \frac{\partial}{\partial \hat{u}_3} \left( \frac{\hat{V}_2}{h_2} \right) \right] \right\} \right. \\
&+ \left. \frac{\partial}{\partial \hat{u}_3} \left\{ 2 \hat{\mu} h_1 h_2 \left[ \frac{1}{h_3} \frac{\partial \hat{V}_3}{\partial \hat{u}_3} + \frac{\hat{V}_1}{h_1 h_3} \frac{\partial h_3}{\partial \hat{u}_1} + \frac{\hat{V}_2}{h_2 h_3} \frac{\partial h_3}{\partial \hat{u}_2} \right] \right\} \right] \\
&+ \frac{\hat{\mu}}{h_1 h_3} \left\{ \frac{h_1}{h_3} \frac{\partial}{\partial \hat{u}_3} \left( \frac{\hat{V}_1}{h_1} \right) + \frac{h_3}{h_1} \frac{\partial}{\partial x_1} \left( \frac{\hat{V}_3}{h_3} \right) \right\} \frac{\partial h_3}{\partial \hat{u}_1} \\
&+ \frac{\hat{\mu}}{h_2 h_3} \left\{ \frac{h_3}{h_2} \frac{\partial}{\partial \hat{u}_2} \left( \frac{\hat{V}_3}{h_3} \right) + \frac{h_2}{h_3} \frac{\partial}{\partial \hat{u}_3} \left( \frac{\hat{V}_2}{h_2} \right) \right\} \frac{\partial h_3}{\partial \hat{u}_2} \\
&- \frac{2 \hat{\mu}}{h_1 h_3} \left\{ \frac{1}{h_1} \frac{\partial \hat{V}_1}{\partial \hat{u}_1} + \frac{\hat{V}_2}{h_1 h_2} \frac{\partial h_1}{\partial \hat{u}_2} + \frac{\hat{V}_3}{h_1 h_3} \frac{\partial h_1}{\partial \hat{u}_3} \right\} \frac{\partial h_1}{\partial \hat{u}_3} \\
&- \frac{2 \hat{\mu}}{h_2 h_3} \left\{ \frac{1}{h_2} \frac{\partial \hat{V}_2}{\partial \hat{u}_2} + \frac{\hat{V}_3}{h_2 h_3} \frac{\partial h_2}{\partial \hat{u}_3} + \frac{\hat{V}_1}{h_1 h_2} \frac{\partial h_2}{\partial \hat{u}_1} \right\} \frac{\partial h_2}{\partial \hat{u}_3} \\
&+ \hat{\rho} \left[ \underbrace{2 \hat{V}_1 \omega_2 - 2 \hat{V}_2 \omega_1}_{\text{Coriolis}} + \underbrace{\hat{u}_3 (\omega_2^2 + \omega_1^2) - \hat{u}_1 \omega_1 \omega_3 - \hat{u}_2 \omega_1 \omega_3}_{\text{Centrifugal}} \right. \\
&+ \underbrace{\hat{u}_1 \omega_2 - \hat{u}_2 \omega_1}_{\text{Euler}} + \hat{u}_1 \omega_2 - \hat{u}_2 \omega_1 + \underbrace{2 V_{e_1} \omega_2 - 2 V_{e_2} \omega_1}_{\text{Magnus}} - \underbrace{\frac{\partial V_{e_3}}{\partial t}}_{\text{Translation}} \left. \right] \\
&\quad \text{Unsteady motion}
\end{aligned}$$

(4.114)

## 4.5 Closure

It was established in this chapter that the Cylindrical and Curvilinear systems, as in the case of the Cartesian system, have an inertial and a non-inertial form. Subsequently the component forms of the non-inertial Navier-Stokes equations were derived in Cartesian, Cylindrical and Curvilinear coordinates respectively. The specific contributions of that followed from the work are as follow:

- The non-inertial momentum equation in incompressible and compressible flow were derived in for the Cartesian, Cylindrical and Curvilinear systems respectively which clearly indicated the
  - differences in the material derivative between the various coordinates systems,
  - forms of the diffusion terms that are dependant on compressibility,
  - subsequent differences in the diffusion terms between coordinates system and
  - formulations of the fictitious forces for each co-ordinate system respectively.
- The continuity equation were determined in component form for the Cartesian, Cylindrical and Curvilinear systems respectively.
- It was shown that the non-inertial equations derived in *Chapter 3* are relevant to all coordinate systems, since the vector form of the Navier-Stokes equations are universal across coordinate systems (White [9]),
- The Cartesian and Cylindrical systems are special cases of the Curvilinear case. The aforementioned can be obtained from the Curvilinear description using the relation shown in *Table 4.1*.

The compressible continuity equation, in Cartesian, Cylindrical and Curvilinear components respectively, were derived and is formulated in *Equations 4.9, 4.35 and 4.110*. In the case of incompressible flow the transient terms can be neglected as well as any terms associated with the change in density.

### Cartesian

$$\frac{\partial \rho}{\partial t} + \frac{\partial \rho u}{\partial x} + \frac{\partial \rho v}{\partial y} + \frac{\partial \rho w}{\partial z} = 0 \quad (4.115)$$

### Cylindrical

$$\frac{\partial \rho}{\partial t} + \frac{\partial \rho u_r}{\partial r} + \frac{\rho u_r}{r} + \frac{1}{r} \frac{\partial \rho u_\theta}{\partial \theta} + \frac{\partial \rho u_z}{\partial z} = 0 \quad (4.116)$$

### Curvilinear

$$\frac{\partial \hat{\rho}}{\partial t} + \frac{\hat{V}_1}{h_1} \frac{\partial \hat{\rho}}{\partial \hat{u}_1} + \frac{\hat{V}_2}{h_2} \frac{\partial \hat{\rho}}{\partial \hat{u}_2} + \frac{\hat{V}_3}{h_3} \frac{\partial \hat{\rho}}{\partial \hat{u}_3} + \frac{\hat{\rho}}{h_1 h_2 h_3} \left[ \frac{\partial}{\partial \hat{u}_1} (h_2 h_3 \hat{V}_1) + \frac{\partial}{\partial \hat{u}_2} (h_1 h_3 \hat{V}_2) + \frac{\partial}{\partial \hat{u}_3} (h_1 h_2 \hat{V}_3) \right] = 0 \quad (4.117)$$

The Curvilinear form of the non-inertial momentum equations is the most general form; the Cartesian and Cylindrical formulations was derived from this using *Table 4.1*. The descriptions of the fictitious forces in the various coordinates systems are shown below for selected directions.

**Curvilinear:  $\hat{u}_1$ -direction**

$$\begin{aligned} \hat{\rho} \left[ \frac{\partial \hat{V}_1}{\partial t} + \dots \right] = & -\frac{1}{h_1} \frac{\partial \hat{\rho}}{\partial \hat{u}_1} + \dots + \hat{\rho} \left[ \underbrace{2\hat{V}_2\omega_3 - 2\hat{V}_3\omega_2}_{\text{Coriolis}} + \underbrace{\hat{u}_1(\omega_3^2 + \omega_2^2) - \hat{u}_2\omega_1\omega_2 - \hat{u}_3\omega_1\omega_3}_{\text{Centrifugal}} \right. \\ & \left. + \underbrace{\hat{u}_2\hat{\omega}_3 - \hat{u}_3\hat{\omega}_2 + \hat{u}_2\omega_3 - \hat{u}_3\omega_2}_{\text{Euler}} + \underbrace{2V_{e_2}\omega_3 - 2V_{e_3}\omega_2}_{\text{Magnus}} - \underbrace{\frac{\partial V_{e_1}}{\partial t}}_{\text{Translation}} \right] \end{aligned} \quad (4.118)$$

Arbitrary Rotation

**Cartesian:  $\hat{x}$ -direction**

$$\begin{aligned} \frac{\partial \hat{\rho}\hat{u}}{\partial t} + \dots = & -\frac{\partial \hat{\rho}}{\partial \hat{x}} + \dots + \underbrace{2\hat{\rho}\hat{v}\omega_z - 2\hat{\rho}\hat{w}\omega_y}_{\text{Coriolis}} + \underbrace{\hat{\rho}\hat{x}(\omega_z^2 + \omega_y^2) - \hat{\rho}\hat{y}\omega_x\omega_y - \hat{\rho}\hat{z}\omega_x\omega_z}_{\text{Centrifugal}} \\ & + \underbrace{\hat{\rho}\hat{y}\hat{\omega}_z - \hat{\rho}\hat{z}\hat{\omega}_y + \hat{\rho}\hat{y}\omega_z - \hat{\rho}\hat{z}\omega_y}_{\text{Euler}} + \underbrace{2\hat{\rho}V_y\omega_z - 2\hat{\rho}V_z\omega_y}_{\text{Magnus}} - \underbrace{\frac{\partial \hat{\rho}V_x}{\partial t}}_{\text{Translation}} \end{aligned} \quad (4.119)$$

Arbitrary Rotation

**Cylindrical:  $\hat{r}$ -direction**

$$\begin{aligned} \frac{\partial \hat{\rho}\hat{u}_r}{\partial t} + \dots = & -\frac{\partial \hat{\rho}}{\partial \hat{r}} + \dots + \underbrace{2\hat{\rho}\hat{u}_\theta\omega_z - 2\hat{\rho}\hat{u}_z\omega_\theta}_{\text{Coriolis}} - \underbrace{\hat{\rho}\hat{z}\omega_r\omega_z + \hat{\rho}\hat{r}\omega_z^2 + \hat{\rho}\hat{r}\omega_\theta^2}_{\text{Centrifugal}} \\ & - \underbrace{\hat{\rho}\hat{z}\hat{\omega}_\theta + \hat{\rho}\hat{u}_\theta\omega_z - \hat{\rho}\hat{u}_z\omega_\theta}_{\text{Euler}} + \underbrace{2\hat{\rho}V_\theta\omega_z - 2\hat{\rho}V_z\omega_\theta}_{\text{Magnus}} - \underbrace{\frac{\partial \hat{\rho}V_r}{\partial t}}_{\text{Translation}} \end{aligned} \quad (4.120)$$

Arbitrary Rotation

The fictitious terms have a common form between the various coordinates systems that are dependant on direction. This can be illustrated with the Coriolis terms from the equations above. The equivalent terms between the coordinates systems are highlighted in the same colour. In a similar manner the equivalence between the other fictitious terms are observed.

$$\begin{aligned} 2\hat{\rho} \hat{V}_2 \omega_3 - 2\hat{\rho} \hat{V}_3 \omega_2 & - \textit{Curvilinear} \\ 2\hat{\rho} \hat{v} \omega_z - 2\hat{\rho} \hat{w} \omega_y & - \textit{Cartesian} \\ 2\hat{\rho} \hat{u}_\theta \omega_z - 2\hat{\rho} \hat{u}_z \omega_\theta & - \textit{Cylindrical} \end{aligned} \quad (4.121)$$



UNIVERSITEIT VAN PRETORIA  
UNIVERSITY OF PRETORIA  
YUNIBESITHI YA PRETORIA



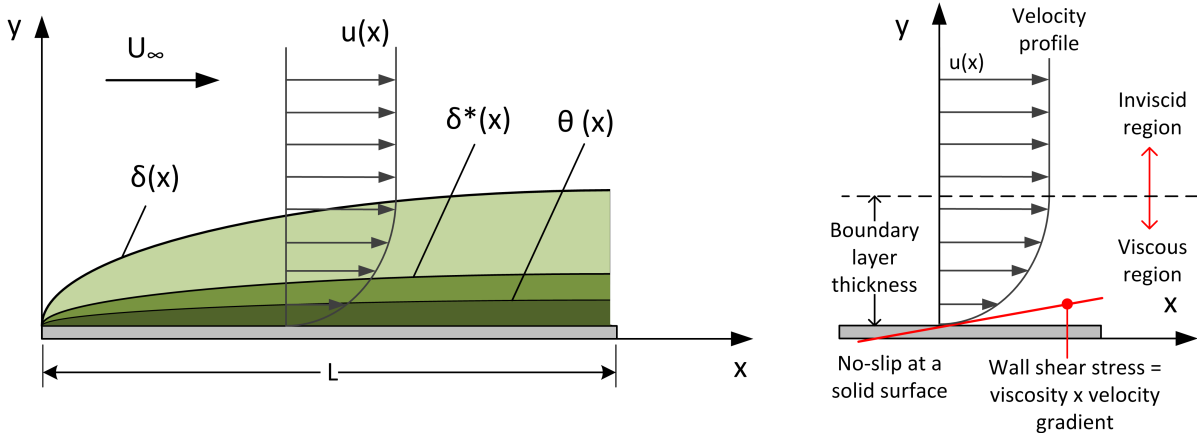
# Chapter 5

## Non-Inertial Boundary Layer Equations

In this chapter the boundary layer equations are determined in a non-inertial frame. Boundary layer theory is well established for inertial cases (Anderson [58], Schlichting [42], White [9]) and is expanded upon to determine the non-inertial formulations.

The boundary layer is the thin layer of viscous fluid close to the wall of a solid surface in a moving fluid. The velocity in the boundary layer approximates zero at the wall (if a no-slip condition is assumed) and increases in a direction perpendicular to the wall to approximate the free stream velocity. The regions associated with the boundary layer are shown in *Figure 5.1*. There are three properties of a boundary layer that characterises it and a fourth that classifies the flow regime; boundary layer thickness  $\delta$ , displacement thickness  $\delta^*$ , momentum thickness  $\theta$  and shape factor  $H$ .

Figure 5.1: Regions Associated with the Laminar Boundary Layer



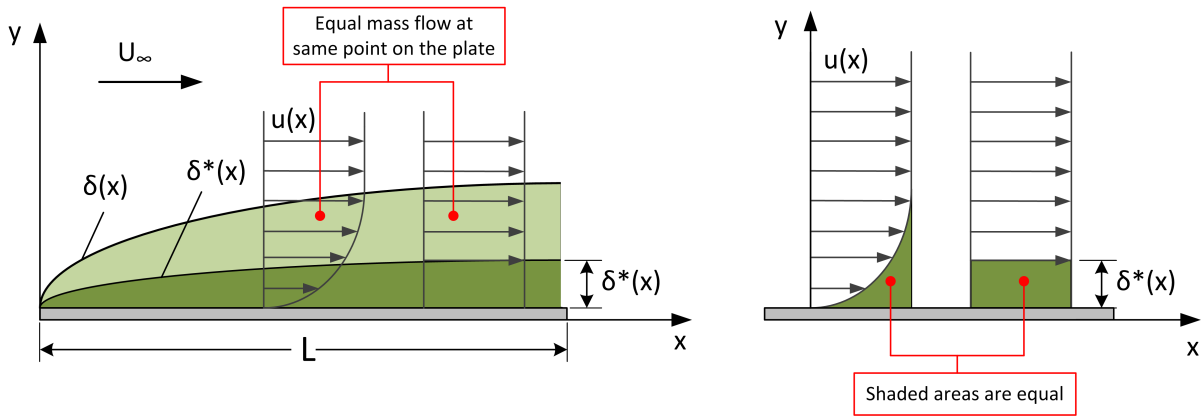
The boundary layer height,  $\delta$ , is the distance from the wall where the velocity is 99% of the free stream velocity. Within boundary layer the viscous effects are dominant during steady state conditions,

while in the outer inviscid flow the momentum effects become dominant.

The displacement thickness,  $\delta^*$ , is the distance by which a surface would have to be moved in the direction perpendicular to its normal vector away from the reference plane, in an inviscid fluid stream of the free stream velocity, to give the same flow rate as occurs between the surface and the reference plane in a real fluid (Schlichting [42]). This definition is mathematically described by *Equation 5.1* (White [9]) and depicted in *Figure 5.2*.

$$\delta^* = \int_0^{y^* \rightarrow \infty} \left(1 - \frac{u}{U_\infty}\right) dy \quad (5.1)$$

Figure 5.2: Graphical Representation of the Displacement Thickness Parameter



The momentum thickness,  $\theta$ , is the distance by which a surface would have to be moved in the direction perpendicular to its normal vector away from the reference plane, in an inviscid fluid stream, of the free stream velocity to give the same momentum as occurs between the surface and the reference plane in a real fluid (Schlichting [42]). This definition is mathematically described by *Equation 5.2* (White [9]) and depicted in *Figure 5.3*.

$$\theta = \int_0^{y^* \rightarrow \infty} \frac{u}{U_\infty} \left(1 - \frac{u}{U_\infty}\right) dy \quad (5.2)$$

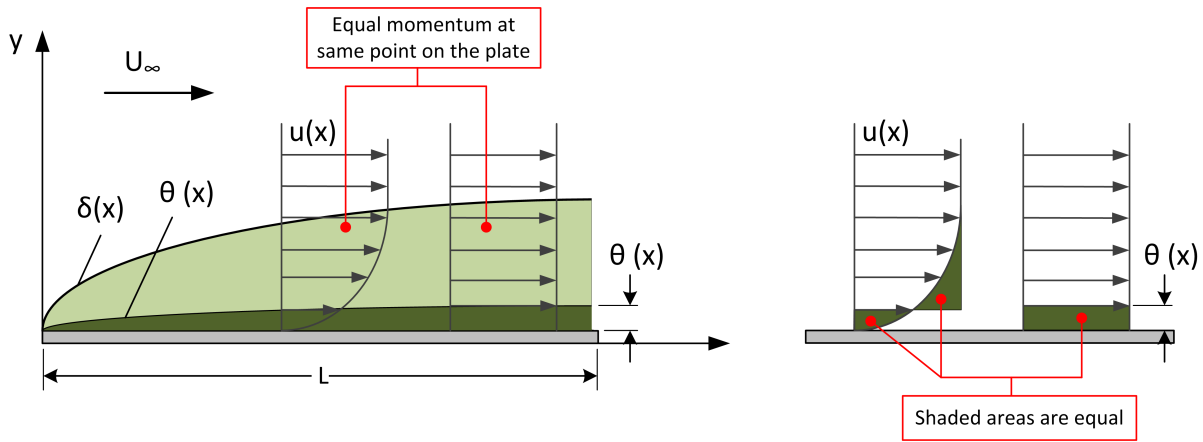
The shape factor is a function of the displacement and momentum thicknesses (*Equation 5.3*). It is used to characterise the flow regime; a value of 2.59 is typical for laminar flows (White [9]). A higher shape factor is associated with a stronger adverse pressure gradient which in turn can lead to flow separation from the solid surface (Wazzan et al. [78]).

$$H = \frac{\delta^*}{\theta} \quad (5.3)$$

The three dimensional boundary layer equations for inertial conditions on a flat plate are derived using a magnitude of order approach (Schlichting [42]). The boundary layer equations for the non-inertial conditions are derived in a similar manner as the inertial equations to determine the effects of the fictitious terms in the near wall region. These equations, along with the boundary layer properties

5.1. NON-INERTIAL BOUNDARY LAYER EQUATIONS FOR A FLAT PLATE - CARTESIAN FORMULATION

Figure 5.3: Graphical Representation of the Momentum Thickness Parameter

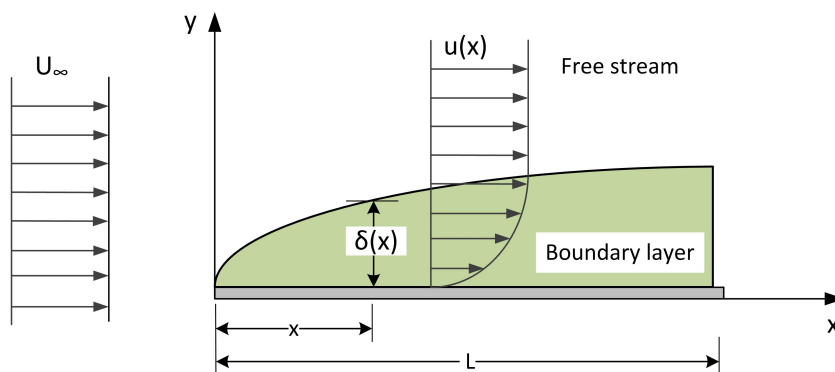


described above, are used in subsequent chapters to enhance the understanding of the flow physics observed in the numerical results of non-inertial flows.

## 5.1 Non-Inertial Boundary Layer Equations for a Flat Plate - Cartesian Formulation

Partial differential equations are analysed by obtaining the non-dimensional form through scaling of the characteristic properties (White [9]). This allows for analysis of the relative magnitudes of the separate terms in the component form of the equation. The characteristic properties of a laminar boundary layer are shown in *Figure 5.4*. It comprises of a reference length ( $L$ ), reference velocity (free stream velocity  $U$ ), boundary layer thickness ( $\delta$ ) and other free stream properties such as viscosity and pressure.

Figure 5.4: Boundary Layer Parameters

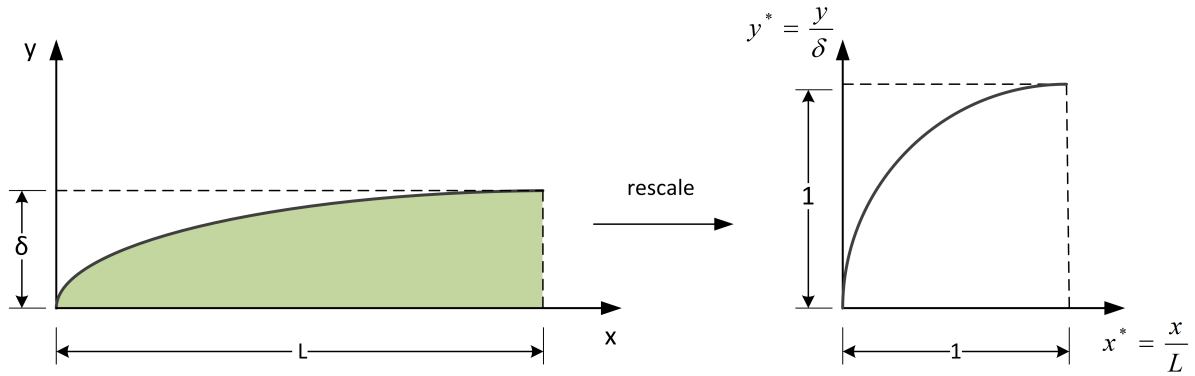


Scaling (see *Figure 5.5*) is aimed at obtaining the relative sizes of the terms in order to identify smaller terms that can be neglected from the equation (Patankar [79], Versteeg and Malalasekera [69]). Elimination of the smaller terms result in a simplified equation. These equations contain the terms that have a significant effect in the near-wall region and are responsible for the behaviour of the flow in the

CHAPTER 5. NON-INERTIAL BOUNDARY LAYER EQUATIONS

boundary layer. The physical responses of the boundary layer to accelerating conditions are explained using the simplified equations.

Figure 5.5: Boundary Layer Scaling Parameters

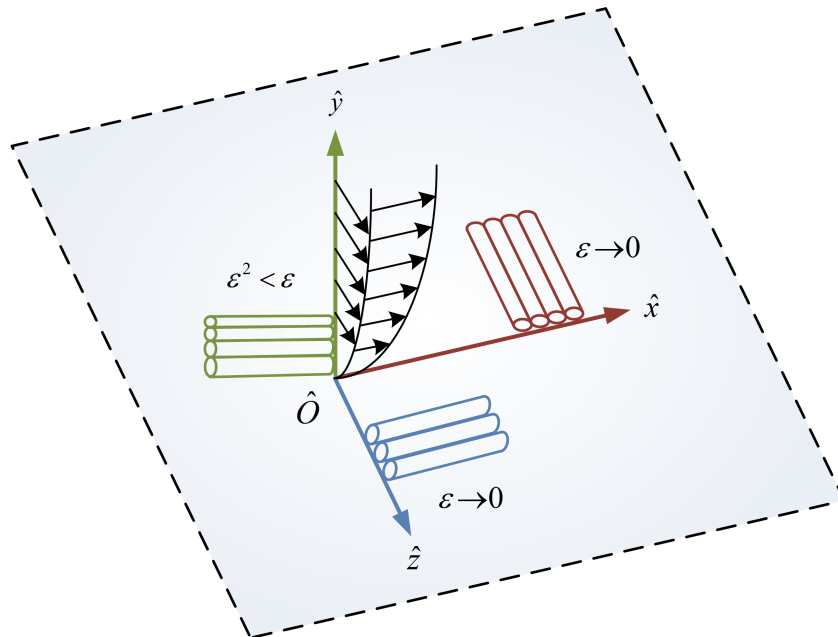


The analysis is based on the assumption that the boundary layer thickness,  $\delta$ , is much smaller in comparison with the body over which the flow is analysed (Schlichting [42]),

$$\frac{\delta}{L} \ll 1 \tag{5.4}$$

A perturbation parameter,  $\varepsilon$  is introduced. This represents a very small disturbance in the flow at the surface that asymptotically approaches zero as indicated in *Figure 5.6*.

Figure 5.6: Perturbation Parameter  $\varepsilon$  on a Flat Surface



The perturbation originates from the surface of the plate continues to propagate along it. Therefore the disturbance approaches  $\varepsilon$  in both the  $\hat{x}$ - and  $\hat{z}$ - directions in the figure above. In the  $\hat{y}$ -direction the

5.1. NON-INERTIAL BOUNDARY LAYER EQUATIONS FOR A FLAT PLATE - CARTESIAN FORMULATION

---

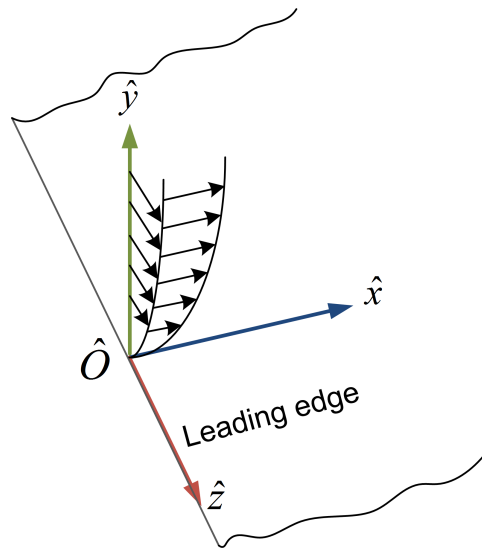
disturbance approaches  $\varepsilon$  close to the wall, but it dissipates further way from the wall since the interaction of the fluid with the solid surface sustains the disturbance. At the flow boundary the disturbance is smaller than  $\varepsilon$  and of order  $\varepsilon^2$ . The boundary layer height is smaller than the disturbance at the wall and asymptotically approaches  $\varepsilon^2$ . It is defined that (Rogers [80], Schlichting [42]),

$$\begin{aligned}
 \varepsilon &\ll 1 \\
 \varepsilon^2 &< \varepsilon \\
 \delta &\rightarrow \varepsilon^2
 \end{aligned}
 \tag{5.5}$$

**5.1.1 NON-DIMENSIONAL ANALYSIS**

Significant work was done by Mager [81] to characterize the laminar boundary layer in turbo-machinery applications. The figure below (*Figure 5.7*) indicates the notation from Mager [81] that are used in this derivation. The boundary layer develops along the  $\hat{x}$ - and  $\hat{z}$ -directions and the rotations occur about the  $\hat{x}$ -,  $\hat{y}$ -, and  $\hat{z}$ -axes with magnitudes  $\omega_1, \omega_2$  and  $\omega_3$  respectively.

Figure 5.7: Flow over a Rotation Flat Surface (Mager [81])



The non-dimensional parameters selected for the spatial variables is as follow (Rogers [80], Schlichting [42], White [9]):

$$\begin{aligned}
 x^* &= \frac{\hat{x}}{L} \\
 y^* &= \frac{\hat{y}}{\delta} \\
 z^* &= \frac{\hat{z}}{L}
 \end{aligned}
 \tag{5.6}$$

$L$  is the reference distance, the assumption is made that the plate is infinite in the  $\hat{x}$ - and  $\hat{z}$ -directions.  $\delta$  is the boundary layer height in the  $\hat{y}$ -direction as a distance of  $L$ .

CHAPTER 5. NON-INERTIAL BOUNDARY LAYER EQUATIONS

---

The velocity components are non-dimensionalized as follow, where  $U$  is the characteristic free-stream velocity (Rogers [80], Schlichting [42], White [9]):

$$\begin{aligned} u^* &= \frac{\hat{u}}{U} \\ v^* &= \frac{\hat{v}}{U} \frac{L}{\delta} \\ w^* &= \frac{\hat{w}}{U} \\ t^* &= t \frac{U}{L} \end{aligned} \tag{5.7}$$

The angular velocity, with the units of radians per second, are non-dimensionalized as follows:

$$\omega_i^* = \omega_i t \left[ \frac{rad}{s} \right] [s] \tag{5.8}$$

The specific pressure and kinematic viscosity are normalized as follows (Rogers [80], Schlichting [42], White [9]):

$$\begin{aligned} \psi^* &= \frac{\psi}{U^2} \left[ \frac{m^2}{s^2} \right] \left[ \frac{s^2}{m^2} \right] \\ \nu^* &= \frac{\nu}{\nu_\infty} \end{aligned} \tag{5.9}$$

### 5.1.2 Continuity Equation for Boundary Layer Flows

The non-inertial continuity equation was derived in *Chapter 4, Equation 4.18*:

$$\frac{\partial \hat{u}}{\partial \hat{x}} + \frac{\partial \hat{v}}{\partial \hat{y}} + \frac{\partial \hat{w}}{\partial \hat{z}} = 0 \tag{5.10}$$

Applying the normalization parameters to this equation result in the non-dimensional form of the equation *Section 5.1.1*:

$$\frac{\partial(u^*U)}{\partial(x^*L)} + \frac{\partial(v^* \frac{U\delta}{L})}{\partial(y^*\delta)} + \frac{\partial(w^*U)}{\partial(z^*L)} = 0 \tag{5.11}$$

The equation above is multiplied by:

$$\frac{L}{U} \tag{5.12}$$

leading to the final non-dimensional form of the equation:

$$[1] \frac{\partial u^*}{\partial x^*} + [1] \frac{\partial v^*}{\partial y^*} + [1] \frac{\partial w^*}{\partial z^*} = 0 \tag{5.13}$$

The coefficients of each term are equal to one and are therefore of the same order of magnitude. No terms can be neglected as all are contributing equally to the flow. The boundary layer continuity equation thus remains the same as the bulk flow equation:

$$\frac{\partial \hat{u}}{\partial \hat{x}} + \frac{\partial \hat{v}}{\partial \hat{y}} + \frac{\partial \hat{w}}{\partial \hat{z}} = 0 \tag{5.14}$$

5.1. NON-INERTIAL BOUNDARY LAYER EQUATIONS FOR A FLAT PLATE - CARTESIAN FORMULATION

**5.1.3 Conservation of Momentum Equation for Boundary Layer Flows**

The non-inertial conservation of momentum equation (*Equation 3.55*) for constant, pure rotation is broken up into its direction components in order to treat the principle directions separately. The  $\hat{x}$ -direction is specified as the first principle directions, and the  $\hat{y}$ - and  $\hat{z}$ -direction the second and third respectively.

$$\frac{\partial \hat{\mathbf{u}}}{\partial t} + (\hat{\mathbf{u}} \cdot \hat{\nabla}) \hat{\mathbf{u}} = -\hat{\nabla} \hat{\psi} + \nu \hat{\nabla}^2 \hat{\mathbf{u}} + \underbrace{2\hat{\mathbf{u}} \wedge \boldsymbol{\Omega}}_{\text{Coriolis}} - \underbrace{\hat{\mathbf{x}} \wedge \boldsymbol{\Omega} \wedge \hat{\mathbf{u}}}_{\text{Centrifugal}} \quad (5.15)$$

**5.1.3.1 First Principle Direction Equation**

The non-inertial conservation of momentum equation in the  $\hat{x}$ -direction is determined using *Equation 4.24* (that established the component form in incompressible flow) and *Equation 4.49* (that indicated the method for determining the component form of the non-inertial components) in *Section 4.3.1.1* :

$$\begin{aligned} \frac{\partial \hat{u}}{\partial t} + \hat{u} \frac{\partial \hat{u}}{\partial \hat{x}} + \hat{v} \frac{\partial \hat{u}}{\partial \hat{y}} + \hat{w} \frac{\partial \hat{u}}{\partial \hat{z}} = & -\frac{\partial \hat{\psi}}{\partial \hat{x}} + \nu \left( \frac{\partial^2 \hat{u}}{\partial \hat{x}^2} + \frac{\partial^2 \hat{u}}{\partial \hat{y}^2} + \frac{\partial^2 \hat{u}}{\partial \hat{z}^2} \right) \\ & + 2\hat{v}\omega_3 - 2\hat{w}\omega_2 + \hat{x}(\omega_3^2 + \omega_2^2) - \hat{y}\omega_1\omega_2 - \hat{z}\omega_1\omega_3 \end{aligned} \quad (5.16)$$

By implementing the normalization parameters as indicated in *Section 5.1.1* and multiplying by,

$$\frac{L}{U^2} \quad (5.17)$$

the equation takes on the non-dimensional form. This allows for order of magnitude analysis of the separate terms:

$$\begin{aligned} \frac{\partial u^*}{\partial t^*} + u^* \frac{\partial u^*}{\partial x^*} + v^* \frac{\partial u^*}{\partial y^*} + w^* \frac{\partial u^*}{\partial z^*} = & -\frac{\partial \psi^*}{\partial x^*} + \nu^* \nu_\infty \left[ \left( \frac{1}{LU} \right) \frac{\partial^2 u^*}{\partial x^{*2}} + \left( \frac{L}{U\delta^2} \right) \frac{\partial^2 u^*}{\partial y^{*2}} + \left( \frac{1}{LU} \right) \frac{\partial^2 u^*}{\partial z^{*2}} \right] \\ & + \left( \frac{\delta}{Ut} \right) 2v^* \omega_3^* - \left( \frac{L}{Ut} \right) 2w^* \omega_2^* + \left( \frac{L^2}{U^2 t^2} \right) x^* [\omega_3^{*2} + \omega_2^{*2}] \\ & - \left( \frac{\delta L}{U^2 t^2} \right) y^* \omega_1^* \omega_2^* - \left( \frac{L^2}{U^2 t^2} \right) z^* \omega_1^* \omega_3^* \end{aligned} \quad (5.18)$$

For the purposes of simplification the assumption is made that the boundary layer thickness approaches a very small number ( $\varepsilon^2$ ) while the characteristic length approaches a very large number (Rogers [80], Schlichting [42]):

$$\begin{aligned} \varepsilon & \ll 1 \\ \delta & \rightarrow \varepsilon^2 \\ L & \rightarrow \infty \end{aligned} \quad (5.19)$$

In order to keep the solution as general as possible, it is assumed that velocity and time has positive values. It then follows that:

$$\begin{aligned} U & \in [\varepsilon, \infty[ \\ t & \in [\varepsilon, \infty[ \end{aligned} \quad (5.20)$$

CHAPTER 5. NON-INERTIAL BOUNDARY LAYER EQUATIONS

From the above relations the following simplifications are made:

$$\begin{aligned}\frac{1}{LU} &\rightarrow \varepsilon \\ \frac{L}{\delta^2} &\rightarrow \infty \\ \frac{\delta}{L} &\rightarrow \varepsilon^2 \\ \delta L &\rightarrow \infty\end{aligned}\tag{5.21}$$

Implementing the above simplifications in *Equation 5.16* lead to the non-dimensional momentum equation with components in the  $\hat{x}$ -direction. The order of magnitude factors and the corresponding orders are indicated below:

$$\begin{aligned}[1]\frac{\partial u^*}{\partial t^*} + [1]u^*\frac{\partial u^*}{\partial x^*} + [1]v^*\frac{\partial u^*}{\partial y^*} + [1]w^*\frac{\partial u^*}{\partial z^*} &= -[1]\frac{\partial \psi^*}{\partial x^*} \\ &+ v^*v_\infty\left[\left(\frac{1}{LU}\right)\frac{\partial^2 u^*}{\partial x^{*2}} + \underbrace{\left(\frac{L}{U\delta^2}\right)}_\infty\frac{\partial^2 u^*}{\partial y^{*2}} + \left(\frac{1}{LU}\right)\frac{\partial^2 u^*}{\partial z^{*2}}\right] \\ &+ \underbrace{\left(\frac{\delta}{Ut}\right)}_{[\varepsilon, \infty[}2v^*\omega_3^* - \underbrace{\left(\frac{L}{Ut}\right)}_{[\varepsilon, \infty[}2w^*\omega_2^* + \underbrace{\left(\frac{L^2}{U^2t^2}\right)}_{[\varepsilon, \infty[}x^*[\omega_3^{*2} + \omega_2^{*2}] \\ &- \underbrace{\left(\frac{\delta L}{U^2t^2}\right)}_{[\varepsilon, \infty[}y^*\omega_1^*\omega_2^* - \underbrace{\left(\frac{L^2}{U^2t^2}\right)}_{[\varepsilon, \infty[}z^*\omega_1^*\omega_3^*\end{aligned}\tag{5.22}$$

The coefficients of the fictitious terms have a temporal component,  $t$ , in the equation. This parameter,  $t \in [\varepsilon, \infty[$ , has been defined for a general solution. The order of magnitude of the coefficients associated with the fictitious terms is undetermined, since it is an element of  $[\varepsilon, \infty[$ . The terms can therefore not be excluded from the equation. None of the fictitious terms could be neglected in this case and in the general solution influences the boundary layer behaviour. The general conservation of momentum for the non-inertial boundary layer equation in the  $\hat{x}$ -direction becomes:

$$\frac{\partial \hat{u}}{\partial t} + \hat{u}\frac{\partial \hat{u}}{\partial \hat{x}} + \hat{v}\frac{\partial \hat{u}}{\partial \hat{y}} + \hat{w}\frac{\partial \hat{u}}{\partial \hat{z}} = -\frac{\partial \hat{\psi}}{\partial \hat{x}} + \nu\left(\frac{\partial^2 \hat{u}}{\partial \hat{y}^2}\right) + 2\hat{v}\omega_3 - 2\hat{w}\omega_2 + \hat{x}(\omega_3^2 + \omega_2^2) - \hat{y}\omega_1\omega_2 - \hat{z}\omega_1\omega_3\tag{5.23}$$

### 5.1.3.2 Second Principle Direction Equation

The non-inertial conservation of momentum equation in the  $\hat{y}$ -direction follows from *Section 4.3.1.1*, *Equation 4.32* and the method for non-inertial component expansion in *Equation 4.49*:

$$\begin{aligned}\frac{\partial \hat{v}}{\partial t} + \hat{u}\frac{\partial \hat{v}}{\partial \hat{x}} + \hat{v}\frac{\partial \hat{v}}{\partial \hat{y}} + \hat{w}\frac{\partial \hat{v}}{\partial \hat{z}} &= -\frac{\partial \hat{\psi}}{\partial \hat{y}} + \nu\left(\frac{\partial^2 \hat{v}}{\partial \hat{x}^2} + \frac{\partial^2 \hat{v}}{\partial \hat{y}^2} + \frac{\partial^2 \hat{v}}{\partial \hat{z}^2}\right) \\ &+ 2\hat{w}\omega_1 - 2\hat{u}\omega_3 + \hat{y}(\omega_3^2 + \omega_1^2) - \hat{x}\omega_1\omega_2 - \hat{z}\omega_2\omega_3\end{aligned}\tag{5.24}$$



5.1. NON-INERTIAL BOUNDARY LAYER EQUATIONS FOR A FLAT PLATE - CARTESIAN FORMULATION

Implementing the non-dimensional parameters previously defined in *Section 5.1.1* and multiplication by:

$$\frac{\delta}{U^2} \quad (5.25)$$

Leads to the non-dimensional form of the equation:

$$\begin{aligned} \left(\frac{\delta^2}{L^2}\right)\frac{\partial v^*}{\partial t^*} + \left(\frac{\delta^2}{L^2}\right)u^*\frac{\partial v^*}{\partial x^*} + \left(\frac{\delta^2}{L^2}\right)v^*\frac{\partial v^*}{\partial y^*} + \left(\frac{\delta^2}{L^2}\right)w^*\frac{\partial v^*}{\partial z^*} &= -\frac{\partial \psi^*}{\partial y^*} \\ + v^*v_\infty\left[\left(\frac{\delta^2}{UL^3}\right)\frac{\partial^2 v^*}{\partial x^{*2}} + \left(\frac{1}{LU}\right)\frac{\partial^2 v^*}{\partial y^{*2}} + \left(\frac{\delta^2}{UL^3}\right)\frac{\partial^2 v^*}{\partial z^{*2}}\right] & \\ + \left(\frac{\delta}{Ut}\right)2w^*\omega_1^* - \left(\frac{\delta}{Ut}\right)2u^*\omega_3^* + y^*\left[\left(\frac{\delta^2}{U^2t^2}\right)\omega_3^{*2} + \left(\frac{\delta^2}{U^2t^2}\right)\omega_1^{*2}\right] & \\ - \left(\frac{\delta L}{U^2t^2}\right)x^*\omega_1^*\omega_2^* - \left(\frac{\delta L}{U^2t^2}\right)z^*\omega_2^*\omega_3^* & \end{aligned} \quad (5.26)$$

When the same simplifications are used as in the  $\hat{x}$ -direction case as shown in *Equation 5.22*, the general conservation of momentum equation for the non-inertial boundary layer equation in the  $\hat{y}$ -direction become:

$$0 = -\frac{\partial \hat{\psi}}{\partial \hat{y}} + 2\hat{w}\omega_1 - 2\hat{u}\omega_3 + \hat{y}(\omega_3^2 + \omega_1^2) - \hat{x}\omega_1\omega_2 - \hat{z}\omega_2\omega_3 \quad (5.27)$$

### 5.1.3.3 Third Principle Direction Equation

The non-inertial conservation of momentum equation in the  $\hat{z}$ -direction is determined using *Section 4.3.1.1*, *Equation 4.32* and *Equation 4.49*:

$$\begin{aligned} \frac{\partial \hat{w}}{\partial t} + \hat{u}\frac{\partial \hat{w}}{\partial \hat{x}} + \hat{v}\frac{\partial \hat{w}}{\partial \hat{y}} + \hat{w}\frac{\partial \hat{w}}{\partial \hat{z}} &= -\frac{\partial \hat{\psi}}{\partial \hat{z}} + v\left(\frac{\partial^2 \hat{w}}{\partial \hat{x}^2} + \frac{\partial^2 \hat{w}}{\partial \hat{y}^2} + \frac{\partial^2 \hat{w}}{\partial \hat{z}^2}\right) \\ + 2\hat{u}\omega_2 - 2\hat{v}\omega_1 + \hat{z}(\omega_2^2 + \omega_1^2) - \hat{x}\omega_1\omega_3 - \hat{y}\omega_2\omega_3 & \end{aligned} \quad (5.28)$$

Implementing the non-dimensional parameters previously defined in *Section 5.1.1* and multiplication by:

$$\frac{L}{U^2} \quad (5.29)$$

lead to the non-dimensional form of the equation:

$$\begin{aligned} \frac{\partial w^*}{\partial t} + u^*\frac{\partial w^*}{\partial x^*} + v^*\frac{\partial w^*}{\partial y^*} + w^*\frac{\partial w^*}{\partial z^*} &= -\frac{\partial \psi^*}{\partial z^*} \\ + v^*v_\infty\left[\left(\frac{1}{LU}\right)\frac{\partial^2 w^*}{\partial x^{*2}} + \left(\frac{L}{\delta U}\right)\frac{\partial^2 w^*}{\partial y^{*2}} + \left(\frac{1}{LU}\right)\frac{\partial^2 w^*}{\partial z^{*2}}\right] & \\ + 2\left(\frac{L}{Ut}\right)u^*\omega_2 - 2\left(\frac{\delta}{Ut}\right)v^*\omega_1 + \left(\frac{L^2}{U^2t^2}\right)z^*(\omega_2^2 + \omega_1^2) & \\ - \left(\frac{L^2}{U^2t^2}\right)x^*\omega_1\omega_3 - \left(\frac{\delta L}{U^2t^2}\right)y^*\omega_2\omega_3 & \end{aligned} \quad (5.30)$$

When the same simplifications are used as in the  $\hat{x}$ -direction case (Equation 5.22), the general conservation of momentum equation for the non-inertial boundary layer equation in the  $\hat{z}$ -direction becomes:

$$\frac{\partial \hat{w}}{\partial t} + \hat{u} \frac{\partial \hat{w}}{\partial \hat{x}} + \hat{v} \frac{\partial \hat{w}}{\partial \hat{y}} + \hat{w} \frac{\partial \hat{w}}{\partial \hat{z}} = -\frac{\partial \hat{\psi}}{\partial \hat{z}} + \nu \left( \frac{\partial^2 \hat{w}}{\partial \hat{y}^2} \right) + 2\hat{u}\omega_2 - 2\hat{v}\omega_1 + \hat{z}(\omega_2^2 + \omega_1^2) - \hat{x}\omega_1\omega_3 - \hat{y}\omega_2\omega_3 \quad (5.31)$$

#### 5.1.3.4 Compressibility Effects on the Boundary Layer Equations

The differences between the compressible and incompressible formulations for the momentum equation were discussed at length in Section 4.2.2.2. It was established that the form of the diffusion terms in compressible and incompressible flow conditions is crucial since the complete deviatoric stress tensor must be used in the compressible case (Equation 4.38):

$$\hat{\boldsymbol{\tau}}(\hat{x}, \hat{y}, \hat{z}) = \begin{bmatrix} 2\hat{\mu} \frac{\partial \hat{u}}{\partial \hat{x}} + \hat{\lambda} \hat{\nabla} \cdot \hat{\mathbf{u}} & \hat{\mu} \left( \frac{\partial \hat{u}}{\partial \hat{y}} + \frac{\partial \hat{v}}{\partial \hat{x}} \right) & \hat{\mu} \left( \frac{\partial \hat{u}}{\partial \hat{z}} + \frac{\partial \hat{w}}{\partial \hat{x}} \right) \\ \hat{\mu} \left( \frac{\partial \hat{u}}{\partial \hat{y}} + \frac{\partial \hat{v}}{\partial \hat{x}} \right) & 2\hat{\mu} \frac{\partial \hat{v}}{\partial \hat{y}} + \hat{\lambda} \hat{\nabla} \cdot \hat{\mathbf{u}} & \hat{\mu} \left( \frac{\partial \hat{v}}{\partial \hat{z}} + \frac{\partial \hat{w}}{\partial \hat{y}} \right) \\ \hat{\mu} \left( \frac{\partial \hat{u}}{\partial \hat{z}} + \frac{\partial \hat{w}}{\partial \hat{x}} \right) & \hat{\mu} \left( \frac{\partial \hat{v}}{\partial \hat{z}} + \frac{\partial \hat{w}}{\partial \hat{y}} \right) & 2\hat{\mu} \frac{\partial \hat{w}}{\partial \hat{z}} + \hat{\lambda} \hat{\nabla} \cdot \hat{\mathbf{u}} \end{bmatrix} \quad (5.32)$$

Here it is determined which of the diffusion terms, that are relevant in the bulk flow, are relevant in the boundary layer. This is done using the order of magnitude analysis (Patankar [79], Schlichting [42], Versteeg and Malalasekera [69], White [9]) that was employed to determine the incompressible boundary layer equations.

The components that pertain to the  $\hat{x}$ -momentum equation is:

$$\frac{\partial}{\partial \hat{x}} \left[ 2\hat{\mu} \frac{\partial \hat{u}}{\partial \hat{x}} + \hat{\lambda} \left( \frac{\partial \hat{u}}{\partial \hat{x}} + \frac{\partial \hat{v}}{\partial \hat{y}} + \frac{\partial \hat{w}}{\partial \hat{z}} \right) \right] + \frac{\partial}{\partial \hat{y}} \left[ \hat{\mu} \left( \frac{\partial \hat{u}}{\partial \hat{y}} + \frac{\partial \hat{v}}{\partial \hat{x}} \right) \right] + \frac{\partial}{\partial \hat{z}} \left[ \hat{\mu} \left( \frac{\partial \hat{u}}{\partial \hat{z}} + \frac{\partial \hat{w}}{\partial \hat{x}} \right) \right] \quad (5.33)$$

The non-dimensional parameters of Section 5.1.1 are substituted in the terms above and multiplied by Equation 5.17,

$$\frac{L}{U^2} \quad (5.34)$$

to obtain the non-dimensional form of the terms:

$$\begin{aligned} \left[ \frac{1}{LU} \right] \frac{\partial}{\partial x^*} \left[ 2\mu \frac{\partial u^*}{\partial x^*} + \lambda \left( \frac{\partial u^*}{\partial x^*} + \frac{\partial v^*}{\partial y^*} + \frac{\partial w^*}{\partial z^*} \right) \right] + \left[ \frac{L}{\delta^2 U} \right] \frac{\partial}{\partial y^*} \left[ \mu \frac{\partial u^*}{\partial y^*} \right] + \left[ \frac{1}{LU} \right] \frac{\partial}{\partial y^*} \left[ \mu \frac{\partial v^*}{\partial x^*} \right] \\ + \left[ \frac{1}{LU} \right] \frac{\partial}{\partial z^*} \left[ \mu \left( \frac{\partial u^*}{\partial z^*} + \frac{\partial w^*}{\partial x^*} \right) \right] \end{aligned} \quad (5.35)$$

An order of magnitude analysis, along with the following simplifications,

$$\begin{aligned} \frac{1}{LU} &\rightarrow \varepsilon \\ \frac{L}{\delta^2 U} &\rightarrow \infty \end{aligned} \quad (5.36)$$

result in a number of the terms being neglected since the coefficients of the terms tends to  $\varepsilon$ .

5.1. NON-INERTIAL BOUNDARY LAYER EQUATIONS FOR A FLAT PLATE - CARTESIAN FORMULATION

$$\begin{aligned} \left[ \frac{1}{LU} \right] \frac{\partial}{\partial x^*} \left[ 2\mu \frac{\partial u^*}{\partial x^*} + \lambda \left( \frac{\partial u^*}{\partial x^*} + \frac{\partial v^*}{\partial y^*} + \frac{\partial w^*}{\partial z^*} \right) \right] + \underbrace{\left[ \frac{L}{\delta^2 U} \right]}_{\infty} \frac{\partial}{\partial y^*} \left[ \mu \frac{\partial u^*}{\partial y^*} \right] + \left[ \frac{1}{LU} \right] \frac{\partial}{\partial y^*} \left[ \mu \frac{\partial v^*}{\partial x^*} \right] \\ + \left[ \frac{1}{LU} \right] \frac{\partial}{\partial z^*} \left[ \mu \left( \frac{\partial u^*}{\partial z^*} + \frac{\partial w^*}{\partial x^*} \right) \right] \end{aligned} \quad (5.37)$$

The diffusive terms in the compressible  $\hat{x}$ -momentum equation are similar to the terms in the incompressible form (Equation 5.23):

$$\frac{\partial}{\partial \hat{y}} \left[ \hat{\mu} \frac{\partial \hat{u}}{\partial \hat{y}} \right] \quad (5.38)$$

The compressible form of the boundary layer equation for the conservation of momentum in the  $\hat{x}$ -direction is similar to the incompressible form determined in Equation 5.23:

$$\begin{aligned} \frac{\partial \hat{\rho} \hat{u}}{\partial t} + \hat{u} \frac{\partial \hat{\rho} \hat{u}}{\partial \hat{x}} + \hat{v} \frac{\partial \hat{\rho} \hat{u}}{\partial \hat{y}} + \hat{w} \frac{\partial \hat{\rho} \hat{u}}{\partial \hat{z}} = - \frac{\partial \hat{p}}{\partial \hat{x}} + \frac{\partial}{\partial \hat{y}} \left[ \hat{\mu} \frac{\partial \hat{u}}{\partial \hat{y}} \right] + 2\hat{\rho} \hat{v} \omega_3 - 2\hat{\rho} \hat{w} \omega_2 + \hat{\rho} \hat{x} (\omega_3^2 + \omega_2^2) \\ - \hat{\rho} \hat{y} \omega_1 \omega_2 - \hat{\rho} \hat{z} \omega_1 \omega_3 \end{aligned} \quad (5.39)$$

The stress components that pertains to the  $\hat{y}$ -momentum equation are:

$$\frac{\partial}{\partial \hat{x}} \left[ \hat{\mu} \left( \frac{\partial \hat{u}}{\partial \hat{y}} + \frac{\partial \hat{v}}{\partial \hat{x}} \right) \right] + \frac{\partial}{\partial \hat{y}} \left[ 2\hat{\mu} \frac{\partial \hat{v}}{\partial \hat{y}} + \hat{\lambda} \left( \frac{\partial \hat{u}}{\partial \hat{x}} + \frac{\partial \hat{v}}{\partial \hat{y}} + \frac{\partial \hat{w}}{\partial \hat{z}} \right) \right] + \frac{\partial}{\partial \hat{z}} \left[ \hat{\mu} \left( \frac{\partial \hat{v}}{\partial \hat{z}} + \frac{\partial \hat{w}}{\partial \hat{y}} \right) \right] \quad (5.40)$$

The non-dimensional parameters of Section 5.1.1 are substituted in the terms above and multiplied by Equation 5.25,

$$\frac{\delta}{U^2} \quad (5.41)$$

to obtain the non-dimensional form of the terms:

$$\begin{aligned} \left[ \frac{1}{LU} \right] \frac{\partial}{\partial x^*} \left[ \mu \frac{\partial u^*}{\partial y^*} \right] + \left[ \frac{\delta^2}{L^3 U} \right] \frac{\partial}{\partial x^*} \left[ \mu \frac{\partial v^*}{\partial x^*} \right] + \left[ \frac{1}{LU} \right] \frac{\partial}{\partial y^*} \left[ 2\mu \frac{\partial v^*}{\partial y^*} + \lambda \left( \frac{\partial u^*}{\partial x^*} + \frac{\partial v^*}{\partial y^*} + \frac{\partial w^*}{\partial z^*} \right) \right] \\ + \left[ \frac{\delta^2}{L^3 U} \right] \frac{\partial}{\partial z^*} \left[ \mu \frac{\partial v^*}{\partial z^*} \right] + \left[ \frac{1}{LU} \right] \frac{\partial}{\partial z^*} \left[ \mu \frac{\partial w^*}{\partial y^*} \right] \end{aligned} \quad (5.42)$$

An order of magnitude analysis, along with the following simplifications,

$$\begin{aligned} \frac{1}{LU} &\rightarrow \varepsilon^2 \\ \frac{\delta^2}{L^3 U} &\rightarrow \varepsilon^2 \end{aligned} \quad (5.43)$$

results in all of the terms being neglected.

$$\begin{aligned}
& \left[ \frac{1}{LU} \right] \frac{\partial}{\partial x^*} \left[ \mu \frac{\partial u^*}{\partial y^*} \right] + \left[ \frac{\delta^2}{L^3 U} \right] \frac{\partial}{\partial x^*} \left[ \mu \frac{\partial v^*}{\partial x^*} \right] + \left[ \frac{1}{LU} \right] \frac{\partial}{\partial y^*} \left[ 2\mu \frac{\partial v^*}{\partial y^*} + \lambda \left( \frac{\partial u^*}{\partial x^*} + \frac{\partial v^*}{\partial y^*} + \frac{\partial w^*}{\partial z^*} \right) \right] \\
& + \left[ \frac{\delta^2}{L^3 U} \right] \frac{\partial}{\partial z^*} \left[ \mu \frac{\partial v^*}{\partial z^*} \right] + \left[ \frac{1}{LU} \right] \frac{\partial}{\partial z^*} \left[ \mu \frac{\partial w^*}{\partial y^*} \right]
\end{aligned} \tag{5.44}$$

The diffusive terms in the compressible  $\hat{y}$ -momentum equation are similar to the terms in the incompressible form; all the terms can be neglected.

The compressible form of the boundary layer equation for the conservation of momentum in the  $\hat{y}$ -direction is similar to the incompressible form determined in *Equation 5.27*:

$$0 = -\frac{\partial \hat{p}}{\partial \hat{y}} + 2\hat{\rho}\hat{w}\omega_1 - 2\hat{\rho}\hat{u}\omega_3 + \hat{\rho}\hat{y}(\omega_3^2 + \omega_1^2) - \hat{\rho}\hat{x}\omega_1\omega_2 - \hat{\rho}\hat{z}\omega_2\omega_3 \tag{5.45}$$

The stress components that pertains to the  $\hat{z}$ -**momentum** equation are:

$$\frac{\partial}{\partial \hat{x}} \left[ \hat{\mu} \left( \frac{\partial \hat{u}}{\partial \hat{z}} + \frac{\partial \hat{w}}{\partial \hat{x}} \right) \right] + \frac{\partial}{\partial \hat{y}} \left[ \hat{\mu} \left( \frac{\partial \hat{v}}{\partial \hat{z}} + \frac{\partial \hat{w}}{\partial \hat{y}} \right) \right] + \frac{\partial}{\partial \hat{z}} \left[ 2\hat{\mu} \frac{\partial \hat{w}}{\partial \hat{z}} + \lambda \left( \frac{\partial \hat{u}}{\partial \hat{x}} + \frac{\partial \hat{v}}{\partial \hat{y}} + \frac{\partial \hat{w}}{\partial \hat{z}} \right) \right] \tag{5.46}$$

The non-dimensional parameters of *Section 5.1.1* are substituted in the terms above and multiplied by *Equation 5.29*,

$$\frac{L}{U^2} \tag{5.47}$$

to obtain the non-dimensional form of the terms:

$$\begin{aligned}
& \left[ \frac{1}{LU} \right] \frac{\partial}{\partial x^*} \left[ \mu \left( \frac{\partial u^*}{\partial z^*} + \frac{\partial w^*}{\partial x^*} \right) \right] + \left[ \frac{1}{LU} \right] \frac{\partial}{\partial y^*} \left[ \mu \frac{\partial v^*}{\partial z^*} \right] + \left[ \frac{L}{\delta^2 U} \right] \frac{\partial}{\partial y^*} \left[ \mu \frac{\partial w^*}{\partial y^*} \right] \\
& + \left[ \frac{1}{LU} \right] \frac{\partial}{\partial z^*} \left[ 2\mu \frac{\partial w^*}{\partial z^*} + \lambda \left( \frac{\partial u^*}{\partial x^*} + \frac{\partial v^*}{\partial y^*} + \frac{\partial w^*}{\partial z^*} \right) \right]
\end{aligned} \tag{5.48}$$

An order of magnitude analysis, along with the following simplifications,

$$\begin{aligned}
\frac{1}{LU} & \rightarrow \varepsilon \\
\frac{L}{\delta^2 U} & \rightarrow \infty
\end{aligned} \tag{5.49}$$

result in a number of the terms being neglected.

$$\begin{aligned}
& \left[ \frac{1}{LU} \right] \frac{\partial}{\partial x^*} \left[ \mu \left( \frac{\partial u^*}{\partial z^*} + \frac{\partial w^*}{\partial x^*} \right) \right] + \left[ \frac{1}{LU} \right] \frac{\partial}{\partial y^*} \left[ \mu \frac{\partial v^*}{\partial z^*} \right] + \underbrace{\left[ \frac{L}{\delta^2 U} \right]}_{\infty} \frac{\partial}{\partial y^*} \left[ \mu \frac{\partial w^*}{\partial y^*} \right] \\
& + \left[ \frac{1}{LU} \right] \frac{\partial}{\partial z^*} \left[ 2\mu \frac{\partial w^*}{\partial z^*} + \lambda \left( \frac{\partial u^*}{\partial x^*} + \frac{\partial v^*}{\partial y^*} + \frac{\partial w^*}{\partial z^*} \right) \right]
\end{aligned} \tag{5.50}$$

## 5.1. NON-INERTIAL BOUNDARY LAYER EQUATIONS FOR A FLAT PLATE - CARTESIAN FORMULATION

The diffusive terms in the compressible  $\hat{z}$ -momentum equation are be similar to the terms in the incompressible form (*Equation 5.31*):

$$\frac{\partial}{\partial \hat{y}} \left[ \hat{\mu} \frac{\partial \hat{w}}{\partial \hat{y}} \right] \quad (5.51)$$

The compressible form of the boundary layer equation for the conservation of momentum in the  $\hat{z}$ -direction is similar to the incompressible form determined in *Equation 5.31*:

$$\begin{aligned} \frac{\partial \hat{\rho} \hat{w}}{\partial t} + \hat{u} \frac{\partial \hat{\rho} \hat{w}}{\partial \hat{x}} + \hat{v} \frac{\partial \hat{\rho} \hat{w}}{\partial \hat{y}} + \hat{w} \frac{\partial \hat{\rho} \hat{w}}{\partial \hat{z}} = & -\frac{\partial \hat{p}}{\partial \hat{z}} + \frac{\partial}{\partial \hat{y}} \left[ \hat{\mu} \frac{\partial \hat{w}}{\partial \hat{y}} \right] + 2\hat{\rho} \hat{u} \omega_2 - 2\hat{\rho} \hat{v} \omega_1 + \hat{\rho} \hat{z} (\omega_2^2 + \omega_1^2) \\ & - \hat{\rho} \hat{x} \omega_1 \omega_3 - \hat{\rho} \hat{y} \omega_2 \omega_3 \end{aligned} \quad (5.52)$$

### 5.1.4 Validation of Equations

In Mager [81] the non-inertial boundary layer equations are defined as follow:

$$\begin{aligned} u_x + u_y + u_z &= 0 \\ uu_x + vu_y + wu_z + 2\omega_2 w - \omega_r^2 r_x &= -\frac{1}{\rho} p_x + \nu u_{yy} \\ 2(\omega_3 u - \omega_1 w) - \omega_r^2 r_y &= -\frac{1}{\rho} p_y \\ uw_x + vw_y + ww_z - 2\omega_2 u - \omega_r^2 r_z &= -\frac{1}{\rho} p_x + \nu w_{yy} \end{aligned} \quad (5.53)$$

Mager [81] however stated that the total change of pressure through out the boundary layer along a principle direction normal to the wall is of the same order as  $\delta$  and may therefore still be neglected as both approximates  $\varepsilon^2$ . The equation in the  $\hat{y}$ -direction can thus be simplified to:

$$-\frac{1}{\rho} p_y \simeq 0 \quad (5.54)$$

The mass conservation equation for the boundary layer agrees with the equation given by Mager [81]:

$$\frac{\partial \hat{u}}{\partial \hat{x}} + \frac{\partial \hat{v}}{\partial \hat{y}} + \frac{\partial \hat{w}}{\partial \hat{z}} = 0 \quad (5.55)$$

The boundary layer equations derived in the previous section represent a general case where no assumptions were made with regards to the order of magnitude of characteristic velocity (U) and time (t). If it is assumed that the product of U and t is greater than one, the term  $\frac{\delta}{U t}$  can be neglected from *Equation 5.22*. This leads to the following boundary layer equation in the  $\hat{x}$ -direction:

$$\begin{aligned} \frac{\partial \hat{u}}{\partial t} + \hat{u} \frac{\partial \hat{u}}{\partial \hat{x}} + \hat{v} \frac{\partial \hat{u}}{\partial \hat{y}} + \hat{w} \frac{\partial \hat{u}}{\partial \hat{z}} = & -\frac{\partial \hat{\psi}}{\partial \hat{x}} + \nu \left( \frac{\partial^2 \hat{u}}{\partial \hat{y}^2} \right) \\ & - 2\hat{w} \omega_2 \\ & + \hat{x} (\omega_3^2 + \omega_2^2) - \hat{y} \omega_1 \omega_2 - \hat{z} \omega_1 \omega_3 \end{aligned} \quad (5.56)$$

CHAPTER 5. NON-INERTIAL BOUNDARY LAYER EQUATIONS

---

This equation agrees with the equation given in Mager [81].

Under the same assumption as above, the boundary layer in the  $\hat{y}$ -direction becomes *Equation 5.27*:

$$0 = -\frac{\partial \hat{\psi}}{\partial \hat{y}} - \hat{x}\omega_1\omega_2 - \hat{z}\omega_2\omega_3 \quad (5.57)$$

In Mager [81] it is assumed that total change of pressure through out the boundary layer long a principle direction normal to the wall is zero. This means that the pressure gradient is only dependant on  $\hat{x}$ - and  $\hat{z}$ -directions. The above equation subsequently becomes:

$$0 = -\frac{\partial \hat{\psi}}{\partial \hat{y}} \quad (5.58)$$

In a similar manner as explained above for the  $\hat{x}$ -direction, the equation in the  $\hat{z}$ -direction becomes (*Equation 5.31*):

$$\begin{aligned} \frac{\partial \hat{w}}{\partial t} + \hat{u} \frac{\partial \hat{w}}{\partial \hat{x}} + \hat{v} \frac{\partial \hat{w}}{\partial \hat{y}} + \hat{w} \frac{\partial \hat{w}}{\partial \hat{z}} &= -\frac{\partial \hat{\psi}}{\partial \hat{z}} + \nu \left( \frac{\partial^2 \hat{w}}{\partial \hat{y}^2} \right) \\ &+ 2\hat{u}\omega_2 \\ &+ \hat{z}(\omega_2^2 + \omega_1^2) - \hat{x}\omega_1\omega_3 - \hat{y}\omega_2\omega_3 \end{aligned} \quad (5.59)$$

This is consistent with the equation given in Mager [81].

Now consider that the rotation on the flat plate is only around the  $\hat{y}$ -axis. In such conditions the values of the angular velocities become:

$$\begin{aligned} \omega_1 &= 0 \\ \omega_2 &= \Omega \\ \omega_3 &= 0 \end{aligned} \quad (5.60)$$

Substituting for these values in Equations 5.56, 5.58 and 5.59 respectively results in the following set of non-inertial boundary layer equations:

$$\begin{aligned} \frac{\partial \hat{u}}{\partial t} + \hat{u} \frac{\partial \hat{u}}{\partial \hat{x}} + \hat{v} \frac{\partial \hat{u}}{\partial \hat{y}} + \hat{w} \frac{\partial \hat{u}}{\partial \hat{z}} &= -\frac{\partial \hat{\psi}}{\partial \hat{x}} + \nu \left( \frac{\partial^2 \hat{u}}{\partial \hat{y}^2} \right) - 2\hat{w}\Omega + \hat{x}\Omega^2 \\ 0 &= -\frac{\partial \hat{\psi}}{\partial \hat{y}} \\ \frac{\partial \hat{w}}{\partial t} + \hat{u} \frac{\partial \hat{w}}{\partial \hat{x}} + \hat{v} \frac{\partial \hat{w}}{\partial \hat{y}} + \hat{w} \frac{\partial \hat{w}}{\partial \hat{z}} &= -\frac{\partial \hat{\psi}}{\partial \hat{z}} + \nu \left( \frac{\partial^2 \hat{w}}{\partial \hat{y}^2} \right) + 2\hat{u}\Omega + \hat{z}\Omega^2 \end{aligned} \quad (5.61)$$

This results in the same equations as in the literature for a rotating blade as described by Bogdanova [82] and Dwyer [83]. The equations derived in this section, provides results that are consistent with the literature (Bogdanova [82], Dwyer [83]).

5.1. NON-INERTIAL BOUNDARY LAYER EQUATIONS FOR A FLAT PLATE - CARTESIAN FORMULATION

**5.1.5 Non-Inertial Boundary Layer Equations for Variable Rotation**

The non-inertial equation for incompressible flow in variable rotation conditions was determined in *Chapter 3, Equation 3.157*:

$$\frac{\partial \hat{\mathbf{u}}}{\partial t} + (\hat{\mathbf{u}} \cdot \hat{\nabla}) \hat{\mathbf{u}} = -\hat{\nabla} \hat{\psi} + \nu \hat{\nabla}^2 \hat{\mathbf{u}} + \underbrace{2\hat{\mathbf{u}} \wedge \hat{\boldsymbol{\Omega}}}_{\text{Coriolis}} - \underbrace{\hat{\mathbf{x}} \wedge \hat{\boldsymbol{\Omega}} \wedge \hat{\boldsymbol{\Omega}}}_{\text{Centrifugal}} + \underbrace{\hat{\mathbf{x}} \wedge \hat{\dot{\boldsymbol{\Omega}}}}_{\text{Euler}} \quad (5.62)$$

The component form of the momentum equations were developed in *Equations 5.23, 5.27 and 5.31*. Component forms of the fictitious forces were determined in *Equation 4.49*. Using the equations mentioned, the Cartesian component form for incompressible flow in variable rotation is expressed as:

**$\hat{x}$ -momentum**

$$\frac{\partial \hat{u}}{\partial t} + \hat{u} \frac{\partial \hat{u}}{\partial \hat{x}} + \hat{v} \frac{\partial \hat{u}}{\partial \hat{y}} + \hat{w} \frac{\partial \hat{u}}{\partial \hat{z}} = -\frac{\partial \hat{\psi}}{\partial \hat{x}} + \hat{v} \frac{\partial^2 \hat{u}}{\partial \hat{y}^2} + 2\hat{v}\hat{\omega}_3 - 2\hat{w}\hat{\omega}_2 + \hat{x}(\hat{\omega}_3^2 + \hat{\omega}_2^2) - \hat{y}\hat{\omega}_1\hat{\omega}_2 - \hat{z}\hat{\omega}_1\hat{\omega}_3 + \hat{y}\hat{\omega}_3 - \hat{z}\hat{\omega}_2 \quad (5.63)$$

**$\hat{y}$ -momentum**

$$0 = -\frac{\partial \hat{\psi}}{\partial \hat{y}} + 2\hat{w}\hat{\omega}_1 - 2\hat{u}\hat{\omega}_3 + \hat{y}(\hat{\omega}_3^2 + \hat{\omega}_1^2) - \hat{x}\hat{\omega}_1\hat{\omega}_2 - \hat{z}\hat{\omega}_2\hat{\omega}_3 + \hat{z}\hat{\omega}_1 - \hat{x}\hat{\omega}_3 \quad (5.64)$$

**$\hat{z}$ -momentum**

$$\frac{\partial \hat{w}}{\partial t} + \hat{u} \frac{\partial \hat{w}}{\partial \hat{x}} + \hat{v} \frac{\partial \hat{w}}{\partial \hat{y}} + \hat{w} \frac{\partial \hat{w}}{\partial \hat{z}} = -\frac{\partial \hat{\psi}}{\partial \hat{z}} + \hat{v} \frac{\partial^2 \hat{w}}{\partial \hat{y}^2} + 2\hat{u}\hat{\omega}_2 - 2\hat{v}\hat{\omega}_1 + \hat{z}(\hat{\omega}_2^2 + \hat{\omega}_1^2) - \hat{x}\hat{\omega}_1\hat{\omega}_3 - \hat{y}\hat{\omega}_2\hat{\omega}_3 + \hat{x}\hat{\omega}_2 - \hat{y}\hat{\omega}_1 \quad (5.65)$$

The non-inertial equation for compressible flow in variable rotation conditions was determined in *Chapter 3, Equation 3.169*:

$$\frac{\partial \hat{\rho} \hat{\mathbf{u}}}{\partial t} + \hat{\nabla} \cdot (\hat{\rho} \hat{\mathbf{u}} \otimes \hat{\mathbf{u}}) = -\hat{\nabla} \hat{p} + \hat{\nabla} \cdot [\hat{\mu}(\hat{\nabla} \hat{\mathbf{u}} + \hat{\nabla} \hat{\mathbf{u}}^T) + \hat{\lambda}(\hat{\nabla} \cdot \hat{\mathbf{u}}) \hat{\mathbf{I}}] + \underbrace{2\hat{\rho} \hat{\mathbf{u}} \wedge \hat{\boldsymbol{\Omega}}}_{\text{Coriolis}} - \underbrace{\hat{\rho} \hat{\mathbf{x}} \wedge \hat{\boldsymbol{\Omega}} \wedge \hat{\boldsymbol{\Omega}}}_{\text{Centrifugal}} + \underbrace{\hat{\rho} \hat{\mathbf{x}} \wedge \hat{\dot{\boldsymbol{\Omega}}}}_{\text{Euler}} \quad (5.66)$$

Using the expression above, along with *Equations 5.39, 5.45, 5.31* and the compressible stress terms determined in *Section 5.1.3.4*, lead to:

**$\hat{x}$ -momentum**

$$\frac{\partial \hat{\rho} \hat{u}}{\partial t} + \hat{u} \frac{\partial \hat{\rho} \hat{u}}{\partial \hat{x}} + \hat{v} \frac{\partial \hat{\rho} \hat{u}}{\partial \hat{y}} + \hat{w} \frac{\partial \hat{\rho} \hat{u}}{\partial \hat{z}} = -\frac{\partial \hat{p}}{\partial \hat{x}} + \frac{\partial}{\partial \hat{y}} \hat{\mu} \frac{\partial \hat{u}}{\partial \hat{y}} + 2\hat{\rho} \hat{v} \hat{\omega}_3 - 2\hat{\rho} \hat{w} \hat{\omega}_2 + \hat{\rho} \hat{x}(\hat{\omega}_3^2 + \hat{\omega}_2^2) - \hat{\rho} \hat{y} \hat{\omega}_1 \hat{\omega}_2 - \hat{\rho} \hat{z} \hat{\omega}_1 \hat{\omega}_3 + \hat{\rho} \hat{y} \hat{\omega}_3 - \hat{\rho} \hat{z} \hat{\omega}_2 \quad (5.67)$$

**$\hat{y}$ -momentum**

$$0 = -\frac{\partial \hat{p}}{\partial \hat{y}} + 2\hat{\rho} \hat{w} \hat{\omega}_1 - 2\hat{\rho} \hat{u} \hat{\omega}_3 + \hat{\rho} \hat{y}(\hat{\omega}_3^2 + \hat{\omega}_1^2) - \hat{\rho} \hat{x} \hat{\omega}_1 \hat{\omega}_2 - \hat{\rho} \hat{z} \hat{\omega}_2 \hat{\omega}_3 + \hat{\rho} \hat{z} \hat{\omega}_1 - \hat{\rho} \hat{x} \hat{\omega}_3 \quad (5.68)$$

**$\hat{z}$ -momentum**

$$\frac{\partial \hat{\rho} \hat{w}}{\partial t} + \hat{u} \frac{\partial \hat{\rho} \hat{w}}{\partial \hat{x}} + \hat{v} \frac{\partial \hat{\rho} \hat{w}}{\partial \hat{y}} + \hat{w} \frac{\partial \hat{\rho} \hat{w}}{\partial \hat{z}} = -\frac{\partial \hat{p}}{\partial \hat{z}} + \frac{\partial}{\partial \hat{y}} \hat{\mu} \frac{\partial \hat{w}}{\partial \hat{y}} + 2\hat{\rho} \hat{u} \hat{\omega}_2 - 2\hat{\rho} \hat{v} \hat{\omega}_1 + \hat{\rho} \hat{z}(\hat{\omega}_2^2 + \hat{\omega}_1^2) - \hat{\rho} \hat{x} \hat{\omega}_1 \hat{\omega}_3 - \hat{\rho} \hat{y} \hat{\omega}_2 \hat{\omega}_3 + \hat{\rho} \hat{x} \hat{\omega}_2 - \hat{\rho} \hat{y} \hat{\omega}_1 \quad (5.69)$$

### 5.1.6 Non-Inertial Boundary Layer Equations for Arbitrary Acceleration

The non-inertial equation for incompressible flow in full arbitrary acceleration conditions was determined in *Chapter 3, Equation 3.239*:

$$\frac{\partial \hat{\mathbf{u}}}{\partial t} + (\hat{\mathbf{u}} \cdot \hat{\nabla}) \hat{\mathbf{u}} = -\hat{\nabla} \hat{\psi} + \nu \hat{\nabla}^2 \hat{\mathbf{u}} + \underbrace{2\hat{\mathbf{u}} \wedge \hat{\boldsymbol{\Omega}}}_{\text{Coriolis}} - \underbrace{\hat{\mathbf{x}} \wedge \hat{\boldsymbol{\Omega}} \wedge \hat{\boldsymbol{\Omega}}}_{\text{Centrifugal}} + \underbrace{\hat{\mathbf{x}} \wedge \hat{\dot{\boldsymbol{\Omega}}}}_{\text{Euler}} + \underbrace{\hat{\mathbf{x}} \wedge \hat{\boldsymbol{\Omega}}}_{\text{Unsteady motion}} + \underbrace{2\mathbf{V}(t) \wedge \hat{\boldsymbol{\Omega}}}_{\text{Magnus}} - \underbrace{\frac{\partial}{\partial t}(\mathbf{V}(t))}_{\text{Translation}} \quad (5.70)$$

This formulation, along with *Equations 5.63, 5.64, 5.65, and 4.49*, result in the following boundary layer expressions:

#### $\hat{\mathbf{x}}$ -momentum

$$\begin{aligned} \frac{\partial \hat{u}}{\partial t} + \hat{u} \frac{\partial \hat{u}}{\partial \hat{x}} + \hat{v} \frac{\partial \hat{u}}{\partial \hat{y}} + \hat{w} \frac{\partial \hat{u}}{\partial \hat{z}} = & -\frac{\partial \hat{\psi}}{\partial \hat{x}} + \hat{v} \frac{\partial^2 \hat{u}}{\partial \hat{y}^2} + 2\hat{v}\omega_3 - 2\hat{w}\omega_2 + \hat{x}(\omega_3^2 + \omega_2^2) - \hat{y}\omega_1\omega_2 - \hat{z}\omega_1\omega_3 \\ & + \hat{y}\omega_3 - \hat{z}\omega_2 + \hat{y}\omega_3 - \hat{z}\omega_2 + 2V_y\omega_3 - 2V_z\omega_2 - \frac{\partial V_x}{\partial t} \end{aligned} \quad (5.71)$$

#### $\hat{\mathbf{y}}$ -momentum

$$\begin{aligned} 0 = & -\frac{\partial \hat{\psi}}{\partial \hat{y}} + 2\hat{w}\omega_1 - 2\hat{u}\omega_3 + \hat{y}(\omega_3^2 + \omega_1^2) - \hat{x}\omega_1\omega_2 - \hat{z}\omega_2\omega_3 + \hat{z}\omega_1 - \hat{x}\omega_3 + \hat{z}\omega_1 - \hat{x}\omega_3 \\ & + 2V_z\omega_1 - 2V_x\omega_3 - \frac{\partial V_y}{\partial t} \end{aligned} \quad (5.72)$$

#### $\hat{\mathbf{z}}$ -momentum

$$\begin{aligned} \frac{\partial \hat{w}}{\partial t} + \hat{u} \frac{\partial \hat{w}}{\partial \hat{x}} + \hat{v} \frac{\partial \hat{w}}{\partial \hat{y}} + \hat{w} \frac{\partial \hat{w}}{\partial \hat{z}} = & -\frac{\partial \hat{\psi}}{\partial \hat{z}} + \hat{v} \frac{\partial^2 \hat{w}}{\partial \hat{y}^2} + 2\hat{u}\omega_2 - 2\hat{v}\omega_1 + \hat{z}(\omega_2^2 + \omega_1^2) - \hat{x}\omega_1\omega_3 - \hat{y}\omega_2\omega_3 \\ & + \hat{x}\omega_2 - \hat{y}\omega_1 + \hat{x}\omega_2 - \hat{y}\omega_1 + 2V_x\omega_2 - 2V_y\omega_1 - \frac{\partial V_z}{\partial t} \end{aligned} \quad (5.73)$$

The non-inertial equation for compressible flow in full arbitrary acceleration conditions was determined in *Chapter 3, Equation 3.227*:

$$\begin{aligned} \frac{\partial \hat{\rho} \hat{\mathbf{u}}}{\partial t} + \hat{\nabla} \cdot (\hat{\rho} \hat{\mathbf{u}} \otimes \hat{\mathbf{u}}) = & -\hat{\nabla} \hat{p} + \hat{\nabla} \cdot [\hat{\mu}(\hat{\nabla} \hat{\mathbf{u}} + \hat{\nabla} \hat{\mathbf{u}}^T) + \hat{\lambda}(\hat{\nabla} \cdot \hat{\mathbf{u}}) \hat{\mathbf{I}}] \\ & - \underbrace{\frac{\partial}{\partial t}(\rho \mathbf{V}(t))}_{\text{Translation}} + \underbrace{\rho \hat{\mathbf{x}} \wedge \hat{\boldsymbol{\Omega}} + \rho \hat{\mathbf{x}} \wedge \hat{\dot{\boldsymbol{\Omega}}}}_{\text{Euler}} + \underbrace{2\rho \hat{\mathbf{u}} \wedge \hat{\boldsymbol{\Omega}}}_{\text{Coriolis}} - \underbrace{\rho \hat{\mathbf{x}} \wedge \hat{\boldsymbol{\Omega}} \wedge \hat{\boldsymbol{\Omega}}}_{\text{Centrifugal}} + \underbrace{2\rho \mathbf{V}(t) \wedge \hat{\boldsymbol{\Omega}}}_{\text{Magnus}} \end{aligned} \quad (5.74)$$

Using this and *Equations 5.71, 5.72, 5.73*, the following boundary layer expressions is obtained for arbitrary motion:

#### $\hat{\mathbf{x}}$ -momentum

$$\begin{aligned} \frac{\partial \hat{\rho} \hat{u}}{\partial t} + \hat{u} \frac{\partial \hat{\rho} \hat{u}}{\partial \hat{x}} + \hat{v} \frac{\partial \hat{\rho} \hat{u}}{\partial \hat{y}} + \hat{w} \frac{\partial \hat{\rho} \hat{u}}{\partial \hat{z}} = & -\frac{\partial \hat{p}}{\partial \hat{x}} + \frac{\partial}{\partial \hat{y}} \hat{\mu} \frac{\partial \hat{u}}{\partial \hat{y}} + 2\hat{\rho} \hat{v} \omega_3 - 2\hat{\rho} \hat{w} \omega_2 + \hat{\rho} \hat{x}(\omega_3^2 + \omega_2^2) \\ & - \hat{\rho} \hat{y} \omega_1 \omega_2 - \hat{\rho} \hat{z} \omega_1 \omega_3 + \hat{\rho} \hat{y} \hat{w}_3 - \hat{\rho} \hat{z} \hat{w}_2 + \hat{\rho} \hat{y} \omega_3 - \hat{\rho} \hat{z} \omega_2 \\ & + 2\hat{\rho} V_y \omega_3 - 2\hat{\rho} V_z \omega_2 - \frac{\partial \hat{\rho} V_x}{\partial t} \end{aligned} \quad (5.75)$$



5.1. NON-INERTIAL BOUNDARY LAYER EQUATIONS FOR A FLAT PLATE - CARTESIAN FORMULATION

---

**$\hat{y}$ -momentum**

$$0 = -\frac{\partial \hat{p}}{\partial \hat{y}} + 2\hat{\rho}\hat{w}\omega_1 - 2\hat{\rho}\hat{u}\omega_3 + \hat{\rho}\hat{y}(\omega_3^2 + \omega_1^2) - \hat{\rho}\hat{x}\omega_1\omega_2 - \hat{\rho}\hat{z}\omega_2\omega_3 + \hat{\rho}\hat{z}\hat{w}_1 - \hat{\rho}\hat{x}\hat{w}_3 + \hat{\rho}\hat{z}\omega_1 - \hat{\rho}\hat{x}\omega_3$$

$$+ 2\hat{\rho}V_z\omega_1 - 2\hat{\rho}V_x\omega_3 - \frac{\partial \hat{\rho}V_y}{\partial t} \quad (5.76)$$

**$\hat{z}$ -momentum**

$$\frac{\partial \hat{\rho}\hat{w}}{\partial t} + \hat{u}\frac{\partial \hat{\rho}\hat{w}}{\partial \hat{x}} + \hat{v}\frac{\partial \hat{\rho}\hat{w}}{\partial \hat{y}} + \hat{w}\frac{\partial \hat{\rho}\hat{w}}{\partial \hat{z}} = -\frac{\partial \hat{p}}{\partial \hat{z}} + \frac{\partial}{\partial \hat{y}} \left[ \hat{\mu} \frac{\partial \hat{w}}{\partial \hat{y}} \right] + 2\hat{\rho}\hat{u}\omega_2 - 2\hat{\rho}\hat{v}\omega_1 + \hat{\rho}\hat{z}(\omega_2^2 + \omega_1^2)$$

$$- \hat{\rho}\hat{x}\omega_1\omega_3 - \hat{\rho}\hat{y}\omega_2\omega_3 + \hat{\rho}\hat{x}\hat{w}_y - \hat{\rho}\hat{y}\hat{w}_x + \hat{\rho}\hat{x}\omega_y - \hat{\rho}\hat{y}\omega_x \quad (5.77)$$

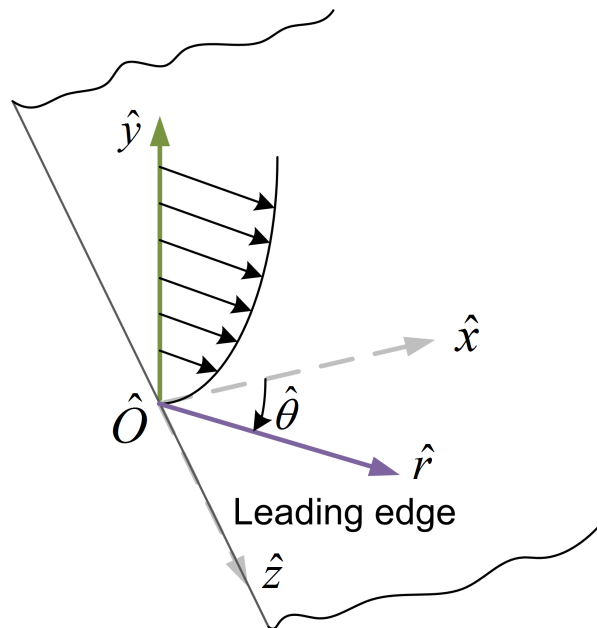
$$+ 2\hat{\rho}V_x\omega_2 - 2\hat{\rho}V_y\omega_1 - \frac{\partial \hat{\rho}V_z}{\partial t}$$

## 5.2 Non-Inertial Boundary Layer Equations for a Flat Plate - Cylindrical Formulation

In some cases for aero-ballistic and aeronautical application, especially when doing asymptotic expansions and similar analytical methods, it is more convenient to make use of a curvilinear formulation for the boundary layer equations. The geometric features of aerodynamic bodies, such as rotating disks and cones, is more efficiently described in a cylindrical system. Analytical solutions for the flow features, specifically of a rotating disk, are available from the literature in cylindrical coordinates (Schlichting [42]).

Consider the same plate as shown in *Figure 5.7*, but with the  $\hat{x}$ - and  $\hat{z}$ -axis written in terms of the  $\hat{r}$ - and  $\hat{\theta}$ - axis cylindrical coordinates ( *Figure 5.8*). The  $\hat{y}$ -axis remains common between the two frames.

Figure 5.8: Flat Plate in Cylindrical Co-ordinates



The cylindrical formulations of the non-inertial Navier-Stokes equations were determined in *Chapter 4* and are used here. The same method of comparative orders that was used in *Section 5.1* are used to obtain the boundary layer equations in a cylindrical co-ordinate system.

### 5.2.1 Non-Dimensional Analysis

The non-dimensional parameters used in this analysis are indicated below.  $R$  is the characteristic distance where, at a characteristic angle of  $\beta$ , the boundary layer height in the  $\hat{y}$ -direction is  $\delta$ . This is

## 5.2. NON-INERTIAL BOUNDARY LAYER EQUATIONS FOR A FLAT PLATE - CYLINDRICAL FORMULATION

---

similar to the non-dimensional parameters of *Section 5.1.1*.

$$\begin{aligned} r^* &= \frac{\hat{r}}{R} \\ y^* &= \frac{\hat{y}}{\delta} \\ \theta^* &= \frac{\hat{\theta}}{\beta}, \beta \in ]0, 2\pi] \end{aligned} \quad (5.78)$$

The normalized velocity components are a function of the characteristic velocity in the free stream and in the case of the velocity in the  $\hat{y}$ -direction,  $R$  and  $\delta$ .

$$\begin{aligned} u_r^* &= \frac{\hat{u}_r}{U_\infty} \\ u_y^* &= \frac{\hat{u}_y}{U_\infty} \frac{R}{\delta} \\ u_\theta^* &= \frac{\hat{u}_\theta}{U_\infty} \end{aligned} \quad (5.79)$$

The remainder of the parameters are normalized in a similar manner as in *Section 5.1.1*:

$$\begin{aligned} t^* &= t \frac{U_\infty}{R} \\ \omega_i^* &= \omega_i t \\ \psi^* &= \frac{\psi}{U_\infty^2} \\ \nu^* &= \frac{\nu}{\nu_\infty} \end{aligned} \quad (5.80)$$

### 5.2.2 Continuity Equation for Boundary Layer Flows

The continuity equation in the cylindrical form was derived in *Equation 4.22*:

$$\frac{\partial \hat{u}_r}{\partial \hat{r}} + \frac{\hat{u}_r}{\hat{r}} + \frac{1}{\hat{r}} \frac{\partial \hat{u}_\theta}{\partial \hat{\theta}} + \frac{\partial \hat{u}_y}{\partial \hat{y}} = 0 \quad (5.81)$$

The non-dimensional form of this equation is obtained by substituting the parameters from *Section 5.2.1* into the equation:

$$\frac{\partial(u_r^* U_\infty)}{\partial(r^* R)} + \frac{u_r^* U_\infty}{r^* R} + \frac{1}{r^* R} \frac{\partial(u_\theta^* U_\infty)}{\partial(\theta^* \beta)} + \frac{\partial(u_y^* \frac{U_\infty \delta}{R})}{\partial(y^* \delta)} = 0 \quad (5.82)$$

The equation above it then multiplied by,

$$\frac{R}{U_\infty} \quad (5.83)$$

CHAPTER 5. NON-INERTIAL BOUNDARY LAYER EQUATIONS

This results in the non-dimensional form of the continuity equation where the order of magnitude, shown in the square brackets, can be used to group the terms that are of comparable order:

$$[1] \frac{\partial u_r^*}{\partial r^*} + [1] \frac{u_r^*}{r^*} + \underbrace{[1] \frac{1}{\beta} \frac{1}{r^*} \frac{\partial u_\theta^*}{\partial \theta^*}}_{]0, 2\pi]} + [1] \frac{\partial u_y^*}{\partial y^*} = 0 \quad (5.84)$$

The parameter  $\beta$  is of finite value since  $\beta \in ]0, 2\pi]$ . The order of the term  $\frac{1}{\beta}$  therefore approximates 1 and can not be neglected from the equation. The boundary layer equation for continuity there remains:

$$\frac{\partial \hat{u}_r}{\partial \hat{r}} + \frac{\hat{u}_r}{\hat{r}} + \frac{1}{\hat{r}} \frac{\partial \hat{u}_\theta}{\partial \hat{\theta}} + \frac{\partial \hat{u}_y}{\partial \hat{y}} = 0 \quad (5.85)$$

### 5.2.3 Conservation of Momentum Equation for Boundary Layer Flows

The tensor form of non-inertial conservation of momentum equation is derived in *Equation 3.55*.

$$\frac{\partial \hat{\mathbf{u}}}{\partial t} + (\hat{\mathbf{u}} \cdot \hat{\nabla}) \hat{\mathbf{u}} = -\hat{\nabla} \hat{\psi} + \nu \hat{\nabla}^2 \hat{\mathbf{u}} + \underbrace{2\hat{\mathbf{u}} \wedge \boldsymbol{\Omega}}_{\text{Coriolis}} - \underbrace{\hat{\mathbf{x}} \wedge \boldsymbol{\Omega} \wedge \boldsymbol{\Omega}}_{\text{Centrifugal}} \quad (5.86)$$

The Cylindrical form of the equations are used here to derive the boundary layer equations.

#### 5.2.3.1 First Principle Direction Equation

The component form of the non-inertial momentum equation in the first principle direction (in this case taken as the  $\hat{r}$ -direction) was derived in *Equation 4.55* for a coordinates system with directions  $(\hat{r}, \hat{\theta}, \hat{z})$ . This formulation is used here for a system  $(\hat{r}, \hat{y}, \hat{\theta})$  to obtain the equation:

$$\begin{aligned} \frac{\partial \hat{u}_r}{\partial t} + \hat{u}_r \frac{\partial \hat{u}_r}{\partial \hat{r}} + \frac{\hat{u}_\theta}{\hat{r}} \frac{\partial \hat{u}_r}{\partial \hat{\theta}} - \frac{\hat{u}_\theta^2}{\hat{r}} + \hat{u}_y \frac{\partial \hat{u}_r}{\partial \hat{y}} = -\frac{\partial \hat{\psi}}{\partial \hat{r}} \\ + \hat{\nu} \left[ \frac{\partial^2 \hat{u}_r}{\partial \hat{r}^2} + \frac{1}{\hat{r}} \frac{\partial \hat{u}_r}{\partial \hat{r}} + \frac{1}{\hat{r}^2} \frac{\partial^2 \hat{u}_r}{\partial \hat{\theta}^2} - \frac{2}{\hat{r}^2} \frac{\partial \hat{u}_\theta}{\partial \hat{\theta}} - \frac{\hat{u}_r}{\hat{r}^2} + \frac{\partial^2 \hat{u}_r}{\partial \hat{y}^2} \right] \\ - \underbrace{2\hat{u}_\theta \omega_y + 2\hat{u}_y \omega_\theta}_{\text{Coriolis}} - \underbrace{\hat{y} \omega_r \omega_y + \hat{r} \omega_y^2 + \hat{r} \omega_\theta^2}_{\text{Centrifugal}} \end{aligned} \quad (5.87)$$

Substitution of the non-dimensional parameters, as defined in *Section 5.2.1*, into the equation, result in the non-dimensional form:

$$\begin{aligned} \left[ \frac{U_\infty^2}{R} \right] \frac{\partial u_r^*}{\partial t^*} + \left[ \frac{U_\infty^2}{R} \right] u_r^* \frac{\partial u_r^*}{\partial r^*} + \left[ \frac{U_\infty^2}{R\beta} \right] \frac{u_\theta^*}{r^*} \frac{\partial u_r^*}{\partial \theta^*} - \left[ \frac{U_\infty^2}{R} \right] \frac{u_\theta^{*2}}{r^*} + \left[ \frac{U_\infty^2}{R} \right] u_y^* \frac{\partial u_r^*}{\partial y^*} = \\ - \left[ \frac{U_\infty^2}{R} \right] \frac{\partial \psi^*}{\partial r^*} + \left[ \frac{U_\infty}{R^2} \right] \nu^* \nu_\infty \frac{\partial^2 u_r^*}{\partial r^{*2}} + \left[ \frac{U_\infty}{R^2} \right] \nu^* \nu_\infty \frac{1}{r^{*2}} \frac{\partial u_r^*}{\partial r^*} \\ + \left[ \frac{U_\infty}{R^2 \beta^2} \right] \nu^* \nu_\infty \frac{1}{r^{*2}} \frac{\partial^2 u_r^*}{\partial \theta^{*2}} - \left[ \frac{U_\infty}{R^2 \beta} \right] \nu^* \nu_\infty \frac{2}{r^{*2}} \frac{\partial u_\theta^*}{\partial \theta^*} - \left[ \frac{U_\infty}{R^2} \right] \nu^* \nu_\infty \frac{u_r^*}{r^{*2}} \\ + \left[ \frac{U_\infty}{\delta^2} \right] \nu^* \nu_\infty \frac{\partial^2 u_r^*}{\partial y^{*2}} - \left[ \frac{U_\infty}{t} \right] 2u_\theta^* \omega_y^* + \left[ \frac{U_\infty \delta}{Rt} \right] 2u_y^* \omega_\theta^* - \left[ \frac{\delta}{t^2} \right] y^* \omega_r^* \omega_y^* \\ + \left[ \frac{R}{t^2} \right] r^* \omega_y^{*2} + \left[ \frac{R}{t^2} \right] r^* \omega_\theta^{*2} \end{aligned} \quad (5.88)$$

5.2. NON-INERTIAL BOUNDARY LAYER EQUATIONS FOR A FLAT PLATE - CYLINDRICAL FORMULATION

Multiplying the equation above with,

$$\frac{R}{U_{\infty}^2} \quad (5.89)$$

results in a non-dimensional form where the order of magnitude of the terms can be evaluated:

$$\begin{aligned} \frac{\partial u_r^*}{\partial t^*} + u_r^* \frac{\partial u_r^*}{\partial r^*} + \left[ \frac{1}{\beta} \right] \frac{u_{\theta}^*}{r^*} \frac{\partial u_r^*}{\partial \theta^*} - \frac{u_{\theta}^{*2}}{r^*} + u_y^* \frac{\partial u_r^*}{\partial y^*} = -\frac{\partial \psi^*}{\partial r^*} + \left[ \frac{1}{U_{\infty} R} \right] v^* v_{\infty} \frac{\partial^2 u_r^*}{\partial r^{*2}} \\ + \left[ \frac{1}{U_{\infty} R} \right] v^* v_{\infty} \frac{1}{r^*} \frac{\partial u_r^*}{\partial r^*} + \left[ \frac{1}{U_{\infty} R \beta^2} \right] v^* v_{\infty} \frac{1}{r^{*2}} \frac{\partial^2 u_r^*}{\partial \theta^{*2}} - \left[ \frac{1}{U_{\infty} R \beta} \right] v^* v_{\infty} \frac{2}{r^{*2}} \frac{\partial u_{\theta}^*}{\partial \theta^*} \\ - \left[ \frac{1}{U_{\infty} R} \right] v^* v_{\infty} \frac{u_r^*}{r^{*2}} + \left[ \frac{R}{U_{\infty} \delta^2} \right] v^* v_{\infty} \frac{\partial^2 u_r^*}{\partial y^{*2}} - \left[ \frac{R}{U_{\infty} t} \right] 2u_{\theta}^* \omega_y^* + \left[ \frac{\delta}{U_{\infty} t} \right] 2u_y^* \omega_{\theta}^* \\ - \left[ \frac{\delta R}{U_{\infty}^2 t^2} \right] y^* \omega_r^* \omega_y^* + \left[ \frac{R^2}{U_{\infty}^2 t^2} \right] r^* \omega_y^{*2} + \left[ \frac{R^2}{U_{\infty}^2 t^2} \right] r^* \omega_{\theta}^{*2} \end{aligned} \quad (5.90)$$

As was done previously, in *Section 5.1* for the purposes of simplification, the assumption is made that the boundary layer thickness approaches a very small number ( $\varepsilon^2$ ) while the characteristic length approaches a very large number ( $\infty$ ):

$$\begin{aligned} \varepsilon &<< 1 \\ \delta &\rightarrow \varepsilon^2 \\ R &\rightarrow \infty \end{aligned} \quad (5.91)$$

In order to keep the solution as general as possible, it is assumed that velocity, time and characteristic angle has positive values:

$$\begin{aligned} U &\in [\varepsilon, \infty [ \\ t &\in [\varepsilon, \infty [ \\ \beta &\in ]0, 2\pi] \end{aligned} \quad (5.92)$$

From the above the following simplifications are made:

$$\begin{aligned} \frac{1}{U_{\infty} R} &\rightarrow \varepsilon \\ \frac{R}{\delta^2} &\rightarrow \infty \\ \delta R &\rightarrow \infty \end{aligned} \quad (5.93)$$

The most general form of the  $\hat{r}$ -momentum boundary layer equation becomes:

$$\begin{aligned} \frac{\partial \hat{u}_r}{\partial \hat{t}} + \hat{u}_r \frac{\partial \hat{u}_r}{\partial \hat{r}} + \frac{\hat{u}_{\theta}}{\hat{r}} \frac{\partial \hat{u}_r}{\partial \hat{\theta}} - \frac{\hat{u}_{\theta}^2}{\hat{r}} + \hat{u}_y \frac{\partial \hat{u}_r}{\partial \hat{y}} = -\frac{\partial \hat{\psi}}{\partial \hat{r}} + \hat{v} \frac{\partial^2 \hat{u}_r}{\partial \hat{y}^2} - 2\hat{u}_{\theta} \omega_y + 2\hat{u}_y \omega_{\theta} \\ - \hat{y} \omega_r \omega_y + \hat{r} \omega_y^2 + \hat{r} \omega_{\theta}^2 \end{aligned} \quad (5.94)$$

None of the fictitious terms could be eliminate and are having an effect in the boundary layer.

### 5.2.3.2 Second Principle Direction Equation

The component form of the conservation of momentum equation in the  $\hat{y}$ -direction is expressed as follow (Equation 4.57):

$$\begin{aligned} \frac{\partial \hat{u}_y}{\partial t} + \hat{u}_r \frac{\partial \hat{u}_y}{\partial \hat{r}} + \frac{\hat{u}_\theta}{\hat{r}} \frac{\partial \hat{u}_y}{\partial \hat{\theta}} + \hat{u}_y \frac{\partial \hat{u}_y}{\partial \hat{y}} = - \frac{\partial \hat{\psi}}{\partial \hat{y}} + v \left[ \frac{\partial^2 \hat{u}_y}{\partial \hat{r}^2} + \frac{1}{\hat{r}} \frac{\partial \hat{u}_y}{\partial \hat{r}} + \frac{1}{\hat{r}^2} \frac{\partial^2 \hat{u}_y}{\partial \hat{\theta}^2} + \frac{\partial^2 \hat{u}_y}{\partial \hat{y}^2} \right] \\ - \underbrace{2\hat{u}_r \omega_\theta + 2\hat{u}_\theta \omega_r}_{\text{Coriolis}} - \underbrace{\hat{r} \omega_r \omega_y + \hat{y} \omega_r^2 + \hat{y} \omega_\theta^2}_{\text{Centrifugal}} \end{aligned} \quad (5.95)$$

Substitution of the equations as shown in Section 5.2.1 result in the expression:

$$\begin{aligned} \left[ \frac{U_\infty^2 \delta}{R^2} \right] \frac{\partial u_y^*}{\partial t^*} + \left[ \frac{U_\infty^2 \delta}{R^2} \right] u_r^* \frac{\partial u_y^*}{\partial r^*} + \left[ \frac{U_\infty^2}{R^2} \right] \frac{u_\theta^*}{r^*} \frac{\partial u_y^*}{\partial \theta^*} + \left[ \frac{U_\infty^2 \delta}{R^2} \right] u_y^* \frac{\partial u_y^*}{\partial y^*} = - \left[ \frac{U_\infty^2}{\delta} \right] \frac{\partial \psi^*}{\partial y^*} \\ + \left[ \frac{U_\infty \delta}{R^3} \right] v^* v_\infty \frac{\partial^2 u_y^*}{\partial r^{*2}} + \left[ \frac{U_\infty \delta}{R^3} \right] v^* v_\infty \frac{1}{r^*} \frac{\partial u_y^*}{\partial r^*} + \left[ \frac{U_\infty \delta}{\beta^2 R^3} \right] v^* v_\infty \frac{1}{r^{*2}} \frac{\partial^2 u_y^*}{\partial \theta^{*2}} \\ + \left[ \frac{U_\infty}{\delta R} \right] v^* v_\infty \frac{\partial^2 u_y^*}{\partial y^{*2}} - \left[ \frac{U_\infty}{t} \right] 2u_r^* \omega_\theta^* + \left[ \frac{U_\infty}{t} \right] 2u_\theta^* \omega_r^* - \left[ \frac{R}{t^2} \right] r^* \omega_r^* \omega_y^* \\ + \left[ \frac{\delta}{t^2} \right] y^* \omega_r^{*2} + \left[ \frac{\delta}{t^2} \right] y^* \omega_\theta^{*2} \end{aligned} \quad (5.96)$$

Multiply the equation above with,

$$\frac{\delta}{U_\infty^2} \quad (5.97)$$

results in the non-dimensional form of the equation:

$$\begin{aligned} \left[ \frac{\delta^2}{R^2} \right] \frac{\partial u_y^*}{\partial t^*} + \left[ \frac{\delta^2}{R^2} \right] u_r^* \frac{\partial u_y^*}{\partial r^*} + \left[ \frac{\delta}{R^2} \right] \frac{u_\theta^*}{r^*} \frac{\partial u_y^*}{\partial \theta^*} + \left[ \frac{\delta^2}{R^2} \right] u_y^* \frac{\partial u_y^*}{\partial y^*} = - \frac{\partial \psi^*}{\partial y^*} \\ + \left[ \frac{\delta^2}{U_\infty R^3} \right] v^* v_\infty \frac{\partial^2 u_y^*}{\partial r^{*2}} + \left[ \frac{\delta^2}{U_\infty R^3} \right] v^* v_\infty \frac{1}{r^*} \frac{\partial u_y^*}{\partial r^*} \\ + \left[ \frac{\delta^2}{U_\infty \beta^2 R^3} \right] v^* v_\infty \frac{1}{r^{*2}} \frac{\partial^2 u_y^*}{\partial \theta^{*2}} + \left[ \frac{1}{U_\infty R} \right] v^* v_\infty \frac{\partial^2 u_y^*}{\partial y^{*2}} - \left[ \frac{\delta}{U_\infty t} \right] 2u_r^* \omega_\theta^* \\ + \left[ \frac{\delta}{U_\infty t} \right] 2u_\theta^* \omega_r^* - \left[ \frac{R \delta}{U_\infty^2 t^2} \right] r^* \omega_r^* \omega_y^* + \left[ \frac{\delta^2}{U_\infty^2 t^2} \right] y^* \omega_r^{*2} + \left[ \frac{\delta^2}{U_\infty^2 t^2} \right] y^* \omega_\theta^{*2} \end{aligned} \quad (5.98)$$

The simplification assumptions that were made in Section 5.2.1 are used here to arrive at the boundary layer equation in the  $\hat{y}$ -direction for cylindrical coordinates:

$$0 = - \frac{\partial \hat{\psi}}{\partial \hat{y}} - 2\hat{u}_r \omega_\theta + 2\hat{u}_\theta \omega_r - \hat{r} \omega_r \omega_y + \hat{y} \omega_r^2 + \hat{y} \omega_\theta^2 \quad (5.99)$$

5.2. NON-INERTIAL BOUNDARY LAYER EQUATIONS FOR A FLAT PLATE - CYLINDRICAL FORMULATION

5.2.3.3 Third Principle Direction Equation

The component form of the momentum equation in the  $\hat{\theta}$ - direction is expressed as shown in Equation 4.56:

$$\begin{aligned} \frac{\partial \hat{u}_\theta}{\partial t} + \hat{u}_r \frac{\partial \hat{u}_\theta}{\partial \hat{r}} + \frac{\hat{u}_\theta}{\hat{r}} \frac{\partial \hat{u}_\theta}{\partial \hat{\theta}} + \frac{\hat{u}_\theta \hat{u}_r}{\hat{r}} + \hat{u}_y \frac{\partial \hat{u}_\theta}{\partial \hat{y}} = -\frac{1}{\hat{r}} \frac{\partial \hat{\psi}}{\partial \hat{\theta}} \\ + \hat{v} \left[ \frac{\partial^2 \hat{u}_\theta}{\partial \hat{r}^2} + \frac{1}{\hat{r}} \frac{\partial \hat{u}_\theta}{\partial \hat{r}} + \frac{1}{\hat{r}^2} \frac{\partial^2 \hat{u}_\theta}{\partial \hat{\theta}^2} - \frac{2}{\hat{r}^2} \frac{\partial \hat{u}_r}{\partial \hat{\theta}} - \frac{\hat{u}_\theta}{\hat{r}^2} + \frac{\partial^2 \hat{u}_\theta}{\partial \hat{y}^2} \right] \\ - \underbrace{2\hat{u}_y \omega_r + 2\hat{u}_r \omega_y}_{\text{Coriolis}} - \underbrace{\hat{r} \omega_r \omega_\theta - \hat{y} \omega_\theta \omega_y}_{\text{Centrifugal}} \end{aligned} \quad (5.100)$$

Substituting the non-dimensional parameters of Section 5.2.1 into the equation above yields:

$$\begin{aligned} \left[ \frac{U_\infty^2}{R} \right] \frac{\partial u_\theta^*}{\partial t^*} + \left[ \frac{U_\infty^2}{R} \right] u_r^* \frac{\partial u_\theta^*}{\partial r^*} + \left[ \frac{U_\infty^2}{\beta R} \right] \frac{u_\theta^*}{r^*} \frac{\partial u_\theta^*}{\partial \theta^*} + \left[ \frac{U_\infty^2}{R} \right] \frac{u_\theta^* u_r^*}{r^*} + \left[ \frac{U_\infty^2}{R} \right] u_y^* \frac{\partial u_\theta^*}{\partial y^*} = \\ - \left[ \frac{U_\infty^2}{\beta R} \right] \frac{1}{r^*} \frac{\partial \psi^*}{\partial \theta^*} + \left[ \frac{U_\infty}{R^2} \right] v^* v_\infty \frac{\partial^2 u_\theta^*}{\partial r^{*2}} + \left[ \frac{U_\infty}{R^2} \right] v^* v_\infty \frac{1}{r^*} \frac{\partial u_\theta^*}{\partial r^*} \\ + \left[ \frac{U_\infty}{\beta^2 R^2} \right] v^* v_\infty \frac{1}{r^{*2}} \frac{\partial^2 u_\theta^*}{\partial \theta^{*2}} - \left[ \frac{U_\infty}{\beta^2 R^2} \right] v^* v_\infty \frac{2}{r^{*2}} \frac{\partial u_r^*}{\partial \theta^*} - \left[ \frac{U_\infty}{R^2} \right] v^* v_\infty \frac{u_\theta^*}{r^{*2}} \\ + \left[ \frac{U_\infty}{\delta^2} \right] v^* v_\infty \frac{\partial^2 u_\theta^*}{\partial y^{*2}} - \left[ \frac{U_\infty \delta}{R t} \right] 2u_y^* \omega_r^* + \left[ \frac{U_\infty}{t} \right] 2u_r^* \omega_y^* \\ - \left[ \frac{R}{t^2} \right] r^* \omega_r^* \omega_\theta^* - \left[ \frac{\delta}{t^2} \right] y^* \omega_\theta^* \omega_y^* \end{aligned} \quad (5.101)$$

Multiplying the non-dimensional expression above with,

$$\frac{\beta R}{U_\infty^2} \quad (5.102)$$

Results in the non-dimensional form of the  $\hat{\theta}$ -momentum equation.

$$\begin{aligned} \beta \frac{\partial u_\theta^*}{\partial t^*} + \beta u_r^* \frac{\partial u_\theta^*}{\partial r^*} + \frac{u_\theta^*}{r^*} \frac{\partial u_\theta^*}{\partial \theta^*} + \beta \frac{u_\theta^* u_r^*}{r^*} + \beta u_y^* \frac{\partial u_\theta^*}{\partial y^*} = -\frac{1}{r^*} \frac{\partial \psi^*}{\partial \theta^*} \\ + \left[ \frac{\beta}{U_\infty R} \right] v^* v_\infty \frac{\partial^2 u_\theta^*}{\partial r^{*2}} + \left[ \frac{\beta}{U_\infty R} \right] v^* v_\infty \frac{1}{r^*} \frac{\partial u_\theta^*}{\partial r^*} + \left[ \frac{1}{U_\infty R \beta} \right] v^* v_\infty \frac{1}{r^{*2}} \frac{\partial^2 u_\theta^*}{\partial \theta^{*2}} \\ - \left[ \frac{1}{U_\infty R \beta} \right] v^* v_\infty \frac{2}{r^{*2}} \frac{\partial u_r^*}{\partial \theta^*} - \left[ \frac{\beta}{U_\infty R} \right] v^* v_\infty \frac{u_\theta^*}{r^{*2}} + \left[ \frac{\beta R}{U_\infty \delta^2} \right] v^* v_\infty \frac{\partial^2 u_\theta^*}{\partial y^{*2}} \\ - \left[ \frac{\beta \delta}{U_\infty t} \right] 2u_y^* \omega_r^* + \left[ \frac{\beta R}{U_\infty t} \right] 2u_r^* \omega_y^* - \left[ \frac{\beta R^2}{U_\infty^2 t^2} \right] r^* \omega_r^* \omega_\theta^* - \left[ \frac{\beta \delta R}{U_\infty^2 t^2} \right] y^* \omega_\theta^* \omega_y^* \end{aligned} \quad (5.103)$$

The same simplifications that were done for the  $\hat{r}$ -momentum equation above are employed here to obtain the final form of  $\hat{\theta}$ -momentum boundary layer equation:

$$\begin{aligned} \frac{\partial \hat{u}_\theta}{\partial t} + \hat{u}_r \frac{\partial \hat{u}_\theta}{\partial \hat{r}} + \frac{\hat{u}_\theta}{\hat{r}} \frac{\partial \hat{u}_\theta}{\partial \hat{\theta}} + \frac{\hat{u}_\theta \hat{u}_r}{\hat{r}} + \hat{u}_y \frac{\partial \hat{u}_\theta}{\partial \hat{y}} = -\frac{1}{\hat{r}} \frac{\partial \hat{\psi}}{\partial \hat{\theta}} + \hat{v} \frac{\partial^2 \hat{u}_\theta}{\partial \hat{y}^2} - 2\hat{u}_y \omega_r + 2\hat{u}_r \omega_y \\ - \hat{r} \omega_r \omega_\theta - \hat{y} \omega_\theta \omega_y \end{aligned} \quad (5.104)$$

Again, as in the case of the  $\hat{r}$ -momentum, none of the fictitious terms could be eliminated from the boundary layer equation.

### 5.2.3.4 Compressibility Effects on the Boundary Layer Equations

The stress tensor in Cylindrical coordinates is described by *Equation 4.43*:

$$\hat{\boldsymbol{\tau}}(\hat{r}, \hat{\theta}, \hat{y}) = \begin{bmatrix} 2\hat{\mu}\frac{\partial\hat{u}_r}{\partial\hat{r}} + \hat{\lambda}\hat{\nabla}\cdot\hat{\mathbf{u}} & \hat{\mu}\left(\frac{1}{\hat{r}}\frac{\partial\hat{u}_r}{\partial\hat{\theta}} - \frac{\hat{u}_\theta}{\hat{r}} + \frac{\partial\hat{u}_\theta}{\partial\hat{r}}\right) & \hat{\mu}\left(\frac{\partial\hat{u}_r}{\partial\hat{y}} + \frac{\partial\hat{u}_y}{\partial\hat{r}}\right) \\ \hat{\mu}\left(\frac{1}{\hat{r}}\frac{\partial\hat{u}_r}{\partial\hat{\theta}} - \frac{\hat{u}_\theta}{\hat{r}} + \frac{\partial\hat{u}_\theta}{\partial\hat{r}}\right) & 2\hat{\mu}\left(\frac{1}{\hat{r}}\frac{\partial\hat{u}_\theta}{\partial\hat{\theta}} + \frac{\hat{u}_r}{\hat{r}}\right) + \hat{\lambda}\hat{\nabla}\cdot\hat{\mathbf{u}} & \hat{\mu}\left(\frac{1}{\hat{r}}\frac{\partial\hat{u}_y}{\partial\hat{\theta}} + \frac{\partial\hat{u}_\theta}{\partial\hat{y}}\right) \\ \hat{\mu}\left(\frac{\partial\hat{u}_r}{\partial\hat{y}} + \frac{\partial\hat{u}_y}{\partial\hat{r}}\right) & \hat{\mu}\left(\frac{1}{\hat{r}}\frac{\partial\hat{u}_y}{\partial\hat{\theta}} + \frac{\partial\hat{u}_\theta}{\partial\hat{y}}\right) & 2\hat{\mu}\frac{\partial\hat{u}_y}{\partial\hat{y}} + \hat{\lambda}\hat{\nabla}\cdot\hat{\mathbf{u}} \end{bmatrix} \quad (5.105)$$

Here it is determined which of the diffusion terms, that are relevant in the bulk flow, are present in the boundary layer. This is done using the order of magnitude analysis that was employed to determined the incompressible boundary layer equations.

The components that pertain to the  $\hat{\mathbf{r}}$ -momentum equation is:

$$\frac{\partial}{\partial\hat{r}}\left[2\hat{\mu}\frac{\partial\hat{u}_r}{\partial\hat{r}} + \hat{\lambda}\left(\frac{\partial\hat{u}_r}{\partial\hat{r}} + \frac{\hat{u}_r}{\hat{r}} + \frac{1}{\hat{r}}\frac{\partial\hat{u}_\theta}{\partial\hat{\theta}} + \frac{\partial\hat{u}_y}{\partial\hat{y}}\right)\right] + \frac{\partial}{\partial\hat{\theta}}\left[\hat{\mu}\left(\frac{1}{\hat{r}}\frac{\partial\hat{u}_r}{\partial\hat{\theta}} - \frac{\hat{u}_\theta}{\hat{r}} + \frac{\partial\hat{u}_\theta}{\partial\hat{r}}\right)\right] + \frac{\partial}{\partial\hat{y}}\left[\hat{\mu}\left(\frac{\partial\hat{u}_r}{\partial\hat{y}} + \frac{\partial\hat{u}_y}{\partial\hat{r}}\right)\right] \quad (5.106)$$

The non-dimensional parameters of *Section 5.2.1* are substituted in the terms above and multiplied by *Equation 5.89*,

$$\frac{R}{U_\infty^2} \quad (5.107)$$

to obtain the non-dimensional form of the terms:

$$\begin{aligned} & \left[\frac{1}{U_\infty R}\right]\frac{\partial}{\partial r^*}2\mu\frac{\partial u_r^*}{\partial r^*} + \left[\frac{1}{U_\infty R}\right]\frac{\partial}{\partial r^*}\lambda\left(\frac{\partial u_r^*}{\partial r^*} + \frac{u_r^*}{r^*}\right) + \left[\frac{1}{U_\infty\beta R}\right]\frac{\partial}{\partial r^*}\lambda\frac{1}{r^*}\frac{\partial u_\theta^*}{\partial\theta^*} + \left[\frac{1}{U_\infty R}\right]\frac{\partial}{\partial r^*}\lambda\frac{\partial u_y^*}{\partial y^*} \\ & + \left[\frac{1}{U_\infty\beta^2}\right]\frac{\partial}{\partial\theta^*}\mu\frac{1}{r^*}\frac{\partial u_r^*}{\partial\theta^*} - \left[\frac{1}{U_\infty\beta}\right]\frac{\partial}{\partial\theta^*}\mu\left(\frac{u_\theta^*}{r^*} + \frac{\partial u_\theta^*}{\partial r^*}\right) + \left[\frac{R}{U_\infty\delta^2}\right]\frac{\partial}{\partial y^*}\mu\frac{\partial u_r^*}{\partial y^*} + \left[\frac{1}{U_\infty R}\right]\frac{\partial}{\partial y^*}\mu\frac{\partial u_y^*}{\partial r^*} \end{aligned} \quad (5.108)$$

An order of magnitude analysis results in a number of the terms being neglected. The diffusive terms in the compressible  $\hat{\mathbf{r}}$ -momentum equation are similar to the terms in the incompressible form (*Equation 5.94*):

$$\frac{\partial}{\partial\hat{y}}\hat{\mu}\frac{\partial\hat{u}_r}{\partial\hat{y}} \quad (5.109)$$

The compressible form of the boundary layer equation for the conservation of momentum in the  $\hat{\mathbf{r}}$ -direction is similar to the incompressible form determined in *Equation 5.94*:

$$\begin{aligned} \frac{\partial\hat{\rho}\hat{u}_r}{\partial t} + \hat{u}_r\frac{\partial\hat{\rho}\hat{u}_r}{\partial\hat{r}} + \frac{\hat{u}_\theta}{\hat{r}}\frac{\partial\hat{\rho}\hat{u}_r}{\partial\hat{\theta}} - \frac{\hat{\rho}\hat{u}_\theta^2}{\hat{r}} + \hat{u}_y\frac{\partial\hat{\rho}\hat{u}_r}{\partial\hat{y}} = & -\frac{\partial\hat{p}}{\partial\hat{r}} + \frac{\partial}{\partial\hat{y}}\hat{\mu}\frac{\partial\hat{u}_r}{\partial\hat{y}} - 2\hat{\rho}\hat{u}_\theta\omega_y + 2\hat{\rho}\hat{u}_y\omega_\theta \\ & - \hat{\rho}\hat{y}\omega_r\omega_y + \hat{\rho}\hat{r}\omega_y^2 + \hat{\rho}\hat{r}\omega_\theta^2 \end{aligned} \quad (5.110)$$

The components that pertain to the  $\hat{\mathbf{y}}$ -momentum equation is:

$$\frac{\partial}{\partial\hat{r}}\left[\hat{\mu}\left(\frac{\partial\hat{u}_r}{\partial\hat{y}} + \frac{\partial\hat{u}_y}{\partial\hat{r}}\right)\right] + \frac{\partial}{\partial\hat{\theta}}\left[\hat{\mu}\left(\frac{1}{\hat{r}}\frac{\partial\hat{u}_y}{\partial\hat{\theta}} + \frac{\partial\hat{u}_\theta}{\partial\hat{y}}\right)\right] + \frac{\partial}{\partial\hat{y}}\left[2\hat{\mu}\frac{\partial\hat{u}_y}{\partial\hat{y}} + \hat{\lambda}\left(\frac{\partial\hat{u}_r}{\partial\hat{r}} + \frac{\hat{u}_r}{\hat{r}} + \frac{1}{\hat{r}}\frac{\partial\hat{u}_\theta}{\partial\hat{\theta}} + \frac{\partial\hat{u}_y}{\partial\hat{y}}\right)\right] \quad (5.111)$$



5.2. NON-INERTIAL BOUNDARY LAYER EQUATIONS FOR A FLAT PLATE - CYLINDRICAL FORMULATION

The non-dimensional parameters of *Section 5.2.1* is substituted in the terms above and multiplied by *Equation 5.97*,

$$\frac{\delta}{U_\infty^2} \quad (5.112)$$

to obtain the non-dimensional form of the terms:

$$\begin{aligned} & \left[ \frac{1}{U_\infty R} \right] \frac{\partial}{\partial r^*} \mu \frac{\partial u_r^*}{\partial y^*} + \left[ \frac{\delta^2}{U_\infty R^3} \right] \frac{\partial}{\partial r^*} \mu \frac{\partial u_y^*}{\partial r^*} + \left[ \frac{\delta^2}{U_\infty \beta^2 R^2} \right] \frac{\partial}{\partial \theta^*} \mu \frac{1}{r^*} \frac{\partial u_y^*}{\partial \theta^*} + \left[ \frac{1}{\beta U_\infty} \right] \frac{\partial}{\partial \theta^*} \mu \frac{\partial u_\theta^*}{\partial y^*} \\ & + \left[ \frac{1}{U_\infty R} \right] \frac{\partial}{\partial y^*} 2\mu \frac{\partial u_y^*}{\partial y^*} + \left[ \frac{1}{U_\infty R} \right] \frac{\partial}{\partial y^*} \lambda \left( \frac{\partial u_r^*}{\partial r^*} + \frac{u_r^*}{r^*} \right) + \left[ \frac{1}{R \beta U_\infty} \right] \frac{\partial}{\partial y^*} \lambda \frac{1}{r^*} \frac{\partial u_\theta^*}{\partial \theta^*} + \left[ \frac{1}{U_\infty R} \right] \frac{\partial}{\partial y^*} \lambda \frac{\partial u_y^*}{\partial y^*} \end{aligned} \quad (5.113)$$

The diffusive terms in the compressible  $\hat{y}$ -momentum equation are similar to the terms in the incompressible form; no diffusion terms are present. The compressible form of the boundary layer equation for the conservation of momentum in the  $\hat{\theta}$ -direction is similar to the incompressible form determined in *Equation 5.99*:

$$0 = -\frac{\partial \hat{\psi}}{\partial \hat{y}} - 2\hat{u}_r \omega_\theta + 2\hat{u}_\theta \omega_r - \hat{r} \omega_r \omega_y + \hat{y} \omega_r^2 + \hat{y} \omega_\theta^2 \quad (5.114)$$

The components that pertain to the  $\hat{\theta}$ -momentum equation is:

$$\frac{\partial}{\partial \hat{r}} \left[ \hat{\mu} \left( \frac{1}{\hat{r}} \frac{\partial \hat{u}_r}{\partial \hat{\theta}} - \frac{\hat{u}_\theta}{\hat{r}} + \frac{\partial \hat{u}_\theta}{\partial \hat{r}} \right) \right] + \frac{\partial}{\partial \hat{\theta}} \left[ 2\hat{\mu} \left( \frac{1}{\hat{r}} \frac{\partial \hat{u}_\theta}{\partial \hat{\theta}} + \frac{\hat{u}_r}{\hat{r}} \right) + \hat{\lambda} \left( \frac{\partial \hat{u}_r}{\partial \hat{r}} + \frac{\hat{u}_r}{\hat{r}} + \frac{1}{\hat{r}} \frac{\partial \hat{u}_\theta}{\partial \hat{\theta}} + \frac{\partial \hat{u}_y}{\partial \hat{y}} \right) \right] + \frac{\partial}{\partial \hat{y}} \left[ \hat{\mu} \left( \frac{1}{\hat{r}} \frac{\partial \hat{u}_y}{\partial \hat{\theta}} + \frac{\partial \hat{u}_\theta}{\partial \hat{y}} \right) \right] \quad (5.115)$$

The non-dimensional parameters of *Section 5.2.1* are substituted in the terms above and multiplied by *Equation 5.102*,

$$\frac{\beta R}{U_\infty^2} \quad (5.116)$$

to obtain the non-dimensional form of the terms:

$$\begin{aligned} & \left[ \frac{1}{U_\infty R} \right] \frac{\partial}{\partial r^*} \mu \frac{1}{r^*} \frac{\partial u_r^*}{\partial \theta^*} + \left[ \frac{\beta}{U_\infty R} \right] \frac{\partial}{\partial r^*} \left[ \mu \left( -\frac{u_\theta^*}{r^*} + \frac{\partial u_\theta^*}{\partial r^*} \right) \right] + \left[ \frac{1}{\beta U_\infty} \right] \frac{\partial}{\partial \theta^*} 2\mu \frac{1}{r^*} \frac{\partial u_\theta^*}{\partial \theta^*} + \left[ \frac{1}{U_\infty} \right] \frac{\partial}{\partial \theta^*} 2\mu \frac{u_r^*}{r^*} \\ & + \left[ \frac{1}{U_\infty} \right] \frac{\partial}{\partial \theta^*} \lambda \left( \frac{\partial u_r^*}{\partial r^*} + \frac{u_r^*}{r^*} \right) + \left[ \frac{1}{\beta U_\infty} \right] \frac{\partial}{\partial \theta^*} \lambda \frac{1}{r^*} \frac{\partial u_\theta^*}{\partial \theta^*} + \left[ \frac{1}{U_\infty} \right] \frac{\partial}{\partial \theta^*} \lambda \frac{\partial u_y^*}{\partial y^*} + \left[ \frac{1}{U_\infty R} \right] \frac{\partial}{\partial y^*} \mu \frac{1}{r^*} \frac{\partial u_y^*}{\partial \theta^*} \\ & + \left[ \frac{\beta R}{\delta^2 U_\infty} \right] \frac{\partial}{\partial y^*} \mu \frac{\partial u_\theta^*}{\partial y^*} \end{aligned} \quad (5.117)$$

An order of magnitude analysis results in a number of the terms being neglected. The diffusive terms in the compressible  $\hat{\theta}$ -momentum equation are similar to the terms in the incompressible form (*Equation 5.104*):

$$\frac{\partial}{\partial \hat{y}} \hat{\mu} \frac{\partial \hat{u}_\theta}{\partial \hat{y}} \quad (5.118)$$

The compressible form of the boundary layer equation for the conservation of momentum in the  $\hat{\theta}$ -direction is similar to the incompressible form determined in *Equation 5.104*:

$$\begin{aligned} \frac{\partial \hat{u}_\theta}{\partial t} + \hat{u}_r \frac{\partial \hat{u}_\theta}{\partial \hat{r}} + \frac{\hat{u}_\theta}{\hat{r}} \frac{\partial \hat{u}_\theta}{\partial \hat{\theta}} + \frac{\hat{u}_\theta \hat{u}_r}{\hat{r}} + \hat{u}_y \frac{\partial \hat{u}_\theta}{\partial \hat{y}} = & -\frac{1}{\hat{r}} \frac{\partial \hat{\psi}}{\partial \hat{\theta}} + \hat{v} \frac{\partial^2 \hat{u}_\theta}{\partial \hat{y}^2} - 2\hat{u}_y \omega_r + 2\hat{u}_r \omega_y \\ & - \hat{r} \omega_r \omega_\theta - \hat{y} \omega_\theta \omega_r \end{aligned} \quad (5.119)$$

### 5.2.4 Validation of Equations

The cylindrical form of the Navier-Stokes equations are expressed, as in the Cartesian case, in the inertial or the non-inertial form. Expressing a set of equations, that was originally in the Cartesian system, in cylindrical coordinates do not place it in the non-inertial frame. This misconception was noted in Anon [84] as shown in Equation 5.120 where certain cylindrical terms (as marked in the equation) were described as the Centrifugal and Coriolis forces respectively. Those terms are merely part of the material derivative in the cylindrical system and bears no relevance to the fictitious forces. This is shown in the sections below.

$$\begin{aligned} \frac{\partial u_r}{\partial t} + u_r \frac{\partial u_r}{\partial r} + \frac{u_\theta}{r} \frac{\partial u_r}{\partial \theta} - \overbrace{\frac{u_\theta^2}{r}}^{\text{Centrifugal}} + u_y \frac{\partial u_r}{\partial y} = & -\frac{\partial \psi}{\partial r} \\ + v \left[ \frac{\partial^2 u_r}{\partial r^2} + \frac{1}{r} \frac{\partial u_r}{\partial r} + \frac{1}{r^2} \frac{\partial^2 u_r}{\partial \theta^2} - \frac{2}{r^2} \frac{\partial u_\theta}{\partial \theta} - \frac{u_r}{r^2} + \frac{\partial^2 u_r}{\partial y^2} \right] & \end{aligned} \quad (5.120)$$

$$\begin{aligned} \frac{\partial u_\theta}{\partial t} + u_r \frac{\partial u_\theta}{\partial r} + \frac{u_\theta}{r} \frac{\partial u_\theta}{\partial \theta} + \overbrace{\frac{u_\theta u_r}{r}}^{\text{Coriolis}} + u_y \frac{\partial u_\theta}{\partial y} = & -\frac{1}{r} \frac{\partial \psi}{\partial \theta} \\ + v \left[ \frac{\partial^2 u_\theta}{\partial r^2} + \frac{1}{r} \frac{\partial u_\theta}{\partial r} + \frac{1}{r^2} \frac{\partial^2 u_\theta}{\partial \theta^2} - \frac{2}{r^2} \frac{\partial u_r}{\partial \theta} - \frac{u_\theta}{r^2} + \frac{\partial^2 u_\theta}{\partial y^2} \right] & \end{aligned}$$

Analytical solutions to classic rotating flow problems, such as the von Karman rotating disk, are done in the Cylindrical system (Schlichting [42]). The vector form of the non-inertial Navier-Stokes equations is independent from coordinates system. The differences in the system of equations (Cartesian and Cylindrical), only becomes apparent when written in component form.

#### 5.2.4.1 Conversion

The Cartesian positions are related to the Cylindrical positions as shown below where it is assumed that the  $\hat{y}$ -axis remains common between the coordinates systems (*Equation 4.15*):

$$\begin{aligned} \hat{x} &= \hat{r} \cos \hat{\theta} \\ \hat{y} &= \hat{y} \\ \hat{z} &= \hat{r} \sin \hat{\theta} \end{aligned} \quad (5.121)$$

## 5.2. NON-INERTIAL BOUNDARY LAYER EQUATIONS FOR A FLAT PLATE - CYLINDRICAL FORMULATION

The velocity components are therefore related by *Equation 4.16*:

$$\begin{aligned}\hat{u} &= \hat{u}_r \cos \hat{\theta} - \hat{u}_\theta \sin \hat{\theta} \\ \hat{v} &= \hat{u}_y \\ \hat{w} &= \hat{u}_r \sin \hat{\theta} + \hat{u}_\theta \cos \hat{\theta}\end{aligned}\quad (5.122)$$

The derivatives of one system are converted by means of the matrix:

$$\begin{bmatrix} \frac{\partial \hat{\phi}}{\partial \hat{x}} \\ \frac{\partial \hat{\phi}}{\partial \hat{y}} \\ \frac{\partial \hat{\phi}}{\partial \hat{z}_v} \end{bmatrix} = \begin{bmatrix} \cos \hat{\theta} & -\frac{\sin \hat{\theta}}{\hat{r}} & 0 \\ 0 & 0 & 1 \\ \sin \hat{\theta} & \frac{\cos \hat{\theta}}{\hat{r}} & 0 \end{bmatrix} \begin{bmatrix} \frac{\partial \hat{\phi}}{\partial \hat{r}} \\ \frac{\partial \hat{\phi}}{\partial \hat{\theta}} \\ \frac{\partial \hat{\phi}}{\partial \hat{y}} \end{bmatrix}\quad (5.123)$$

The relations above are used to convert between the coordinates systems in the section below to obtain the non-inertial boundary layer equations.

### 5.2.4.2 Continuity

The continuity equation for the boundary layer was derived in *Section 5.1.2* and resulted in *Equation 5.14*:

$$\frac{\partial \hat{u}}{\partial \hat{x}} + \frac{\partial \hat{v}}{\partial \hat{y}} + \frac{\partial \hat{w}}{\partial \hat{z}} = 0\quad (5.124)$$

Substitution with the equations as shown in the previous section lead to the following expressions:

$$\begin{aligned}(\cos \hat{\theta} \frac{\partial}{\partial \hat{r}} - \frac{\sin \hat{\theta}}{\hat{r}} \frac{\partial}{\partial \hat{\theta}})(\hat{u}_r \cos \hat{\theta} - \hat{u}_\theta \sin \hat{\theta}) + (\sin \hat{\theta} \frac{\partial}{\partial \hat{r}} + \frac{\cos \hat{\theta}}{\hat{r}} \frac{\partial}{\partial \hat{\theta}})(\hat{u}_r \sin \hat{\theta} + \hat{u}_\theta \cos \hat{\theta}) \\ + \frac{\partial \hat{u}_y}{\partial \hat{y}} = 0\end{aligned}\quad (5.125)$$

$$\frac{\partial \hat{u}_r}{\partial \hat{r}} (\cos^2 \hat{\theta} + \sin^2 \hat{\theta}) + \frac{\hat{u}_r}{\hat{r}} (\cos^2 \hat{\theta} + \sin^2 \hat{\theta}) + \frac{1}{\hat{r}} \frac{\partial \hat{u}_\theta}{\partial \hat{\theta}} (\cos^2 \hat{\theta} + \sin^2 \hat{\theta}) + \frac{\partial \hat{u}_y}{\partial \hat{y}} = 0$$

Using,

$$\cos^2 \hat{\theta} + \sin^2 \hat{\theta} = 1\quad (5.126)$$

the final equation becomes:

$$\frac{\partial \hat{u}_r}{\partial \hat{r}} + \frac{\hat{u}_r}{\hat{r}} + \frac{1}{\hat{r}} \frac{\partial \hat{u}_\theta}{\partial \hat{\theta}} + \frac{\partial \hat{u}_y}{\partial \hat{y}} = 0\quad (5.127)$$

This is the equation for the boundary layer in cylindrical coordinates. This is the same as *Equation 5.85* derived in *Section 5.2.2*.

### 5.2.4.3 Momentum Equations

The non-inertial  $\hat{x}$ -momentum equation, as derived in *Section 5.1.3.1*, *Equation 5.23* is:

$$\begin{aligned}\frac{\partial \hat{u}}{\partial t} + \hat{u} \frac{\partial \hat{u}}{\partial \hat{x}} + \hat{v} \frac{\partial \hat{u}}{\partial \hat{y}} + \hat{w} \frac{\partial \hat{u}}{\partial \hat{z}} = -\frac{\partial \hat{\psi}}{\partial \hat{x}} + \nu \left( \frac{\partial^2 \hat{u}}{\partial \hat{y}^2} \right) + 2\hat{v}\omega_3 - 2\hat{w}\omega_2 \\ + \hat{x}(\omega_3^2 + \omega_2^2) - \hat{y}\omega_1\omega_2 - \hat{z}\omega_1\omega_3\end{aligned}\quad (5.128)$$

CHAPTER 5. NON-INERTIAL BOUNDARY LAYER EQUATIONS

This is converted to the Cylindrical coordinates system piece by piece to result in the final equation.

The transient term, with substitution of the conversions indicated in *Section 5.4.1* is expanded to the following:

$$\frac{\partial \hat{u}}{\partial t} \rightarrow \frac{\partial}{\partial t}(\hat{u}_r \cos \hat{\theta} - \hat{u}_\theta \sin \hat{\theta}) \frac{\partial}{\partial t}(\hat{u}_r \cos \hat{\theta} - \hat{u}_\theta \sin \hat{\theta}) = \frac{\partial \hat{u}_r}{\partial t} \cos \hat{\theta} + \frac{\partial \cos \hat{\theta}}{\partial t} \hat{u}_r - \frac{\partial \hat{u}_\theta}{\partial t} \sin \hat{\theta} - \frac{\partial \sin \hat{\theta}}{\partial t} \hat{u}_\theta \quad (5.129)$$

If it is assumed that  $\hat{\theta} \rightarrow \varepsilon$  where  $\varepsilon \rightarrow 0$ , then  $\cos \hat{\theta} \rightarrow 1$  and  $\sin \hat{\theta} \rightarrow 0$ . The equation above simplifies to:

$$\frac{\partial \hat{u}}{\partial t} \rightarrow \frac{\partial \hat{u}_r}{\partial t} \quad (5.130)$$

The remainder of the terms is converted in a similar manner:

**Advection terms:**

$$\begin{aligned} \hat{u} \frac{\partial \hat{u}}{\partial \hat{x}} &\rightarrow \hat{u}_r \frac{\partial \hat{u}_r}{\partial \hat{r}} \\ \hat{v} \frac{\partial \hat{u}}{\partial \hat{y}} &\rightarrow \hat{u}_y \frac{\partial \hat{u}_r}{\partial \hat{y}} \\ \hat{w} \frac{\partial \hat{u}}{\partial \hat{z}} &\rightarrow \frac{\hat{u}_\theta}{\hat{r}} \frac{\partial \hat{u}_r}{\partial \hat{\theta}} - \frac{\hat{u}_\theta^2}{\hat{r}} \end{aligned} \quad (5.131)$$

**Pressure term:**

$$\frac{\partial \hat{\psi}}{\partial \hat{x}} \rightarrow \frac{\partial \hat{\psi}}{\partial \hat{r}} \quad (5.132)$$

**Diffusion term:**

$$\frac{\partial^2 \hat{u}}{\partial \hat{y}^2} \rightarrow \frac{\partial^2 \hat{u}_r}{\partial \hat{y}^2} \quad (5.133)$$

**Fictitious terms:**

**Coriolis terms,**

$$\begin{aligned} 2\hat{v}\hat{\omega}_3 - 2\hat{w}\hat{\omega}_2 &\rightarrow [2\hat{u}_y(\hat{\omega}_r \sin \hat{\theta} + \hat{\omega}_\theta \cos \hat{\theta}) - 2(\hat{u}_r \sin \hat{\theta} + \hat{u}_\theta \cos \hat{\theta})\hat{\omega}_z] \\ &\rightarrow 2\hat{u}_y \omega_\theta - 2\hat{u}_\theta \omega_y \end{aligned} \quad (5.134)$$

**Centrifugal terms,**

$$\hat{x}(\hat{\omega}_3^2 + \hat{\omega}_2^2) - \hat{y}\hat{\omega}_1\hat{\omega}_2 - \hat{z}\hat{\omega}_1\hat{\omega}_3 \rightarrow -\hat{y}\hat{\omega}_r\hat{\omega}_y + \hat{r}\hat{\omega}_y^2 + \hat{r}\hat{\omega}_\theta^2$$

This conversion leads to the non-inertial form of the  $\hat{r}$ -momentum, which is the same as the derived Equation 5.94:

$$\begin{aligned} \frac{\partial \hat{u}_r}{\partial t} + \hat{u}_r \frac{\partial \hat{u}_r}{\partial \hat{r}} + \frac{\hat{u}_\theta}{\hat{r}} \frac{\partial \hat{u}_r}{\partial \hat{\theta}} - \frac{\hat{u}_\theta^2}{\hat{r}} + \hat{u}_y \frac{\partial \hat{u}_r}{\partial \hat{y}} &= -\frac{\partial \hat{\psi}}{\partial \hat{r}} + \hat{v} \frac{\partial^2 \hat{u}_r}{\partial \hat{y}^2} - 2\hat{u}_\theta \omega_y + 2\hat{u}_y \omega_\theta \\ &\quad - \hat{y}\omega_r \omega_y + \hat{r}\omega_y^2 + \hat{r}\omega_\theta^2 \end{aligned} \quad (5.135)$$

## 5.2. NON-INERTIAL BOUNDARY LAYER EQUATIONS FOR A FLAT PLATE - CYLINDRICAL FORMULATION

In a similar manner the conversion of *Equations 5.27* and *5.31* lead to a set of equations that are the same as *Equations 5.99* and *5.104* respectively.

$$\begin{aligned}
0 &= -\frac{\partial \hat{\psi}}{\partial \hat{y}} - 2\hat{u}_r \hat{\omega}_\theta + 2\hat{u}_\theta \hat{\omega}_r - \hat{r} \hat{\omega}_r \hat{\omega}_y + \hat{y} \hat{\omega}_r^2 + \hat{y} \hat{\omega}_\theta^2 \\
\frac{\partial \hat{u}_\theta}{\partial t} + \hat{u}_r \frac{\partial \hat{u}_\theta}{\partial \hat{r}} + \frac{\hat{u}_\theta}{\hat{r}} \frac{\partial \hat{u}_\theta}{\partial \hat{\theta}} + \frac{\hat{u}_\theta \hat{u}_r}{\hat{r}} + \hat{u}_y \frac{\partial \hat{u}_\theta}{\partial \hat{y}} &= -\frac{1}{\hat{r}} \frac{\partial \hat{\psi}}{\partial \hat{\theta}} + \hat{v} \frac{\partial^2 \hat{u}_\theta}{\partial \hat{y}^2} - 2\hat{u}_y \hat{\omega}_r \\
&+ 2\hat{u}_r \hat{\omega}_y - \hat{r} \hat{\omega}_r \hat{\omega}_\theta - \hat{y} \hat{\omega}_\theta \hat{\omega}_r
\end{aligned} \tag{5.136}$$

Implementing the same conditions as in Equation 5.60 where rotation about the  $\hat{y}$ -axis was considered,

$$\begin{aligned}
\hat{\omega}_r &= 0 \\
\hat{\omega}_y &= \Omega \\
\hat{\omega}_\theta &= 0
\end{aligned} \tag{5.137}$$

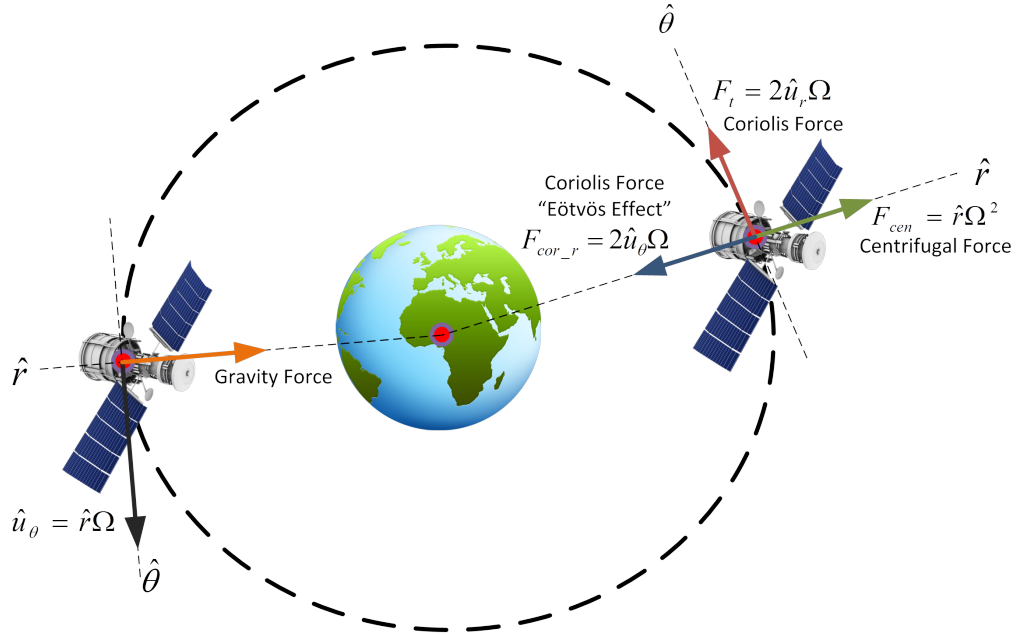
results in the following set of non-inertial boundary layer equations:

$$\begin{aligned}
\frac{\partial \hat{u}_r}{\partial t} + \hat{u}_r \frac{\partial \hat{u}_r}{\partial \hat{r}} + \frac{\hat{u}_\theta}{\hat{r}} \frac{\partial \hat{u}_r}{\partial \hat{\theta}} - \frac{\hat{u}_\theta^2}{\hat{r}} + \hat{u}_y \frac{\partial \hat{u}_r}{\partial \hat{y}} &= -\frac{\partial \hat{\psi}}{\partial \hat{r}} + \hat{v} \frac{\partial^2 \hat{u}_r}{\partial \hat{y}^2} - 2\hat{u}_\theta \Omega + \hat{r} \Omega^2 \\
0 &= -\frac{\partial \hat{\psi}}{\partial \hat{y}} \\
\frac{\partial \hat{u}_\theta}{\partial t} + \hat{u}_r \frac{\partial \hat{u}_\theta}{\partial \hat{r}} + \frac{\hat{u}_\theta}{\hat{r}} \frac{\partial \hat{u}_\theta}{\partial \hat{\theta}} + \frac{\hat{u}_\theta \hat{u}_r}{\hat{r}} + \hat{u}_y \frac{\partial \hat{u}_\theta}{\partial \hat{y}} &= -\frac{1}{\hat{r}} \frac{\partial \hat{\psi}}{\partial \hat{\theta}} + \hat{v} \frac{\partial^2 \hat{u}_\theta}{\partial \hat{y}^2} + 2\hat{u}_r \Omega
\end{aligned} \tag{5.138}$$

For exactly the same conditions, Dumitrescu et al. [85] made use of a set of boundary layer equations where both the Coriolis and Centrifugal terms were present in the  $\hat{r}$ - and  $\hat{\theta}$ -momentum equations respectively. The work of Martinez et al. [86] on the other hand has the Centrifugal force only present in the  $\hat{r}$ -direction and the Coriolis force only in the  $\hat{\theta}$ -direction. The derivation above indicates that in pure rotation about the  $\hat{y}$ -axis, the Coriolis force is present in both the  $\hat{r}$ - and  $\hat{\theta}$ -directions. It was shown in the mathematical development that the centrifugal term should only be present in the  $\hat{r}$ -momentum equation. This is depicted in *Figure 5.9* using a satellite orbiting earth.

It is assumed that the satellite is in pure rotation about the earth. The satellite is also travelling at a constant rotational speed. The centrifugal force points in the positive  $\hat{r}$ -direction away from earth's centre. There are two components for the Coriolis force. The first one is the component responsible for the Eötvös effect pointing in the negative  $\hat{r}$ -direction. The second one is the most general component. It is similar to the Coriolis force responsible for deflections on the surface of the earth. This component points in the positive  $\hat{\theta}$ -direction.

Figure 5.9: Visualization of Physical Meaning of Fictitious Forces



### 5.2.5 Non-Inertial Boundary Layer Equations for Variable Rotation

The non-inertial equation for incompressible flow in variable rotation conditions were determined in Chapter 3, Equation 3.157:

$$\frac{\partial \hat{\mathbf{u}}}{\partial t} + (\hat{\mathbf{u}} \cdot \hat{\nabla}) \hat{\mathbf{u}} = -\hat{\nabla} \hat{\psi} + \nu \hat{\nabla}^2 \hat{\mathbf{u}} + \underbrace{2\hat{\mathbf{u}} \wedge \boldsymbol{\Omega}}_{\text{Coriolis}} - \underbrace{\hat{\mathbf{x}} \wedge \boldsymbol{\Omega} \wedge \boldsymbol{\Omega}}_{\text{Centrifugal}} + \underbrace{\hat{\mathbf{x}} \wedge \dot{\boldsymbol{\Omega}}}_{\text{Euler}} \quad (5.139)$$

The component form of the incompressible momentum equations were determined in Equations 5.94, 5.99 and 5.104. Additional non-inertial components related to this case are obtained from Equations 4.60, 4.62 and 4.61. Combining the relations previously obtained, lead to the component form of the incompressible momentum equations for variable rotation:

**$\hat{r}$ -momentum**

$$\frac{\partial \hat{u}_r}{\partial t} + \hat{u}_r \frac{\partial \hat{u}_r}{\partial \hat{r}} + \frac{\hat{u}_\theta}{\hat{r}} \frac{\partial \hat{u}_r}{\partial \hat{\theta}} - \frac{\hat{u}_\theta^2}{\hat{r}} + \hat{u}_y \frac{\partial \hat{u}_r}{\partial \hat{y}} = -\frac{\partial \hat{\psi}}{\partial \hat{r}} + \hat{\nu} \frac{\partial^2 \hat{u}_r}{\partial \hat{y}^2} - 2\hat{u}_\theta \omega_y + 2\hat{u}_y \omega_\theta - \hat{y} \omega_r \omega_y + \hat{r} \omega_y^2 + \hat{r} \omega_\theta^2 + \hat{y} \dot{\omega}_\theta \quad (5.140)$$

**$\hat{y}$ -momentum**

$$0 = -\frac{\partial \hat{\psi}}{\partial \hat{y}} - 2\hat{u}_r \omega_\theta + 2\hat{u}_\theta \omega_r - \hat{r} \omega_r \omega_y + \hat{y} \omega_r^2 + \hat{y} \omega_\theta^2 - \hat{r} \dot{\omega}_\theta \quad (5.141)$$

**$\hat{\theta}$ -momentum**

$$\frac{\partial \hat{u}_\theta}{\partial t} + \hat{u}_r \frac{\partial \hat{u}_\theta}{\partial \hat{r}} + \frac{\hat{u}_\theta}{\hat{r}} \frac{\partial \hat{u}_\theta}{\partial \hat{\theta}} + \frac{\hat{u}_\theta \hat{u}_r}{\hat{r}} + \hat{u}_y \frac{\partial \hat{u}_\theta}{\partial \hat{y}} = -\frac{1}{\hat{r}} \frac{\partial \hat{\psi}}{\partial \hat{\theta}} + \hat{\nu} \frac{\partial^2 \hat{u}_\theta}{\partial \hat{y}^2} - 2\hat{u}_y \omega_r + 2\hat{u}_r \omega_y - \hat{r} \omega_r \omega_\theta - \hat{y} \omega_\theta \omega_y - \hat{y} \dot{\omega}_r + \hat{r} \dot{\omega}_y \quad (5.142)$$

## 5.2. NON-INERTIAL BOUNDARY LAYER EQUATIONS FOR A FLAT PLATE - CYLINDRICAL FORMULATION

The non-inertial equation for compressible flow in variable rotation was determined in *Chapter 3, Equation 3.169*:

$$\frac{\partial \hat{\rho} \hat{\mathbf{u}}}{\partial t} + \hat{\nabla} \cdot (\hat{\rho} \hat{\mathbf{u}} \otimes \hat{\mathbf{u}}) = -\hat{\nabla} \hat{p} + \hat{\nabla} \cdot [\hat{\mu}(\hat{\nabla} \hat{\mathbf{u}} + \hat{\nabla} \hat{\mathbf{u}}^T) + \hat{\lambda}(\hat{\nabla} \cdot \hat{\mathbf{u}}) \hat{\mathbf{I}}] + \underbrace{2\rho \hat{\mathbf{u}} \wedge \boldsymbol{\Omega}}_{\text{Coriolis}} - \underbrace{\rho \hat{\mathbf{x}} \wedge \boldsymbol{\Omega} \wedge \boldsymbol{\Omega}}_{\text{Centrifugal}} + \underbrace{\rho \hat{\mathbf{x}} \wedge \dot{\boldsymbol{\Omega}}}_{\text{Euler}} \quad (5.143)$$

Using the component forms developed in *Equations 5.110, 5.114 and 5.119*, and the non-inertial terms of *Equations 4.77, 4.78 and 4.79* lead to the compressible component formulations for variable, pure rotation:

### $\hat{r}$ -momentum

$$\frac{\partial \hat{\rho} \hat{u}_r}{\partial t} + \hat{u}_r \frac{\partial \hat{\rho} \hat{u}_r}{\partial \hat{r}} + \frac{\hat{u}_\theta}{\hat{r}} \frac{\partial \hat{\rho} \hat{u}_r}{\partial \hat{\theta}} - \frac{\hat{\rho} \hat{u}_\theta^2}{\hat{r}} + \hat{u}_y \frac{\partial \hat{\rho} \hat{u}_r}{\partial \hat{y}} = -\frac{\partial \hat{p}}{\partial \hat{r}} + \frac{\partial}{\partial \hat{y}} \hat{\mu} \frac{\partial \hat{u}_r}{\partial \hat{y}} - 2\hat{\rho} \hat{u}_\theta \omega_y + 2\hat{\rho} \hat{u}_y \omega_\theta - \hat{\rho} \hat{y} \omega_r \omega_y + \hat{\rho} \hat{r} \omega_y^2 + \hat{\rho} \hat{r} \omega_\theta^2 + \hat{\rho} \hat{y} \dot{\omega}_\theta \quad (5.144)$$

### $\hat{y}$ -momentum

$$0 = -\frac{\partial \hat{p}}{\partial \hat{y}} - 2\hat{\rho} \hat{u}_r \omega_\theta + 2\hat{\rho} \hat{u}_\theta \omega_r - \hat{\rho} \hat{r} \omega_r \omega_y + \hat{\rho} \hat{y} \omega_r^2 + \hat{\rho} \hat{y} \omega_\theta^2 - \hat{\rho} \hat{r} \dot{\omega}_\theta \quad (5.145)$$

### $\hat{\theta}$ -momentum

$$\frac{\partial \hat{\rho} \hat{u}_\theta}{\partial t} + \hat{u}_r \frac{\partial \hat{\rho} \hat{u}_\theta}{\partial \hat{r}} + \frac{\hat{u}_\theta}{\hat{r}} \frac{\partial \hat{\rho} \hat{u}_\theta}{\partial \hat{\theta}} + \frac{\hat{\rho} \hat{u}_\theta \hat{u}_r}{\hat{r}} + \hat{u}_y \frac{\partial \hat{\rho} \hat{u}_\theta}{\partial \hat{y}} = -\frac{1}{\hat{r}} \frac{\partial \hat{p}}{\partial \hat{\theta}} + \frac{\partial}{\partial \hat{y}} \hat{\mu} \frac{\partial \hat{u}_\theta}{\partial \hat{y}} - 2\hat{\rho} \hat{u}_y \omega_r + 2\hat{\rho} \hat{u}_r \omega_y - \hat{\rho} \hat{r} \omega_r \omega_\theta - \hat{\rho} \hat{y} \omega_\theta \omega_y - \hat{\rho} \hat{y} \dot{\omega}_r + \hat{\rho} \hat{r} \dot{\omega}_y \quad (5.146)$$

## 5.2.6 Non-Inertial Boundary Layer Equations for Arbitrary Acceleration

The non-inertial equation for incompressible flow in full arbitrary acceleration conditions was determined in *Chapter 3, Equation 3.239*,

$$\frac{\partial \hat{\mathbf{u}}}{\partial t} + (\hat{\mathbf{u}} \cdot \hat{\nabla}) \hat{\mathbf{u}} = -\hat{\nabla} \hat{\psi} + \nu \hat{\nabla}^2 \hat{\mathbf{u}} - \underbrace{\frac{\partial}{\partial t} (\mathbf{V}(t))}_{\text{Translation}} + \underbrace{\hat{\mathbf{x}} \wedge \boldsymbol{\Omega} + \hat{\mathbf{x}} \wedge \dot{\boldsymbol{\Omega}}}_{\text{Unsteady motion}} + \underbrace{2\hat{\mathbf{u}} \wedge \boldsymbol{\Omega}}_{\text{Coriolis}} - \underbrace{\hat{\mathbf{x}} \wedge \boldsymbol{\Omega} \wedge \boldsymbol{\Omega}}_{\text{Centrifugal}} + \underbrace{2\mathbf{V}(t) \wedge \boldsymbol{\Omega}}_{\text{Magnus}} \quad (5.147)$$

Using *Equations 4.69, 4.70, 4.71, 5.140, 5.141 and 5.142* the incompressible component form for arbitrary acceleration can be obtained:

### $\hat{r}$ -momentum

$$\frac{\partial \hat{u}_r}{\partial t} + \hat{u}_r \frac{\partial \hat{u}_r}{\partial \hat{r}} + \frac{\hat{u}_\theta}{\hat{r}} \frac{\partial \hat{u}_r}{\partial \hat{\theta}} - \frac{\hat{u}_\theta^2}{\hat{r}} + \hat{u}_y \frac{\partial \hat{u}_r}{\partial \hat{y}} = -\frac{\partial \hat{\psi}}{\partial \hat{r}} + \hat{\nu} \frac{\partial^2 \hat{u}_r}{\partial \hat{y}^2} - 2\hat{u}_\theta \omega_y + 2\hat{u}_y \omega_\theta - \hat{y} \omega_r \omega_y + \hat{r} \omega_y^2 + \hat{r} \omega_\theta^2 + \hat{y} \dot{\omega}_\theta - \hat{u}_\theta \omega_y + \hat{u}_y \omega_\theta - 2V_\theta \omega_y + 2V_y \omega_\theta - \frac{\partial V_r}{\partial t} \quad (5.148)$$

### $\hat{y}$ -momentum

$$0 = -\frac{\partial \hat{\psi}}{\partial \hat{y}} - 2\hat{u}_r \omega_\theta + 2\hat{u}_\theta \omega_r - \hat{r} \omega_r \omega_y + \hat{y} \omega_r^2 + \hat{y} \omega_\theta^2 - \hat{r} \dot{\omega}_\theta - \hat{u}_r \omega_\theta + \hat{u}_\theta \omega_r - 2V_r \omega_\theta + 2V_\theta \omega_r - \frac{\partial V_z}{\partial t} \quad (5.149)$$



CHAPTER 5. NON-INERTIAL BOUNDARY LAYER EQUATIONS

**$\hat{\theta}$ -momentum**

$$\begin{aligned} \frac{\partial \hat{u}_\theta}{\partial t} + \hat{u}_r \frac{\partial \hat{u}_\theta}{\partial \hat{r}} + \frac{\hat{u}_\theta}{\hat{r}} \frac{\partial \hat{u}_\theta}{\partial \hat{\theta}} + \frac{\hat{u}_\theta \hat{u}_r}{\hat{r}} + \hat{u}_y \frac{\partial \hat{u}_\theta}{\partial \hat{y}} = & -\frac{1}{\hat{r}} \frac{\partial \hat{\psi}}{\partial \hat{\theta}} + \hat{v} \frac{\partial^2 \hat{u}_\theta}{\partial \hat{y}^2} - 2\hat{u}_y \omega_r + 2\hat{u}_r \omega_y \\ & - \hat{r} \omega_r \omega_\theta - \hat{y} \omega_\theta \omega_y - \hat{y} \dot{\omega}_r + \hat{r} \dot{\omega}_y \\ & - \hat{u}_y \omega_r + \hat{u}_r \omega_y - 2V_y \omega_r + 2V_r \omega_y - \frac{\partial V_\theta}{\partial t} \end{aligned} \quad (5.150)$$

The non-inertial equation for compressible flow in full arbitrary acceleration conditions was determined in *Chapter 3, Equation 3.227*:

$$\begin{aligned} \frac{\partial \hat{\rho} \hat{\mathbf{u}}}{\partial t} + \hat{\mathbf{v}} \cdot (\hat{\rho} \hat{\mathbf{u}} \otimes \hat{\mathbf{u}}) = & -\hat{\nabla} \hat{p} + \hat{\mathbf{v}} \cdot [\hat{\mu}(\hat{\nabla} \hat{\mathbf{u}} + \hat{\nabla} \hat{\mathbf{u}}^T) + \hat{\lambda}(\hat{\nabla} \cdot \hat{\mathbf{u}}) \hat{\mathbf{I}}] \\ & - \underbrace{\frac{\partial}{\partial t}(\rho \mathbf{V}(t))}_{\text{Translation}} + \underbrace{\rho \hat{\mathbf{x}} \wedge \boldsymbol{\Omega} + \rho \hat{\mathbf{x}} \wedge \dot{\boldsymbol{\Omega}}}_{\text{Unsteady motion}} + \underbrace{2\rho \hat{\mathbf{u}} \wedge \boldsymbol{\Omega}}_{\text{Coriolis}} - \underbrace{\rho \hat{\mathbf{x}} \wedge \boldsymbol{\Omega} \wedge \boldsymbol{\Omega}}_{\text{Centrifugal}} + \underbrace{2\rho \mathbf{V}(t) \wedge \boldsymbol{\Omega}}_{\text{Magnus}} \end{aligned} \quad (5.151)$$

The formulation above, along with *Equations 5.148, 5.149, 5.150* result in the following boundary layer expressions:

**$\hat{r}$ -momentum**

$$\begin{aligned} \frac{\partial \hat{\rho} \hat{u}_r}{\partial t} + \hat{u}_r \frac{\partial \hat{\rho} \hat{u}_r}{\partial \hat{r}} + \frac{\hat{u}_\theta}{\hat{r}} \frac{\partial \hat{\rho} \hat{u}_r}{\partial \hat{\theta}} - \frac{\hat{\rho} \hat{u}_\theta^2}{\hat{r}} + \hat{u}_y \frac{\partial \hat{\rho} \hat{u}_r}{\partial \hat{y}} = & -\frac{\partial \hat{p}}{\partial \hat{r}} + \frac{\partial}{\partial \hat{y}} \hat{\mu} \frac{\partial \hat{u}_r}{\partial \hat{y}} - 2\hat{\rho} \hat{u}_\theta \omega_y + 2\hat{\rho} \hat{u}_y \omega_\theta \\ & - \hat{\rho} \hat{y} \omega_r \omega_y + \hat{\rho} \hat{r} \omega_y^2 + \hat{\rho} \hat{r} \omega_\theta^2 + \hat{\rho} \hat{y} \dot{\omega}_\theta - \hat{\rho} \hat{u}_\theta \omega_y + \hat{\rho} \hat{u}_y \omega_\theta \\ & - 2\hat{\rho} V_\theta \omega_y + 2\hat{\rho} V_y \omega_\theta - \frac{\partial \hat{\rho} V_r}{\partial t} \end{aligned} \quad (5.152)$$

**$\hat{y}$ -momentum**

$$\begin{aligned} 0 = & -\frac{\partial \hat{p}}{\partial \hat{y}} - 2\hat{\rho} \hat{u}_r \omega_\theta + 2\hat{\rho} \hat{u}_\theta \omega_r - \hat{\rho} \hat{r} \omega_r \omega_y + \hat{\rho} \hat{y} \omega_r^2 + \hat{\rho} \hat{y} \omega_\theta^2 - \hat{\rho} \hat{r} \dot{\omega}_\theta - \hat{\rho} \hat{u}_r \omega_\theta + \hat{\rho} \hat{u}_\theta \omega_r \\ & - 2\hat{\rho} V_r \omega_\theta + 2\hat{\rho} V_\theta \omega_r - \frac{\partial \hat{\rho} V_z}{\partial t} \end{aligned} \quad (5.153)$$

**$\hat{\theta}$ -momentum**

$$\begin{aligned} \frac{\partial \hat{\rho} \hat{u}_\theta}{\partial t} + \hat{u}_r \frac{\partial \hat{\rho} \hat{u}_\theta}{\partial \hat{r}} + \frac{\hat{u}_\theta}{\hat{r}} \frac{\partial \hat{\rho} \hat{u}_\theta}{\partial \hat{\theta}} + \frac{\hat{\rho} \hat{u}_\theta \hat{u}_r}{\hat{r}} + \hat{u}_y \frac{\partial \hat{\rho} \hat{u}_\theta}{\partial \hat{y}} = & -\frac{1}{\hat{r}} \frac{\partial \hat{p}}{\partial \hat{\theta}} + \frac{\partial}{\partial \hat{y}} \hat{\mu} \frac{\partial \hat{u}_\theta}{\partial \hat{y}} - 2\hat{\rho} \hat{u}_y \omega_r + 2\hat{\rho} \hat{u}_r \omega_y \\ & - \hat{\rho} \hat{r} \omega_r \omega_\theta - \hat{\rho} \hat{y} \omega_\theta \omega_y - \hat{\rho} \hat{y} \dot{\omega}_r + \hat{\rho} \hat{r} \dot{\omega}_y - \hat{\rho} \hat{y} \dot{\omega}_r + \hat{\rho} \hat{r} \dot{\omega}_y - \hat{\rho} \hat{u}_y \omega_r + \hat{\rho} \hat{u}_r \omega_y \\ & - 2\hat{\rho} V_y \omega_r + 2\hat{\rho} V_r \omega_y - \frac{\partial \hat{\rho} V_\theta}{\partial t} \end{aligned} \quad (5.154)$$



## 5.3 Non-Inertial Boundary Layer Equations for a Flat Plate - Curvilinear Formulation

### 5.3.1 Continuity Equation

The continuity equation in the boundary layer was determined in Cartesian and Cylindrical coordinates in *Equations 5.14* and *5.85* respectively. The continuity equation in curvilinear coordinates takes a form similar to *Equation 4.110*:

$$\frac{\partial \hat{\rho}}{\partial t} + \frac{1}{h_1 h_2 h_3} \left[ \frac{\partial}{\partial \hat{u}_1} (h_2 h_3 \hat{\rho} \hat{V}_1) + \frac{\partial}{\partial \hat{u}_2} (h_1 h_3 \hat{\rho} \hat{V}_2) + \frac{\partial}{\partial \hat{u}_3} (h_1 h_2 \hat{\rho} \hat{V}_3) \right] = 0 \quad (5.155)$$

### 5.3.2 Conservation of Momentum Equation for Boundary Layer Flows

In *Sections 5.1* and *5.2* the conservation of momentum equation was determined in the boundary layer region for Cartesian and Cylindrical components respectively. These sections indicated that the material derivative remains unchanged in the longitudinal and transversal direction, but is eliminated in the direction normal to the surface. The pressure gradient terms, as well as all the terms related to fictitious effects are present in the boundary layer equations. The diffusion terms originating from the divergence of the stress tensor, showed that all terms are neglected except for specific terms of  $\tau_{12}$  and  $\tau_{23}$ .

$$\boldsymbol{\tau}(1, 2, 3) = \begin{bmatrix} \tau_{11} & \tau_{12} & \tau_{13} \\ \tau_{21} & \tau_{22} & \tau_{23} \\ \tau_{31} & \tau_{23} & \tau_{33} \end{bmatrix} \quad (5.156)$$

The remaining diffusion terms have been identified in *Equations 5.38* and *5.51* as  $\frac{\partial}{\partial \hat{y}} \hat{\mu} \frac{\partial \hat{u}}{\partial \hat{y}}$  and  $\frac{\partial}{\partial \hat{y}} \hat{\mu} \frac{\partial \hat{w}}{\partial \hat{y}}$  for the  $\hat{x}$ - and  $\hat{z}$ -momentum equations respectively. These terms are components of  $\tau_{12}$  and  $\tau_{23}$  of the Cartesian stress tensor described in *Equation 4.38*.

$$\hat{\boldsymbol{\tau}}(\hat{x}, \hat{y}, \hat{z}) = \begin{bmatrix} \dots & \hat{\mu} \left( \frac{\partial \hat{u}}{\partial \hat{y}} + \frac{\partial \hat{w}}{\partial \hat{x}} \right) & \dots \\ \dots & 2\hat{\mu} \frac{\partial \hat{u}}{\partial \hat{y}} + \hat{\lambda} \hat{\nabla} \cdot \hat{\mathbf{u}} & \dots \\ \dots & \hat{\mu} \left( \frac{\partial \hat{w}}{\partial \hat{z}} + \frac{\partial \hat{u}}{\partial \hat{y}} \right) & \dots \end{bmatrix} \quad (5.157)$$

Similarly, in the Cylindrical Stress Tensor (*Equation 4.43*) the equivalent components of  $\tau_{12}$  and  $\tau_{23}$  remain relevant in the boundary layer as indicated by *Equations 5.109* and *5.118*.

$$\hat{\boldsymbol{\tau}}(\hat{r}, \hat{y}, \hat{\theta}) = \begin{bmatrix} \dots & \hat{\mu} \left( \frac{\partial \hat{u}_r}{\partial \hat{y}} + \frac{\partial \hat{u}_y}{\partial \hat{r}} \right) & \dots \\ \dots & 2\hat{\mu} \frac{\partial \hat{u}_y}{\partial \hat{y}} + \hat{\lambda} \hat{\nabla} \cdot \hat{\mathbf{u}} & \dots \\ \dots & \hat{\mu} \left( \frac{1}{\hat{r}} \frac{\partial \hat{u}_y}{\partial \hat{\theta}} + \frac{\partial \hat{u}_\theta}{\partial \hat{y}} \right) & \dots \end{bmatrix} \quad (5.158)$$

CHAPTER 5. NON-INERTIAL BOUNDARY LAYER EQUATIONS

The equivalent terms of  $\tau_{12}$  and  $\tau_{23}$  are relevant in the boundary layer when expressed in Curvilinear coordinates. The components of the Curvilinear stress tensor were described in *Equation 4.104*, with  $\tau_{12}$  and  $\tau_{32}$  defined as:

$$\begin{aligned}\hat{\tau}_{12} &= \hat{\mu} \left[ \frac{h_2}{h_1} \frac{\partial}{\partial \hat{u}_1} \left( \frac{\hat{V}_2}{h_2} \right) + \frac{h_1}{h_2} \frac{\partial}{\partial \hat{u}_2} \left( \frac{\hat{V}_1}{h_1} \right) \right] \\ \hat{\tau}_{32} &= \hat{\mu} \left[ \frac{h_3}{h_2} \frac{\partial}{\partial \hat{u}_2} \left( \frac{\hat{V}_3}{h_3} \right) + \frac{h_2}{h_3} \frac{\partial}{\partial \hat{u}_3} \left( \frac{\hat{V}_2}{h_2} \right) \right]\end{aligned}\quad (5.159)$$

*Table 4.1* gave the conversion from a Curvilinear system to a Cartesian or Cylindrical system. The table are based on the third principal direction ( $\hat{z}$ -direction) being normal to the surface. Here the second principal direction ( $\hat{y}$ -direction) is taken a normal to the wall. The conversion between the systems changes as follow:

Table 5.1: Relations between the Curvilinear Coordinate System and Other Systems

Curvilinear	$u_1$	$u_2$	$u_3$	$x$	$y$	$z$	$h_1$	$h_2$	$h_3$
Cartesian	$x$	$y$	$z$	$x$	$y$	$z$	1	1	1
Cylindrical	$r$	$y$	$\theta$	$r \cos \theta$	$z$	$r \sin \theta$	1	1	$r$

The conversion of  $\tau_{12}$  indicates that equivalent terms to be included in the boundary layer equation.

$$\begin{aligned}\hat{\tau}_{12_{curvilinear}} &= \hat{\mu} \left[ \frac{h_2}{h_1} \frac{\partial}{\partial \hat{u}_1} \left( \frac{\hat{V}_2}{h_2} \right) + \frac{h_1}{h_2} \frac{\partial}{\partial \hat{u}_2} \left( \frac{\hat{V}_1}{h_1} \right) \right] \\ \hat{\tau}_{12_{cartesian}} &= \hat{\mu} \left[ \frac{1}{1} \frac{\partial}{\partial \hat{x}} \left( \frac{\hat{v}}{1} \right) + \frac{1}{1} \frac{\partial}{\partial \hat{y}} \left( \frac{\hat{u}}{1} \right) \right] \\ \hat{\tau}_{12_{cylindrical}} &= \hat{\mu} \left[ \frac{1}{1} \frac{\partial}{\partial \hat{r}} \left( \frac{\hat{u}_y}{1} \right) + \frac{1}{1} \frac{\partial}{\partial \hat{y}} \left( \frac{\hat{u}_r}{1} \right) \right]\end{aligned}\quad (5.160)$$

Using the above relations, it is seen that the term  $\hat{\mu} \frac{h_1}{h_2} \frac{\partial}{\partial \hat{u}_2} \left( \frac{\hat{V}_1}{h_1} \right)$  must be included in the boundary layer equation for the first principle direction. In a similar manner the equivalent term in  $\tau_{32}$  can be determined as  $\hat{\mu} \frac{1}{1} \frac{\partial}{\partial \hat{r}} \left( \frac{\hat{u}_y}{1} \right)$ .

$$\hat{\boldsymbol{\tau}}(\hat{u}_1, \hat{u}_2, \hat{u}_3) = \begin{bmatrix} \dots & \hat{\mu} \left[ \frac{h_2}{h_1} \frac{\partial}{\partial \hat{u}_1} \left( \frac{\hat{V}_2}{h_2} \right) + \frac{h_1}{h_2} \frac{\partial}{\partial \hat{u}_2} \left( \frac{\hat{V}_1}{h_1} \right) \right] & \dots \\ \dots & 2\hat{\mu} \left( \frac{1}{h_2} \frac{\partial \hat{V}_2}{\partial \hat{u}_2} + \frac{\hat{V}_3}{h_2 h_3} \frac{\partial h_2}{\partial \hat{u}_3} + \frac{\hat{V}_1}{h_1 h_2} \frac{\partial h_2}{\partial \hat{u}_1} \right) + \hat{\lambda} \hat{\nabla} \cdot \hat{\nabla} & \dots \\ \dots & \hat{\mu} \left[ \frac{h_3}{h_2} \frac{\partial}{\partial \hat{u}_2} \left( \frac{\hat{V}_3}{h_3} \right) + \frac{h_2}{h_3} \frac{\partial}{\partial \hat{u}_3} \left( \frac{\hat{V}_2}{h_2} \right) \right] & \dots \end{bmatrix}\quad (5.161)$$

5.3. NON-INERTIAL BOUNDARY LAYER EQUATIONS FOR A FLAT PLATE - CURVILINEAR FORMULATION

Using *Equations 4.112, 4.113 and 4.114* the non-inertial Curvilinear set of equations for the conservation of momentum in the boundary layer for compressible flow are determined:

**$\hat{u}_1$ -momentum:**

$$\begin{aligned}
& \hat{\rho} \left[ \frac{\partial \hat{V}_1}{\partial t} + \frac{\hat{V}_1}{h_1} \frac{\partial \hat{V}_1}{\partial \hat{u}_1} + \frac{\hat{V}_2}{h_2} \frac{\partial \hat{V}_1}{\partial \hat{u}_2} + \frac{\hat{V}_3}{h_3} \frac{\partial \hat{V}_1}{\partial \hat{u}_3} - \hat{V}_2 \left( \frac{\hat{V}_2}{h_1 h_2} \frac{\partial h_2}{\partial \hat{u}_1} - \frac{\hat{V}_1}{h_1 h_2} \frac{\partial h_1}{\partial \hat{u}_2} \right) + \hat{V}_3 \left( \frac{\hat{V}_1}{h_1 h_3} \frac{\partial h_1}{\partial \hat{u}_3} - \frac{\hat{V}_3}{h_1 h_3} \frac{\partial h_3}{\partial \hat{u}_1} \right) \right] \\
& = -\frac{1}{h_1} \frac{\partial \hat{p}}{\partial \hat{u}_1} + \frac{1}{h_2} \frac{\partial}{\partial \hat{u}_2} \hat{\mu} \frac{h_1}{h_2} \frac{\partial \hat{u}_2}{\partial \hat{u}_1} \frac{\hat{V}_1}{h_1} \\
& + \hat{\rho} \left[ \underbrace{2\hat{V}_2 \omega_3 - 2\hat{V}_3 \omega_2}_{\text{Coriolis}} + \underbrace{\hat{u}_1(\omega_3^2 + \omega_2^2) - \hat{u}_2 \omega_1 \omega_2 - \hat{u}_3 \omega_1 \omega_3}_{\text{Centrifugal}} \right. \\
& \left. + \underbrace{\hat{u}_2 \dot{\omega}_3 - \hat{u}_3 \dot{\omega}_2 + \hat{u}_2 \omega_3 - \hat{u}_3 \omega_2}_{\text{Euler}} + \underbrace{2V_{e_2} \omega_3 - 2V_{e_3} \omega_2}_{\text{Magnus}} - \underbrace{\frac{\partial V_{e_1}}{\partial t}}_{\text{Translation}} \right]
\end{aligned} \tag{5.162}$$

**$\hat{u}_2$ -momentum:**

$$\begin{aligned}
0 = & -\frac{1}{h_2} \frac{\partial \hat{p}}{\partial \hat{u}_2} + \hat{\rho} \left[ \underbrace{2\hat{V}_3 \omega_1 - 2\hat{V}_1 \omega_3}_{\text{Coriolis}} + \underbrace{\hat{u}_2(\omega_3^2 + \omega_1^2) - \hat{u}_1 \omega_1 \omega_2 - \hat{u}_3 \omega_2 \omega_3}_{\text{Centrifugal}} \right. \\
& \left. + \underbrace{\hat{u}_3 \dot{\omega}_1 - \hat{u}_1 \dot{\omega}_3 + \hat{u}_3 \omega_1 - \hat{u}_1 \omega_3}_{\text{Euler}} + \underbrace{2V_{e_3} \omega_1 - 2V_{e_1} \omega_3}_{\text{Magnus}} - \underbrace{\frac{\partial V_{e_2}}{\partial t}}_{\text{Translation}} \right]
\end{aligned} \tag{5.163}$$

**$\hat{u}_3$ -momentum:**

$$\begin{aligned}
& \hat{\rho} \left[ \frac{\partial \hat{V}_3}{\partial t} + \frac{\hat{V}_1}{h_1} \frac{\partial \hat{V}_3}{\partial \hat{u}_1} + \frac{\hat{V}_2}{h_2} \frac{\partial \hat{V}_3}{\partial \hat{u}_2} + \frac{\hat{V}_3}{h_3} \frac{\partial \hat{V}_3}{\partial \hat{u}_3} - \hat{V}_1 \left( \frac{\hat{V}_1}{h_1 h_3} \frac{\partial h_1}{\partial \hat{u}_3} - \frac{\hat{V}_3}{h_1 h_3} \frac{\partial h_3}{\partial \hat{u}_1} \right) + \hat{V}_2 \left( \frac{\hat{V}_3}{h_2 h_3} \frac{\partial h_2}{\partial \hat{u}_1} - \frac{\hat{V}_2}{h_2 h_3} \frac{\partial h_2}{\partial \hat{u}_3} \right) \right] \\
& = -\frac{1}{h_1} \frac{\partial \hat{p}}{\partial \hat{u}_3} + \frac{1}{h_2} \frac{\partial}{\partial \hat{u}_2} \hat{\mu} \frac{h_3}{h_2} \frac{\partial \hat{u}_2}{\partial \hat{u}_3} \frac{\hat{V}_3}{h_3} \\
& + \hat{\rho} \left[ \underbrace{2\hat{V}_1 \omega_2 - 2\hat{V}_2 \omega_1}_{\text{Coriolis}} + \underbrace{\hat{u}_3(\omega_2^2 + \omega_1^2) - \hat{u}_1 \omega_1 \omega_3 - \hat{u}_2 \omega_1 \omega_3}_{\text{Centrifugal}} \right. \\
& \left. + \underbrace{\hat{u}_1 \dot{\omega}_2 - \hat{u}_2 \dot{\omega}_1 + \hat{u}_1 \omega_2 - \hat{u}_2 \omega_1}_{\text{Euler}} + \underbrace{2V_{e_1} \omega_2 - 2V_{e_2} \omega_1}_{\text{Magnus}} - \underbrace{\frac{\partial V_{e_3}}{\partial t}}_{\text{Translation}} \right]
\end{aligned} \tag{5.164}$$

### 5.3.3 Validation of Equations

The conservation of momentum equations for incompressible flow in Curvilinear coordinates are derived using *Equations 5.162, 5.163 and 5.164*:

**$\hat{u}_1$ -momentum:**

$$\begin{aligned}
& \frac{\partial \hat{V}_1}{\partial t} + \frac{\hat{V}_1}{h_1} \frac{\partial \hat{V}_1}{\partial \hat{u}_1} + \frac{\hat{V}_2}{h_2} \frac{\partial \hat{V}_1}{\partial \hat{u}_2} + \frac{\hat{V}_3}{h_3} \frac{\partial \hat{V}_1}{\partial \hat{u}_3} - \hat{V}_2 \left( \frac{\hat{V}_2}{h_1 h_2} \frac{\partial h_2}{\partial \hat{u}_1} - \frac{\hat{V}_1}{h_1 h_2} \frac{\partial h_1}{\partial \hat{u}_2} \right) + \hat{V}_3 \left( \frac{\hat{V}_1}{h_1 h_3} \frac{\partial h_1}{\partial \hat{u}_3} - \frac{\hat{V}_3}{h_1 h_3} \frac{\partial h_3}{\partial \hat{u}_1} \right) \\
&= -\frac{1}{h_1} \frac{\partial \hat{\psi}}{\partial \hat{u}_1} + \frac{1}{h_2} \frac{\partial}{\partial \hat{u}_2} \hat{v} \frac{h_1}{h_2} \frac{\partial \hat{u}_2}{\partial \hat{u}_2} \frac{\hat{V}_1}{h_1} \\
&+ \underbrace{2\hat{V}_2 \omega_3 - 2\hat{V}_3 \omega_2}_{\text{Coriolis}} + \underbrace{\hat{u}_1(\omega_3^2 + \omega_2^2) - \hat{u}_2 \omega_1 \omega_2 - \hat{u}_3 \omega_1 \omega_3}_{\text{Centrifugal}} \\
&+ \underbrace{\hat{u}_2 \dot{\omega}_3 - \hat{u}_3 \dot{\omega}_2 + \hat{u}_2 \omega_3 - \hat{u}_3 \omega_2}_{\text{Euler}} + \underbrace{2V_{e_2} \omega_3 - 2V_{e_3} \omega_2}_{\text{Magnus}} - \underbrace{\frac{\partial V_{e_1}}{\partial t}}_{\text{Translation}}
\end{aligned} \tag{5.165}$$

**$\hat{u}_2$ -momentum:**

$$\begin{aligned}
0 &= -\frac{1}{h_2} \frac{\partial \hat{\psi}}{\partial \hat{u}_2} + \underbrace{2\hat{V}_3 \omega_1 - 2\hat{V}_1 \omega_3}_{\text{Coriolis}} + \underbrace{\hat{u}_2(\omega_3^2 + \omega_1^2) - \hat{u}_1 \omega_1 \omega_2 - \hat{u}_3 \omega_2 \omega_3}_{\text{Centrifugal}} \\
&+ \underbrace{\hat{u}_3 \dot{\omega}_1 - \hat{u}_1 \dot{\omega}_3 + \hat{u}_3 \omega_1 - \hat{u}_1 \omega_3}_{\text{Euler}} + \underbrace{2V_{e_3} \omega_1 - 2V_{e_1} \omega_3}_{\text{Magnus}} - \underbrace{\frac{\partial V_{e_2}}{\partial t}}_{\text{Translation}}
\end{aligned} \tag{5.166}$$

**$\hat{u}_3$ -momentum:**

$$\begin{aligned}
& \frac{\partial \hat{V}_3}{\partial t} + \frac{\hat{V}_1}{h_1} \frac{\partial \hat{V}_3}{\partial \hat{u}_1} + \frac{\hat{V}_2}{h_2} \frac{\partial \hat{V}_3}{\partial \hat{u}_2} + \frac{\hat{V}_3}{h_3} \frac{\partial \hat{V}_3}{\partial \hat{u}_3} - \hat{V}_1 \left( \frac{\hat{V}_1}{h_1 h_3} \frac{\partial h_1}{\partial \hat{u}_3} - \frac{\hat{V}_3}{h_1 h_3} \frac{\partial h_3}{\partial \hat{u}_1} \right) + \hat{V}_2 \left( \frac{\hat{V}_3}{h_2 h_3} \frac{\partial h_2}{\partial \hat{u}_1} - \frac{\hat{V}_2}{h_2 h_3} \frac{\partial h_2}{\partial \hat{u}_3} \right) \\
&= -\frac{1}{h_3} \frac{\partial \hat{\psi}}{\partial \hat{u}_3} + \frac{1}{h_2} \frac{\partial}{\partial \hat{u}_2} \hat{v} \frac{h_3}{h_2} \frac{\partial \hat{u}_2}{\partial \hat{u}_2} \frac{\hat{V}_3}{h_3} \\
&+ \underbrace{2\hat{V}_1 \omega_2 - 2\hat{V}_2 \omega_1}_{\text{Coriolis}} + \underbrace{\hat{u}_3(\omega_2^2 + \omega_1^2) - \hat{u}_1 \omega_1 \omega_3 - \hat{u}_2 \omega_1 \omega_3}_{\text{Centrifugal}} \\
&+ \underbrace{\hat{u}_1 \dot{\omega}_2 - \hat{u}_2 \dot{\omega}_1 + \hat{u}_1 \omega_2 - \hat{u}_2 \omega_1}_{\text{Euler}} + \underbrace{2V_{e_1} \omega_2 - 2V_{e_2} \omega_1}_{\text{Magnus}} - \underbrace{\frac{\partial V_{e_3}}{\partial t}}_{\text{Translation}}
\end{aligned} \tag{5.167}$$

### 5.3. NON-INERTIAL BOUNDARY LAYER EQUATIONS FOR A FLAT PLATE - CURVILINEAR FORMULATION

In *Equation 5.60* a set of rotation parameters were defined for rotation about the  $\hat{y}$ -axis in the Cartesian direction. The same set of equations are applied here to *Equations 5.165, 5.166 and 5.167*.

$$\begin{aligned}\omega_1 &= 0 \\ \omega_2 &= \Omega \\ \omega_3 &= 0\end{aligned}\tag{5.168}$$

A set of boundary layer equations for incompressible flow with no translation and steady rotation about the second principal direction in Curvilinear coordinates are obtained:

**$\hat{u}_1$ -momentum:**

$$\begin{aligned}\frac{\partial \hat{V}_1}{\partial t} + \frac{\hat{V}_1}{h_1} \frac{\partial \hat{V}_1}{\partial \hat{u}_1} + \frac{\hat{V}_2}{h_2} \frac{\partial \hat{V}_1}{\partial \hat{u}_2} + \frac{\hat{V}_3}{h_3} \frac{\partial \hat{V}_1}{\partial \hat{u}_3} - \hat{V}_2 \left( \frac{\hat{V}_2}{h_1 h_2} \frac{\partial h_2}{\partial \hat{u}_1} - \frac{\hat{V}_1}{h_1 h_2} \frac{\partial h_1}{\partial \hat{u}_2} \right) + \hat{V}_3 \left( \frac{\hat{V}_1}{h_1 h_3} \frac{\partial h_1}{\partial \hat{u}_3} - \frac{\hat{V}_3}{h_1 h_3} \frac{\partial h_3}{\partial \hat{u}_1} \right) \\ = -\frac{1}{h_1} \frac{\partial \hat{\psi}}{\partial \hat{u}_1} + \frac{1}{h_2} \frac{\partial}{\partial \hat{u}_2} \hat{v} \frac{h_1}{h_2} \frac{\partial \hat{u}_2}{\partial \hat{u}_2} \frac{\hat{V}_1}{h_1} - \underbrace{2\hat{V}_3 \Omega}_{\text{Coriolis}} + \underbrace{\hat{u}_1 \Omega^2}_{\text{Centrifugal}}\end{aligned}\tag{5.169}$$

**$\hat{u}_2$ -momentum:**

$$0 = -\frac{1}{h_2} \frac{\partial \hat{\psi}}{\partial \hat{u}_2}\tag{5.170}$$

**$\hat{u}_3$ -momentum:**

$$\begin{aligned}\frac{\partial \hat{V}_3}{\partial t} + \frac{\hat{V}_1}{h_1} \frac{\partial \hat{V}_3}{\partial \hat{u}_1} + \frac{\hat{V}_2}{h_2} \frac{\partial \hat{V}_3}{\partial \hat{u}_2} + \frac{\hat{V}_3}{h_3} \frac{\partial \hat{V}_3}{\partial \hat{u}_3} - \hat{V}_1 \left( \frac{\hat{V}_1}{h_1 h_3} \frac{\partial h_1}{\partial \hat{u}_3} - \frac{\hat{V}_3}{h_1 h_3} \frac{\partial h_3}{\partial \hat{u}_1} \right) + \hat{V}_2 \left( \frac{\hat{V}_3}{h_2 h_3} \frac{\partial h_2}{\partial \hat{u}_1} - \frac{\hat{V}_2}{h_2 h_3} \frac{\partial h_2}{\partial \hat{u}_3} \right) \\ = -\frac{1}{h_3} \frac{\partial \hat{\psi}}{\partial \hat{u}_3} + \frac{1}{h_2} \frac{\partial}{\partial \hat{u}_2} \hat{v} \frac{h_3}{h_2} \frac{\partial \hat{u}_2}{\partial \hat{u}_2} \frac{\hat{V}_3}{h_3} + \underbrace{2\hat{V}_1 \Omega}_{\text{Coriolis}} + \underbrace{\hat{u}_3 \Omega^2}_{\text{Centrifugal}}\end{aligned}\tag{5.171}$$

The Curvilinear geometry is a flat plate in this case. The equations above are written in the Cartesian or Cylindrical form using *Table 5.1*.

The Cartesian description then becomes:

CHAPTER 5. NON-INERTIAL BOUNDARY LAYER EQUATIONS

---

$$\begin{aligned}
 \frac{\partial \hat{u}}{\partial t} + \hat{u} \frac{\partial \hat{u}}{\partial \hat{x}} + \hat{v} \frac{\partial \hat{u}}{\partial \hat{y}} + \hat{w} \frac{\partial \hat{u}}{\partial \hat{z}} &= -\frac{\partial \hat{\psi}}{\partial \hat{x}} + \nu \frac{\partial^2 \hat{u}}{\partial \hat{y}^2} - 2\hat{w}\Omega + \hat{x}\Omega^2 \\
 0 &= -\frac{\partial \hat{\psi}}{\partial \hat{y}} \\
 \frac{\partial \hat{w}}{\partial t} + \hat{u} \frac{\partial \hat{w}}{\partial \hat{x}} + \hat{v} \frac{\partial \hat{w}}{\partial \hat{y}} + \hat{w} \frac{\partial \hat{w}}{\partial \hat{z}} &= -\frac{\partial \hat{\psi}}{\partial \hat{z}} + \nu \frac{\partial^2 \hat{w}}{\partial \hat{y}^2} + 2\hat{u}\Omega + \hat{z}\Omega^2
 \end{aligned} \tag{5.172}$$

This is the same as the set of equations in *Equation 5.61* which were used in *Section 5.1.4* to validate the boundary layer equations in the Cartesian co-ordinate system.

In a similar manner the Cylindrical equations are obtained:

$$\begin{aligned}
 \frac{\partial \hat{u}_r}{\partial t} + \hat{u}_r \frac{\partial \hat{u}_r}{\partial \hat{r}} + \frac{\hat{u}_\theta}{\hat{r}} \frac{\partial \hat{u}_r}{\partial \hat{\theta}} - \frac{\hat{u}_\theta^2}{\hat{r}} + \hat{u}_y \frac{\partial \hat{u}_r}{\partial \hat{y}} &= -\frac{\partial \hat{\psi}}{\partial \hat{r}} + \hat{\nu} \frac{\partial^2 \hat{u}_r}{\partial \hat{y}^2} - 2\hat{u}_\theta\Omega + \hat{r}\Omega^2 \\
 0 &= -\frac{\partial \hat{\psi}}{\partial \hat{y}} \\
 \frac{\partial \hat{u}_\theta}{\partial t} + \hat{u}_r \frac{\partial \hat{u}_\theta}{\partial \hat{r}} + \frac{\hat{u}_\theta}{\hat{r}} \frac{\partial \hat{u}_\theta}{\partial \hat{\theta}} + \frac{\hat{u}_\theta \hat{u}_r}{\hat{r}} + \hat{u}_y \frac{\partial \hat{u}_\theta}{\partial \hat{y}} &= -\frac{1}{\hat{r}} \frac{\partial \hat{\psi}}{\partial \hat{\theta}} + \hat{\nu} \frac{\partial^2 \hat{u}_\theta}{\partial \hat{y}^2} + 2\hat{u}_r\Omega
 \end{aligned} \tag{5.173}$$

The equations above are similar to *Equation 5.138* which were used in *Section 5.2.5* to validate the boundary layer equations in the Cylindrical co-ordinate system.

## 5.4 Closure

This chapter provided a framework for the analysis of the non-inertial boundary layer in Cartesian, Cylindrical and Curvilinear coordinates respectively. The main results are:

- The continuity equations in the boundary layer for both compressible and incompressible flows were obtained. No terms are neglected from the continuity equation. Therefore the form remains the same as in the bulk flow.

$$\frac{\partial \hat{\rho}}{\partial t} + \frac{1}{h_1 h_2 h_3} \left[ \frac{\partial}{\partial \hat{u}_1} (h_2 h_3 \hat{\rho} \hat{V}_1) + \frac{\partial}{\partial \hat{u}_2} (h_1 h_3 \hat{\rho} \hat{V}_2) + \frac{\partial}{\partial \hat{u}_3} (h_1 h_2 \hat{\rho} \hat{V}_3) \right] = 0 \quad (5.174)$$

- The momentum equations in the boundary layer for compressible and incompressible flow were determined for Cartesian, Cylindrical and Curvilinear co-ordinate systems.

### $\hat{x}$ -momentum

$$\begin{aligned} \frac{\partial \hat{\rho} \hat{u}}{\partial t} + \hat{u} \frac{\partial \hat{\rho} \hat{u}}{\partial \hat{x}} + \hat{v} \frac{\partial \hat{\rho} \hat{u}}{\partial \hat{y}} + \hat{w} \frac{\partial \hat{\rho} \hat{u}}{\partial \hat{z}} = & -\frac{\partial \hat{p}}{\partial \hat{x}} + \frac{\partial}{\partial \hat{y}} \left[ \hat{\mu} \frac{\partial \hat{u}}{\partial \hat{y}} \right] + 2\hat{\rho} \hat{v} \omega_3 - 2\hat{\rho} \hat{w} \omega_2 + \hat{\rho} \hat{x} (\omega_3^2 + \omega_2^2) \\ & - \hat{\rho} \hat{y} \omega_1 \omega_2 - \hat{\rho} \hat{z} \omega_1 \omega_3 + \hat{\rho} \hat{y} \hat{\omega}_3 - \hat{\rho} \hat{z} \hat{\omega}_2 + \hat{\rho} \hat{y} \omega_3 - \hat{\rho} \hat{z} \omega_2 \\ & + 2\hat{\rho} \hat{V}_y \omega_3 - 2\hat{\rho} \hat{V}_z \omega_2 - \frac{\partial \hat{\rho} \hat{V}_x}{\partial t} \end{aligned} \quad (5.175)$$

### $\hat{y}$ -momentum

$$\begin{aligned} 0 = & -\frac{\partial \hat{p}}{\partial \hat{y}} + 2\hat{\rho} \hat{w} \omega_1 - 2\hat{\rho} \hat{u} \omega_3 + \hat{\rho} \hat{y} (\omega_3^2 + \omega_1^2) - \hat{\rho} \hat{x} \omega_1 \omega_2 - \hat{\rho} \hat{z} \omega_2 \omega_3 + \hat{\rho} \hat{z} \hat{\omega}_1 - \hat{\rho} \hat{x} \hat{\omega}_3 + \hat{\rho} \hat{z} \omega_1 - \hat{\rho} \hat{x} \omega_3 \\ & + 2\hat{\rho} \hat{V}_z \omega_1 - 2\hat{\rho} \hat{V}_x \omega_3 - \frac{\partial \hat{\rho} \hat{V}_y}{\partial t} \end{aligned} \quad (5.176)$$

### $\hat{z}$ -momentum

$$\begin{aligned} \frac{\partial \hat{\rho} \hat{w}}{\partial t} + \hat{u} \frac{\partial \hat{\rho} \hat{w}}{\partial \hat{x}} + \hat{v} \frac{\partial \hat{\rho} \hat{w}}{\partial \hat{y}} + \hat{w} \frac{\partial \hat{\rho} \hat{w}}{\partial \hat{z}} = & -\frac{\partial \hat{p}}{\partial \hat{z}} + \frac{\partial}{\partial \hat{y}} \left[ \hat{\mu} \frac{\partial \hat{w}}{\partial \hat{y}} \right] + 2\hat{\rho} \hat{u} \omega_2 - 2\hat{\rho} \hat{v} \omega_1 + \hat{\rho} \hat{z} (\omega_2^2 + \omega_1^2) \\ & - \hat{\rho} \hat{x} \omega_1 \omega_3 - \hat{\rho} \hat{y} \omega_2 \omega_3 + \hat{\rho} \hat{x} \hat{\omega}_y - \hat{\rho} \hat{y} \hat{\omega}_x + \hat{\rho} \hat{x} \omega_y - \hat{\rho} \hat{y} \omega_x \\ & + 2\hat{\rho} \hat{V}_x \omega_2 - 2\hat{\rho} \hat{V}_y \omega_1 - \frac{\partial \hat{\rho} \hat{V}_z}{\partial t} \end{aligned} \quad (5.177)$$

- The following similarities were observed for all co-ordinate systems:
  - The material derivative (left hand side of the Navier-Stokes equation) are unchanged in the longitudinal and transversal directions. However, all left hand side terms are neglected in the direction normal to the surface.
  - The pressure gradient terms are present in all directions.

CHAPTER 5. NON-INERTIAL BOUNDARY LAYER EQUATIONS

◦ The diffusion terms in the boundary layer originate from specific components in the stress tensor of the  $\tau_{12}$  and  $\tau_{32}$  terms.

$$\begin{aligned}\hat{\tau}_{12} &= \hat{\mu} \left[ \frac{h_2}{h_1} \frac{\partial}{\partial \hat{u}_1} \left( \frac{\hat{V}_2}{h_2} \right) + \frac{h_1}{h_2} \frac{\partial}{\partial \hat{u}_2} \left( \frac{\hat{V}_1}{h_1} \right) \right] \\ \hat{\tau}_{32} &= \hat{\mu} \left[ \frac{h_3}{h_2} \frac{\partial}{\partial \hat{u}_2} \left( \frac{\hat{V}_3}{h_3} \right) + \frac{h_2}{h_3} \frac{\partial}{\partial \hat{u}_3} \left( \frac{\hat{V}_2}{h_2} \right) \right]\end{aligned}\quad (5.178)$$

◦ The fictitious terms can not be neglected from the boundary layer equations. Therefore the terms have an influence on the boundary layer velocity profile during acceleration and deceleration of the object.

**$\hat{u}_1$ -momentum:**

$$\begin{aligned}& \frac{\partial \hat{V}_1}{\partial t} + \frac{\hat{V}_1}{h_1} \frac{\partial \hat{V}_1}{\partial \hat{u}_1} + \frac{\hat{V}_2}{h_2} \frac{\partial \hat{V}_1}{\partial \hat{u}_2} + \frac{\hat{V}_3}{h_3} \frac{\partial \hat{V}_1}{\partial \hat{u}_3} - \hat{V}_2 \left( \frac{\hat{V}_2}{h_1 h_2} \frac{\partial h_2}{\partial \hat{u}_1} - \frac{\hat{V}_1}{h_1 h_2} \frac{\partial h_1}{\partial \hat{u}_2} \right) + \hat{V}_3 \left( \frac{\hat{V}_1}{h_1 h_3} \frac{\partial h_1}{\partial \hat{u}_3} - \frac{\hat{V}_3}{h_1 h_3} \frac{\partial h_3}{\partial \hat{u}_1} \right) \\ &= -\frac{1}{h_1} \frac{\partial \hat{\psi}}{\partial \hat{u}_1} + \frac{1}{h_2} \frac{\partial}{\partial \hat{u}_2} \hat{v} \frac{h_1}{h_2} \frac{\partial \hat{V}_1}{\partial \hat{u}_2} \\ &+ \underbrace{2\hat{V}_2 \omega_3 - 2\hat{V}_3 \omega_2}_{\text{Coriolis}} + \underbrace{\hat{u}_1(\omega_3^2 + \omega_2^2) - \hat{u}_2 \omega_1 \omega_2 - \hat{u}_3 \omega_1 \omega_3}_{\text{Centrifugal}} \\ &+ \underbrace{\hat{u}_2 \omega_3 - \hat{u}_3 \omega_2}_{\text{Euler}} + \hat{u}_2 \omega_3 - \hat{u}_3 \omega_2 + \underbrace{2V_{e_2} \omega_3 - 2V_{e_3} \omega_2}_{\text{Magnus}} - \underbrace{\frac{\partial V_{e_1}}{\partial t}}_{\text{Translation}} \\ &\quad \text{Unsteady motion}\end{aligned}\quad (5.179)$$

**$\hat{u}_2$ -momentum:**

$$\begin{aligned}0 &= -\frac{1}{h_2} \frac{\partial \hat{\psi}}{\partial \hat{u}_2} + \underbrace{2\hat{V}_3 \omega_1 - 2\hat{V}_1 \omega_3}_{\text{Coriolis}} + \underbrace{\hat{u}_2(\omega_3^2 + \omega_1^2) - \hat{u}_1 \omega_1 \omega_2 - \hat{u}_3 \omega_2 \omega_3}_{\text{Centrifugal}} \\ &+ \underbrace{\hat{u}_3 \omega_1 - \hat{u}_1 \omega_3}_{\text{Euler}} + \hat{u}_3 \omega_1 - \hat{u}_1 \omega_3 + \underbrace{2V_{e_3} \omega_1 - 2V_{e_1} \omega_3}_{\text{Magnus}} - \underbrace{\frac{\partial V_{e_1}}{\partial t}}_{\text{Translation}} \\ &\quad \text{Unsteady motion}\end{aligned}\quad (5.180)$$

The boundary layer equations were validated with examples from the literature (Bogdanova [82], Dumitrescu et al. [85], Dwyer [83] and Mager [81]) for cases with zero translation and steady rotation. The components of the fictitious forces in Cylindrical coordinates were visualized in *Figure 5.9* by indicating the direction of the Centrifugal force and the two components of the Coriolis force.

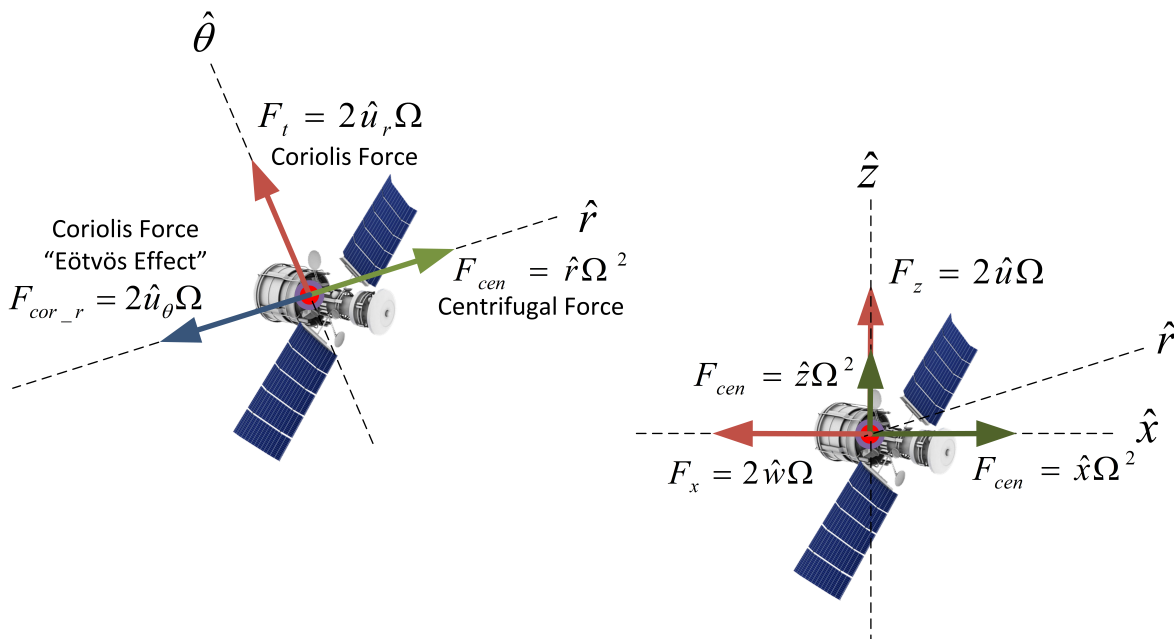
$$\begin{aligned}\frac{\partial \hat{u}_r}{\partial t} + \hat{u}_r \frac{\partial \hat{u}_r}{\partial \hat{r}} + \frac{\hat{u}_\theta}{\hat{r}} \frac{\partial \hat{u}_r}{\partial \hat{\theta}} - \frac{\hat{u}_\theta^2}{\hat{r}} + \hat{u}_y \frac{\partial \hat{u}_r}{\partial \hat{y}} &= -\frac{\partial \hat{\psi}}{\partial \hat{r}} + \hat{v} \frac{\partial^2 \hat{u}_r}{\partial \hat{y}^2} - 2\hat{u}_\theta \Omega + \hat{r} \Omega^2 \\ \frac{\partial \hat{u}_\theta}{\partial t} + \hat{u}_r \frac{\partial \hat{u}_\theta}{\partial \hat{r}} + \frac{\hat{u}_\theta}{\hat{r}} \frac{\partial \hat{u}_\theta}{\partial \hat{\theta}} + \frac{\hat{u}_\theta \hat{u}_r}{\hat{r}} + \hat{u}_y \frac{\partial \hat{u}_\theta}{\partial \hat{y}} &= -\frac{1}{\hat{r}} \frac{\partial \hat{\psi}}{\partial \hat{\theta}} + \hat{v} \frac{\partial^2 \hat{u}_\theta}{\partial \hat{y}^2} + 2\hat{u}_r \Omega\end{aligned}\quad (5.181)$$



In a similar manner the components of the fictitious forces in Cartesian coordinates can be visualized using the same analogy as *Figure 5.9*. This is shown in *Figure 5.10*.

$$\begin{aligned}
 \frac{\partial \hat{u}}{\partial t} + \hat{u} \frac{\partial \hat{u}}{\partial \hat{x}} + \hat{v} \frac{\partial \hat{u}}{\partial \hat{y}} + \hat{w} \frac{\partial \hat{u}}{\partial \hat{z}} &= -\frac{\partial \hat{\psi}}{\partial \hat{x}} + \nu \frac{\partial^2 \hat{u}}{\partial \hat{y}^2} - 2\hat{w}\Omega + \hat{x}\Omega^2 \\
 \frac{\partial \hat{w}}{\partial t} + \hat{u} \frac{\partial \hat{w}}{\partial \hat{x}} + \hat{v} \frac{\partial \hat{w}}{\partial \hat{y}} + \hat{w} \frac{\partial \hat{w}}{\partial \hat{z}} &= -\frac{\partial \hat{\psi}}{\partial \hat{z}} + \nu \frac{\partial^2 \hat{w}}{\partial \hat{y}^2} + 2\hat{u}\Omega + \hat{z}\Omega^2
 \end{aligned}
 \tag{5.182}$$

Figure 5.10: Visualization of the Fictitious Forces in Cylindrical and Cartesian Co-ordinates



In a Cylindrical system the Centrifugal force has one component in the positive  $\hat{r}$ -direction. In a Cartesian system it has two components. The Coriolis force consists of two components in both Cylindrical and Cartesian systems. The Eötvös effect and the Coriolis force tangential to the satellite motion can be distinguished separately in the Cylindrical system. In the Cartesian system these effects cannot be separated.



UNIVERSITEIT VAN PRETORIA  
UNIVERSITY OF PRETORIA  
YUNIBESITHI YA PRETORIA

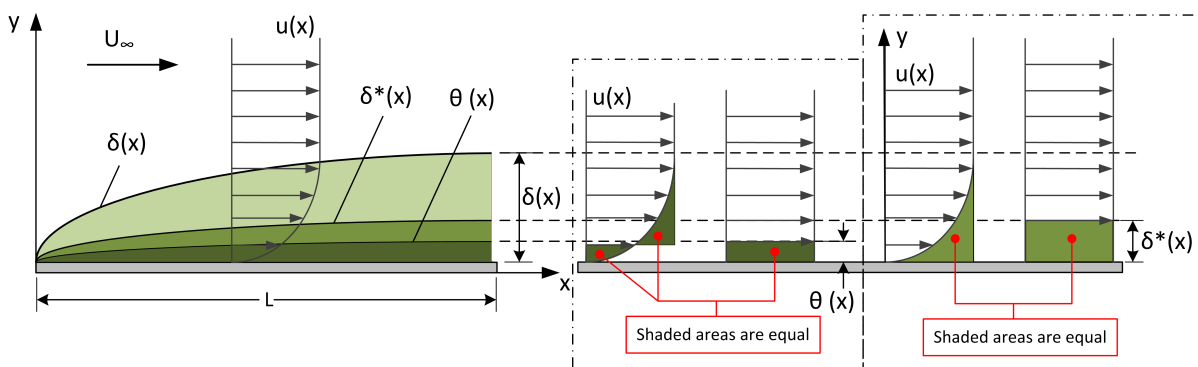
## Non-Inertial Solver Implementation and Validation

The open source code OpenFOAM was utilized as a platform for the non-inertial solver development and subsequent numerical analysis. Implementation of the solver is discussed in a manner that facilitates reproduction of the code. The theoretical formulation and numerical methods used in the subsequent analysis are provided to add to the reproducibility of results.

Two validation cases were conducted to assess the functionality of the developed solver; a laminar flat plate and a laminar rotating disk. Analytical results for these cases are available from the literature (Blasius [37], Monaghan [87], von Karman [41]). This is compared with the steady state numerical results.

The boundary layer behaviour is discussed in terms of the boundary layer height,  $\delta$ , displacement thickness,  $\delta^*$ , momentum thickness,  $\theta$ , and the Shape Factor,  $H$  (Figure 6.1).

Figure 6.1: Physical Interpretation of the Boundary Layer Parameters



The boundary layer height is the distance from the wall where the stream-wise velocity is 99% of the free stream velocity. The mathematical definitions of the displacement and momentum thickness was shown in Equations 5.1 and 5.2.

CHAPTER 6. NON-INERTIAL SOLVER IMPLEMENTATION AND VALIDATION

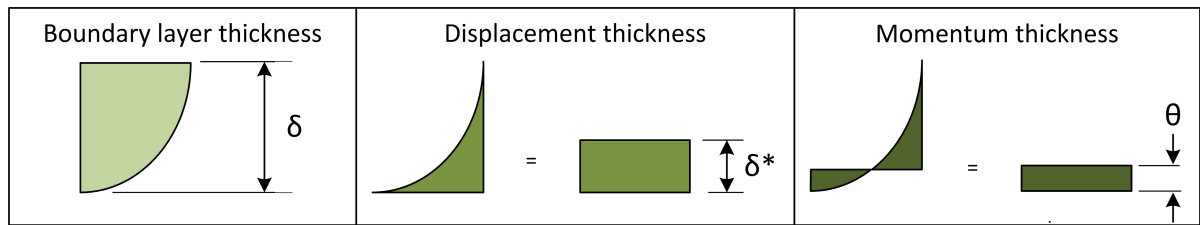
$$\delta^* = \int_0^{y^* \rightarrow \infty} \left(1 - \frac{u}{U_\infty}\right) dy \tag{6.1}$$

$$\theta = \int_0^{y^* \rightarrow \infty} \frac{u}{U_\infty} \left(1 - \frac{u}{U_\infty}\right) dy \tag{6.2}$$

A comparison of the parameters is shown in *Figure 6.2*. This indicates that the boundary layer thickness is higher than the displacement thickness which in turn is higher than the momentum thickness.

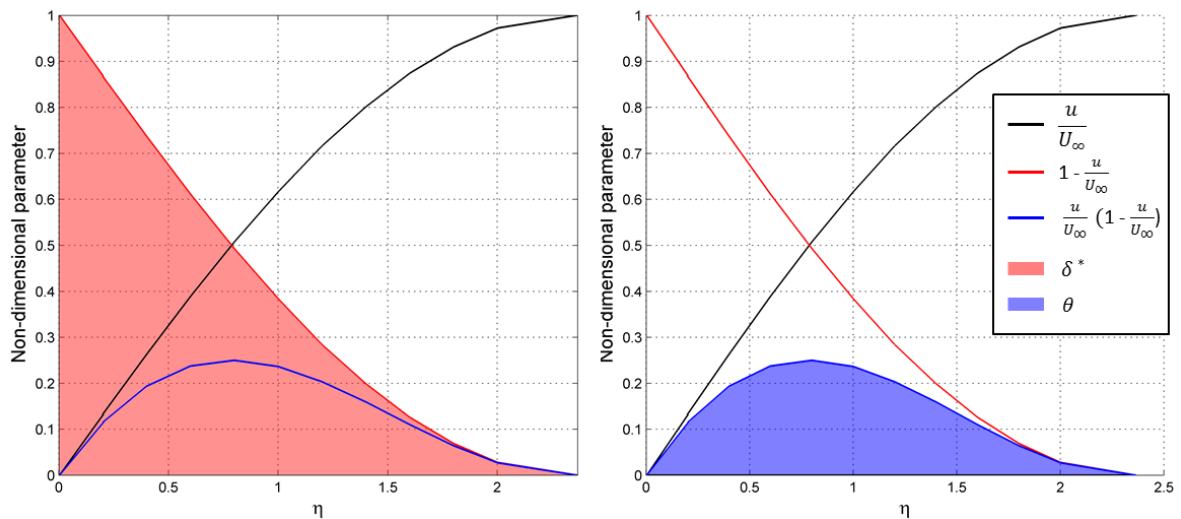
$$\delta > \delta^* > \theta \tag{6.3}$$

Figure 6.2: Comparison between the Boundary Layer, Displacement and Momentum Thicknesses



The parameters above are used to obtain a numerical approximation of the displacement and momentum thicknesses. The displacement thickness is the area under the  $1 - \frac{u}{U_\infty}$  curve. The momentum thickness is the area under the  $\frac{u}{U_\infty} \left(1 - \frac{u}{U_\infty}\right)$  curve. This is demonstrated in *Figure 6.3*.

Figure 6.3: Boundary Layer Parameters on a Flat Plate

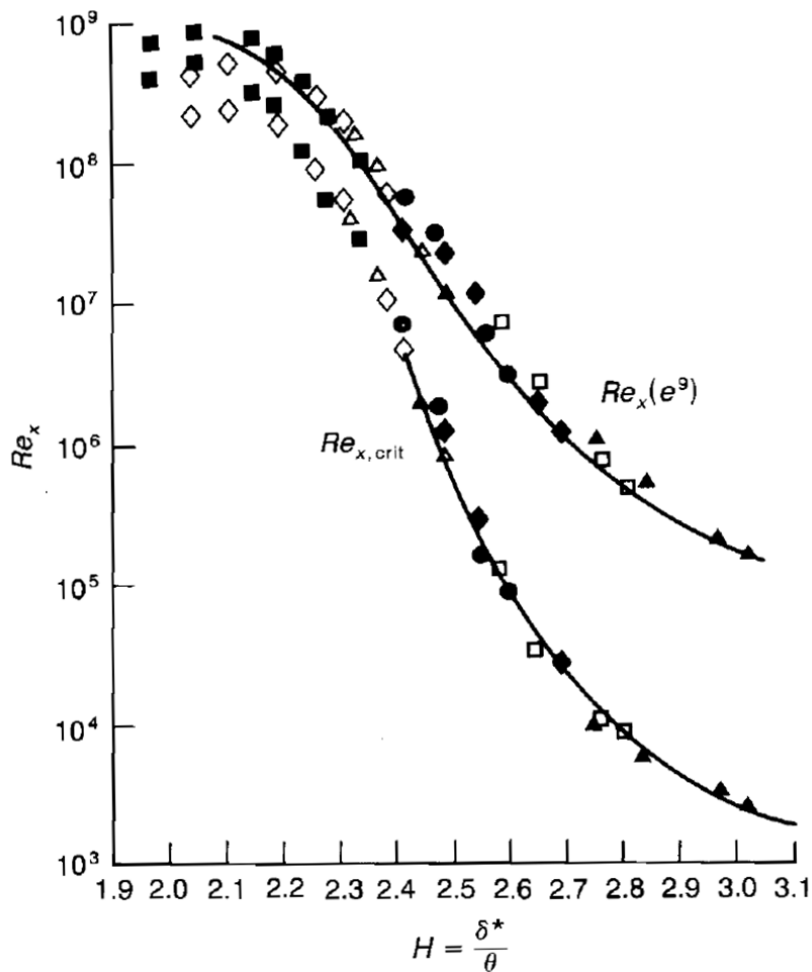


The Shape factor is determined from the displacement and momentum thicknesses.

$$H = \frac{\delta^*}{\theta} \tag{6.4}$$

The purpose of the Shape Factor is to characterize the regime of the flow. Wazzan et al. [78] determined the Shape Factor curve as a function of the critical and transition Reynolds numbers (*Figure 6.4*).

Figure 6.4: Correlation of Critical Reynolds Number, Transition Reynolds Number versus Shape Factor from Wazzan et al. [78]



In *Figure 6.4* it is shown that at lower Reynolds numbers, the critical Reynolds number occur at a higher Shape Factor value. Similarly, at high Reynolds numbers the Shape Factors are much lower for corresponding critical Reynolds number. The Shape Factor is used in steady state analyses to determine if the flow has separated. It is also used to determine if the flow is turbulent or laminar. The critical Reynolds number for a Blasius Flat plate is approximately 2.59 (White [9]).

## 6.1 Code Implementation

### 6.1.1 Open Source Field Operation And Manipulation - OPENFOAM®

OpenFOAM (OpenFOAM [88]) is a acronym for Open Source Field operation and Manipulation. It is a C++ toolbox that provides a platform for the development of customized numerical solvers related to continuum mechanics problems using the finite volume method. It is released under the Open Source Software GNU General Public License (GNU [89]).

The code was originally developed by Henry Weller at Imperial College in London. The commercial Computational Fluid Dynamic (CFD) codes StarCD (CD-adapco [90]) and Fluent (ANSYS [91]) also originates from this college.

Numerical analysis of aerospace and defence applications requires a significant level of code flexibility to make the desired changes to existing subroutines or to develop new routines. OpenFOAM® consist of many solvers, utilities and libraries that provide an ideal platform of development. Its object orientated code architecture allows for re-use of existing code blocks and objects and therefore eases the overhead of new developments.

OpenFOAM provides a good alternative to commercial software since it has been extensively validated and there is no direct costs involved to operate it.

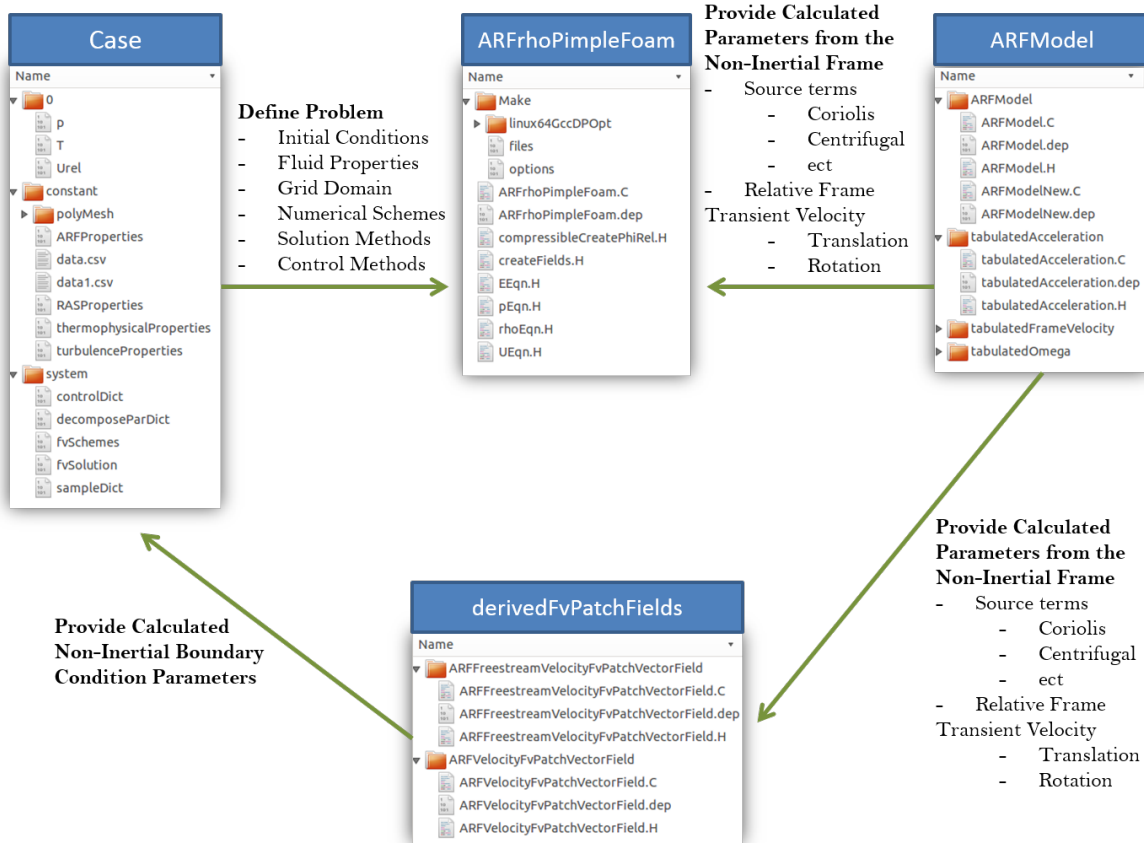
### 6.1.2 Code Architecture

The non-inertial solver is designated **ARFrhoPimpleFoam**. The code architecture consist of three main code blocks and the case set-up files (*Figure 6.5*). The baseline of the OpenFOAM solver, rhoPimpleFoam, were used since it already had the source terms for steady rotation implemented. Although the solver methodology is based on the PIMPLE method (SIMPLE-PISO hybrid with pseudo-transient implementation (Ferziger and Peric [92], Versteeg and Malalasekera [69])), it can be operated in the PISO mode (Pressure Implicit with Splitting of Operator (Ferziger and Peric [92], Versteeg and Malalasekera [69])) as was done in this analysis. The quasi-transient transient implementation of PIMPLE is not be able to capture transient behaviour accurately as no parameter relaxation should be used in time accurate cases. The baseline of the existing **SRFModel** library was used to developed the **ARFModel** library. This library contains all the non-inertial source terms for an object in arbitrary acceleration but in pure rotation.

In this architecture the case set-up defines the problem, which include the initial conditions, fluid properties, grid domain, numerical schemes, solution methods and control measures. This information is provided to the solver, ARFrhoPimpleFoam and the library, ARFModel. The solver contains the compiled source code for the solution algorithm. Parameters in the solver points to the ARFModel that calculates the non-inertial source terms and determines the frame velocity through interpolation of the table provided in the case set-up.

The case set-up can make use of specialized non-inertial boundary conditions which is obtained in the ARFModel/derivedFvPatchFields library. It provides the non-inertial velocity boundary condition with information obtained from the ARFModel library.

Figure 6.5: Accelerating Reference Frame (ARF) Model Code Architecture



The resulting application for solving cases in a non-inertial frame has the following attributes:

- **Non-Inertial Momentum Equation Implementation.** The momentum equations implementation in the existing **SRFModel** was for steady rotations only. This was modified to contain the relevant source terms as derived in *Equation 3.227*. The term  $\rho \hat{\mathbf{x}} \wedge \boldsymbol{\Omega}$  was not included since only pure rotation are investigated here. The non-inertial momentum equation implemented in the **ARFModel** is:

$$\begin{aligned}
 \frac{\partial \hat{\rho} \hat{\mathbf{u}}}{\partial t} + \hat{\nabla} \cdot (\hat{\rho} \hat{\mathbf{u}} \otimes \hat{\mathbf{u}}) = & -\hat{\nabla} \hat{p} + \hat{\nabla} \cdot [\hat{\mu}(\hat{\nabla} \hat{\mathbf{u}} + \hat{\nabla} \hat{\mathbf{u}}^T) + \hat{\lambda}(\hat{\nabla} \cdot \hat{\mathbf{u}}) \hat{\mathbf{I}}] \\
 & - \underbrace{\frac{\partial}{\partial t}(\rho \mathbf{V}(t))}_{\text{Translation}} + \underbrace{\rho \hat{\mathbf{x}} \wedge \dot{\boldsymbol{\Omega}}}_{\text{Euler}} + \underbrace{2\rho \hat{\mathbf{u}} \wedge \boldsymbol{\Omega}}_{\text{Coriolis}} - \underbrace{\rho \hat{\mathbf{x}} \wedge \boldsymbol{\Omega} \wedge \boldsymbol{\Omega}}_{\text{Centrifugal}} + \underbrace{2\rho \mathbf{V}(t) \wedge \boldsymbol{\Omega}}_{\text{Magnus}}
 \end{aligned}$$

- **Non-inertial Operation.** The code solves entirely in the non-inertial frame therefore the velocity vectors are calculated in terms of the relative frame. The code calculates the absolute velocities

## CHAPTER 6. NON-INERTIAL SOLVER IMPLEMENTATION AND VALIDATION

---

by transformation of the relative velocities.

- Prescribed Motion. The solver requires the time dependant translational and rotational velocities as inputs for the prescribed motion of the system.
- Stationary Mesh. The uniqueness of this implementation lies in the non-inertial nature where the object is completely stationary and the flow is in motion. This eliminates the need for a moving mesh or level set methods that can cause large computational overheads. The cells in the near wall region can be made sufficiently small to capture the boundary layer response to changing bulk flow conditions.
- Specialized Boundary Conditions. The boundary conditions are able to adapt to the changing relative motion of the non-inertial frame when in acceleration. This is achieved by specifying the boundary conditions in the absolute frame (of which the far field is stationary) and transforming the conditions according to the prescribed motion to the non-inertial frame.
- Compressible. The governing equations are in the compressible form, which make is applicable to a wider range of applications.

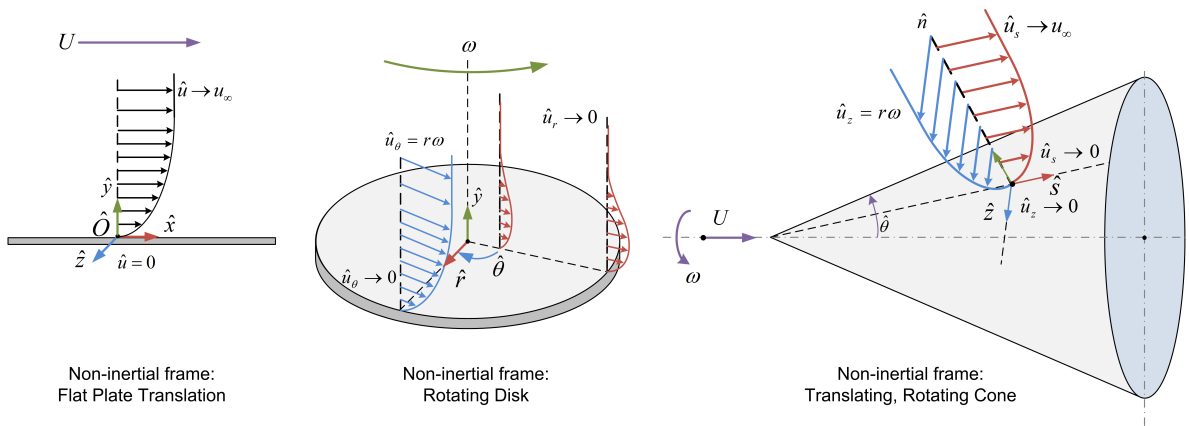
A detailed account of the implementation, with code examples, are given in *Appendix B*.



## 6.2 Theoretical Formulation

The theoretical formulation and numerical method used to analyse the three cases in this thesis (Figure 6.6) is discussed in this section. This includes the assumptions made regarding the flow, the governing equations implemented and the closure models used. The grid independent computational domains and boundary conditions for each case is shown. The numerical methods that was used to solve the system of equations, as already implemented in openFOAM, is discussed.

Figure 6.6: Graphical Representation of Test Cases; Translating Plate, Rotating Disk and Translating, Rotating Cone



### 6.2.1 Assumptions

The following assumptions were made with regards to the flow field:

- The flow can be completely described in the non-inertial reference frame.
- The fluid is Newtonian i.e. the viscous stresses in the fluid is linearly proportional to the strain rate.
- The ideal gas law is an appropriate equation of state to utilize as a closure model.
- The compressible form of the governing equations accurately describes the flow.
- The flow is well within the laminar regime, no turbulence models are employed.
- Viscous dissipation terms,  $\hat{\phi}$ , in the energy equation can be neglected since this is a laminar case and the dissipation term is associated with turbulent behaviour.
- The bulk viscosity is zero, as per Stoke's Law.
- Heat conduction is described by Fourier's Law.

## 6.2.2 Governing Equations

The governing equations used in the analysis was derived in *Chapter 3*.

The conservation of mass, also referred to as the continuity equation, made use of the formulation of *Equation 3.192*.

$$\frac{\partial \hat{\rho}}{\partial t} + \hat{\nabla} \cdot \hat{\rho} \hat{\mathbf{u}} = 0 \quad (6.5)$$

In the source code this equation is solved in the inclusion of the header file, *rhoEqn.H* (shown in *Appendix B*).

The non-inertial energy equation was derived in *Equation 3.237*.

$$\frac{\partial \hat{\rho} \hat{e}}{\partial t} + (\hat{\nabla} \cdot \hat{\rho} \hat{e} \hat{\mathbf{u}}) = -\hat{p}(\hat{\nabla} \cdot \hat{\mathbf{u}}) + \hat{\nabla} \cdot (\hat{k} \hat{\nabla} \hat{T}) + \hat{\phi} \quad (6.6)$$

The implementation of this equation in openFOAM was done using a different form. The viscous dissipation term,  $\hat{\phi}$ , is assumed to be negligible as discussed in the assumptions. The energy equation is expressed either in the internal energy form or the enthalpy form.

The **internal energy** form of the equation is described as,

$$\frac{\partial \hat{\rho} \hat{e}_s}{\partial t} + (\hat{\nabla} \cdot \hat{\rho} \hat{e}_s \hat{\mathbf{u}}) + \frac{\partial \hat{\rho} \hat{K}}{\partial t} + (\hat{\nabla} \cdot \hat{\rho} \hat{K} \hat{\mathbf{u}}) + \hat{p}(\hat{\nabla} \cdot \hat{\mathbf{u}}) - \hat{\nabla} \cdot (\hat{k} \hat{\nabla} \hat{T}) = 0 \quad (6.7)$$

where K represents the potential energy.

The **enthalpy** form of the energy equation is described as follow:

$$\frac{\partial \hat{\rho} \hat{h}_s}{\partial t} + (\hat{\nabla} \cdot \hat{\rho} \hat{h}_s \hat{\mathbf{u}}) + \frac{\partial \hat{\rho} \hat{K}}{\partial t} + (\hat{\nabla} \cdot \hat{\rho} \hat{K} \hat{\mathbf{u}}) - \frac{\partial \hat{p}}{\partial t} - \hat{\nabla} \cdot (\hat{k} \hat{\nabla} \hat{T}) = 0 \quad (6.8)$$

In the source code this equation is solved in the inclusion of the header file, *EEqn.H* (shown in *Appendix B*).

The non-inertial momentum equation for fully arbitrary flow was derived in *Equation 3.227*. The equation had an additional term that represented a moving axis formulation,  $\hat{\rho} \hat{\mathbf{x}} \wedge \hat{\boldsymbol{\Omega}}$ . In this case that term was neglected since only cases in pure rotation are considered. Therefore the equation below was implemented:

$$\begin{aligned} \frac{\partial \hat{\rho} \hat{\mathbf{u}}}{\partial t} + \hat{\nabla} \cdot (\hat{\rho} \hat{\mathbf{u}} \otimes \hat{\mathbf{u}}) - \hat{\nabla} \cdot [\hat{\mu}(\hat{\nabla} \hat{\mathbf{u}} + \hat{\nabla} \hat{\mathbf{u}}^T) + \hat{\lambda}(\hat{\nabla} \cdot \hat{\mathbf{u}}) \hat{\mathbf{I}}] \\ + \underbrace{\frac{\partial}{\partial t}(\hat{\rho} \mathbf{V}(t))}_{\text{Translation}} - \underbrace{\hat{\rho} \hat{\mathbf{x}} \wedge \hat{\boldsymbol{\Omega}}}_{\text{Euler}} - \underbrace{2\hat{\rho} \hat{\mathbf{u}} \wedge \hat{\boldsymbol{\Omega}}}_{\text{Coriolis}} + \underbrace{\hat{\rho} \hat{\mathbf{x}} \wedge \hat{\boldsymbol{\Omega}} \wedge \hat{\boldsymbol{\Omega}}}_{\text{Centrifugal}} - \underbrace{2\hat{\rho} \mathbf{V}(t) \wedge \hat{\boldsymbol{\Omega}}}_{\text{Magnus}} = -\hat{\nabla} \hat{p} \end{aligned} \quad (6.9)$$

In the source code this equation is solved in the inclusion of the header file, *UEqn.H* (shown in *Appendix B*).

### 6.2.3 Closure Models

The system of governing equations above requires additional equation to close the system of equations. An equation of state, transport model and thermodynamic model is required to ensure that for the number of unknowns, there are the same number of equations.

Closure models to be used are defined in the *thermophysicalProperties* dictionary in the openFOAM set up files. This specifies the equation of the state, transport model and thermodynamic model.

The equation of state used in this case is the ideal gas law. This relates the pressure to the density, gas constant and temperature of the fluid.

$$p = \rho RT \quad (6.10)$$

The transport model makes use the equation below, where the Prandtl number is expressed as a ratio of viscous diffusion rate over the thermal diffusion rate:

$$P_r = \frac{C_p \mu}{\kappa} \quad (6.11)$$

In this implementation either the internal energy or enthalpy can be used to determine the temperature profile in the fluid.

The enthalpy is a function of internal energy and pressure.

$$h_s = e_s + \frac{p}{\rho} \quad (6.12)$$

This equation can be re-written to make the internal energy the subject of the equation. The known quantities in the flow is then used to model the internal energy.

$$\begin{aligned} e_s &= h_s - \frac{p}{\rho} \\ &= \int_{T_0}^T C_p T - \frac{r_u T_0}{M_w} \end{aligned} \quad (6.13)$$

The total enthalpy can also be expressed as the sum of the static enthalpy and the enthalpy of the dynamic pressure (Sontagg and Borgnakke [93]).

$$h_t = h_s + 0.5 \mathbf{U} \cdot \mathbf{U} \quad (6.14)$$

The static enthalpy is replaced with known quantities in the flow, and the equation becomes:

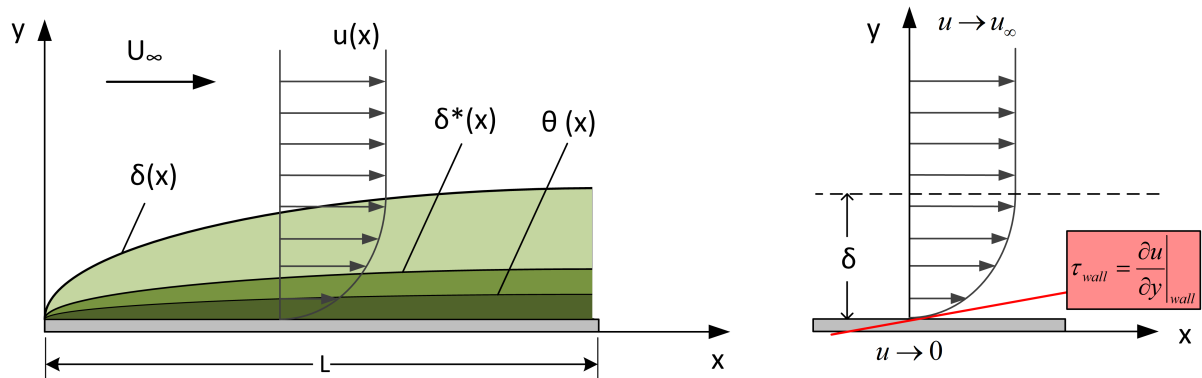
$$h_t = \int_{T_0}^T C_p dT + 0.5 \mathbf{U} \cdot \mathbf{U} \quad (6.15)$$

## 6.3 Case Set-up

### 6.3.1 Computational Domains

The objective of the analyses is to characterise the response of the laminar boundary layer to prescribed motion. Computational grids are required with a sufficient amount of cells in the near-wall viscous region (*Figure 6.7*).

Figure 6.7: Orientating Image of the Boundary Layer



In the near-wall region a sufficient resolution between discrete points are required to obtain a solution that is representative on the flow. At least 15 cells are required in the boundary layer region on a steady solution to achieve this. In accelerating and decelerating flows, more cells are required. Grids were generated with between 25 - 50 cells in the boundary layer. The first dimensionless cell node height is in the order of  $y^+ = 1$  (Ferziger and Peric [92]). Grids were designed according to these parameters.

$$y^+ = \frac{u^* y}{\nu} \approx 1 \quad (6.16)$$

The computational domains for the three cases (translating plate, rotating disk and translating, rotating cone) are described in *Figures 6.8, 6.9* and *6.10* below.

The grids have been designed and tested to ensure grid independence. Results from the grid independence study is shown in *Figures 6.11, 6.12* and *6.13*.

Figure 6.8: Computational Domain for Translating Plate Case

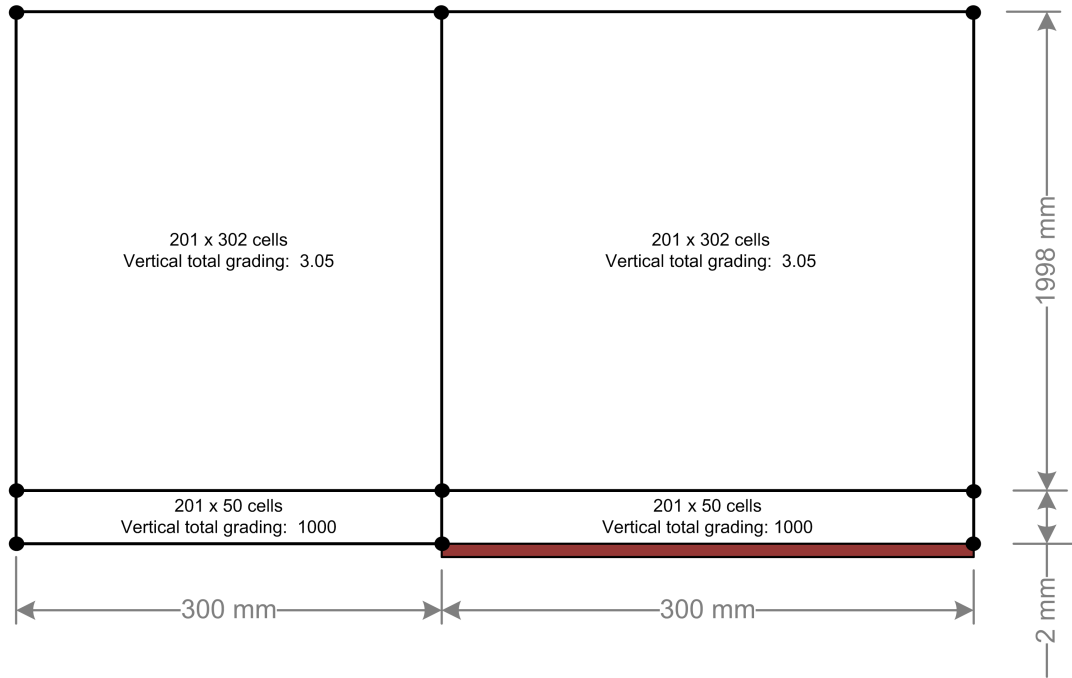
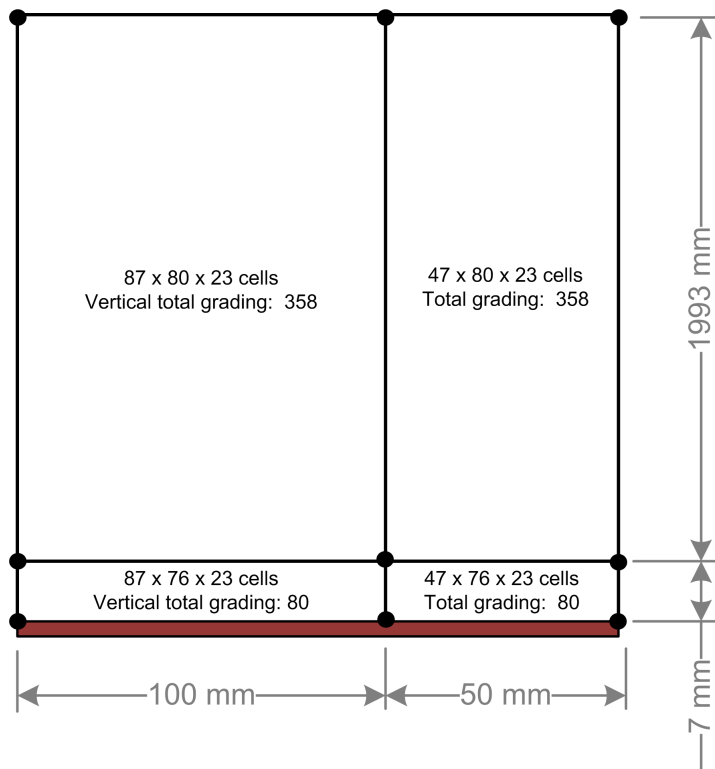


Figure 6.9: Computational Domain for Rotating Disk Case



CHAPTER 6. NON-INERTIAL SOLVER IMPLEMENTATION AND VALIDATION

Figure 6.10: Computational Domain for Translating, Rotating Cone Case

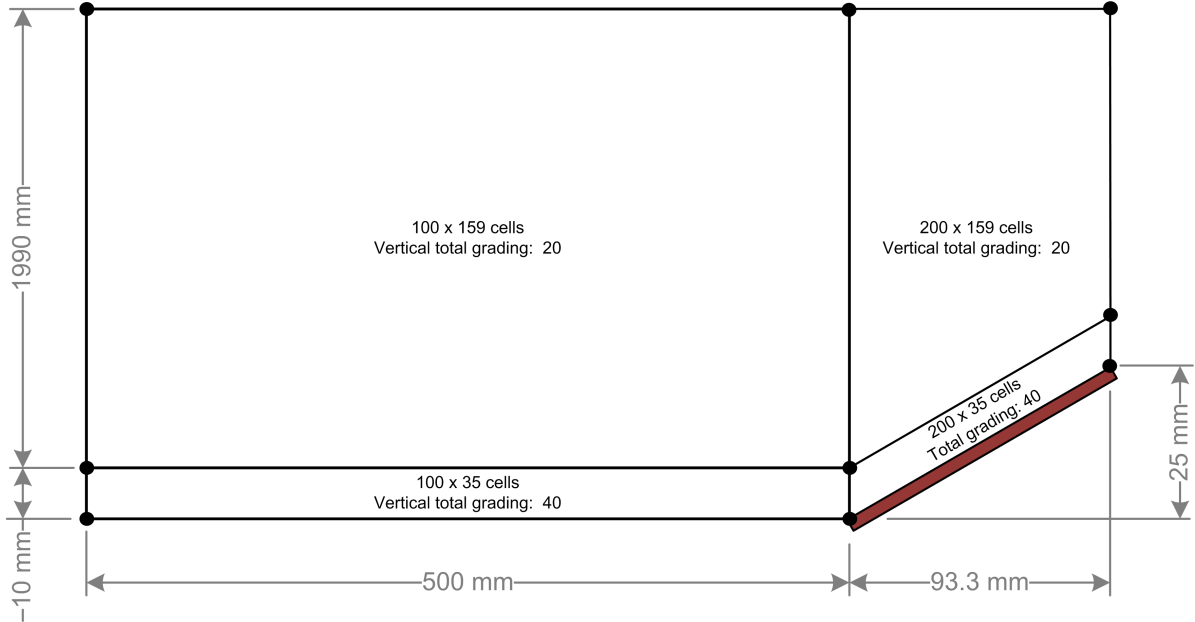


Figure 6.11: Grid independence of the laminar flat plate

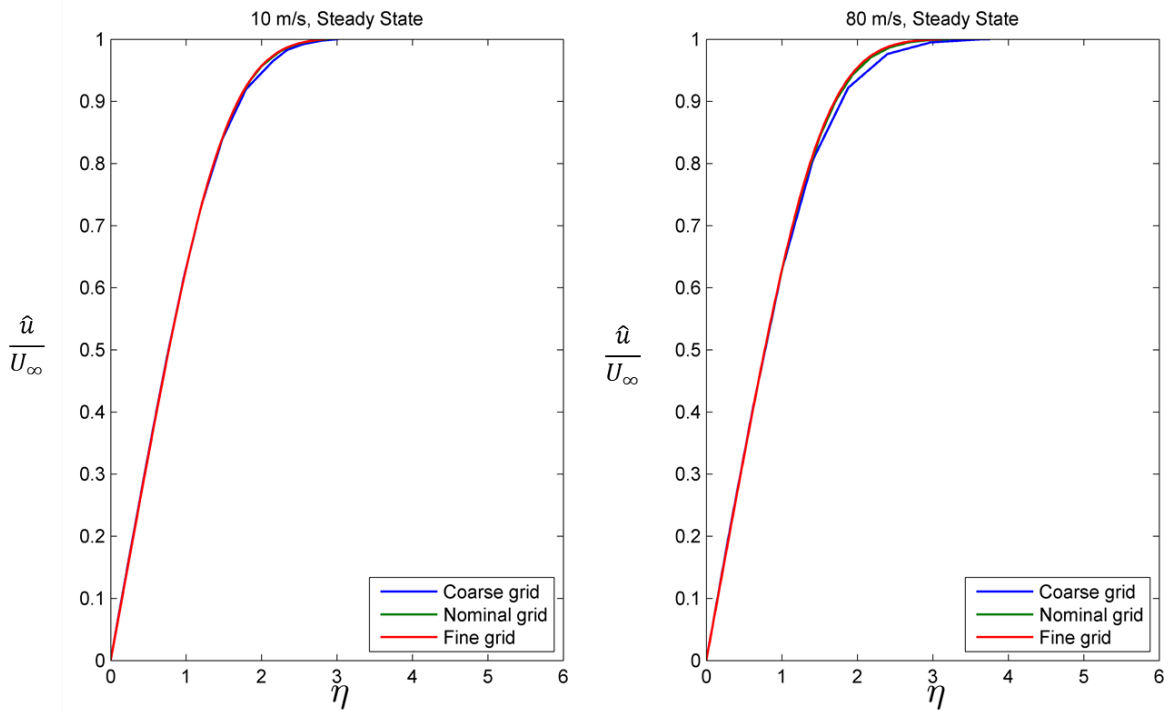


Figure 6.12: Grid independence of the laminar rotating disk

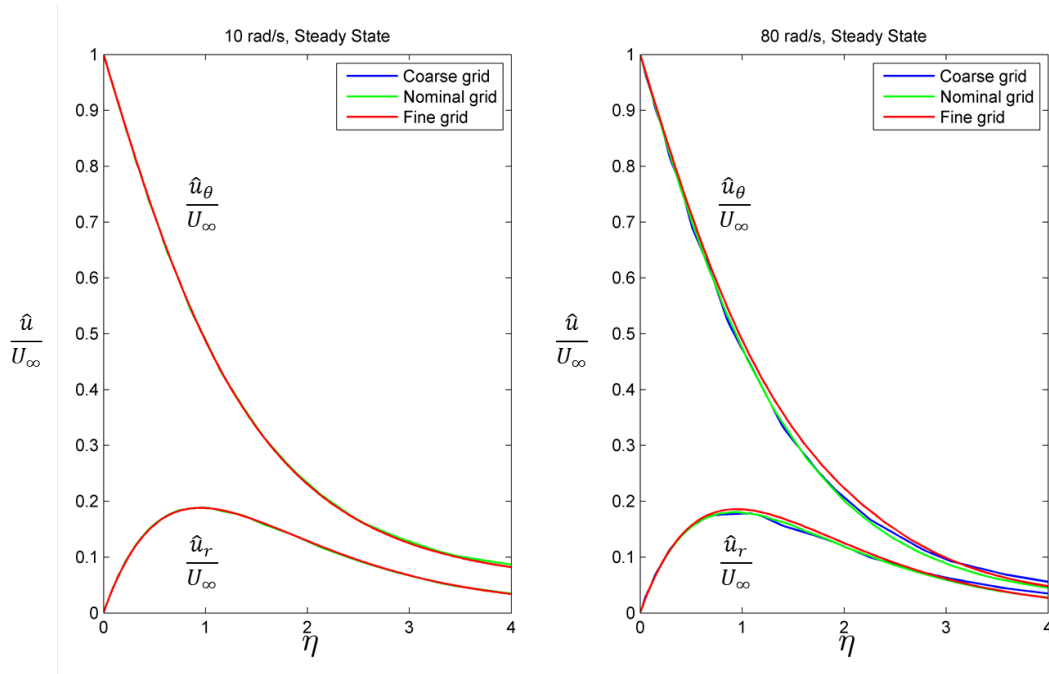
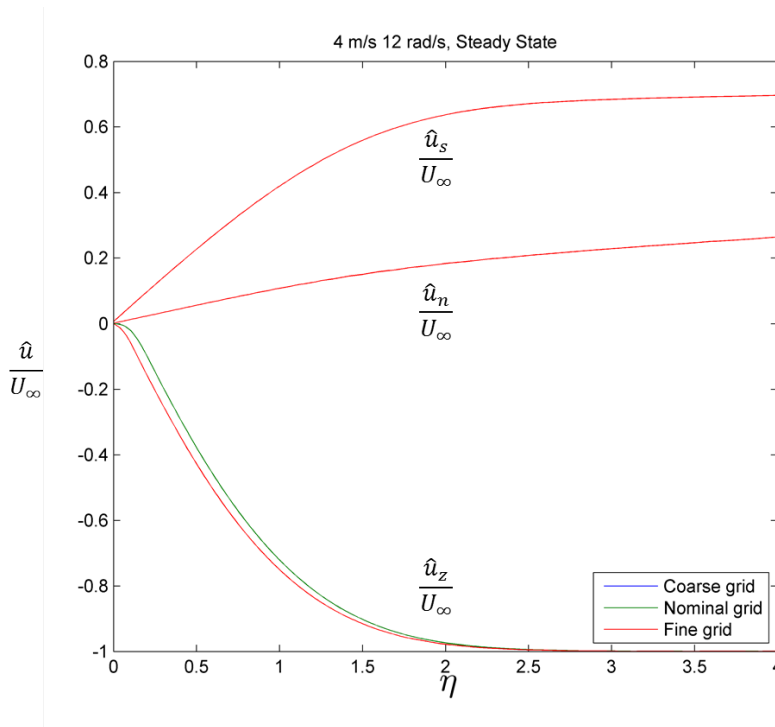


Figure 6.13: Grid independence of the translating, rotating cone

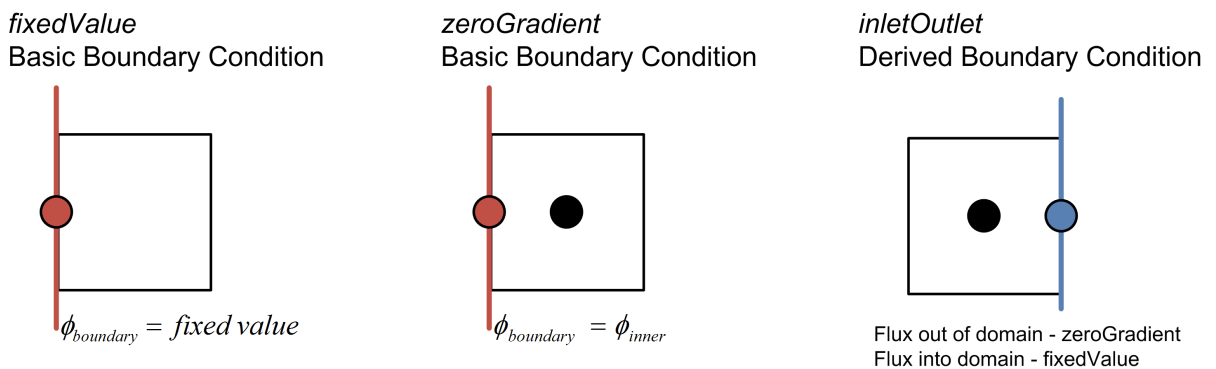


### 6.3.2 Boundary Conditions

OpenFOAM has vast libraries of boundary conditions that can be used. Boundary conditions can also be augmented from existing source codes or newly developed. Three classes of boundary conditions are defined: basic, derived and constraint conditions.

**Basic boundary conditions** are independent from any other utilities and all the mathematical equation to used this library is in its root source code. Examples of this is the *fixedValue* condition and the *zeroGradient* conditions as shown in *Figure 6.14*.

Figure 6.14: Boundary Condition Definition for *fixedValue*, *zeroGradient* and *inletOutlet*

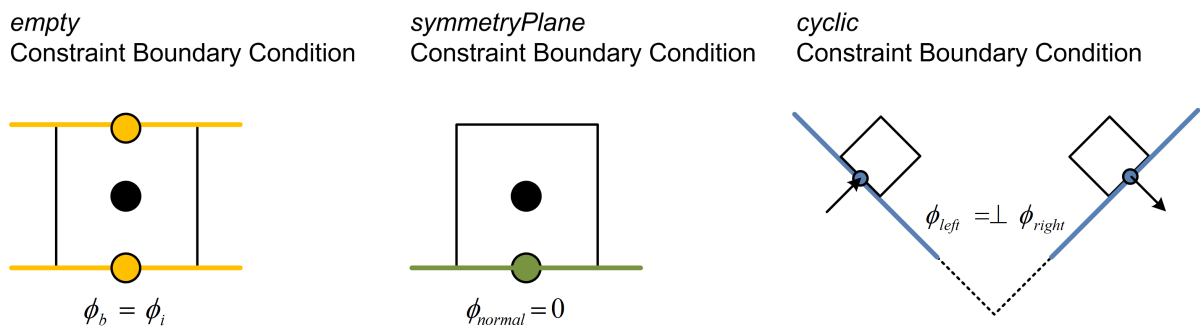


The *fixedValue* condition enforces a fixed value on the boundary, while the *zeroGradient* condition obtains the boundary value from the internal node.

**Derived boundary conditions** are dependent on either the basic boundary condition specification or on another external library. The *inletOutlet* condition is an example of an outlet derived boundary where a *fixedValue* condition is enforce on the boundary if the flux is into the computational domain and a *zeroGradient* condition when the flux is out of the domain.

**Constraint type boundary conditions** allows for reduction of dimensions or computational domain due to axis-symmetry, symmetry or two dimensionality (see examples in *Figure 6.15*.)

Figure 6.15: Boundary Condition Definition for *empty*, *symmetryPlane* and *cyclic*



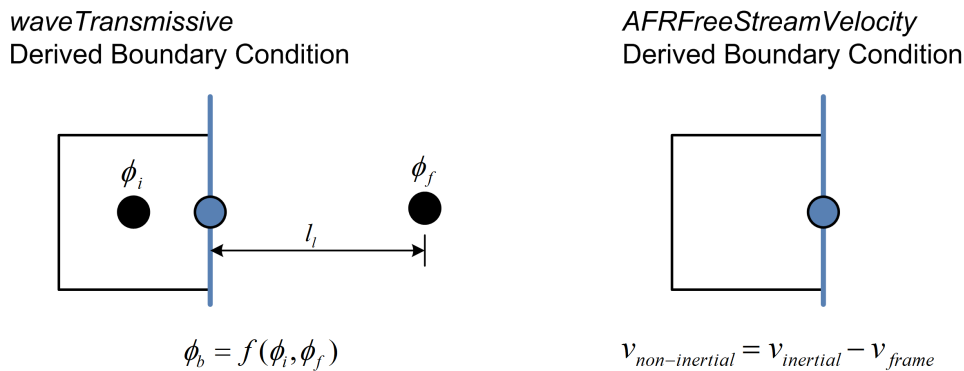
The *empty* condition allow for the reduction of dimensions where no solution is required on the empty patch pairs. A *symmetryPlane* condition is used at the mirror line of a symmetrical object to



reduce the size and extend of the computational domain. This condition sets all the normal components of vectors to zero. The *cyclic* condition requires that a pair of boundaries be identified and treats these patches as if it is physically connected. This allows for the reduction of the computational grid in axis-symmetrical cases.

Two special boundary conditions were also used as shown in *Figure 6.16*.

Figure 6.16: Boundary Condition Definition for *waveTransmissive* and *ARFFreeStreamVelocity*



The first is the *waveTransmissive* condition. This conditions allows for less stringent pressure conditions on the outlet boundary where the boundary value assigned is a function of the inner node and a far-field ghost node. Interpolation between the inner node and the ghost node is used to obtain the value for the boundary. The second is a boundary that was modified for the purposes of this work and is designated the *ARFFreeStreamVelocity* condition. In this condition the value of the velocity vector in the inertial frame is specified. The value for the non-inertial frame is calculated by subtracting the frame velocity vector from the specified inertial velocity vector. Specifying the far-field inertial velocity vector is simple since the flow in the inertial far-fields is stationary. In *Appendix C* the partial source code for this implementation is shown.

The boundary condition locations for the flat plate, rotating disk and cone are graphically represented in *Figures 6.17, 6.18 and 6.19*. *Tables 6.1, 6.3 and 6.5* indicate the velocity, pressure and temperature boundary conditions for each case respectively.

The flow conditions was select to ensure that the fluid remains well within the laminar regime. To this effect the Reynolds number for a flat plate in translation must be below 300 000 (Crowe et al. [94]) and a rotating disk below 500 (Imayama [43], Schmid and Henningson [44]). A rotating cone with a 15 degree half-angle separates at a Reynolds number of approximately 249.64 (Mansour and Kargar [57]). Axial flow delays the onset of transition, therefore if the rotational Reynolds numbers are kept below 250, the flow is laminar for low axial velocities (Garret and Peake [52] Kobayashi and Kohama [95]). *Tables 6.2, 6.4 and 6.6* show the Reynolds numbers of the separate cases.

Figure 6.17: Graphical Representation of Translating Plate Boundary Condition

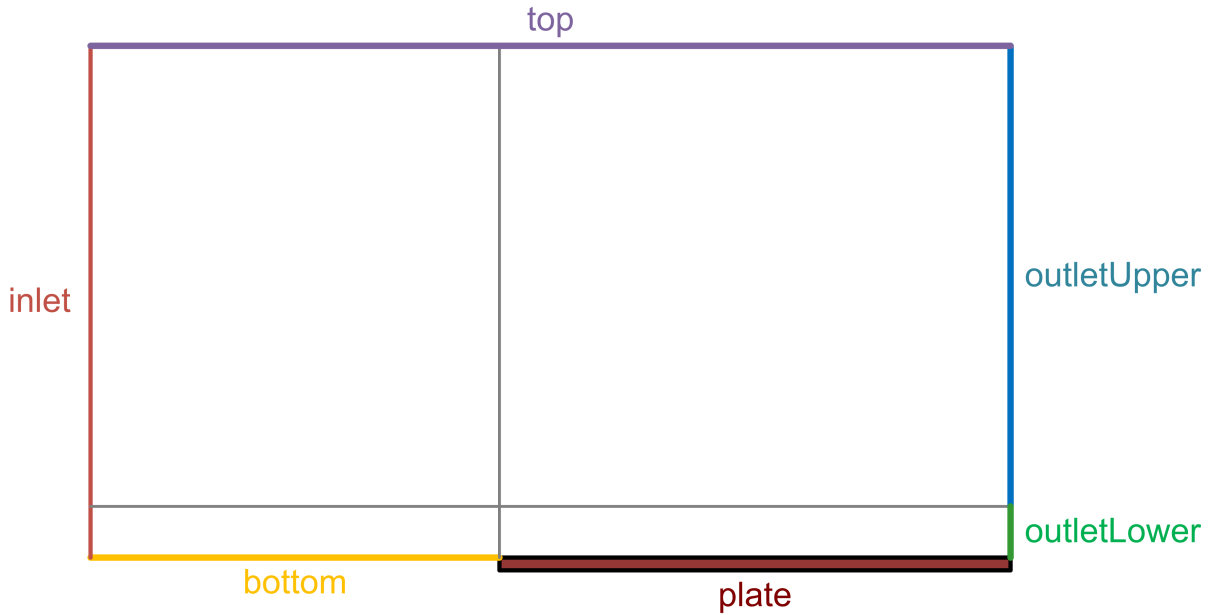


Table 6.1: Boundary Conditions of the Translating Plate

Boundary	Velocity	Pressure	Temperature
inlet	ARFFreeStreamVelocity	zeroGradient	fixedValue
bottom	symmetryPlane	symmetryPlane	symmetryPlane
plate	no-slip wall	zeroGradient	zeroGradient
outletLower	zeroGradient	zeroGradient	inletOutlet
outletUpper	ARFFreeStreamVelocity	zeroGradient	inletOutlet
top	ARFFreeStreamVelocity	zeroGradient	inletOutlet
front/back	empty	empty	empty

$$Re_x = \frac{\rho U x}{\mu} \quad (6.17)$$

Table 6.2: Minimum and Maximum Reynolds Numbers of the Translating Plate

Condition	$U[m/s]$	$Re_x$	$Re_{crit}$
min	10	35 100	300 000
max	80	280 800	300 000

Figure 6.18: Graphical Representation of Rotating Disk Boundary Condition

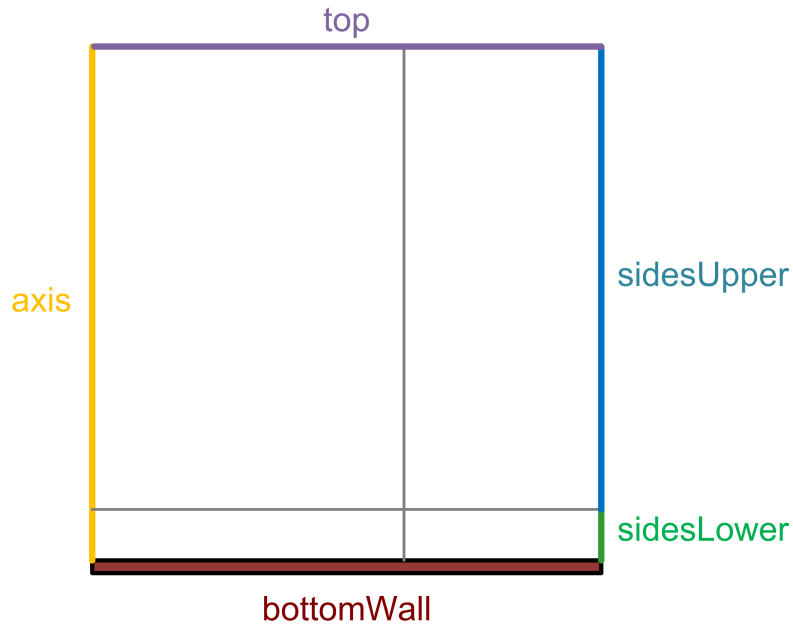


Table 6.3: Boundary Conditions of the Rotating Disk

Boundary	Velocity	Pressure	Temperature
axis	symmetryPlane	symmetryPlane	symmetryPlane
bottomWall	no-slip wall	zeroGradient	zeroGradient
sidesLower	zeroGradient	zeroGradient	inletOutlet
sidesUpper	ARFFreeStreamVelocity	zeroGradient	inletOutlet
top	ARFFreeStreamVelocity	zeroGradient	inletOutlet
front/back	cyclic	cyclic	cyclic

$$Re_r = r \sqrt{\frac{\omega}{\nu}} \quad (6.18)$$

Table 6.4: Minimum and Maximum Reynolds Numbers of the Rotating Disk

Condition	$\omega[rad/s]$	$Re_r$	$Re_{crit}$
min	10	150	500
max	80	424.2	500

Figure 6.19: Graphical Representation of Translating, Rotating Cone Boundary Condition

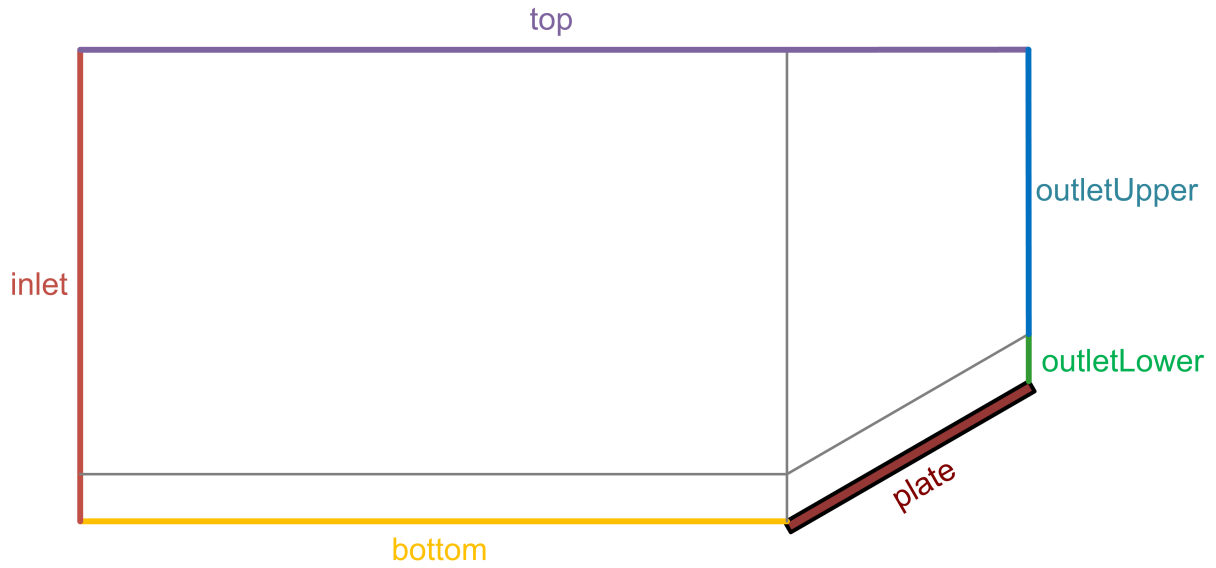


Table 6.5: Boundary Conditions of the Translating, Rotating Cone

Boundary	Velocity	Pressure	Temperature
inlet	ARFFreeStreamVelocity	waveTransmissive	inletOutlet
bottom	symmetryPlane	symmetryPlane	symmetryPlane
plate	no-slip wall	zeroGradient	zeroGradient
outletLower	zeroGradient	zeroGradient	inletOutlet
outletUpper	ARFFreeStreamVelocity	waveTransmissive	inletOutlet
top	ARFFreeStreamVelocity	waveTransmissive	inletOutlet
front/back	cyclic	cyclic	cyclic

$$Re_{4m/s} = \frac{\rho UL}{\mu} \quad (6.19)$$

$$Re_{12rad/s} = r \sqrt{\frac{\omega}{\nu}} \quad (6.20)$$

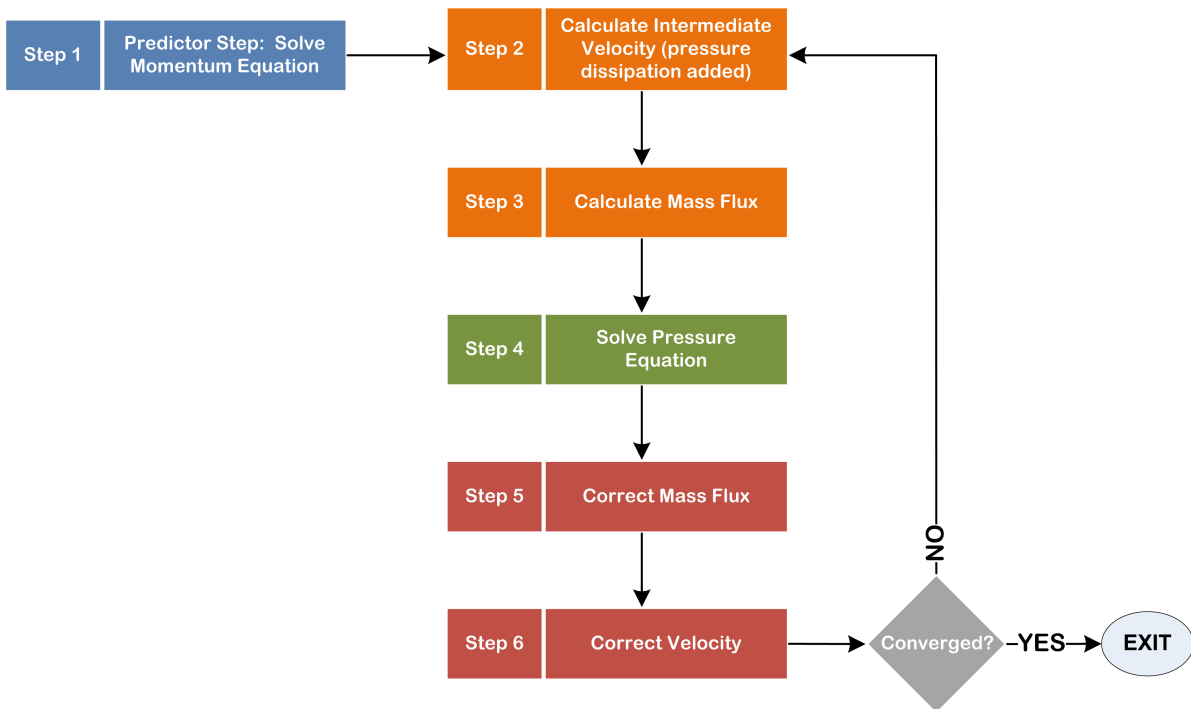
Table 6.6: Maximum Reynolds Numbers of the Translating, Rotating Cone

Condition	Value	$Re_x$	$Re_{crit}$
Plate	4m/s	4 520.412	300 000
Cone	12rad/s	9.37	249.63

### 6.3.3 Numerical Method

The solution algorithm that is used in the simulation is the Pressure Implicit Method with Splitting of operators, referred to as the PISO method. The algorithm is shown in *Figure 6.20*. The method consist of one predictor and two corrector steps for each local iteration and was used in its standard implementation in openFOAM.

Figure 6.20: Pressure Implicit with Splitting of Operator (PISO) Solution Algorithm



The openFOAM code allows for the separate discretization treatments of divergence, gradient and laplacian terms. This is selected in the *fvSchemes* file in the *system* folder of the case set-up.

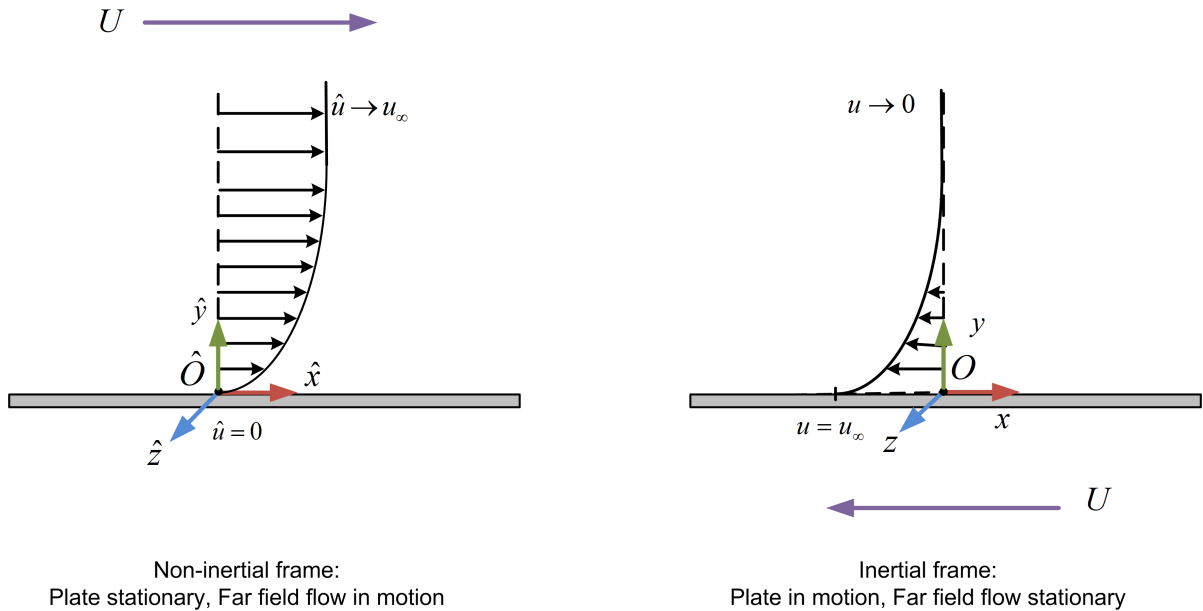
Time integration was done using the implicit Euler method (Ferziger and Peric [92], Versteeg and Malalasekera [69]). In the steady state solutions the Courant number was kept below 0.9 and in the accelerating and decelerating cases a constant time step was used since time accurate results were required. Discretization of the divergence terms were done using Gauss's theorem (Ferziger and Peric [92], Versteeg and Malalasekera [69]) with a total variate diminishing (TVD) scheme. The gradient and laplacian term terms were both discretised with Gauss's theorem and a central differencing scheme (Ferziger and Peric [92], Versteeg and Malalasekera [69]).

## 6.4 Validation Results

### 6.4.1 Laminar Flat Plate

The first validation case utilized to test the functionality of the developed solver was the laminar flat plate. The boundary layer on a flat plate is self-similar. It means that along the plate the shape of the velocity distribution differs in scale but the form of the profile remains the same. The profile shape is also similar between the non-inertial and inertial frames, with the exception of directionality. This is elaborated on in the next chapter. A graphical representation of the boundary layer in the non-inertial and inertial frames is shown in *Figure 6.21*.

Figure 6.21: Graphical Representation of the Boundary Layer on a Flat Plate



The laminar flat plate is a classic problem in Fluid Mechanics for which a similarity solution was developed by Blasius [37]. The boundary layer equations are simplified by introduction of a non-dimensional similarity variable  $\eta$ ,

$$\eta = \frac{1}{2} \frac{y}{x} \sqrt{Re_x} \quad (6.21)$$

that reduces the partial differential boundary layer equation to a non-dimensional ordinary differential equation.

$$2f''' + f''f = 0 \quad (6.22)$$

The first derivative of the non-dimensional function  $f(\eta)$ , become the non-dimensional velocity:

$$f'(\eta) = \frac{U}{U_\infty} \quad (6.23)$$

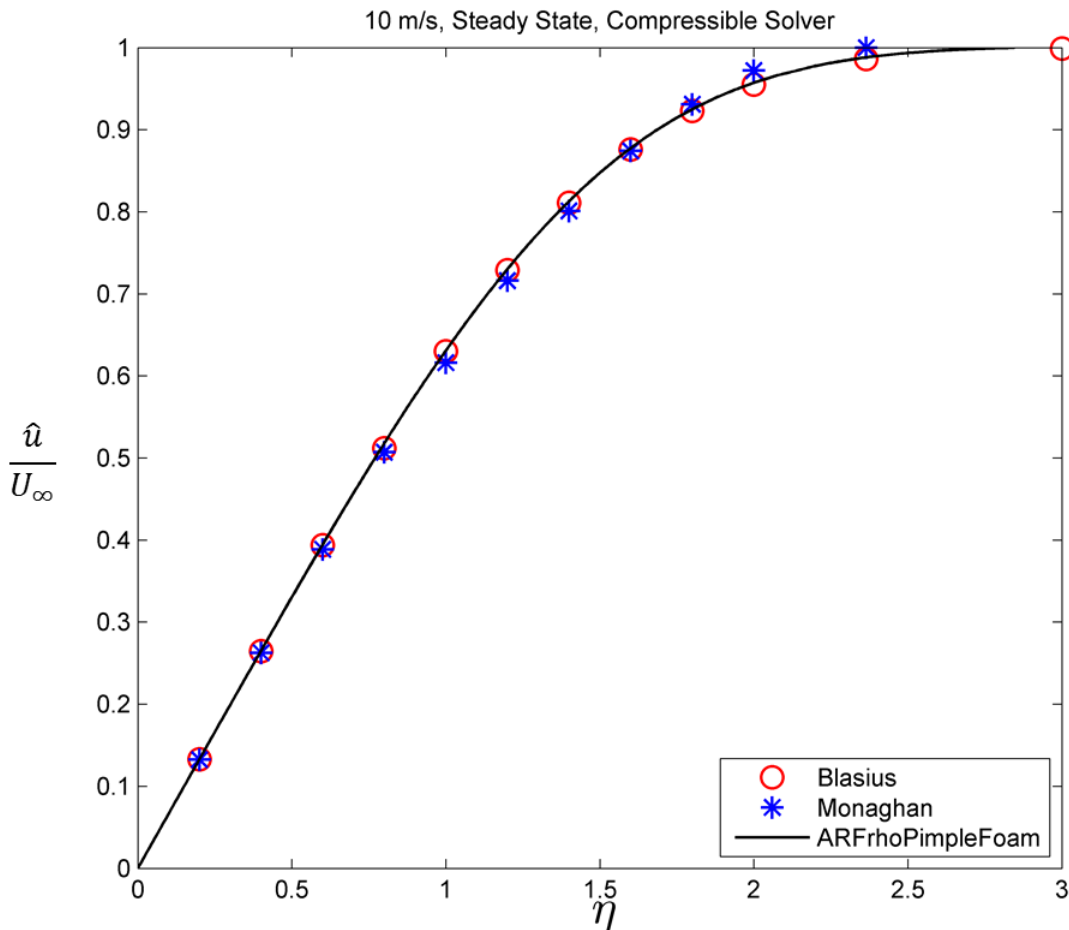
The algebraic equation can numerical be solved with an integration routine, such as the Runge Kutta method, using the initial values below.

$$\begin{aligned}
 f(0) &= 0 \\
 f'(0) &= 0 \\
 f'(\infty) &\approx 1
 \end{aligned}
 \tag{6.24}$$

In a similar manner used to determine the Blasius solution to an incompressible, laminar flat plate, Monaghan [87] derived a solution for laminar compressible boundary layer.

Numerical simulations for steady state conditions were conducted for free stream velocities of 10 m/s, 45 m/s and 80 m/s. The simulation results were compared against the solutions of Blasius [37] and Monaghan [87]. The results of the comparisons obtained are depicted in *Figures 6.22, 6.23 and 6.24*.

Figure 6.22: Steady State Solution for a Laminar Flat Plate at 10 m/s



CHAPTER 6. NON-INERTIAL SOLVER IMPLEMENTATION AND VALIDATION

Figure 6.23: Steady State Solution for a Laminar Flat Plate at 45 m/s

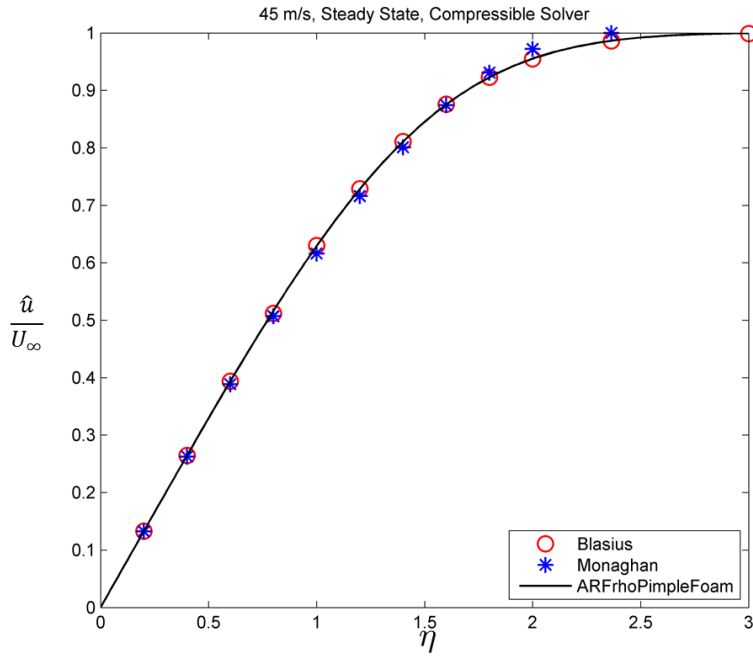
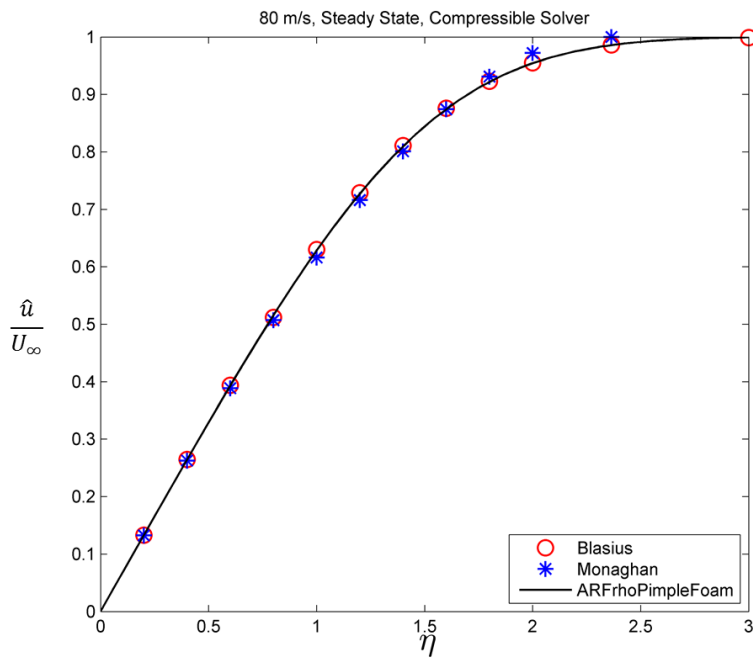


Figure 6.24: Steady State Solution for a Laminar Flat Plate at 80 m/s





The simulated results compares well with the analytical results of the Blasius [37] and Monaghan [87] solutions. The results from this test case are be used in the next chapter as steady state starting conditions. The flow is accelerated or decelerated from these initial conditions.

The boundary layer characteristic profiles,

$$\begin{aligned} & \frac{\hat{u}}{U_\infty} \\ & 1 - \frac{\hat{u}}{U_\infty} \\ & \frac{\hat{u}}{U_\infty} \left(1 - \frac{\hat{u}}{U_\infty}\right) \end{aligned} \tag{6.25}$$

are compared to the analytical results in *Figures 6.25, 6.26 and 6.27*. The numerical results compare well with the analytical results.

In *Table 6.7* the boundary layer parameters are compared with the analytical results. The differences between the numerical and analytical results are within acceptable parameters as determined by:

$$Difference\% = \frac{Result_{Analytical} - Result_{Numerical}}{Result_{Analytical}} * 100 \tag{6.26}$$

Figure 6.25: Comparison of Boundary Layer Parameters at 10 m/s

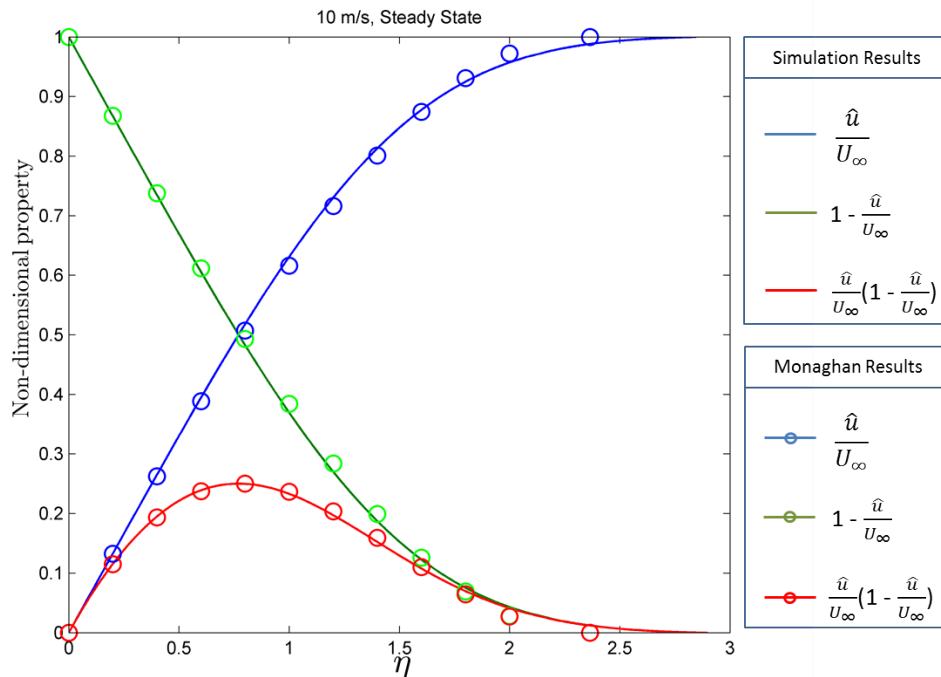


Figure 6.26: Comparison of Boundary Layer Parameters at 45 m/s

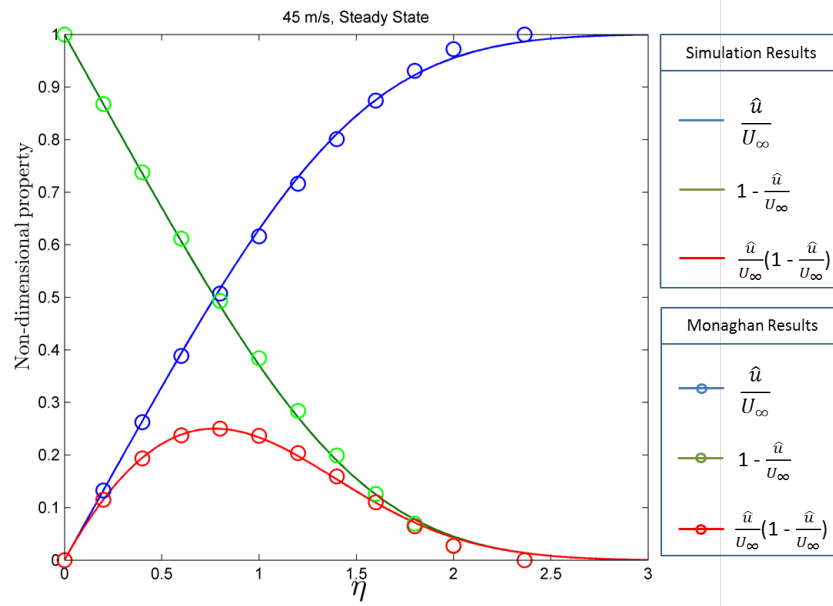


Figure 6.27: Comparison of Boundary Layer Parameters at 80 m/s

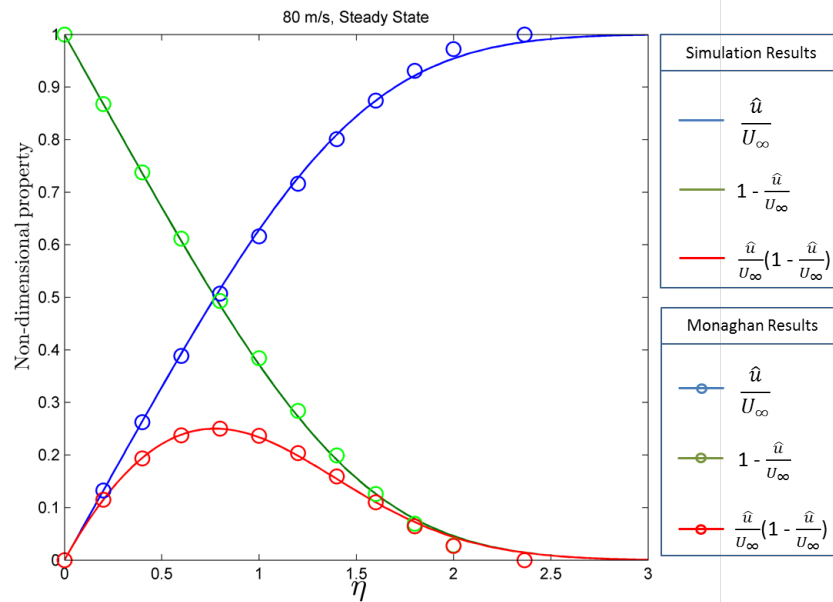


Table 6.7: Boundary Layer Properties of the Translating Plate 0.2 m

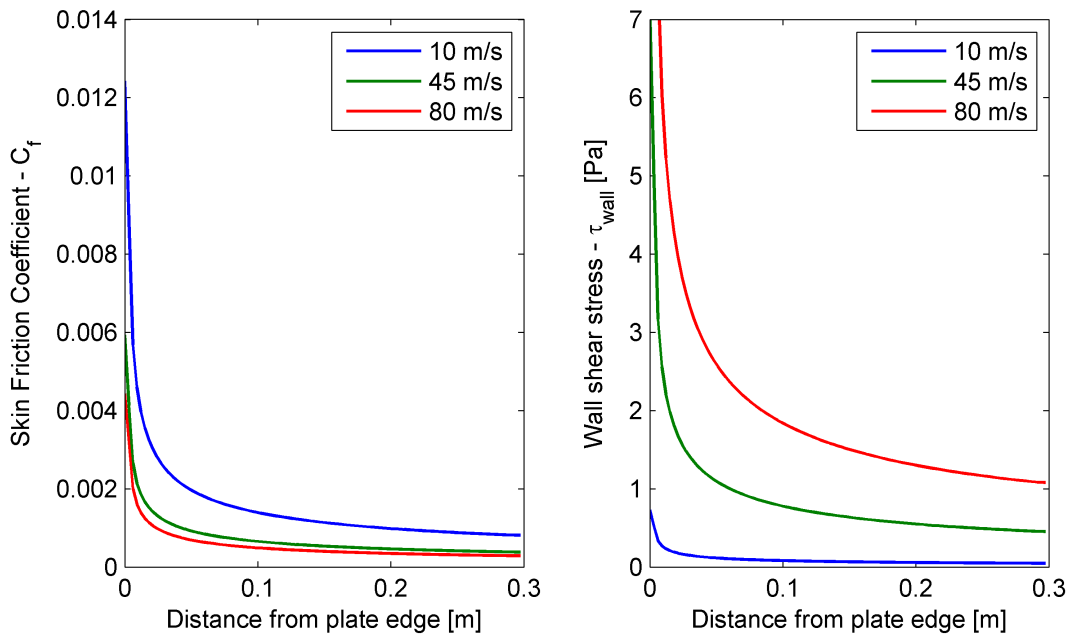
		$\delta$ [m]	$\delta^*$ [m]	$\theta$ [m]	H
10 m/s	Analytical	$2.2054e^{-3}$	$0.8040e^{-3}$	$0.2999e^{-3}$	2.68
	Numerical	$2.6526e^{-3}$	$0.7941e^{-3}$	$0.3025e^{-3}$	2.62
	Difference %	-16.86	-1.22	0.85	-2.06
45 m/s	Analytical	$1.0396e^{-3}$	$0.3790e^{-3}$	$0.1414e^{-3}$	2.68
	Numerical	$1.3363e^{-3}$	$0.3749e^{-3}$	$0.1423e^{-3}$	2.63
	Difference %	-22.20	-1.10	0.64	-1.73
80 m/s	Analytical	$0.7797e^{-3}$	$0.2843e^{-3}$	$0.1060e^{-3}$	2.68
	Numerical	$1.0260e^{-3}$	$0.2816e^{-3}$	$0.1069e^{-3}$	2.63
	Difference %	-24.01	-0.93	0.79	-1.71

The wall shear stress is calculated during the numerical simulations. This is used to determine the skin friction coefficient. The skin friction coefficient is directly proportional to the skin friction drag on the translating plate. This is used to determine the effect of unsteady motion on the skin friction drag. The skin friction coefficient and wall shear stress for steady state conditions are shown in *Figure 6.28*.

$$\tau_{wall} = \mu \frac{\partial u}{\partial y}$$

$$C_f = \frac{\tau_{wall}}{0.5\rho U_{\infty}^2} \tag{6.27}$$

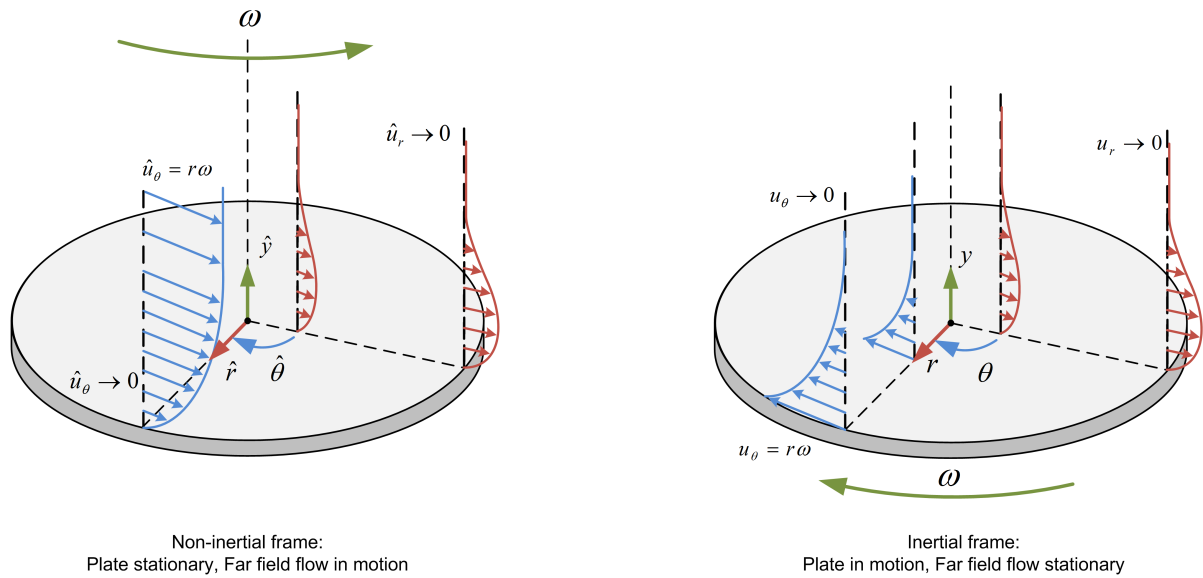
Figure 6.28: Skin Friction Coefficients and Wall Shear Stress



## 6.4.2 Laminar Rotating Disk

The second validation case concerns the boundary layer on a rotating disk. In *Figure 6.29* a graphical representation of the boundary layer on the rotating disk is shown for the radial and tangential directions.

Figure 6.29: Graphical Representation of the Boundary Layer on a Rotating Disk



In von Karman [41] a similarity solution is derived for the boundary layer on a rotating disk. This solution is discussed in detail by Schlichting [42]. A solution is obtained by introducing a similarity variable,  $\eta$ , to the boundary layer equations (in cylindrical coordinates).

$$\eta = y \sqrt{\frac{\omega y}{\nu}} \quad (6.28)$$

In the above equation  $y$  is the height normal to the wall,  $\omega_y$  is the rotational velocity (in rad/s) about the  $y$ -axis and  $\nu$  is the kinematic viscosity. Using this equation the partial differential equations (PDE) is reduced to a set of ordinary differential equations (ODE), as shown by Schlichting [42]. This is solved numerically to obtain the velocity profiles.

Simulations were conducted for rotational velocities of 10 rad/s, 45 rad/s and 80 rad/s to obtain the steady state solution in the non-inertial frame (*Figures 6.30* and *6.32*). This solution was transformed to the inertial frame in order to compare it with the analytical result (Schlichting [42], von Karman [41]) presented in *Figures 6.31* and *6.33*.

Figure 6.30: Non-Inertial Tangential Velocity Profiles

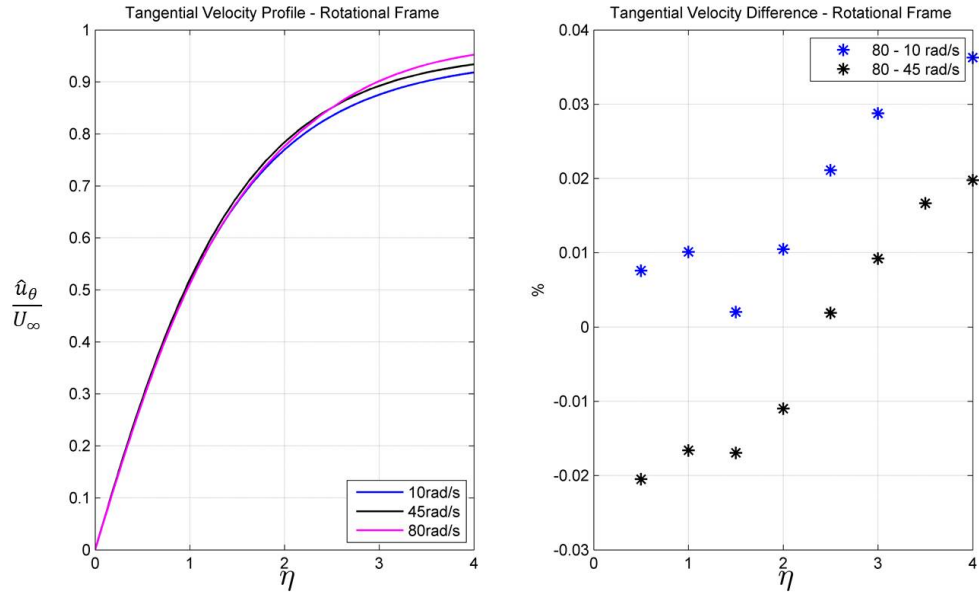
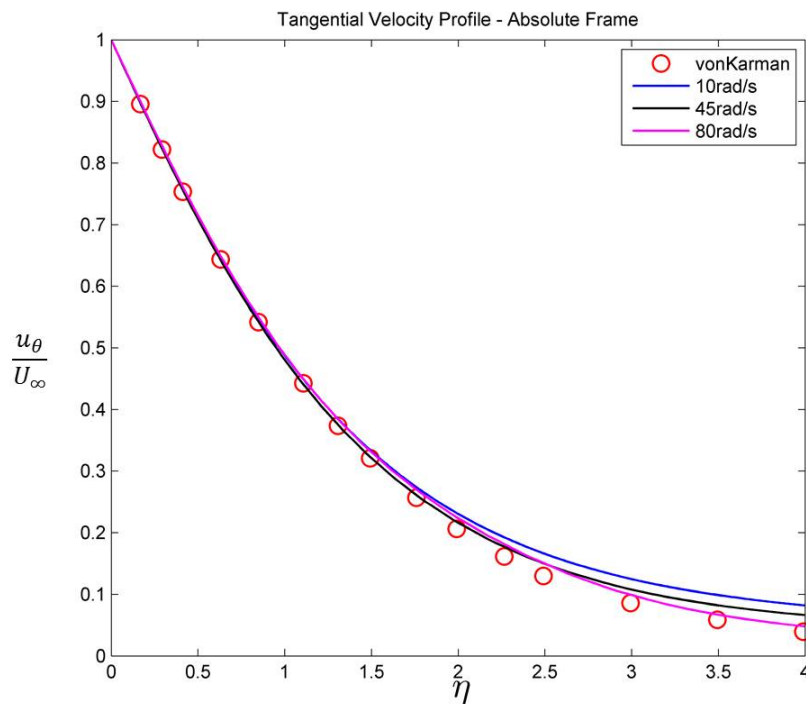


Figure 6.31: Comparison between Numerical and Analytical Tangential Velocity Results



CHAPTER 6. NON-INERTIAL SOLVER IMPLEMENTATION AND VALIDATION

Figure 6.32: Non-Inertial Radial Velocity Profiles

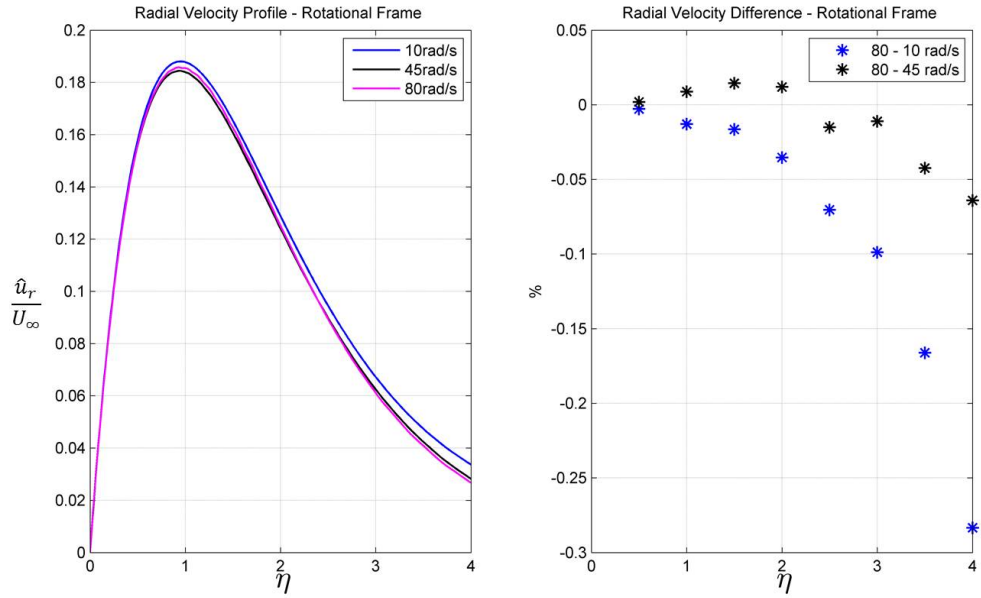
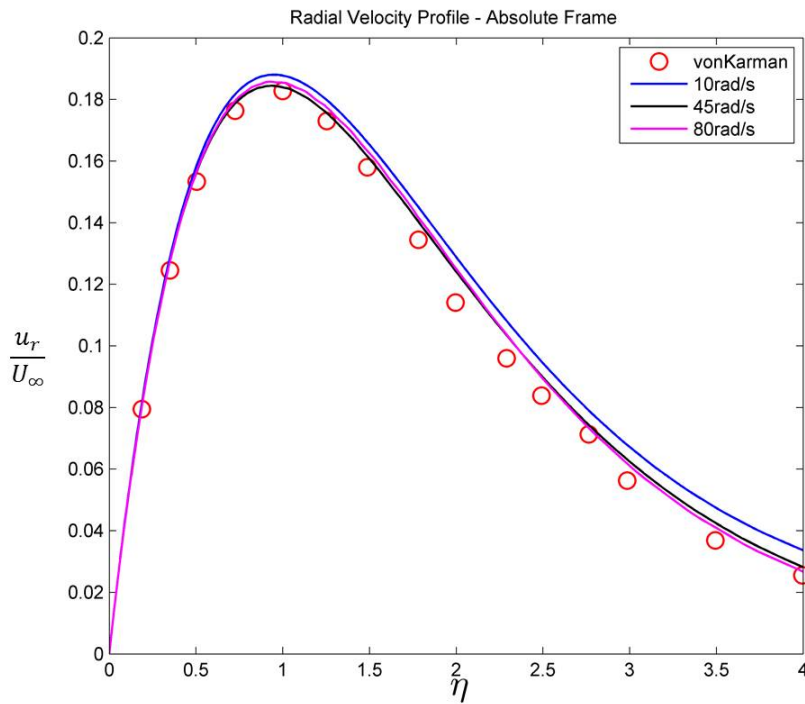


Figure 6.33: Comparison between Numerical and Analytical Radial Velocity Results



The tangential non-dimensional velocity profile is consistent with the analytical result near the wall region. Slight differences are observed in the far-field of the boundary layer. The non-dimensional value is slightly higher than the analytical value. This difference is increased with decreasing rotational velocity.

Similar behaviour is observed for in the radial direction. The radial non-dimensional velocity profile is overall consistent with the profile of the analytical result. The apex of the simulated curves are in the same order as the analytical apex. However, the simulated results are slightly higher than the analytical result.

The von Karman equations do not account for instabilities in the flow. The differences between the numerical and analytical results are due to the formation of laminar instabilities. Instabilities associated with rotating disks are mostly of Type I and Type II (Chefranov [96], Zoueshtiagh et al. [48]). Type I instabilities occur due to inviscid cross flow interactions. An example of Type I is the spiral vortices occurring above a Reynold number of 500. These vortices facilitates flow transition. Type II is instabilities that occur due to interaction between the Coriolis and viscous forces in the boundary layer. The differences observed here are due to cyclonic vortices at the centre of rotation. Moulin and Flór [47] investigated the sudden start of rotating disks. They experimentally observed the growth of the cyclonic vortices due to Ekman suction. It was noted that the growth rate of the vortices diminishes over time for steady state spin up conditions. This indicates that the cyclonic vortices are stationary in steady state conditions. This instability is classified as Type I since it operates in the inviscid region of the flow.

An increase in rotational velocity, adds to the momentum in the inviscid regions of the flow. The effect of the cyclonic vortice on the boundary layer are reduced since the increased momentum dominates the formation of cyclonic vortices. Therefore, with increasing rotational velocity, the cyclonic vortices decrease and the numerical solution approximates the von Karman solution.

The boundary characteristic properties in the radial and tangential directions were determined for the numerical and analytical results.

$$\begin{aligned} & \frac{\hat{u}_\theta}{U_\infty} \\ & 1 - \frac{\hat{u}_\theta}{U_\infty} \\ & \frac{\hat{u}_\theta}{U_\infty} \left(1 - \frac{\hat{u}_\theta}{U_\infty}\right) \end{aligned} \quad (6.29)$$

$$\begin{aligned} & \frac{\hat{u}_r}{U_\infty} \\ & 1 - \frac{\hat{u}_r}{U_\infty} \\ & \frac{\hat{u}_r}{U_\infty} \left(1 - \frac{\hat{u}_r}{U_\infty}\right) \end{aligned} \quad (6.30)$$

The comparison of the boundary layer properties are shown in *Tables 6.8* and *6.9* for the tangential and radial direction respectively.

Table 6.8: Tangential Boundary Layer Properties of the Rotating Disk at 0.14 m radius

		$\delta_\theta$ [m]	$\delta_\theta^*$ [m]	$\theta_\theta$ [m]	$H_\theta$
10 rad/s	Analytical	$6.0e^{-3}$	$1.283e^{-3}$	$6.0102e^{-4}$	2.13
	Numerical	$6.2e^{-3}$	$1.475e^{-3}$	$7.5953e^{-4}$	1.94
	Difference %	3	15.01	26.37	-8.98
45 rad/s	Analytical	$2.8e^{-3}$	$6.0482e^{-4}$	$2.8332e^{-4}$	2.13
	Numerical	$2.83e^{-3}$	$6.5632e^{-4}$	$3.2964e^{-4}$	1.99
	Difference %	1.14	8.51	16.34	-6.73
80 rad/s	Analytical	$2.1e^{-3}$	$4.5362e^{-4}$	$2.1249e^{-4}$	2.13
	Numerical	$2.12e^{-3}$	$4.7743e^{-4}$	$2.2977e^{-4}$	2.07
	Difference %	1.05	5.25	8.13	-2.66

Table 6.9: Radial Boundary Layer Properties of the Rotating Disk at 0.14 m radius

		$\delta_r$ [m]	$\delta_r^*$ [m]	$\theta_r$ [m]	$H_r$
10 rad/s	Analytical	$6.0e^{-3}$	$5.5865e^{-3}$	$3.6386e^{-4}$	15.35
	Numerical	$6.2e^{-3}$	$5.7001e^{-3}$	$4.2472e^{-4}$	13.42
	Difference %	3	2.03	16.72	-12.58
45 rad/s	Analytical	$2.8e^{-3}$	$2.6335e^{-3}$	$1.7152e^{-4}$	15.35
	Numerical	$2.83e^{-3}$	$2.6184e^{-3}$	$1.8724e^{-4}$	13.98
	Difference %	1.14	-0.57	9.16	-8.91
80 rad/s	Analytical	$2.1e^{-3}$	$1.9751e^{-3}$	$1.2864e^{-4}$	15.35
	Numerical	$2.12e^{-3}$	$1.9619e^{-3}$	$1.3964e^{-4}$	14.04
	Difference %	1.05	-0.66	8.55	-8.49

Comparisons are graphically represented for 10 rad/s, 45 rad/s and 80 rad/s in *Figures 6.34-6.39*. The effect of the cyclonic vortices on the boundary layer can be observed in the graphs. In the near wall regions deviation from the von Karman results are small. The regions near the free-stream flow deviated from the analytical result. The deviation is indirectly proportional to rotational velocity.



Figure 6.34: Comparison of Tangential Boundary Layer Characteristic Profiles for 10 rad/s

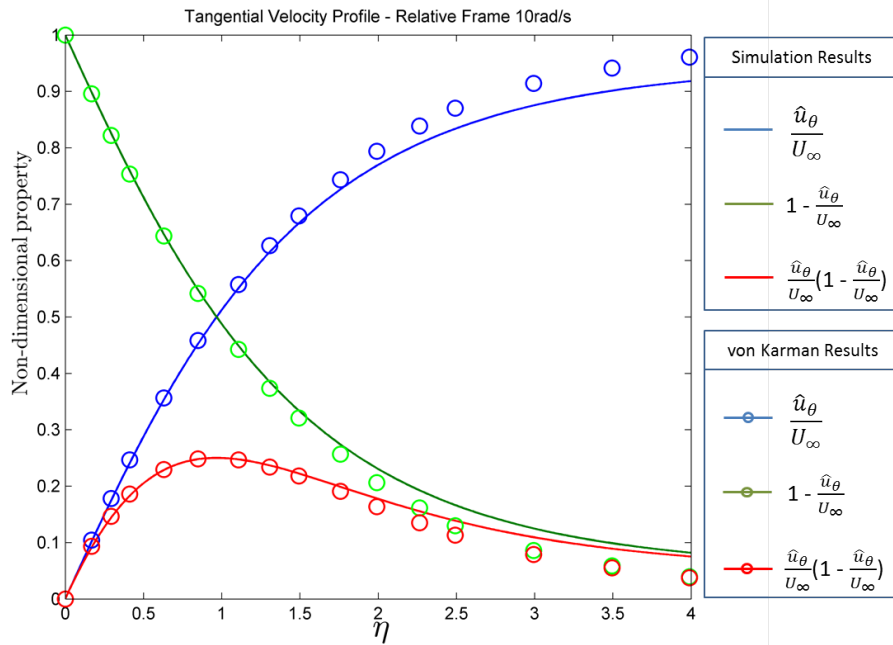
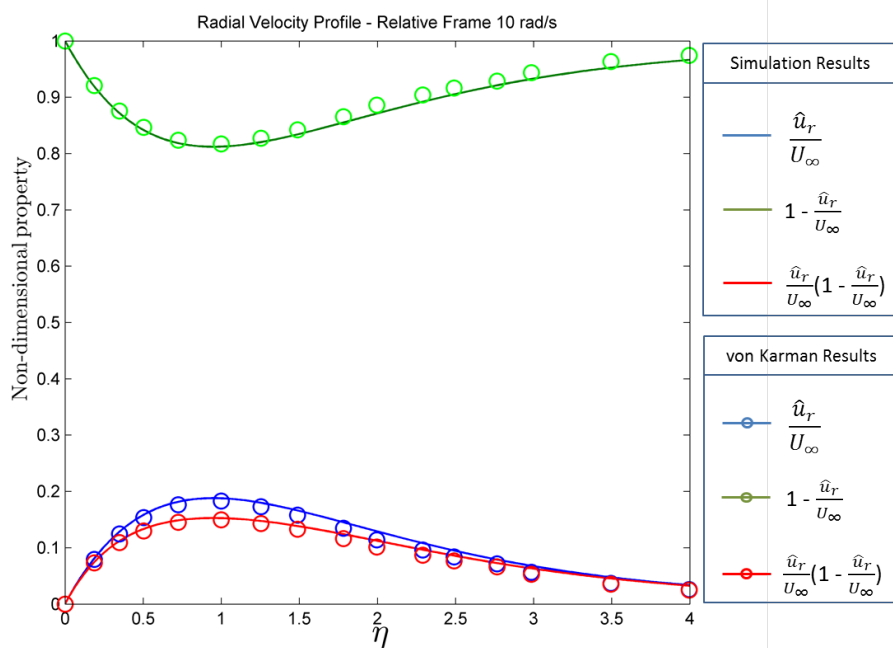


Figure 6.35: Comparison of Radial Boundary Layer Characteristic Profiles for 10 rad/s



CHAPTER 6. NON-INERTIAL SOLVER IMPLEMENTATION AND VALIDATION

Figure 6.36: Comparison of Tangential Boundary Layer Characteristic Profiles for 45 rad/s

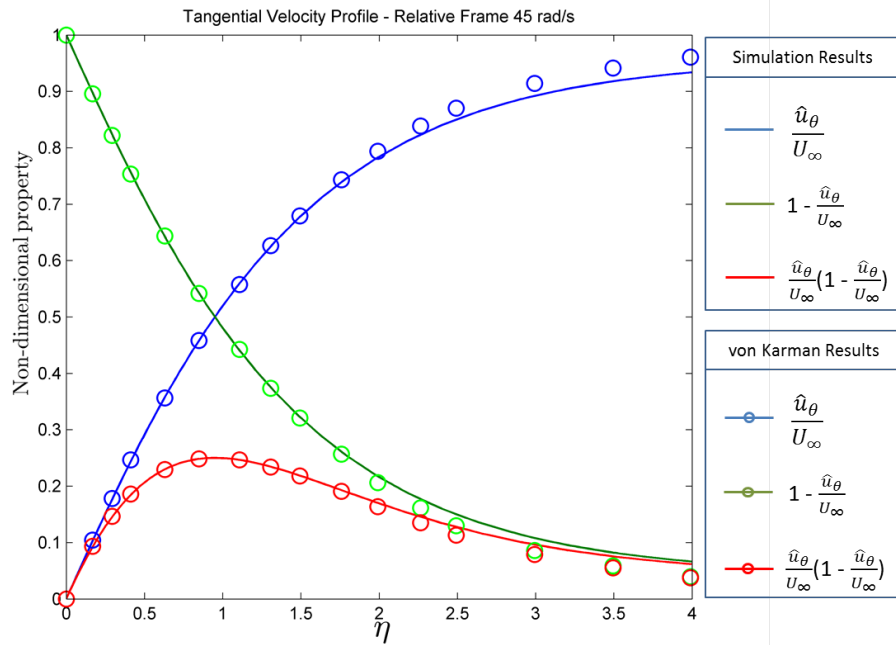


Figure 6.37: Comparison of Radial Boundary Layer Characteristic Profiles for 45 rad/s

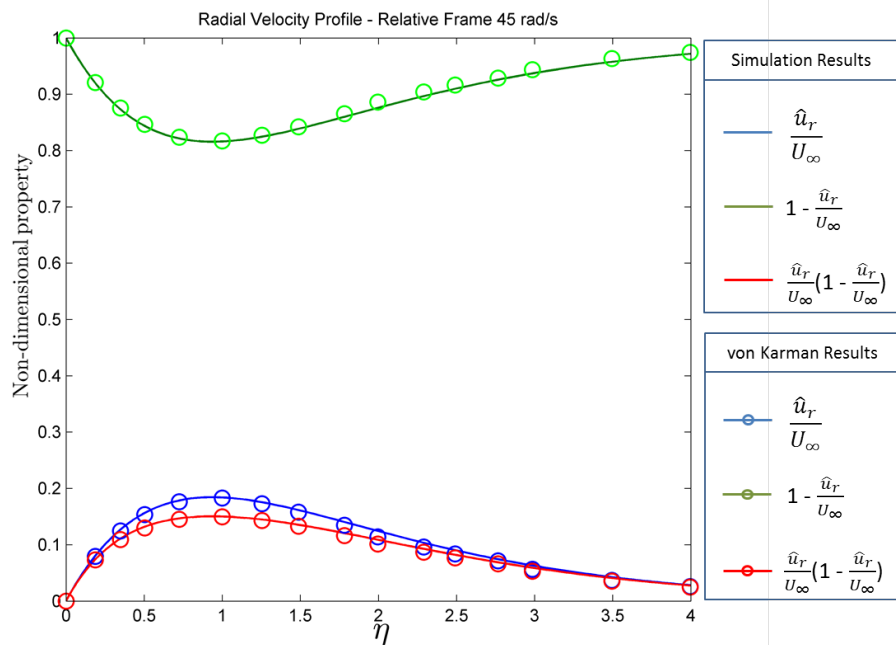


Figure 6.38: Comparison of Tangential Boundary Layer Characteristic Profiles for 80 rad/s

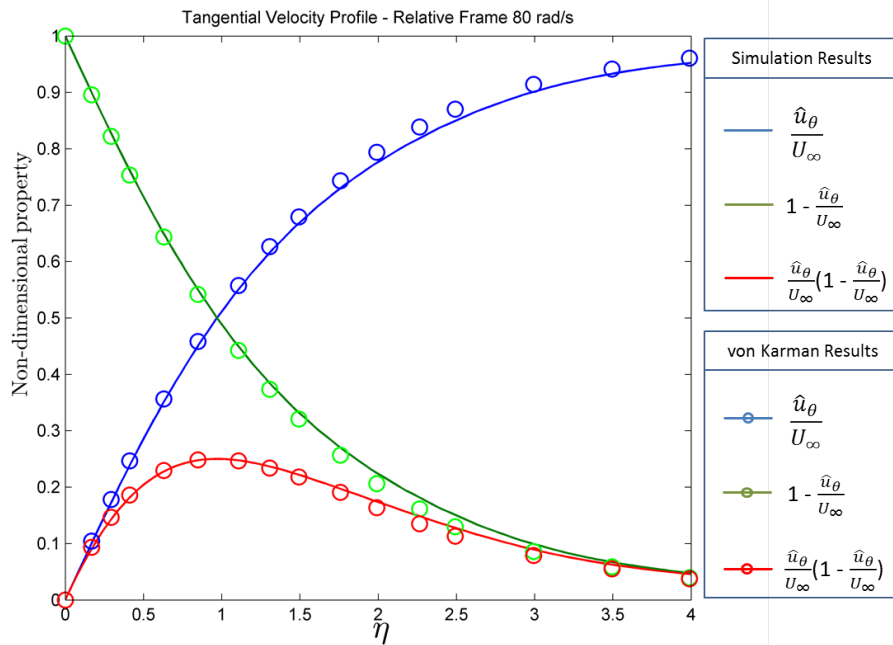
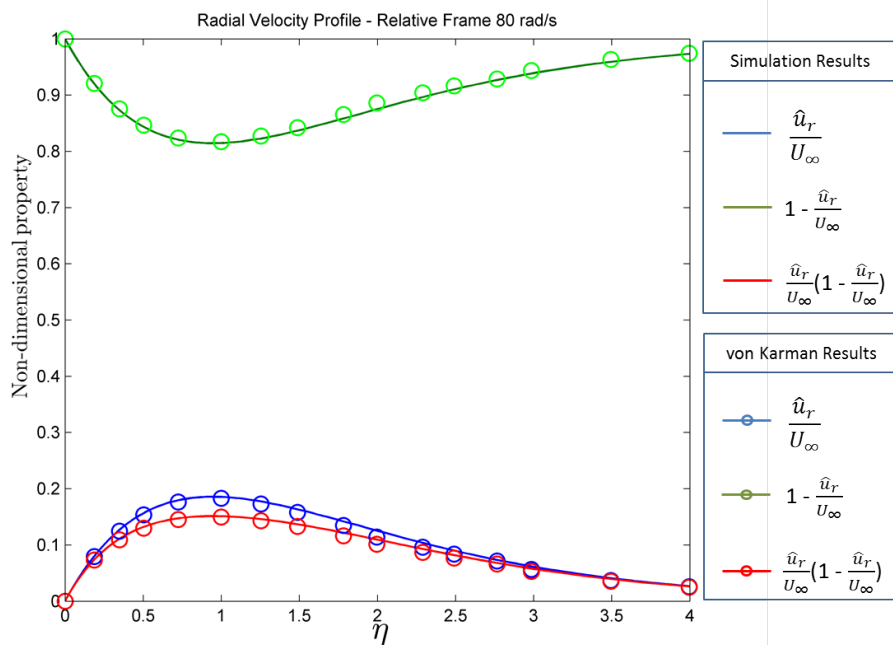


Figure 6.39: Comparison of Radial Boundary Layer Characteristic Profiles for 80 rad/s

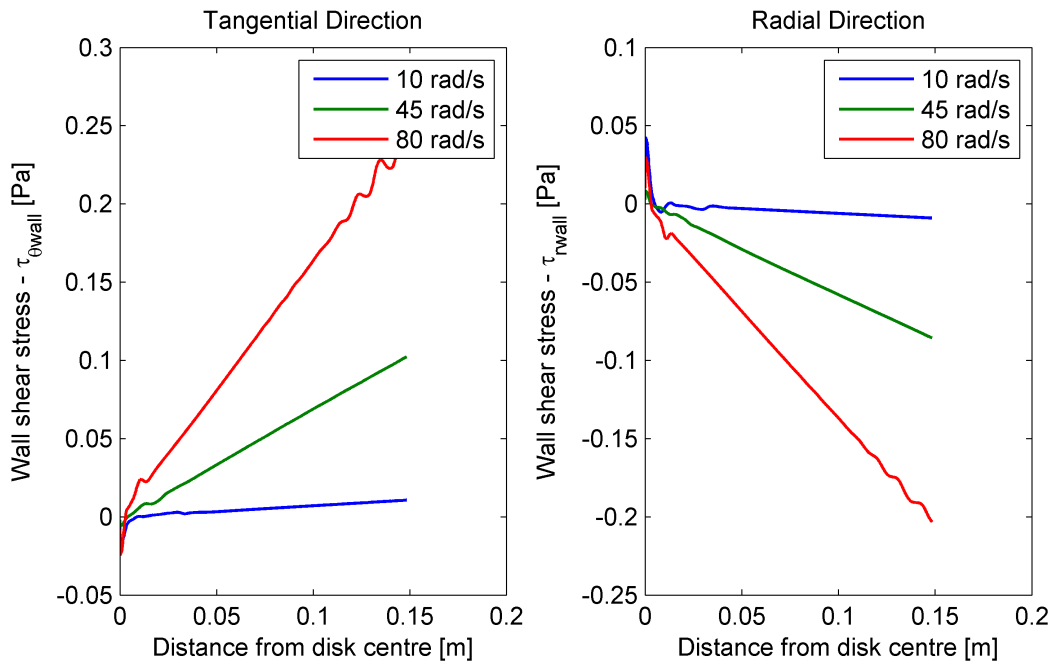


CHAPTER 6. NON-INERTIAL SOLVER IMPLEMENTATION AND VALIDATION

The wall shear stress was calculated in the tangential and radial directions. This was used to determine the total skin friction on the rotating plate. The effect of acceleration and deceleration on skin friction coefficient, and subsequently the skin friction drag, is determined in *Chapter 8*.

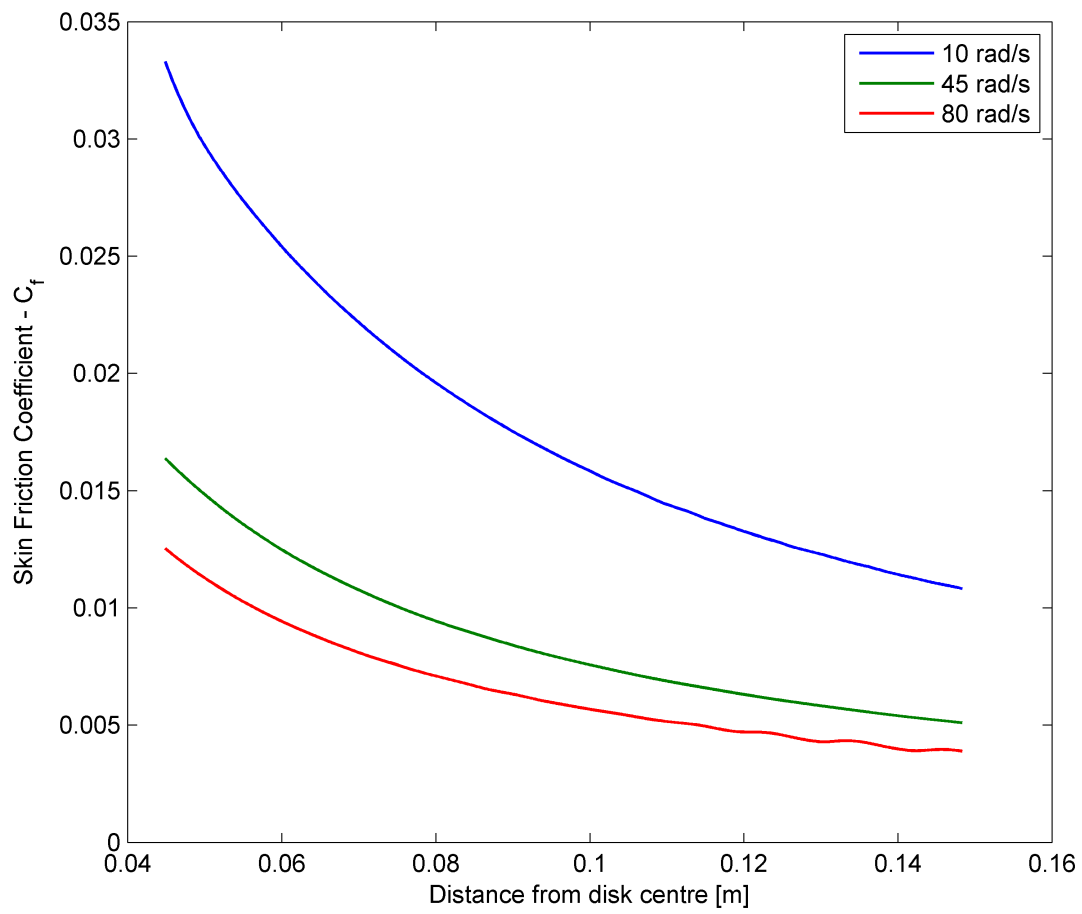
$$\begin{aligned}\tau_{\theta_{wall}} &= \mu \frac{\partial u_{\theta}}{\partial y} \\ \tau_{r_{wall}} &= \mu \frac{\partial u_r}{\partial y} \\ \tau_{wall} &= \sqrt{\tau_{\theta_{wall}}^2 + \tau_{r_{wall}}^2} \\ C_f &= \frac{\tau_{wall}}{0.5\rho U_{\infty}^2}\end{aligned}\tag{6.31}$$

Figure 6.40: Wall Shear Stress in the Tangential (left) and Radial (right) Directions



Overall the simulated results compares well with the analytical results and can be used in *Chapter 8* as initial conditions for subsequent analyses.

Figure 6.41: Skin Friction Coefficients for Steady State Conditions



## 6.5 Closure

This chapter reported on the non-inertial solver development and validation test cases related to the solver functionality. The contributions of this chapter is:

- **Development of a non-inertial solver.** The non-inertial equations derived in *Chapter 3* were implemented in the open source platform OpenFOAM. The governing equations that was implemented are the conservation of mass, momentum and energy equations respectively:

$$\begin{aligned} \frac{\partial \hat{\rho}}{\partial t} + \hat{\nabla} \cdot \hat{\rho} \hat{\mathbf{u}} &= 0 \\ \frac{\partial \hat{\rho} \hat{\mathbf{u}}}{\partial t} + \hat{\nabla} \cdot (\hat{\rho} \hat{\mathbf{u}} \otimes \hat{\mathbf{u}}) - \hat{\nabla} \cdot [\hat{\mu}(\hat{\nabla} \hat{\mathbf{u}} + \hat{\nabla} \hat{\mathbf{u}}^T) + \hat{\lambda}(\hat{\nabla} \cdot \hat{\mathbf{u}}) \hat{\mathbf{I}}] \\ &+ \underbrace{\frac{\partial}{\partial t}(\hat{\rho} \mathbf{V}(t))}_{\text{Translation}} - \underbrace{\hat{\rho} \hat{\mathbf{x}} \wedge \hat{\boldsymbol{\Omega}}}_{\text{Euler}} - \underbrace{2\hat{\rho} \hat{\mathbf{u}} \wedge \hat{\boldsymbol{\Omega}}}_{\text{Coriolis}} + \underbrace{\hat{\rho} \hat{\mathbf{x}} \wedge \hat{\boldsymbol{\Omega}} \wedge \hat{\boldsymbol{\Omega}}}_{\text{Centrifugal}} - \underbrace{2\hat{\rho} \mathbf{V}(t) \wedge \hat{\boldsymbol{\Omega}}}_{\text{Magnus}} = -\hat{\nabla} \hat{p} \\ \frac{\partial \hat{\rho} \hat{h}_s}{\partial t} + (\hat{\nabla} \cdot \hat{\rho} \hat{h}_s \hat{\mathbf{u}}) + \frac{\partial \hat{\rho} \hat{K}}{\partial t} + (\hat{\nabla} \cdot \hat{\rho} \hat{K} \hat{\mathbf{u}}) - \frac{\partial \hat{p}}{\partial t} - \hat{\nabla} \cdot (\hat{k} \hat{\nabla} \hat{T}) &= 0 \end{aligned}$$

The source code and case set-up are shown in *Appendix B*. The resulting code had the properties of:

- Non-inertial momentum equation implementation,
  - Prescribed motion definitions required,
  - Operating on a stationary mesh,
  - Using specialized boundary conditions and
  - Capability of resolving compressible flow.
- **Development of a non-inertial boundary condition.** A special boundary condition, **ARFFreeStreamVelocity**, was developed that allows for defining the free stream velocity conditions in the inertial frame. It is a simplified manner of describing the flow boundaries where the inertial velocity is stationary. The code transforms the boundary values to the non-inertial frame using the prescribed motion definitions.
  - **Validation of the non-inertial code.** Two validation cases were conducted to assess the functionality of the solver; a flat plate and a rotating cone. Numerical results from these analyses were compared with analytical results from Blasius [37], Monaghan [87] and von Karman [41] respectively. The simulated results compared well with the analytical results, the solver can therefore be used in the subsequent chapter to analyse the behaviour of the boundary layer under various accelerating conditions.

## Boundary Layer Response in Pure Rotation - Flat Plate Flow

The aim of this chapter is to characterise the response of the laminar boundary layer to arbitrary translations on a flat plate. This is accomplished through a multitude of simulation results that are interpreted using the non-inertial boundary layer equations established in previous chapters.

Acceleration of objects takes place over a variety of magnitudes. The lowest orders are represented by accelerating trains while the highest orders are found in the Large Hadron Collider and accelerations from a Wakefield plasma accelerator (*Table 7.1*). In this chapter the acceleration and deceleration parameters have been varied from 70 g to 700 000 g to obtain results over a large spectrum.

Table 7.1: Examples of Accelerating Objects

Order of Magnitude	Example
0-1 g	Train or car acceleration
1 - 10 g	F1 race cars
10 - 100 g	Ejection seat of aircraft
100 - 1 000 g	Missile in acceleration
1 000 - 10 000 g	Artillery projectile
10 000 - 100 000 g	Small calibre bullets
> 100 000 g	Theoretical Space guns

Acceleration and deceleration are analysed separately. In the first instance the flow is accelerated from a fully converged, steady state solution at 10 m/s ( $Re = 3.5 \times 10^4$ ) to a final velocity of 80 m/s ( $Re = 2.81 \times 10^5$ ). Here this is referred to as the *Acceleration Event*. Acceleration from 70 g to 70000 g at increasing orders of 10 is investigated. The second instance is analysed through deceleration from a fully converged, steady state solution at 80 m/s ( $Re = 2.81 \times 10^5$ ) to a final velocity of 10 m/s ( $Re = 3.5 \times 10^4$ ). This is referred to as the *Deceleration Event*. Decelerations from 70 g to 70000 g at increasing orders of 10 are investigated. In *Table 7.2*, the simulations conducted for an accelerating and decelerating flat

plate are respectively tabulated.

Table 7.2: Flat Plate Test Matrix

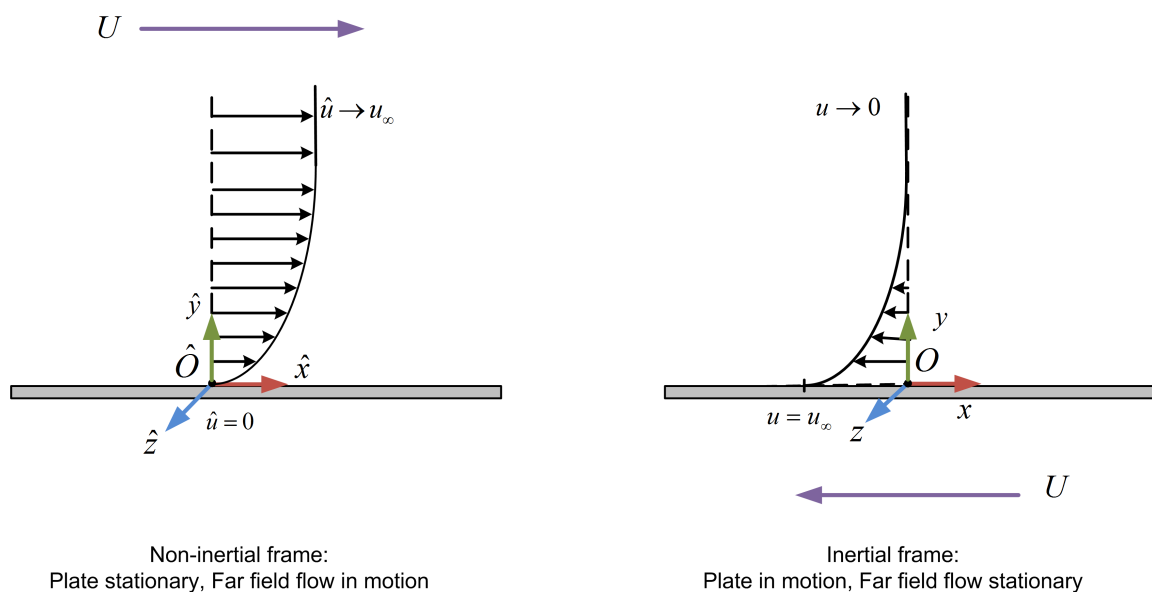
	Acceleration Event	Deceleration Event
Velocity [m/s]	10 to 80	80 to 10
Reynolds Number	$3.5 \times 10^4$ to $2.81 \times 10^5$	$2.81 \times 10^5$ to $3.5 \times 10^4$
	70g	70g
	700g	700g
	7 000g	7 000g
	70 000g	70 000g
	700 000g	700 000g

The acceleration conditions were selected to represent a large operational envelope. The minimum acceleration, 70g, is typical of ejection seats of aircraft. A lower value was not taken as the focus of this work is applications in the aero-ballistic environment where higher accelerations are present. The maximum value, 700 000g, was selected beyond that limit of known applications ensuring proper coverage of the range of applications. The flow conditions were select to ensure that the fluid remains well within the laminar regime. To this effect the Reynolds number of the flat plate in translation are kept below 300 000 (Crowe et al. [94]).

## 7.1 Case Description

The laminar boundary layer on a flat plate in steady motion was discussed in *Chapter 6*. Analytical solutions are available from the literature (Blasius [37], Monaghan [87]) against which the non-inertial solver was validated. The case analysed in this chapter is depicted in *Figure 7.1*.

Figure 7.1: Graphical Representation of the Boundary Layer on a Flat Plate

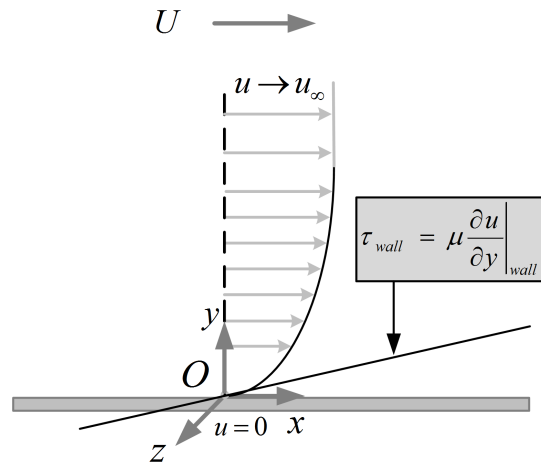




The difference between the velocity vectors in the inertial frame and non-inertial frame can be observed in *Figure 7.1*. In the inertial frame the plate is in motion with a velocity  $U$  in the negative  $x$ -direction. In the near-wall region the boundary layer assumes an absolute velocity of  $U$  in the negative  $x$ -direction - the velocity at which the plate is moving. In the far field the absolute velocity approaches zero. In the non-inertial frame the perspective of the observer has changed; the plate is stationary and the fluid is in motion. In the near-wall region the fluid velocity approaches zero on the no-slip wall and in the far field the fluid velocity approaches  $U$  - the relative velocity of the moving plate.

The velocity profile of the boundary layer is a function of the diffusion term in the Navier-Stokes equations. This originates from the shear stress on the wall which is a function of the velocity gradient on the wall (*Figure 7.2*).

Figure 7.2: Wall Shear Stress as a Function of Velocity Gradient



Mathematically, the diffusion term is responsible for the existence of the boundary layer. If this term is excluded from the equation, the Navier-Stokes equations are reduced to the inviscid Euler equations. Without viscosity in the flow, there is no boundary layer. The influence of the diffusion term is used in later sections to explain the behaviour of the boundary layer in accelerating conditions.

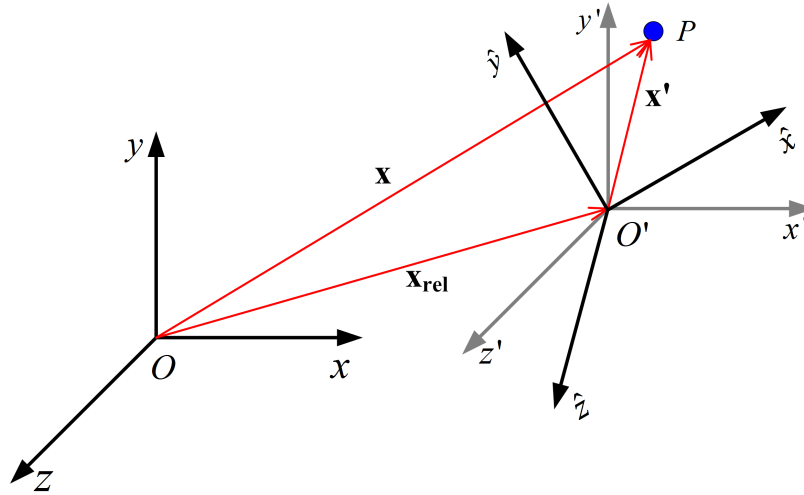
$$\underbrace{\frac{\partial \rho u}{\partial t} + u \frac{\partial \rho u}{\partial x} + v \frac{\partial \rho u}{\partial y}}_{\text{Material Derivative}} = -\frac{\partial p}{\partial x} + \frac{\partial}{\partial y} \left( \mu \frac{\partial u}{\partial y} \right) \tag{7.1}$$

In order to interpret the response of the boundary layer to acceleration and deceleration, the non-inertial equations are required. In *Chapter 3* the non-inertial momentum equation was derived for arbitrary acceleration using the frame description in *Figure 7.3*.

Relationships between the inertial and orientation preserving frames were derived in *Equation 3.180*, which in turn was used to find an expression for the motion in the non-inertial frame (*Equation 3.183*).

$$\mathbf{u}'(\mathbf{x}', t) = G^{\mathbf{M}^t} \mathbf{u}(\mathbf{x}, t) = \mathbf{u}(\mathbf{x}, t) - \mathbf{V}(t) + \mathbf{x}' \wedge \boldsymbol{\Omega} - [\mathbf{a}(t) + \dot{\boldsymbol{\Omega}} \wedge \mathbf{x}' + \boldsymbol{\Omega} \wedge \dot{\mathbf{x}}'] \Delta t \tag{7.2}$$

Figure 7.3: Frame Definitions for Non-Inertial Flow



$$\hat{\mathbf{u}}(\hat{\mathbf{x}}, t) = R^{\mathbf{M}}[\mathbf{u}(\mathbf{x}, t) - \mathbf{V}(t) + \mathbf{x}' \wedge \boldsymbol{\Omega} - [\mathbf{a}(t) + \dot{\boldsymbol{\Omega}} \wedge \mathbf{x}' + \boldsymbol{\Omega} \wedge \dot{\mathbf{x}}'] \Delta t] \quad (7.3)$$

Through elimination of terms that are not applicable in this case, the equations above can be used to determine an expression for this specific case of arbitrary translation:

$$\mathbf{u}'(\mathbf{x}', t) = \mathbf{u}(\mathbf{x}, t) - \mathbf{V}(t) \quad (7.4)$$

$$\hat{\mathbf{u}}(\hat{\mathbf{x}}, t) = R^{\mathbf{M}}[\mathbf{u}(\mathbf{x}, t) - \mathbf{V}(t)] \quad (7.5)$$

Further simplification, taken into account that no rotation is involved in this case, leads to a relation for the absolute velocity in terms of the relative frame velocity and non-inertial velocity:

$$\mathbf{u}(\mathbf{x}, t) = \hat{\mathbf{u}}(\hat{\mathbf{x}}, t) + \mathbf{V}(t) \quad (7.6)$$

The momentum equation for unsteady relative translation can be obtained by eliminating the rotational terms from *Equation 3.246*:

$$\underbrace{\frac{\partial \hat{\rho} \hat{\mathbf{u}}}{\partial t} + \hat{\nabla} \cdot (\hat{\rho} \hat{\mathbf{u}} \otimes \hat{\mathbf{u}})}_{\text{Material Derivative}} = -\hat{\nabla} \hat{p} + \hat{\nabla} \cdot [\hat{\mu}(\hat{\nabla} \hat{\mathbf{u}} + \hat{\nabla} \hat{\mathbf{u}}^T) + \hat{\lambda}(\hat{\nabla} \cdot \hat{\mathbf{u}}) \hat{\mathbf{I}}] - \underbrace{\frac{\partial}{\partial t}(\rho \mathbf{V}(t))}_{\text{Translation}} \quad (7.7)$$

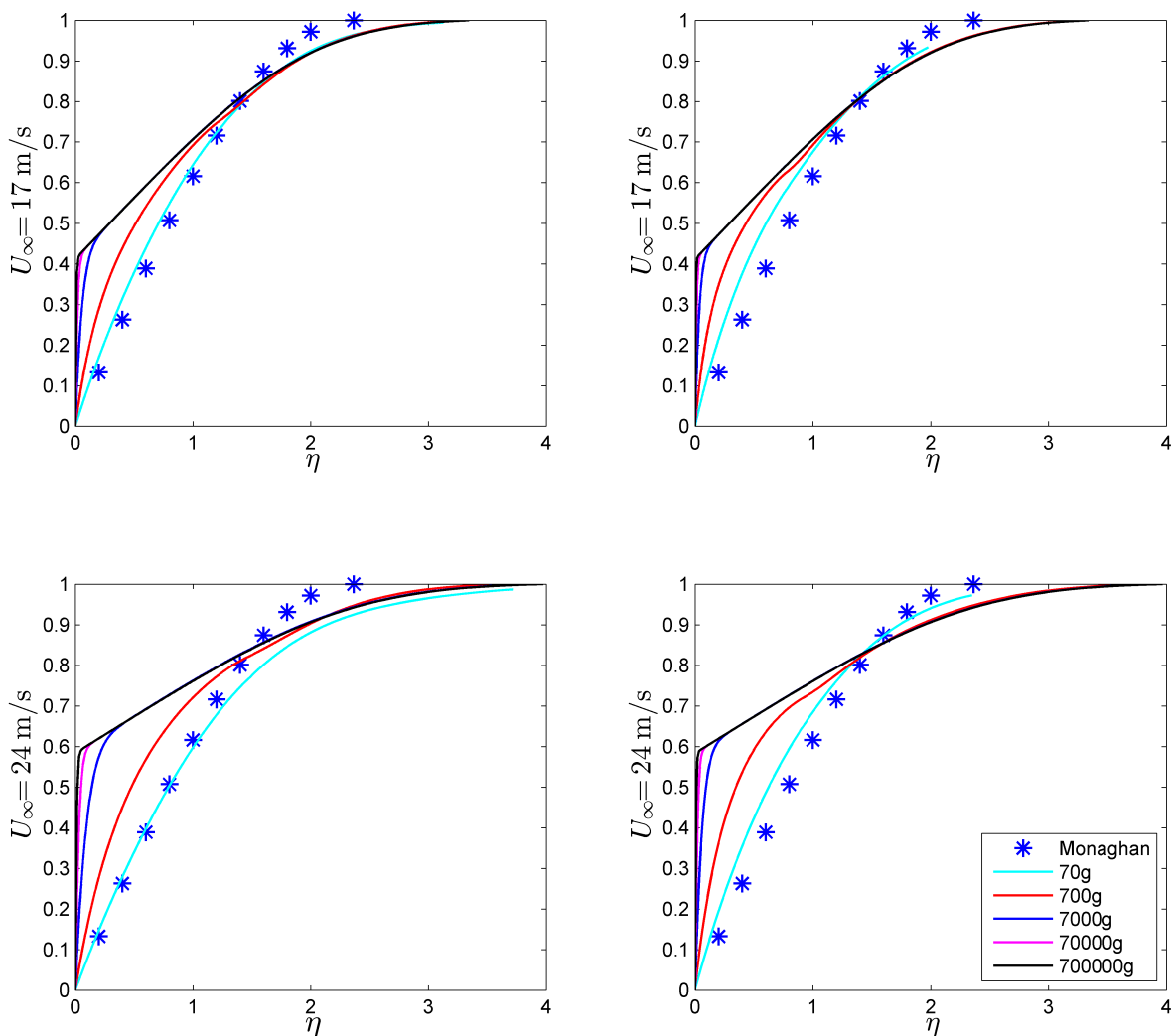
The only fictitious term remaining in the momentum equation is the unsteady frame acceleration. It acts as a momentum source when in the plate is in acceleration and a momentum sink in decelerating conditions.

## 7.2 Results and Discussion - Acceleration

### 7.2.1 Velocity Profiles

The accelerating flow analysis was done for the laminar flat plate in accordance with *Table 7.2*. Comparisons were drawn between the non-dimensional velocity profiles at common free stream velocities for different accelerations. The non-dimensional distance from the wall,  $\eta$ , is determined by *Equation 6.21*. Results are indicated in three grouping in *Figures 7.4-7.6*. The three groupings were selected to represent the results in a concise manner.

Figure 7.4: Non-Dimensional Velocity Profiles: Translating Flat Plate - Acceleration Grouping I



CHAPTER 7. BOUNDARY LAYER RESPONSE IN PURE ROTATION - FLAT PLATE FLOW

Figure 7.5: Non-Dimensional Velocity Profiles: Translating Flat Plate - Acceleration Grouping II

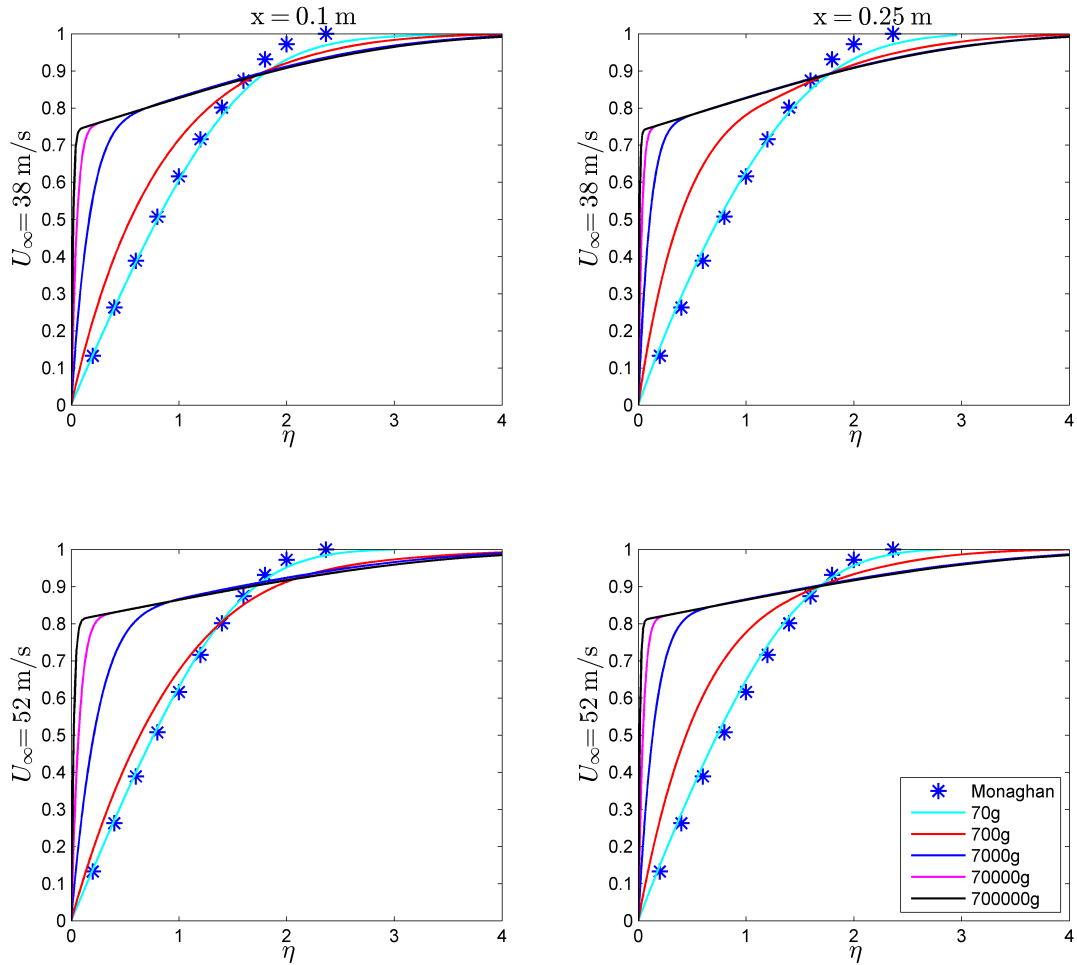
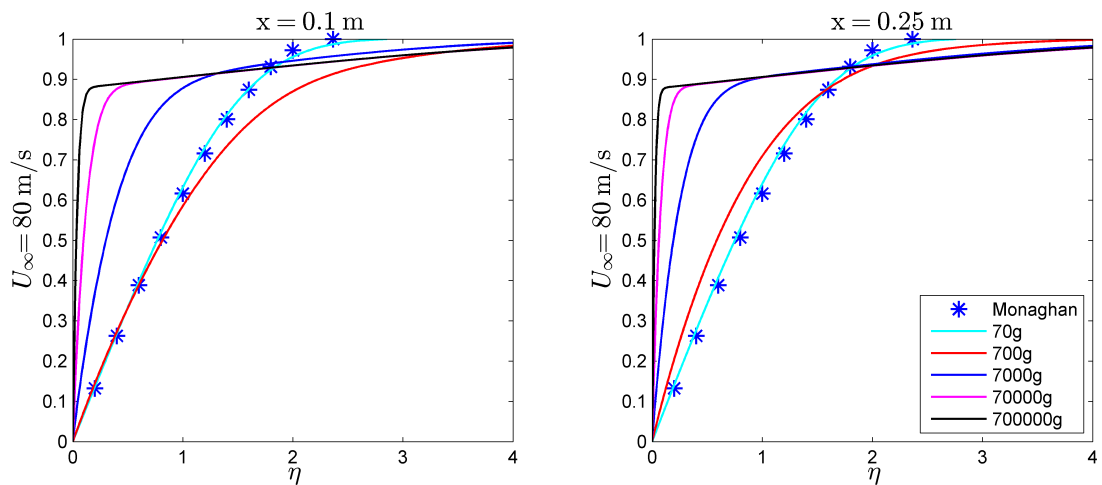
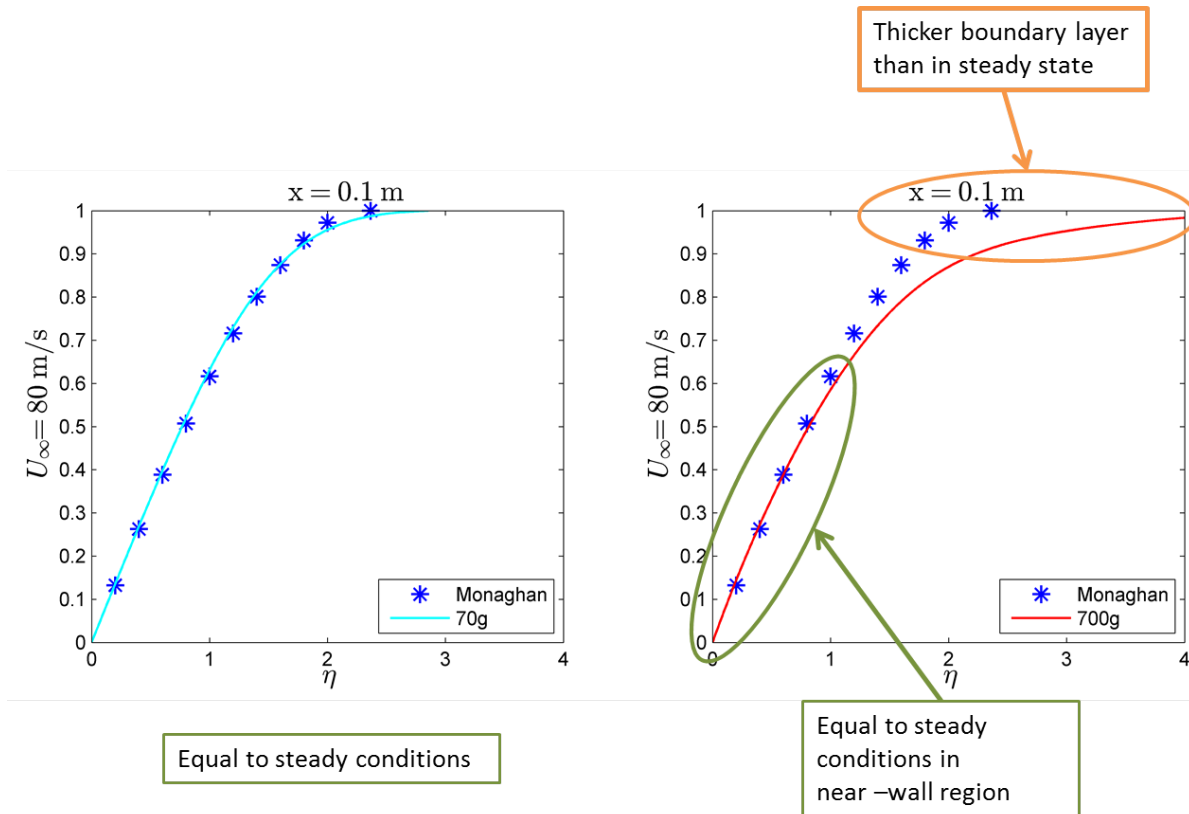


Figure 7.6: Non-Dimensional Velocity Profiles: Translating Flat Plate - Acceleration Grouping III



Sample results that are representative of the boundary layer responses are shown for explanation purpose in *Figures 7.7* and *7.8*.

Figure 7.7: Sample Results and Observations for the Lower Acceleration Cases



In *Figure 7.7* it is shown that the 70g acceleration case remains very close to the steady state results. In the near-wall region the velocity gradient is maintained at steady state values. The boundary layer thickness is the same since the free-stream velocity is reached at the same value for non-dimensional height,  $\eta$ , than in the steady state case. In *Figure 7.4* it is seen that the profile deviated from the steady state conditions in the middle boundary layer region between free stream values of 17 m/s and 24 m/s, but by 38 m/s the deviations subsided and a steady profile was resumed. The diffusion term dominates the 70g acceleration case to maintain near steady state conditions.

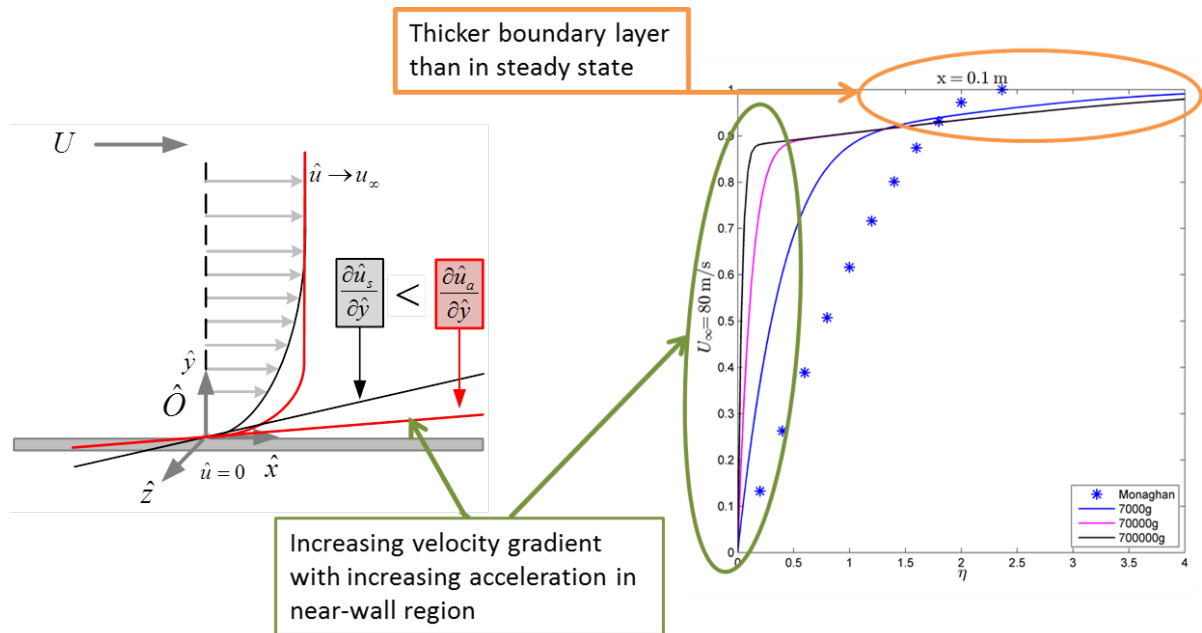
The 700 g acceleration case maintains the steady state profiles in the near-wall regions, but deviates as the flow approaches the free stream conditions in the far field (*Figure 7.7*). This leads to a thicker boundary layer than the steady state where the free-stream velocity value is achieved at a higher non-dimensional height,  $\eta$ , than in the steady state case. This response is a combination of the diffusion term dominating in the near-wall region and the material derivative of momentum (all the terms on the left hand side of the equation) dominating in the far field.

The higher acceleration cases ( $> 1000 \text{ g}$ ) is characterised by an increased velocity gradient in the near wall region resulting in a higher wall shear stress (*Figure 7.8*). This increase in near-wall

CHAPTER 7. BOUNDARY LAYER RESPONSE IN PURE ROTATION - FLAT PLATE FLOW

velocity gradient is directly proportional to the acceleration - higher acceleration causes higher wall shear stresses. The boundary layer is thicker than in the steady state conditions since the free-stream condition (a non-dimensional velocity of 1) is reached at a higher non-dimensional distance,  $\eta$ , than in the steady state case. The flow in all regions is dominated by the momentum of the acceleration.

Figure 7.8: Sample Results and Observations for the Higher Acceleration Cases



The observed behaviour was shown in the non-inertial frame. It can also be explained from the inertial perspective. In the inertial frame the flat plate is initially in a fully developed steady state condition. The plate is moving while the far field flow is standing still. The velocity profile has an identical shape to the velocity profile in the non-inertial frame. However, the velocity at the wall has the value of the non-inertial free stream value. The far-field velocity in the inertial frame is zero. As the plate accelerates the velocity at the wall increases rapidly. Since the motion is unsteady, the velocity gradient near the wall becomes steeper. The velocity in the free stream remains at zero. The thickening of the boundary layer occurs due to the momentum effects dominating the viscous effect. Furthermore, the time scale of the event is too high for the viscous effects to dominate the flow. Subsequently, the viscous effects are not able to adjust the boundary layer flow to assume the steady state profile in these changing conditions.

The observed results can further be interpreted mathematically using the boundary layer equations derived in *Chapter 5*. In *Equations 5.75* and *5.76* the Cartesian component from the non-inertial momentum equations were derived for arbitrary accelerating conditions.

7.2. RESULTS AND DISCUSSION - ACCELERATION

**x-momentum**

$$\underbrace{\frac{\partial \hat{\rho} \hat{u}}{\partial t} + \hat{u} \frac{\partial \hat{\rho} \hat{u}}{\partial \hat{x}} + \hat{v} \frac{\partial \hat{\rho} \hat{u}}{\partial \hat{y}} + \hat{w} \frac{\partial \hat{\rho} \hat{u}}{\partial \hat{z}}}_{\text{Material Derivative}} = -\frac{\partial \hat{p}}{\partial \hat{x}} + \frac{\partial}{\partial \hat{y}} \left( \hat{\mu} \frac{\partial \hat{u}}{\partial \hat{y}} \right) + 2\hat{\rho} \hat{v} \omega_3 - 2\hat{\rho} \hat{w} \omega_2 + \hat{\rho} \hat{x} (\omega_3^2 + \omega_2^2)$$

$$\begin{aligned}
 & -\hat{\rho} \hat{y} \omega_1 \omega_2 - \hat{\rho} \hat{z} \omega_1 \omega_3 + \hat{\rho} \hat{y} \hat{\omega}_3 - \hat{\rho} \hat{z} \hat{\omega}_2 + \hat{\rho} \hat{y} \omega_3 - \hat{\rho} \hat{z} \omega_2 \\
 & + 2\hat{\rho} V_y \omega_3 - 2\hat{\rho} V_z \omega_2 - \frac{\partial \hat{\rho} V_x}{\partial t}
 \end{aligned}
 \tag{7.8}$$

**y-momentum**

$$\begin{aligned}
 0 = & -\frac{\partial \hat{p}}{\partial \hat{y}} + 2\hat{\rho} \hat{w} \omega_1 - 2\hat{\rho} \hat{u} \omega_3 + \hat{\rho} \hat{y} (\omega_3^2 + \omega_1^2) - \hat{\rho} \hat{x} \omega_1 \omega_2 - \hat{\rho} \hat{z} \omega_2 \omega_3 + \hat{\rho} \hat{z} \hat{\omega}_1 - \hat{\rho} \hat{x} \hat{\omega}_3 + \hat{\rho} \hat{z} \omega_1 - \hat{\rho} \hat{x} \omega_3 \\
 & + 2\hat{\rho} V_z \omega_1 - 2\hat{\rho} V_x \omega_3 - \frac{\partial \hat{\rho} V_y}{\partial t}
 \end{aligned}
 \tag{7.9}$$

The equations above can be simplified by eliminating the terms that is not relevant to flat plate translation in the x-direction. All terms associated with rotation and translational acceleration in the y-direction is removed from the equation, resulting in the following set of boundary layer equations:

**x-momentum**

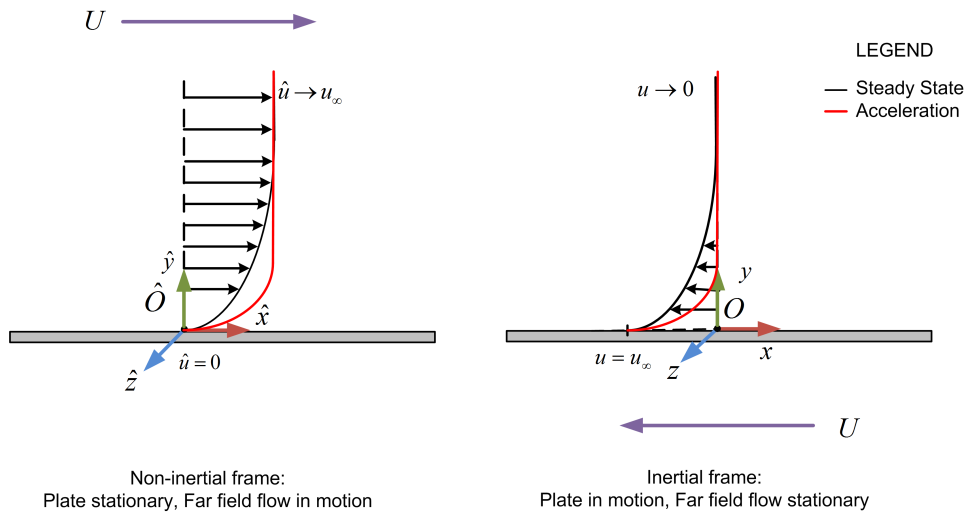
$$\frac{\partial \hat{\rho} \hat{u}}{\partial t} + \hat{u} \frac{\partial \hat{\rho} \hat{u}}{\partial \hat{x}} + \hat{v} \frac{\partial \hat{\rho} \hat{u}}{\partial \hat{y}} = -\frac{\partial \hat{p}}{\partial \hat{x}} + \frac{\partial}{\partial \hat{y}} \left( \hat{\mu} \frac{\partial \hat{u}}{\partial \hat{y}} \right) - \frac{\partial \hat{\rho} V_x}{\partial t}
 \tag{7.10}$$

**y-momentum**

$$0 = -\frac{\partial \hat{p}}{\partial \hat{y}}
 \tag{7.11}$$

The equation set above is responsible for the observed behaviour and from this a mechanism can be devised to explain the boundary layer response (*Figure 7.9*).

Figure 7.9: Boundary Layer Profiles for Steady and Accelerating Conditions



In *Equation 7.6* the absolute and relative velocities were related to each other for this case.

$$\mathbf{u}(\mathbf{x}, t) = \hat{\mathbf{u}}(\hat{\mathbf{x}}, t) + \mathbf{V}(t)
 \tag{7.12}$$

CHAPTER 7. BOUNDARY LAYER RESPONSE IN PURE ROTATION - FLAT PLATE FLOW

The meaning of this relationship become clear when the component form of the inertial and non-inertial x-momentum equations are compared. An increase in the relative frame velocity (velocity of the plate in the negative x-direction) results in an increase in the non-inertial velocity and subsequently the absolute velocity.

- Absolute acceleration

$$\frac{\partial \rho u}{\partial t} + u \frac{\partial \rho u}{\partial x} + v \frac{\partial \rho u}{\partial y} = -\frac{\partial p}{\partial x} + \frac{\partial}{\partial y} \left( \mu \frac{\partial u}{\partial y} \right)$$

- Non-inertial acceleration

$$\frac{\partial \hat{\rho} \hat{u}}{\partial t} + \hat{u} \frac{\partial \hat{\rho} \hat{u}}{\partial \hat{x}} + \hat{v} \frac{\partial \hat{\rho} \hat{u}}{\partial \hat{y}} = -\frac{\partial \hat{p}}{\partial \hat{x}} + \frac{\partial}{\partial \hat{y}} \left( \hat{\mu} \frac{\partial \hat{u}}{\partial \hat{y}} \right) - \frac{\partial \hat{\rho} V_x}{\partial t}$$

- Frame acceleration prescribed

The prescribed frame velocity, here acting in the negative x-direction, acts as a source of momentum. An increase in this term on the right hand side of the momentum equation, results in an overall increase in the material derivative on the left hand side of the equation.

$$\frac{\partial \hat{\rho} \hat{u}}{\partial t} + \hat{u} \frac{\partial \hat{\rho} \hat{u}}{\partial \hat{x}} + \hat{v} \frac{\partial \hat{\rho} \hat{u}}{\partial \hat{y}} = -\frac{\partial \hat{p}}{\partial \hat{x}} + \frac{\partial}{\partial \hat{y}} \left( \hat{\mu} \frac{\partial \hat{u}}{\partial \hat{y}} \right) - \frac{\partial \hat{\rho} V_x}{\partial t}$$

An increase in the material derivative results in an increase in  $\hat{u}$ , which in term results in an increase in the wall velocity gradient (Figure 7.10) which is the observed effect in the accelerating boundary layer profile.

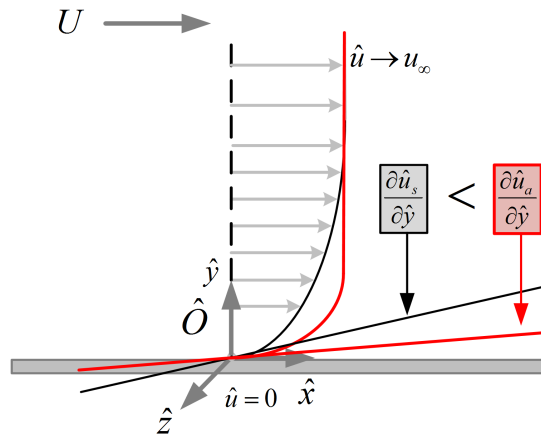
$$\frac{\partial \hat{\rho} \hat{u}}{\partial t} + \hat{u} \frac{\partial \hat{\rho} \hat{u}}{\partial \hat{x}} + \hat{v} \frac{\partial \hat{\rho} \hat{u}}{\partial \hat{y}} = -\frac{\partial \hat{p}}{\partial \hat{x}} + \frac{\partial}{\partial \hat{y}} \left( \hat{\mu} \frac{\partial \hat{u}}{\partial \hat{y}} \right) - \frac{\partial \hat{\rho} V_x}{\partial t}$$

The strength of this mechanism is dependant on the magnitude of the frame acceleration. Three distinct acceleration regions are identified in the translation case; a viscous dominant, a viscous-momentum interaction and a momentum dominant region.

- **Region I - Viscous Dominant.** The 70 g case falls within this region. There is almost no divergence from the steady state non-dimensional result (Monaghan [87]). The viscous effects dominate the boundary layer flow and any disturbances in the boundary layer is neutralized by the much larger viscous forces. This can be seen the Grouping I (Figure 7.4) results at 20.5 m/s where



Figure 7.10: Increased Wall Velocity Gradient for Accelerating Conditions



the disturbance occurs, the upstream propagation at 24 m/s. At Grouping II (Figure 7.5) 38 m/s the disturbance has been dissipated and the profile is on the steady state baseline again. In this region the rate of change in velocity due to acceleration is small enough to allow the flow the adjust to steady state conditions. The induced momentum effects, due to acceleration, is not high enough to result in changes in the boundary layer properties.

Acceleration Response - Type I:

$$\frac{\partial \hat{\rho} \hat{u}}{\partial t} + \hat{u} \frac{\partial \hat{\rho} \hat{u}}{\partial \hat{x}} + \hat{v} \frac{\partial \hat{\rho} \hat{u}}{\partial \hat{y}} = -\frac{\partial \hat{p}}{\partial \hat{x}} + \frac{\partial}{\partial \hat{y}} \hat{\mu} \frac{\partial \hat{u}}{\partial \hat{y}} - \frac{\partial \hat{\rho} V_x}{\partial t}$$

- **Region II - Viscous-Momentum Interaction.** In the near wall region the viscous effects originates from the wall and dominates the flow close to the wall. This effect becomes smaller further away from the wall. In the free-stream the viscous effects are negligible and the momentum effects dominate. In region II, the time scales of the viscous and momentum forces in the boundary layer are approximately equal leading the two effects being of comparable order. This causes disturbance of the boundary layer since neither force is dominant. The 700 g case falls within this region. The region (for this specific case) extends from approximately 500 g - 1100 g. It is characterized by unsteady disturbance propagation that originates from the wall which causes erratic behaviour in the boundary layer.

Acceleration Response - Type II:

$$\frac{\partial \hat{\rho} \hat{u}}{\partial t} + \hat{u} \frac{\partial \hat{\rho} \hat{u}}{\partial \hat{x}} + \hat{v} \frac{\partial \hat{\rho} \hat{u}}{\partial \hat{y}} = -\frac{\partial \hat{p}}{\partial \hat{x}} + \frac{\partial}{\partial \hat{y}} \hat{\mu} \frac{\partial \hat{u}}{\partial \hat{y}} - \frac{\partial \hat{\rho} V_x}{\partial t}$$

CHAPTER 7. BOUNDARY LAYER RESPONSE IN PURE ROTATION - FLAT PLATE FLOW

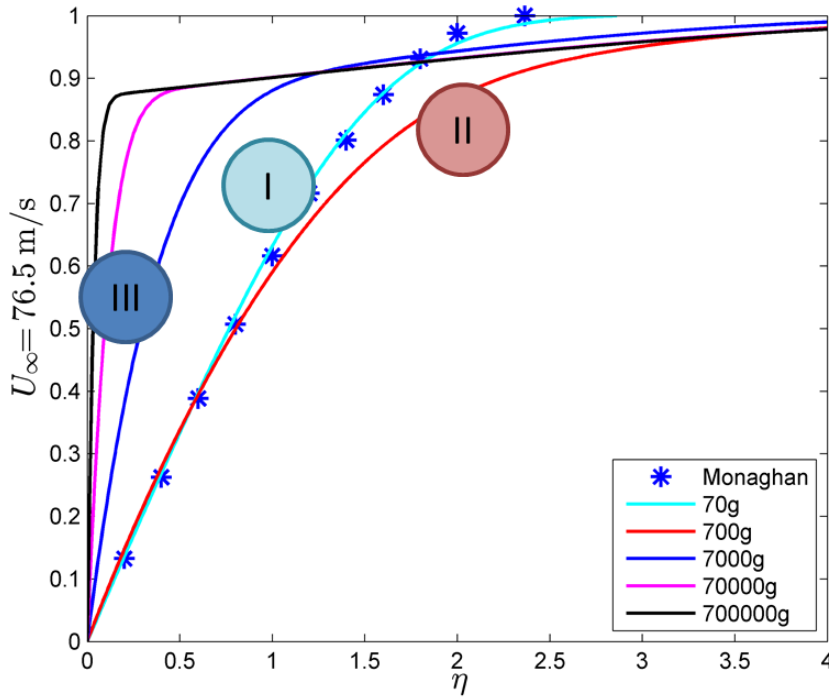
- Region III - Momentum Dominant.** The three higher acceleration cases falls within this region - 7000 g, 70000 g and 700000 g. The region is characterized by a sharp increase in the near-wall velocity gradient that is directly proportional to the acceleration. The boundary layer velocity profile resembles that of a fully developed, turbulent profile with the steep gradient that becomes almost parallel with the free stream in the regions close to the boundary layer edge. An increase in boundary layer height is observed. The general form of the profiles are comparable with similar studies in literature (Back [28], Mager [97]).

Acceleration Response - Type III:

$$\frac{\partial \hat{\rho} \hat{u}}{\partial t} + \hat{u} \frac{\partial \hat{\rho} \hat{u}}{\partial \hat{x}} + \hat{v} \frac{\partial \hat{\rho} \hat{u}}{\partial \hat{y}} = -\frac{\partial \hat{p}}{\partial \hat{x}} + \frac{\partial}{\partial \hat{y}} \hat{\mu} \frac{\partial \hat{u}}{\partial \hat{y}} - \frac{\partial \hat{\rho} V_x}{\partial t}$$

The accelerating results is grouped in the three regions as shown in (Figure 7.11).

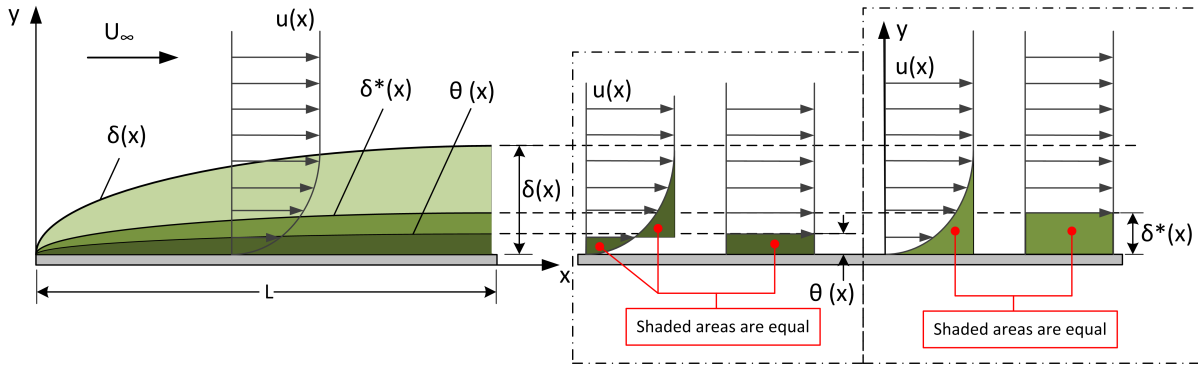
Figure 7.11: Acceleration Response Regions by Type in Simulation Results



### 7.2.2 Boundary Layer Parameters

The boundary layer properties that are considered here have been shown in *Figure 6.1*:

Figure 7.12: Physical Interpretation of the Boundary Layer Parameters



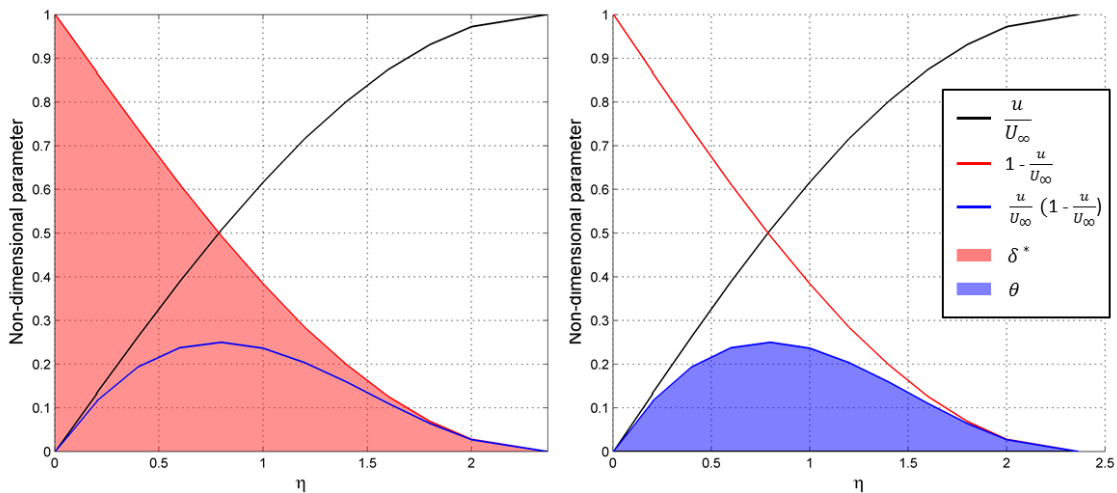
The effect of acceleration on the boundary layer thickness have been discussed in the previous section along with the boundary layer shape. The definitions of the displacement thickness,  $\delta^*$  and the momentum thickness,  $\theta$ , follow directly from the non-dimensional boundary layer profile,  $\frac{\hat{u}}{U_\infty}$ . The mechanism described in the previous section, that effects the boundary layer profile, therefore influences these parameters as well.

$$\delta^* = \int_0^{y^* \rightarrow \infty} \left(1 - \frac{\hat{u}}{U_\infty}\right) dy \quad (7.13)$$

$$\theta = \int_0^{y^* \rightarrow \infty} \frac{\hat{u}}{U_\infty} \left(1 - \frac{\hat{u}}{U_\infty}\right) dy \quad (7.14)$$

The displacement and momentum thicknesses are determined by integrating the area under the relevant curve as shown below:

Figure 7.13: Boundary Layer Parameters on a Flat Plate



CHAPTER 7. BOUNDARY LAYER RESPONSE IN PURE ROTATION - FLAT PLATE FLOW

Comparisons of the displacement thickness for various accelerations are shown in *Figures 7.14 - 7.17*.

Figure 7.14: Displacement Thickness Comparison for the Accelerating Flat Plate

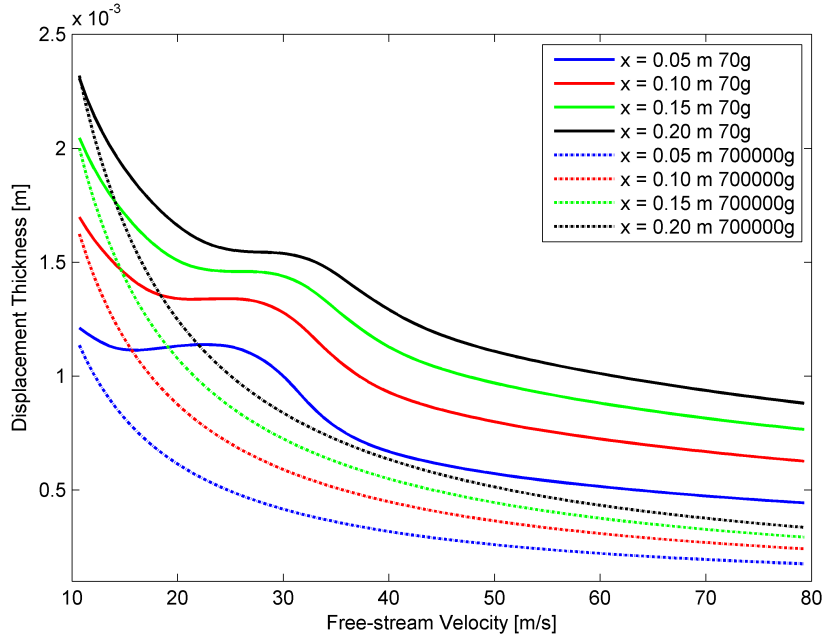


Figure 7.15: Displacement Thickness Derivatives Comparison for the Accelerating Flat Plate

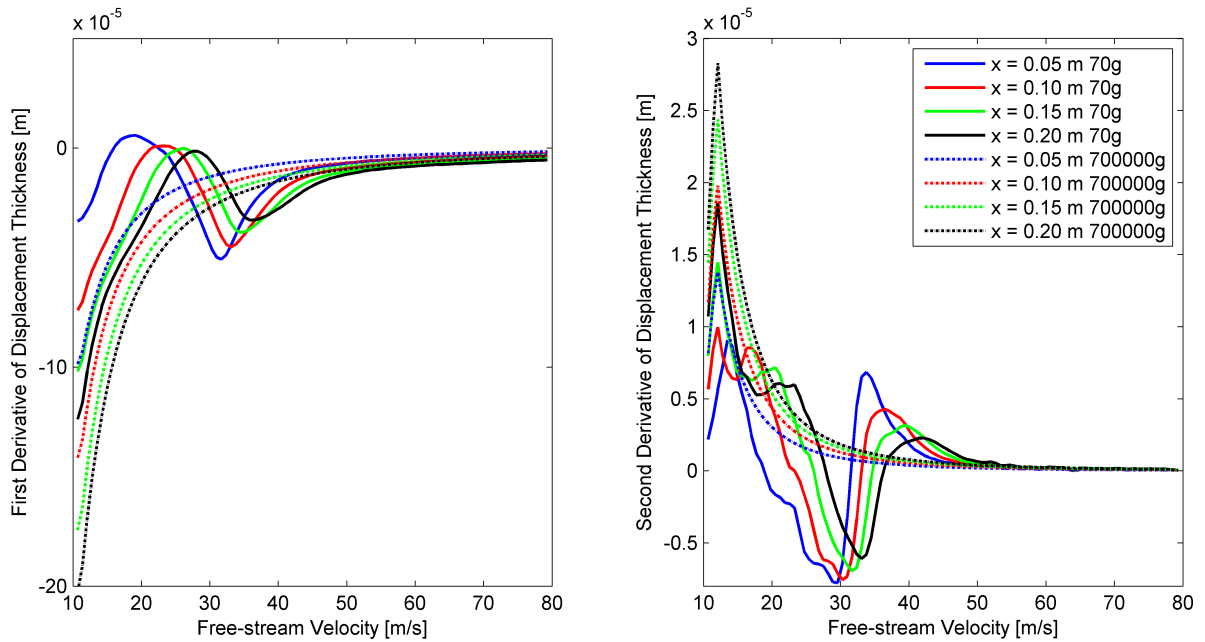


Figure 7.16: Displacement Thickness Comparison at  $x = 0.05$  m in Accelerating Conditions

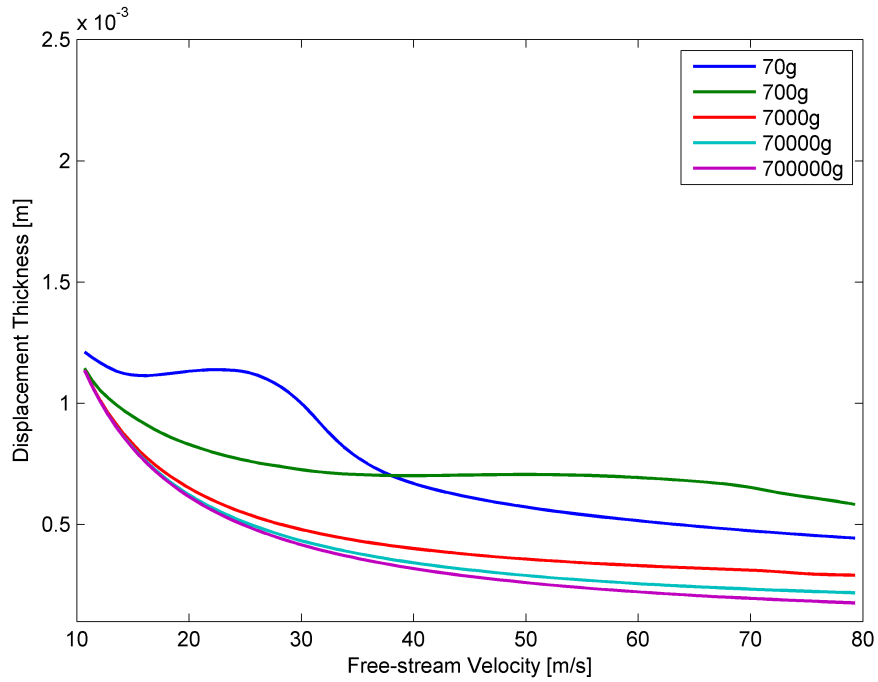
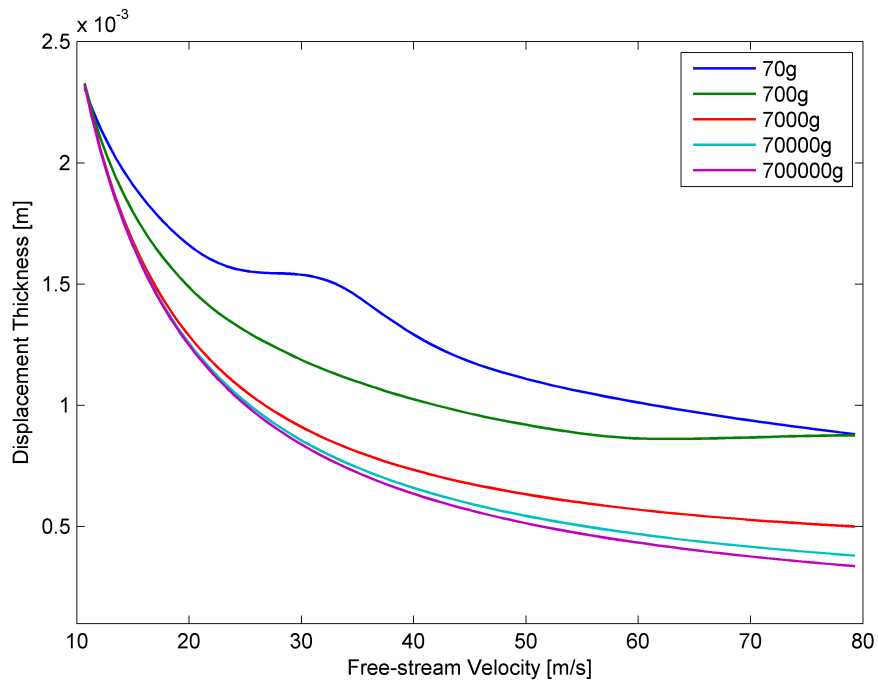


Figure 7.17: Displacement Thickness Comparison at  $x = 0.2$  m in Accelerating Conditions



Since the boundary layer properties are directly linked to the boundary layer profile, the behaviour of the parameters can be grouped in the same three regions as identified in the previous section.

**Region I - Viscous Dominant Region** - has a displacement thickness that is on average monotonically decreasing with increased free-stream velocity. A slight disturbance in the early stages of the acceleration event, at approximately 20 m/s to 30 m/s free-stream velocity, is observed. It was noted in the previous section that the velocity profile deviated from the steady state conditions between free stream values of 17 m/s and 24 m/s. At a velocity of 38 m/s the deviations subsided and a steady profile was resumed. This was due to viscous-momentum force interactions and is the origin of the disturbance. The first derivative of the displacement thickness indicates that this disturbance is time related. The local maximum and minimum values of displacement thickness, between 17 m/s and 38 m/s, occurs consecutively in time for successive points on the plate (*Figure 7.15*). The disturbance dissipates after 50 m/s. The first derivative approximates zero near the completion of the event at 80 m/s. This is an indication that the displacement thickness approaches an asymptotic value. The second derivative has an inflection point at the start of the acceleration event. This is a response to the sudden acceleration of flow in a steady condition, similar to the mass flow conditions of a sudden start case. Sudden acceleration is here defined as the initial response of the flow in the first instance of the acceleration event. This region showed no plate edge effects in the boundary layer.

**Region II - Viscous-Momentum Interaction Region** - is characterised by erratic behaviour of the displacement thickness. Disturbances are noted in the first and second derivative. On average the first derivative of the displacement thickness, *Figures 7.16* and *7.17*, approximates zero at the end of the event. Although there are disturbances in the displacement thickness value near 80 m/s, it approximates an averaged asymptotic value. The inflection point in the second derivative is larger than the other acceleration case. This indicates that in this region the boundary layer is sensitive to sudden acceleration and responds accordingly. Edge disturbances of the plate were not observed in this region.

In **Region III - Momentum Dominant Region** - the displacement thickness is monotonically decreasing with increasing free-stream velocity. There are no observed disturbances in the displacement thickness in this region. The first derivative is monotonically increasing. It approximates zero, which indicates that the displacement thickness approaches an asymptote during the acceleration event. An inflection point is present in the second derivative. The value of the inflection point is equal between the 7000g, 70000g and 700000g cases. The displacement thickness inflection point is a measure of the response of the mass flow to sudden acceleration. Here it indicates that the mass flow response to sudden acceleration from a steady state condition is independent from the strength of the acceleration. No plate edge effects are observed in this region.

7.2. RESULTS AND DISCUSSION - ACCELERATION

The momentum thickness responds in a similar manner than the displacement thickness over the three acceleration regions. The results are shown in *Figures 7.18-7.21*.

Figure 7.18: Momentum Thickness Comparison for the Accelerating Flat Plate

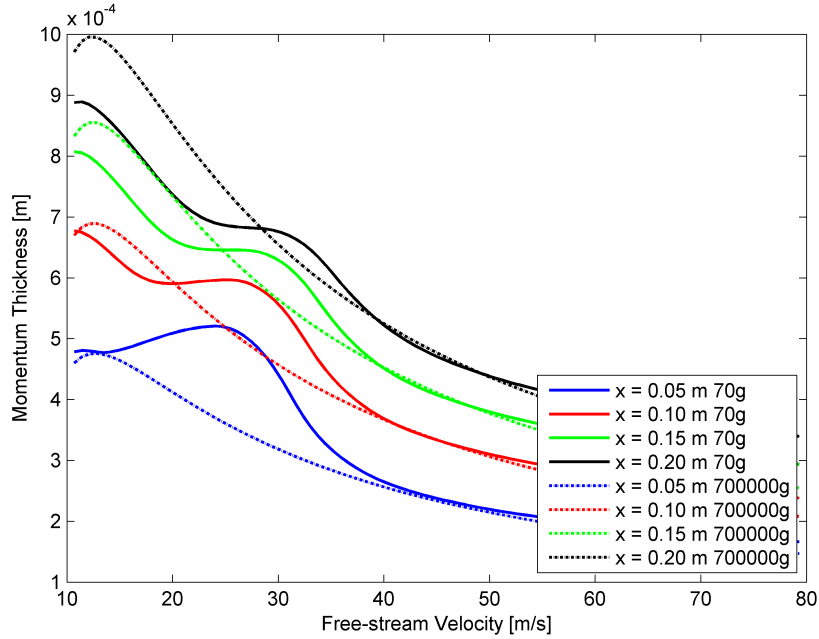
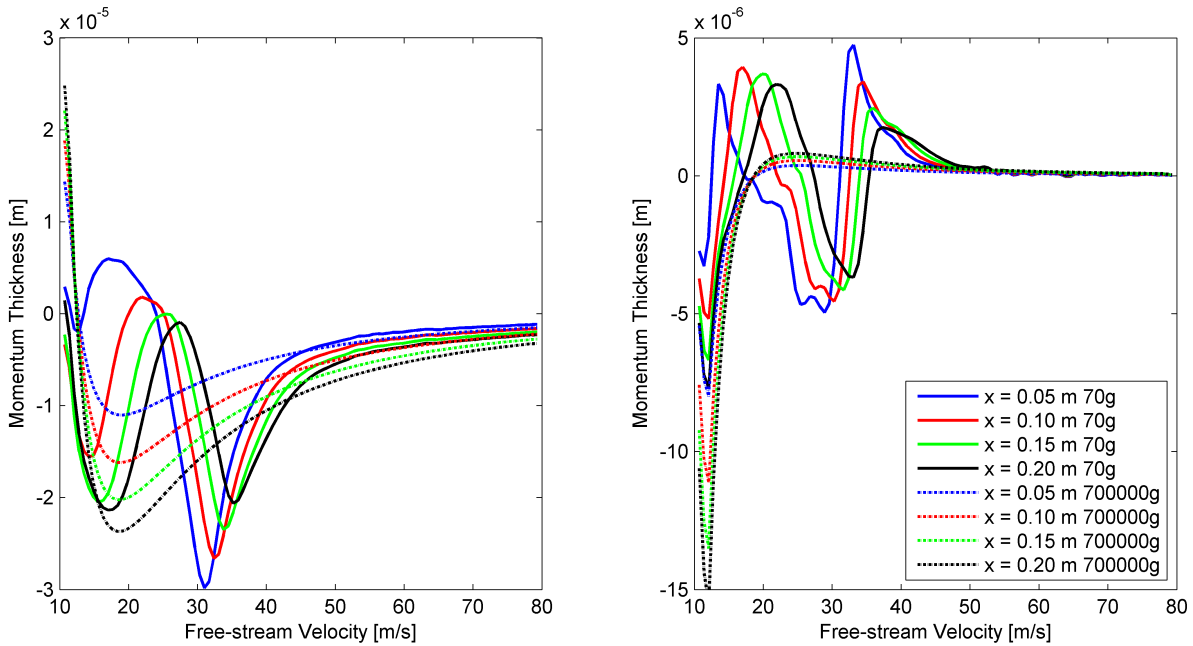


Figure 7.19: Momentum Thickness Derivatives Comparison for the Accelerating Flat Plate



CHAPTER 7. BOUNDARY LAYER RESPONSE IN PURE ROTATION - FLAT PLATE FLOW

Figure 7.20: Momentum Thickness Comparison at  $x = 0.05$  m in Accelerating Conditions

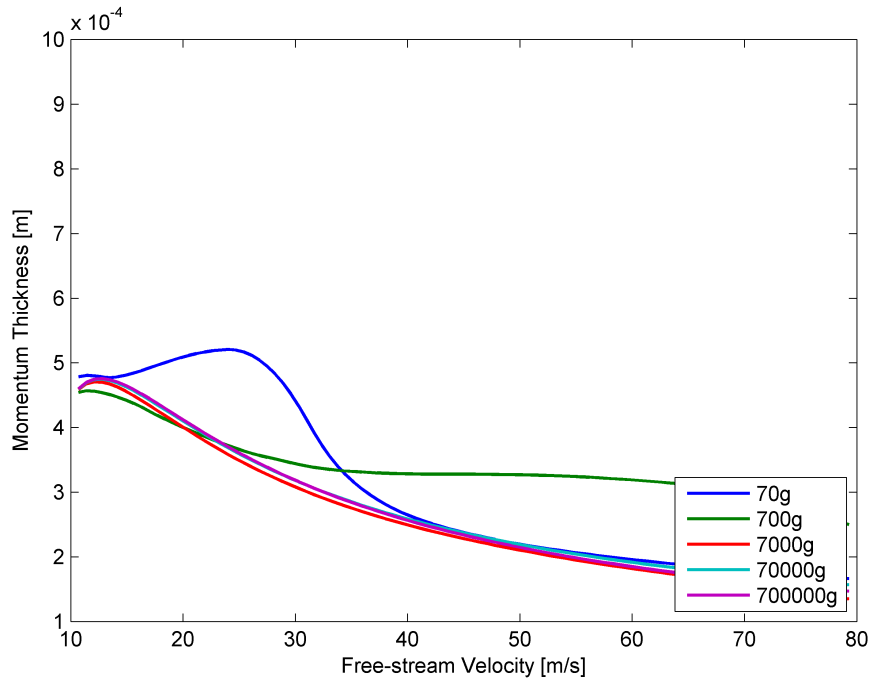
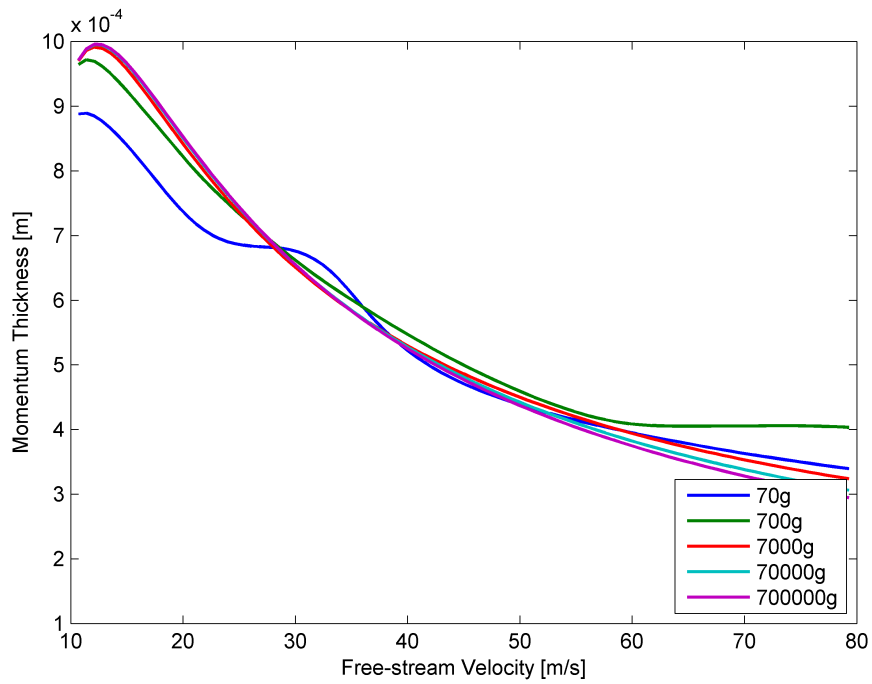


Figure 7.21: Momentum Thickness Comparison at  $x = 0.2$  m in Accelerating Conditions





In **Region I - Viscous Dominant Region** - the average momentum thickness is monotonically decreasing with increased free-stream velocity. The same disturbance that was noted in the displacement thickness between 17 m/s and 38 m/s is observed here. This disturbance is also time dependant as shown in the consecutive maxima in the first derivative *Figure 7.20*. The momentum thickness approaches an asymptote as indicated by the first derivative approximating zero at the end of the event. An small inflection point is observed in the second derivative. This is an indication of the response of the momentum in the boundary layer to sudden acceleration. Edge effects of the plate is not observed in this region.

**Region II - Viscous-Momentum Interaction Region** - shows erratic behaviour in the momentum thickness. The average first and second derivative approaches zero, but with visible disturbances in the result. This is especially seen at the end of the acceleration event. No momentum edge effects are observed in this region.

A slight increase in the momentum thickness at the beginning of the acceleration event is present in **Region III - Momentum Dominant Region**. After this increase the momentum thickness monotonically decreases without disturbances. The first derivative shows a minimum value in the early stages of the acceleration event. After this, it monotonically increases and approximates zero near the end of the event. This indicates that the momentum thickness approaches an asymptotic value. An inflection point is noted in the second derivative. This point has the same value for all the Region III cases. Furthermore, the momentum thickness in this region varies very little between all the acceleration cases that fall in this category. The momentum in the boundary layer shows minimal response to the initial stages of sudden acceleration from steady state conditions. In this region there are no plate edge effects on the momentum thickness.

The shape factor is calculated from the displacement and momentum thickness parameters.

$$H = \frac{\delta^*}{\theta} \quad (7.15)$$

The results are shown in *Figures 7.22-7.24*.

The **Region I - Viscous Dominant Region** - starts with the steady state value of approximately 2.68 as determined in the previous chapter. In the initial stages of the acceleration event the shape factor value decreases to a minimum. After the minimum was reached, the shape factor increases and approximates the steady state shape factor value. The first derivative approximates zero near the end of the event. Therefore, the shape factor approaches an asymptotic value at the end of the acceleration event. The disturbances due to viscous-momentum interaction are present in the second derivative. These are damped out as was seen in the displacement and momentum thickness graphs.

**Region II - Viscous-Momentum Interaction Region** - shape factor graphs displays similar behaviour as Region I. The value starts at the steady state condition and reduces to a minimum value. The value then increases and recovers a percentage of the steady state value. The first derivative approaches zero, indicating that the shape factor approximates an asymptotic value. The second derivative shows disturbances near the plate edge at the end of the event. This indicates that distance from the plate edge affects the shape factor.

Figure 7.22: Shape Factor Comparison for the Accelerating Flat Plate

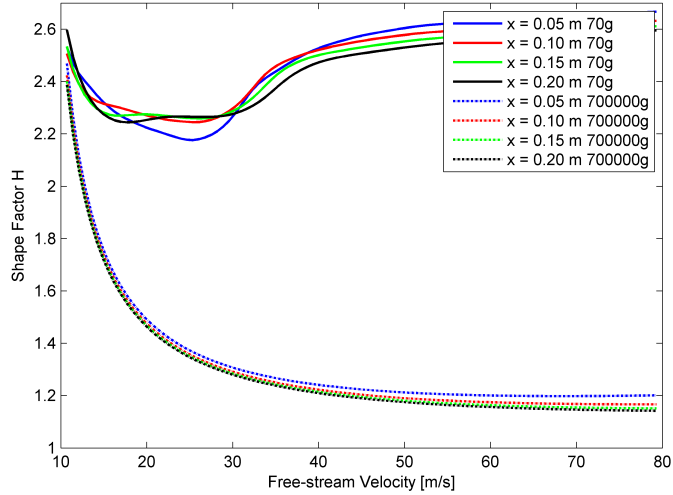
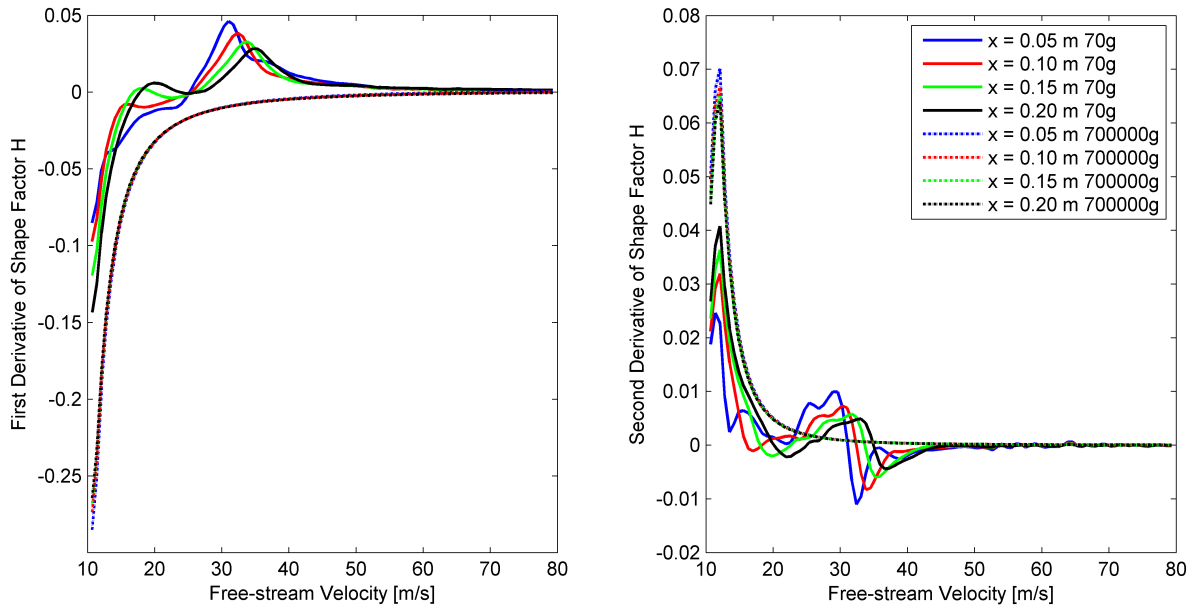


Figure 7.23: Shape Factor Derivative Comparison for the Accelerating Flat Plate



In **Region III - Momentum Dominant** - the 7000g case shape factor responds differently to acceleration than the other two cases in this category. At the location close to the plate edge, the 7000g case has a similar response to Region I and Region II. Further away from the plate edge, the response is similar to the higher acceleration cases. The shape factors of the 70000g and 700000g cases are monotonically decreasing. There is no turning point in the result and no attempt to recover the steady state value. The first derivative shows that an asymptotic value is approached. There are no disturbances in

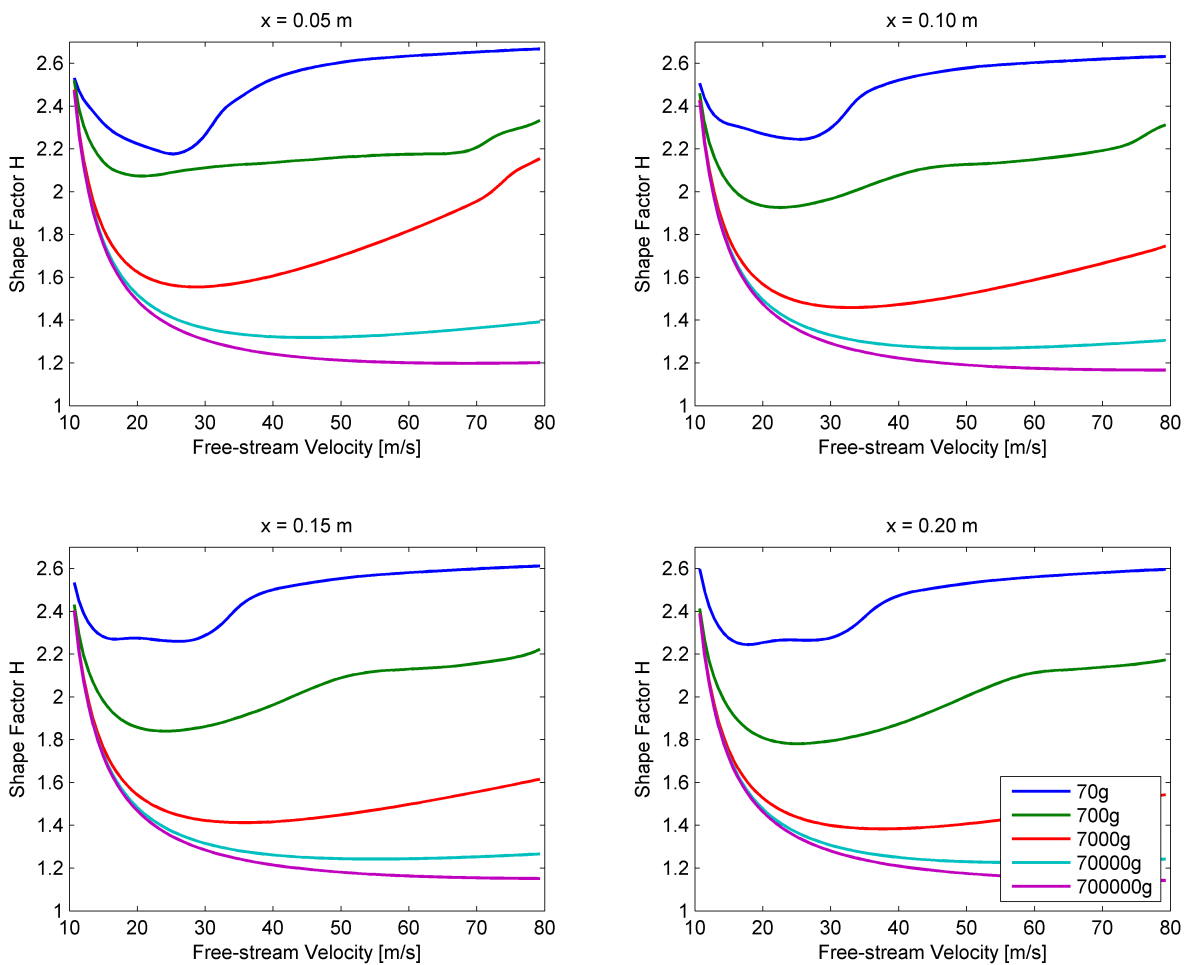
7.2. RESULTS AND DISCUSSION - ACCELERATION

the second derivative.

In *Figure 7.24* a comparison between the shape factors at various points on the plate indicate that the shape factor is dependant on position on the plate. The value at the end of the event is higher close to the plate edge.

The results of the displacement thickness, momentum thickness and shape factor indicates that steady acceleration flow can be equated to developing flow. The flow approaches asymptotic values if the steady acceleration condition is maintained for a period of time. The shape factor is dependant on both the size of the acceleration and the position on the plate.

Figure 7.24: Shape Factor Comparison at Various Plate Positions for the Accelerating Plate

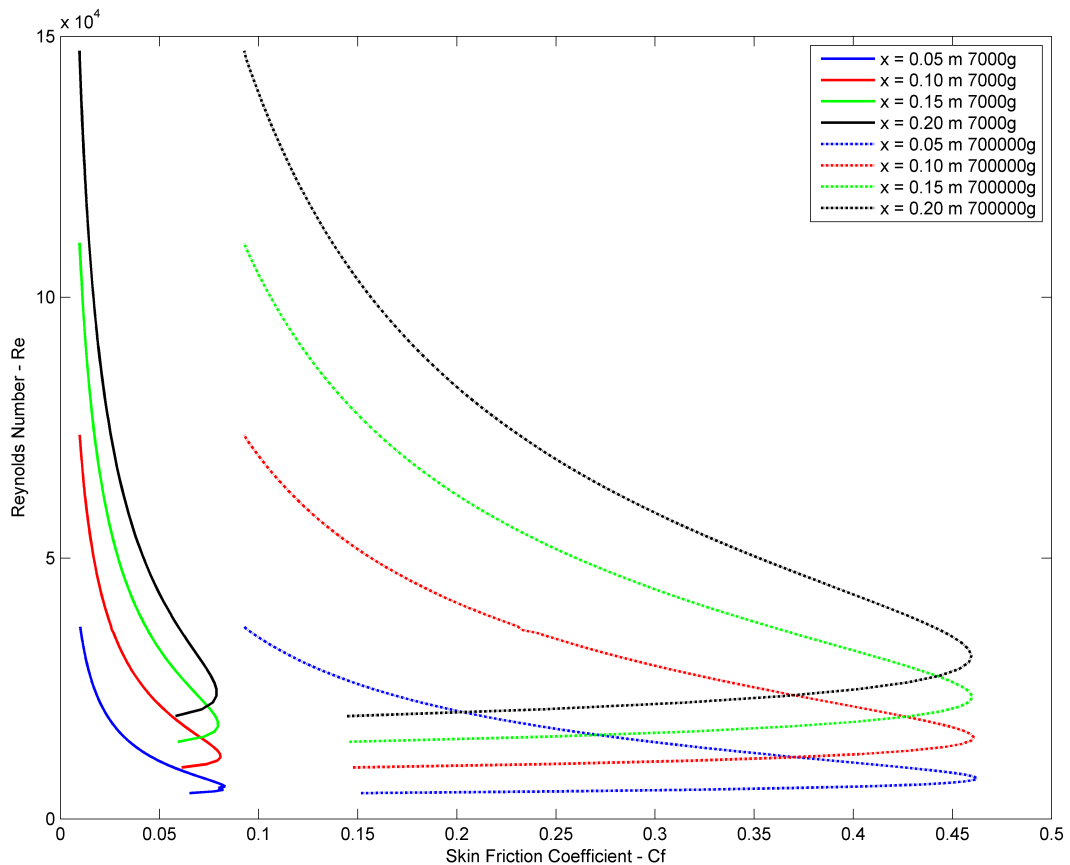


### 7.2.3 Skin Friction Coefficients

The skin friction coefficient is a function of the wall shear stress, the fluid density and the free-stream velocity. It is calculated from the wall shear stress results obtained from the simulation. The skin friction drag is directly proportional to the skin friction coefficient. Skin friction plots give an indication of the drag behaviour of the plate during acceleration. Results for the skin friction coefficient plotted against Reynold number are shown in *Figures 7.25 and 7.26*.

$$\begin{aligned}
 \tau_{wall} &= \mu \left. \frac{\partial \hat{u}}{\partial y} \right|_{wall} \\
 C_f &= \frac{\tau_{wall}}{0.5 \rho U_{\infty}^2} \\
 F_{drag} &= C_f \frac{\rho U_{\infty}^2}{2} A_{wetted}
 \end{aligned}
 \tag{7.16}$$

Figure 7.25: Comparison between Skin Friction Coefficients at Various Free-Stream Reynolds Numbers for Accelerating Conditions



The behaviour of the skin friction coefficient is the same across all regions of the flow. An initial increase is observed and a maximum value reached. The skin friction coefficient is then decreased to a value lower than the value at commencement of the acceleration event. The first derivative approximates

7.2. RESULTS AND DISCUSSION - ACCELERATION

zero at the end of the event, indicating that the skin friction coefficient approaches an asymptotic value (Figure 7.27). The second derivative shows an inflection point at commencement of the event. This is a response to the sudden acceleration of the flat plate. In accelerating flows, from steady state conditions, the skin friction drag have a similar response as the skin friction coefficient. The response is an initial increase in drag. A maximum value is reached early in the event. This maximum drag is dependant on acceleration strength - stronger accelerations lead to higher drag forces. The drag force is reduced to a value lower than the initial starting condition provided that steady acceleration is maintained for a sufficient time duration.

Figure 7.26: Comparison between Skin Friction Coefficients at Various Plate Positions for Accelerating Conditions

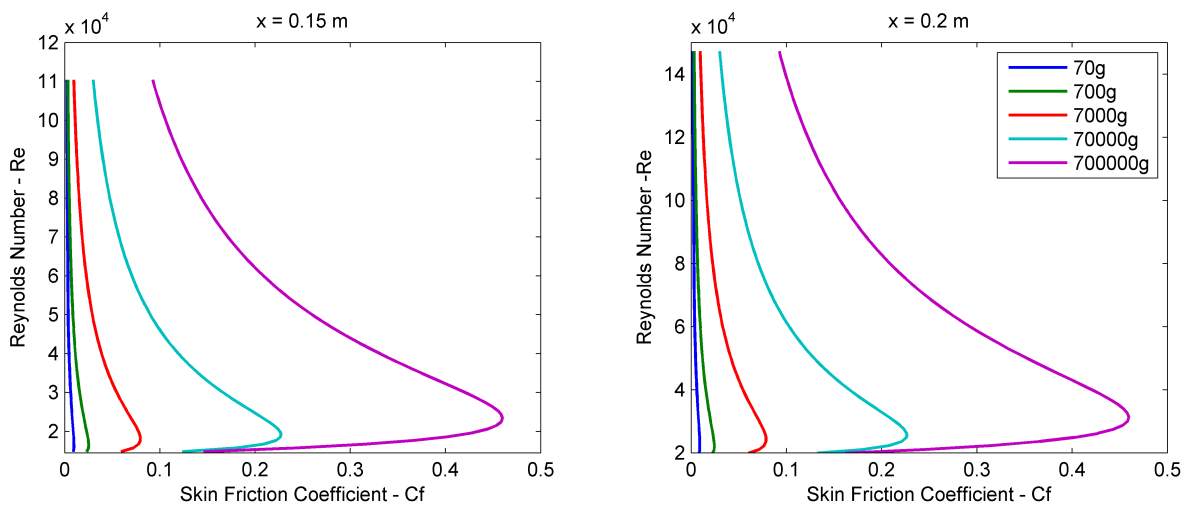
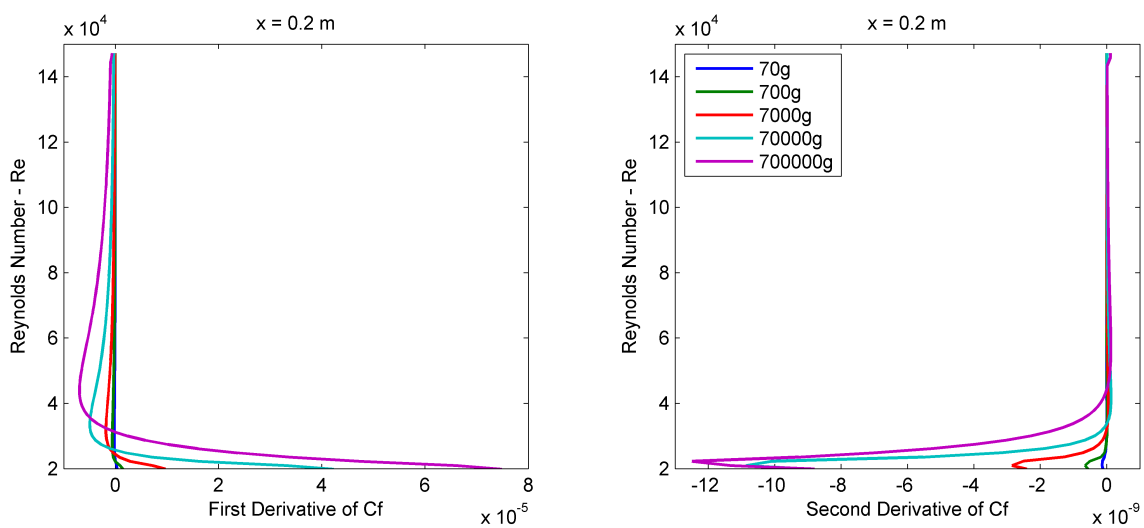


Figure 7.27: First and Second Derivatives of the Skin Friction Coefficients in Accelerating Conditions

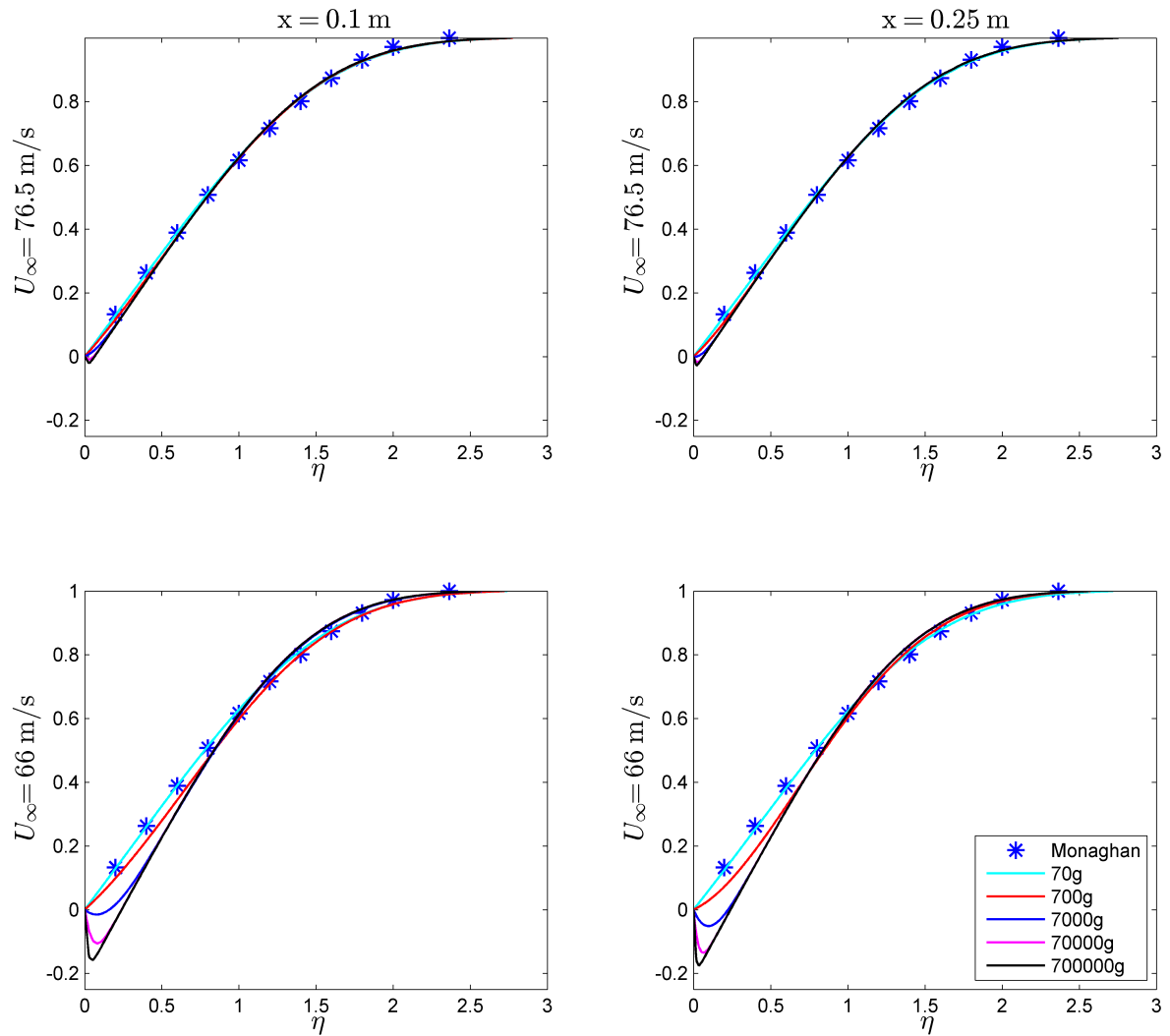


## 7.3 Results and Discussion - Deceleration

### 7.3.1 Velocity Profiles

The decelerating flow analysis was done according to *Table 7.2*. Comparisons were drawn between the non-dimensional velocity profiles at common free stream velocities for different decelerations. The results are indicated in three grouping in *Figures 7.28-7.30*. The groupings were selected to be representative of the total result and for explanation purposes.

Figure 7.28: Non-Dimensional Velocity Profiles: Translating Flat Plate - Deceleration Grouping I





7.3. RESULTS AND DISCUSSION - DECELERATION

Figure 7.29: Non-Dimensional Velocity Profiles: Translating Flat Plate - Deceleration Grouping II

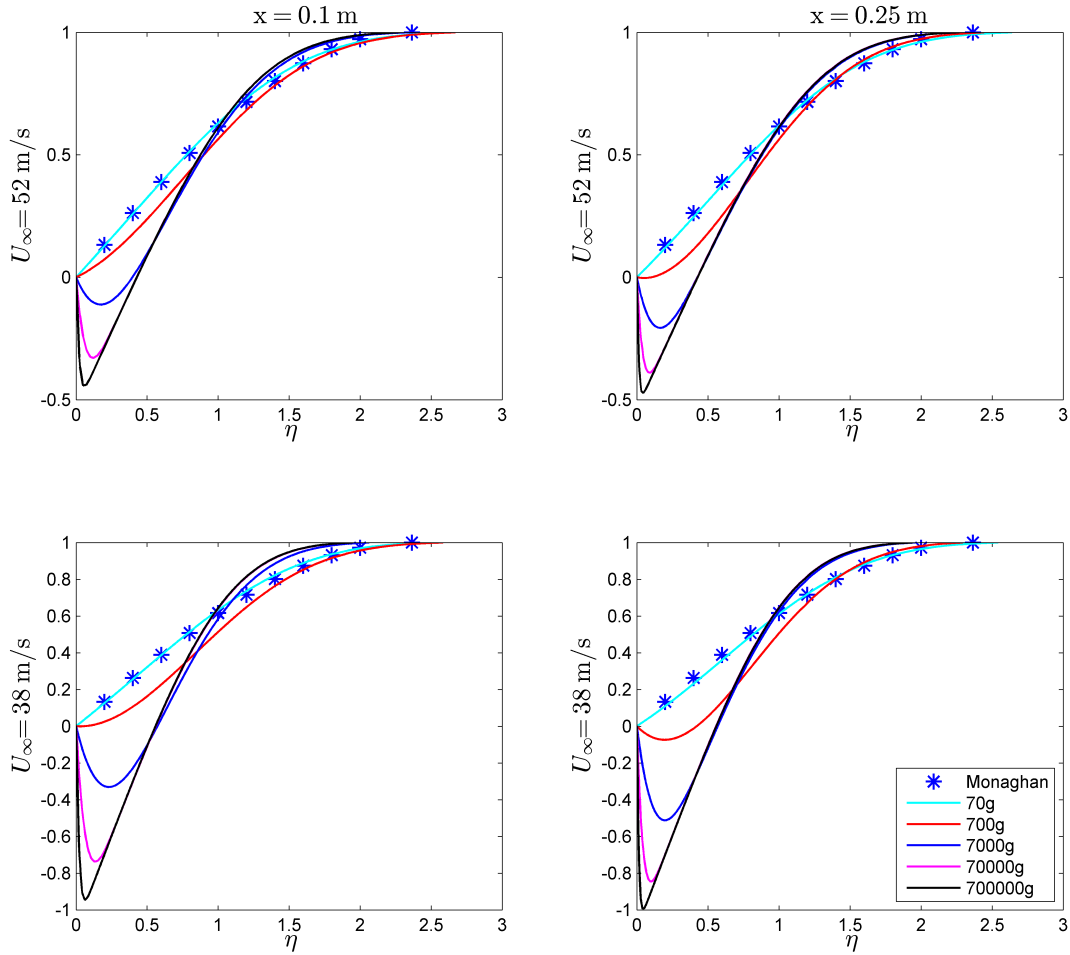
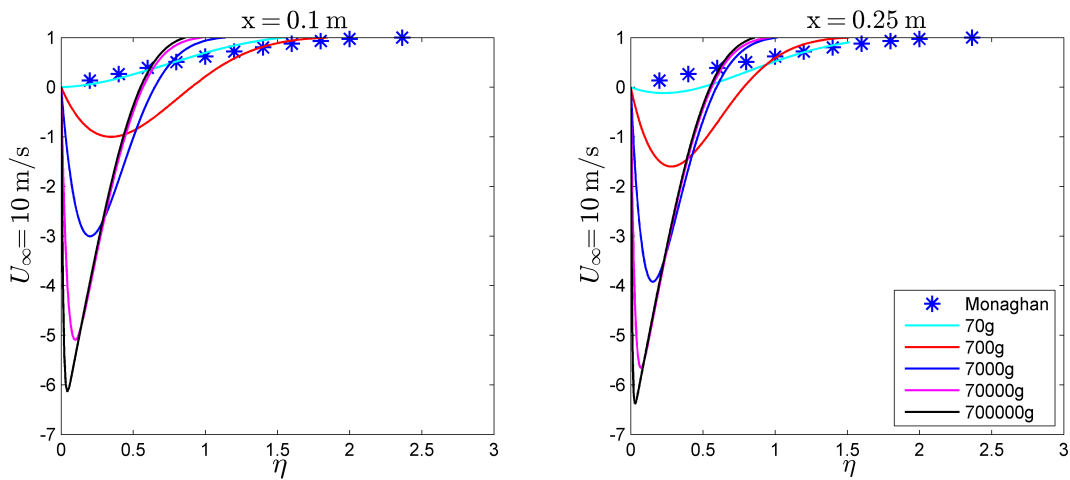


Figure 7.30: Non-Dimensional Velocity Profiles: Translating Flat Plate - Deceleration Grouping III

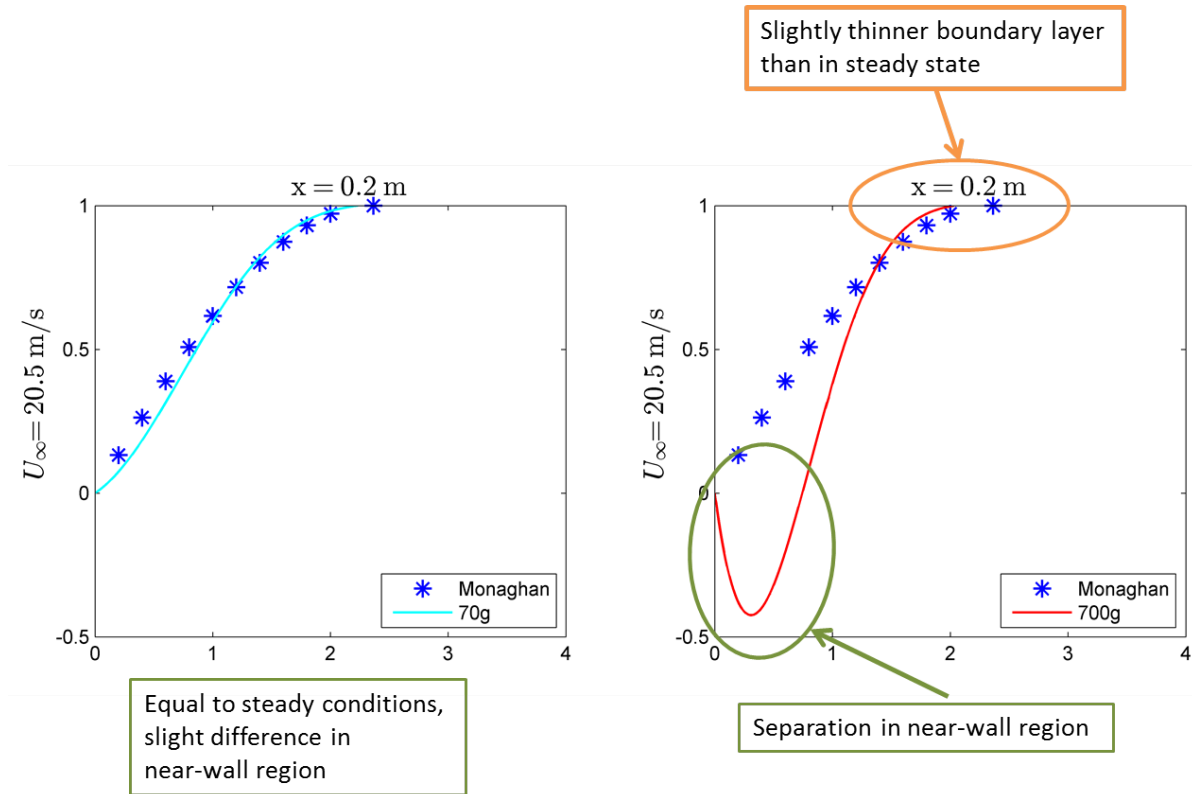


CHAPTER 7. BOUNDARY LAYER RESPONSE IN PURE ROTATION - FLAT PLATE FLOW

Sample results that are representative of the boundary layer responses are shown for explanation purpose in *Figures 7.31* and *7.32*.

The 70 g deceleration case remains equal to steady state conditions for the greatest part of the simulations *Figure 7.31* . There is a slight difference in the near-wall region, but the flow is considered to be marginally dominated by the viscosity.

Figure 7.31: Sample Results and Observations for the Lower Deceleration Cases



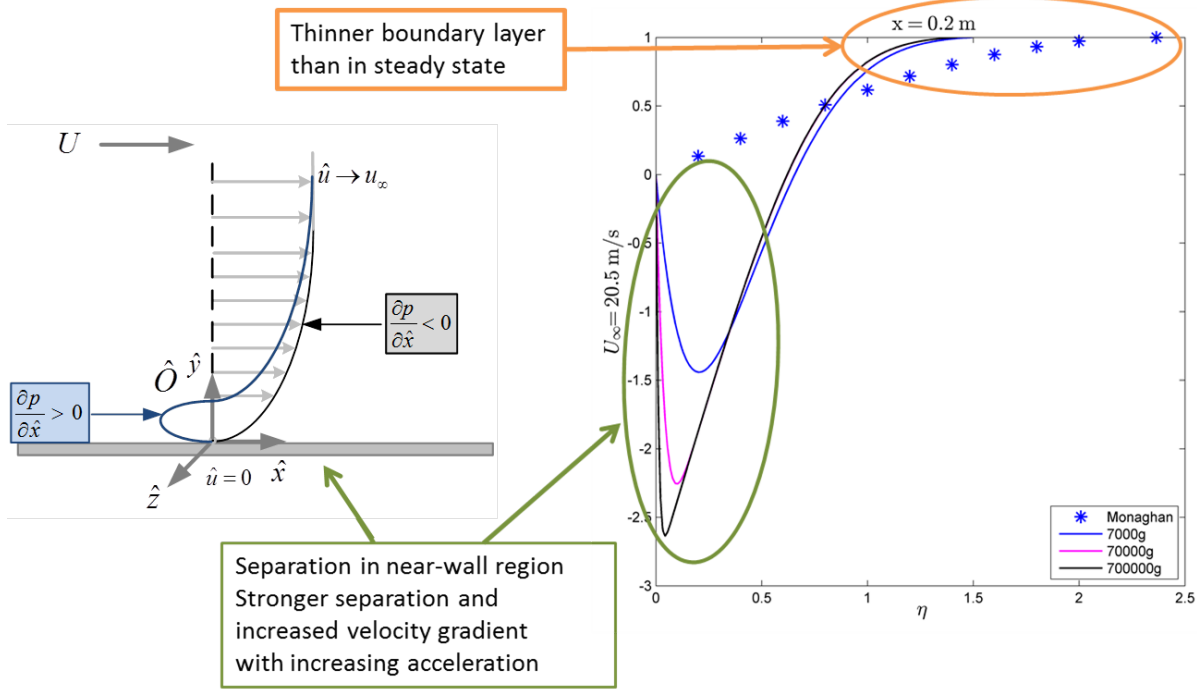
Separation is observed in the near-wall region of the 700 g case (*Figure 7.31*). In the far field the boundary layer is slightly thinner. The non-dimensional free-stream velocity is reached at a slightly lower non-dimensional distance,  $\eta$ , than in the steady state solution. This is due to momentum effects further away from the wall.

In the higher deceleration cases separation is prevalent. The flow reversal becomes stronger with increasing deceleration (*Figure 7.32*). The non-dimensional velocity approximates one at a much lower non-dimensional distance,  $\eta$ . This indicates that the boundary layer is significantly thinner in deceleration than in the steady state. The flow is dominated by the momentum which originates from flow deceleration.

The result in this section are comparable with a study done by Back [28]. He obtained similar profiles by investigating the effect of inducing pressure changes in the boundary layer. In the Navier-Stokes equations, changes in deceleration have a similar effect on the boundary layer since it is also located on the right hand side of *Equation 7.8*. The phenomenon can be explained in the inertial frame.



Figure 7.32: Sample Results and Observations for the Higher Deceleration Cases



The plate wall has a certain velocity and the bulk flow is stationary. The velocity profile extends from the high velocity to zero. Now the plate is decelerated, for instance from 80 m/s to 70 m/s. The velocity at the wall are then 70 m/s, but due to the historic profile at 80 m/s there is a certain amount of momentum and energy in the boundary layer. This momentum and energy is subjected to the laws of conservation of momentum and energy. If the deceleration is low enough (in this case below 70g) the boundary layer have time to adjust to the changing conditions and the "excess" momentum and energy diffuse into the bulk flow. However, if the deceleration is high enough (in this case above 70g) there is not time for diffusion to take place and the boundary layer separates. The mechanism for this is further discussed in the paragraphs below.

Equations 5.75 and 5.76 was used to determined the boundary layer equations that pertain to flow in arbitrary translation. The same equations are relevant here.

**x-momentum**

$$\frac{\partial \hat{\rho} \hat{u}}{\partial t} + \hat{u} \frac{\partial \hat{\rho} \hat{u}}{\partial \hat{x}} + \hat{v} \frac{\partial \hat{\rho} \hat{u}}{\partial \hat{y}} = -\frac{\partial \hat{p}}{\partial \hat{x}} + \frac{\partial}{\partial \hat{y}} \left( \hat{\mu} \frac{\partial \hat{u}}{\partial \hat{y}} \right) - \frac{\partial \hat{\rho} V_x}{\partial t} \quad (7.17)$$

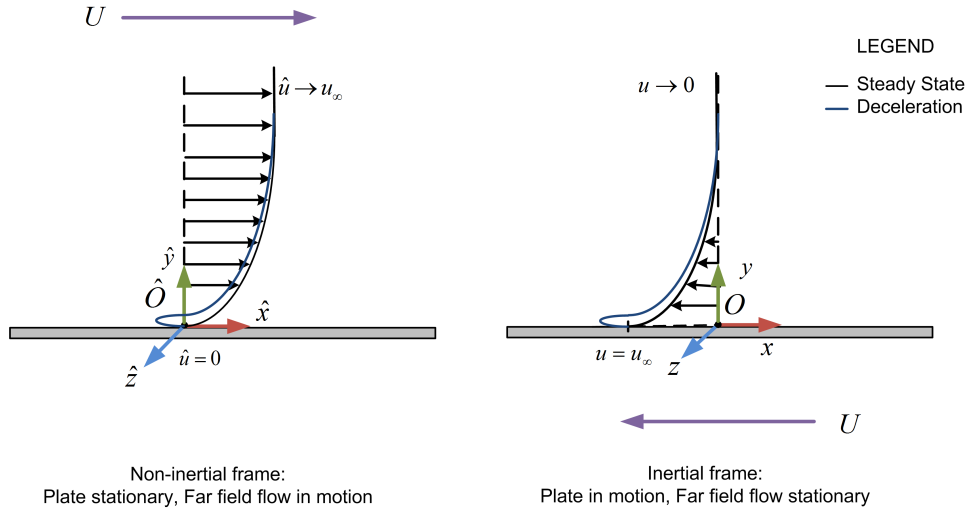
**y-momentum**

$$0 = -\frac{\partial \hat{p}}{\partial \hat{y}} \quad (7.18)$$

In this case however, the non-inertial terms on the right hand side of the equation becomes a sink which causes the separation of the flow (Figure 7.33).

CHAPTER 7. BOUNDARY LAYER RESPONSE IN PURE ROTATION - FLAT PLATE FLOW

Figure 7.33: Boundary Layer Profiles for Steady and Deceleration Conditions



- Absolute Deceleration

$$\frac{\partial \rho u}{\partial t} + u \frac{\partial \rho u}{\partial x} + v \frac{\partial \rho u}{\partial y} = -\frac{\partial p}{\partial x} + \frac{\partial}{\partial y} \left( \mu \frac{\partial u}{\partial y} \right)$$

- Relative Deceleration

$$\frac{\partial \hat{\rho} \hat{u}}{\partial t} + \hat{u} \frac{\partial \hat{\rho} \hat{u}}{\partial \hat{x}} + \hat{v} \frac{\partial \hat{\rho} \hat{u}}{\partial \hat{y}} = -\frac{\partial \hat{p}}{\partial \hat{x}} + \frac{\partial}{\partial \hat{y}} \left( \hat{\mu} \frac{\partial \hat{u}}{\partial \hat{y}} \right) - \frac{\partial \hat{\rho} V_x}{\partial t}$$

- Frame Deceleration prescribed

The deceleration of the relative frame causes a momentum sink on the right hand side of the momentum equation. This leads to a decrease on the left hand side in the material derivative.

$$\frac{\partial \hat{\rho} \hat{u}}{\partial t} + \hat{u} \frac{\partial \hat{\rho} \hat{u}}{\partial \hat{x}} + \hat{v} \frac{\partial \hat{\rho} \hat{u}}{\partial \hat{y}} = -\frac{\partial \hat{p}}{\partial \hat{x}} + \frac{\partial}{\partial \hat{y}} \left( \hat{\mu} \frac{\partial \hat{u}}{\partial \hat{y}} \right) - \frac{\partial \hat{\rho} V_x}{\partial t}$$

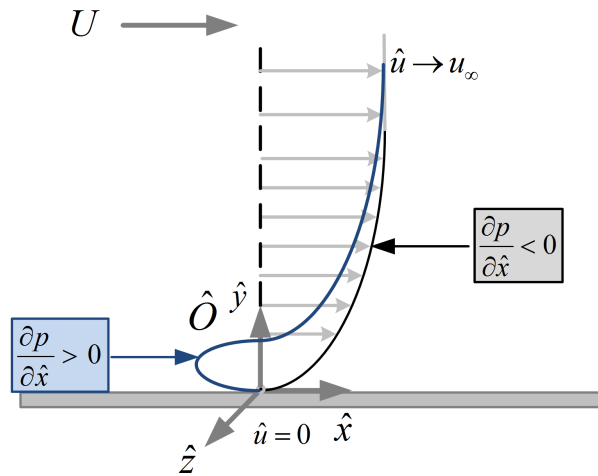
The decrease of the material derivative lead to a decrease in  $\hat{u}$ , which in turn causes a decrease in the velocity gradient at the wall.

$$\frac{\partial \hat{\rho} \hat{u}}{\partial t} + \hat{u} \frac{\partial \hat{\rho} \hat{u}}{\partial \hat{x}} + \hat{v} \frac{\partial \hat{\rho} \hat{u}}{\partial \hat{y}} = -\frac{\partial \hat{p}}{\partial \hat{x}} + \frac{\partial}{\partial \hat{y}} \left( \hat{\mu} \frac{\partial \hat{u}}{\partial \hat{y}} \right) - \frac{\partial \hat{\rho} V_x}{\partial t}$$

A decrease in the near-wall velocity gradient causes an increase in the pressure gradient, since the terms have opposite signs. The pressure gradient increases to such an extent that an adverse pressure gradient forms and the flow separates.

$$\frac{\partial \hat{\rho} \hat{u}}{\partial t} + \hat{u} \frac{\partial \hat{\rho} \hat{u}}{\partial \hat{x}} + \hat{v} \frac{\partial \hat{\rho} \hat{u}}{\partial \hat{y}} = - \frac{\partial \hat{p}}{\partial \hat{x}} + \frac{\partial}{\partial \hat{y}} \left( \hat{\mu} \frac{\partial \hat{u}}{\partial \hat{y}} \right) - \frac{\partial \hat{\rho} V_x}{\partial t}$$

Figure 7.34: Adverse Pressure Gradient for Decelerating Conditions



The same three distinct regions that were identified in the accelerating case, presented itself here (Figure 7.35):

- Region I - Viscous Dominant.** The 70 g case falls within this region. In comparison with the steady state non-dimensional result, there is no observed difference in the profile. The time scale at which the event occurs is low enough to allow time for the viscous forces in the boundary layer to adjust to the changes and keep the steady state profile.

Deceleration Reaction - Type I:

$$\frac{\partial \hat{\rho} \hat{u}}{\partial t} + \hat{u} \frac{\partial \hat{\rho} \hat{u}}{\partial \hat{x}} + \hat{v} \frac{\partial \hat{\rho} \hat{u}}{\partial \hat{y}} = - \frac{\partial \hat{p}}{\partial \hat{x}} + \frac{\partial}{\partial \hat{y}} \left( \hat{\mu} \frac{\partial \hat{u}}{\partial \hat{y}} \right) - \frac{\partial \hat{\rho} V_x}{\partial t}$$

- Region II - Viscous-Momentum Interaction.** The 700 g deceleration case falls within this region. The region is characterized by disturbances in the boundary layer due to the interaction between the viscous and momentum effects. Separation of the boundary layer occurs almost immediately and are directly proportional to the deceleration. In the near-wall regions the momentum effects dominates, while close to the boundary layer edge, the viscous effects dominate. In the upper regions of the boundary layer the profile conforms to the steady state result.

CHAPTER 7. BOUNDARY LAYER RESPONSE IN PURE ROTATION - FLAT PLATE FLOW

Deceleration Response - Type II:

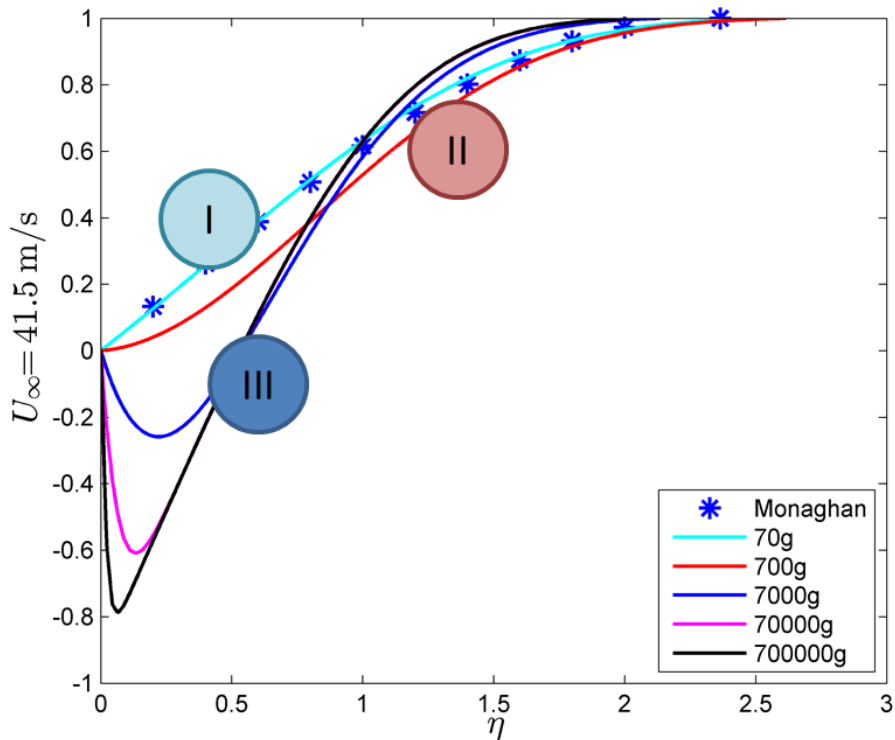
$$\frac{\partial \hat{\rho} \hat{u}}{\partial t} + \hat{u} \frac{\partial \hat{\rho} \hat{u}}{\partial \hat{x}} + \hat{v} \frac{\partial \hat{\rho} \hat{u}}{\partial \hat{y}} = -\frac{\partial \hat{p}}{\partial \hat{x}} + \frac{\partial}{\partial \hat{y}} \hat{\mu} \frac{\partial \hat{u}}{\partial \hat{y}} - \frac{\partial \hat{\rho} V_x}{\partial t}$$

- **Region III - Momentum Dominant.** The three higher deceleration cases falls within this region. The momentum effects due to deceleration dominates here. Separation occurs very early and the boundary layer remains separated throughout the plate. The velocity gradient close to the wall is very steep and directly proportional to the deceleration. The boundary layer height is decreased with almost the same distance for all the cases in this region. Similarity, that depends on the time scales involved, is present in the region.

Deceleration Response - Type III:

$$\frac{\partial \hat{\rho} \hat{u}}{\partial t} + \hat{u} \frac{\partial \hat{\rho} \hat{u}}{\partial \hat{x}} + \hat{v} \frac{\partial \hat{\rho} \hat{u}}{\partial \hat{y}} = -\frac{\partial \hat{p}}{\partial \hat{x}} + \frac{\partial}{\partial \hat{y}} \hat{\mu} \frac{\partial \hat{u}}{\partial \hat{y}} - \frac{\partial \hat{\rho} V_x}{\partial t}$$

Figure 7.35: Acceleration Response Regions by Type in Simulation Results



### 7.3.2 Boundary Layer Parameters

The boundary layer parameters were determined here in the same manner as discussed in *Section 7.2.2*. The results of the displacement thickness for a decelerating plate are shown in *Figures 7.36-7.39*.

Figure 7.36: Displacement Thickness Comparison for the Decelerating Flat Plate

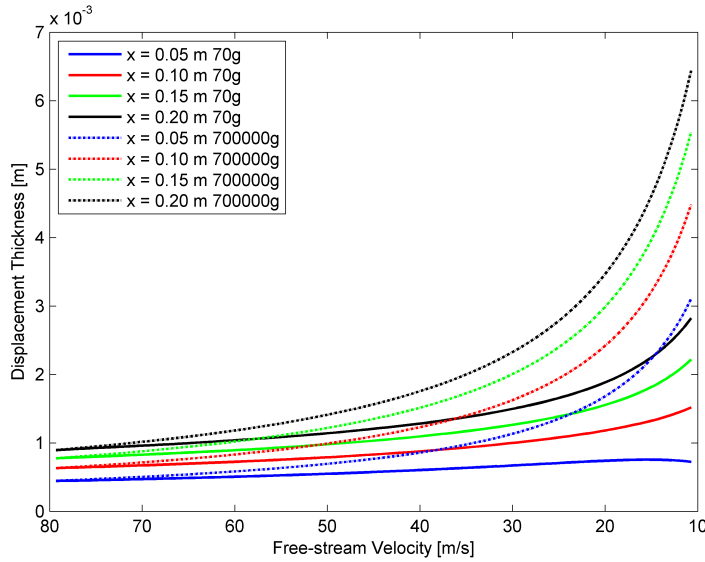
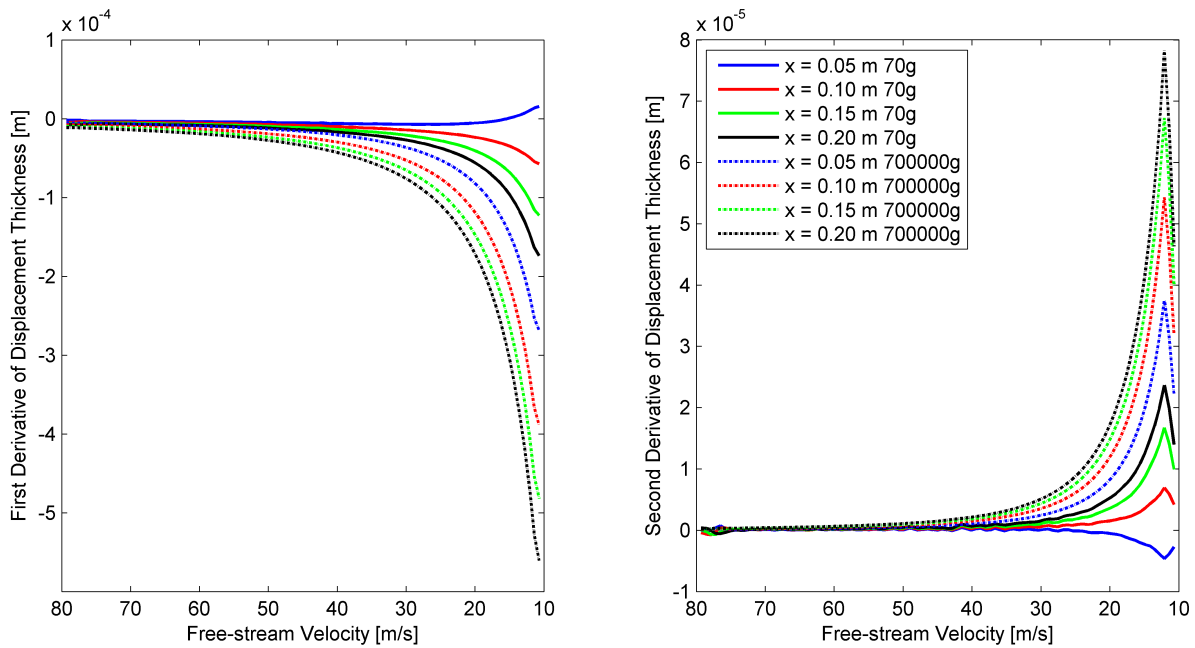


Figure 7.37: Displacement Thickness Comparison for the Decelerating Flat Plate



CHAPTER 7. BOUNDARY LAYER RESPONSE IN PURE ROTATION - FLAT PLATE FLOW

Figure 7.38: Displacement Thickness Comparison at  $x = 0.05$  m in Decelerating Conditions

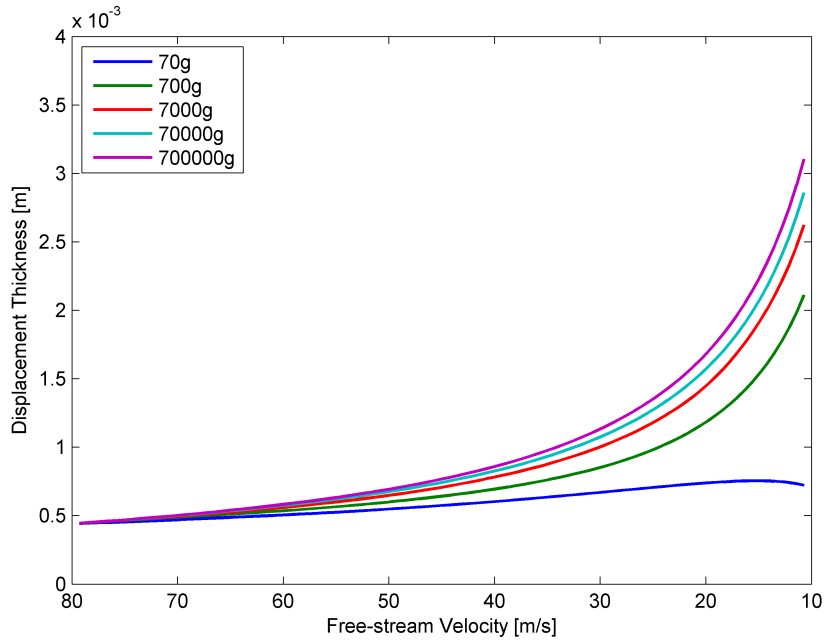
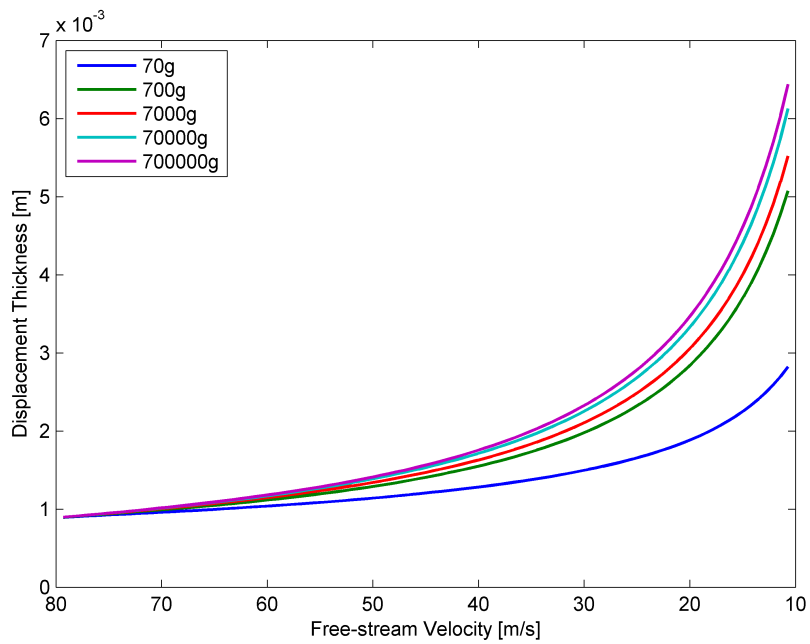


Figure 7.39: Displacement Thickness Comparison at  $x = 0.2$  m in Decelerating Conditions

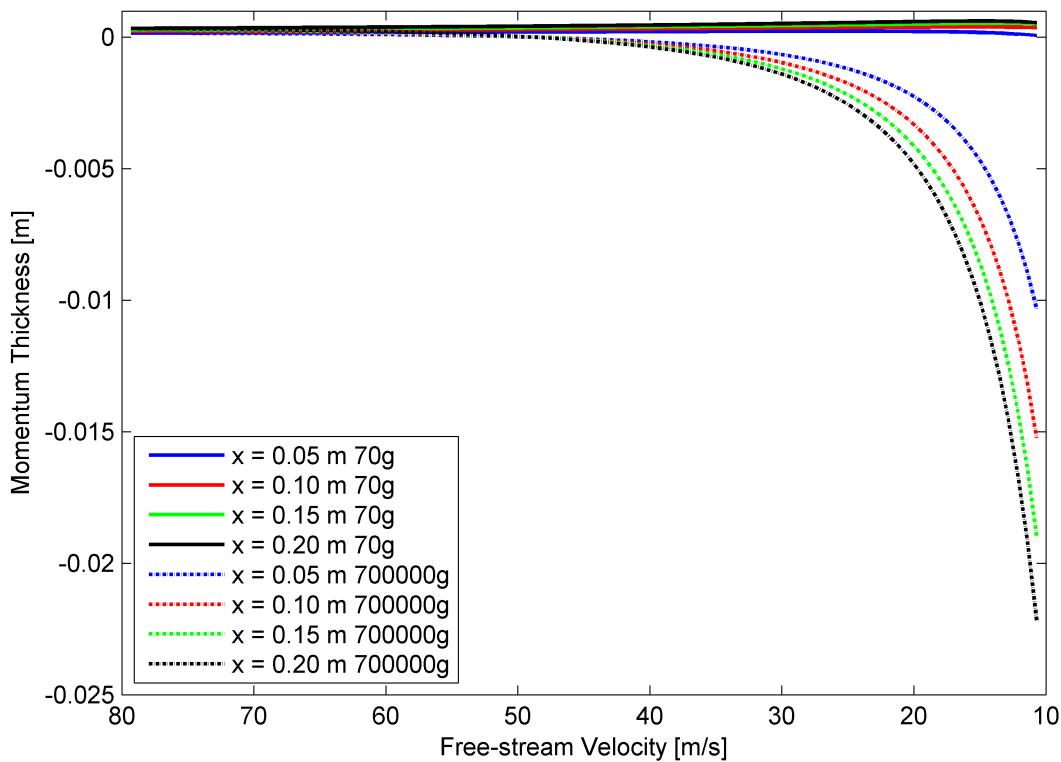


7.3. RESULTS AND DISCUSSION - DECELERATION

The plots indicate that all three regions, as previously defined, react similarly to the deceleration event. The displacement thickness increases in decreasing free-stream velocity. The displaced value is directly proportional to deceleration strength. The first derivative is divergent, indicating that the displacement value do not approximate an asymptotic value. It continues to increase in decelerating flow. The second derivative shows an inflection point near the end of the deceleration event. This is in contrast to the acceleration case where the inflection point occurred at the beginning of the acceleration event. The inflection point here is a result of a hysteresis-like response of the boundary layer mass flow to deceleration and is dependant on the strength of deceleration.

The momentum thickness plots are displayed in *Figures 7.40-7.43*. The momentum thickness for all three regions, as previously defined, responds in a similar manner to deceleration. The momentum thickness diverges with decreasing free-stream velocity. This is confirmed with the diverging first derivative. An inflection point is shown in the second derivative. As in the displacement thickness, this is a hysteresis like response to deceleration of the plate.

Figure 7.40: Momentum Thickness Comparison for the Decelerating Flat Plate



CHAPTER 7. BOUNDARY LAYER RESPONSE IN PURE ROTATION - FLAT PLATE FLOW

Figure 7.41: Momentum Thickness Comparison for the Decelerating Flat Plate

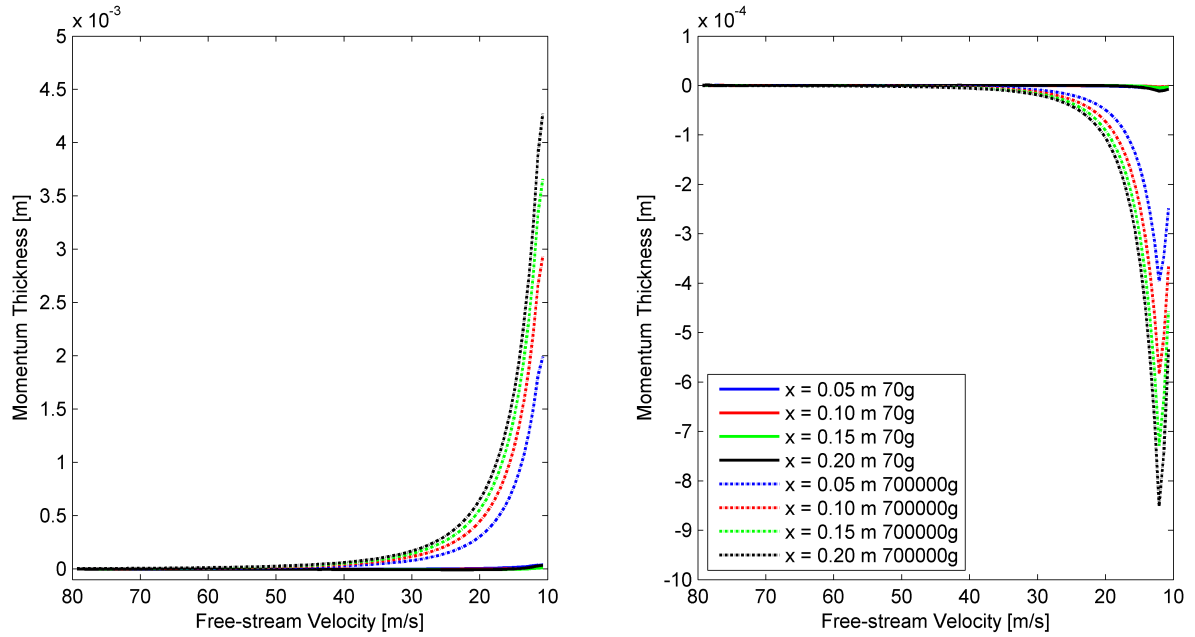


Figure 7.42: Momentum Thickness Comparison at  $x = 0.05$  m in Decelerating Conditions

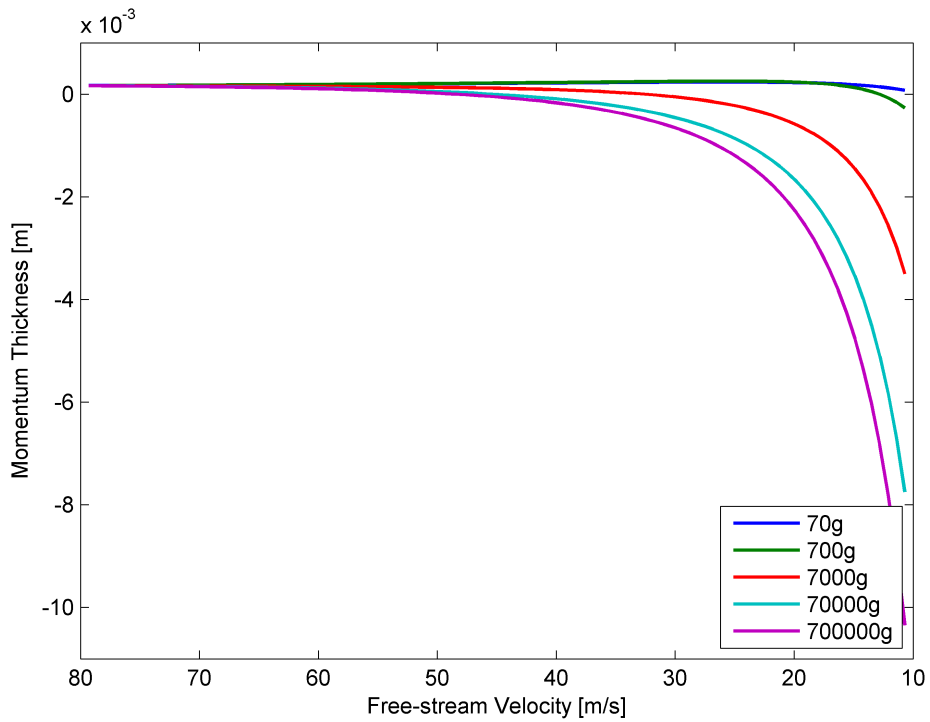
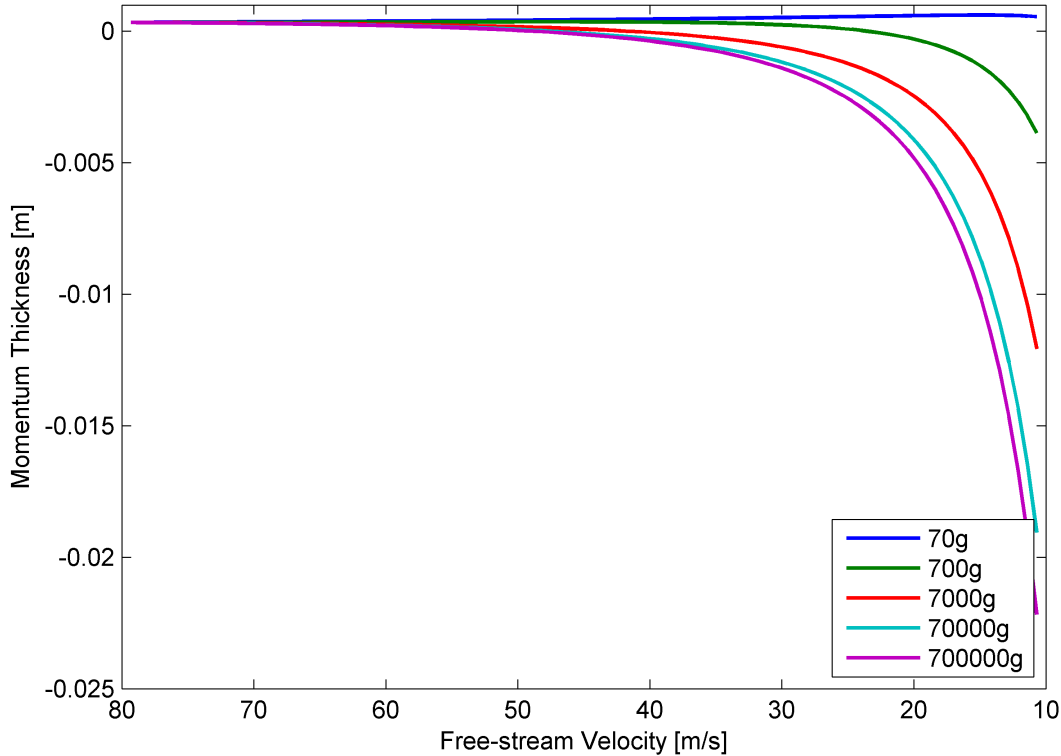




Figure 7.43: Momentum Thickness Comparison at  $x = 0.2$  m in Decelerating Conditions



The shape factor was determined from the results above. The response of the shape factor to deceleration is depicted in *Figures 7.44-7.46*.

The shape factors of all three previously defined regions response to deceleration in the same manner. At commencement of the deceleration event, the shape factor is at the steady state value. It is then increased to a point where a discontinuity is present. The shape factor value approaches the asymptote on the left hand side of the discontinuity. On the right hand side of the discontinuity, the shape factor approaches the asymptote with a negative value. It continue to increase, whilst remaining negative until the end of the event. The occurrence of the discontinuity is dependant on the strength of the deceleration. In higher deceleration cases, the onset of the discontinuity is earlier than for lower decelerations. It occurs at all positions on the flat plate. This behaviour is a result of the flow reversal. Flow reversal takes place at shape factor values between 2.6 and 2.8 for steady state conditions. From the previous subsection it was observed that the flow in this case separates very early in the deceleration event. The subsequent strength of the reversal causes a negative momentum thickness, which is where the discontinuity manifests. A negative shape factor value is undefined in the literature both for computational and numerical work. This condition is not physically possible. A negative shape factor can be define here as a flow with abnormally strong reversal to the extent that the momentum thickness is negative. Furthermore, it is a flow characterised by the resultant momentum in the boundary layer being in the reversed

CHAPTER 7. BOUNDARY LAYER RESPONSE IN PURE ROTATION - FLAT PLATE FLOW

flow direction. However, the occurrence of the discontinuity provides an indication of the strength of the reversal. It subsequently also provides the point where the momentum in the reversed component of the boundary layer, is equal to the momentum that has not yet reversed.

Figure 7.44: Shape Factor Comparison for the Decelerating Flat Plate

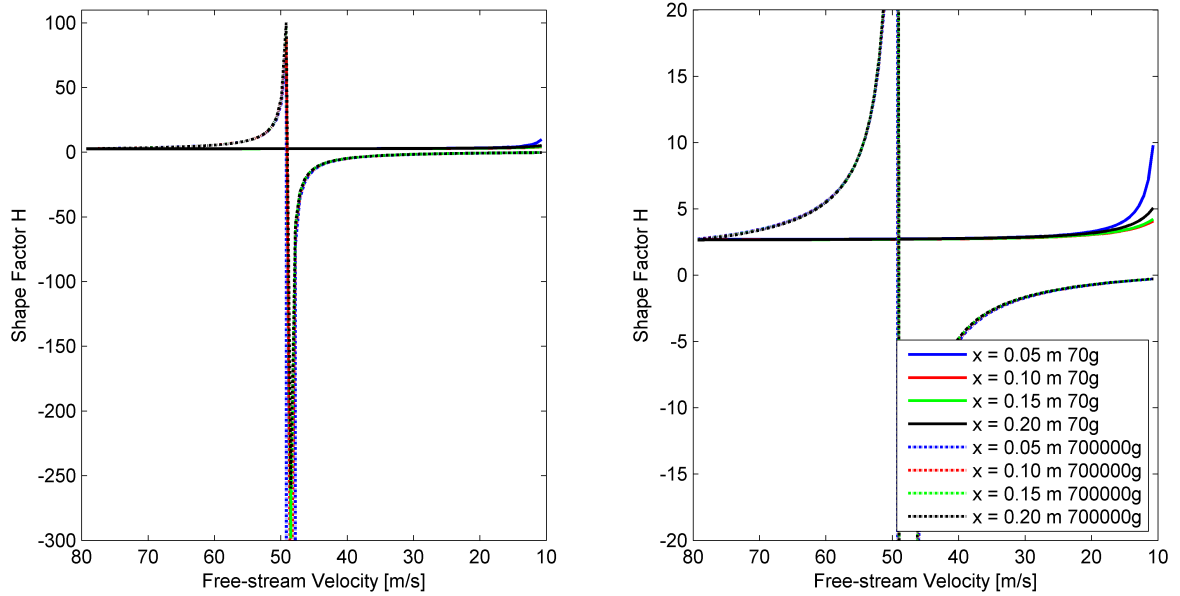
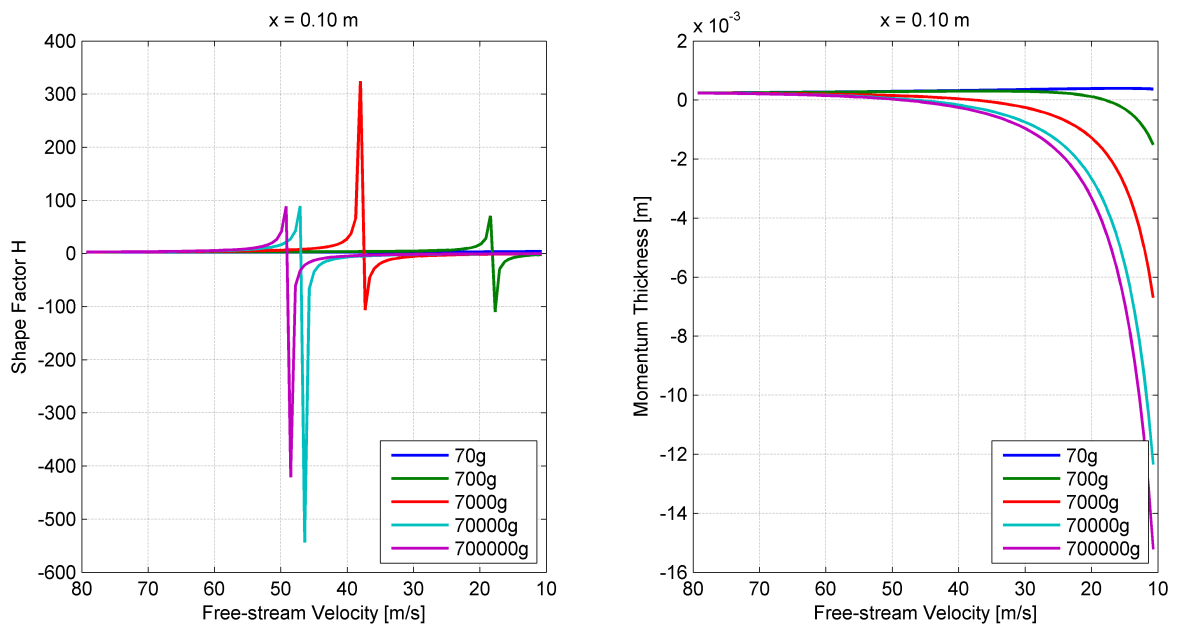
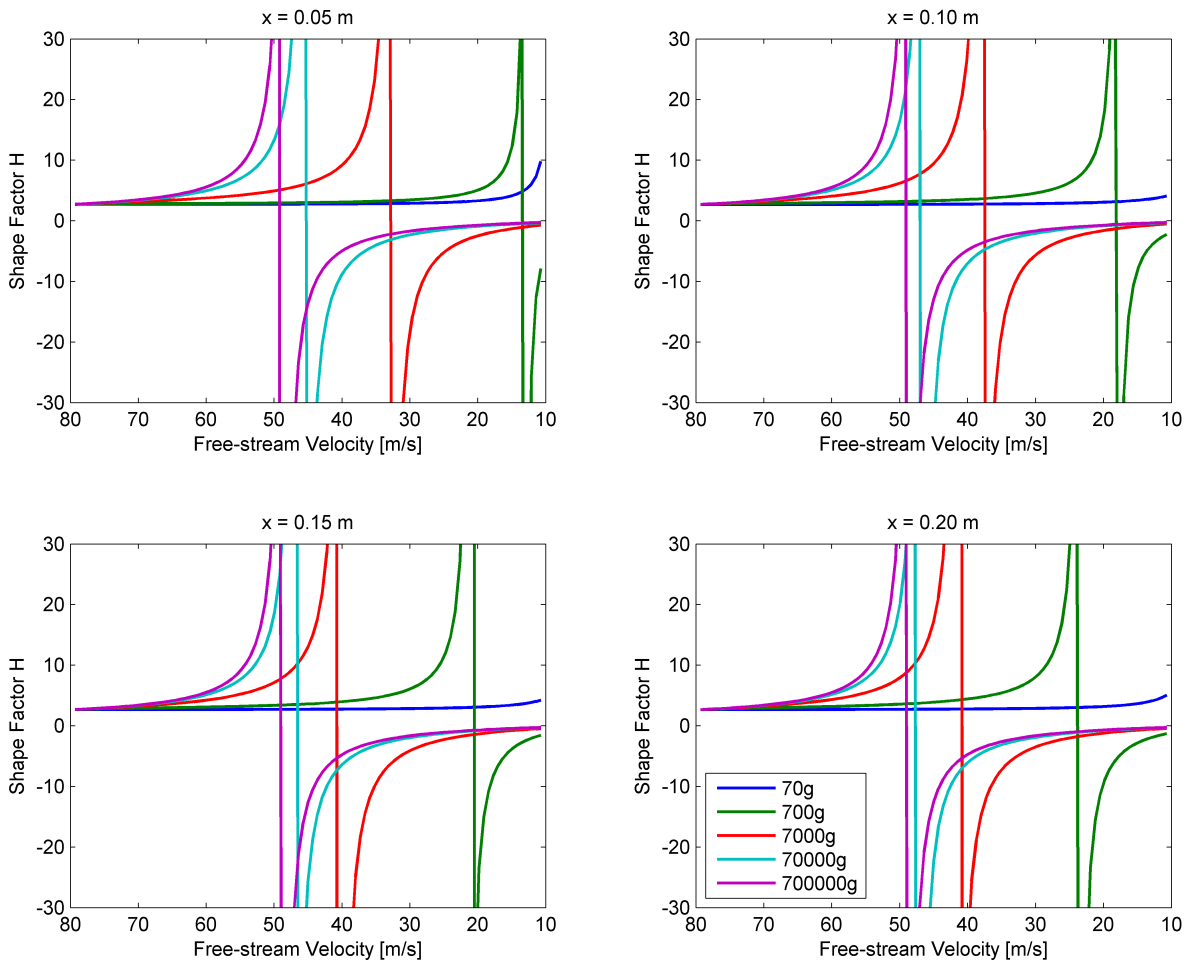


Figure 7.45: Comparison of Shape Factor Discontinuities and Momentum Thickness for the Decelerating Flat Plate



7.3. RESULTS AND DISCUSSION - DECELERATION

Figure 7.46: Shape Factor Comparison at Various Plate Positions in Decelerating Conditions



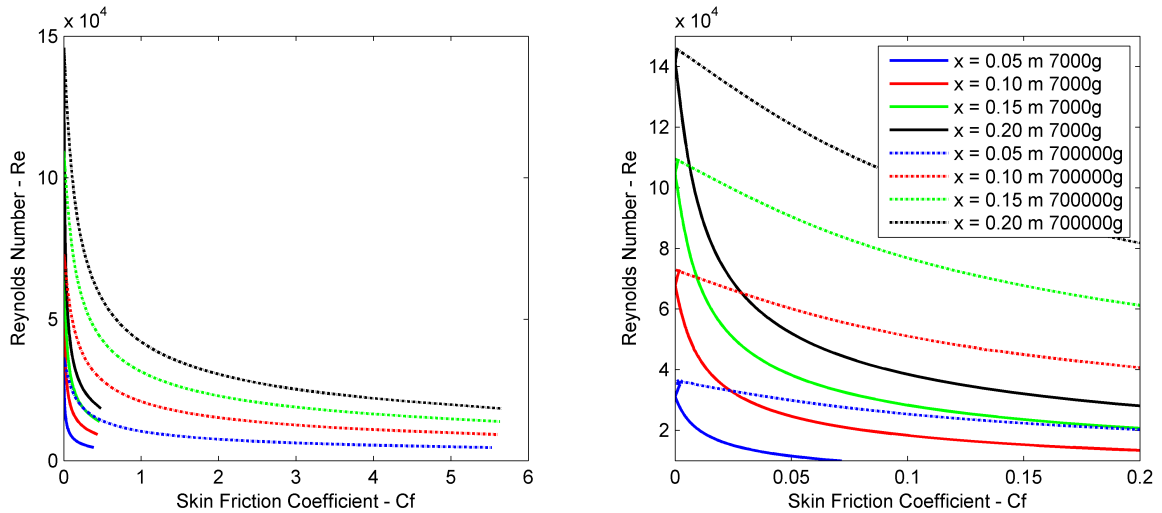
### 7.3.3 Skin Friction Coefficients

The skin friction coefficients were determined in the same manner as for the accelerating cases.

$$\begin{aligned}
 \tau_{wall} &= \mu \frac{\partial \hat{u}}{\partial y} \Big|_{wall} \\
 C_f &= \frac{\tau_{wall}}{0.5 \rho U_{\infty}^2} \\
 F_{drag} &= C_f \frac{\rho U_{\infty}^2}{2} A_{wetted}
 \end{aligned}
 \tag{7.19}$$

The results are shown in *Figures 7.47-7.49*.

Figure 7.47: Comparison between Skin Friction Coefficients at Various Free-Stream Reynolds Numbers for Decelerating Conditions



The skin friction coefficients associated with the three respective regions, reacts in a similar manner to decelerating conditions. At high Reynolds numbers, at commencement of the deceleration event, the skin friction is equal to the steady state value. The value for skin friction increases rapidly as the event progresses. The first derivative is divergent, which indicates that the skin friction coefficient continues to increase (*Figure 7.49*). The value are directly proportional to deceleration strength. The stronger the deceleration is the higher the skin friction values (and subsequently the drag force) are on the plate.

7.3. RESULTS AND DISCUSSION - DECELERATION

Figure 7.48: Comparison between Skin Friction Coefficients at Various Plate Positions for Decelerating Conditions

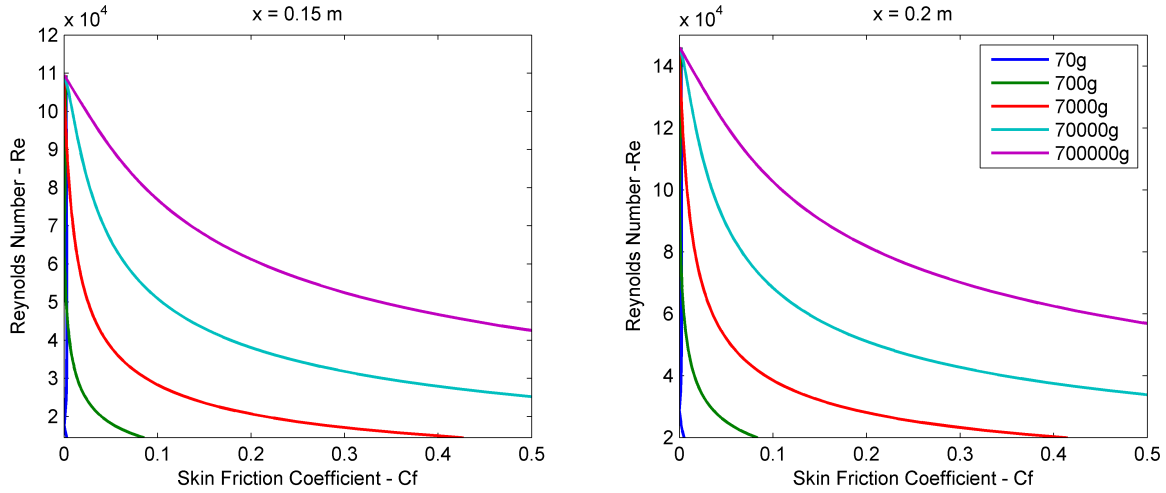
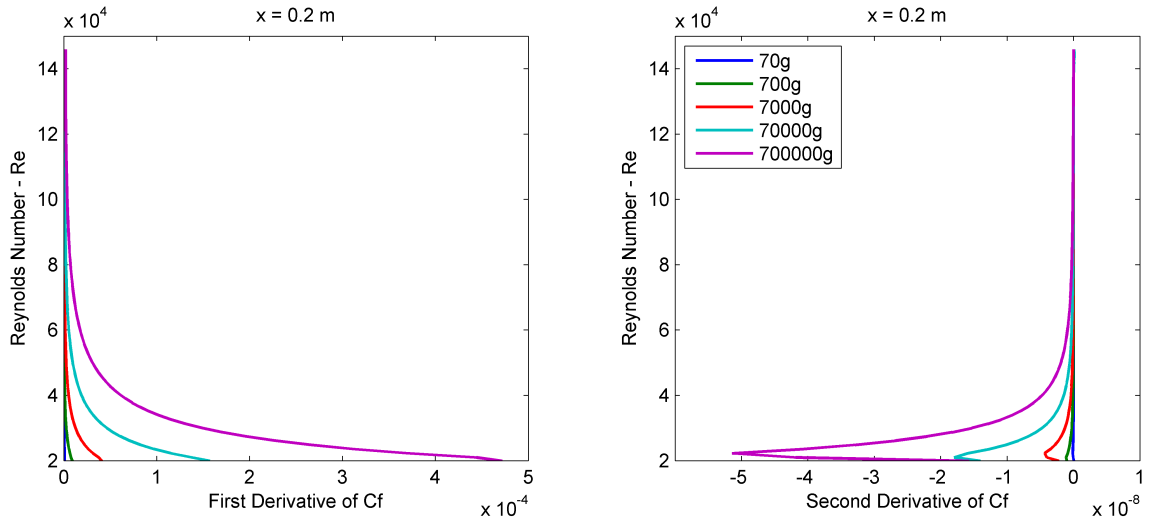


Figure 7.49: First and Second Derivatives of the Skin Friction Coefficients in Decelerating Conditions



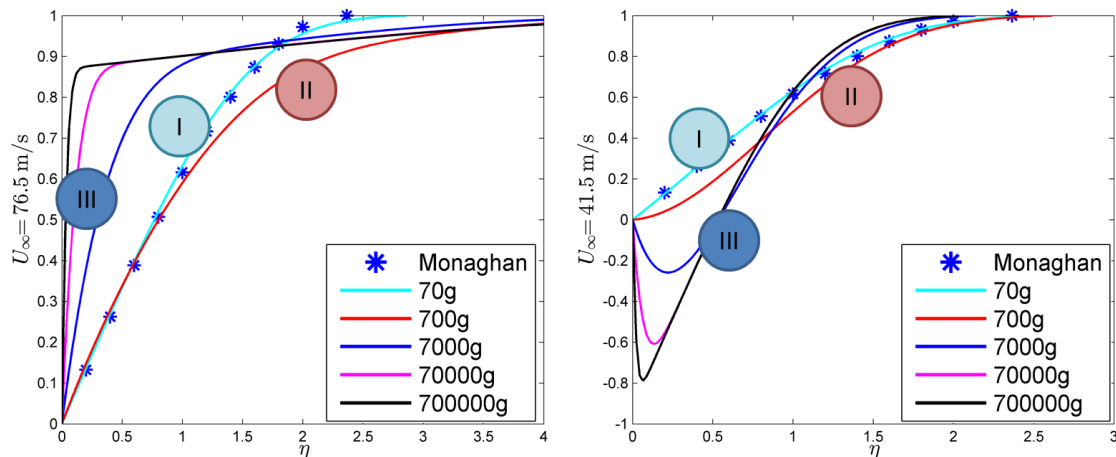
## 7.4 Closure

This chapter aimed at characterising the response of the laminar boundary layer to arbitrary translation. The most important results are as follows:

- 1) The definition of three types of responses to arbitrary translation for a flat plate.
- 2) The proposal of a mechanism proving an explanation for response types.
- 3) The characterisation of the response of the shape factor to arbitrary translation.
- 4) The characterisation of the response of the skin friction coefficient to arbitrary translation.

Three types of responses to changing conditions in the relative velocity have been identified as shown in *Figure 7.50*.

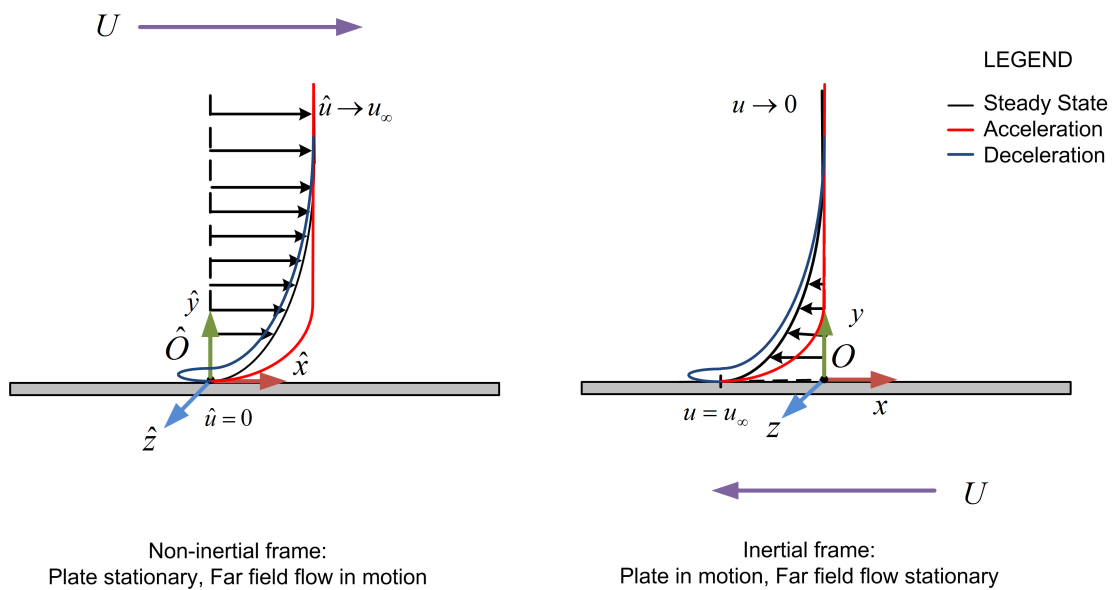
Figure 7.50: Response Types for Accelerating and Decelerating Conditions on a Flat Plate



- **Response Type I**, which is viscous dominant. The time scale at which the event occurs is low enough to allow time for the viscous forces in the boundary layer to adjust to the changes and keep the steady state profile.
- **Response Type II**, where the time scales of the viscous and momentum forces are of the same order. Certain regions of the boundary layer are dominated by viscosity and others by momentum. In acceleration the viscosity dominates in the near-wall region and momentum in the far field regions. In deceleration momentum dominates in the near-wall region and viscosity in the far field.
- **Response Type III**, which is dominated by momentum. The time scale at which the event occurs is too high for viscous forces in the boundary layer to adjust to the changes and keep the steady state profile. In deceleration the near-wall velocity profile increases with increasing deceleration. In deceleration separation occurs as a result of momentum changes in the flow.

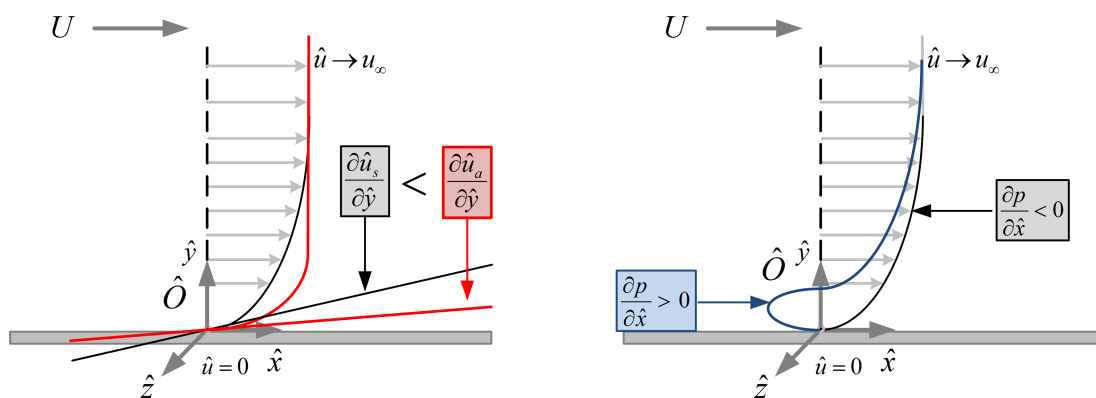
The generalised behaviour of a flat plate subjected to arbitrary translation is depicted in *Figure 7.51*. Accelerating velocity profiles has steeper gradients in the near wall region and a lightly thicker boundary layer when compared to the steady state result. The gradient are proportional to the acceleration parameter. Decelerating velocity profiles indicates that flow reversal takes place (which is proportional to the deceleration) and the boundary layer are thinner than calculated in the steady state case.

Figure 7.51: Boundary Layer Profiles for Steady, Acceleration and Deceleration Conditions on a Flat Plate



A mechanism was proposed for the response of the boundary layer using the boundary layer equation below. The mechanism is depicted in *Figure 7.52*.

Figure 7.52: Accelerating and Decelerating Mechanisms of Boundary Layer Response on a Flat Plate



$$\frac{\partial \rho \hat{u}}{\partial t} + \hat{u} \frac{\partial \rho \hat{u}}{\partial \hat{x}} + \hat{v} \frac{\partial \rho \hat{u}}{\partial \hat{y}} = - \frac{\partial \hat{p}}{\partial \hat{x}} + \frac{\partial}{\partial \hat{y}} \left( \hat{\mu} \frac{\partial \hat{u}}{\partial \hat{y}} \right) - \frac{\partial \rho V_x}{\partial t}$$

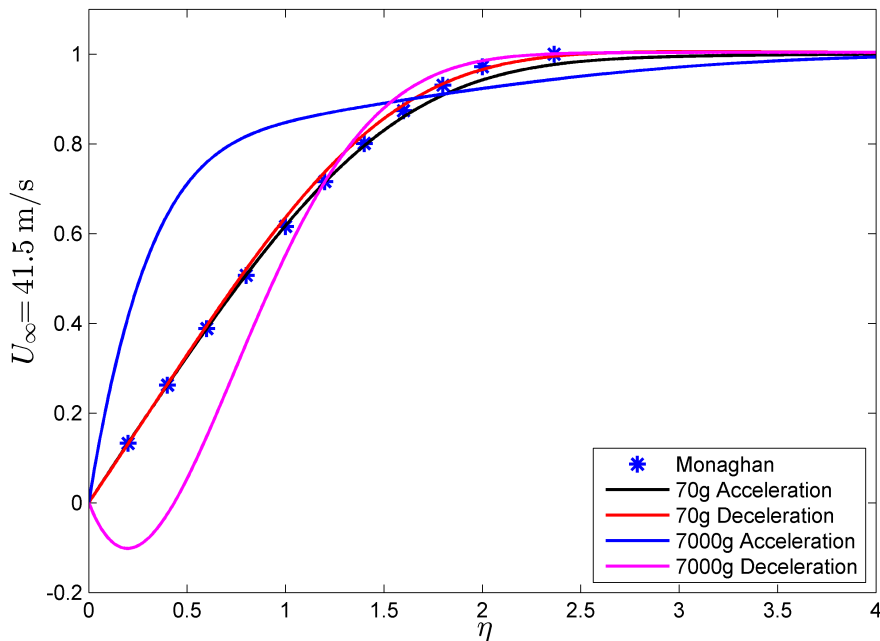
CHAPTER 7. BOUNDARY LAYER RESPONSE IN PURE ROTATION - FLAT PLATE FLOW

In acceleration the relative frame acceleration term becomes a momentum source. An increase in momentum on the right hand side of the equation leads to an increase in the material derivative on the left hand side of the equation. This increase results in an increase in velocity  $u$ . In turn it causes the velocity gradient at the wall to increase. This is the effect observed in the simulation results.

The opposite occurs in deceleration where the relative frame acceleration term becomes a momentum sink. A decrease in momentum on the right hand side of the equation leads to a decrease in the material derivative on the left hand side of the equation. This decrease results in a decrease in velocity  $u$ . In turn it causes the velocity gradient at the wall to decrease. The pressure gradient has an opposite sign to the diffusion term and increases to such an extent that an adverse pressure gradient form. This results in flow separation as observed in the simulation results.

Figure 7.53 is presented to depict the variability in the boundary layer profiles for different starting and acceleration conditions. The flow history has an influence on the boundary layer behaviour and must be considered in aerodynamic studies.

Figure 7.53: Variability in Boundary Layer Profiles for Different Starting and Acceleration Conditions on a Flat Plate

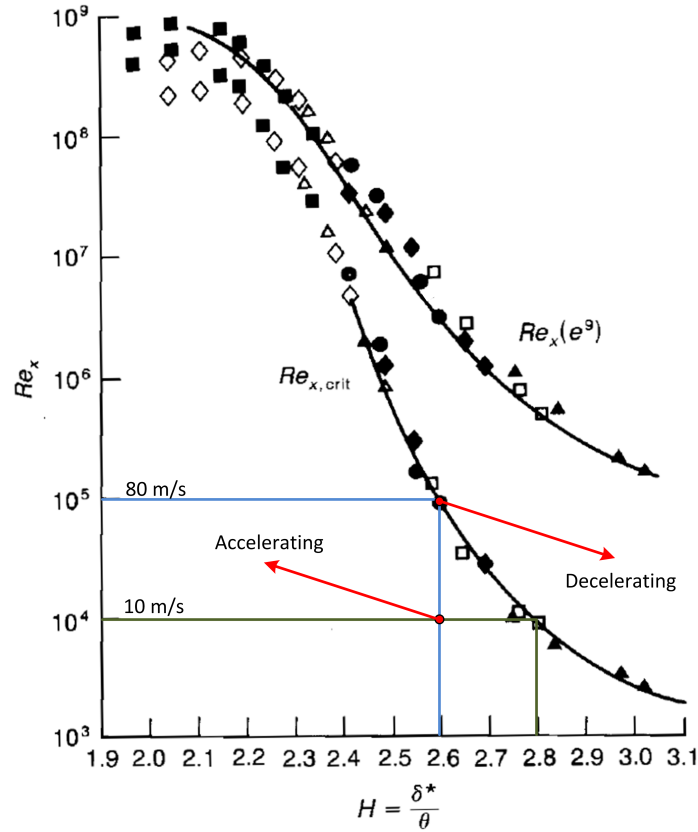


The response of the shape factor to acceleration and decelerating conditions have been determined. A graph that characterises the critical shape factor versus Reynolds numbers are available from the literature (Wazzan et al. [78]). This is limited to steady flow conditions, but it still gives a good indication of where flow separation can be expected (Figure 7.54).

For the conditions analysed here, the flow is expected to separate for shape factor between 2.6 and 2.8. The general tendency of the shape factor is to decrease in acceleration and increase in deceleration (Figure 7.55).



Figure 7.54: Shape Factor Changes for Accelerating and Decelerating Flow Mapped on the Graph of Wazzan et al. [78]



The responses can be further broken down according to response type, as discussed in the body of this chapter. There exists a limit of acceleration strength that is related to the shape factor response. Below this limit the shape factor attempts to recover the initial value as the event progresses. At acceleration above the limit the shape factor decreases and approximate a low asymptotic value. In deceleration there is a discontinuity in the deceleration event. This marks the point where the shape factor becomes negative due to the negative value of the momentum thickness. At this point the resultant momentum in the boundary layer points in the direction of the reverse flow.

The response of the skin friction coefficient to arbitrary translation is shown in *Figure 7.56*. In acceleration the skin friction coefficient initial increases, reaches a maximum and then decrease at the event continues. It approximates an asymptotic value near the end of the event. Deceleration increase the skin friction coefficient significantly. The response is divergent and continues for the duration of the event. The skin friction drag is directly proportional to the skin friction coefficient and thus have a similar response to arbitrary translation.

Figure 7.55: Results of the Shape Factor Response for Acceleration (left) and Deceleration (Right) Events on a Flat Plate

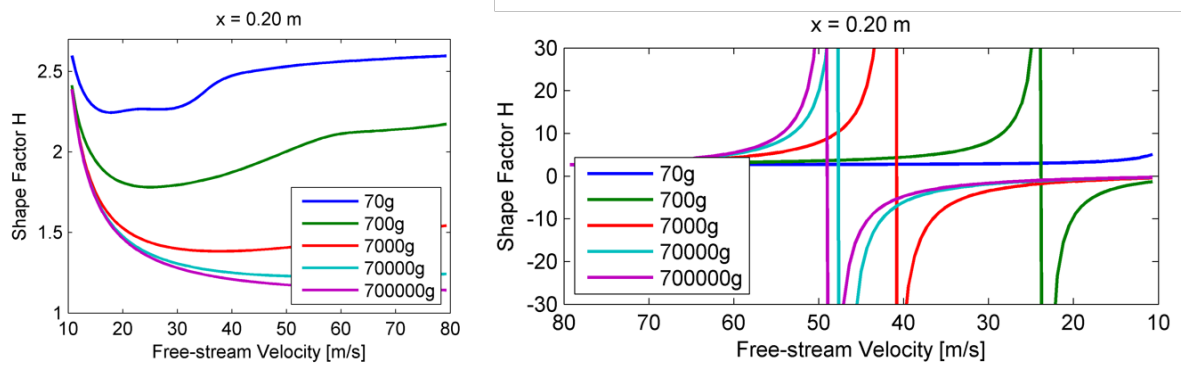
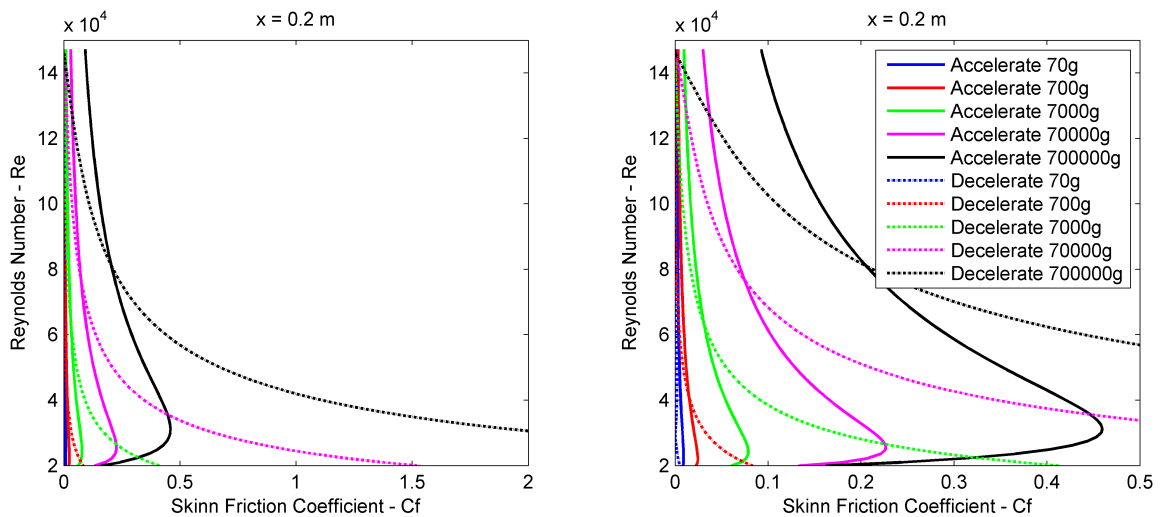


Figure 7.56: Result of the Skin Friction Coefficient Response to Arbitrary Translation on a Flat Plate



## Boundary Layer Response in Pure Rotation - Rotating Disk Flow

This chapter investigates the response of a laminar boundary layer on a rotating disk to changes in angular velocity. Arbitrary angular acceleration occurs over a range of magnitudes for various applications. Examples include spin stabilize projectiles, missiles conducting high acceleration manoeuvres, spin up or spin down of turbo-machines, ship propellers, helicopter blades and wind turbines to name a few. The highest angular acceleration is found in ultra-centrifuges where accelerations of up to 1 000 000 g is possible. The angular acceleration and deceleration in this case is varied from 70g to 700 000g. A wide range a values is covered in the same manner as done in the previous chapter.

The accelerating cases are initialized from a steady state solution at 10 rad/s ( $Re_{rot} = 150$ ) and accelerated to 80 rad/s ( $Re_{rot} = 424.3$ ). Five acceleration cases are done with constant acceleration from 70g to 700 000g at increments of 10. Similarly, the deceleration cases commence from a steady state solution or 80 rad/s ( $Re_{rot} = 424.3$ ) and decelerated to 10 rad/s ( $Re_{rot} = 150$ ) with decelerations as shown below in *Table 8.1*.

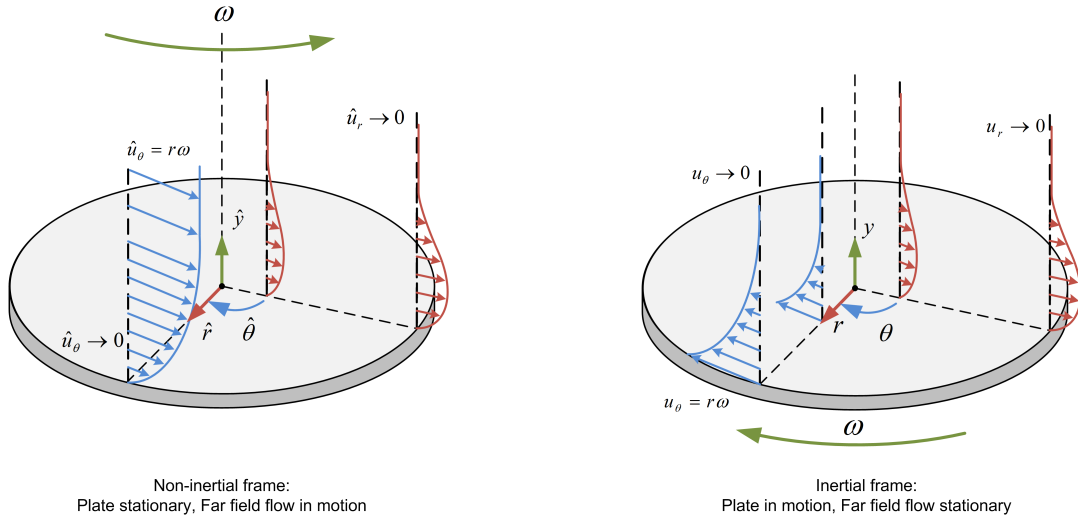
Table 8.1: Rotating Disk Test Matrix

	Acceleration Event	Deceleration Event
Velocity [rad/s]	10 to 80	80 to 10
Reynolds Number	150 to 424.3	424.3 to 150
	70g	70g
	700g	700g
	7 000g	7 000g
	70 000g	70 000g
	700 000g	700 000g

## 8.1 Case Description

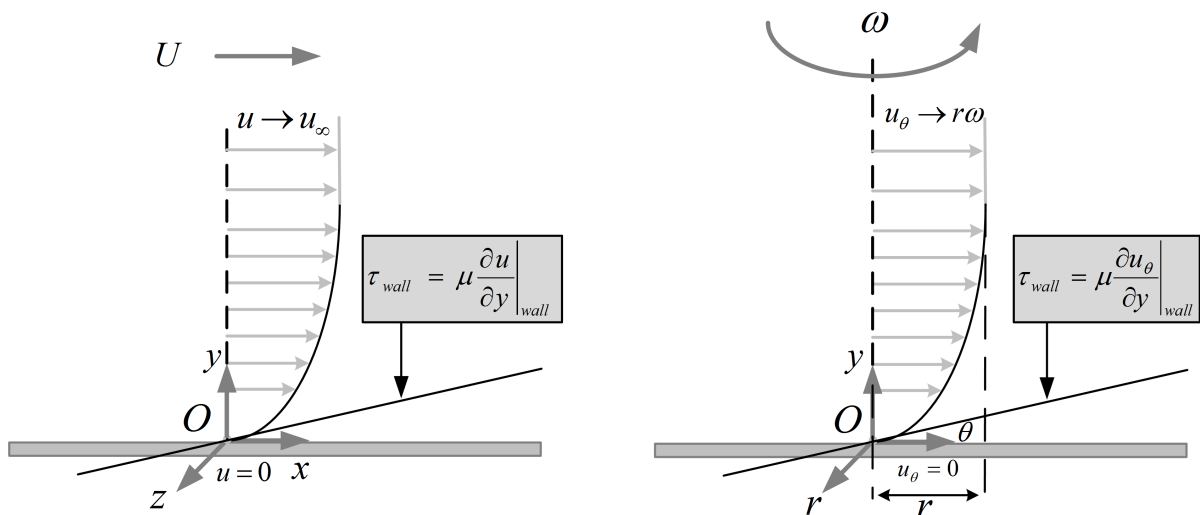
The steady state solution of the rotating disk was discussed in *Chapter 6*. Analytical results are available from the literature (Schlichting [42], von Karman [41]). The boundary layer the forms on the rotating disk in steady, pure rotation is depicted in *Figure 8.1*.

Figure 8.1: Graphical Representation of the Boundary Layer on a Rotating Disk



Parallels can be drawn between the boundary layer on the rotating disk in the tangential direction and the boundary layer on the laminar flat plate (*Figure 8.2*).

Figure 8.2: Depiction of the laminar boundary layer on the flat plate (left) and in the tangential direction on a rotating disk (right)



At the wall, the velocity is zero since no-slip conditions is assumed. The velocity profile further away from the wall increases monotonically to approach the free-stream value in the far field. In the

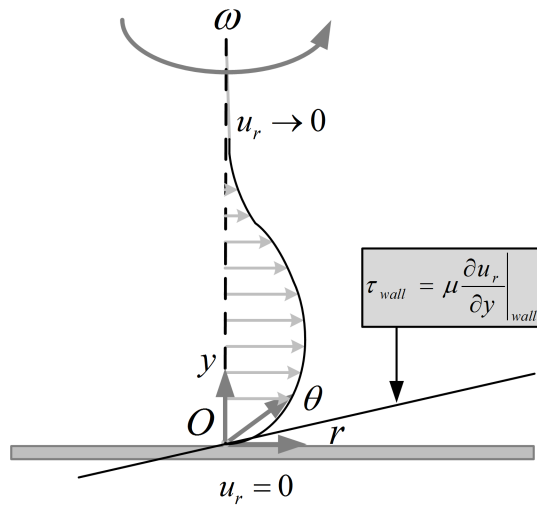
case of the flat plate, the free-stream value is the translational velocity at which the plate is moving. The rotating plate free-stream value is dependant on the distance from the centre of rotation and the rotational velocity.

The wall shear stress is dependant on the velocity gradient at the wall. This term is present in the boundary layer equation and is responsible for the shape of the boundary layer. The non-inertial form the equation was derived in *Equation 5.148* and is expressed in the inertial frame as follow:

$$\frac{\partial \rho u_\theta}{\partial t} + u_r \frac{\partial \rho u_\theta}{\partial r} + \frac{u_\theta}{r} \frac{\partial \rho u_\theta}{\partial \theta} + \frac{\rho u_\theta u_r}{r} + u_y \frac{\partial \rho u_\theta}{\partial y} = -\frac{1}{r} \frac{\partial p}{\partial \theta} + \frac{\partial}{\partial y} \left( \mu \frac{\partial u_\theta}{\partial y} \right) \quad (8.1)$$

The boundary layer in the radial direction occurs as a result of secondary effects of due to tangential rotation (*Figure 8.3*). In an ideal flow  $u_r$  is zero through the entire domain. Viscous and secondary flow effects results in a boundary layer that is approaches zero velocity in the near-wall and far-field respectively. In the central regions of the boundary layer, the velocity profile is monotonically increasing closer to the wall, and monotonically decreasing closer to the boundary layer edge.

Figure 8.3: Depiction of the laminar boundary layer on a rotating disk in the radial direction

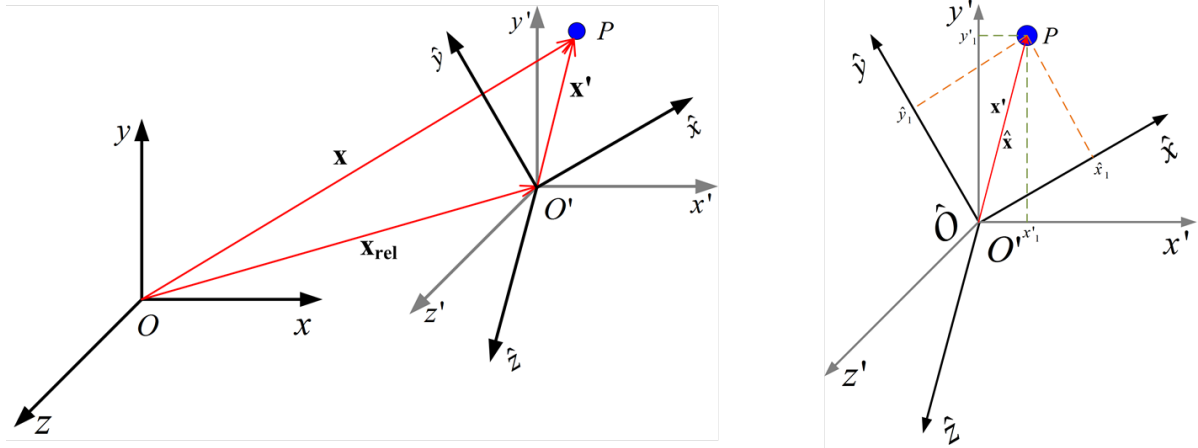


The non-inertial boundary layer equation for a rotating disk in the radial direction was determined in *Equation 5.152*. This equation can be written in the inertial frame as shown below. The term responsible for the formation of the boundary layer is  $\frac{\partial}{\partial y} \left( \mu \frac{\partial u_r}{\partial y} \right)$ .

$$\frac{\partial \rho u_r}{\partial t} + u_r \frac{\partial \rho u_r}{\partial r} + \frac{u_\theta}{r} \frac{\partial \rho u_r}{\partial \theta} - \frac{\rho u_\theta^2}{r} + u_y \frac{\partial \rho u_r}{\partial y} = -\frac{\partial p}{\partial r} + \frac{\partial}{\partial y} \left( \mu \frac{\partial u_r}{\partial y} \right) \quad (8.2)$$

The boundary layer equations are required in the non-inertial form. This is used to interpret the results from the simulations. In *Chapter 3* the non-inertial momentum equation was derived using the frame description in *Figure 8.4*.

Figure 8.4: Frame definitions for non-inertial flow



The full momentum equation that is used to solve unsteady rotational flow was determined in Equation 3.169:

$$\frac{\partial \hat{\rho} \hat{\mathbf{u}}}{\partial t} + \hat{\nabla} \cdot (\hat{\rho} \hat{\mathbf{u}} \otimes \hat{\mathbf{u}}) = -\hat{\nabla} \hat{p} + \hat{\nabla} \cdot [\hat{\mu} (\hat{\nabla} \hat{\mathbf{u}} + \hat{\nabla} \hat{\mathbf{u}}^T) + \hat{\lambda} (\hat{\nabla} \cdot \hat{\mathbf{u}}) \hat{\mathbf{I}}] + \underbrace{2\rho \hat{\mathbf{u}} \wedge \boldsymbol{\Omega}}_{\text{Coriolis}} - \underbrace{\rho \hat{\mathbf{x}} \wedge \boldsymbol{\Omega} \wedge \boldsymbol{\Omega}}_{\text{Centrifugal}} + \underbrace{\rho \hat{\mathbf{x}} \wedge \dot{\boldsymbol{\Omega}}}_{\text{Euler}} \quad (8.3)$$

This equation was expanded in Equation 5.144-5.146 to obtain the formulations in cylindrical components. The equations can be reduced to a set that applies to this specific case:

**r-momentum**

$$\frac{\partial \hat{\rho} \hat{u}_r}{\partial t} + \hat{u}_r \frac{\partial \hat{\rho} \hat{u}_r}{\partial \hat{r}} + \frac{\hat{u}_\theta}{\hat{r}} \frac{\partial \hat{\rho} \hat{u}_r}{\partial \hat{\theta}} - \frac{\hat{\rho} \hat{u}_\theta^2}{\hat{r}} + \hat{u}_y \frac{\partial \hat{\rho} \hat{u}_r}{\partial \hat{y}} = -\frac{\partial \hat{p}}{\partial \hat{r}} + \frac{\partial}{\partial \hat{y}} \left( \hat{\mu} \frac{\partial \hat{u}_r}{\partial \hat{y}} \right) - 2\hat{\rho} \hat{u}_\theta \omega_y + \hat{\rho} \hat{r} \omega_y^2 \quad (8.4)$$

**y-momentum**

$$0 = -\frac{\partial \hat{p}}{\partial \hat{y}} \quad (8.5)$$

**$\theta$ -momentum**

$$\frac{\partial \hat{\rho} \hat{u}_\theta}{\partial t} + \hat{u}_r \frac{\partial \hat{\rho} \hat{u}_\theta}{\partial \hat{r}} + \frac{\hat{u}_\theta}{\hat{r}} \frac{\partial \hat{\rho} \hat{u}_\theta}{\partial \hat{\theta}} + \frac{\hat{\rho} \hat{u}_\theta \hat{u}_r}{\hat{r}} + \hat{u}_y \frac{\partial \hat{\rho} \hat{u}_\theta}{\partial \hat{y}} = -\frac{1}{\hat{r}} \frac{\partial \hat{p}}{\partial \hat{\theta}} + \frac{\partial}{\partial \hat{y}} \left( \hat{\mu} \frac{\partial \hat{u}_\theta}{\partial \hat{y}} \right) + 2\hat{\rho} \hat{u}_r \omega_y + \hat{\rho} \hat{r} \dot{\omega}_y \quad (8.6)$$

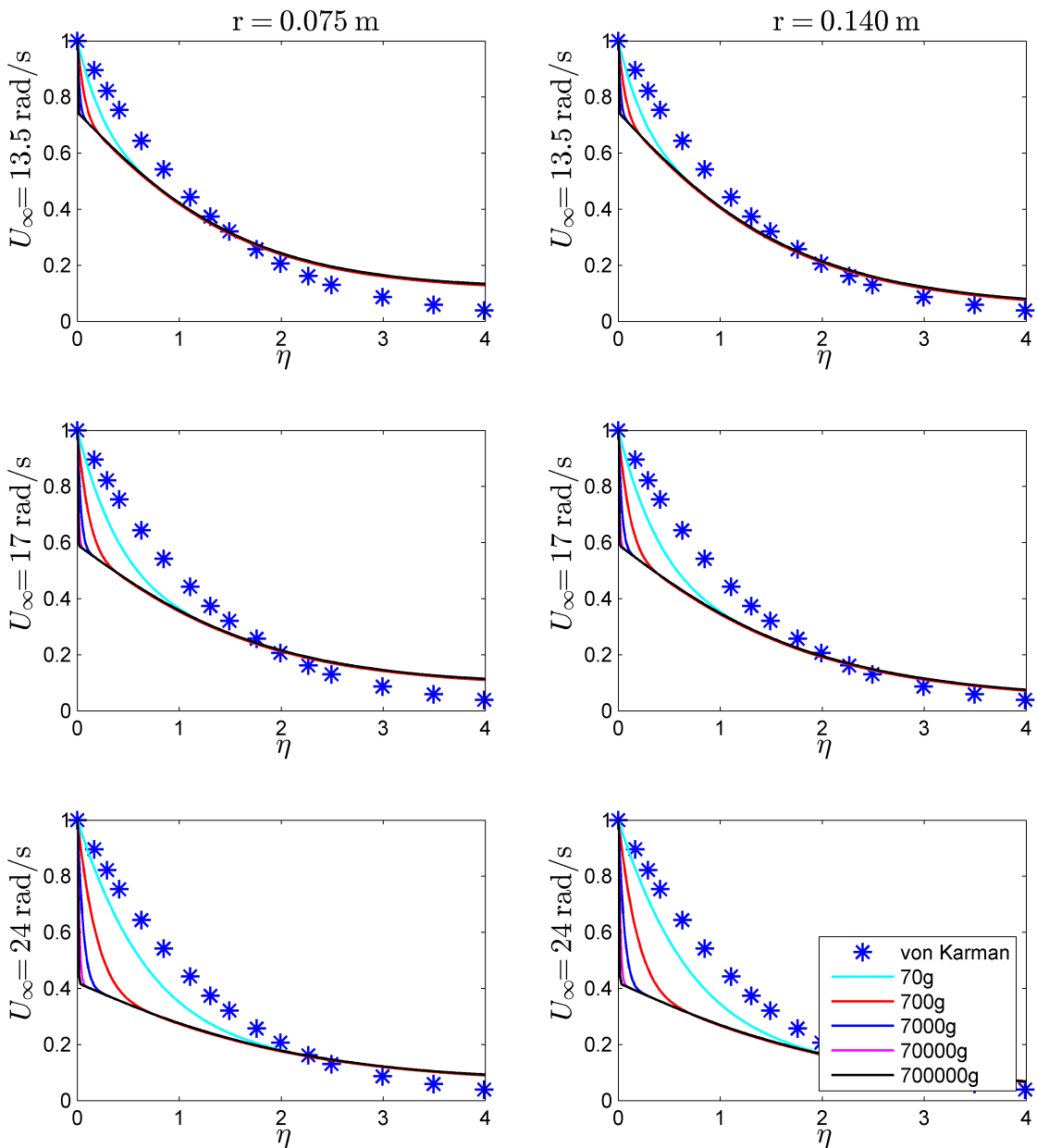
The case description that was used to perform the numerical simulation with was described in Chapter 6. The results are interpreted using the boundary layer formulations above.

## 8.2 Results and Discussion - Acceleration

### 8.2.1 Velocity Profiles

The result from the acceleration simulation for the rotating disk in the **tangential direction** is shown in *Figures 8.5-8.7* respectively. The results are displayed in the absolute frame in order to compare it with the von Karman solution. The non-dimensional distance from the wall,  $\eta$ , is determined by *Equation 6.28*.

Figure 8.5: Non-Dimensional Tangential Velocity Profiles: Rotating Disk - Acceleration Grouping I



CHAPTER 8. BOUNDARY LAYER RESPONSE IN PURE ROTATION - ROTATING DISK FLOW

Figure 8.6: Non-Dimensional Tangential Velocity Profiles: Rotating Disk - Acceleration Grouping II

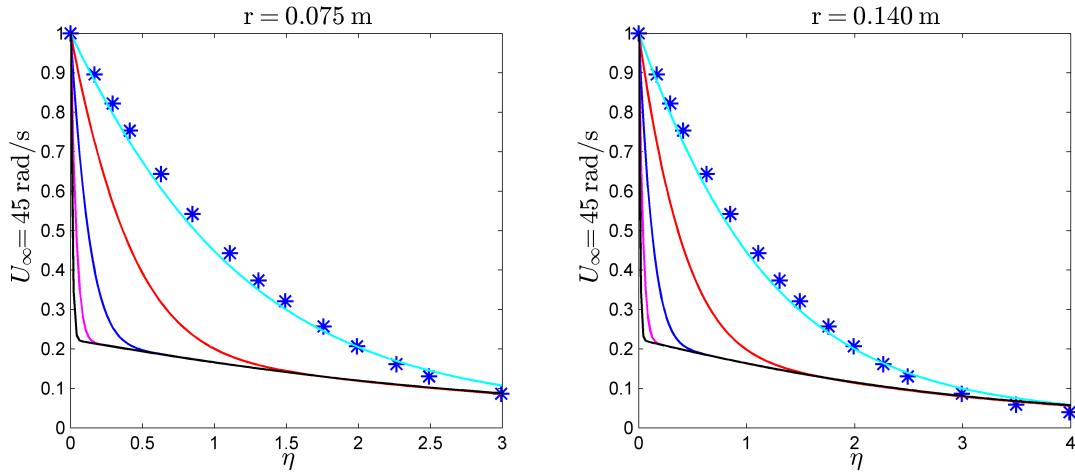
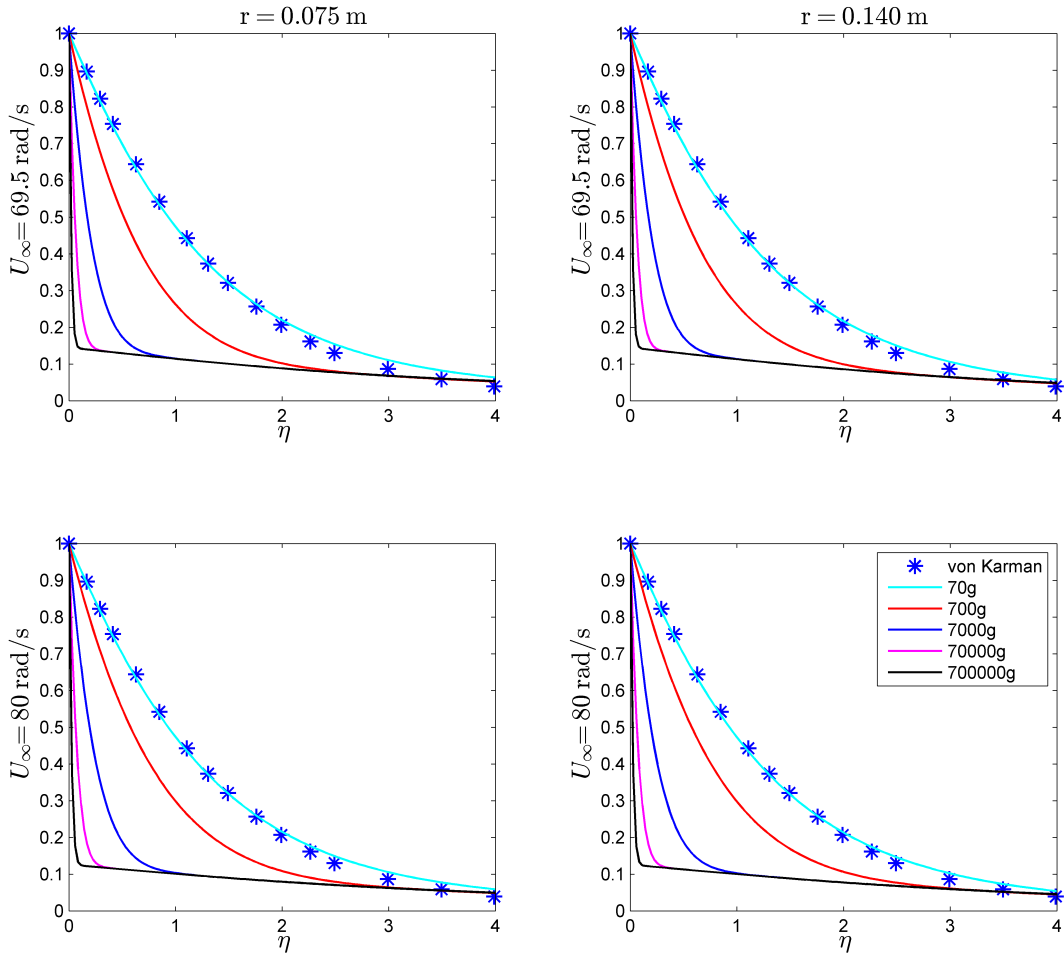


Figure 8.7: Non-Dimensional Tangential Velocity Profiles: Rotating Disk - Acceleration Grouping III

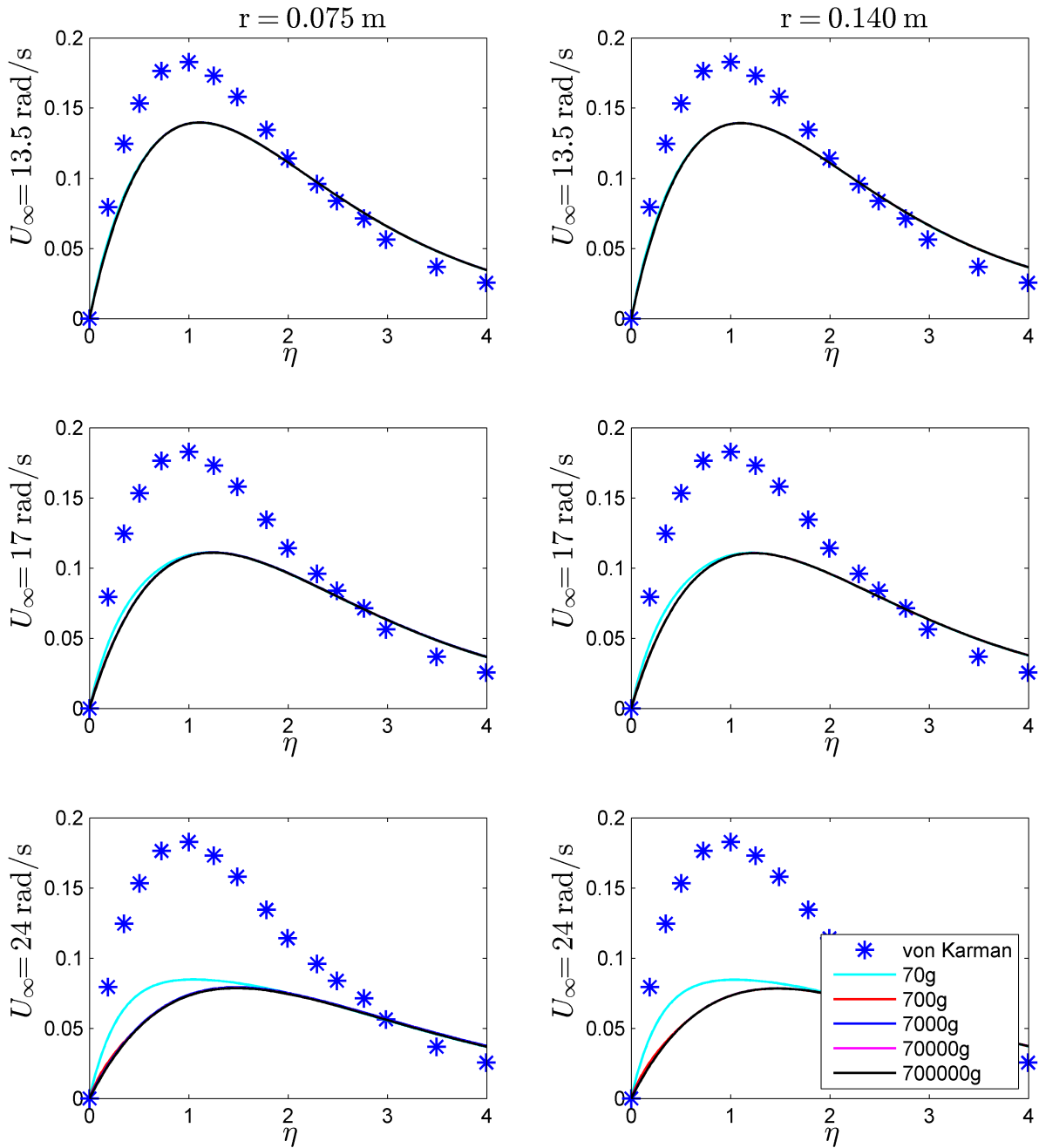




8.2. RESULTS AND DISCUSSION - ACCELERATION

The result from the acceleration simulation for the rotating disk in the **radial direction** is shown in Figures 8.8-8.10 respectively.

Figure 8.8: Non-Dimensional Radial Velocity Profiles: Rotating Disk - Acceleration Grouping I



CHAPTER 8. BOUNDARY LAYER RESPONSE IN PURE ROTATION - ROTATING DISK FLOW

Figure 8.9: Non-Dimensional Radial Velocity Profiles: Rotating Disk - Acceleration Grouping II

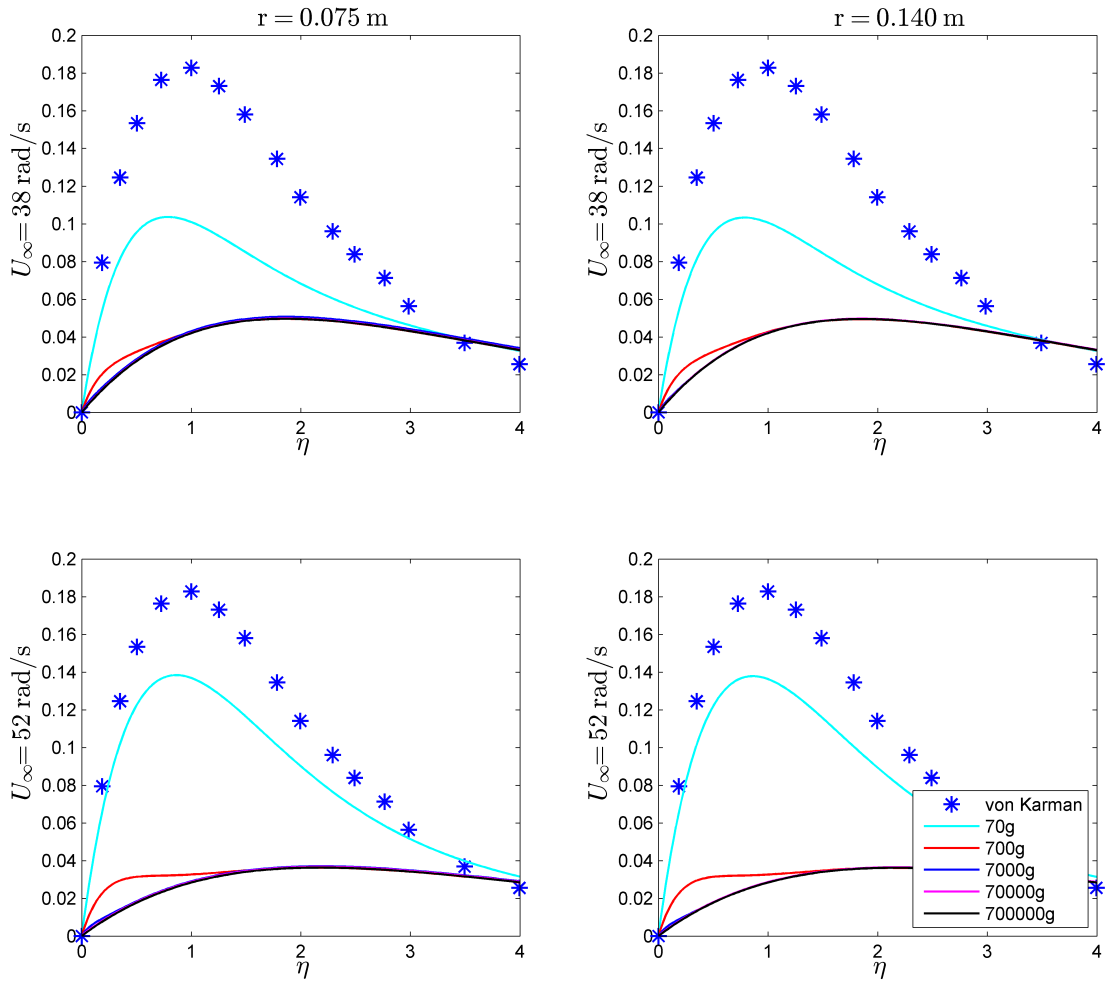
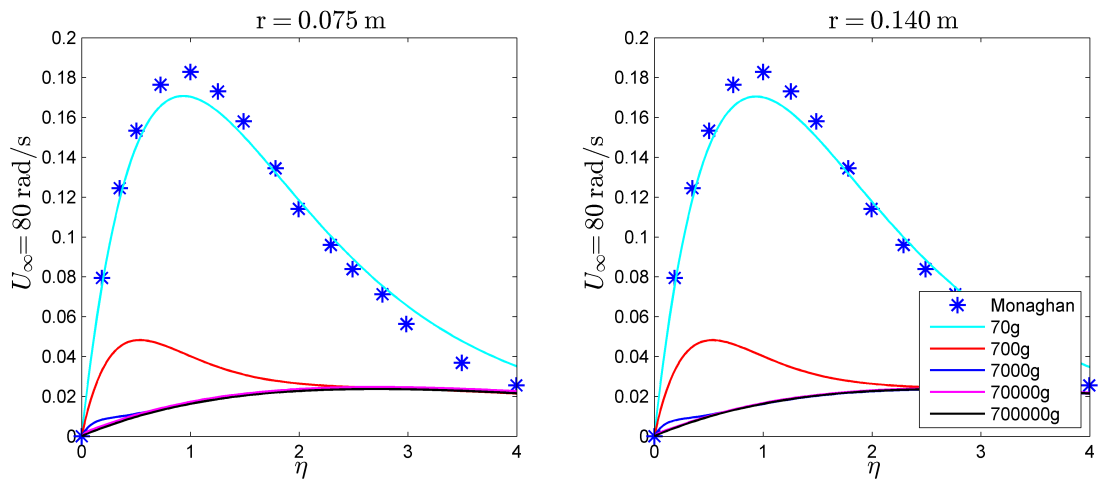


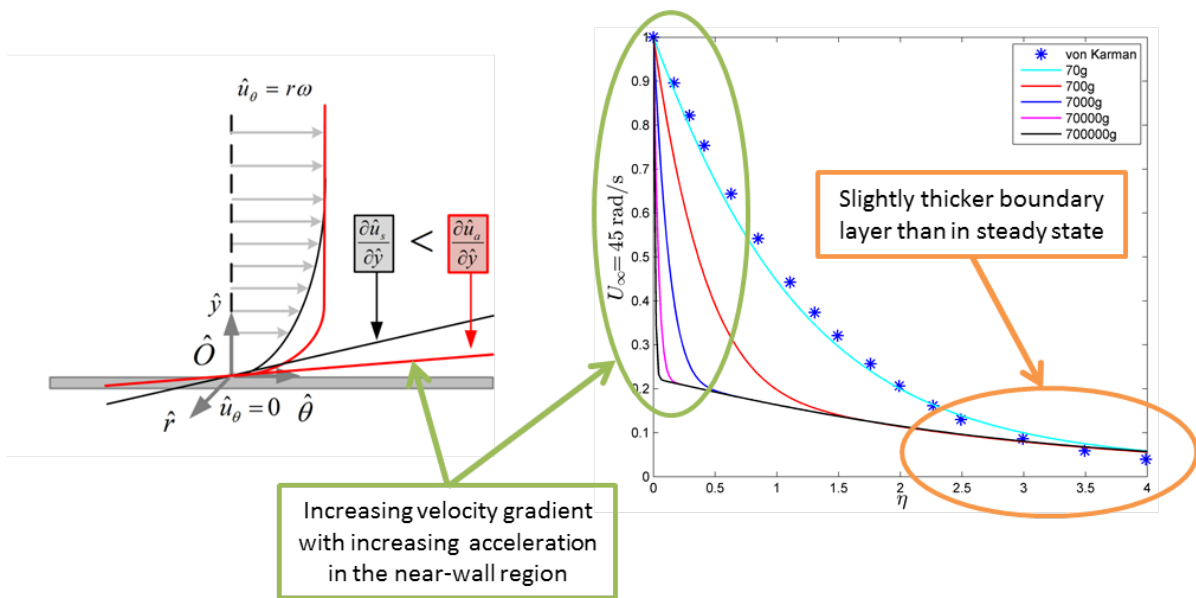
Figure 8.10: Non-Dimensional Radial Velocity Profiles: Rotating Disk - Acceleration Grouping III



8.2. RESULTS AND DISCUSSION - ACCELERATION

The results from the acceleration simulation for the rotating disk in the **tangential direction** have many similarities with the flat plate in acceleration. It can be seen that the boundary layer has an immediate reaction to acceleration in the near-wall region. Initially the boundary layer thickens (Grouping I), but reduces and becomes slightly thicker than the steady state solution as the acceleration event progresses. In the far-field, close to the free stream values, all the acceleration cases displays similar non-dimensional values. In the near-wall regions the velocity gradient of the boundary layer becomes steeper with increased acceleration (Figure 8.11).

Figure 8.11: Sample results and observations for tangential flow in acceleration



The results from the acceleration simulation for the rotating disk in the **radial direction** showed limited reaction to tangential acceleration. The first grouping of results indicates that the far-fields values shows an initial thickening of the boundary layer when compared to steady state results. In the near-wall region the apex of the profile is lower than the steady state result and decreases as the simulation progress. All the accelerating profiles have the same values, with the exception of the 70g case that breaks away. The second and third grouping displays similar patterns where the boundary layer becomes thinner and the apex is reduced. The profile lines are common between the acceleration cases with the exception of the 70g case, as before, and the 700g that also breaks away. These results are an indication that the radial velocity profile is very slow to react to acceleration. The profiles that remain on top of each other are an indication that the boundary layer is maintaining the initial conditions. The boundary layer profile of the high acceleration cases (7000g, 70 000g and 700 000g) are frozen in the initial conditions of the acceleration event. The lower acceleration cases to however show a response. The lowest acceleration case, 70g, is first to respond. The response is initiated in the near-wall region and then propagates to the upper areas of the boundary layer. The 700g case responds in a similar manner, but much later in the

CHAPTER 8. BOUNDARY LAYER RESPONSE IN PURE ROTATION - ROTATING DISK FLOW

acceleration event.

The boundary layer equations for unsteady rotation were shown in *Section 8.1*:

**r-momentum**

$$\frac{\partial \hat{\rho} \hat{u}_r}{\partial t} + \hat{u}_r \frac{\partial \hat{\rho} \hat{u}_r}{\partial \hat{r}} + \frac{\hat{u}_\theta}{\hat{r}} \frac{\partial \hat{\rho} \hat{u}_r}{\partial \hat{\theta}} - \frac{\hat{\rho} \hat{u}_\theta^2}{\hat{r}} + \hat{u}_y \frac{\partial \hat{\rho} \hat{u}_r}{\partial \hat{y}} = -\frac{\partial \hat{p}}{\partial \hat{r}} + \frac{\partial}{\partial \hat{y}} \left( \hat{\mu} \frac{\partial \hat{u}_r}{\partial \hat{y}} \right) - 2\hat{\rho} \hat{u}_\theta \omega_y + \hat{\rho} \hat{r} \omega_y^2 \quad (8.7)$$

**y-momentum**

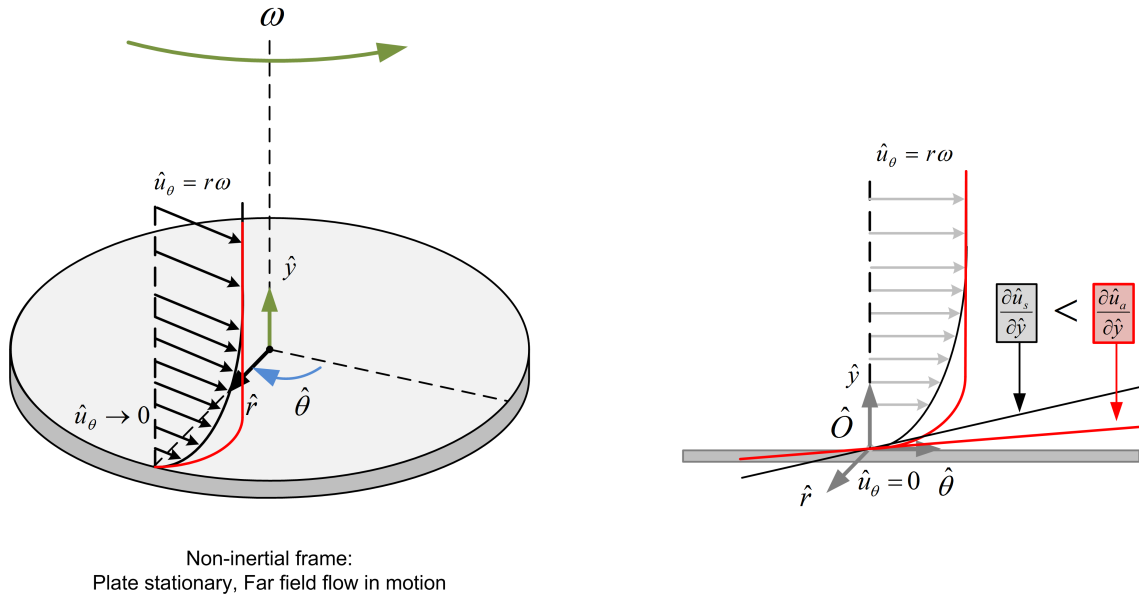
$$0 = -\frac{\partial \hat{p}}{\partial \hat{y}} \quad (8.8)$$

**$\theta$ -momentum**

$$\frac{\partial \hat{\rho} \hat{u}_\theta}{\partial t} + \hat{u}_r \frac{\partial \hat{\rho} \hat{u}_\theta}{\partial \hat{r}} + \frac{\hat{u}_\theta}{\hat{r}} \frac{\partial \hat{\rho} \hat{u}_\theta}{\partial \hat{\theta}} + \frac{\hat{\rho} \hat{u}_\theta \hat{u}_r}{\hat{r}} + \hat{u}_y \frac{\partial \hat{\rho} \hat{u}_\theta}{\partial \hat{y}} = -\frac{1}{\hat{r}} \frac{\partial \hat{p}}{\partial \hat{\theta}} + \frac{\partial}{\partial \hat{y}} \left( \hat{\mu} \frac{\partial \hat{u}_\theta}{\partial \hat{y}} \right) + 2\hat{\rho} \hat{u}_r \omega_y + \hat{\rho} \hat{r} \omega_y \quad (8.9)$$

These equations are responsible for the boundary layer response of the rotating disk to angular acceleration (*Figure 8.12*). It is used to propose a physical mechanism for the observed behaviour.

Figure 8.12: Boundary layer profile for steady angular acceleration



In accelerating conditions, the Coriolis and Euler forces increase. These are located on the right hand side of the equation below and therefore becomes momentum sources.

$$\frac{\partial \hat{\rho} \hat{u}_\theta}{\partial t} + \hat{u}_r \frac{\partial \hat{\rho} \hat{u}_\theta}{\partial \hat{r}} + \frac{\hat{u}_\theta}{\hat{r}} \frac{\partial \hat{\rho} \hat{u}_\theta}{\partial \hat{\theta}} + \frac{\hat{\rho} \hat{u}_\theta \hat{u}_r}{\hat{r}} + \hat{u}_y \frac{\partial \hat{\rho} \hat{u}_\theta}{\partial \hat{y}} = -\frac{1}{\hat{r}} \frac{\partial \hat{p}}{\partial \hat{\theta}} + \frac{\partial}{\partial \hat{y}} \left( \hat{\mu} \frac{\partial \hat{u}_\theta}{\partial \hat{y}} \right) + \underbrace{2\hat{\rho} \hat{u}_r \omega_y}_{\text{Coriolis}} + \underbrace{\hat{\rho} \hat{r} \omega_y}_{\text{Euler}}$$

8.2. RESULTS AND DISCUSSION - ACCELERATION

The momentum sources causes an imbalance on the left hand side on the equation. To maintain equality between the right and left hand sides, the material derivative (all the terms on the left hand side) increases.

$$\frac{\partial \hat{\rho} \hat{u}_\theta}{\partial t} + \hat{u}_r \frac{\partial \hat{\rho} \hat{u}_\theta}{\partial \hat{r}} + \frac{\hat{u}_\theta}{\hat{r}} \frac{\partial \hat{\rho} \hat{u}_\theta}{\partial \hat{\theta}} + \frac{\hat{\rho} \hat{u}_\theta \hat{u}_r}{\hat{r}} + \hat{u}_y \frac{\partial \hat{\rho} \hat{u}_\theta}{\partial \hat{y}} = -\frac{1}{\hat{r}} \frac{\partial \hat{p}}{\partial \hat{\theta}} + \frac{\partial}{\partial \hat{y}} \left( \hat{\mu} \frac{\partial \hat{u}_\theta}{\partial \hat{y}} \right) + 2\hat{\rho} \hat{u}_r \omega_y + \hat{\rho} \hat{r} \dot{\omega}_y$$

An increase in the material derivative leads to an increase in the tangential velocity. This in turn lead to an increase in the velocity gradient. The pressure decreases to compensate for the additional momentum on the right hand side.

$$\frac{\partial \hat{\rho} \hat{u}_\theta}{\partial t} + \hat{u}_r \frac{\partial \hat{\rho} \hat{u}_\theta}{\partial \hat{r}} + \frac{\hat{u}_\theta}{\hat{r}} \frac{\partial \hat{\rho} \hat{u}_\theta}{\partial \hat{\theta}} + \frac{\hat{\rho} \hat{u}_\theta \hat{u}_r}{\hat{r}} + \hat{u}_y \frac{\partial \hat{\rho} \hat{u}_\theta}{\partial \hat{y}} = -\frac{1}{\hat{r}} \frac{\partial \hat{p}}{\partial \hat{\theta}} + \frac{\partial}{\partial \hat{y}} \left( \hat{\mu} \frac{\partial \hat{u}_\theta}{\partial \hat{y}} \right) + 2\hat{\rho} \hat{u}_r \omega_y + \hat{\rho} \hat{r} \dot{\omega}_y$$

In the flat plate accelerating case of *Chapter 7* three response types were identified.

- **Response Type I**, which is viscous dominant.
- **Response Type II**, which is certain regions in the boundary layer are dominated by viscosity and other regions by momentum.
- **Response Type III**, which is dominated by momentum.

The same response types are relevant here. There is no occurrence of Response Type I where the steady state conditions are maintained for the duration of the event. The 70g case fall into the Response Type II category, since it is dominates by viscosity in some regions and momentum in others. The remainder of the higher acceleration cases are all of Response Type III.

An alternative explanation for the behaviour is to recognize that an increase in the angular velocity,  $\omega_y$ , results in an increase in the tangential velocity,  $u_\theta$ .

$$u_\theta = r\omega_y \tag{8.10}$$

The increase of  $u_\theta$  results in an increase in both the material derivative and the viscous terms.

$$\frac{\partial \hat{\rho} \hat{u}_\theta}{\partial t} + \hat{u}_r \frac{\partial \hat{\rho} \hat{u}_\theta}{\partial \hat{r}} + \frac{\hat{u}_\theta}{\hat{r}} \frac{\partial \hat{\rho} \hat{u}_\theta}{\partial \hat{\theta}} + \frac{\hat{\rho} \hat{u}_\theta \hat{u}_r}{\hat{r}} + \hat{u}_y \frac{\partial \hat{\rho} \hat{u}_\theta}{\partial \hat{y}} = -\frac{1}{\hat{r}} \frac{\partial \hat{p}}{\partial \hat{\theta}} + \frac{\partial}{\partial \hat{y}} \left( \hat{\mu} \frac{\partial \hat{u}_\theta}{\partial \hat{y}} \right) + 2\hat{\rho} \hat{u}_r \omega_y + \hat{\rho} \hat{r} \dot{\omega}_y$$

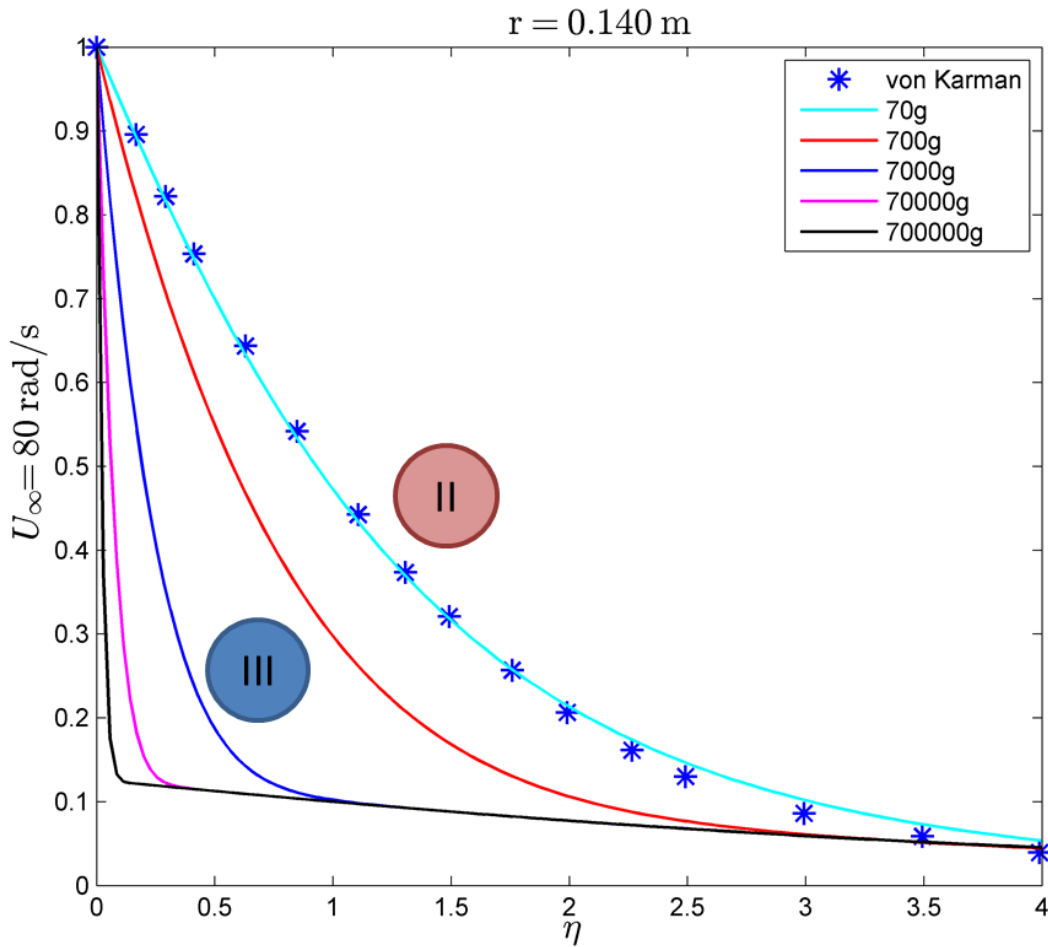
CHAPTER 8. BOUNDARY LAYER RESPONSE IN PURE ROTATION - ROTATING DISK FLOW

The magnitude of the increase in the left hand side momentum terms are larger than the increase in the viscous term. A  $\frac{\partial \hat{u}_\theta}{\partial \hat{y}}$  term is seen on both side of the equation. On the right hand side the gradient of the term is taken. This value is smaller than the magnitude of all the momentum terms on the left hand side.

$$\frac{\partial \hat{\rho} \hat{u}_\theta}{\partial t} + \hat{u}_r \frac{\partial \hat{\rho} \hat{u}_\theta}{\partial \hat{r}} + \frac{\hat{u}_\theta}{\hat{r}} \frac{\partial \hat{\rho} \hat{u}_\theta}{\partial \hat{\theta}} + \frac{\hat{\rho} \hat{u}_\theta \hat{u}_r}{\hat{r}} + \hat{u}_y \left( \frac{\partial \hat{\rho} \hat{u}_\theta}{\partial \hat{y}} \right) = -\frac{1}{\hat{r}} \frac{\partial \hat{p}}{\partial \hat{\theta}} + \frac{\partial}{\partial \hat{y}} \left( \hat{\mu} \frac{\partial \hat{u}_\theta}{\partial \hat{y}} \right) + \underbrace{2 \hat{\rho} \hat{u}_r \omega_y}_{\text{Coriolis}} + \underbrace{\hat{\rho} \hat{r} \dot{\omega}_y}_{\text{Euler}}$$

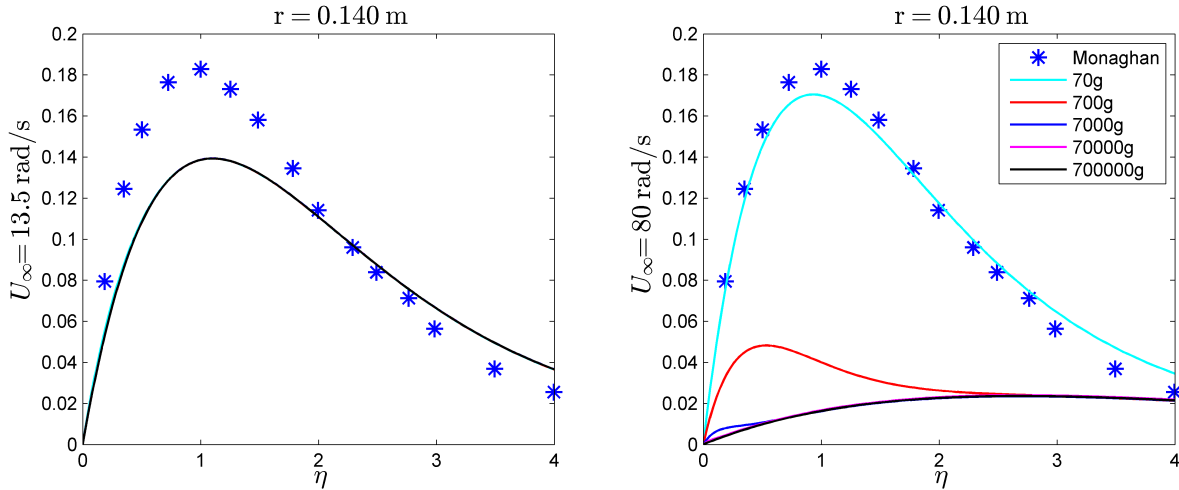
In light of the above it is postulated that the response of the tangential boundary layer largely falls in the Type III category (*Figure 8.13*). The 70g case falls within the Type II category. At accelerations smaller than 70g it is possible that a Type I response will be observed. Smaller than 70g accelerations are not within the scope of this study and are suggested for further work in this field.

Figure 8.13: Acceleration Response Types of the Rotating Disk



The flow in the radial direction is slow to respond to the changing condition, where the lower acceleration cases responds first (Figure 8.14).

Figure 8.14: Sample Results of the Radial Velocity Profiles in Acceleration



The boundary layer in the radial direction has two non-inertial terms, the Coriolis and the Centrifugal force.

$$\frac{\partial \hat{\rho} \hat{u}_r}{\partial t} + \hat{u}_r \frac{\partial \hat{\rho} \hat{u}_r}{\partial \hat{r}} + \frac{\hat{u}_\theta}{\hat{r}} \frac{\partial \hat{\rho} \hat{u}_r}{\partial \hat{\theta}} - \frac{\hat{\rho} \hat{u}_\theta^2}{\hat{r}} + \hat{u}_y \frac{\partial \hat{\rho} \hat{u}_r}{\partial \hat{y}} = -\frac{\partial \hat{p}}{\partial \hat{r}} + \frac{\partial}{\partial \hat{y}} \left( \hat{\mu} \frac{\partial \hat{u}_r}{\partial \hat{y}} \right) - \underbrace{2 \hat{\rho} \hat{u}_\theta \omega_y}_{\text{Coriolis}} + \underbrace{\hat{\rho} \hat{r} \omega_y^2}_{\text{Centrifugal}}$$

The radial boundary layer forms due to secondary effects. It is not directly influenced by the tangential velocity and has no unsteady terms (i.e. Euler) in the equation. The flow remains in the initial state for the higher acceleration cases. Changes occur first in the 70 g case in the near-wall regions. This is an indication that the response originates from an increase of the velocity gradient.

During tangential acceleration, the tangential velocity increases. This results in an increase on the left hand side of the equation. The increase is balanced on the right hand side by an increase in the viscous terms.

$$\frac{\partial \hat{\rho} \hat{u}_r}{\partial t} + \hat{u}_r \frac{\partial \hat{\rho} \hat{u}_r}{\partial \hat{r}} + \frac{\hat{u}_\theta}{\hat{r}} \frac{\partial \hat{\rho} \hat{u}_r}{\partial \hat{\theta}} - \frac{\hat{\rho} \hat{u}_\theta^2}{\hat{r}} + \hat{u}_y \frac{\partial \hat{\rho} \hat{u}_r}{\partial \hat{y}} = -\frac{\partial \hat{p}}{\partial \hat{r}} + \frac{\partial}{\partial \hat{y}} \left( \hat{\mu} \frac{\partial \hat{u}_r}{\partial \hat{y}} \right) - 2 \hat{\rho} \hat{u}_\theta \omega_y + \hat{\rho} \hat{r} \omega_y^2$$

The Coriolis and Centrifugal forces have opposite signs. It is postulated that the magnitude of the terms are of the same order. This creates a feedback loop where the Centrifugal term is a momentum source and the Coriolis is a momentum sink. The effect of these terms in the boundary layer are minimal.

CHAPTER 8. BOUNDARY LAYER RESPONSE IN PURE ROTATION - ROTATING DISK FLOW

The eventual increase of the viscous term on the right hand side of the equation leads to an increase on left hand side. Subsequently, the radial velocity,  $u_r$ , is also increase.

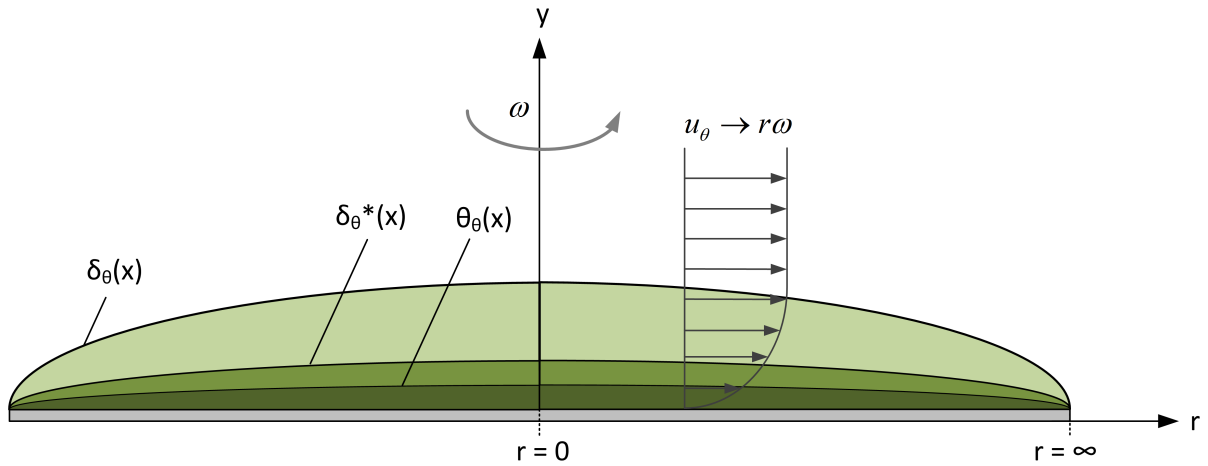
$$\frac{\partial \hat{\rho} \hat{u}_r}{\partial t} + \hat{u}_r \frac{\partial \hat{\rho} \hat{u}_r}{\partial \hat{r}} + \frac{\hat{u}_\theta}{\hat{r}} \frac{\partial \hat{\rho} \hat{u}_r}{\partial \theta} - \frac{\hat{\rho} \hat{u}_\theta^2}{\hat{r}} + \hat{u}_y \frac{\partial \hat{\rho} \hat{u}_r}{\partial \hat{y}} = -\frac{\partial \hat{p}}{\partial \hat{r}} + \frac{\partial}{\partial \hat{y}} \left( \hat{\mu} \frac{\partial \hat{u}_r}{\partial \hat{y}} \right) - 2\hat{\rho} \hat{u}_\theta \omega_y + \hat{\rho} \hat{r} \omega_y^2$$

The increase of  $u_r$  depends on the strength of the acceleration and is therefore time dependant. In higher accelerations there is not sufficient time for the radial velocity profile to respond to the changing conditions.

**8.2.2 Boundary Layer Parameters**

The boundary layer parameters on the rotating disk (*Figure 8.15*) were determined in a similar manner as the flat plate.

Figure 8.15: Tangential Boundary Layer on a Rotating Disk



The parameters were calculated in the tangential and radial directions respectively:

**Tangential Parameters**

$$\begin{aligned}
 \delta_\theta^* &= \int_0^{y^* \rightarrow \infty} \left(1 - \frac{u_\theta}{U_\infty}\right) dy \\
 \theta_\theta &= \int_0^{y^* \rightarrow \infty} \frac{u_\theta}{U_\infty} \left(1 - \frac{u_\theta}{U_\infty}\right) dy \\
 H_\theta &= \frac{\delta_\theta^*}{\theta_\theta}
 \end{aligned} \tag{8.11}$$



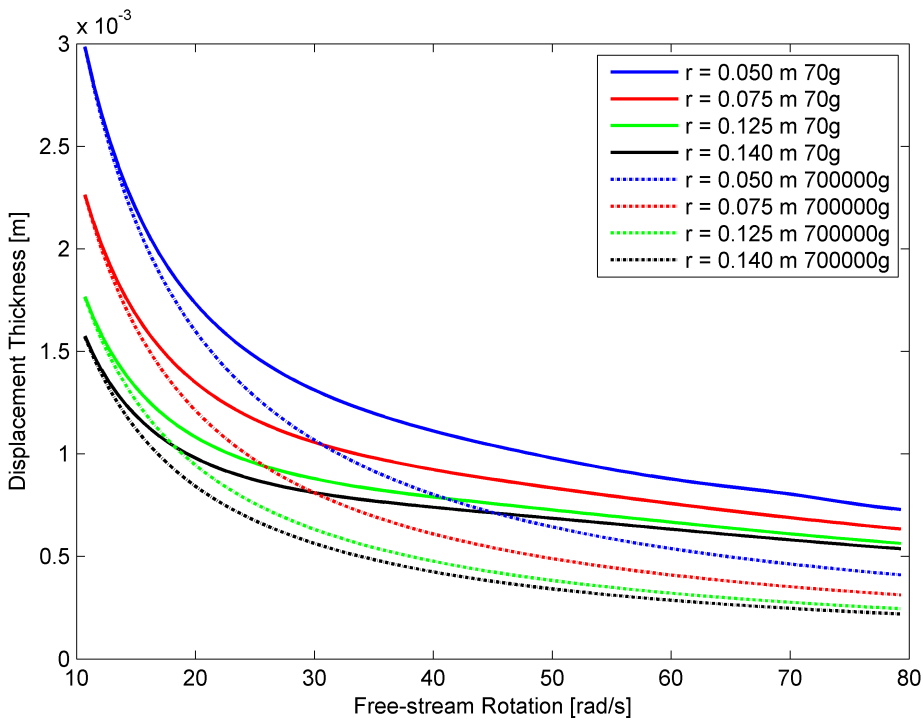
### Radial Parameters

$$\begin{aligned}
 \delta_r^* &= \int_0^{y^* \rightarrow \infty} \left(1 - \frac{u_r}{U_\infty}\right) dy \\
 \theta_r &= \int_0^{y^* \rightarrow \infty} \frac{u_r}{U_\infty} \left(1 - \frac{u_r}{U_\infty}\right) dy \\
 H_r &= \frac{\delta_r^*}{\theta_r}
 \end{aligned}
 \tag{8.12}$$

#### 8.2.2.1 Tangential Parameters

Displacement Thickness result in the tangential direction is shown in *Figures 8.16-8.18*.

Figure 8.16: Tangential Displacement Thickness Comparison for the Accelerating Rotating Disk



The rotating disk displays behaviour similar to the flat plate. The displacement thickness is monotonically decreasing. It approaches an asymptote near the end of the acceleration event that is indirectly proportional to the acceleration strength. The approach of an asymptote is evident from the first derivative results that approximates zero. An inclination point is seen in the second derivative at the beginning of the event. This is a response to the sudden acceleration. At 70g a disturbance is seen at the point closest to the plate centre near the end of the event. The second derivative displays unsteady behaviour at this point. This is due to the effect of a stationary vortex in the middle of the plate.

CHAPTER 8. BOUNDARY LAYER RESPONSE IN PURE ROTATION - ROTATING DISK FLOW

Figure 8.17: Tangential Displacement Thickness Derivatives Comparison for the Accelerating Rotating Disk

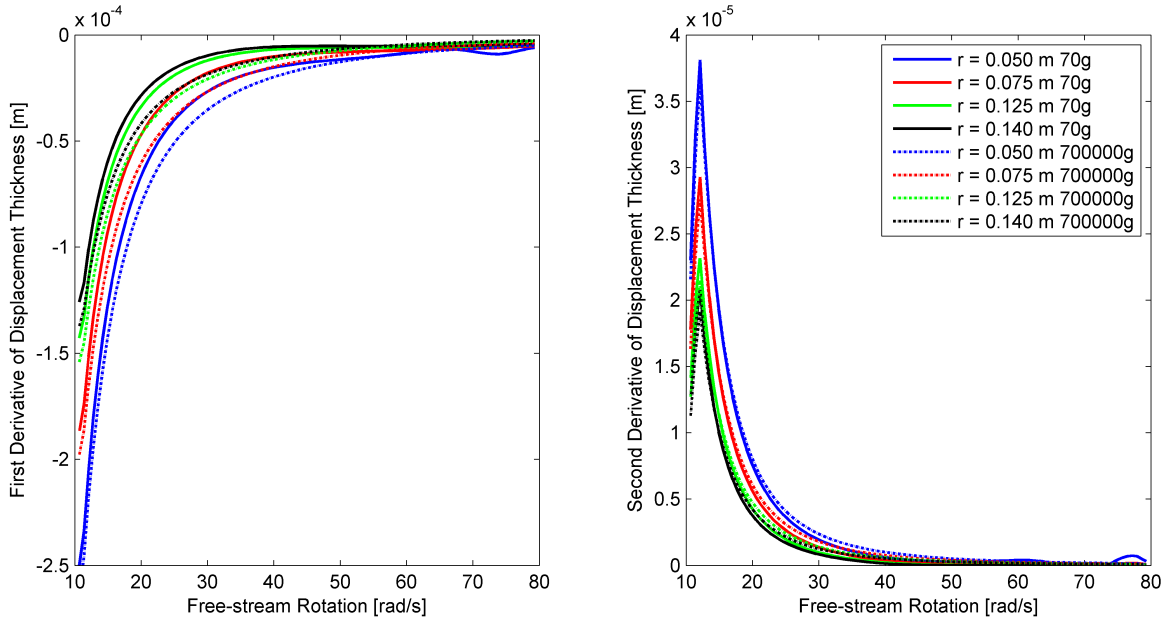
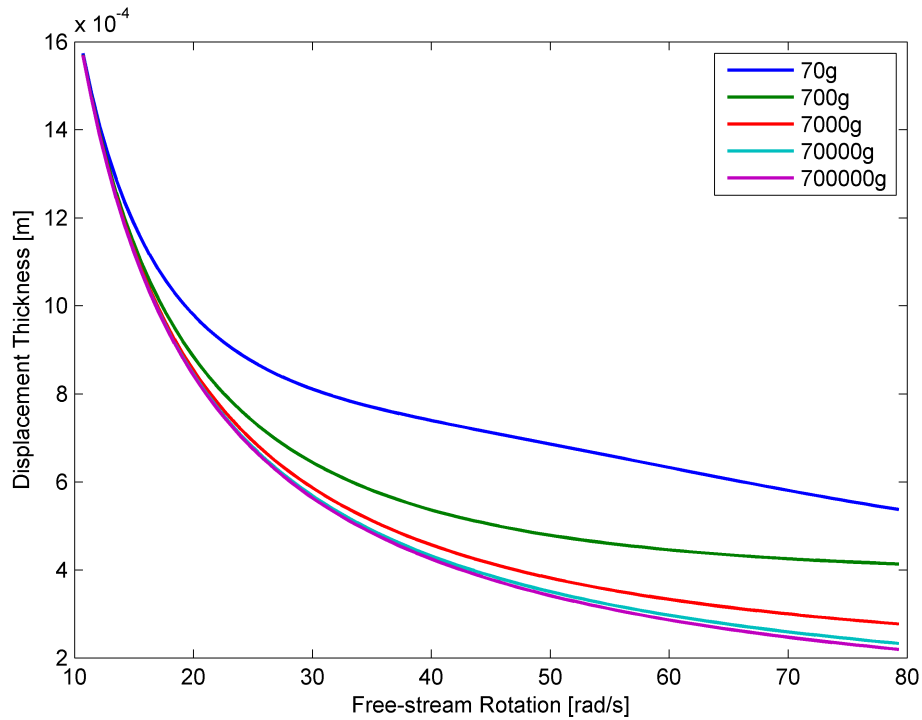


Figure 8.18: Tangential Displacement Thickness Comparison at  $r = 0.14$  m in Accelerating Conditions



8.2. RESULTS AND DISCUSSION - ACCELERATION

The tangential momentum thickness is shown in *Figures 8.19-8.21*.

Figure 8.19: Tangential Momentum Thickness Comparison for the Accelerating Rotating Disk

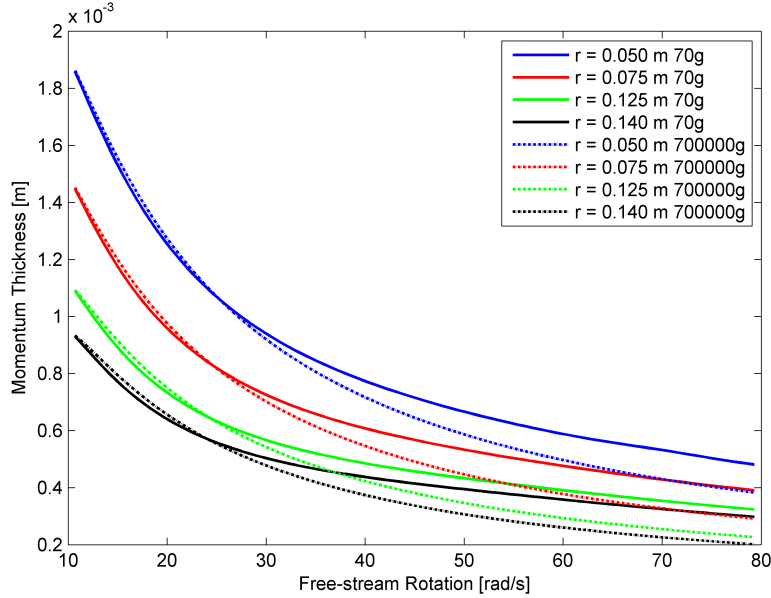
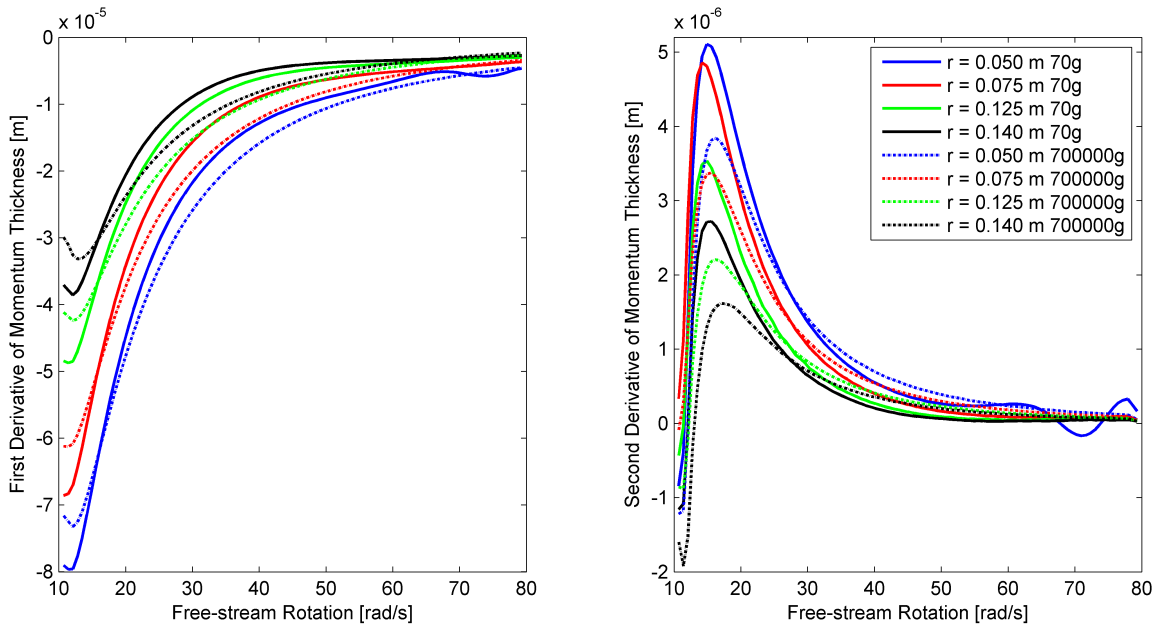
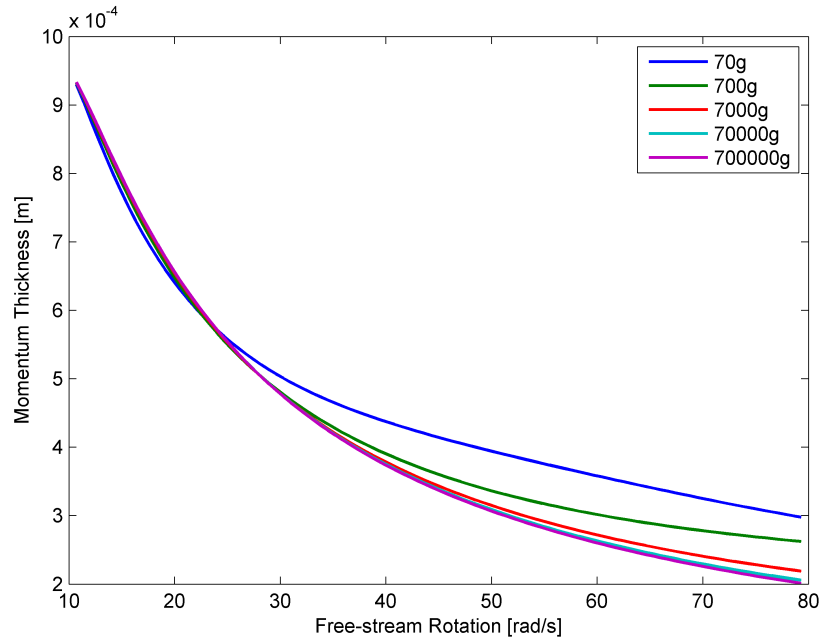


Figure 8.20: Tangential Momentum Thickness Derivative Comparison for the Accelerating Rotating Disk



The behaviour is similar to a flat plate in acceleration. The momentum thickness is monotonically decreasing. The first derivative approaches zero near the end of the acceleration event. This is an indica-

Figure 8.21: Tangential Momentum Thickness Comparison at  $r = 0.14$  m in Accelerating Conditions



tion that the momentum thickness approaches an asymptotic value. The value is indirectly proportional to acceleration strength. The rotating disk boundary layer is sensitive to sudden acceleration. The first derivative decrease at the beginning stages of the event before it increases and approach zero. The leads to two inflection points in the second derivative as a response to sudden acceleration. At low accelerations, i.e. 70g a disturbance is seen in the final stages of the acceleration event. This is due to effects of the centre stationary vortex.

The Shape Factor results for the tangential direction is shown in *Figures 8.22 and 8.23*.

Since the displacement and momentum thickness results are similar to the acceleration flat plate results, the shape factor displays similar trends as well. At the lower accelerations, 70g and 700g, the shape factor decrease to a minimum value. It then increases an attempt to recover the starting value. At the plate edge, the value is not fully recovered, while further away form the edge, the value is overshoot. The first derivative indicates that an asymptotic value is approached near the end of the event. The higher acceleration cases, 70 000g and 700 000g, is monotonically decreasing an approaches a minimum value. While the 7000g displays behaviour is between the lower acceleration and higher acceleration cases. It is monotonically decreasing of the first half of the event, after which it has a slight upward tendency. All the value tend towards and asymptotic limit that is dependant on acceleration strength. The second derivatives of all results show that the shape factor is affected by sudden acceleration. This effect is independent on acceleration strength.

8.2. RESULTS AND DISCUSSION - ACCELERATION

Figure 8.22: Tangential Shape Factor Comparison for the Accelerating Rotating Disk

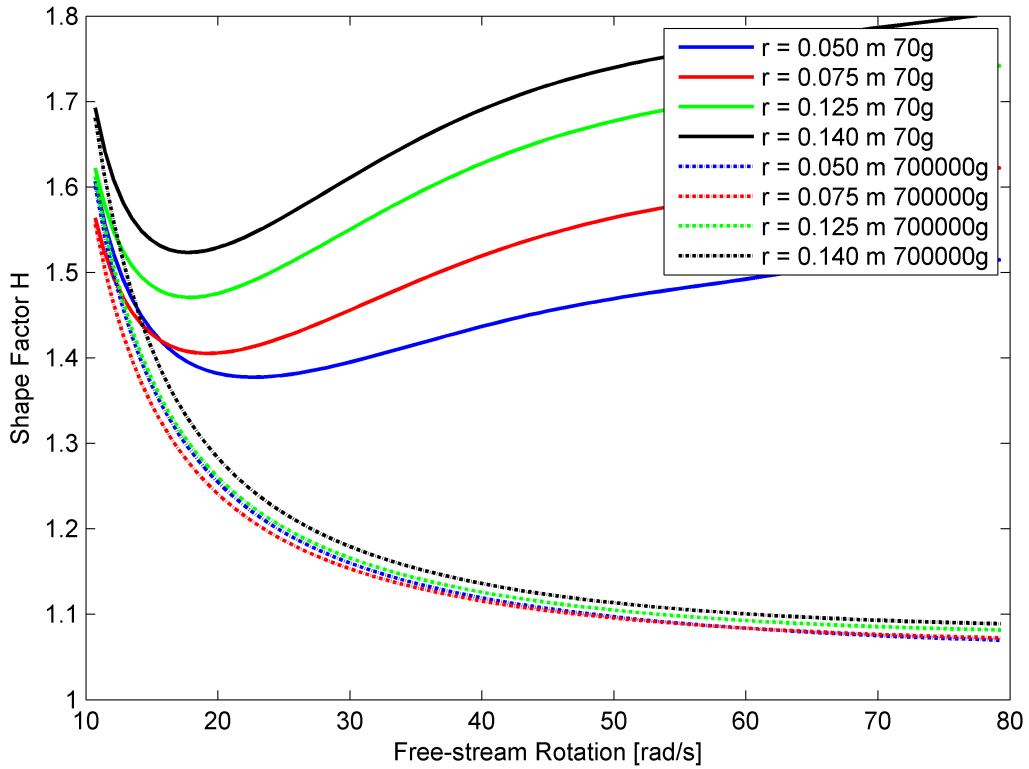
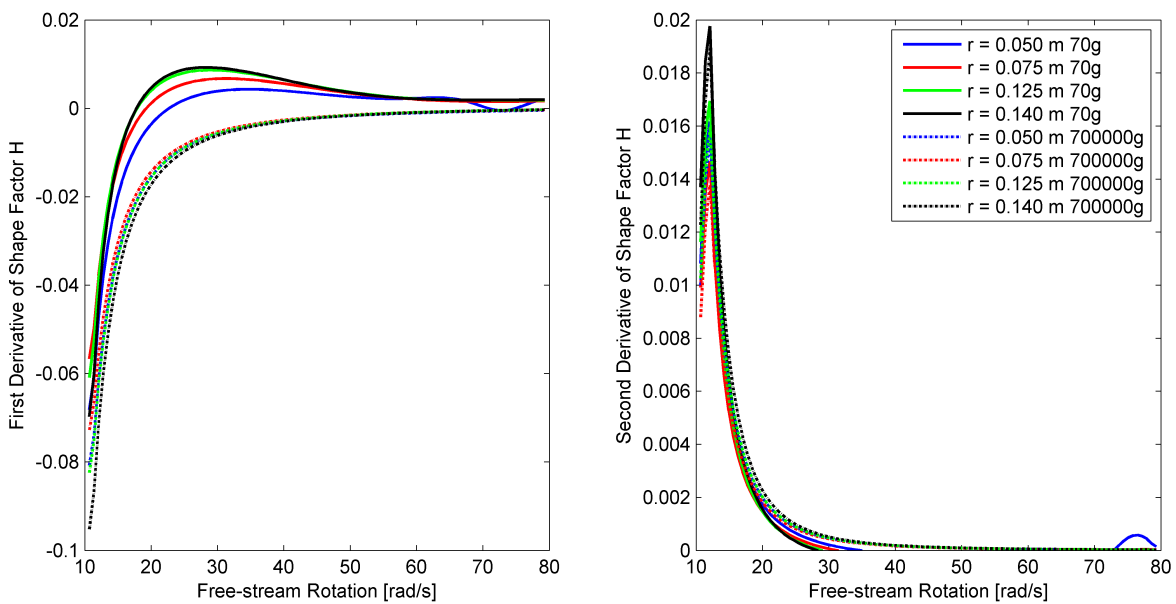


Figure 8.23: Tangential Shape Factor Derivative Comparison for the Accelerating Rotating Disk



### 8.2.2.2 Radial Parameters

Displacement Thickness results for the radial direction is shown in *Figures 8.24-8.26*.

Figure 8.24: Radial Displacement Thickness Comparison for the Accelerating Rotating Disk

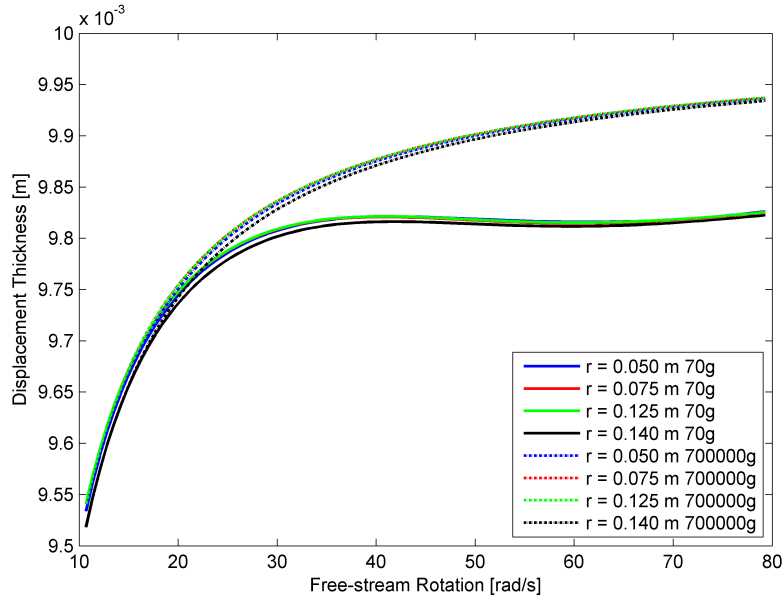
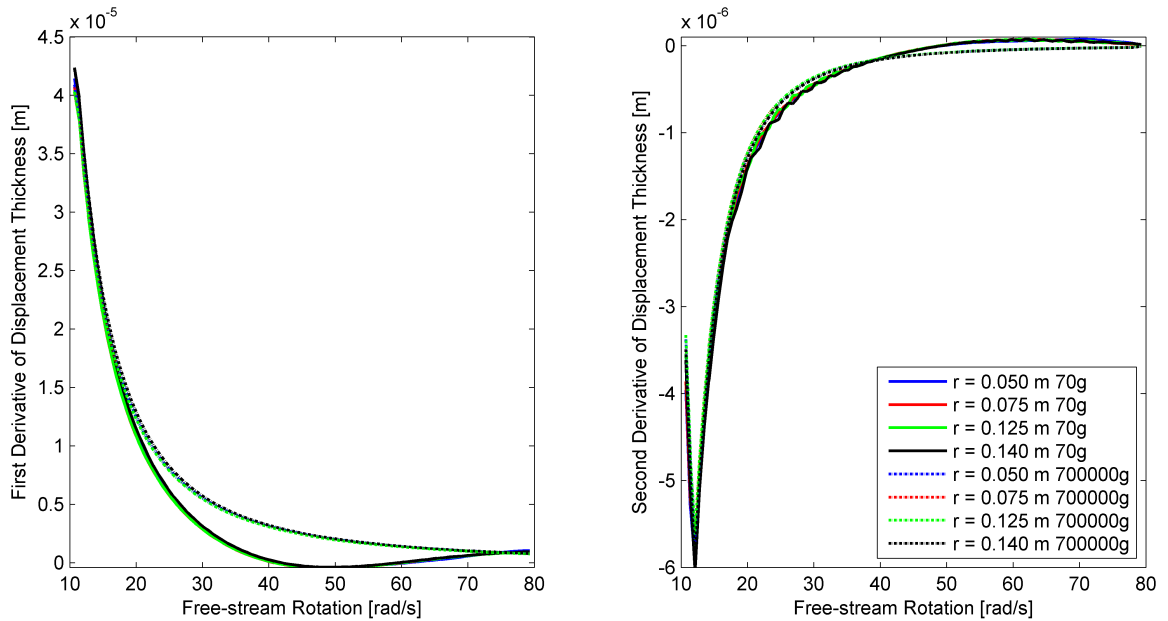
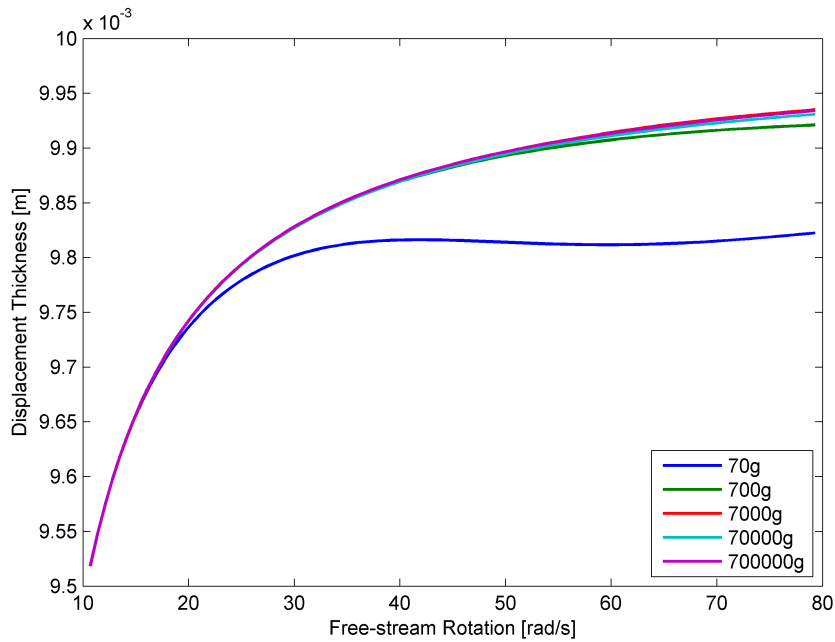


Figure 8.25: Radial Displacement Thickness Derivatives Comparison for the Accelerating Rotating Disk



The displacement thickness is monotonically increasing. The 70g acceleration case has a lower re-

Figure 8.26: Radial Displacement Thickness Comparison at  $r = 0.14$  m in Accelerating Conditions



sults, while all the other cases have results that is almost on top of each other. The first derivative shows that the 70g case has small disturbances near the end of the event. For this case the final result may approximate an asymptotic value if the event is carried on for long enough. The existence of such an asymptote can not be conclusively proved with the results here. The first derivatives of the accelerations higher than 70g do however approximate zero indicating the existence of the asymptote. An inflection point is present in the second derivative. This is a result of the response to sudden acceleration. It is not dependant on acceleration strength. At the point closest to the centre, the 70g, 700g and 7 000g cases shown unsteady behaviour. This behaviour is damped out further away from the centre. This is a result of the interference of the station vortex at the centre of the plate.

The momentum thickness results in the radial direction are shown in *Figures 8.27-8.29*.

The momentum thickness is monotonically decreasing. It show similar tendencies as the displacement thickness. The 70g case result is higher than the remainder of the acceleration cases. The other case results are of the same order and have values than are close together. The 70g case shows small disturbances in the first derivative. This occurs near the end of the acceleration event. The first derivatives of the other cases approximates zero. An inflection point is noted in all cases of the second derivative. The same unsteady behaviour that was seen in the displacement thickness is seen here. Closer to the centre of the plate, the flow is affected by the central stationary vortex, this is evident in the low frequency oscillations of the second derivative.

CHAPTER 8. BOUNDARY LAYER RESPONSE IN PURE ROTATION - ROTATING DISK FLOW

Figure 8.27: Radial Momentum Thickness Comparison for the Accelerating Rotating Disk

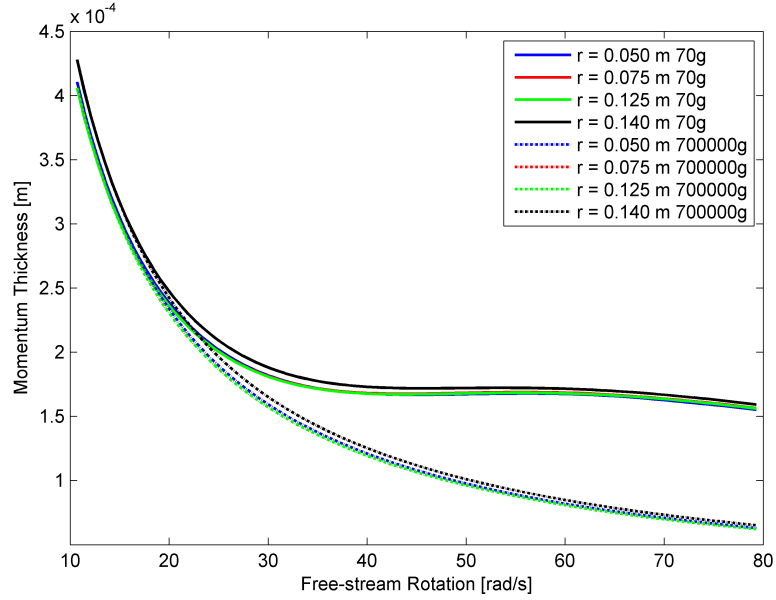
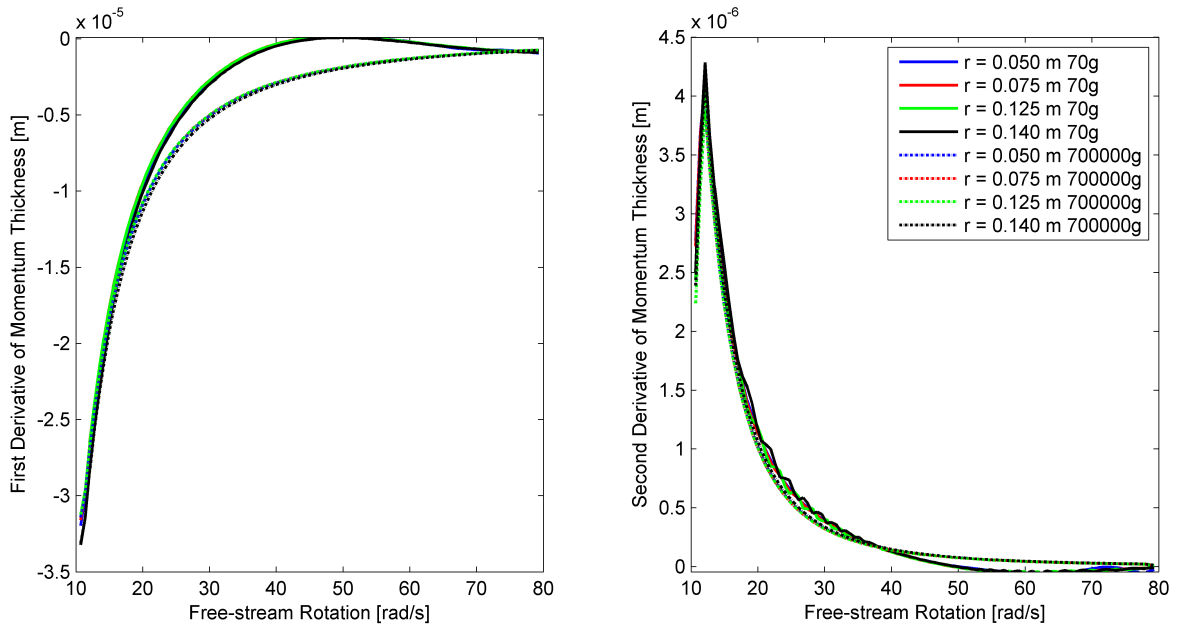


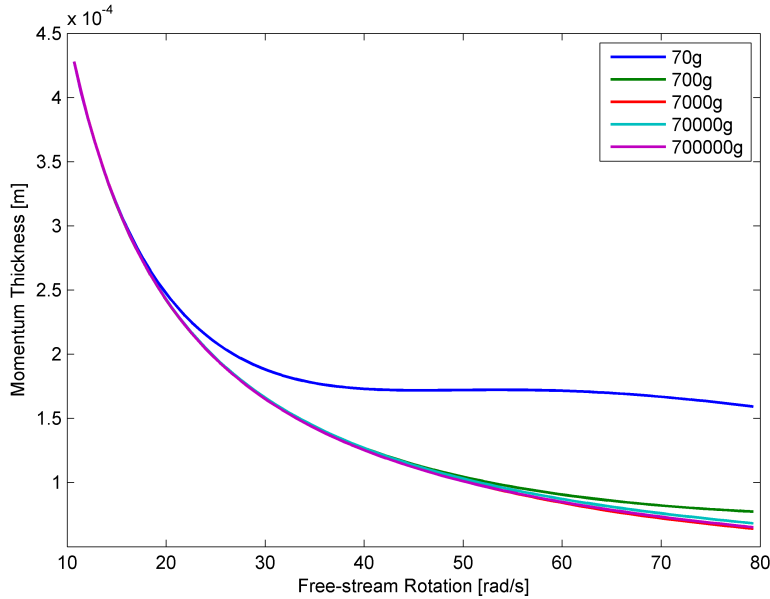
Figure 8.28: Radial Momentum Thickness Derivative Comparison for the Accelerating Rotating Disk





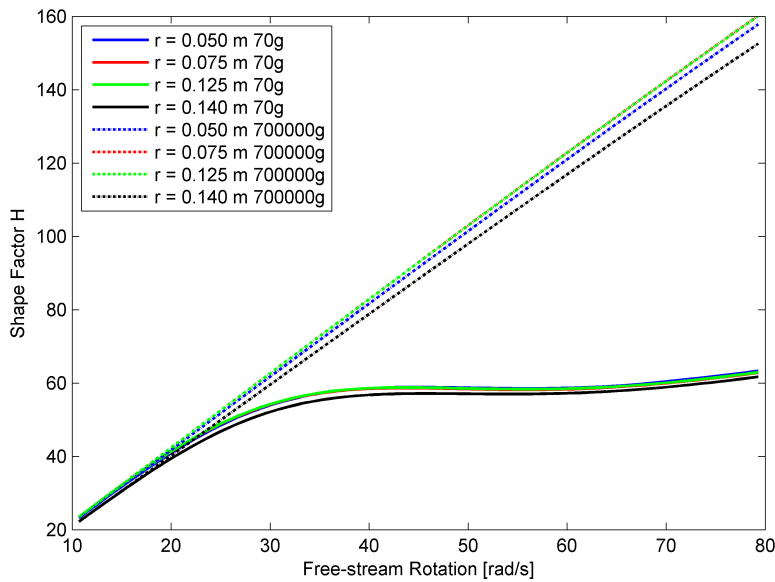
8.2. RESULTS AND DISCUSSION - ACCELERATION

Figure 8.29: Radial Momentum Thickness Comparison at  $r = 0.14$  m in Accelerating Conditions



Shape factor results for the radial direction are shown in *Figures 8.30*.

Figure 8.30: Radial Shape Factor Comparison for the Accelerating Rotating Disk



The shape factor response of the radial direction can be divided in three groupings; linear behaviour, non-linear behaviour and mixed linear/non-linear behaviour. This behaviour is dependant on distance from the centre of the plate. Close to the centre the flow is affected by the central vortex, while it has a lesser effect further away.

## CHAPTER 8. BOUNDARY LAYER RESPONSE IN PURE ROTATION - ROTATING DISK FLOW

---

In the regions further away from the centre the higher acceleration cases, 700 000g, 70 000g and 7 000g, displays linear behaviour in the shape factor. The values increase linearly along the trajectory of the event. The 70g case shows non-linear behaviour and has a much lower value than the other cases. The 700g case appears to have a mixed response. At first it has similar values to the higher acceleration cases, but at later stages in the event, the behaviour becomes non-linear.

In the regions closer to the centre of the disk, the 700 000g shows linear behaviour, the 70g non-linear and the remainder of the cases shows mixed behaviour.

The behaviour as described above is reflected in the first and second derivatives for the shape factor.

In the first derivative, the linear grouping has near-steady values of the same order. The non-linear grouping (70g), has variable result. Initially the mixed grouping has the same results as the linear grouping. In the later stages of the acceleration event the result tend toward the value of the non-linear.

The second derivative shows sinusoidal behaviour for the 70g case with low frequency disturbances. The 700g case shows high frequency disturbances near the disk centre, that is damped out further away from the centre. The same disturbance is present in the 7 000g cases, but with a lower frequency and amplitude. The higher acceleration cases approximates zero.

The flow in the radial direction is a secondary effect of the tangential acceleration. The shape factor therefore dependant on secondary effect. It is dependant on acceleration strength and is affected by its position on the plate. The central stationary vortex on the plate influences the boundary layer parameters. This effect of the influence is indirectly proportional to acceleration strength.

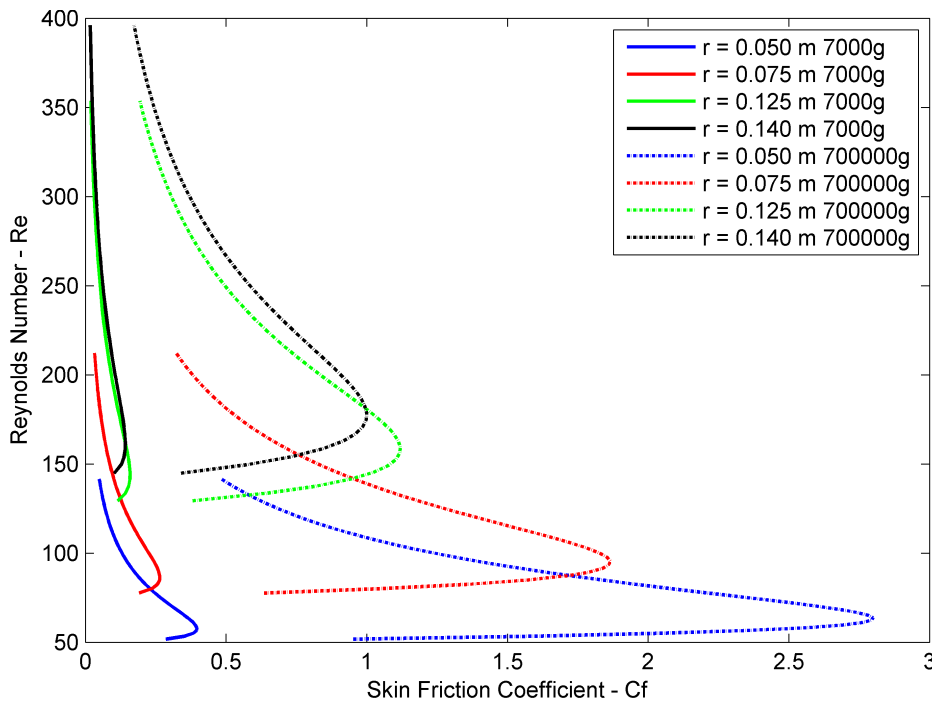
### 8.2.3 Skin Friction Coefficients

The skin friction coefficients on the rotating disk were determined in a similar manner as for the flat plate.

$$\begin{aligned}
 \tau_{\theta_{wall}} &= \left( \mu \frac{\partial u_{\theta}}{\partial y} \right) \Big|_{wall} \\
 \tau_{r_{wall}} &= \mu \frac{\partial u_r}{\partial y} \Big|_{wall} \\
 \tau_{wall} &= \sqrt{\tau_{\theta_{wall}}^2 + \tau_{r_{wall}}^2} \\
 C_f &= \frac{\tau_{wall}}{0.5\rho U_{\infty}^2}
 \end{aligned}
 \tag{8.13}$$

The results are indicated in *Figures 8.31-8.32*.

Figure 8.31: Comparison between Skin Friction Coefficients at Various Free-Stream Rotational Reynolds Numbers for Accelerating Conditions



The behaviour of the skin friction coefficient is similar to the general tendencies seen for the flat plate. There is an initial increase in the skin friction coefficient. After a maximum value is reached, the skin friction coefficient decreases and approaches an asymptotic value. Higher accelerations result in higher skin friction coefficients. The skin friction is lower at positions further from the centre of the plate. The values are dependant both on position on the plate and acceleration strength.

CHAPTER 8. BOUNDARY LAYER RESPONSE IN PURE ROTATION - ROTATING DISK FLOW

Figure 8.32: Comparison between Skin Friction Coefficients at Various Disk Positions for Accelerating Conditions

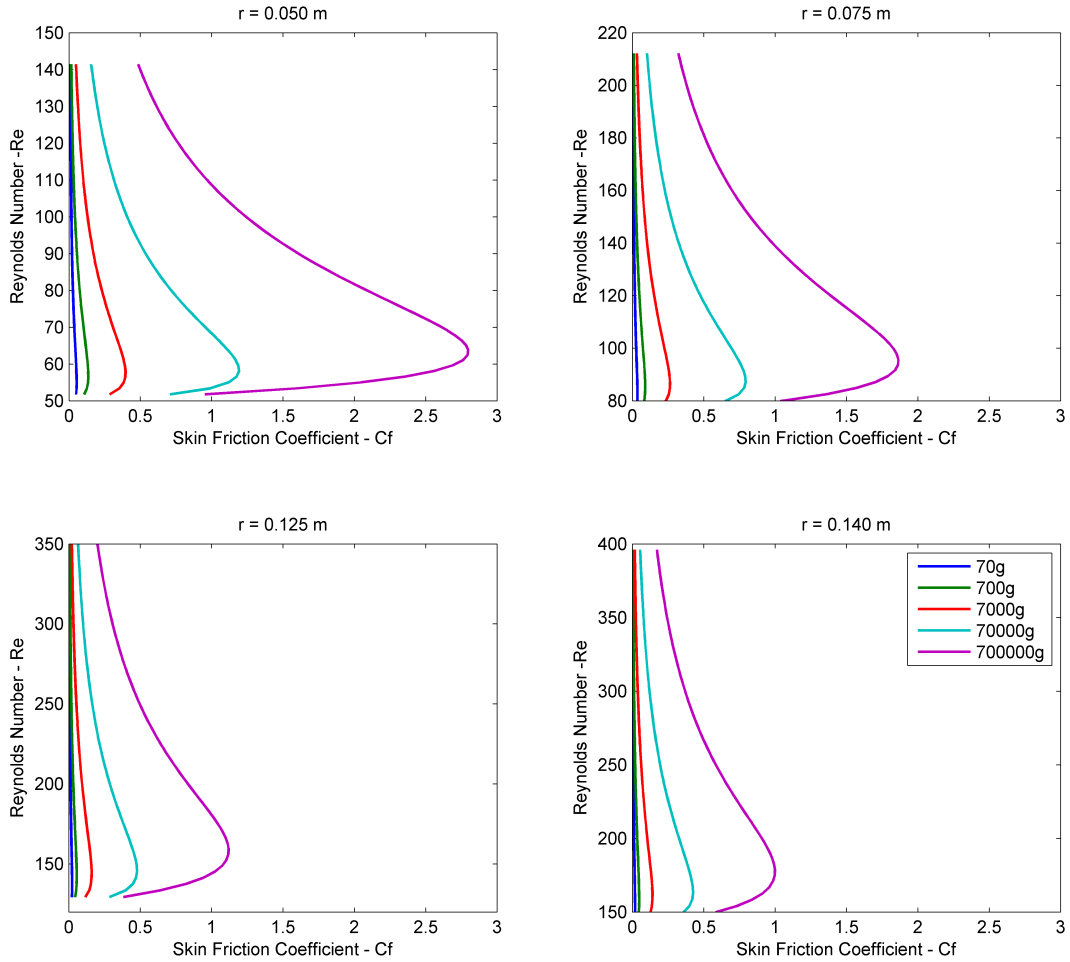
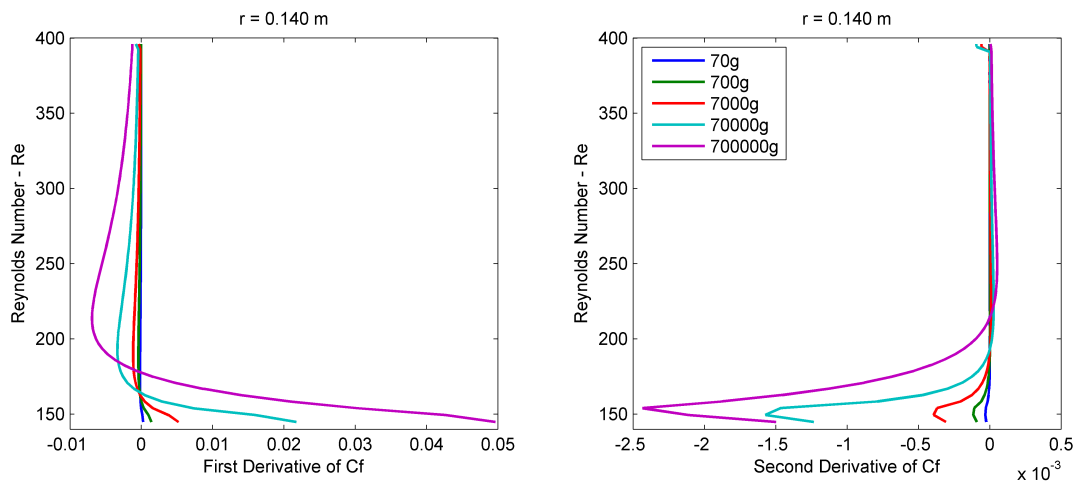


Figure 8.33: Derivatives of Skin Friction Coefficient for Accelerating Conditions

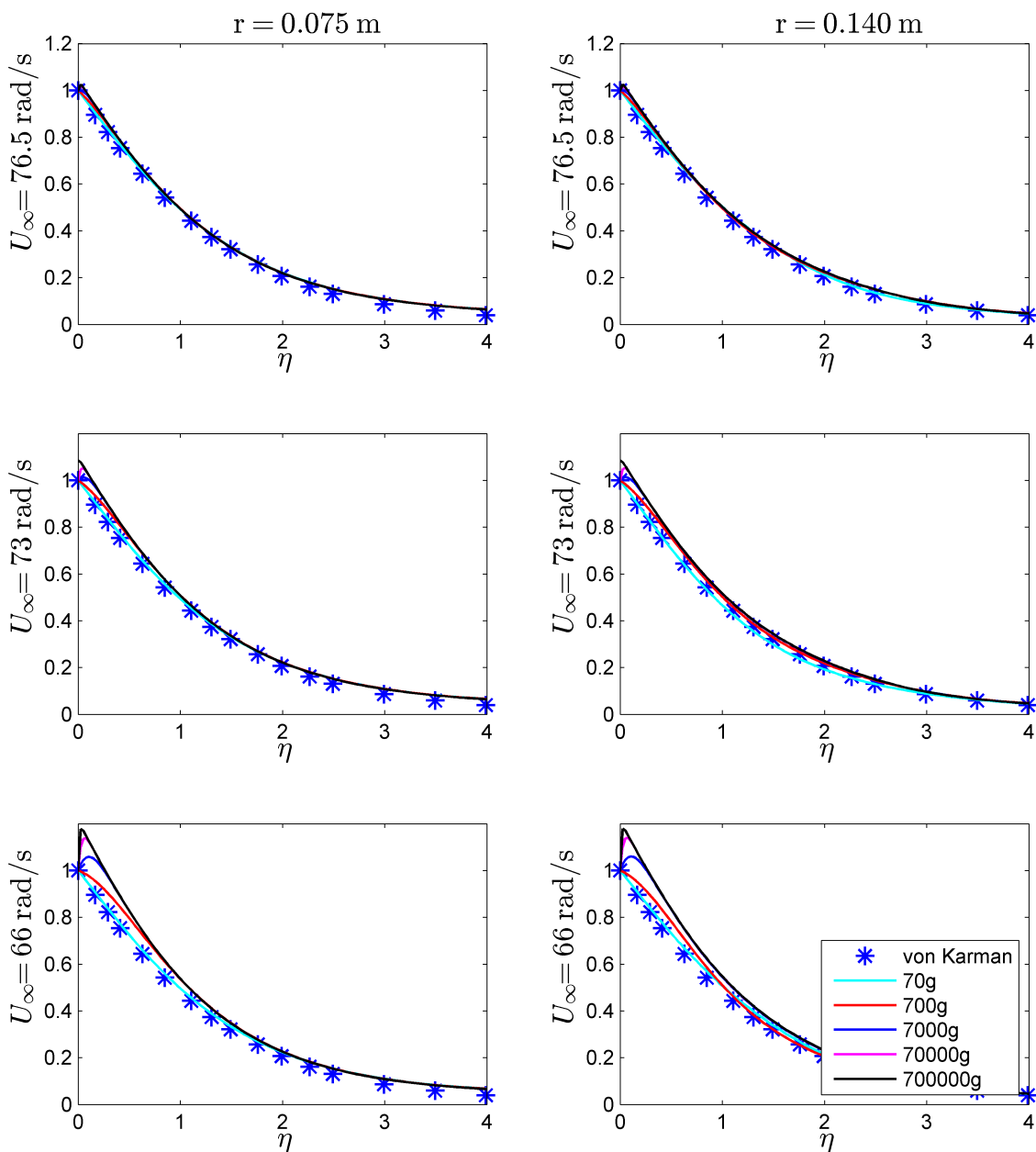


## 8.3 Results and Discussion - Deceleration

### 8.3.1 Velocity Profiles

The result from the decelerating simulation for the rotating disk in the **tangential direction** is shown in *Figures 8.34-8.36* respectively. The non-dimensional distance from the wall,  $\eta$ , is determined by *Equation 6.28*.

Figure 8.34: Non-Dimensional Tangential Velocity Profiles: Rotating Disk - Deceleration Grouping I



CHAPTER 8. BOUNDARY LAYER RESPONSE IN PURE ROTATION - ROTATING DISK FLOW

Figure 8.35: Non-Dimensional Tangential Velocity Profiles: Rotating Disk - Deceleration Grouping II

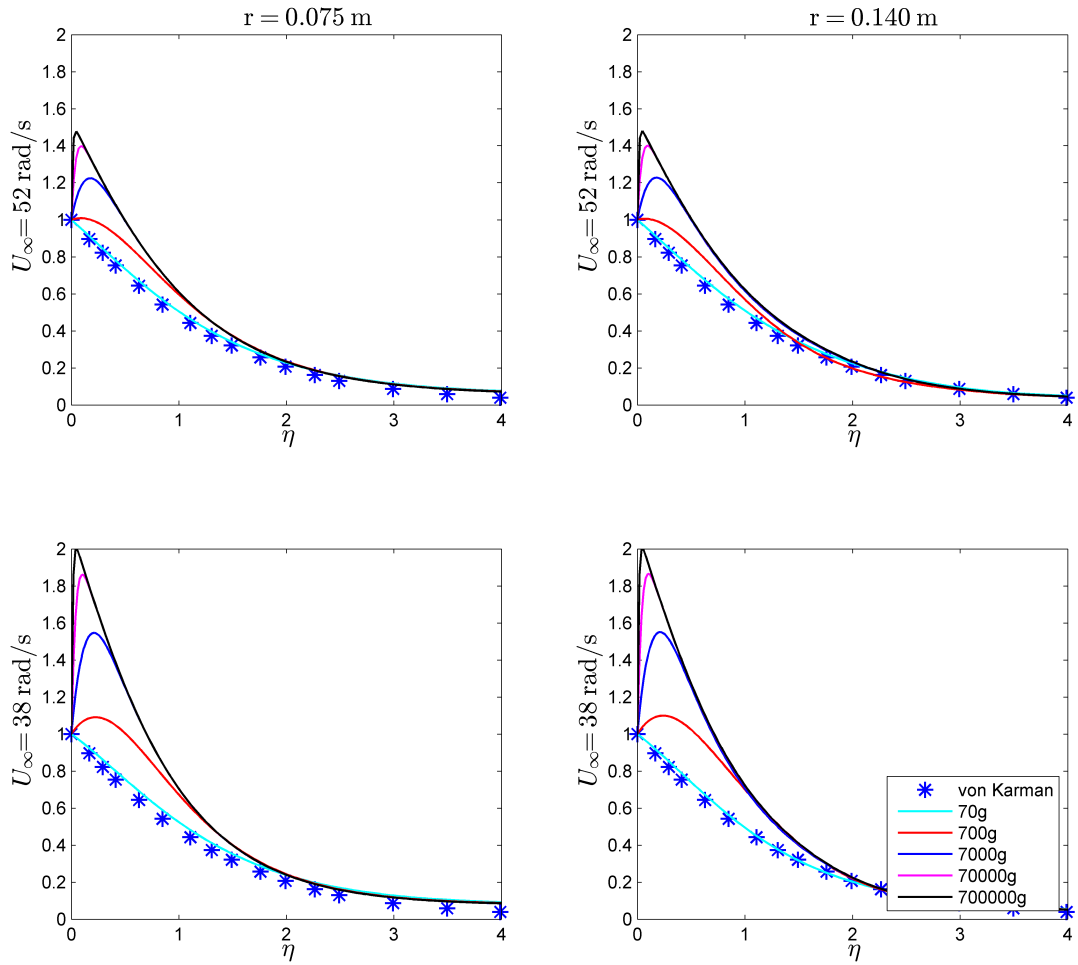
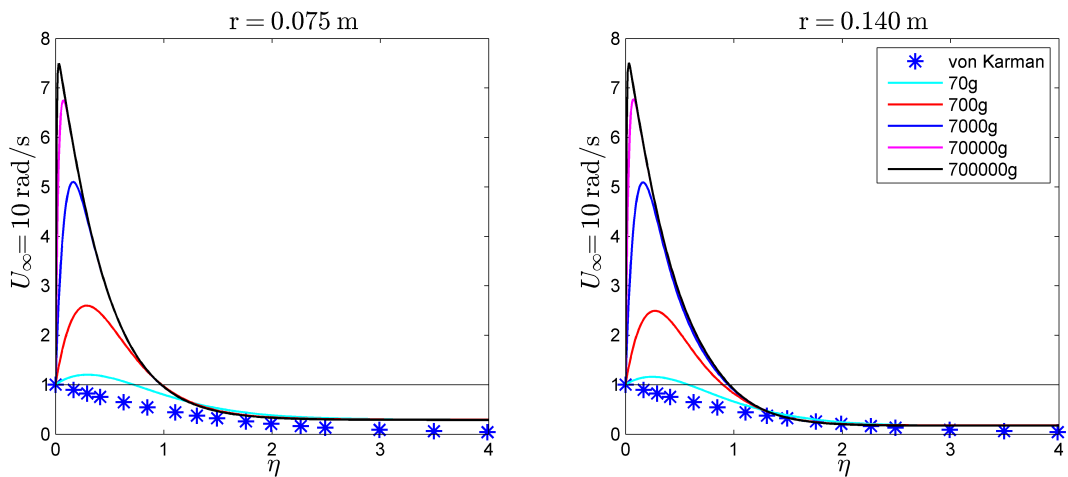


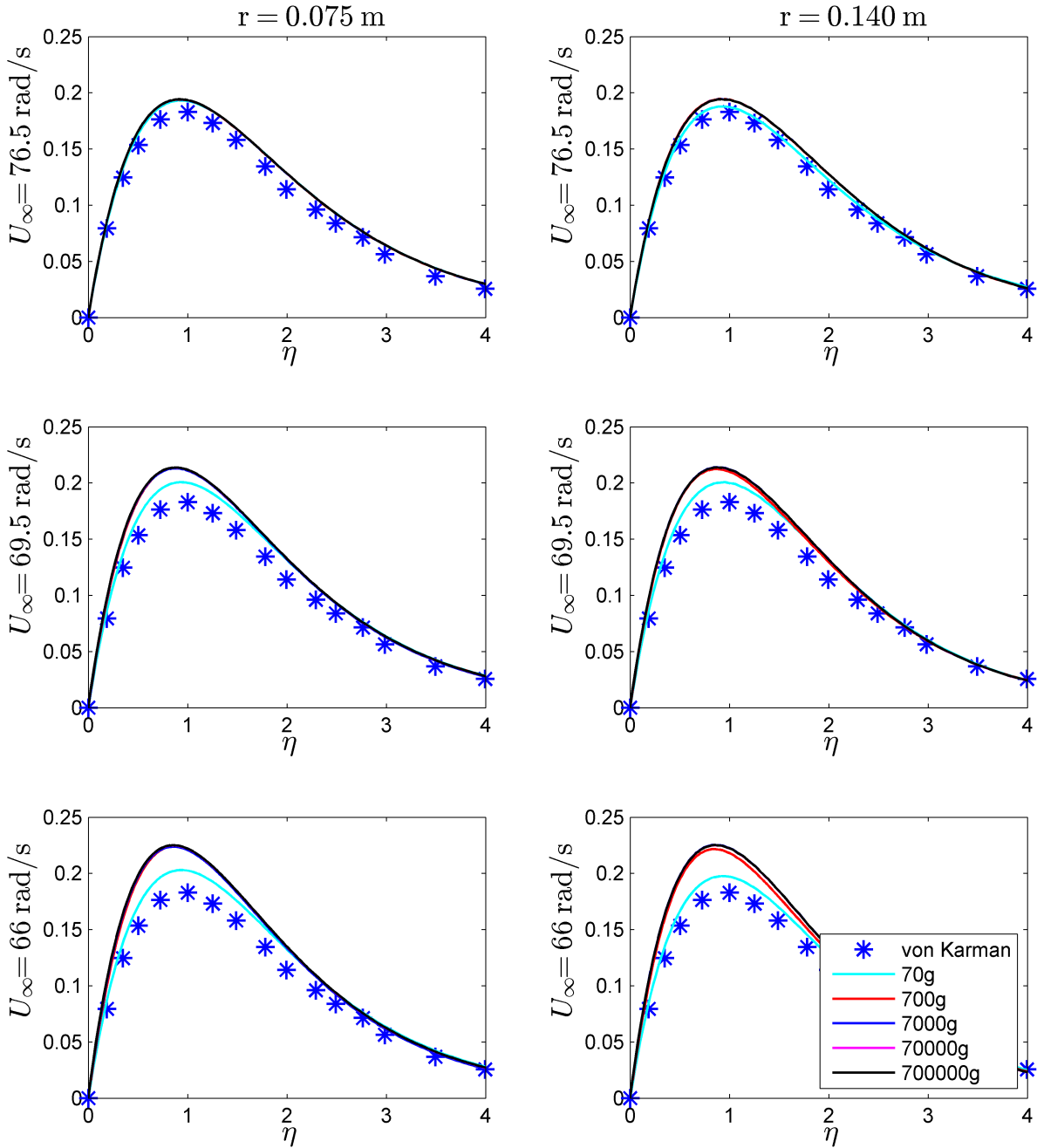
Figure 8.36: Non-Dimensional Tangential Velocity Profiles: Rotating Disk - Deceleration Grouping III



8.3. RESULTS AND DISCUSSION - DECELERATION

The result from the decelerating simulation for the rotating disk in the **radial direction** is shown in Figures 8.37-8.39 respectively.

Figure 8.37: Non-Dimensional Radial Velocity Profiles: Rotating Disk - Deceleration Grouping I



CHAPTER 8. BOUNDARY LAYER RESPONSE IN PURE ROTATION - ROTATING DISK FLOW

Figure 8.38: Non-Dimensional Radial Velocity Profiles: Rotating Disk - Deceleration Grouping II

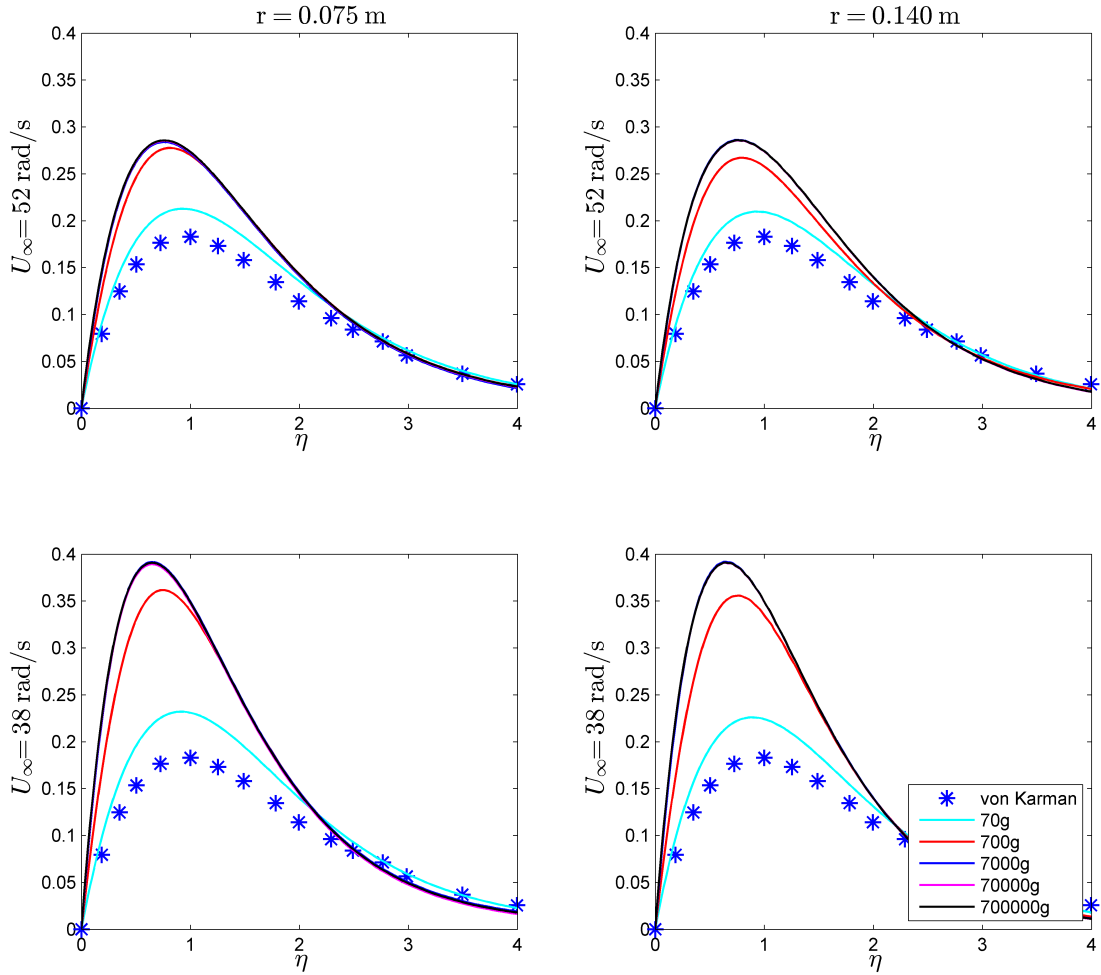
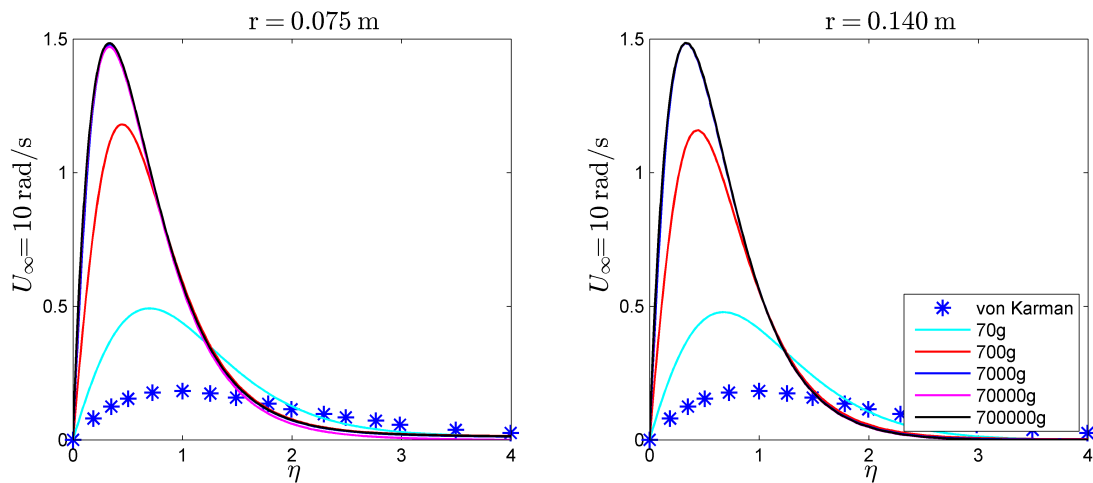


Figure 8.39: Non-Dimensional Radial Velocity Profiles: Rotating Disk - Deceleration Grouping III

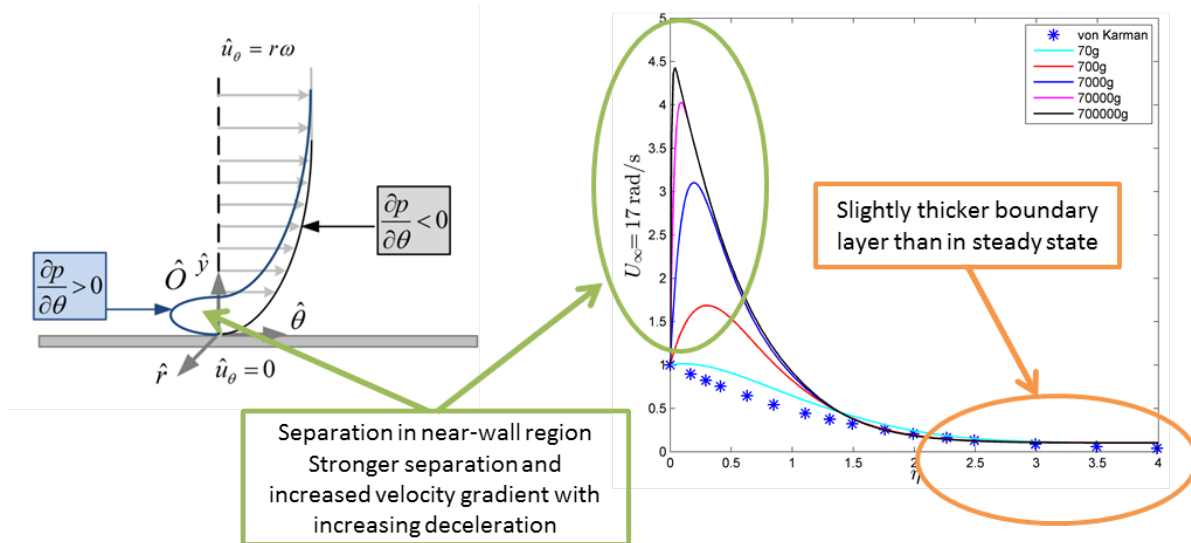




8.3. RESULTS AND DISCUSSION - DECELERATION

The result from the decelerating simulation for the rotating disk showed that there is a slight thickening of the boundary layer in the far-field across all the cases of deceleration. The boundary layer reverses almost immediately, except in the 70g cases where minimal reversals is observed. The strength of the flow reversal is directly proportional to the magnitude of the deceleration. The non-dimensional far-field values of the simulated profiles are all equal in value.

Figure 8.40: Sample results and observations for tangential flow in deceleration



The result from the decelerating simulation for the rotating disk in the **radial direction** indicates an immediate reaction to the deceleration. The boundary layer height is comparable to steady state results, but there is an increased apex value. In the Grouping I results, all the deceleration cases are of the same value, with the exception of the 70g result that breaks away. In the grouping II and III results further thinning of the boundary layer is seen and the 70g as well as the 700g case breaks away from the commonly shared profile values. This is an indication that the radial flow, being a secondary flow effect, is slow to respond to changing conditions in the tangential direction.

The results obtained for the rotating disk in deceleration has similarities to the decelerating flat plat. The flow reversal is common behaviour between the cases. This flow is also mostly momentum dominant, with the exception of the 70g deceleration analysis, as in the case of the accelerating disk. The reaction to deceleration has immediate effects on the boundary layer profile.

CHAPTER 8. BOUNDARY LAYER RESPONSE IN PURE ROTATION - ROTATING DISK FLOW

The boundary layer equations for unsteady rotation were shown in *Section 8.1*:

**r-momentum**

$$\frac{\partial \hat{\rho} \hat{u}_r}{\partial t} + \hat{u}_r \frac{\partial \hat{\rho} \hat{u}_r}{\partial \hat{r}} + \frac{\hat{u}_\theta}{\hat{r}} \frac{\partial \hat{\rho} \hat{u}_r}{\partial \hat{\theta}} - \frac{\hat{\rho} \hat{u}_\theta^2}{\hat{r}} + \hat{u}_y \frac{\partial \hat{\rho} \hat{u}_r}{\partial \hat{y}} = -\frac{\partial \hat{p}}{\partial \hat{r}} + \frac{\partial}{\partial \hat{y}} \left( \hat{\mu} \frac{\partial \hat{u}_r}{\partial \hat{y}} \right) - 2\hat{\rho} \hat{u}_\theta \omega_y + \hat{\rho} \hat{r} \omega_y^2 \quad (8.14)$$

**$\theta$ -momentum**

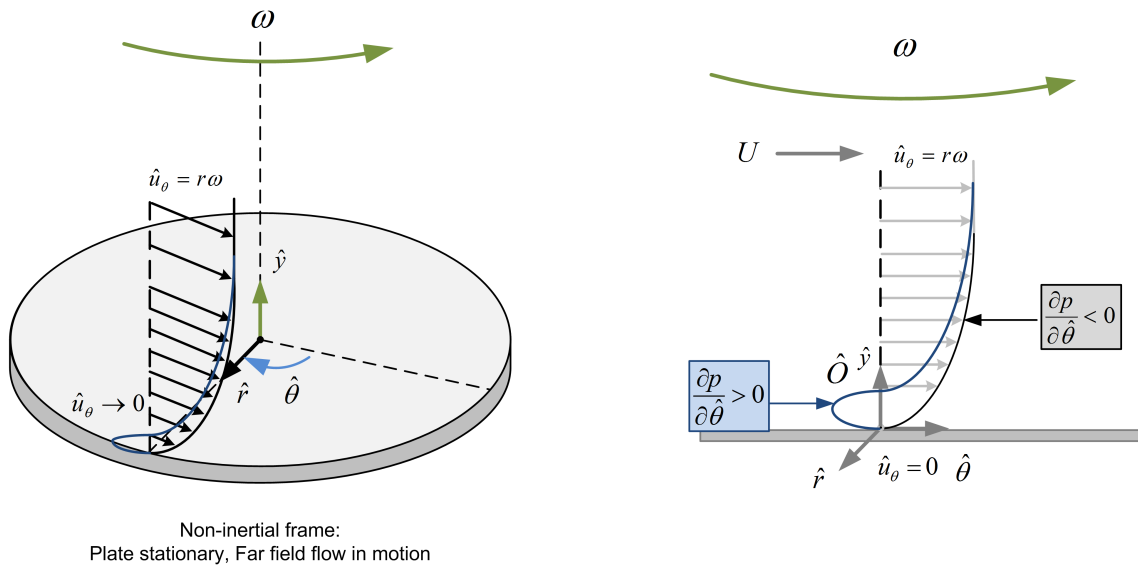
$$\frac{\partial \hat{\rho} \hat{u}_\theta}{\partial t} + \hat{u}_r \frac{\partial \hat{\rho} \hat{u}_\theta}{\partial \hat{r}} + \frac{\hat{u}_\theta}{\hat{r}} \frac{\partial \hat{\rho} \hat{u}_\theta}{\partial \hat{\theta}} + \frac{\hat{\rho} \hat{u}_\theta \hat{u}_r}{\hat{r}} + \hat{u}_y \frac{\partial \hat{\rho} \hat{u}_\theta}{\partial \hat{y}} = -\frac{1}{\hat{r}} \frac{\partial \hat{p}}{\partial \hat{\theta}} + \frac{\partial}{\partial \hat{y}} \left( \hat{\mu} \frac{\partial \hat{u}_\theta}{\partial \hat{y}} \right) - 2\hat{\rho} \hat{u}_r \omega_y - \hat{\rho} \hat{r} \dot{\omega}_y \quad (8.15)$$

**y-momentum**

$$0 = -\frac{\partial \hat{p}}{\partial \hat{y}} \quad (8.16)$$

These equations are responsible for the observed behaviour of the flow in deceleration as depicted in *Figure 8.41*.

Figure 8.41: Boundary layer profile for steady angular deceleration



In the tangential direction, the Coriolis and Euler forces are the only non-inertial force components present. In the accelerating case these forces acted as momentum sources. Here, in the decelerating case the forces act as momentum sinks.

$$\frac{\partial \hat{\rho} \hat{u}_\theta}{\partial t} + \hat{u}_r \frac{\partial \hat{\rho} \hat{u}_\theta}{\partial \hat{r}} + \frac{\hat{u}_\theta}{\hat{r}} \frac{\partial \hat{\rho} \hat{u}_\theta}{\partial \hat{\theta}} + \frac{\hat{\rho} \hat{u}_\theta \hat{u}_r}{\hat{r}} + \hat{u}_y \frac{\partial \hat{\rho} \hat{u}_\theta}{\partial \hat{y}} = -\frac{1}{\hat{r}} \frac{\partial \hat{p}}{\partial \hat{\theta}} + \frac{\partial}{\partial \hat{y}} \left( \hat{\mu} \frac{\partial \hat{u}_\theta}{\partial \hat{y}} \right) + \underbrace{2\hat{\rho} \hat{u}_r \omega_y}_{\text{Coriolis}} + \underbrace{\hat{\rho} \hat{r} \dot{\omega}_y}_{\text{Euler}}$$

In deceleration the Euler force becomes negative since  $\dot{\omega}_y$  is acting in a direction opposite to the tangential rotation  $\omega_y$  of the plate. The tangential rotation decreases as a result of the deceleration. This results in a decrease in momentum on the right hand side of the equation. To balance the left hand side with the right, there is a decrease in momentum on the left hand side.

8.3. RESULTS AND DISCUSSION - DECELERATION

$$\frac{\partial \hat{\rho} \hat{u}_\theta}{\partial t} + \hat{u}_r \frac{\partial \hat{\rho} \hat{u}_\theta}{\partial \hat{r}} + \frac{\hat{u}_\theta}{\hat{r}} \frac{\partial \hat{\rho} \hat{u}_\theta}{\partial \hat{\theta}} + \frac{\hat{\rho} \hat{u}_\theta \hat{u}_r}{\hat{r}} + \hat{u}_y \frac{\partial \hat{\rho} \hat{u}_\theta}{\partial \hat{y}} = -\frac{1}{\hat{r}} \frac{\partial \hat{p}}{\partial \hat{\theta}} + \frac{\partial}{\partial \hat{y}} \left( \hat{\mu} \frac{\partial \hat{u}_\theta}{\partial \hat{y}} \right) + 2\hat{\rho} \hat{u}_r \omega_y + \hat{\rho} \hat{r} \dot{\omega}_y$$

Subsequently, the tangential velocity,  $\hat{u}_\theta$ , decreases as it is a function of the rotational velocity:

$$\hat{u}_\theta = \hat{r} \omega_y \quad (8.17)$$

The velocity gradient in the near-wall region decreases.

$$\frac{\partial \hat{\rho} \hat{u}_\theta}{\partial t} + \hat{u}_r \frac{\partial \hat{\rho} \hat{u}_\theta}{\partial \hat{r}} + \frac{\hat{u}_\theta}{\hat{r}} \frac{\partial \hat{\rho} \hat{u}_\theta}{\partial \hat{\theta}} + \frac{\hat{\rho} \hat{u}_\theta \hat{u}_r}{\hat{r}} + \hat{u}_y \frac{\partial \hat{\rho} \hat{u}_\theta}{\partial \hat{y}} = -\frac{1}{\hat{r}} \frac{\partial \hat{p}}{\partial \hat{\theta}} + \frac{\partial}{\partial \hat{y}} \left( \hat{\mu} \frac{\partial \hat{u}_\theta}{\partial \hat{y}} \right) + \hat{\rho} \hat{u}_r \omega_y + \hat{\rho} \hat{r} \dot{\omega}_y$$

In order to balance the decrease in the near-wall region, the pressure gradient is adjusted. At a certain point an adverse pressure gradient forms and the flow in the near-wall region separates.

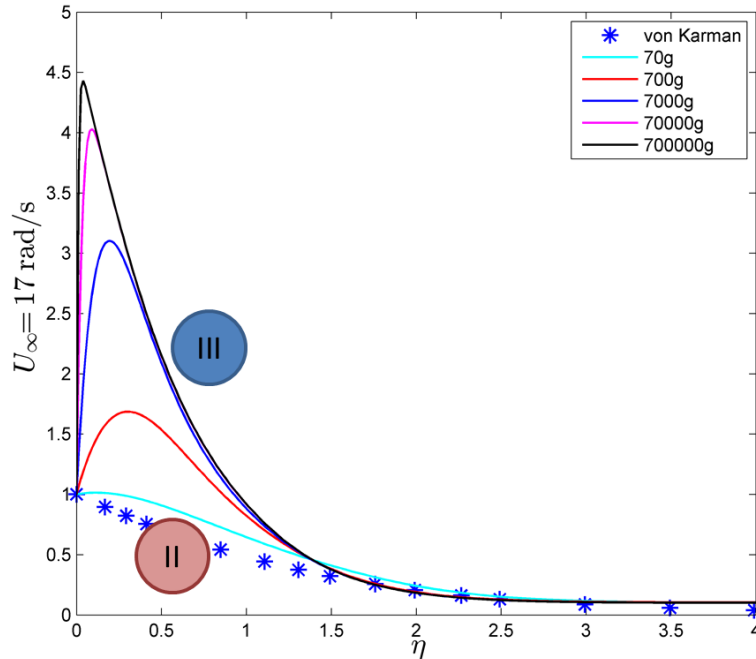
$$\frac{\partial \hat{\rho} \hat{u}_\theta}{\partial t} + \hat{u}_r \frac{\partial \hat{\rho} \hat{u}_\theta}{\partial \hat{r}} + \frac{\hat{u}_\theta}{\hat{r}} \frac{\partial \hat{\rho} \hat{u}_\theta}{\partial \hat{\theta}} + \frac{\hat{\rho} \hat{u}_\theta \hat{u}_r}{\hat{r}} + \hat{u}_y \frac{\partial \hat{\rho} \hat{u}_\theta}{\partial \hat{y}} = -\frac{1}{\hat{r}} \frac{\partial \hat{p}}{\partial \hat{\theta}} + \frac{\partial}{\partial \hat{y}} \left( \hat{\mu} \frac{\partial \hat{u}_\theta}{\partial \hat{y}} \right) + \hat{\rho} \hat{u}_r \omega_y + \hat{\rho} \hat{r} \dot{\omega}_y$$

In the case of the flat plate three types of responses to decelerating flow was proposed. The regions are similar to those of an accelerating case:

- **Response Type I**, which is viscous dominant.
- **Response Type II**, which is certain regions in the boundary layer are dominated by viscosity and other regions by momentum.
- **Response Type III**, which is dominated by momentum.

The rotating disk is showing a **Deceleration Response Type III** for all cases of deceleration from 700g to 700 000g analysed here. This flow is momentum dominant (*Figure 8.42*). The 70g case fall within the Response Type II category as it the neither dominated by viscous forces nor by momentum forces. As in the accelerating disk case, it is postulated that responses mostly fall within the third category.

Figure 8.42: Deceleration Response Types of the Rotating Disk



A decrease in the angular velocity,  $\omega_y$ , results in a decrease in the tangential velocity,  $u_\theta$ . This results in decrease in both the material derivative and the viscous terms.

$$\frac{\partial \hat{\rho} \hat{u}_\theta}{\partial t} + \hat{u}_r \frac{\partial \hat{\rho} \hat{u}_\theta}{\partial \hat{r}} + \frac{\hat{u}_\theta}{\hat{r}} \frac{\partial \hat{\rho} \hat{u}_\theta}{\partial \hat{\theta}} + \frac{\hat{\rho} \hat{u}_\theta \hat{u}_r}{\hat{r}} + \hat{u}_y \frac{\partial \hat{\rho} \hat{u}_\theta}{\partial \hat{y}} = -\frac{1}{\hat{r}} \frac{\partial \hat{p}}{\partial \hat{\theta}} + \frac{\partial}{\partial \hat{y}} \left( \hat{\mu} \frac{\partial \hat{u}_\theta}{\partial \hat{y}} \right) + 2\hat{\rho} \hat{u}_r \omega_y + \hat{\rho} \hat{r} \dot{\omega}_y$$

The magnitude of the decrease in the left hand side momentum terms are larger than the decrease in the viscous term. A  $\frac{\partial \hat{u}_\theta}{\partial \hat{y}}$  term is seen on both side of the equation. On the right hand side the gradient of the term is taken. This value is smaller than the magnitude of all the momentum terms on the left hand side.

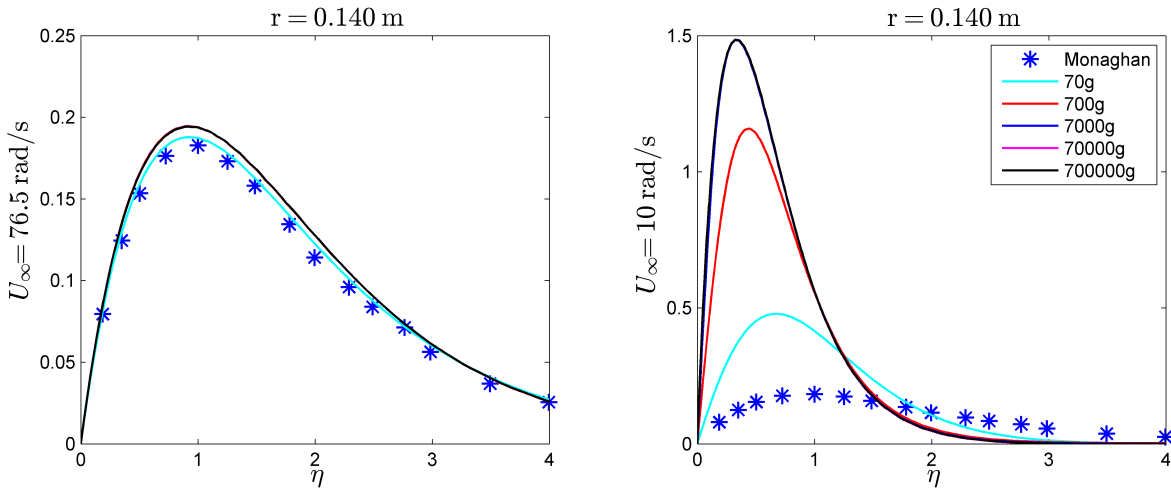
$$\frac{\partial \hat{\rho} \hat{u}_\theta}{\partial t} + \hat{u}_r \frac{\partial \hat{\rho} \hat{u}_\theta}{\partial \hat{r}} + \frac{\hat{u}_\theta}{\hat{r}} \frac{\partial \hat{\rho} \hat{u}_\theta}{\partial \hat{\theta}} + \frac{\hat{\rho} \hat{u}_\theta \hat{u}_r}{\hat{r}} + \hat{u}_y \frac{\partial \hat{\rho} \hat{u}_\theta}{\partial \hat{y}} = -\frac{1}{\hat{r}} \frac{\partial \hat{p}}{\partial \hat{\theta}} + \frac{\partial}{\partial \hat{y}} \left( \hat{\mu} \frac{\partial \hat{u}_\theta}{\partial \hat{y}} \right) + \underbrace{2\hat{\rho} \hat{u}_r \omega_y}_{\text{Coriolis}} + \underbrace{\hat{\rho} \hat{r} \dot{\omega}_y}_{\text{Euler}}$$

The response of the tangential boundary layer to deceleration therefore largely falls in the Type III category. At very small deceleration it is possible that a Type I or Type II response will be observed. Small decelerations are suggested for further work in this field.

The response the deceleration flow in the radial direction displays the same trends as in the acceleration case. The flow in the higher deceleration cases remains in the initial state, while the lower decelerations reacts has a delayed reaction (Figure 8.43).

8.3. RESULTS AND DISCUSSION - DECELERATION

Figure 8.43: Sample Results of the Radial Velocity Profiles in Deceleration



The Coriolis and Centrifugal forces represent the non-inertial effects in the radial direction.

$$\frac{\partial \hat{\rho} \hat{u}_r}{\partial t} + \hat{u}_r \frac{\partial \hat{\rho} \hat{u}_r}{\partial \hat{r}} + \frac{\hat{u}_\theta}{\hat{r}} \frac{\partial \hat{\rho} \hat{u}_r}{\partial \hat{\theta}} - \frac{\hat{\rho} \hat{u}_\theta^2}{\hat{r}} + \hat{u}_y \frac{\partial \hat{\rho} \hat{u}_r}{\partial \hat{y}} = -\frac{\partial \hat{p}}{\partial \hat{r}} + \frac{\partial}{\partial \hat{y}} \left( \hat{\mu} \frac{\partial \hat{u}_r}{\partial \hat{y}} \right) - \underbrace{2 \hat{\rho} \hat{u}_\theta \omega_y}_{\text{Coriolis}} + \underbrace{\hat{\rho} \hat{r} \omega_y^2}_{\text{Centrifugal}}$$

In the same manner as explained for the acceleration case, the Coriolis and Centrifugal forces create a feedback loop between each other. Changes in the tangential velocity eventually lead to a reduction in momentum in the radial velocity gradient.

$$\frac{\partial \hat{\rho} \hat{u}_r}{\partial t} + \hat{u}_r \frac{\partial \hat{\rho} \hat{u}_r}{\partial \hat{r}} + \frac{\hat{u}_\theta}{\hat{r}} \frac{\partial \hat{\rho} \hat{u}_r}{\partial \hat{\theta}} - \frac{\hat{\rho} \hat{u}_\theta^2}{\hat{r}} + \hat{u}_y \frac{\partial \hat{\rho} \hat{u}_r}{\partial \hat{y}} = -\frac{\partial \hat{p}}{\partial \hat{r}} + \frac{\partial}{\partial \hat{y}} \left( \hat{\mu} \frac{\partial \hat{u}_r}{\partial \hat{y}} \right) - \diamond 2 \hat{\rho} \hat{u}_\theta \omega_y + \diamond \hat{\rho} \hat{r} \omega_y^2$$

The eventual decrease on the right hand side of the equation leads to a decrease in momentum on the left hand side. The radial velocity,  $u_r$ , decreases as a result. This mechanism is time dependant and depends on the strength of the deceleration parameter.

$$\frac{\partial \hat{\rho} \hat{u}_r}{\partial t} + \hat{u}_r \frac{\partial \hat{\rho} \hat{u}_r}{\partial \hat{r}} + \frac{\hat{u}_\theta}{\hat{r}} \frac{\partial \hat{\rho} \hat{u}_r}{\partial \hat{\theta}} - \frac{\hat{\rho} \hat{u}_\theta^2}{\hat{r}} + \hat{u}_y \frac{\partial \hat{\rho} \hat{u}_r}{\partial \hat{y}} = -\frac{\partial \hat{p}}{\partial \hat{r}} + \frac{\partial}{\partial \hat{y}} \left( \hat{\mu} \frac{\partial \hat{u}_r}{\partial \hat{y}} \right) - \diamond 2 \hat{\rho} \hat{u}_\theta \omega_y + \diamond \hat{\rho} \hat{r} \omega_y^2$$

### 8.3.2 Boundary Layer Parameters

#### 8.3.2.1 Tangential Parameters

The tangential displacement thickness results for the decelerating disk are shown in *Figures 8.44-8.46*.

Figure 8.44: Tangential Displacement Thickness Comparison for the Decelerating Rotating Disk

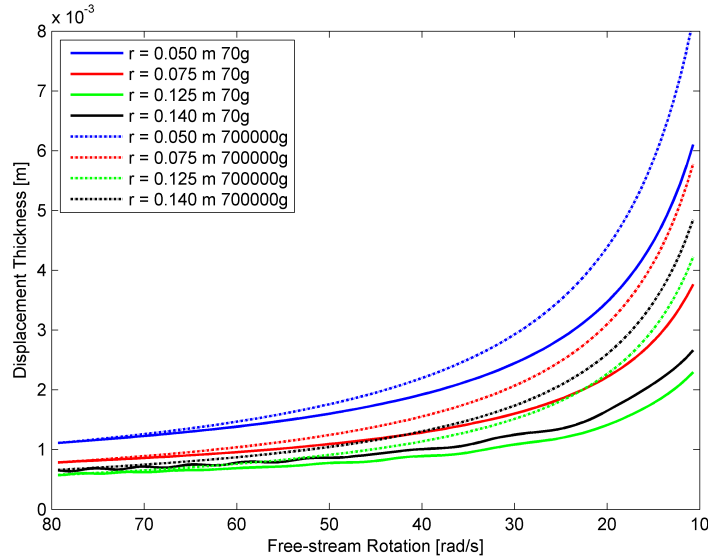


Figure 8.45: Tangential Displacement Thickness Derivative Comparison for the Decelerating Rotating Disk

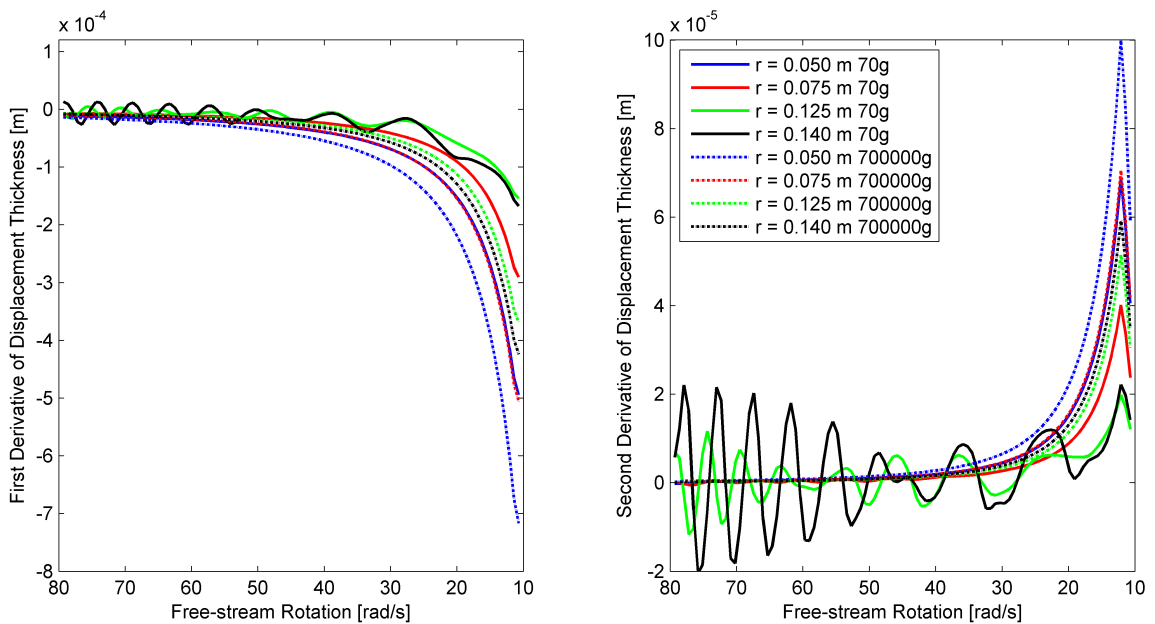
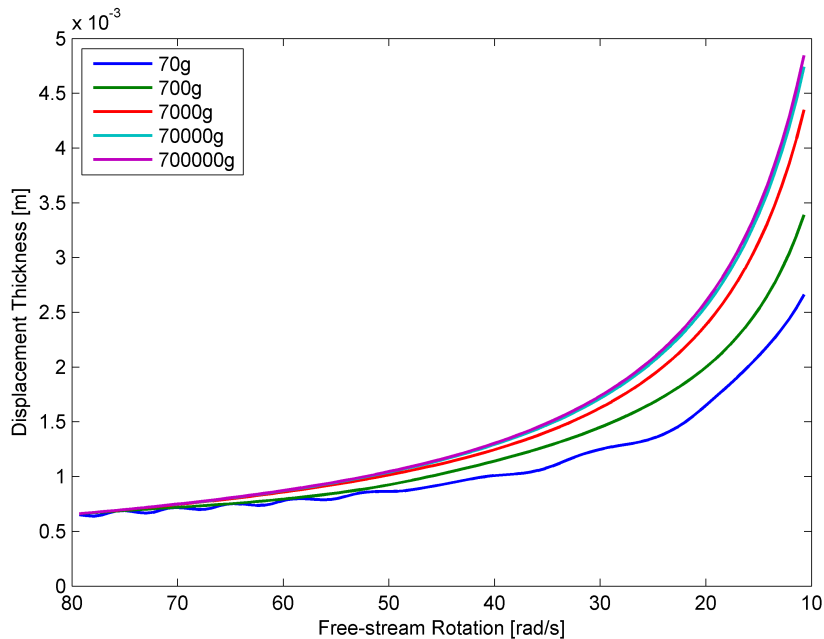


Figure 8.46: Tangential Displacement Thickness Comparison at  $r = 0.14$  m in Decelerating Conditions



The displacement thickness on the decelerating disk is monotonically increasing. The values are directly proportional to acceleration strength; a higher acceleration results in a higher displacement thickness. The values are divergent. This can be seen in the first derivative. An inflection point is noted in the second derivative near the end of the deceleration event. This is due to a hysteresis effect of the flow response to deceleration. In the 70g case, unsteady behaviour is seen throughout the deceleration event. This occurs at the sample locations further away from centre of the disk. The 70g case has a Type II response to deceleration. In this type of flow the boundary layer is dominated by momentum forces in some parts and viscous forces in other parts of the profile. The results is an unsteady flow that presents as oscillations in the first derivative of the displacement thickness. The effect is damped out later in the deceleration event when the viscous forces becomes more dominant and stabilizes the boundary layer profile.

Momentum thickness in the tangential direction for deceleration is shown in *Figures 8.47-8.49* .

The response of the momentum thickness to deceleration in the tangential direction can be divided into two groups. The 70g and 700g is in the first grouping, while the cases equal to 7 000g and higher fall in the second grouping. In the first grouping there is a very slight increase in momentum thickness up until a free-stream rotation of 40 rad/s. In the first derivative it can be seen that the gradient is very small in the initial stages of the deceleration event. After a maximum values is reached the results becomes monotonically decreasing. This value is divergent as can be seen from the first derivative. The same unsteady behaviour that was noted in to 70g case is present here. At points further away from the disk centre the momentum thickness is oscillating. This effect is damped out further along the deceleration event. The second grouping presents with a momentum thickness that is monotonically decreasing. The

CHAPTER 8. BOUNDARY LAYER RESPONSE IN PURE ROTATION - ROTATING DISK FLOW

Figure 8.47: Tangential Momentum Thickness Comparison for the Decelerating Rotating Disk

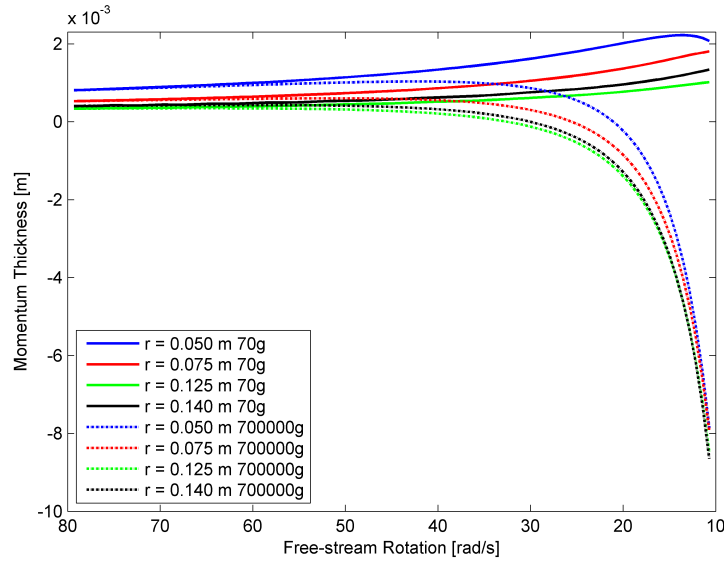
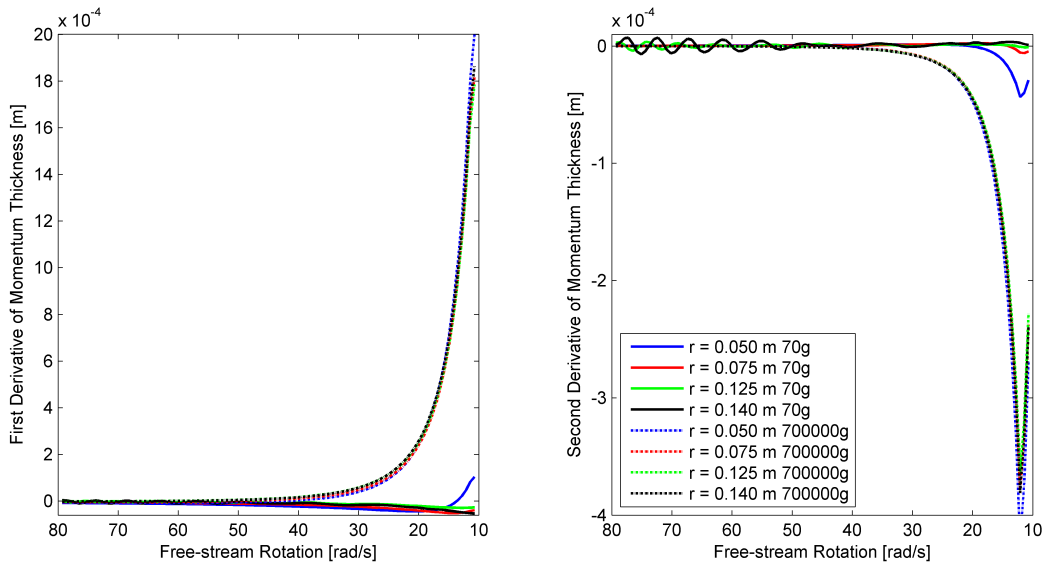


Figure 8.48: Tangential Momentum Thickness Derivative Comparison for the Decelerating Rotating Disk

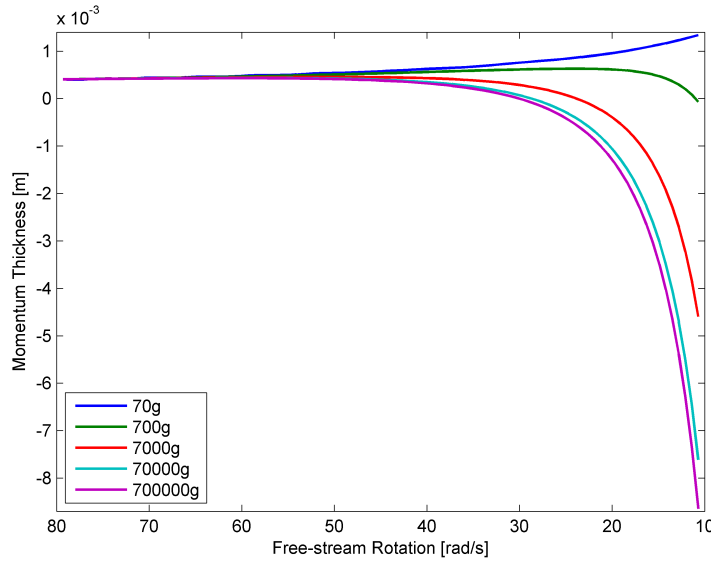


result is divergent and is proportional to the acceleration strength. An inflection point is again present in the second derivative in the later stages of the acceleration event.



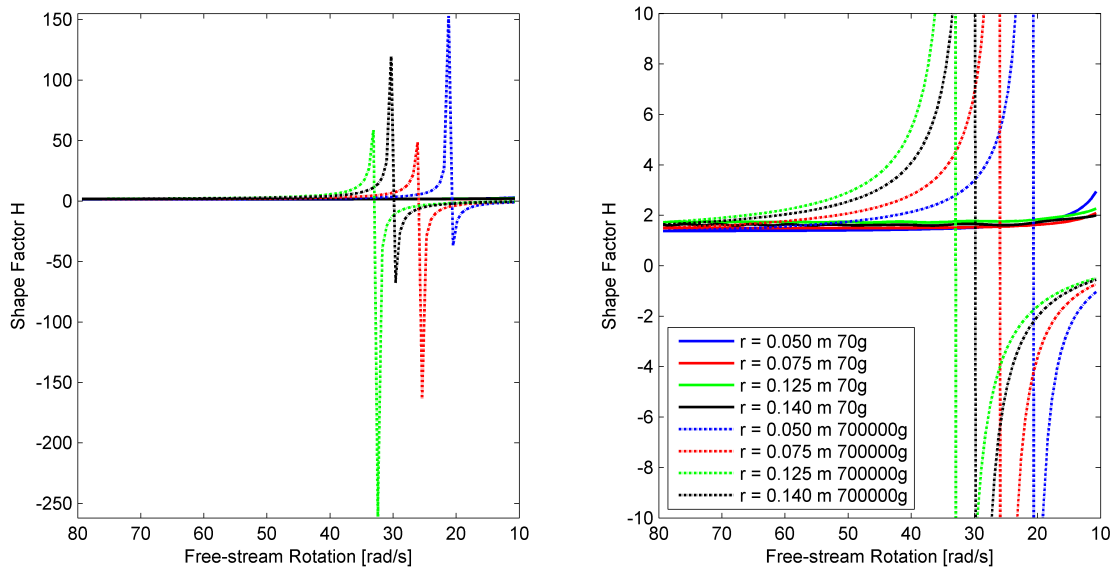
8.3. RESULTS AND DISCUSSION - DECELERATION

Figure 8.49: Tangential Momentum Thickness Comparison at  $r = 0.14$  m in Decelerating Conditions



The tangential shape factor results are shown in *Figures 8.50-8.51*.

Figure 8.50: Tangential Shape Factor Derivative Comparison for the Decelerating Rotating Disk



The shape factor behaviour for the decelerating disk has many parallels to the shape factor for the decelerating plate. The discontinuity that characterized the decelerating flat plate shape factor is present here. The shape factor is monotonically increasing as the beginning of the deceleration event. It approaches an asymptote. After the asymptote the shape factor becomes negative and approaches zero near the end of the acceleration event. The discontinuity is dependent on deceleration; a stronger

CHAPTER 8. BOUNDARY LAYER RESPONSE IN PURE ROTATION - ROTATING DISK FLOW

Figure 8.51: Comparison of Tangential Shape Factor Discontinuities and Momentum Thickness for the Decelerating Disk

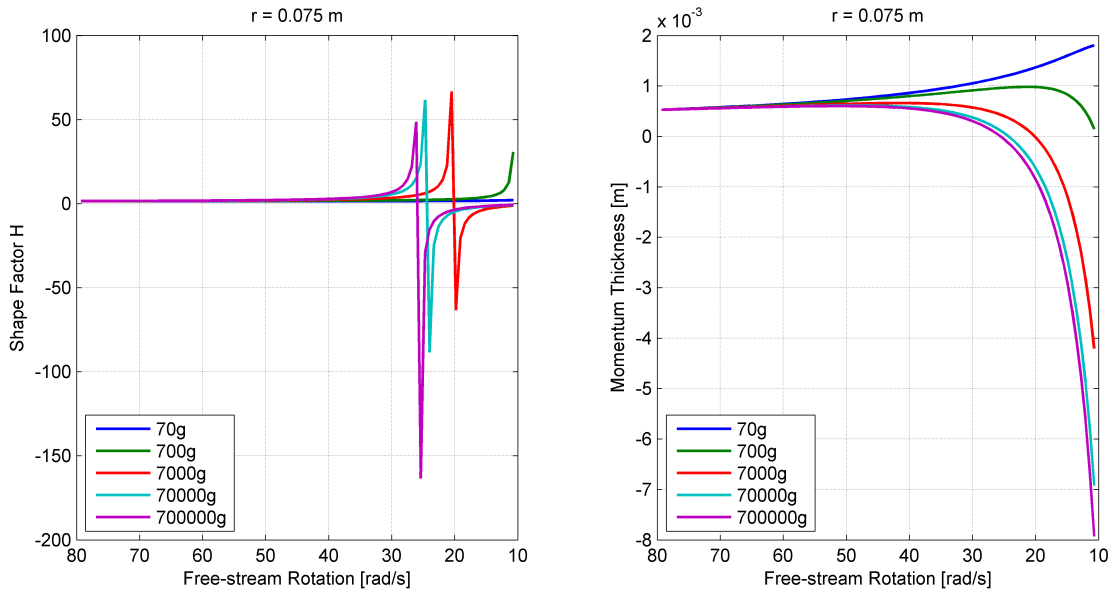
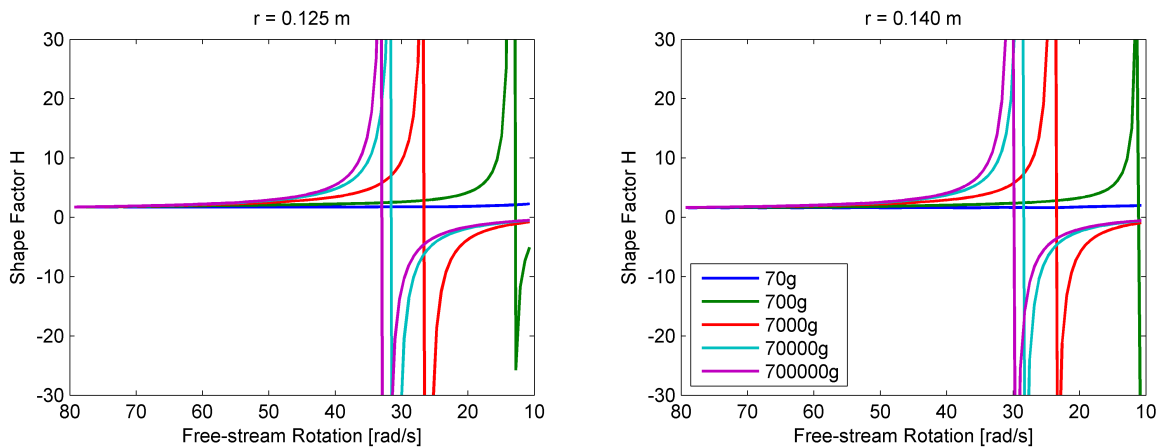


Figure 8.52: Tangential Shape Factor Comparison at Various Radial Positions for the Decelerating Disk



deceleration approaches its asymptote earlier in the event than a weaker deceleration. It presents when the momentum thickness becomes negative. A negative shape factor is not achievable in the physical world. Mathematically it is an indication that the flow regime is changing. The models applied can no longer sufficiently describe the flow. It is postulate here that the asymptote is an indication that the flow has become turbulent. Flow reversal leads to turbulence and a high shape factor.

### 8.3.2.2 Radial Parameters

In Figures 8.53-8.55 the displacement thickness in the radial direction is shown.

Figure 8.53: Radial Displacement Thickness Comparison for the Decelerating Rotating Disk

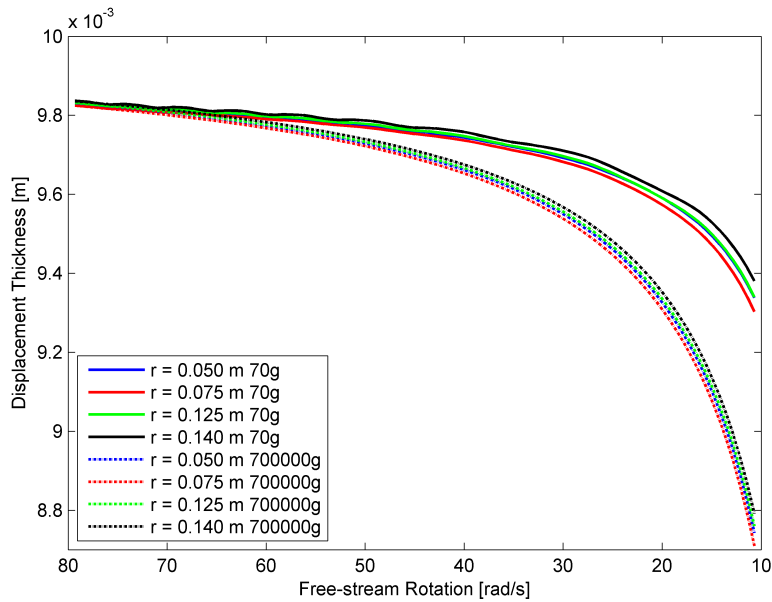


Figure 8.54: Radial Displacement Thickness Derivative Comparison for the Decelerating Rotating Disk

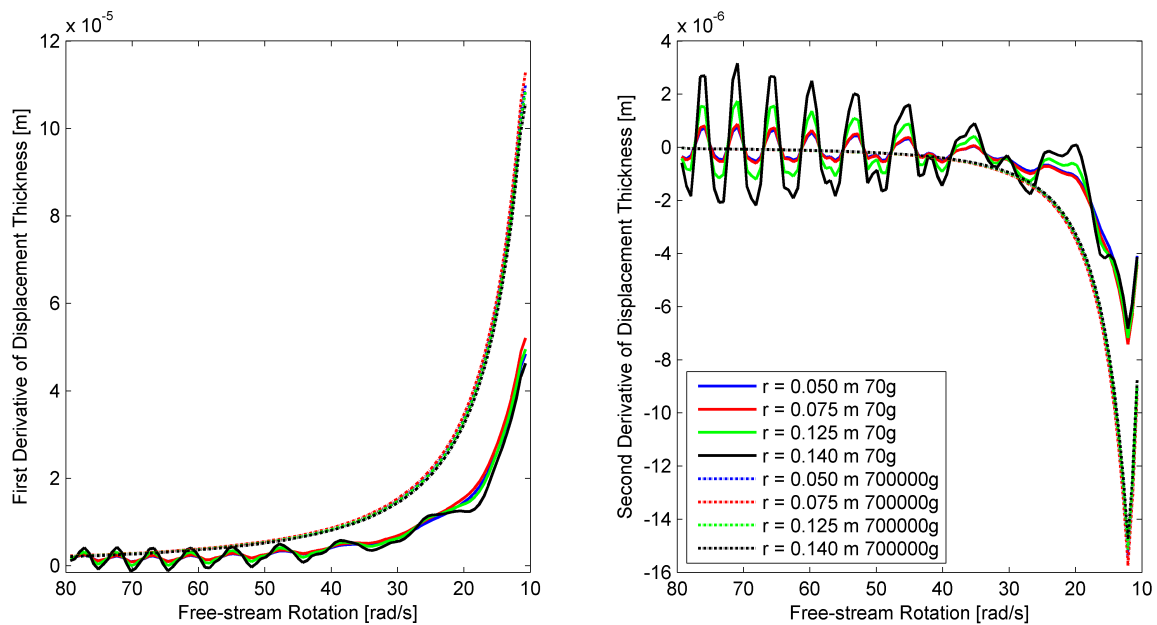
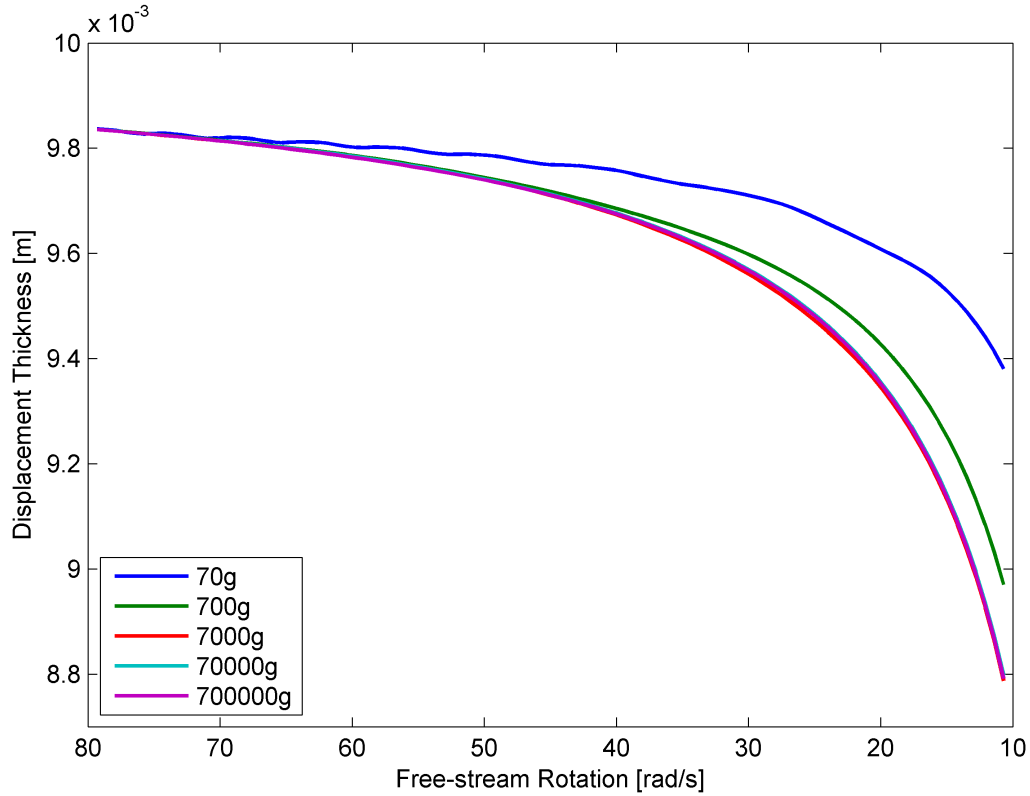


Figure 8.55: Radial Displacement Thickness Comparison at  $r = 0.14$  m in Decelerating Conditions



The displacement thickness is monotonically decreasing. It is indirectly proportional to deceleration strength; a higher deceleration have a lower displacement thickness value. The values are divergent as can be seen in the first derivative. The inflection point in the second derivative is present here as it was for all cases of deceleration in the tangential direction. The 70g case displays disturbances in the first and second derivative. This is similar to behaviour noted in the tangential direction for deceleration. The exception here is that it occurs at all points on the disk and not just at the exterior points further away from the centre. The disturbances is in phase with each other. Higher amplitudes is observed at the exterior point. This typifies the Type II behaviour where neither viscous force nor momentum forces and dominant in the boundary layer. The effect is damped out further along the deceleration event.

Momentum thickness result in the radial direction is displayed in *Figures 8.56-8.58* .

Figure 8.56: Radial Momentum Thickness Comparison for the Decelerating Rotating Disk

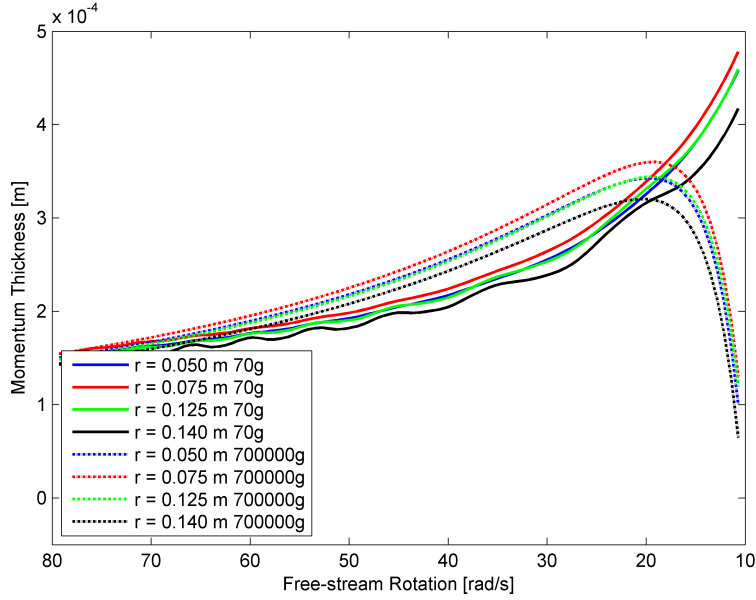


Figure 8.57: Radial Momentum Thickness Derivative Comparison for the Decelerating Rotating Disk

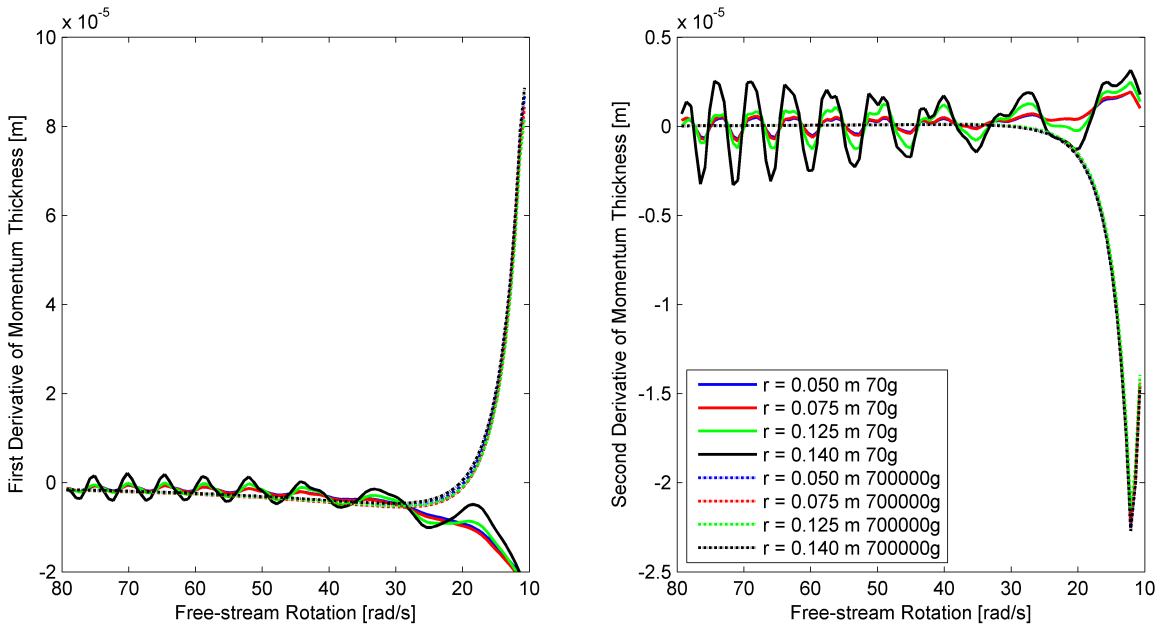
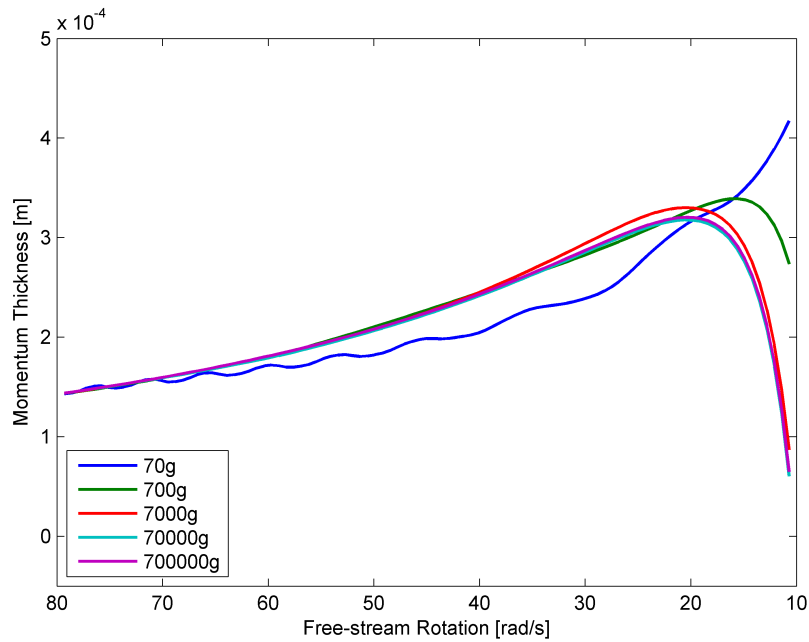


Figure 8.58: Radial Momentum Thickness Comparison at  $r = 0.14$  m in Decelerating Conditions



The radial momentum thickness displays two groupings of behaviour for decelerating conditions. The 70g case (Type II) responds differently to changing conditions than the remainder of the cases (Type III). The cases all respond in a similar manner up to a free-stream rotation of 30 rad/s. At this point the profiles are monotonically increasing. The momentum thickness is directly proportional to deceleration strength. The 70g case continues to increase until the completion of the deceleration event. The higher acceleration cases reach a maximum value and rapidly decrease. In all cases the results are divergent. The first derivative of the 70g case approaches negative infinity, while the higher cases approach positive infinity. The same disturbances that was noted in the radial displacement thickness for the 70g case is noted here. The disturbances occur at all points on the disk. It is in phase with each other, but with higher amplitudes at points further away from the centre of the plate.

The radial shape factor for decelerating conditions on a rotating disk is displayed in *Figures 8.59* and *8.60*.

The shape factor is influenced by the behaviour of the momentum thickness and displays similar trends. The 70g deceleration, which is of Deceleration Response Type II, has a shape factor that is monotonically decreasing. It is divergent and displays the disturbances as noted in the momentum thickness. The remainder of the deceleration cases, which are all of Deceleration Response Type III, have shape factors that is decreasing, reaches a minimum after which it rapidly diverges.

8.3. RESULTS AND DISCUSSION - DECELERATION

Figure 8.59: Radial Shape Factor Comparison for the Decelerating Rotating Disk

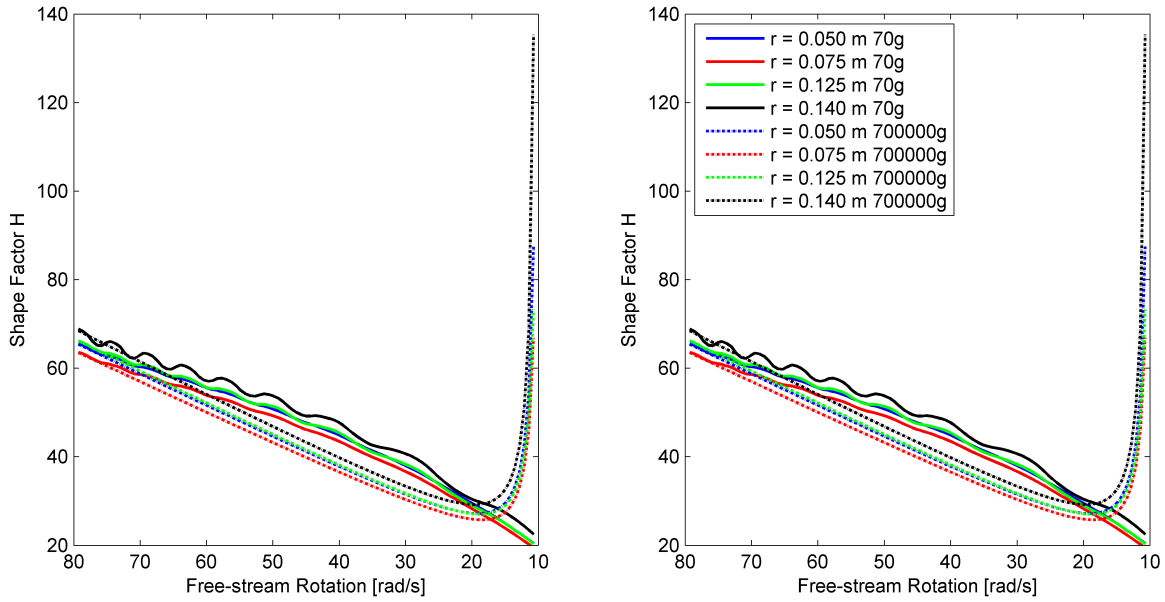
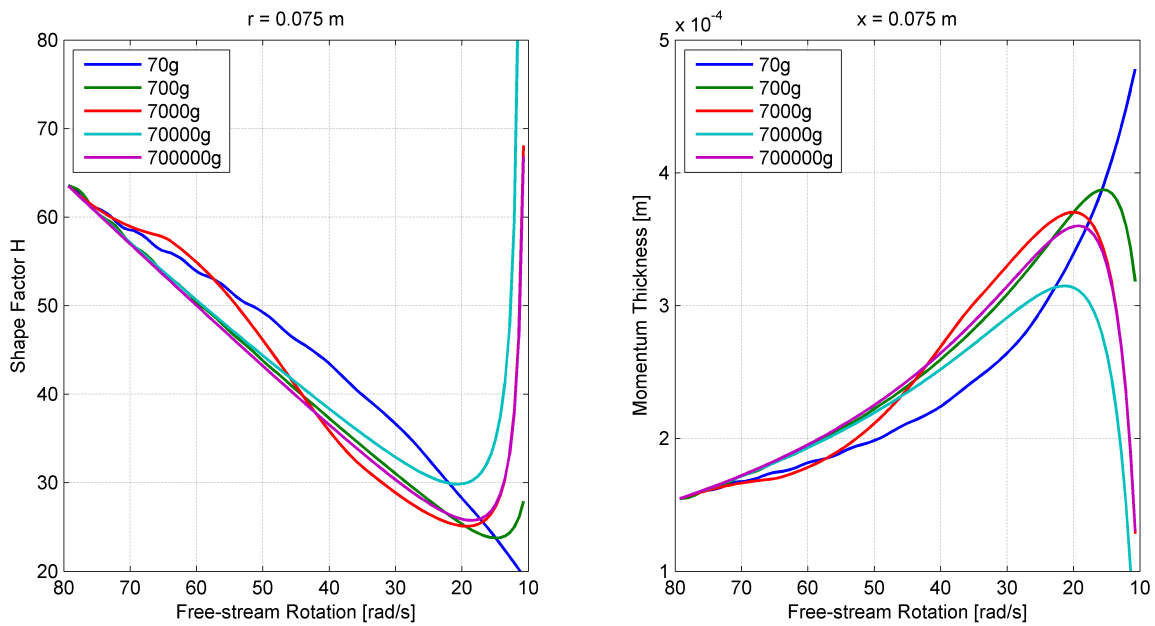


Figure 8.60: Comparison of Radial Shape Factor Values and Momentum Thickness for the Decelerating Disk



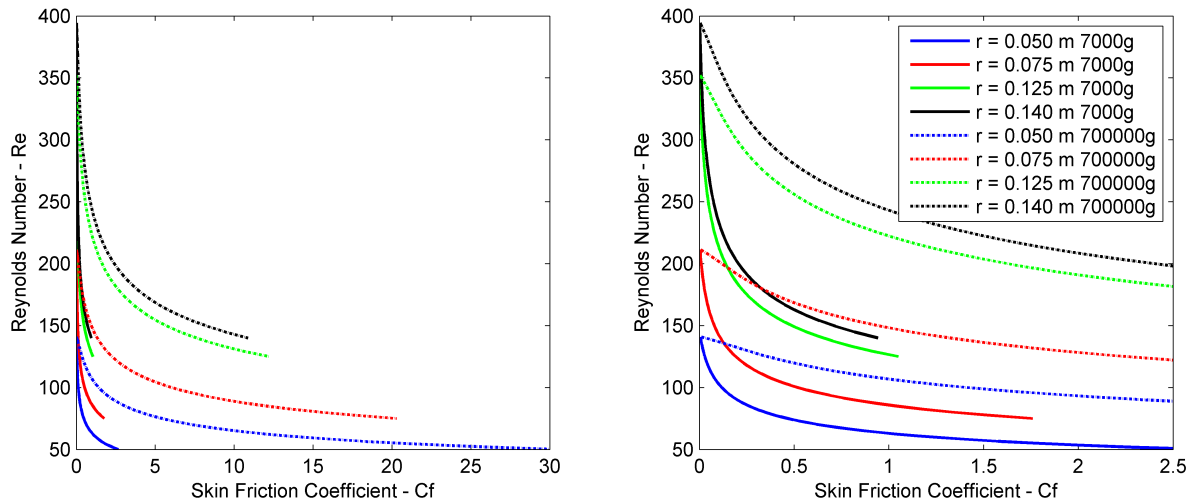
### 8.3.3 Skin Friction Coefficients

The skin friction coefficients were determined in the same manner as for the acceleration cases.

$$\begin{aligned}\tau_{\theta_{wall}} &= \left(\mu \frac{\partial u_{\theta}}{\partial y}\right) \Big|_{wall} \\ \tau_{r_{wall}} &= \mu \frac{\partial u_r}{\partial y} \Big|_{wall} \\ \tau_{wall} &= \sqrt{\tau_{\theta_{wall}}^2 + \tau_{r_{wall}}^2} \\ C_f &= \frac{\tau_{wall}}{0.5\rho U_{\infty}^2}\end{aligned}\tag{8.18}$$

The results are displayed in *Figures 8.61-8.62*.

Figure 8.61: Comparison between Skin Friction Coefficients at Various Free-Stream Rotational Reynolds Numbers for Decelerating Conditions



The decelerating disk skin friction coefficients have similar trends than the decelerating flat plate. Skin friction coefficient values are divergent in deceleration and directly proportional to deceleration strength. On a rotating disk it is also dependant on position, since rotational velocity is a function of location on the disk. The values are at a maximum at the interior points (closest to the disk centre) and becomes smaller at the exterior points (further away from the centre).





8.3. RESULTS AND DISCUSSION - DECELERATION

Figure 8.62: Comparison between Skin Friction Coefficients at Various Disk Positions for Decelerating Condition

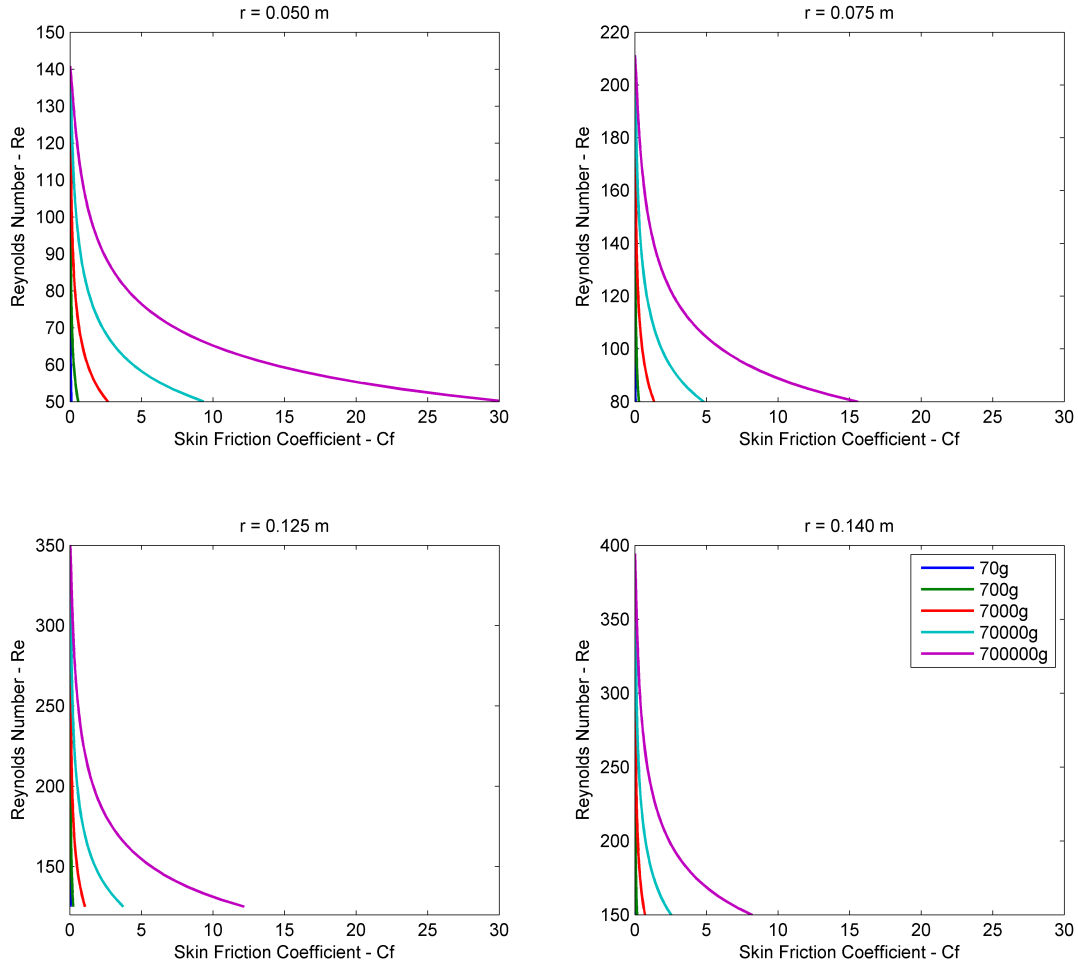
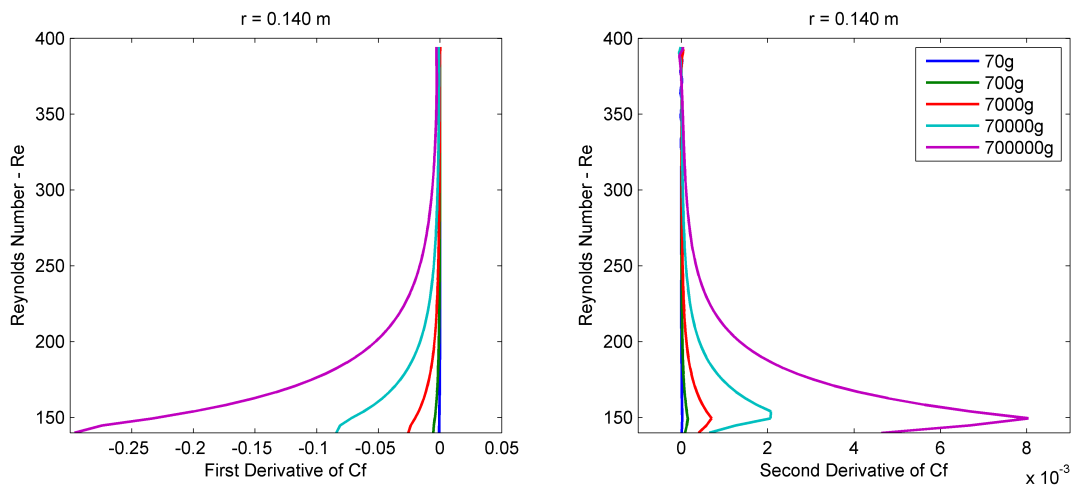


Figure 8.63: Derivatives of Skin Friction Coefficient for Decelerating Conditions



## 8.4 Closure

This chapter aimed at characterising the response of the laminar boundary layer to arbitrary rotation. The contribution of this chapter are as follows:

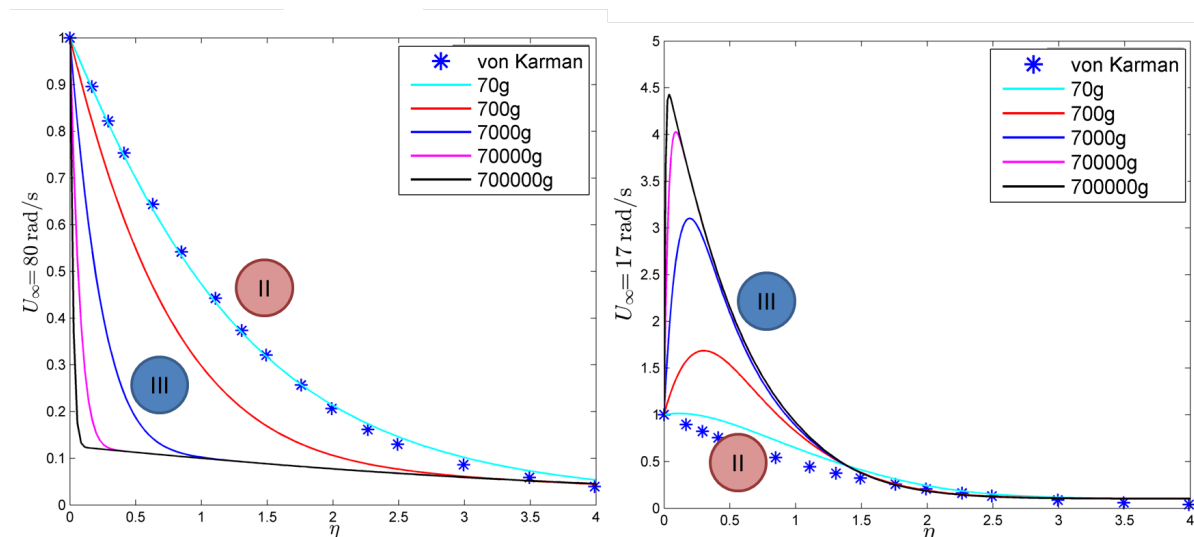
- 1) The characterisation of the boundary layer behaviour in terms of the three types of responses to arbitrary motion as define *Chapter 7*.
- 2) The proposal of a mechanism providing an explanation for response types.
- 3) The characterisation of the response of the shape factor to arbitrary rotation.
- 4) The characterisation of the response of the skin friction coefficient to arbitrary rotation.

The same three response regions that were defined in *Chapter 7* is applicable to the flow behaviour in this chapter:

- **Response Type I**, which is viscous dominant.
- **Response Type II**, which is certain regions in the boundary layer are dominated by viscosity and other regions by momentum.
- **Response Type III**, which is dominated by momentum.

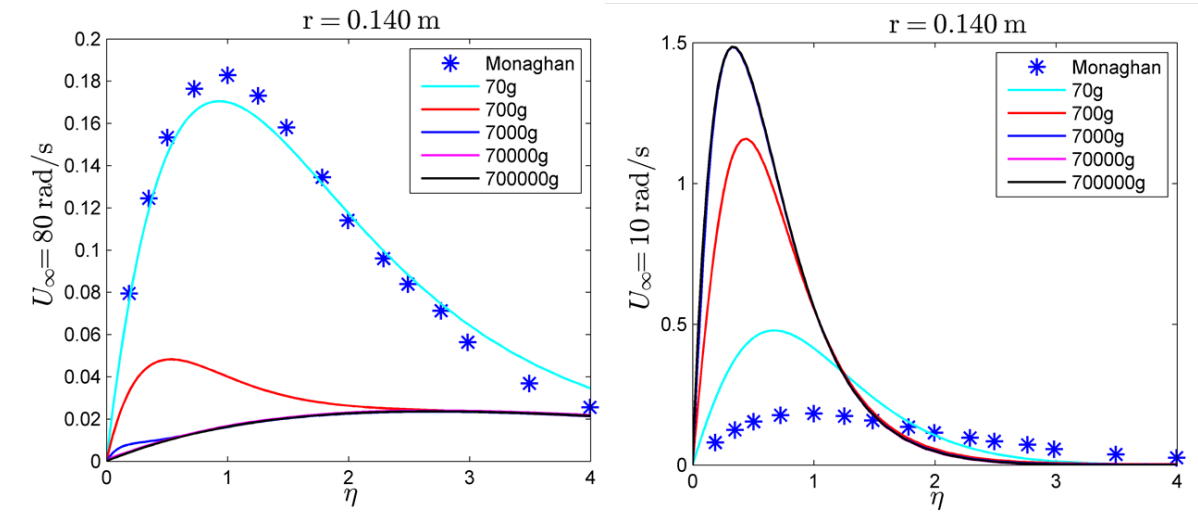
The response to acceleration and deceleration in the tangential direction behaves similar to the flat plate (*Figure 8.64*). However, a Type I response was not observed in the rotating disk case.

Figure 8.64: Response types for accelerating (left) and decelerating (right) conditions on a rotating disk in the tangential direction



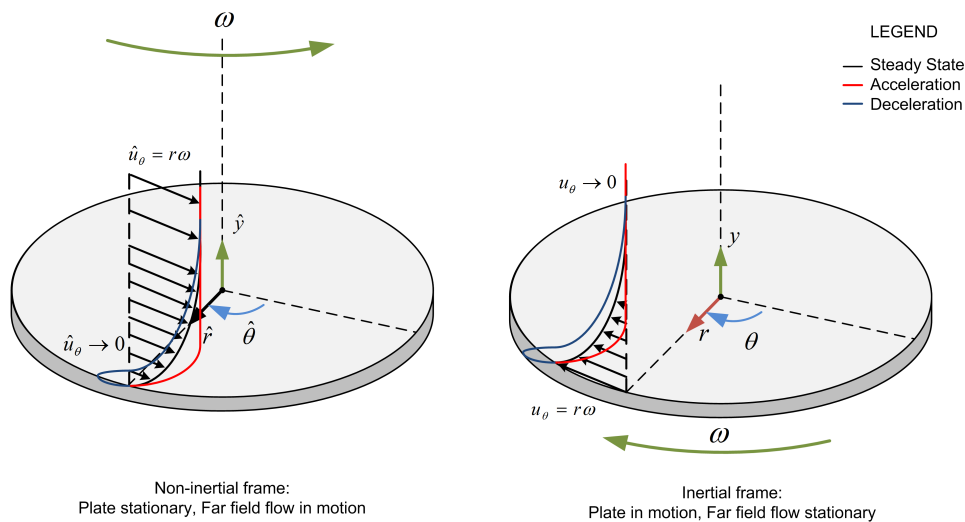
Boundary layer behaviour in the radial direction indicated a slow response to changing conditions. The lower acceleration cases responds first. This was also the case in deceleration. At high accelerations and decelerations the radial profile remains in the initial state.

Figure 8.65: Response to accelerating (left) and decelerating (right) conditions on a rotating disk in the radial direction



The general trends in tangential velocity behaviour on the rotating disk, both in acceleration and deceleration, are depicted in *Figure 8.66*.

Figure 8.66: Boundary layer profiles for steady, acceleration and deceleration conditions on a rotating disk

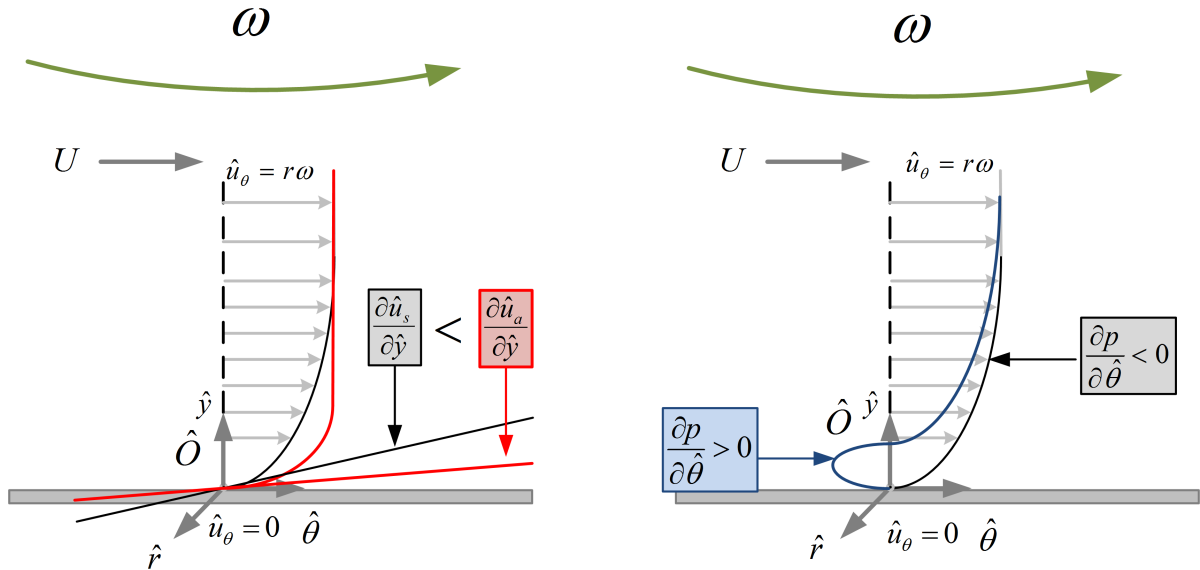


Parallels can be drawn between the flat plate and rotating disk in changing conditions. In acceleration the velocity profiles have steeper gradients in the near-wall region. This gradient is proportional to the acceleration strength. Decelerating velocity profiles is characterized by flow reversal. The reversal is directly proportional to the deceleration strength. A mechanism was proposed for the response of the boundary layer using the boundary layer equations below. The mechanism is depicted in *Figure 8.67*.

In acceleration the fictitious forces become sources of momentum. An increase in momentum on

CHAPTER 8. BOUNDARY LAYER RESPONSE IN PURE ROTATION - ROTATING DISK FLOW

Figure 8.67: Accelerating and decelerating mechanisms of boundary layer response on a rotating disk



the right hand side of the equation leads to an increase in on the left hand side. This results in an increase in tangential velocity,  $u_\theta$ , which in turn causes the velocity gradient at the wall to increase. The effect is observed in the simulation results.

The opposite occurs in deceleration when the fictitious forces becomes momentum sinks. A decrease in momentum on the right hand side of the equation leads to a decrease on the left hand side. This results in a decrease in tangential velocity  $u_\theta$ , which in turn causes the velocity gradient at the wall to decrease. The pressure gradient has an opposite sign to the diffusion term. When it increases to such an extent that an adverse pressure gradient form, separation is observed. This is the separation observed in the simulation results.

$$\frac{\partial \hat{\rho} \hat{u}_\theta}{\partial t} + \hat{u}_r \frac{\partial \hat{\rho} \hat{u}_\theta}{\partial \hat{r}} + \frac{\hat{u}_\theta}{\hat{r}} \frac{\partial \hat{\rho} \hat{u}_\theta}{\partial \hat{\theta}} + \frac{\hat{\rho} \hat{u}_\theta \hat{u}_r}{\hat{r}} + \hat{u}_y \frac{\partial \hat{\rho} \hat{u}_\theta}{\partial \hat{y}} = - \underbrace{\frac{1}{\hat{r}} \frac{\partial \hat{p}}{\partial \hat{\theta}}}_{\text{Blue Star}} + \underbrace{\frac{\partial}{\partial \hat{y}} \left( \hat{\mu} \frac{\partial \hat{u}_\theta}{\partial \hat{y}} \right)}_{\text{Pink Oval}} + \underbrace{2 \hat{\rho} \hat{u}_r \omega_y + \hat{\rho} \hat{r} \dot{\omega}_y}_{\text{Fictitious Forces}}$$

The same mechanism as described above was responsible for the behaviour of the flat plate in arbitrary translation. Since the mechanism is the same, the tangential boundary behave like a boundary layer on a flat plate.

$$\frac{\partial \hat{\rho} \hat{u}}{\partial t} + \hat{u} \frac{\partial \hat{\rho} \hat{u}}{\partial \hat{x}} + \hat{v} \frac{\partial \hat{\rho} \hat{u}}{\partial \hat{y}} = - \underbrace{\frac{\partial \hat{p}}{\partial \hat{x}}}_{\text{Blue Star}} + \underbrace{\frac{\partial}{\partial \hat{y}} \left( \hat{\mu} \frac{\partial \hat{u}}{\partial \hat{y}} \right)}_{\text{Pink Oval}} - \underbrace{\frac{\partial \hat{\rho} V_x}{\partial t}}_{\text{Yellow Oval}}$$

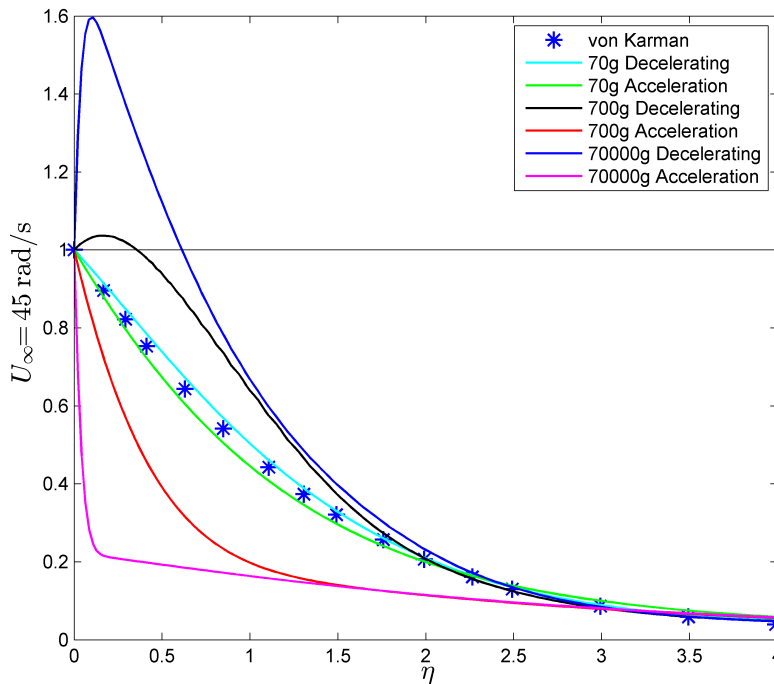
The radial mechanism of response is much simpler. The fictitious forces are of the same order, but with difference mathematical signs. Changes in the fictitious forces creates a feedback loop where

the one component is a momentum source and the other is a momentum sink. Response in the radial boundary layer are not caused by the fictitious components, but rather by changes in the rotational velocity,  $u_\theta$ . This affects the balance between the right and left hand side of the equation. The viscous term adjusts to counter the changes. Subsequently the value of the radial velocity increases or decreases. This mechanism is highly dependant on the acceleration or deceleration strength. In cases where high rates of change is present, the radial velocity profile remains in the initial state.

$$\frac{\partial \hat{\rho} \hat{u}_r}{\partial t} + \hat{u}_r \frac{\partial \hat{\rho} \hat{u}_r}{\partial \hat{r}} + \frac{\hat{u}_\theta}{\hat{r}} \frac{\partial \hat{\rho} \hat{u}_r}{\partial \hat{\theta}} - \frac{\hat{\rho} \hat{u}_\theta^2}{\hat{r}} + \hat{u}_y \frac{\partial \hat{\rho} \hat{u}_r}{\partial \hat{y}} = - \frac{\partial \hat{p}}{\partial \hat{r}} + \frac{\partial}{\partial \hat{y}} \left( \hat{\mu} \frac{\partial \hat{u}_r}{\partial \hat{y}} \right) - \left[ 2\hat{\rho} \hat{u}_\theta \omega_y \right] + \left[ \hat{\rho} \hat{r} \omega_y^2 \right]$$

Figure 8.68 is presented here to show the variability in velocity profiles.

Figure 8.68: Variability in boundary layer profiles for different starting and acceleration conditions on a rotating disk



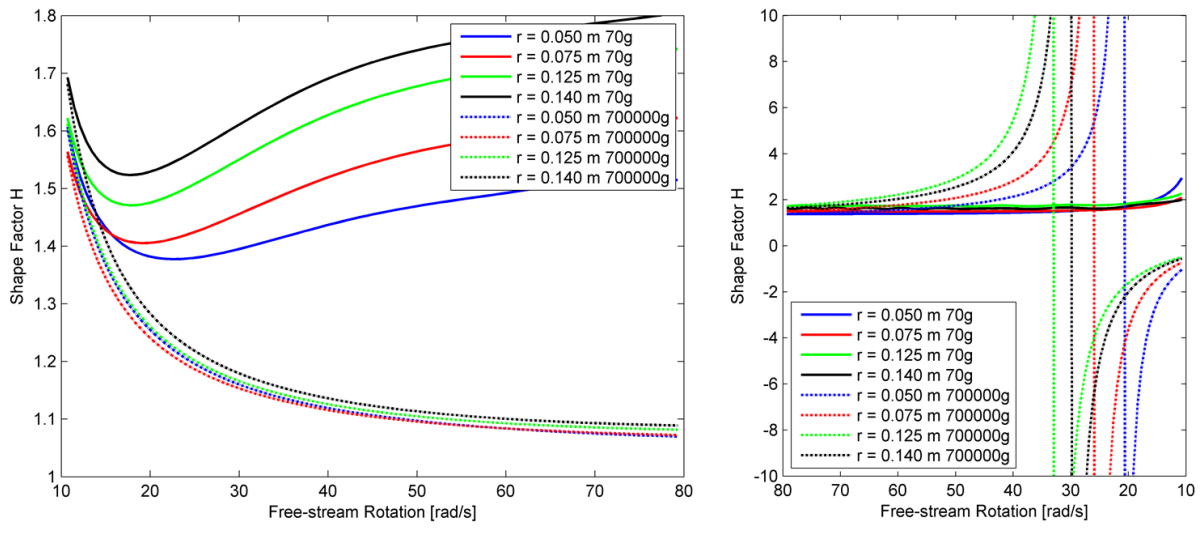
The profile is dependent on the history of the flow as well as the strength of acceleration or deceleration. At values of 70g the profile in unsteady velocity varies little from the steady state result. However, this still has a major impact on the shape factor and more importantly the skin friction coefficient. The effects of arbitrary motion should still be included in mathematical models.

The shape factor in tangential direction is shown in Figure 8.69 for accelerating and decelerating conditions. The behaviour is similar to the flat plate results. The higher acceleration cases is monotonically decreasing and approximates a minimum value. In contract, the lower acceleration cases reach a

CHAPTER 8. BOUNDARY LAYER RESPONSE IN PURE ROTATION - ROTATING DISK FLOW

minimum value very early in the event. It then recovers the initial value and approaches an asymptotic shape factor value. In deceleration the shape factor displays a discontinuity. The shape factor approaches positive infinity at this point. A discontinuity in the mathematics is an indication that the flow regime has changed. It is therefore postulated that the discontinuity is the point where the flow becomes turbulent.

Figure 8.69: Results of the tangential shape factor response for acceleration (left) and deceleration (right) events on a rotating disk



The shape factor in radial direction, as shown in *Figure 8.70* is divergent in all cases. Type II flows, such as the 70g case, responds in a different manner than the Type III flows. Type II approaches negative infinity in deceleration while Type III approaches positive infinity. The 70g is characterized by unsteady oscillations in the shape factor.

The skin friction coefficients (*Figure 8.71*) on a rotating disk reacts in the same manner as it would on a flat plate in translation. In acceleration the value first increase. It reach a maximum after which it is reduced. An asymptote is approximated as the acceleration event continues. The skin friction coefficient in deceleration is divergent and continues to increase. The values in both cases are dependant on position on the disk.

Figure 8.70: Results of the radial shape factor response for acceleration (left) and deceleration (right) events on a rotating disk

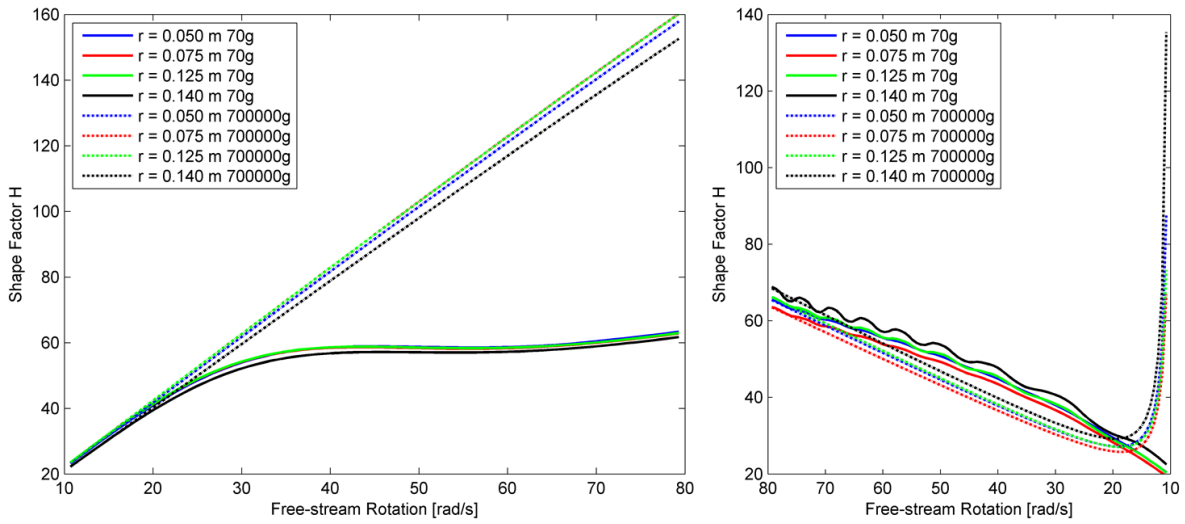
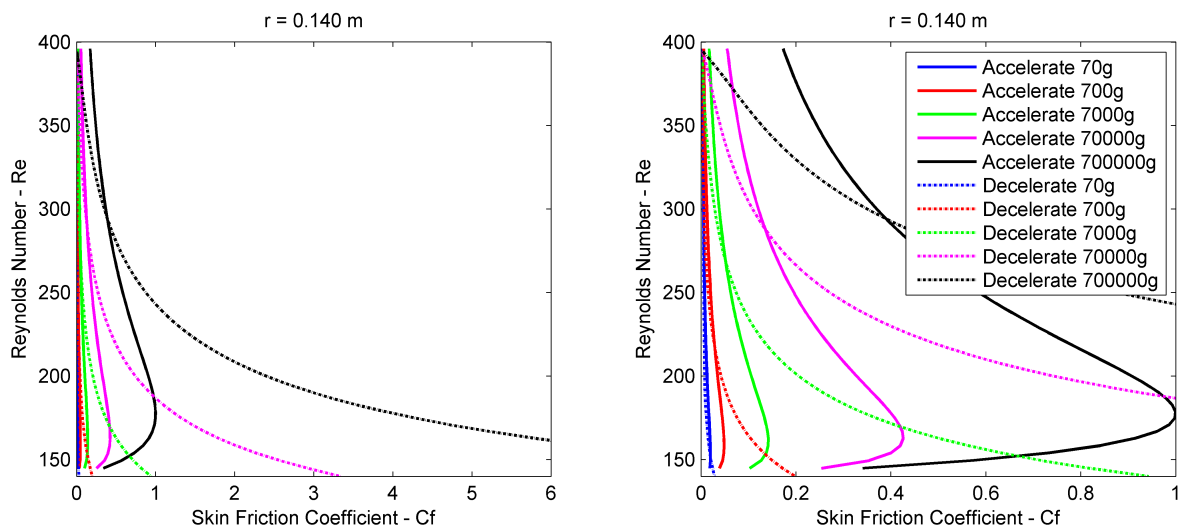


Figure 8.71: Result of the skin friction coefficient response to arbitrary rotation on a rotating disk





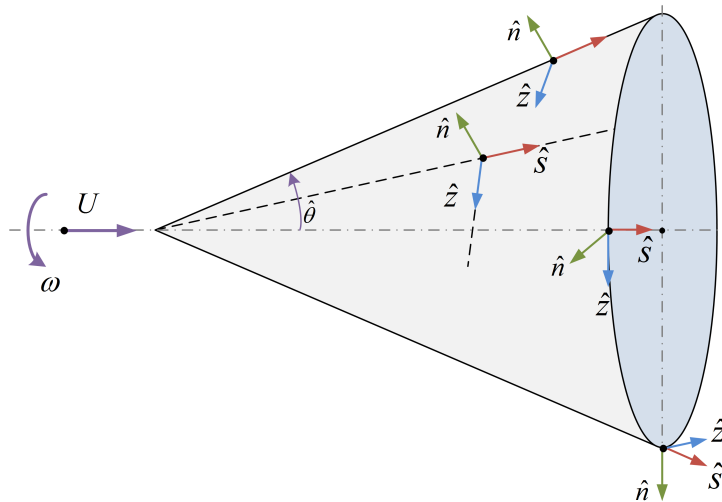
UNIVERSITEIT VAN PRETORIA  
UNIVERSITY OF PRETORIA  
YUNIBESITHI YA PRETORIA



## Boundary Layer Response in Combined Translation and Rotation - Arbitrary Cone Flow

The boundary layer response to acceleration and deceleration of a rotating cone in axial flow is analysed in this chapter. The cone has a half angle of  $15^\circ$  and is subjected to arbitrary translating and rotating conditions. The boundary layer profiles is depicted in terms of a curvilinear coordinate system as shown in *Figure 9.1*.

Figure 9.1: Orientating Image of the Rotating Cone in Axial Flow



Rotating cones in axial flow are commonly found in engineering environments such as turbo-machinery, aerial vehicles and defence systems. Applications range from missile nose cones and projectile front ends to engine intakes and rotor configurations of wind turbines. The function of the cone is to direct the flow and facilitate maximum pressure recovery in the system.

CHAPTER 9. BOUNDARY LAYER RESPONSE IN COMBINED TRANSLATION AND ROTATION - ARBITRARY CONE FLOW

---

Since cones are commonly used, the theory of cone flow is well established in terms of the shock wave angles (when applicable), streamline curvatures and pressure losses. Most studies are focussed on predicting transition from laminar to turbulent flow (Mansour and Kargar [57], Garret and Peake [52], Kobayashi and Kohama [95]), while few studies investigate the boundary layer (Back [28]).

A number of test conditions have been selected to investigate the behaviour of the boundary layer in arbitrary changing flow. The test cases have been divided into several groupings that test various aspects of the response to acceleration and deceleration in translation and rotation. The groupings are as follow:

- **Group I - Steady Translation with No Rotation.** The results from this grouping is for comparative purposes with other groups that include rotation. Free-stream velocities of 1 m/s, 2 m/s, 3 m/s and 4 m/s were simulated.
- **Groups II & III - Variable Translation, Steady Rotation.** The effect of acceleration and deceleration in translation on the boundary layer of the cone at two constant rotations (10 rad/s and 2 rad/s respectively) are determined, see *Table 9.1*.
- **Group IV & V - Steady Translation, Variable Rotation/** The effect of acceleration and deceleration in rotation on the boundary layer of the cone at two constant translations (1 m/s and 4 m/s respectively) are determined, see *Table 9.2*.
- **Group VI - Mixed Acceleration and Decelerating Conditions.** In *Table 9.3* the conditions for this case is shown to indicate the response of the boundary layer to a mixture of accelerating and decelerating conditions. A number of simulation sets are defined in accordance *Table 9.3*. The event of *Set 2* takes place over a time frame where  $\Delta t = 1e - 02s$ . Similarly *Set 3* corresponds to  $\Delta t = 1e - 03s$  up to *Set 6* that takes  $\Delta t = 1e - 06s$  to complete.

Table 9.1: Translating, Rotating Cone Test Matrix Group II and Group III

Groups	Steady Solution	Acceleration Event	Deceleration Event
II	1, 2, 3 & 4 m/s at 10 rad/s 10 rad/s	1 m/s - 4 m/s 70g - 700 000g	4 m/s - 1 m/s 700 000g - 70g
III	1, 2, 3 & 4 m/s at 2 rad/s 2 rad/s	1 m/s - 4 m/s 70g - 700 000g	4 m/s - 1 m/s 700 000g - 70g

Table 9.2: Translating, Rotating Cone Test Matrix Group IV and Group V

Groups	Steady Solution	Acceleration Event	Deceleration Event
IV	1 m/s at 2, 6, 10 & 12 rad/s 1 m/s	2 rad/s - 12 rad/s 70g - 700 000g	12 rad/s - 2 rad/s 700 000g - 70g
V	4 m/s at 2, 6, 10 & 12 rad/s 4 m/s	2 rad/s - 12 rad/s 70g - 700 000g	12 rad/s - 2 rad/s 70g - 700 000g

Table 9.3: Translating, Rotating Cone Test Matrix Group VI

Groups	Steady Solution	Acceleration	Deceleration	Mixed
VI	1.75 m/s at 4.5 & 9.5 rad/s 2 m/s 7 rad/s 3.25 m/s at 4.5 & 9.5 rad/s	1 m/s 2 rad/s to 4 m/s 12 rad/s $\Delta t : 1e-02s - 1e-06s$ Set2 - Set6	4 m/s 12 rad/s to 1 m/s 2 rad/s $\Delta t : 1e-02s - 1e-06s$ Set2 - Set6	1 m/s 12 rad/s to 4 m/s 2 rad/s $\Delta t : 1e-02s - 1e-06s$ Set2 - Set6
a				
b				
c				
d				

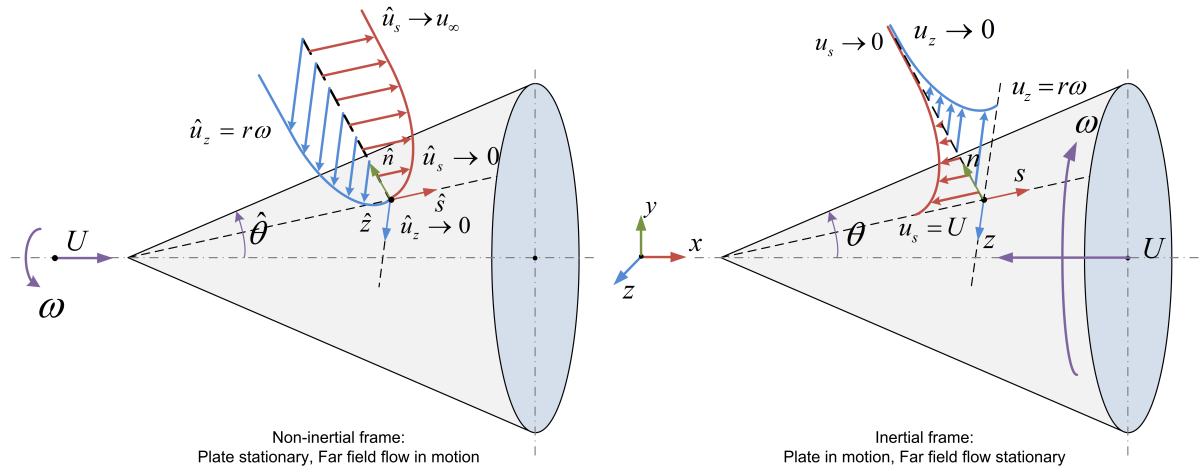
## 9.1 Case Description

In *Figure 9.2* a graphical representation of the boundary layer on a rotating cone in axial flow is given. The rotation is about Cartesian  $x$ -axis at the centre of the cone. Translation occurs along this axis as well.

The cone geometry and boundary layer is expressed here in curvilinear co-ordinates as discussed in *Section 4.4*. The  $s$ ,  $n$  and  $z$ -directions from an orthogonal set. The  $s$ -direction is on the surface on the

CHAPTER 9. BOUNDARY LAYER RESPONSE IN COMBINED TRANSLATION AND ROTATION - ARBITRARY CONE FLOW

Figure 9.2: Graphical Representation of the Boundary Layer on a Rotating Cone in Axial Flow



cone parallel to the longitudinal plane. Perpendicular to this is the  $z$ -direction which is parallel to the transverse plane. The  $n$ -direction is normal to the surface of the cone.

The boundary layer is divided into two components in the  $s$ -direction and the  $z$ -direction respectively. The steady state boundary profile is equivalent to the laminar flat plate profile in the  $s$ -direction, while the profile in the  $z$ -direction is similar to the rotating disk case.

The full momentum equation in the non-inertial frame, as derived in *Equation 3.227*, is applicable to this case. However, the term  $\rho \hat{\mathbf{x}} \wedge \boldsymbol{\Omega}$  is not applicable, since rotation is around a stationary axis.

$$\begin{aligned}
 \frac{\partial \hat{\rho} \hat{\mathbf{u}}}{\partial t} + \hat{\nabla} \cdot (\hat{\rho} \hat{\mathbf{u}} \otimes \hat{\mathbf{u}}) = & -\hat{\nabla} \hat{p} + \hat{\nabla} \cdot [\hat{\mu}(\hat{\nabla} \hat{\mathbf{u}} + \hat{\nabla} \hat{\mathbf{u}}^T) + \hat{\lambda}(\hat{\nabla} \cdot \hat{\mathbf{u}}) \hat{\mathbf{I}}] \\
 & - \underbrace{\frac{\partial}{\partial t}(\rho \mathbf{V}(t))}_{\text{Translation}} + \underbrace{\rho \hat{\mathbf{x}} \wedge \boldsymbol{\Omega}}_{\text{Euler}} + \underbrace{2\rho \hat{\mathbf{u}} \wedge \boldsymbol{\Omega}}_{\text{Coriolis}} - \underbrace{\rho \hat{\mathbf{x}} \wedge \boldsymbol{\Omega} \wedge \boldsymbol{\Omega}}_{\text{Centrifugal}} + \underbrace{2\rho \mathbf{V}(t) \wedge \boldsymbol{\Omega}}_{\text{Magnus}} \quad (9.1)
 \end{aligned}$$

The theoretical formulation and numerical methods used were described in *Chapter 6*.

The non-dimensional distance perpendicular to the cone surface is determined in a similar manner as for the flat plate in *Equation 6.21*.

$$\eta = \frac{\hat{n}}{\hat{s}} \sqrt{\frac{\rho U_{\infty} \hat{s}}{\hat{\mu}}} \quad (9.2)$$

This parameter is used through out this chapter to obtain non-dimensional profiles for the cone.

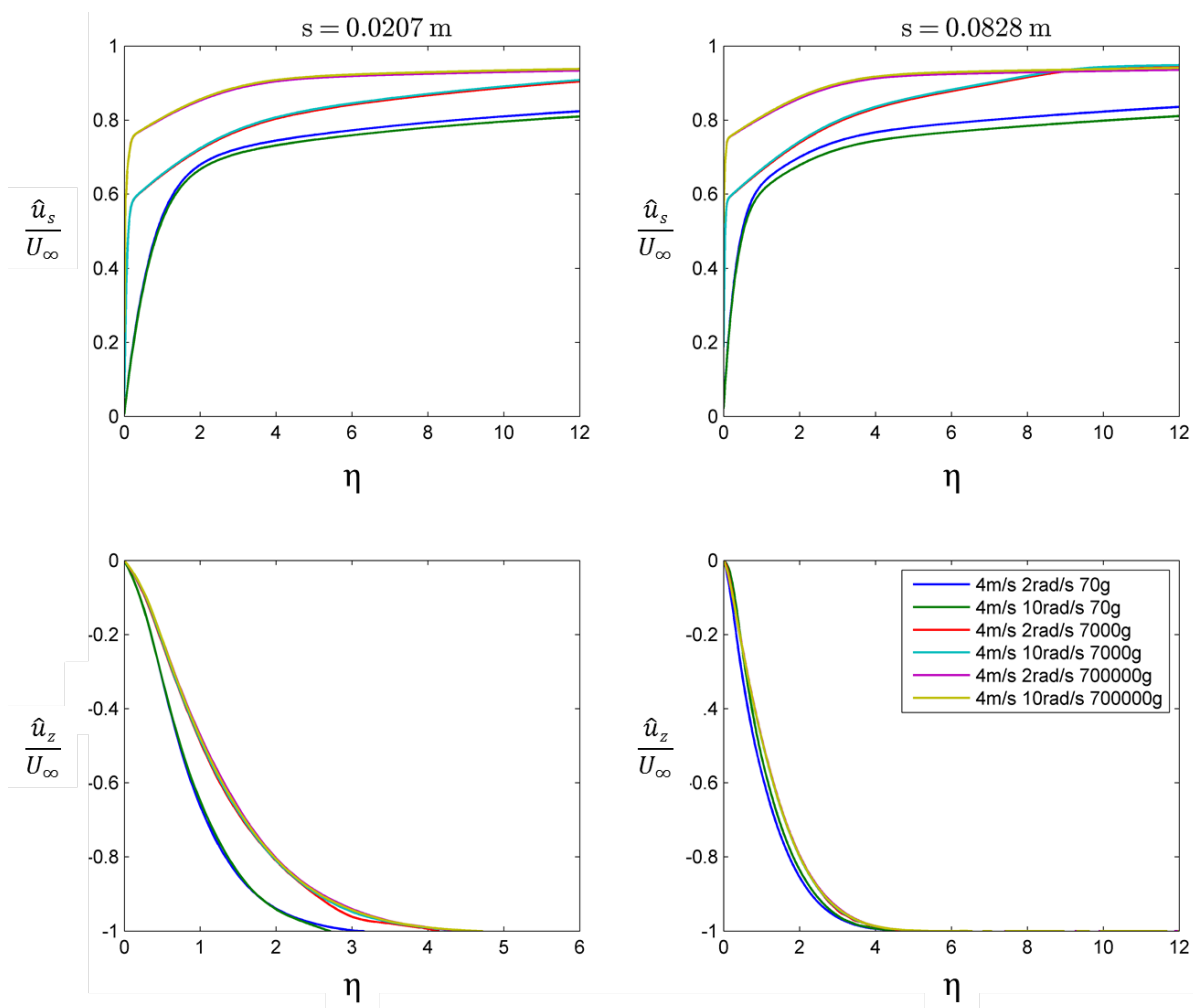
## 9.2 Results and Discussion - Acceleration

### 9.2.1 Velocity Profiles

#### 9.2.1.1 Accelerating Translation with Steady Rotation

In *Figure 9.3*, a comparison is drawn between the results of the Group 2 and Group 3 simulations. That the acceleration groupings between the cases (e.g. 4 m/s 2 rad/s 70 g versus 4 m/s 10 rad/s 70 g) in the  $s$ -direction has similar results. This indicates that the flow is dominated by the translational velocity for this selection of parameters. The rotational velocity is much smaller than the translational velocity. In the case of rotating large calibre projectiles, the translational velocity dominates as well. The translation velocity is in the order of Mach 2.8, while the rotational speed - depending on the barrel rifling, is in the order of 15000 rpm. The general tendencies of the velocity profiles are similar to those observed for the flat plate (*Figure 7.8*). An increase in near wall velocity gradient is observed with increased acceleration.

Figure 9.3: Comparison between Group 2 and Group 3 Simulation Results for Acceleration



CHAPTER 9. BOUNDARY LAYER RESPONSE IN COMBINED TRANSLATION AND ROTATION - ARBITRARY CONE FLOW

Figures 9.4 and 9.5 show the results of the non-dimensional  $s$ -direction velocity profiles for Group 2 and Group 3 respectively.

Figure 9.4: Non-Dimensional  $s$ -Direction Velocity Profiles: Group 2 Accelerating Cone

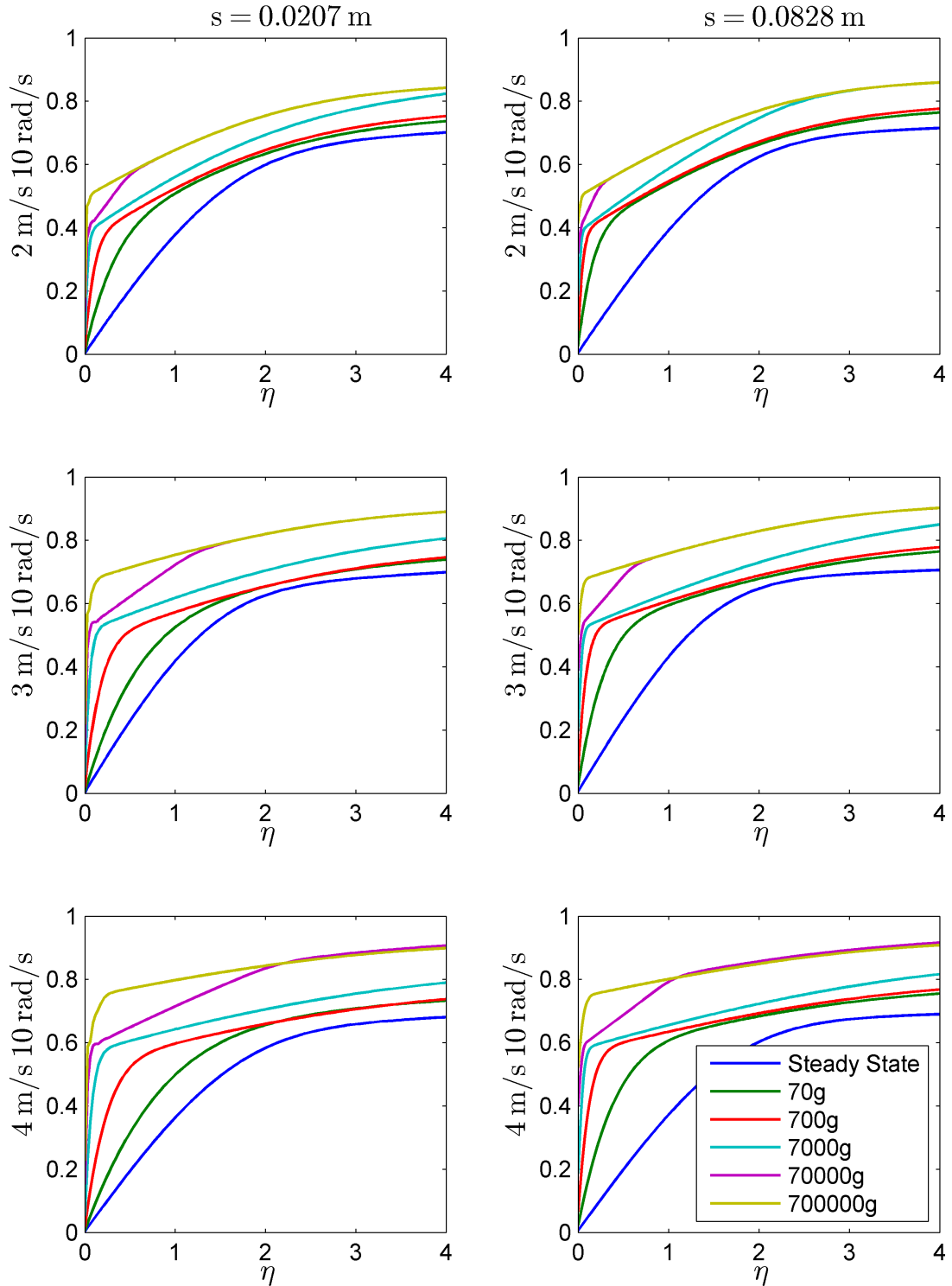
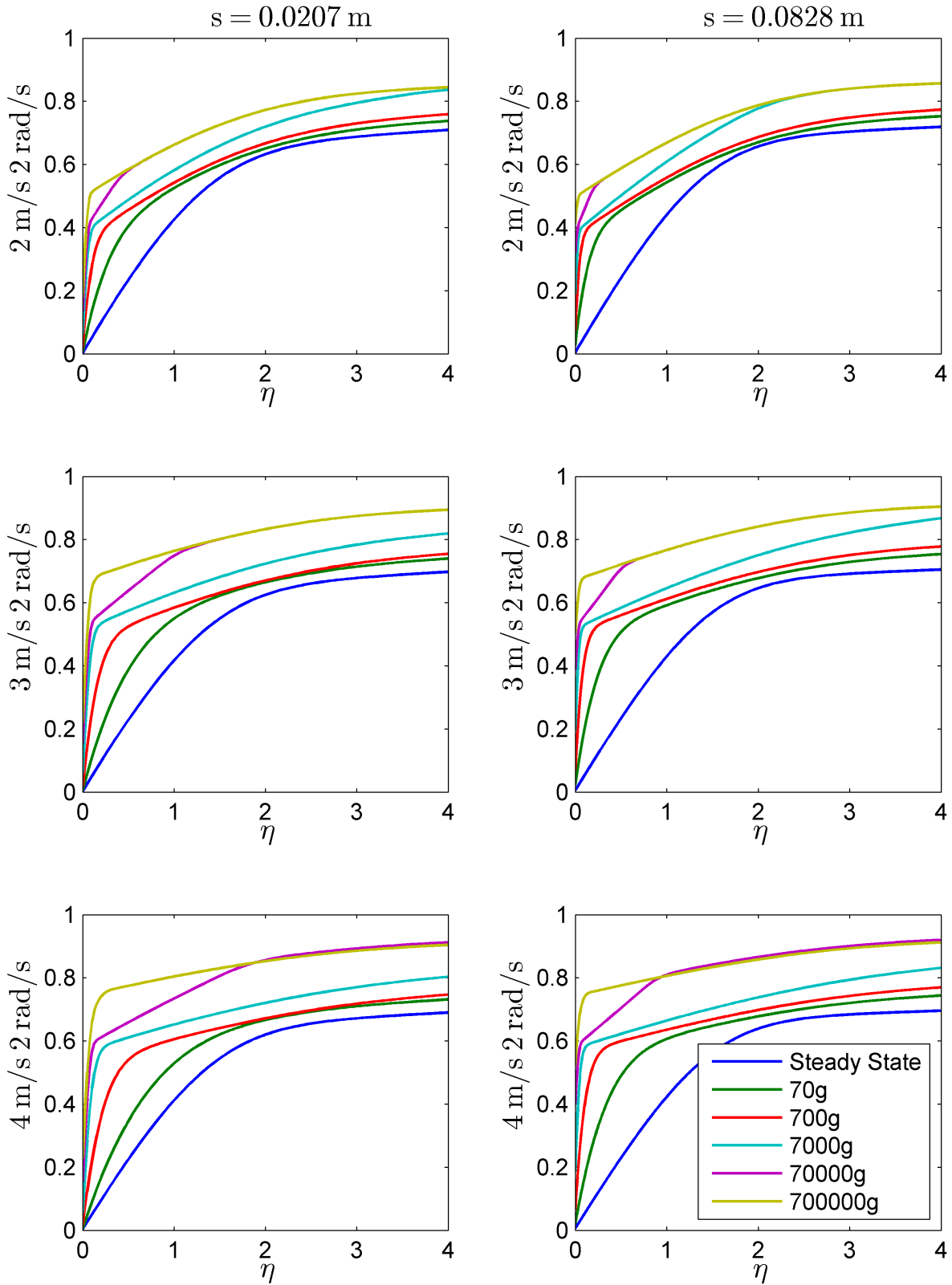


Figure 9.5: Non-Dimensional  $s$ -Direction Velocity Profiles: Group 3 Accelerating Cone



CHAPTER 9. BOUNDARY LAYER RESPONSE IN COMBINED TRANSLATION AND ROTATION - ARBITRARY CONE FLOW

Figures 9.6 and 9.7 show the results of the non-dimensional  $z$ -direction velocity profiles for Group 2 and Group 3 respectively.

Figure 9.6: Non-Dimensional  $z$ -Direction Velocity Profiles: Group 2 Accelerating Cone

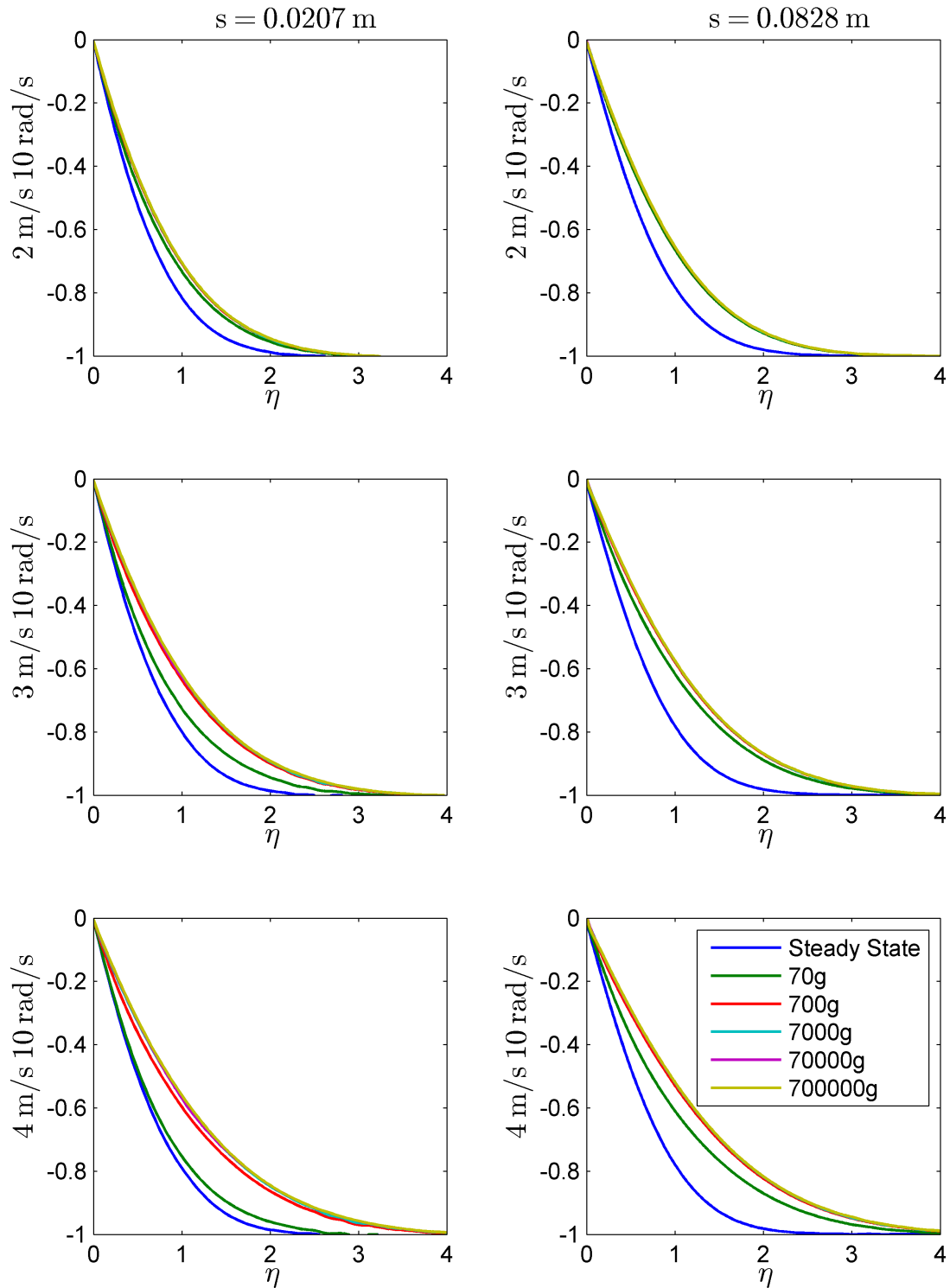
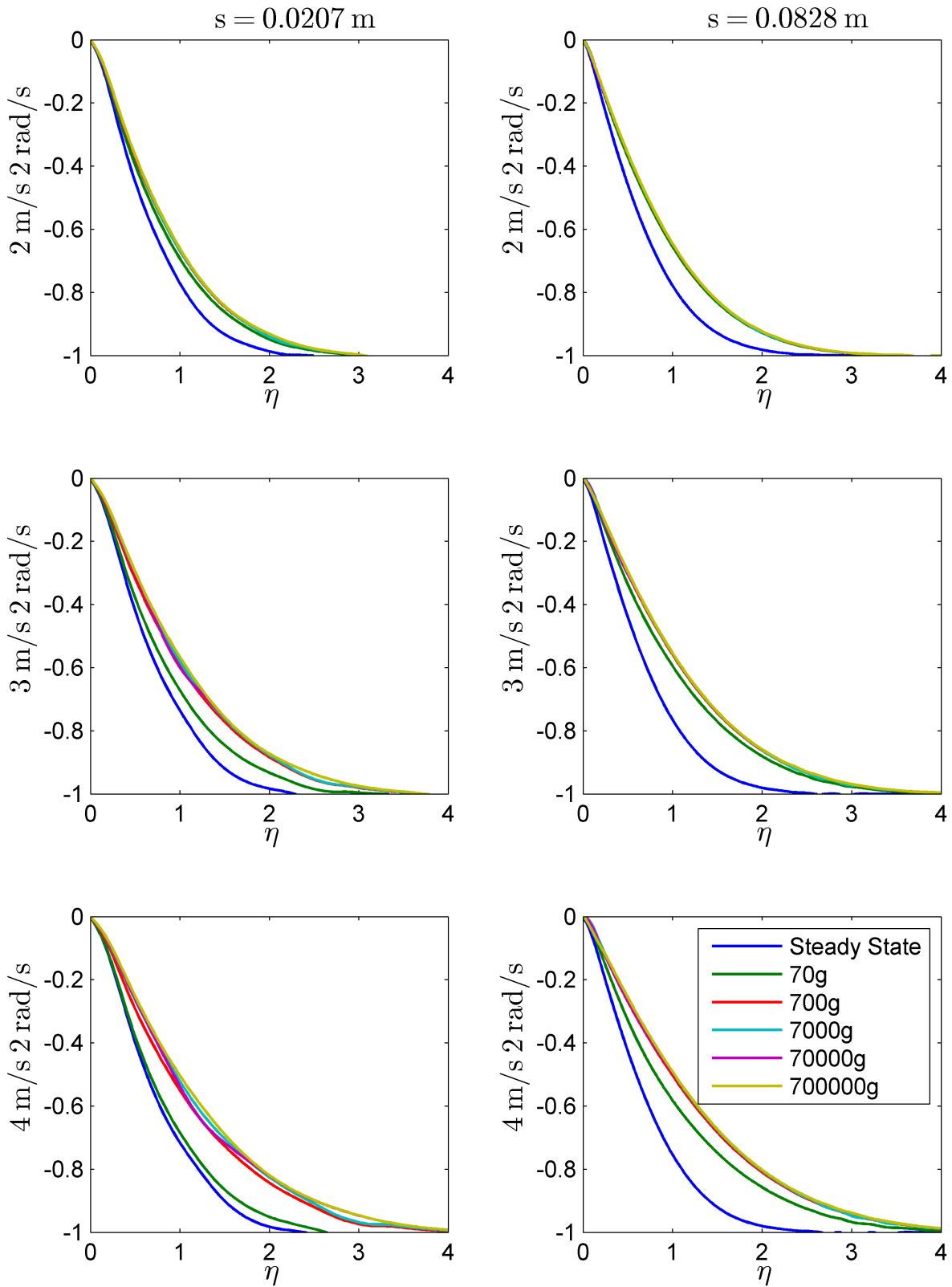




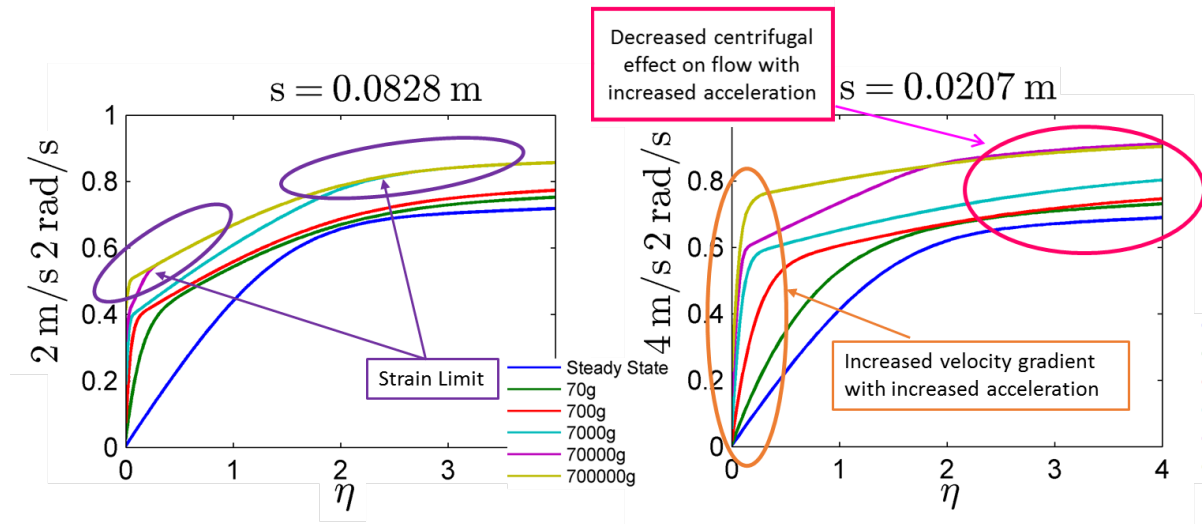
Figure 9.7: Non-Dimensional z-Direction Velocity Profiles: Group 3 Accelerating Cone



CHAPTER 9. BOUNDARY LAYER RESPONSE IN COMBINED TRANSLATION AND ROTATION - ARBITRARY CONE FLOW

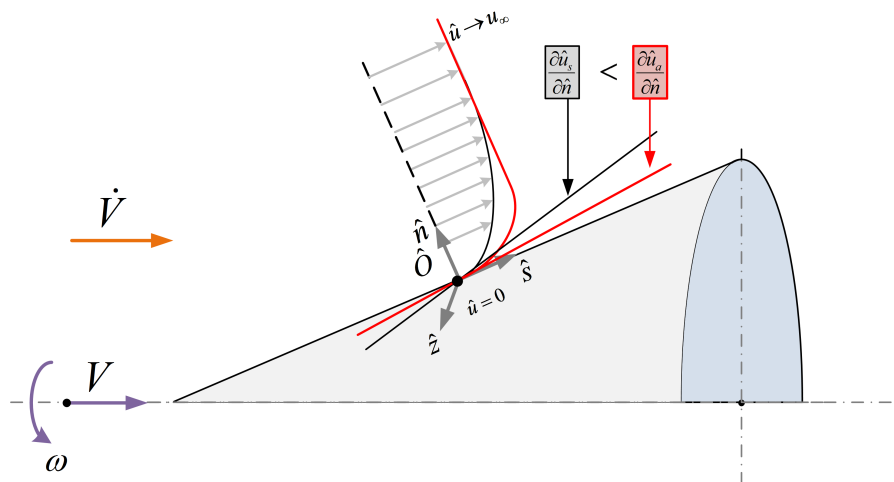
In the longitudinal  $s$ -direction three key responses have been observed (*Figure 9.8*); 1) an increase velocity gradient in the near-wall region, 2) a change in non-dimensional velocity in the far-field and 3) the presence of a strain limit at higher accelerations typically from 7000 g upwards.

Figure 9.8: Responses of the Boundary Layer on the Cone to Acceleration in Translation



The cone in translational acceleration reacts in a similar manner than the flat plate subjected to the same conditions. In *Figure 9.9* the velocity profile along the  $s$ -direction is shown. The profile is equivalent to the profile of the flat plate shown *Figure 7.8* where an increase in translational velocity lead to an increase in the velocity gradient in the near-wall region.

Figure 9.9: Accelerating Velocity Profile in the  $s$ -Direction on the Cone



*Equation 5.162* provided a mathematical description of the boundary layer in the  $s$ -direction for arbitrary acceleration. In this case the equation is reduced to:

$$\begin{aligned}
& \hat{\rho} \left[ \frac{\partial \hat{V}_1}{\partial t} + \frac{\hat{V}_1}{h_1} \frac{\partial \hat{V}_1}{\partial \hat{u}_1} + \frac{\hat{V}_2}{h_2} \frac{\partial \hat{V}_1}{\partial \hat{u}_2} + \frac{\hat{V}_3}{h_3} \frac{\partial \hat{V}_1}{\partial \hat{u}_3} - \hat{V}_2 \left( \frac{\hat{V}_2}{h_1 h_2} \frac{\partial h_2}{\partial \hat{u}_1} - \frac{\hat{V}_1}{h_1 h_2} \frac{\partial h_1}{\partial \hat{u}_2} \right) + \hat{V}_3 \left( \frac{\hat{V}_1}{h_1 h_3} \frac{\partial h_1}{\partial \hat{u}_3} - \frac{\hat{V}_3}{h_1 h_3} \frac{\partial h_3}{\partial \hat{u}_1} \right) \right] \\
& = -\frac{1}{h_1} \frac{\partial \hat{p}}{\partial \hat{u}_1} + \frac{1}{h_2} \frac{\partial}{\partial \hat{u}_2} \hat{\mu} \frac{h_1}{h_2} \frac{\partial \hat{u}_2}{\partial \hat{u}_2} \frac{\hat{V}_1}{h_1} + \hat{\rho} \left[ \underbrace{\hat{u}_1 \omega_2^2 - \hat{u}_2 \omega_1 \omega_2}_{\text{Centrifugal}} - \underbrace{\frac{\partial V_{e1}}{\partial t}}_{\text{Translation}} \right]
\end{aligned} \tag{9.3}$$

The same mechanism as described for the flat plate in *Chapter 7* applies. The non-inertial translation term on the right hand side acts as a momentum source in the equations. This results in an overall increase on the left hand side which is balanced by an increase in the near-wall velocity profile.

$$\begin{aligned}
& \hat{\rho} \left[ \frac{\partial \hat{V}_1}{\partial t} + \frac{\hat{V}_1}{h_1} \frac{\partial \hat{V}_1}{\partial \hat{u}_1} + \frac{\hat{V}_2}{h_2} \frac{\partial \hat{V}_1}{\partial \hat{u}_2} + \frac{\hat{V}_3}{h_3} \frac{\partial \hat{V}_1}{\partial \hat{u}_3} - \hat{V}_2 \left( \frac{\hat{V}_2}{h_1 h_2} \frac{\partial h_2}{\partial \hat{u}_1} - \frac{\hat{V}_1}{h_1 h_2} \frac{\partial h_1}{\partial \hat{u}_2} \right) + \hat{V}_3 \left( \frac{\hat{V}_1}{h_1 h_3} \frac{\partial h_1}{\partial \hat{u}_3} - \frac{\hat{V}_3}{h_1 h_3} \frac{\partial h_3}{\partial \hat{u}_1} \right) \right] \\
& = -\frac{1}{h_1} \frac{\partial \hat{p}}{\partial \hat{u}_1} + \frac{1}{h_2} \frac{\partial}{\partial \hat{u}_2} \hat{\mu} \frac{h_1}{h_2} \frac{\partial \hat{u}_2}{\partial \hat{u}_2} \frac{\hat{V}_1}{h_1} + \hat{\rho} \left[ \underbrace{\hat{u}_1 \omega_2^2 - \hat{u}_2 \omega_1 \omega_2}_{\text{Centrifugal}} - \underbrace{\frac{\partial V_{e1}}{\partial t}}_{\text{Translation}} \right]
\end{aligned} \tag{9.4}$$

The second response observed is an increase in non-dimensional velocity values with increasing acceleration. This occurs due to the interaction between the Coriolis and Translation non-inertial terms during acceleration.

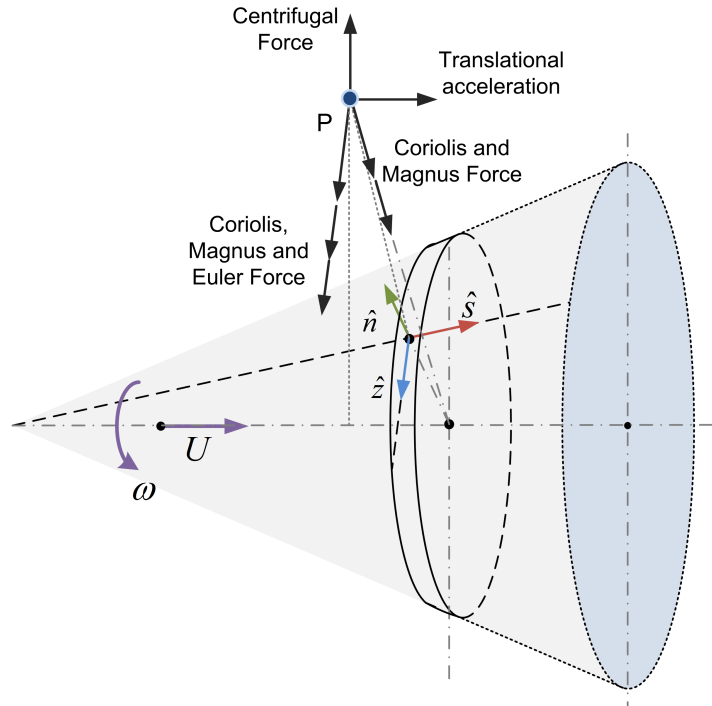
$$\begin{aligned}
& \hat{\rho} \left[ \frac{\partial \hat{V}_1}{\partial t} + \frac{\hat{V}_1}{h_1} \frac{\partial \hat{V}_1}{\partial \hat{u}_1} + \frac{\hat{V}_2}{h_2} \frac{\partial \hat{V}_1}{\partial \hat{u}_2} + \frac{\hat{V}_3}{h_3} \frac{\partial \hat{V}_1}{\partial \hat{u}_3} - \hat{V}_2 \left( \frac{\hat{V}_2}{h_1 h_2} \frac{\partial h_2}{\partial \hat{u}_1} - \frac{\hat{V}_1}{h_1 h_2} \frac{\partial h_1}{\partial \hat{u}_2} \right) + \hat{V}_3 \left( \frac{\hat{V}_1}{h_1 h_3} \frac{\partial h_1}{\partial \hat{u}_3} - \frac{\hat{V}_3}{h_1 h_3} \frac{\partial h_3}{\partial \hat{u}_1} \right) \right] \\
& = -\frac{1}{h_1} \frac{\partial \hat{p}}{\partial \hat{u}_1} + \frac{1}{h_2} \frac{\partial}{\partial \hat{u}_2} \hat{\mu} \frac{h_1}{h_2} \frac{\partial \hat{u}_2}{\partial \hat{u}_2} \frac{\hat{V}_1}{h_1} + \hat{\rho} \left[ \underbrace{\hat{u}_1 \omega_2^2 - \hat{u}_2 \omega_1 \omega_2}_{\text{Centrifugal}} - \underbrace{\frac{\partial V_{e1}}{\partial t}}_{\text{Translation}} \right]
\end{aligned} \tag{9.5}$$

In steady state conditions, the effects of all the non-inertial terms are in balance *Figure 9.10*. The effects all occur at the same time scale. An increase in the translational velocity, while the rotational velocity remains constant, causes the translation non-inertial term to dominate the Centrifugal forces. The time scale of the translation term is increased to become higher than the time scale of the centrifugal force, leading to a higher non-dimensional velocity in the  $s$ -direction.

The final response of the boundary layer involves strain limit that a boundary layer in acceleration can be subjected to. In the derivation of the Navier-Stokes equations for first principles, the infinitesimal strain theory is applied to a fluid parcel to obtain the stress tensor (Schlichting [42]). In a solid undergoing deformation, the strain is initially directly proportional to the stress. This condition only applies in the elastic portion of deformation up to the strain value that is associated with the plastic limit. From that point forward the material would undergo plastic deformation from which the material

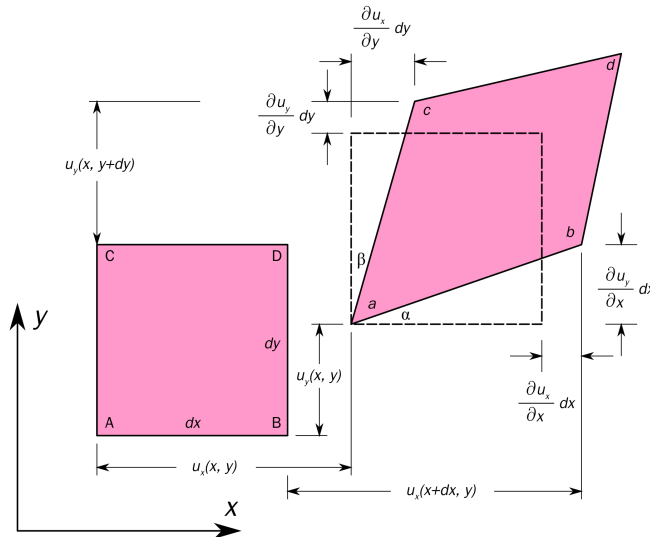
CHAPTER 9. BOUNDARY LAYER RESPONSE IN COMBINED TRANSLATION AND ROTATION - ARBITRARY CONE FLOW

Figure 9.10: Non-inertial Force Acting on a Cone in Arbitrary Motion



can not recover. A solid material therefore has a strain limit that separates the elastic deformation from the plastic deformation. In the Navier-Stokes equations the analogy is made that a fluid parcel deforms under external forces in the same manner as a solid parcel would in the elastic regime (Figure 9.11).

Figure 9.11: Strained Element



The strain limit of the fluid is the point where the fluid parcel has reached maximum deformation. This limit manifests in the accelerating boundary layer as a conglomeration of the boundary profiles for

various acceleration strengths. At this point the velocity profile becomes independent from the current acceleration strength. There is therefore a limit to how fast the particles can be accelerated in certain regions of the boundary layer. The profile is bounded by the strain limit. In the inviscid part of the flow, which is external of the boundary layer, the same limits does not apply.

The flow in the  $z$ -direction (transverse direction) reacts very similar to the rotating disk flow in the radial direction (*Figure 8.14*). The accelerating profiles are all of the same value, but not equal to the steady state result. As the simulation progresses the 70g profile separates from bundle results in the direction of the steady state result. This shows that there is a delay in the reaction of the tangential velocity profile to adjust to the accelerating boundary layer. The 70g profile has sufficient time to start adjusting to the changing conditions, while the remainder of the profiles remain at values similar to the starting condition. The general equation for boundary layer flow in the tangential direction was determined in *Equation 5.164*. This equation is reduced to obtain the non-inertial forces relevant to this case. the observed behaviour is due to an interaction between the Coriolis, Centrifugal and Magnus forces in a similar manner as discussed in *Section 8.2.1*.

$$\begin{aligned}
 & \hat{\rho} \left[ \frac{\partial \hat{V}_3}{\partial t} + \frac{\hat{V}_1}{h_1} \frac{\partial \hat{V}_3}{\partial \hat{u}_1} + \frac{\hat{V}_2}{h_2} \frac{\partial \hat{V}_3}{\partial \hat{u}_2} + \frac{\hat{V}_3}{h_3} \frac{\partial \hat{V}_3}{\partial \hat{u}_3} - \hat{V}_1 \left( \frac{\hat{V}_1}{h_1 h_3} \frac{\partial h_1}{\partial \hat{u}_3} - \frac{\hat{V}_3}{h_1 h_3} \frac{\partial h_3}{\partial \hat{u}_1} \right) + \hat{V}_2 \left( \frac{\hat{V}_3}{h_2 h_3} \frac{\partial h_2}{\partial \hat{u}_1} - \frac{\hat{V}_2}{h_2 h_3} \frac{\partial h_2}{\partial \hat{u}_3} \right) \right] \\
 & = -\frac{1}{h_1} \frac{\partial \hat{p}}{\partial \hat{u}_3} + \frac{1}{h_2} \frac{\partial}{\partial \hat{u}_2} \hat{\mu} \frac{h_3}{h_2} \frac{\partial \hat{u}_2}{\partial \hat{u}_2} \frac{\hat{V}_3}{h_3} \\
 & + \hat{\rho} \left[ \underbrace{2\hat{V}_1 \omega_2 - 2\hat{V}_2 \omega_1}_{\text{Coriolis}} + \underbrace{\hat{u}_3 (\omega_2^2 + \omega_1^2)}_{\text{Centrifugal}} + \underbrace{2V_{e1} \omega_2 - 2V_{e2} \omega_1}_{\text{Magnus}} \right]
 \end{aligned} \tag{9.6}$$

The same acceleration response types that were defined *Chapter 7* and used in *Chapter 8* are relevant to this case. The responses are:

- **Response Type I**, which is viscous dominant.
- **Response Type II**, which is certain regions in the boundary layer are dominated by viscosity and other regions by momentum.
- **Response Type III**, which is dominated by momentum.

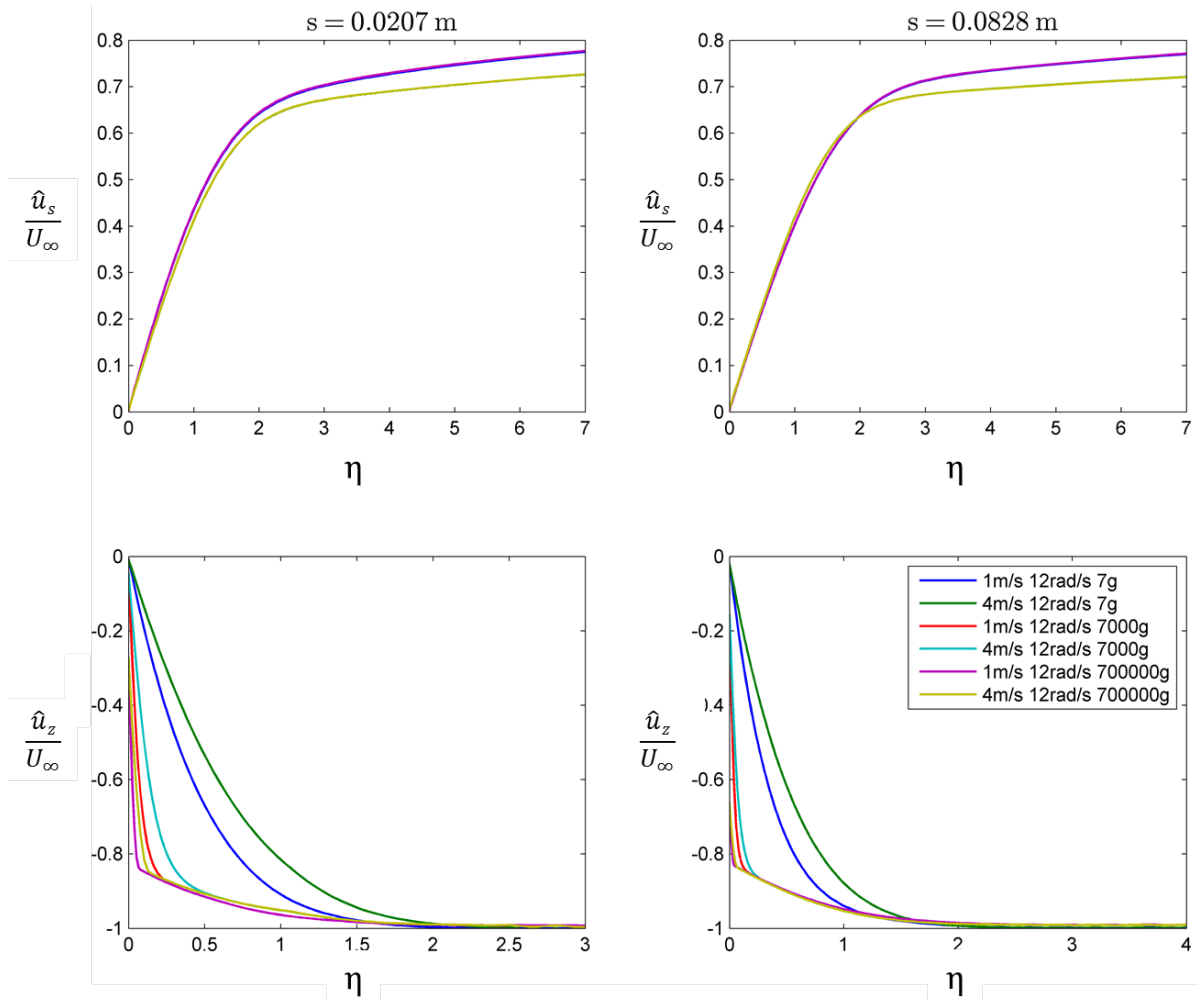
The flow in this case fall exclusively in the **Response Type III** category. The accelerating boundary layer deviates from the steady state profile. The two profiles do not overlap, neither in the near-wall nor far-field regions of the boundary layer. The flow for this selection of conditions are therefore dominated by momentum effects.

CHAPTER 9. BOUNDARY LAYER RESPONSE IN COMBINED TRANSLATION AND ROTATION - ARBITRARY CONE FLOW

9.2.1.2 Steady Translation with Accelerating Rotation

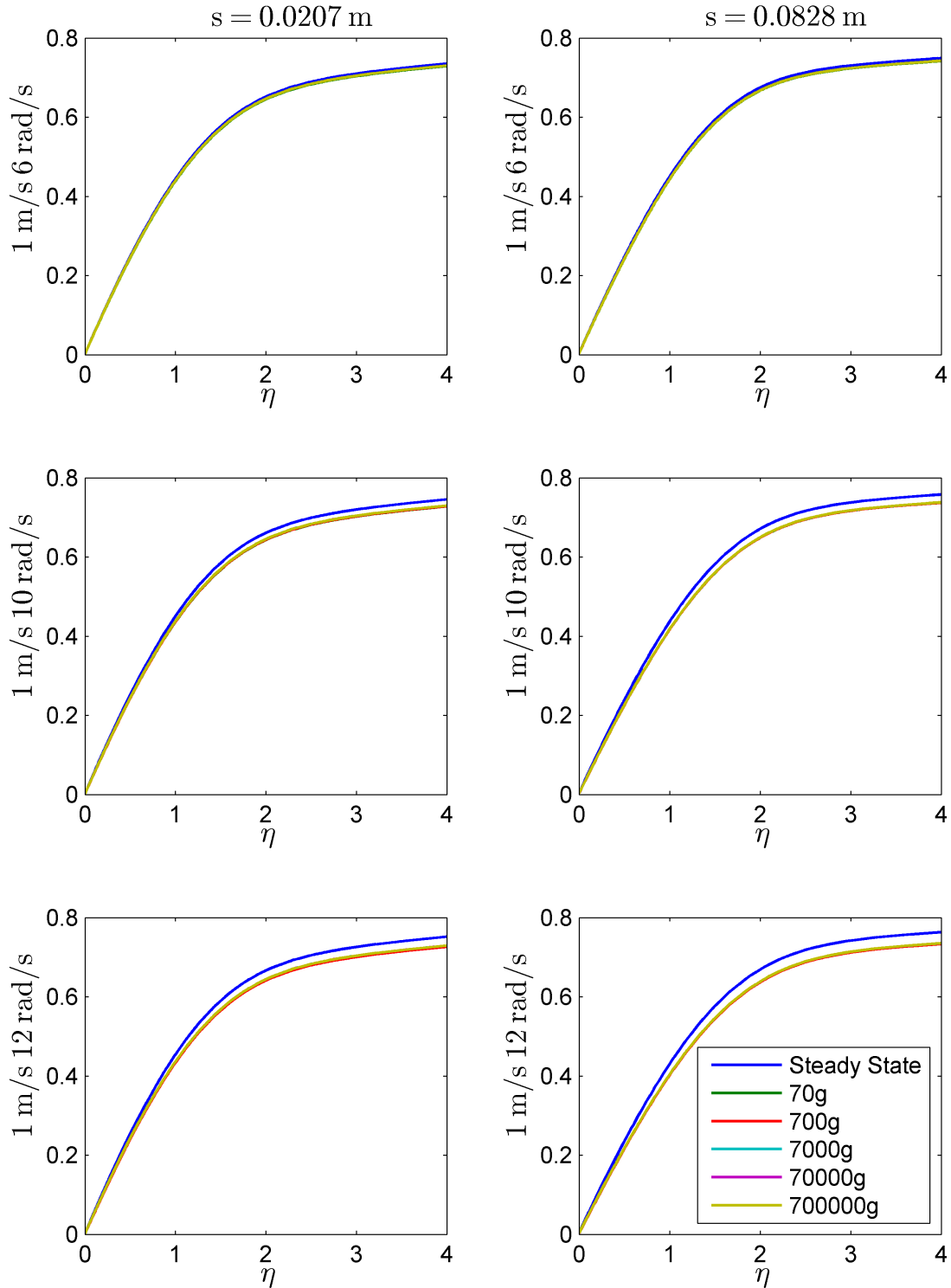
In Figure 9.12 the results from the accelerating part of Table 9.2 is shown. In the  $s$ -direction the boundary layers are divided into two regions;  $\eta < 2$  and  $\eta > 2$ . In the region closer to the wall,  $\eta < 2$ , the profiles are dominated by viscous forces. Here the 1 m/s and 4 m/s profiles are approximately equal. In the far-field of the boundary layer,  $\eta > 2$ , the flow is influenced by the Centrifugal acceleration. This is a similar mechanism as discussed in the previous subsection. Translation dominates the flow and the profiles are independent from the strength of the acceleration. The velocity profiles in the  $z$ -direction displays similar behaviour as the rotating disk in the tangential direction. The velocity gradients become larger closer to the wall with increasing acceleration. The strain limit that was discussed in the previous subsection is observed here as well.

Figure 9.12: Comparison between Group 4 and Group 5 Simulation Results for Acceleration



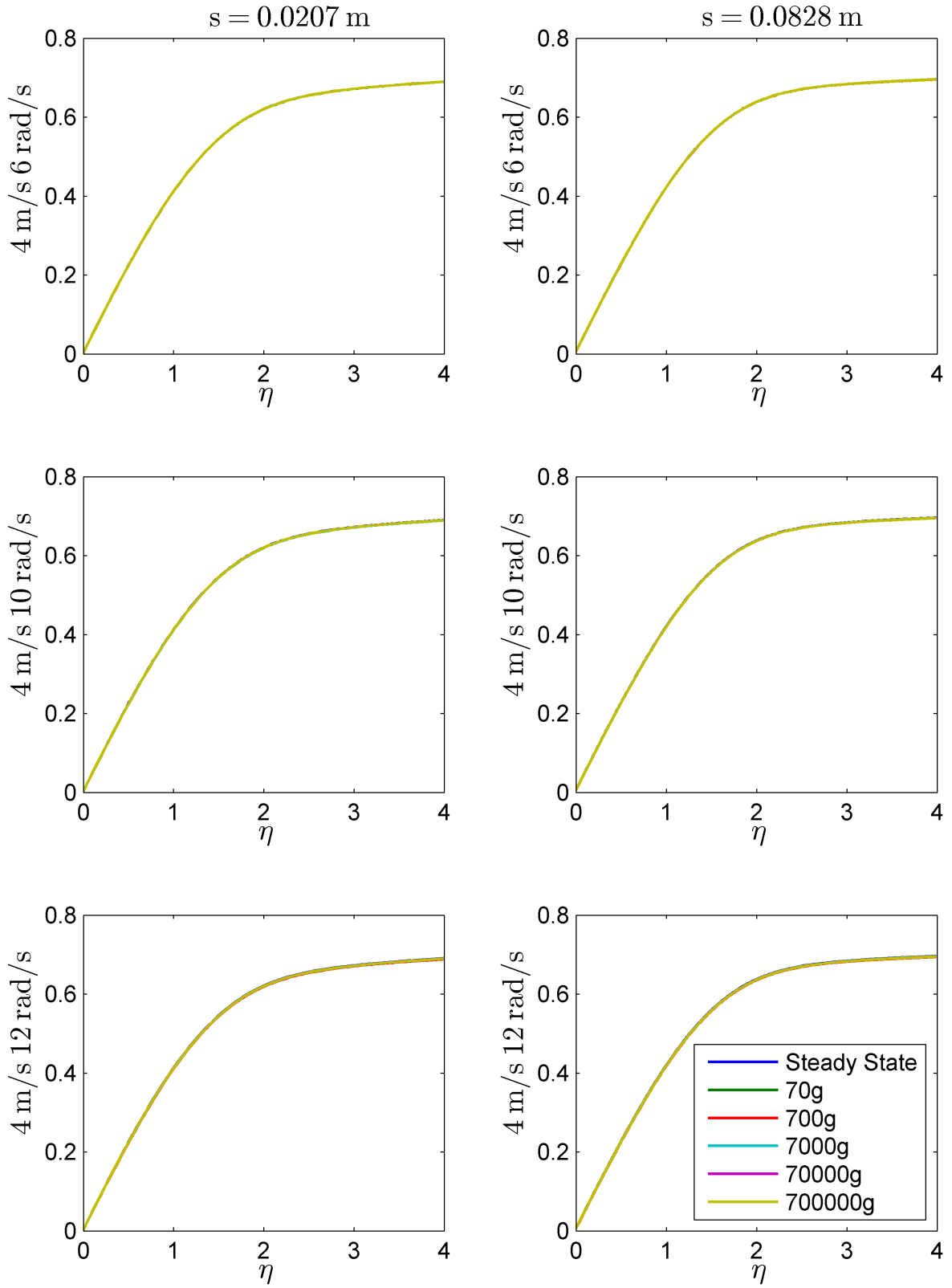
Figures 9.13 and 9.14 show the results of the non-dimensional  $s$ -direction velocity profiles for Group 4 and Group 5 respectively.

Figure 9.13: Non-Dimensional  $s$ -Direction Velocity Profiles: Group 4 Accelerating Cone



CHAPTER 9. BOUNDARY LAYER RESPONSE IN COMBINED TRANSLATION AND ROTATION - ARBITRARY CONE FLOW

Figure 9.14: Non-Dimensional  $s$ -Direction Velocity Profiles: Group 5 Accelerating Cone

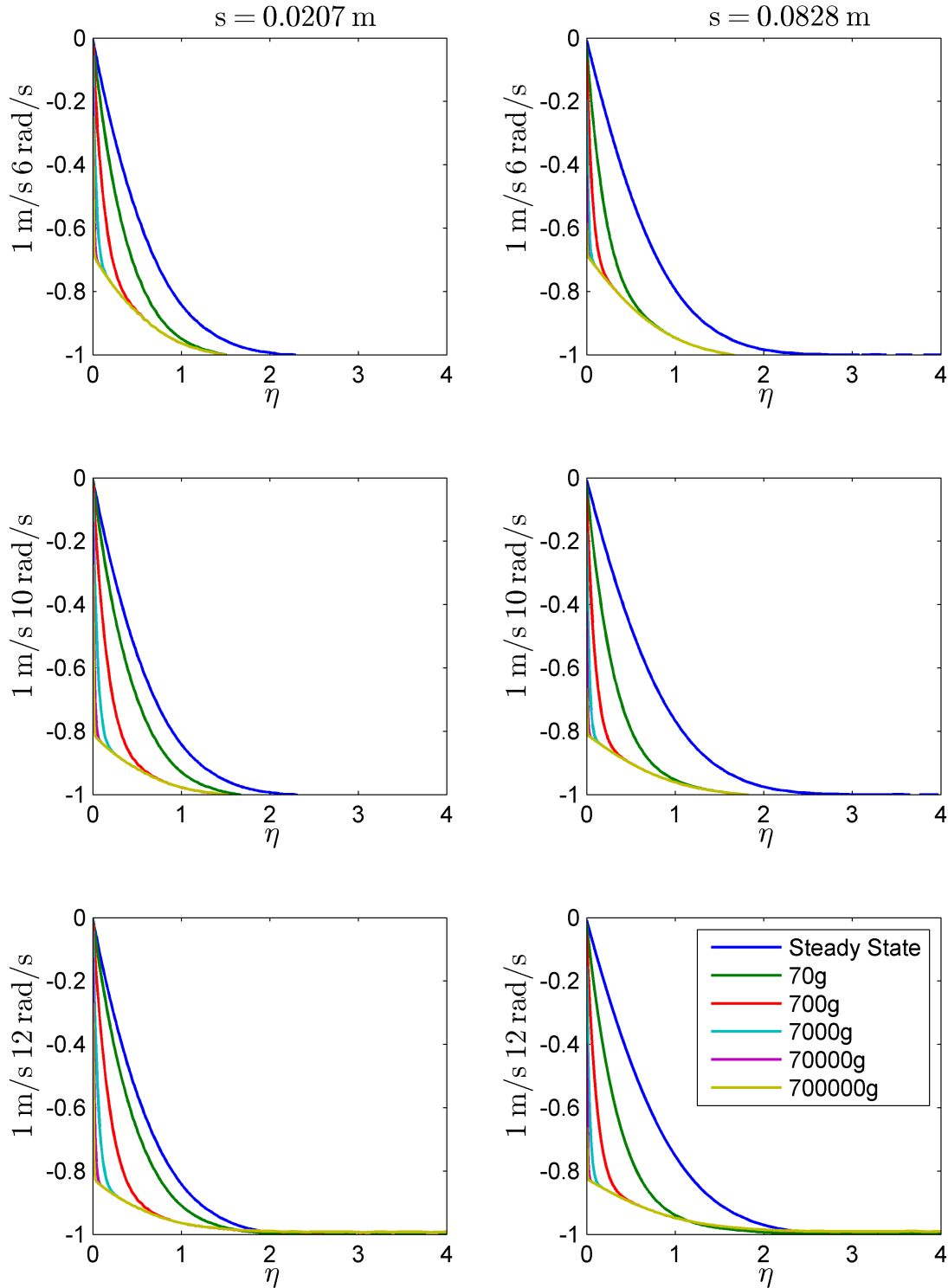




9.2. RESULTS AND DISCUSSION - ACCELERATION

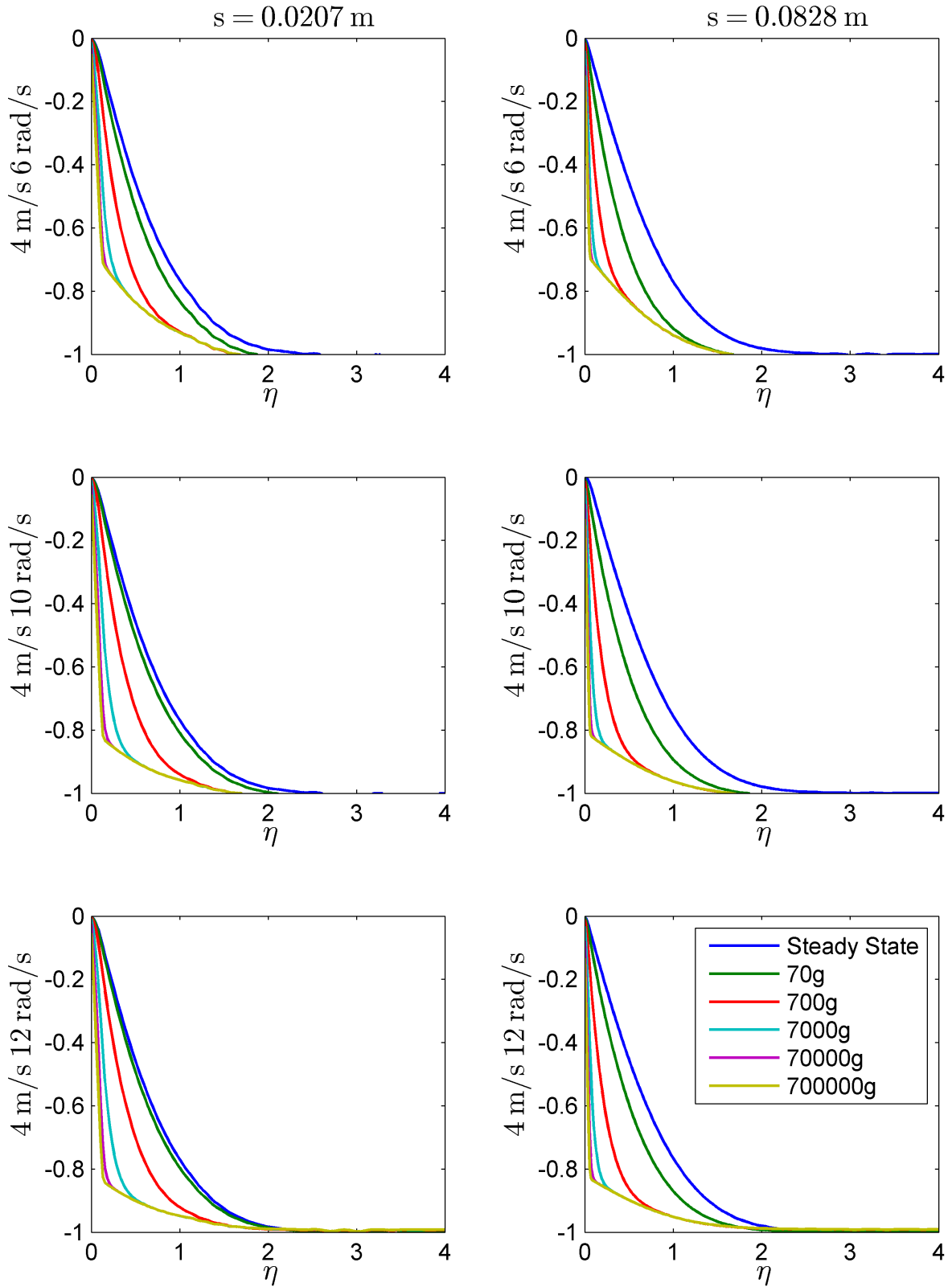
Figures 9.15 and 9.16 show the results of the non-dimensional tangential velocity profiles for Group 4 and Group 5 respectively.

Figure 9.15: Non-Dimensional  $z$ -Direction Velocity Profiles: Group 4 Accelerating Cone



CHAPTER 9. BOUNDARY LAYER RESPONSE IN COMBINED TRANSLATION AND ROTATION - ARBITRARY CONE FLOW

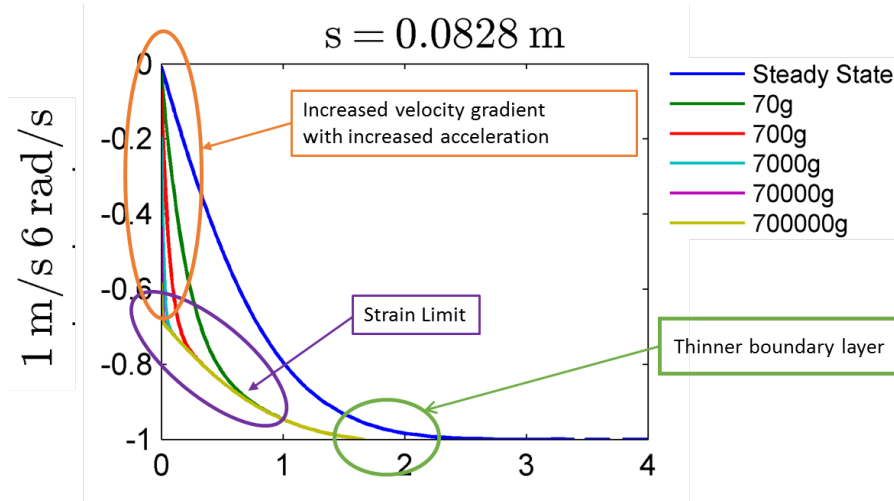
Figure 9.16: Non-Dimensional  $z$ -Direction Velocity Profiles: Group 5 Accelerating Cone



9.2. RESULTS AND DISCUSSION - ACCELERATION

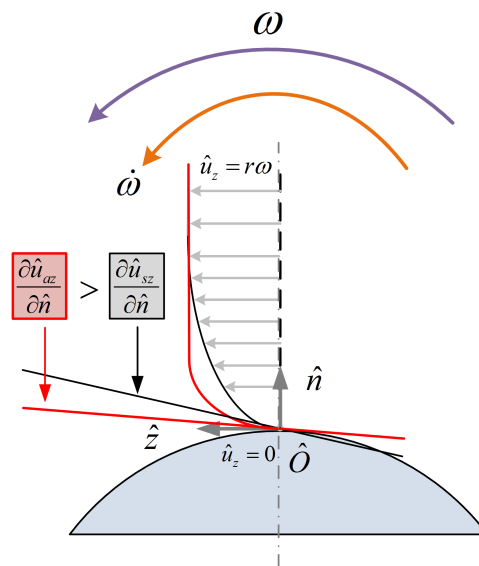
The result of the cone in the  $z$ -direction is consistent with the rotating disk in the tangential direction. This is displayed in *Figure 9.17* where an increased velocity gradient is observed that is directly proportional to the acceleration strength. The presence of the strain limit, as discussed in the previous subsection, is also present in this case. The boundary layer response to acceleration is momentum dominant and therefore of **Type III**.

Figure 9.17: Responses of the Boundary Layer on the Cone to Acceleration in Rotation



The mechanism responsible for the increased velocity gradient in the near-wall region is similar to the mechanism that causes the same effect on the rotating disk (*Figure 9.18*). The increase in the velocity gradient near the wall is a direct result of the acceleration of the flow.

Figure 9.18: Accelerating Velocity Profile in the  $z$ -Direction on the Cone



The governing equation for the momentum in the  $z$ -direction was determined in *Equation 5.164*.

CHAPTER 9. BOUNDARY LAYER RESPONSE IN COMBINED TRANSLATION AND ROTATION - ARBITRARY CONE FLOW

For the current case this equation is reduced to the following:

$$\begin{aligned}
& \hat{\rho} \left[ \frac{\partial \hat{V}_3}{\partial t} + \frac{\hat{V}_1}{h_1} \frac{\partial \hat{V}_3}{\partial \hat{u}_1} + \frac{\hat{V}_2}{h_2} \frac{\partial \hat{V}_3}{\partial \hat{u}_2} + \frac{\hat{V}_3}{h_3} \frac{\partial \hat{V}_3}{\partial \hat{u}_3} - \hat{V}_1 \left( \frac{\hat{V}_1}{h_1 h_3} \frac{\partial h_1}{\partial \hat{u}_3} - \frac{\hat{V}_3}{h_1 h_3} \frac{\partial h_3}{\partial \hat{u}_1} \right) + \hat{V}_2 \left( \frac{\hat{V}_3}{h_2 h_3} \frac{\partial h_2}{\partial \hat{u}_1} - \frac{\hat{V}_2}{h_2 h_3} \frac{\partial h_2}{\partial \hat{u}_3} \right) \right] \\
& = -\frac{1}{h_1} \frac{\partial \hat{p}}{\partial \hat{u}_3} + \frac{1}{h_2} \frac{\partial}{\partial \hat{u}_2} \hat{\mu} \frac{h_3}{h_2} \frac{\partial \hat{u}_2}{\partial \hat{u}_3} \frac{\hat{V}_3}{h_3} \\
& + \hat{\rho} \left[ \underbrace{2\hat{V}_1 \omega_2 - 2\hat{V}_2 \omega_1}_{\text{Coriolis}} + \underbrace{\hat{u}_3 (\omega_2^2 + \omega_1^2)}_{\text{Centrifugal}} + \underbrace{\hat{u}_1 \omega_2 - \hat{u}_2 \omega_1}_{\text{Euler}} + \underbrace{2V_{e1} \omega_2 - 2V_{e2} \omega_1}_{\text{Magnus}} \right]
\end{aligned} \tag{9.7}$$

Rotational acceleration causes an increase in the non-inertial terms on the right hand side of the equation. In response the momentum terms on the left hand side increase. The velocity,  $V_3$  subsequently increases. This results in an increase in the near-wall velocity profile.

$$\begin{aligned}
& \hat{\rho} \left[ \frac{\partial \hat{V}_3}{\partial t} + \frac{\hat{V}_1}{h_1} \frac{\partial \hat{V}_3}{\partial \hat{u}_1} + \frac{\hat{V}_2}{h_2} \frac{\partial \hat{V}_3}{\partial \hat{u}_2} + \frac{\hat{V}_3}{h_3} \frac{\partial \hat{V}_3}{\partial \hat{u}_3} - \hat{V}_1 \left( \frac{\hat{V}_1}{h_1 h_3} \frac{\partial h_1}{\partial \hat{u}_3} - \frac{\hat{V}_3}{h_1 h_3} \frac{\partial h_3}{\partial \hat{u}_1} \right) + \hat{V}_2 \left( \frac{\hat{V}_3}{h_2 h_3} \frac{\partial h_2}{\partial \hat{u}_1} - \frac{\hat{V}_2}{h_2 h_3} \frac{\partial h_2}{\partial \hat{u}_3} \right) \right] \\
& = -\frac{1}{h_1} \frac{\partial \hat{p}}{\partial \hat{u}_3} + \frac{1}{h_2} \frac{\partial}{\partial \hat{u}_2} \hat{\mu} \frac{h_3}{h_2} \frac{\partial \hat{u}_2}{\partial \hat{u}_3} \frac{\hat{V}_3}{h_3} \\
& + \hat{\rho} \left[ \underbrace{2\hat{V}_1 \omega_2 - 2\hat{V}_2 \omega_1}_{\text{Coriolis}} + \underbrace{\hat{u}_3 (\omega_2^2 + \omega_1^2)}_{\text{Centrifugal}} + \underbrace{\hat{u}_1 \omega_2 - \hat{u}_2 \omega_1}_{\text{Euler}} + \underbrace{2V_{e1} \omega_2 - 2V_{e2} \omega_1}_{\text{Magnus}} \right]
\end{aligned} \tag{9.8}$$

Equation 5.162 is reduced to described the flow in the  $s$ -direction for this case.

$$\begin{aligned}
& \hat{\rho} \left[ \frac{\partial \hat{V}_1}{\partial t} + \frac{\hat{V}_1}{h_1} \frac{\partial \hat{V}_1}{\partial \hat{u}_1} + \frac{\hat{V}_2}{h_2} \frac{\partial \hat{V}_1}{\partial \hat{u}_2} + \frac{\hat{V}_3}{h_3} \frac{\partial \hat{V}_1}{\partial \hat{u}_3} - \hat{V}_2 \left( \frac{\hat{V}_2}{h_1 h_2} \frac{\partial h_2}{\partial \hat{u}_1} - \frac{\hat{V}_1}{h_1 h_2} \frac{\partial h_1}{\partial \hat{u}_2} \right) + \hat{V}_3 \left( \frac{\hat{V}_1}{h_1 h_3} \frac{\partial h_1}{\partial \hat{u}_3} - \frac{\hat{V}_3}{h_1 h_3} \frac{\partial h_3}{\partial \hat{u}_1} \right) \right] \\
& = -\frac{1}{h_1} \frac{\partial \hat{p}}{\partial \hat{u}_1} + \frac{1}{h_2} \frac{\partial}{\partial \hat{u}_2} \hat{\mu} \frac{h_1}{h_2} \frac{\partial \hat{u}_2}{\partial \hat{u}_1} \frac{\hat{V}_1}{h_1} \\
& + \hat{\rho} \left[ \underbrace{\hat{u}_1 \omega_2^2 - \hat{u}_2 \omega_1 \omega_2}_{\text{Centrifugal}} \right] - \hat{u}_3 \dot{\omega}_2
\end{aligned} \tag{9.9}$$

The effect of the Centrifugal force in the equation below is seen in *Figure 9.13* and depicted in *Figure 9.10*. The flow is dominated by translation. If the translational velocity is low enough the Centrifugal force influences the shape of the velocity profile. In the Group 4 case, with 1 m/s translational velocity the far-field non-dimensional velocity is reduced with higher rotations. However, in the Group 5 case, with 4 m/s translation completely dominates the flow and no differences is observed (*Figure 9.14*). In both cases the flow in the  $s$ -direction is independent of the acceleration since no variation is seen in the profiles for different accelerations.

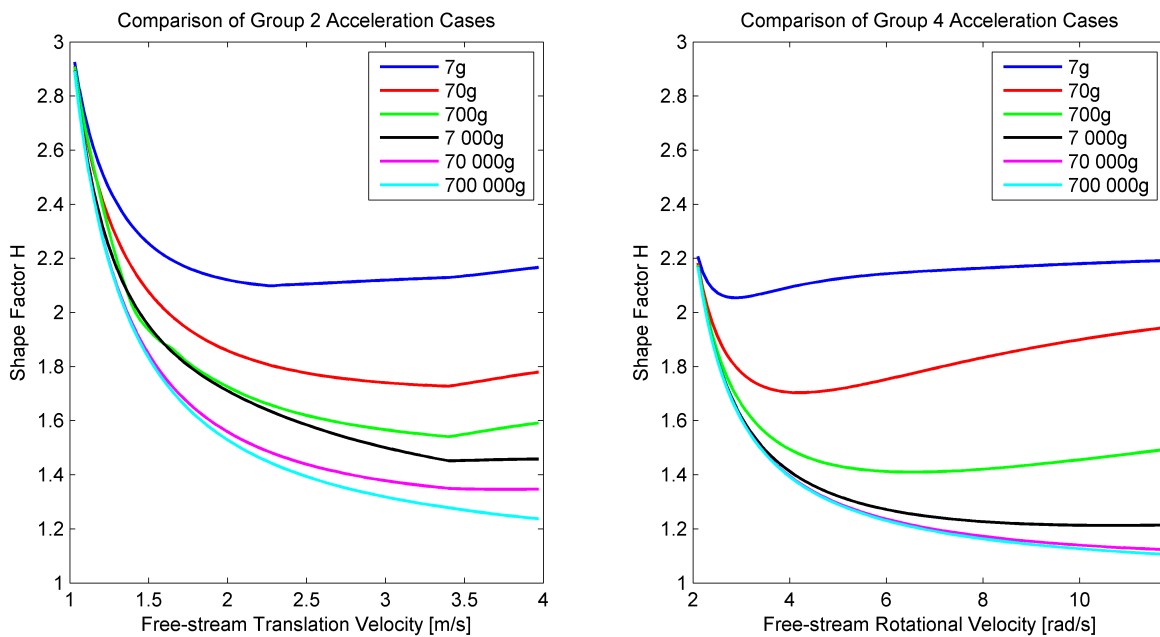
### 9.2.2 Boundary Layer Parameters

The shape factor was calculated here as shown in *Chapters 7 and 8* from the displacement and momentum thickness parameters.

$$H = \frac{\delta^*}{\theta} \tag{9.10}$$

In *Figure 9.19* a comparison of the results for different accelerations is shown for Group 2 in the *s*-direction and Group 4 in the *z*-direction. *Figures 9.20 -9.23* show the results for the *s*-direction of Groups 2 and 3 and the *z*-direction of the Groups 4 and 5 respectively.

Figure 9.19: Comparison of Shape Factor for the Group 2 (left) and Group 4 (right) Cases



The results are consistent with those of the flat plate and rotating disk in acceleration. Two types of behaviour are seen in the profiles. The first is observed in the lower accelerations. The shape factor initially decreases to reach a minimum value, after which it is increasing and attempts to recover the steady state value. The second type of behaviour is seen in the higher acceleration cases. Here the shape factor decreases to approach an minimum asymptotic value. In both cases the first derivative approaches zero, indicating that an asymptotic values is approached.

CHAPTER 9. BOUNDARY LAYER RESPONSE IN COMBINED TRANSLATION AND ROTATION - ARBITRARY CONE FLOW

Figure 9.20: Shape Factor in  $s$ -Direction for Translational Acceleration

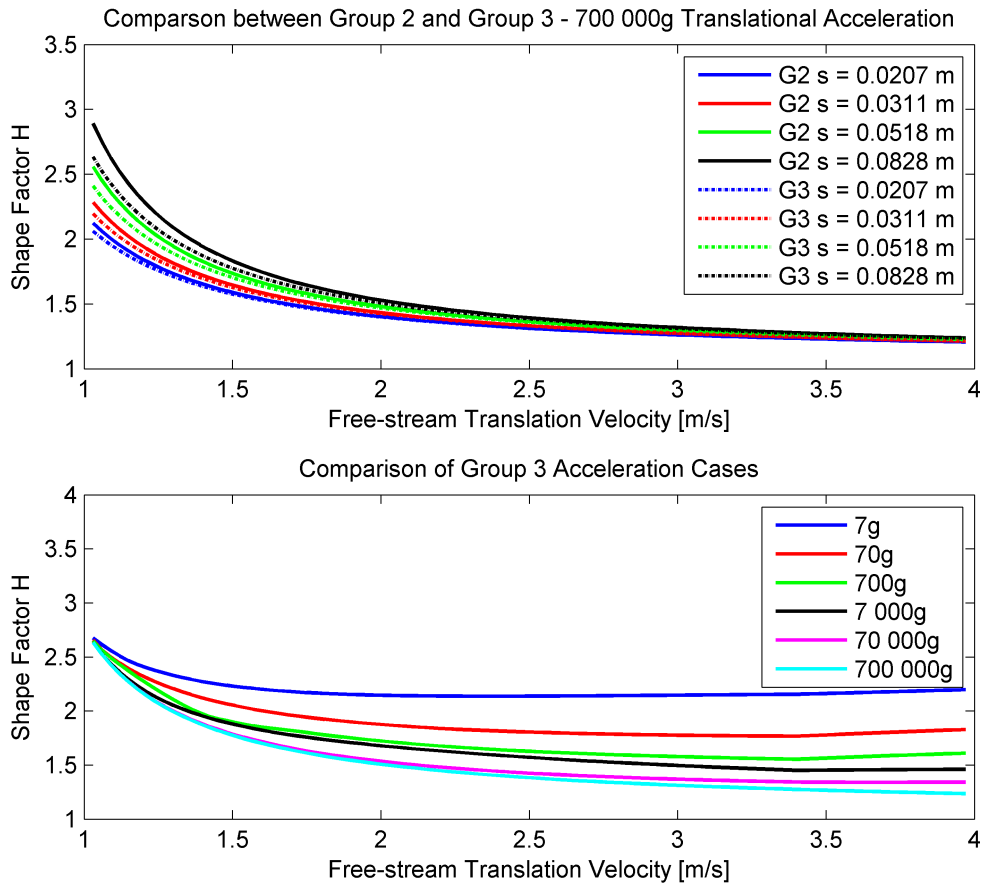
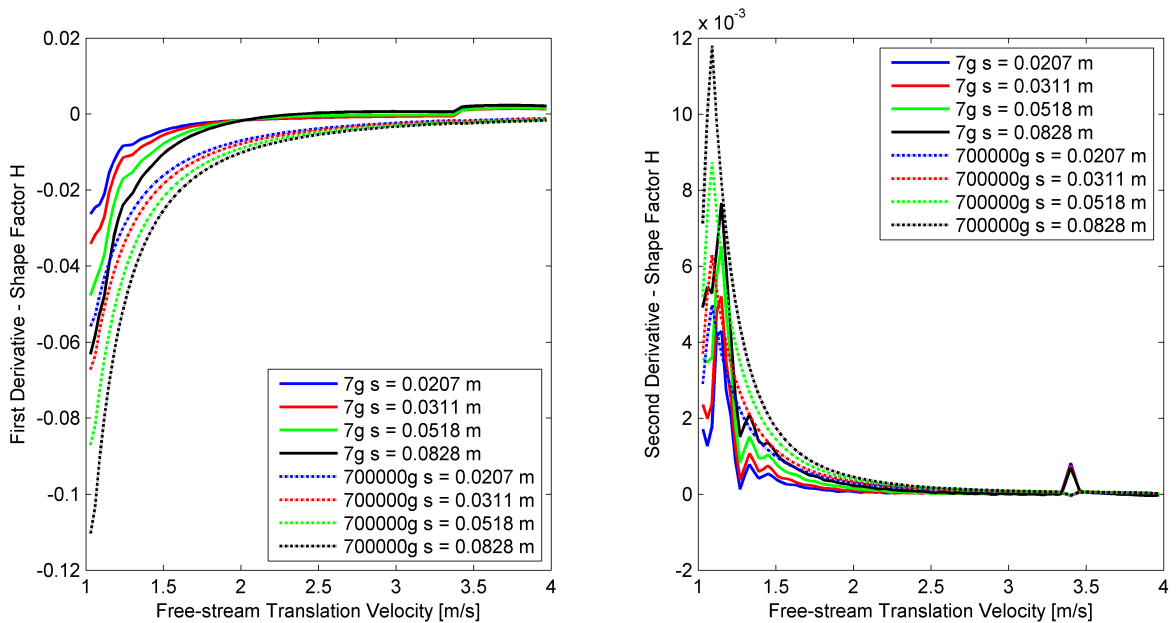


Figure 9.21: Derivatives of Shape Factor in  $s$ -Direction for Translational Acceleration



9.2. RESULTS AND DISCUSSION - ACCELERATION

Figure 9.22: Shape Factor in z-Direction for Rotational Acceleration

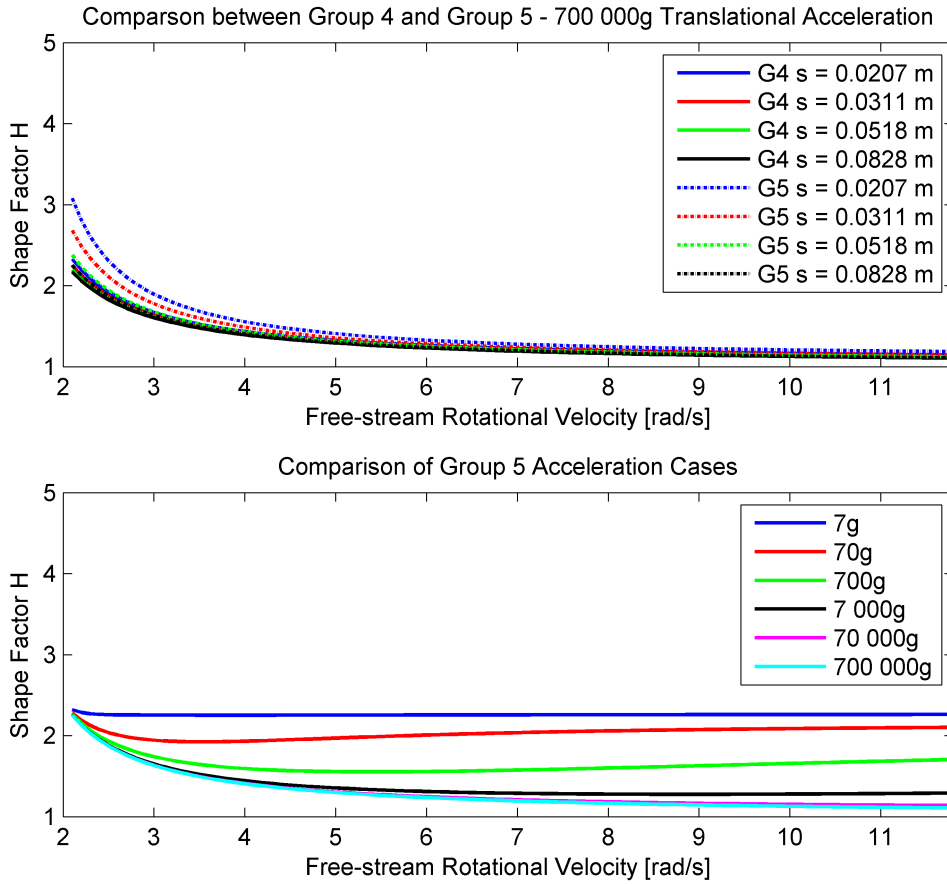
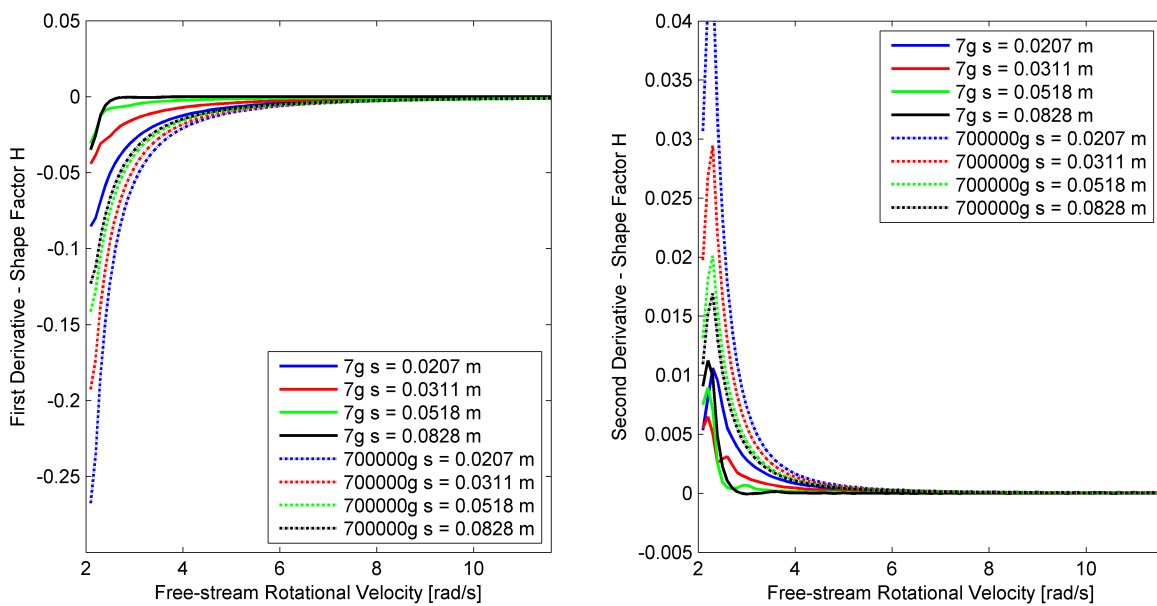


Figure 9.23: Derivatives of Shape Factor in z-Direction for Rotational Acceleration



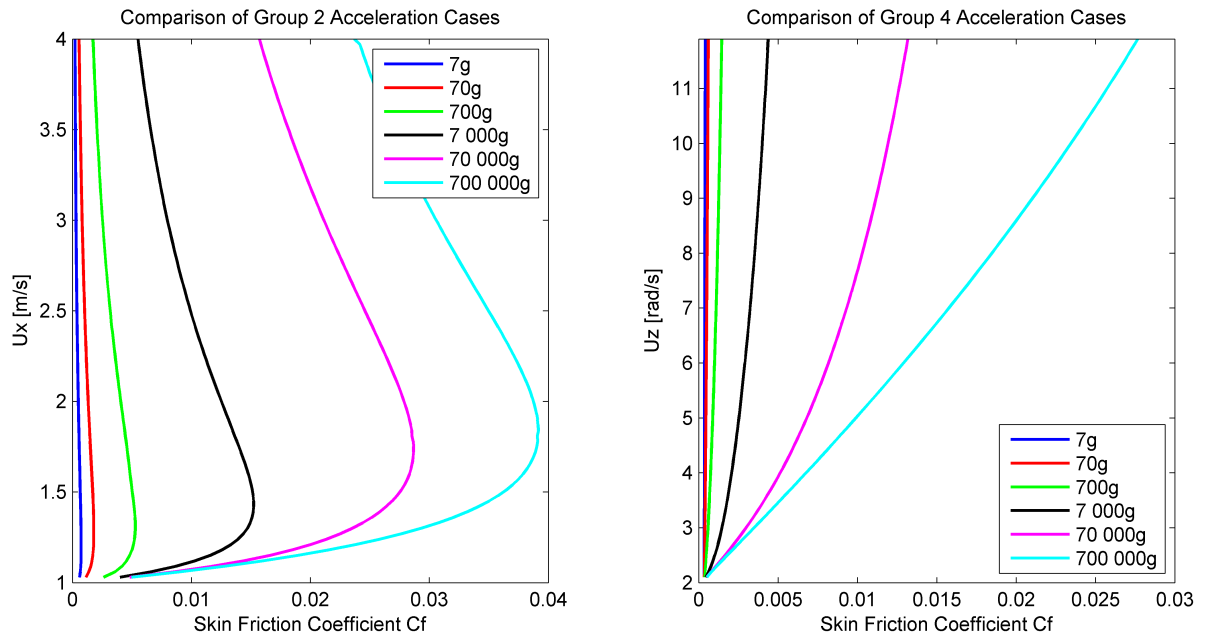
### 9.2.3 Skin Friction Coefficients

The skin friction coefficients were determined using the equation of in *Chapters 7 and 8*. The results are shown in *Figures 9.24-9.28*.

$$\tau_{wall} = \mu \left. \frac{\partial \hat{u}}{\partial y} \right|_{wall} \tag{9.11}$$

$$C_f = \frac{\tau_{wall}}{0.5 \rho U_\infty^2}$$

Figure 9.24: Comparison of Skin Friction Coefficient for the Group 2 (left) and Group 4 (right) Cases



The Group 2 and Group 3 cases display similar responses at the flat plate in acceleration. The skin friction coefficient has an initial increase at the start of the acceleration event. The value reaches a maximum after which it steadily decreases to approach an asymptote. Higher accelerations leads to higher skin friction coefficient values.

The Group 4 and Group 5 cases do not compare with any results previously observed, neither for the flat plate nor the rotating disk. At low accelerations the change in skin friction coefficient values is very small, with the biggest changes seen in the accelerations above 7 000g.



9.2. RESULTS AND DISCUSSION - ACCELERATION

Figure 9.25: Skin Friction Coefficient in *s*-Direction for Translational Acceleration

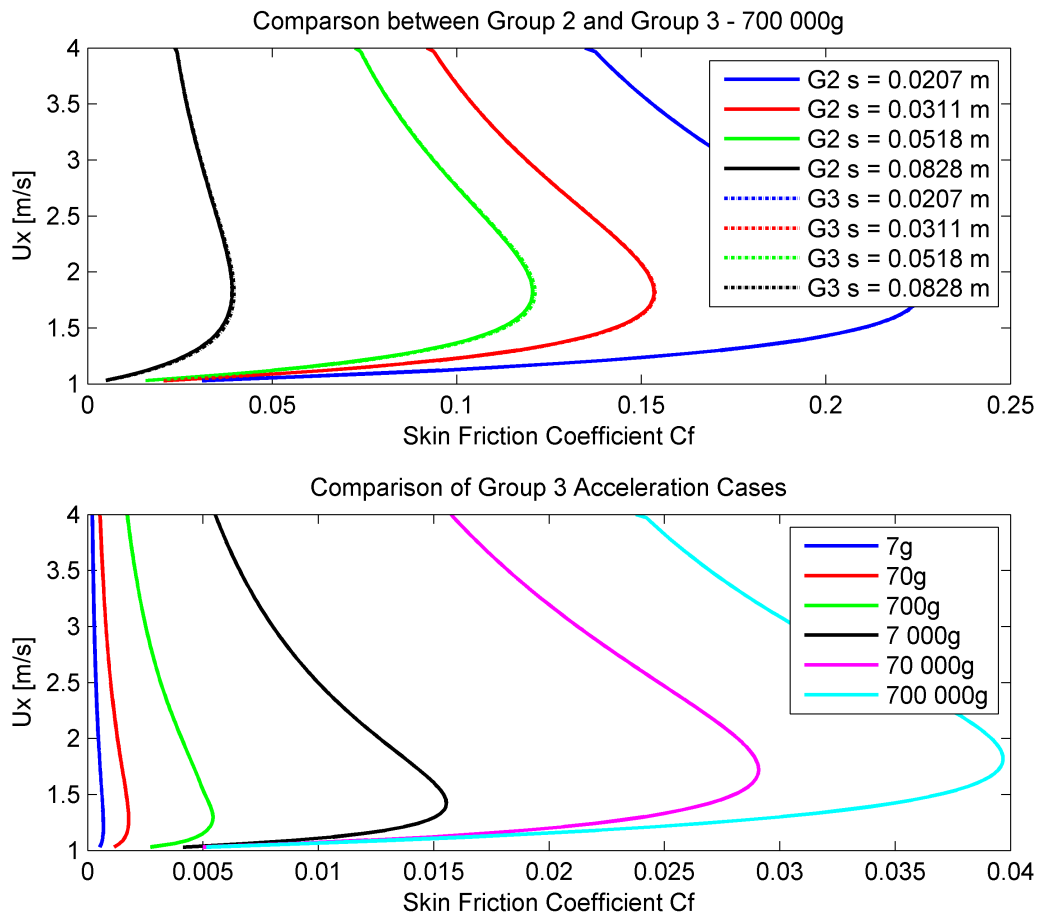
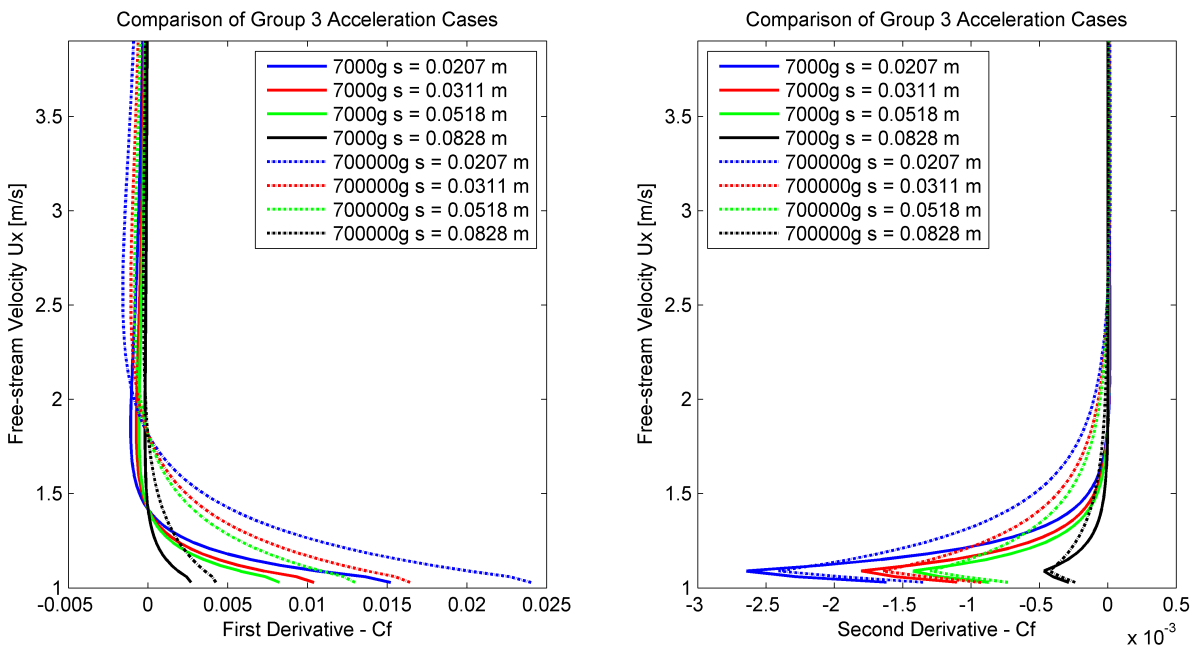


Figure 9.26: Derivatives of Skin Friction Coefficient in *s*-Direction for Translational Acceleration



CHAPTER 9. BOUNDARY LAYER RESPONSE IN COMBINED TRANSLATION AND ROTATION - ARBITRARY CONE FLOW

Figure 9.27: Skin Friction Coefficient in z-Direction for Rotational Acceleration

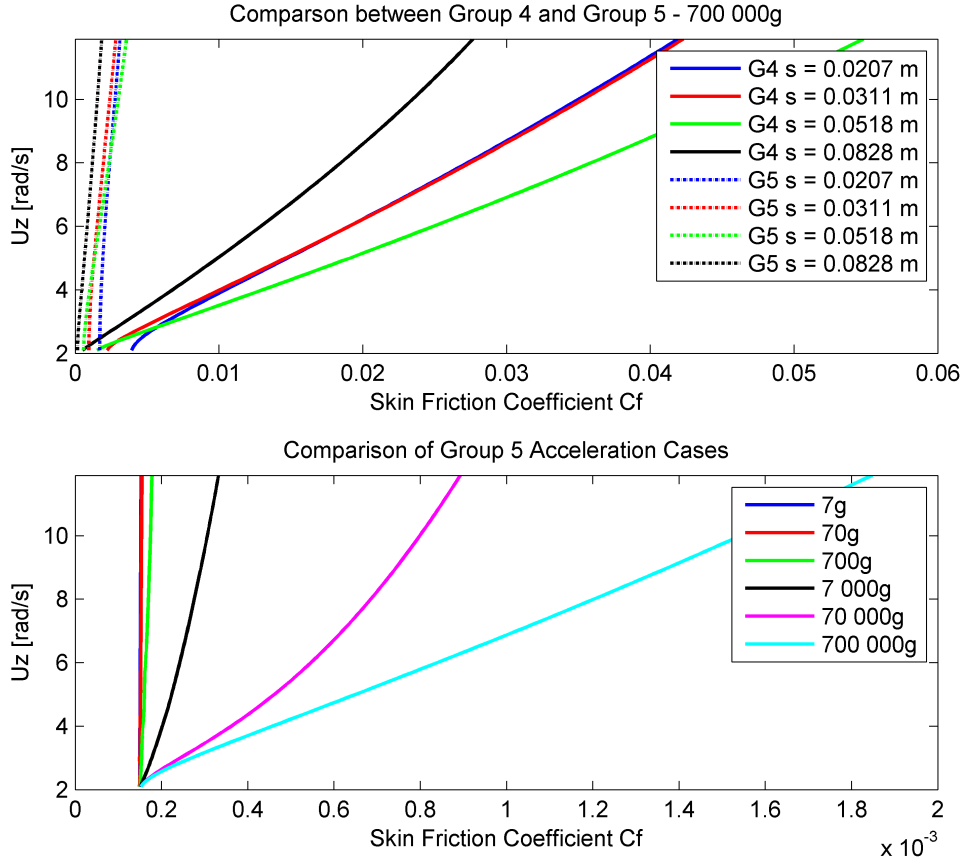
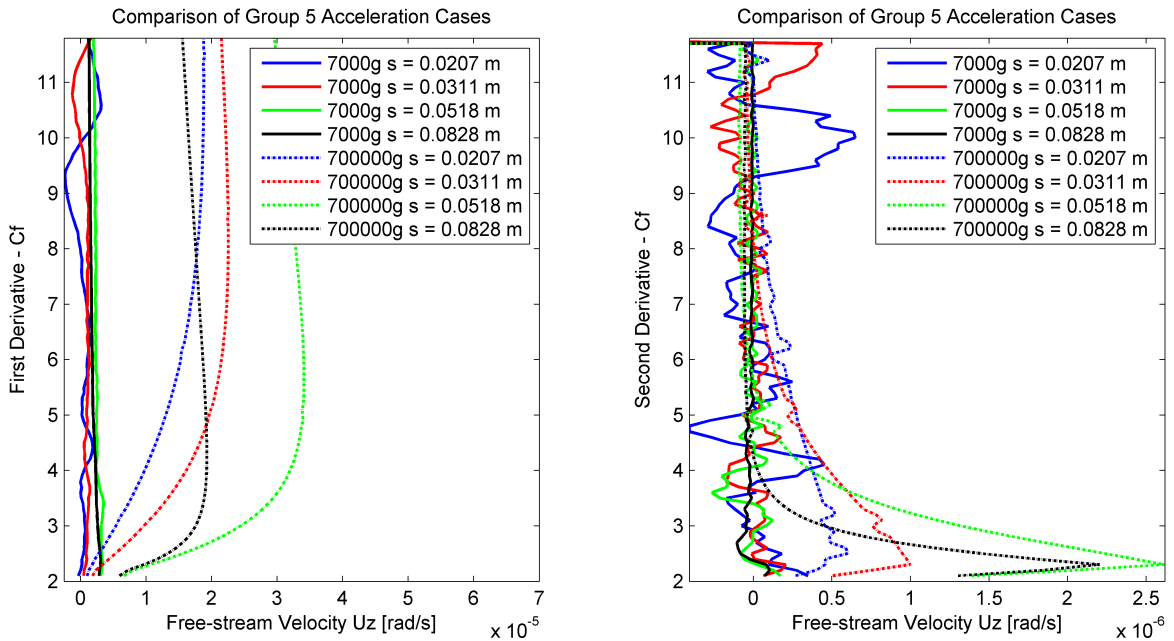


Figure 9.28: Derivatives of Skin Friction Coefficient in z-Direction for Rotational Acceleration



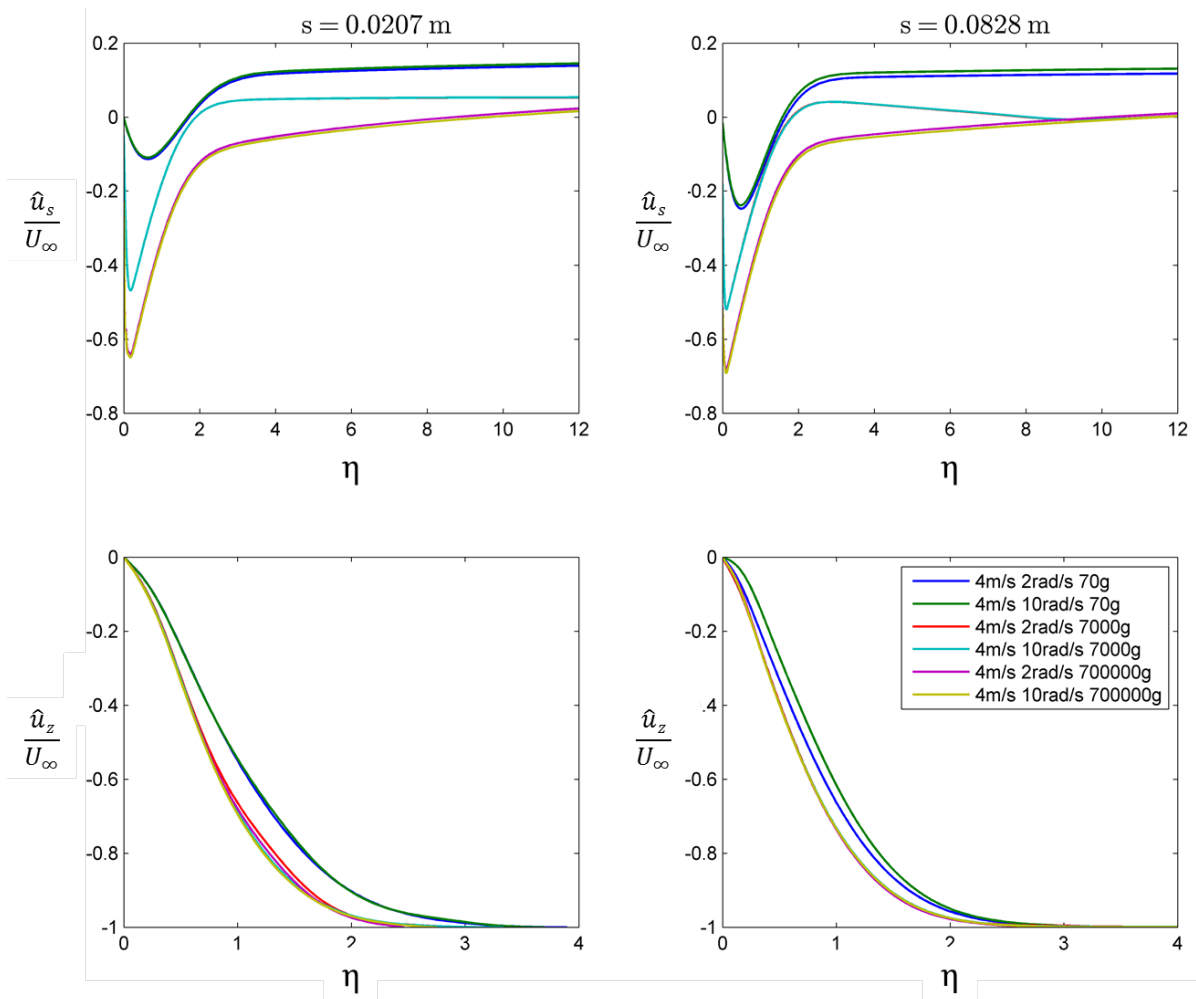
## 9.3 Results and Discussion - Deceleration

### 9.3.1 Velocity Profiles

#### 9.3.1.1 Decelerating Translation with Steady Rotation

The deceleration of the axial velocity for the cone was done in accordance with *Table 9.1*. A comparison between the result for the Group 2 and Group 3 results are shown in *Figure 9.29*. The velocity profiles in the  $s$ -direction is minimally influenced by the difference in rotational velocity. Profiles with the same deceleration however, have similar values. Strong separation of the flow is seen. The separation strength is directly proportional to the deceleration. The Centrifugal force lowers the non-dimensional velocity value in the far-field of the boundary layer. The tangential velocity profile (in the  $z$ -direction) are only slightly affected by the change in axial velocity. The flow is overall dominated by the larger translational velocity.

Figure 9.29: Comparison between Group 2 and Group 3 Simulation Results for Deceleration



CHAPTER 9. BOUNDARY LAYER RESPONSE IN COMBINED TRANSLATION AND ROTATION - ARBITRARY CONE FLOW

In *Figures 9.30 and 9.31* the  $s$ -direction velocities for the Group 2 and Group 3 results are shown.

Figure 9.30: Non-Dimensional  $s$ -Direction Velocity Profiles: Group 2 Decelerating Cone

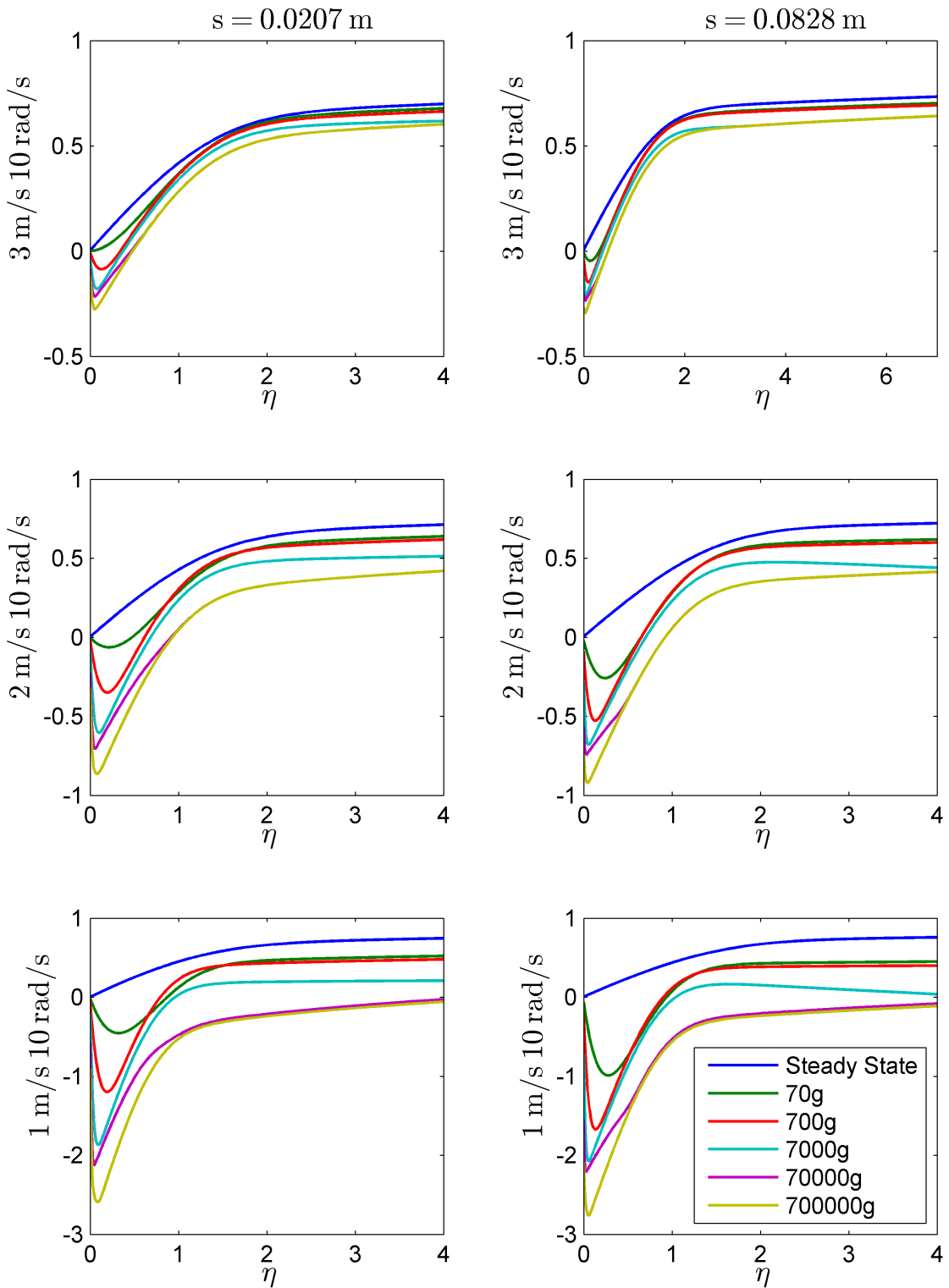
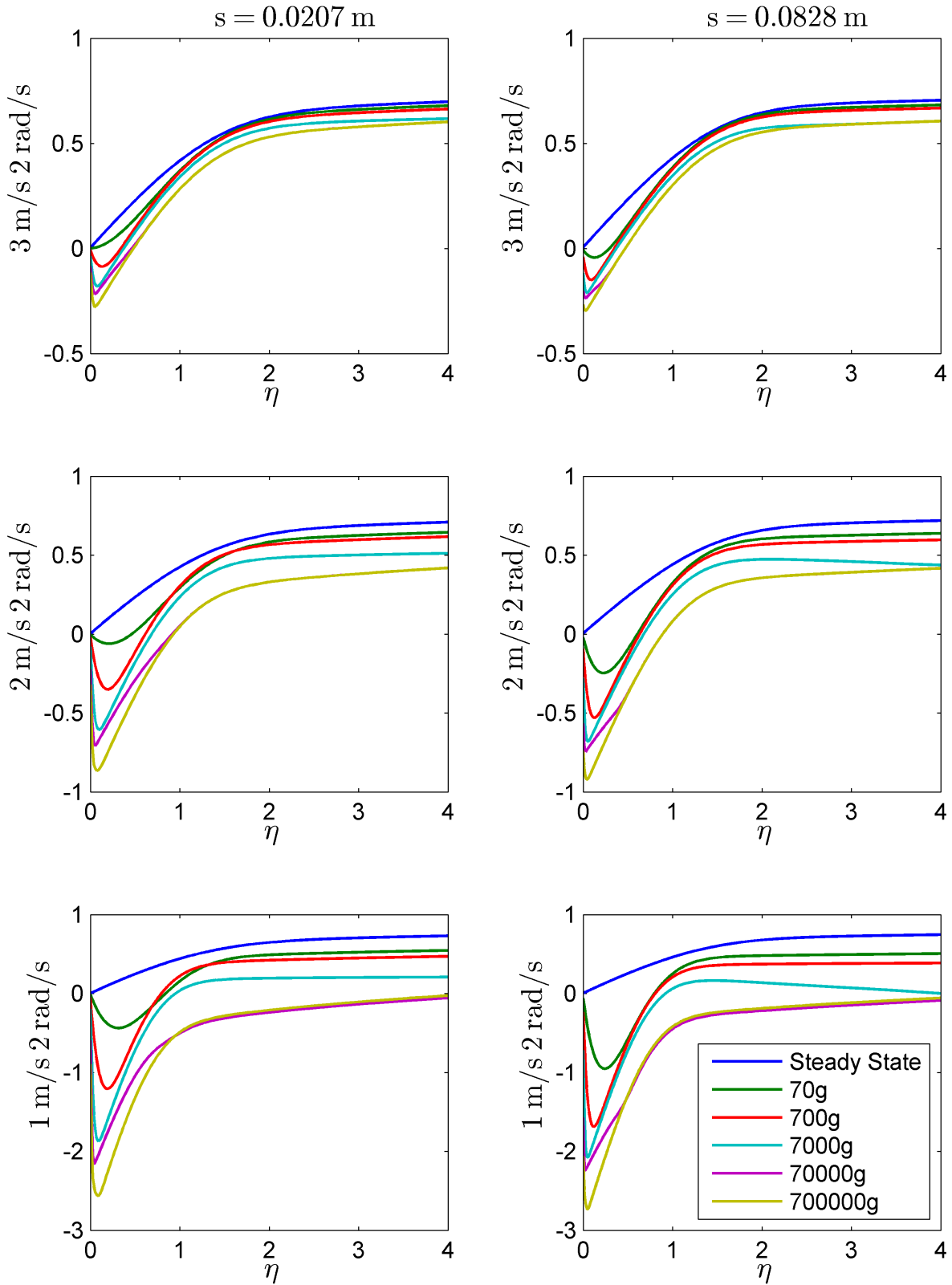


Figure 9.31: Non-Dimensional  $s$ -Direction Velocity Profiles: Group 3 Decelerating Cone



CHAPTER 9. BOUNDARY LAYER RESPONSE IN COMBINED TRANSLATION AND ROTATION - ARBITRARY CONE FLOW

In *Figures 9.32 and 9.33* the tangential velocities for the Group 2 and Group 3 results are shown.

Figure 9.32: Non-Dimensional  $z$ -Direction Velocity Profiles: Group 2 Decelerating Cone

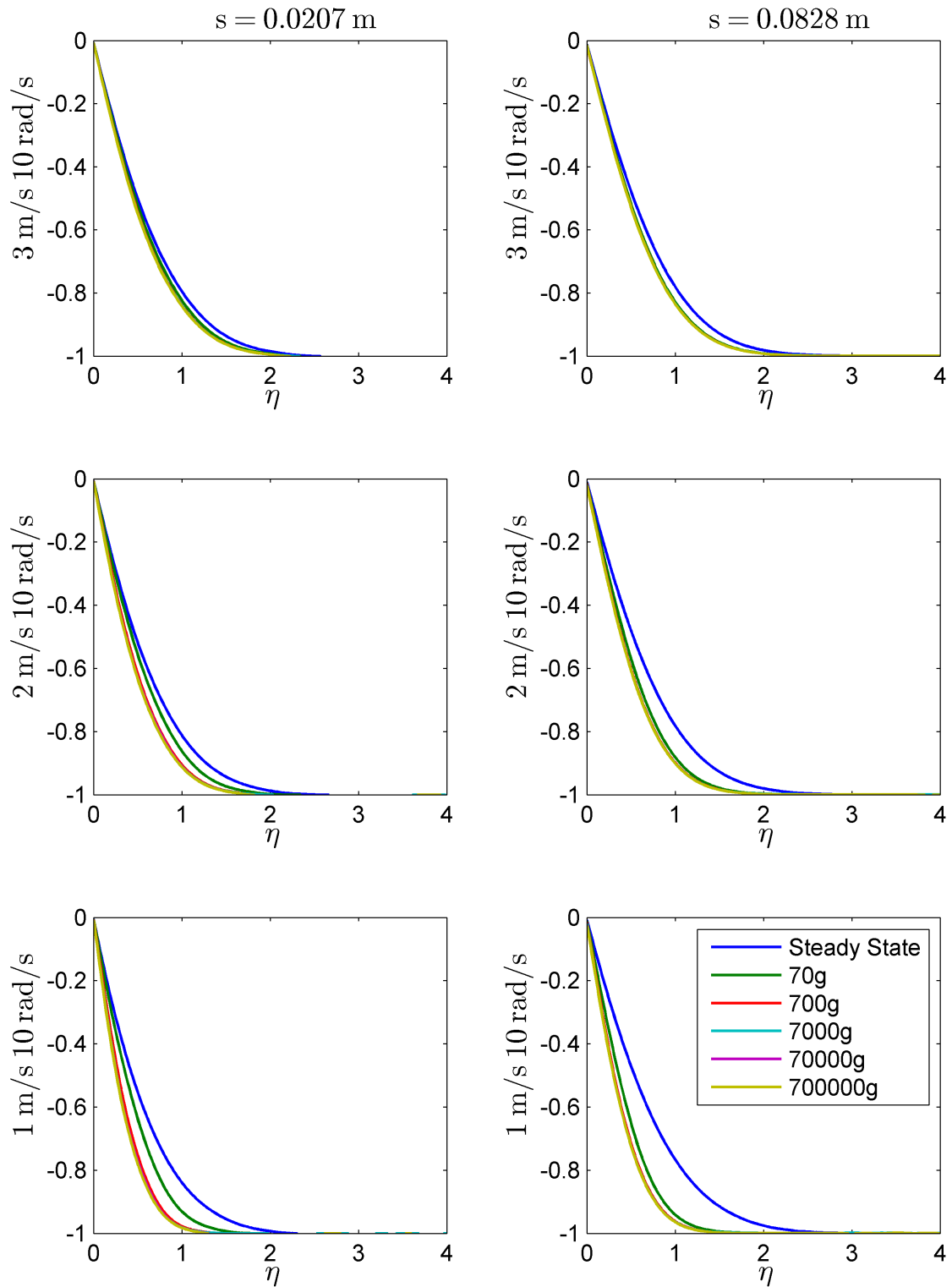
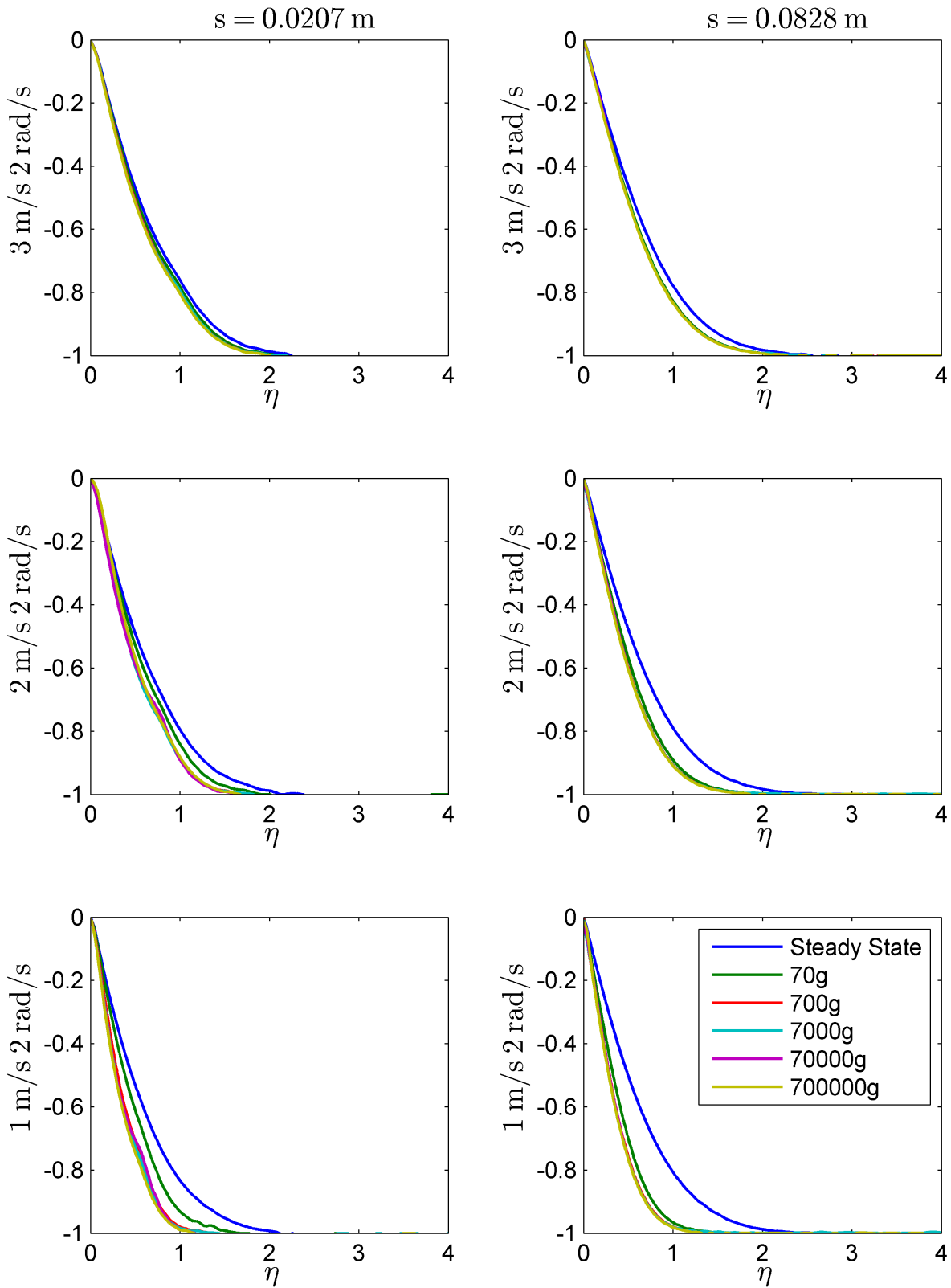


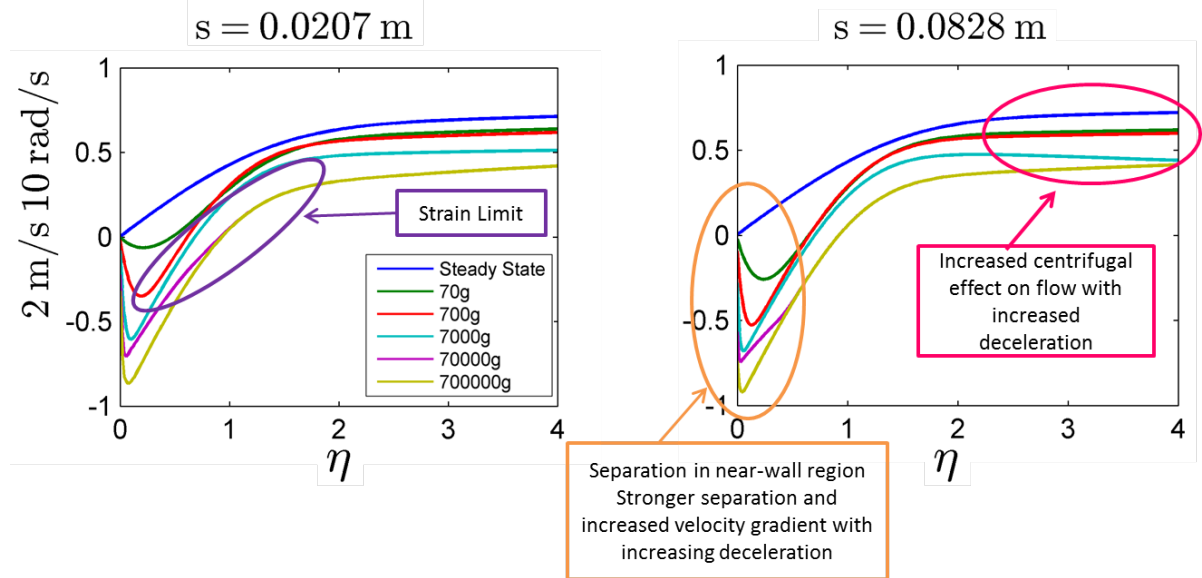
Figure 9.33: Non-Dimensional  $z$ -Direction Velocity Profiles: Group 3 Decelerating Cone



CHAPTER 9. BOUNDARY LAYER RESPONSE IN COMBINED TRANSLATION AND ROTATION - ARBITRARY CONE FLOW

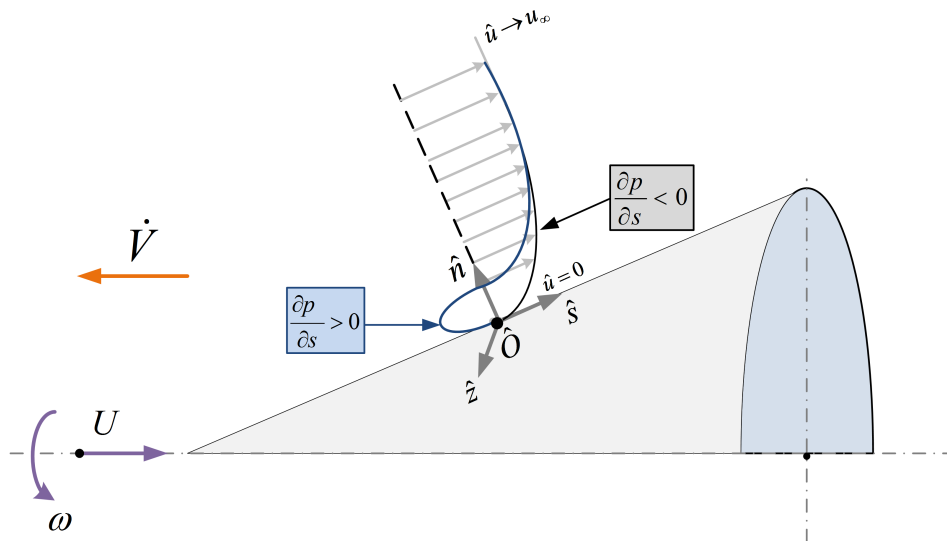
The flow reacts immediately to the decelerating conditions. The deceleration response is classified as **Type III** since no part of the profile remains close to the steady state result. Three profile responses have been observed similar to the responses in acceleration; separation in the near-wall region, influence of the centrifugal effect in the boundary far-field and the presence of a strain limit (*Figure 9.34*).

Figure 9.34: Responses of the Boundary Layer on the Cone to Deceleration in Translation



The mechanism responsible for the flow reversal is similar to those for the flat plate and rotating disk where an adverse pressure gradient is the underlying cause (*Figure 9.35*).

Figure 9.35: Decelerating Velocity Profile in the  $s$ -Direction on the Cone



The governing equation for the boundary layer flow in the  $s$ -direction was determined in 5.162. This equation is can be reduced to show only the terms that are relevant in this case:





9.3. RESULTS AND DISCUSSION - DECELERATION

$$\begin{aligned}
& \hat{\rho} \left[ \frac{\partial \hat{V}_1}{\partial t} + \frac{\hat{V}_1}{h_1} \frac{\partial \hat{V}_1}{\partial \hat{u}_1} + \frac{\hat{V}_2}{h_2} \frac{\partial \hat{V}_1}{\partial \hat{u}_2} + \frac{\hat{V}_3}{h_3} \frac{\partial \hat{V}_1}{\partial \hat{u}_3} - \hat{V}_2 \left( \frac{\hat{V}_2}{h_1 h_2} \frac{\partial h_2}{\partial \hat{u}_1} - \frac{\hat{V}_1}{h_1 h_2} \frac{\partial h_1}{\partial \hat{u}_2} \right) + \hat{V}_3 \left( \frac{\hat{V}_1}{h_1 h_3} \frac{\partial h_1}{\partial \hat{u}_3} - \frac{\hat{V}_3}{h_1 h_3} \frac{\partial h_3}{\partial \hat{u}_1} \right) \right] \\
& = -\frac{1}{h_1} \frac{\partial \hat{p}}{\partial \hat{u}_1} + \frac{1}{h_2} \frac{\partial}{\partial \hat{u}_2} \hat{\mu} \frac{h_1}{h_2} \frac{\partial \hat{u}_2}{\partial \hat{u}_2} \frac{\hat{V}_1}{h_1} \\
& + \hat{\rho} \left[ \underbrace{\hat{u}_1 \omega_2^2 - \hat{u}_2 \omega_1 \omega_2}_{\text{Centrifugal}} - \underbrace{\frac{\partial V_{e1}}{\partial t}}_{\text{Translation}} \right]
\end{aligned} \tag{9.12}$$

In deceleration conditions the non-inertial terms on the right hand side of the equation becomes a momentum sink. The reduction on the right hand side of the equation leads to a decrease on the left hand side momentum terms. As a result, the velocity  $\hat{V}_1$  decreases. In turn this leads to a decrease in the velocity gradient in the stress tensor. The flow compensates for the reduced velocity gradient by increasing the pressure gradient. This results in an adverse pressure gradient. In these conditions the flow separates from the wall and flow in the opposite direction.

$$\begin{aligned}
& \hat{\rho} \left[ \frac{\partial \hat{V}_1}{\partial t} + \frac{\hat{V}_1}{h_1} \frac{\partial \hat{V}_1}{\partial \hat{u}_1} + \frac{\hat{V}_2}{h_2} \frac{\partial \hat{V}_1}{\partial \hat{u}_2} + \frac{\hat{V}_3}{h_3} \frac{\partial \hat{V}_1}{\partial \hat{u}_3} - \hat{V}_2 \left( \frac{\hat{V}_2}{h_1 h_2} \frac{\partial h_2}{\partial \hat{u}_1} - \frac{\hat{V}_1}{h_1 h_2} \frac{\partial h_1}{\partial \hat{u}_2} \right) + \hat{V}_3 \left( \frac{\hat{V}_1}{h_1 h_3} \frac{\partial h_1}{\partial \hat{u}_3} - \frac{\hat{V}_3}{h_1 h_3} \frac{\partial h_3}{\partial \hat{u}_1} \right) \right] \\
& = -\frac{1}{h_1} \frac{\partial \hat{p}}{\partial \hat{u}_1} + \frac{1}{h_2} \frac{\partial}{\partial \hat{u}_2} \hat{\mu} \frac{h_1}{h_2} \frac{\partial \hat{u}_2}{\partial \hat{u}_2} \frac{\hat{V}_1}{h_1} \\
& + \hat{\rho} \left[ \underbrace{\hat{u}_1 \omega_2^2 - \hat{u}_2 \omega_1 \omega_2}_{\text{Centrifugal}} - \underbrace{\hat{u}_3 \omega_2}_{\text{Euler}} - \underbrace{\frac{\partial V_{e1}}{\partial t}}_{\text{Translation}} \right]
\end{aligned} \tag{9.13}$$

In the tangential direction a delay in the reaction of the tangential velocities can be seen (*Figures 9.32 and 9.33*). However the 70g profile reacts to the changing conditions. This is a similar effect as was seen in the radial direction of the rotating disk. Since there are no direct changes in this direction, the flow changes due to secondary effects. The lower deceleration cases react first, while in the higher decelerations the profile in this direction remains in it's initial state.

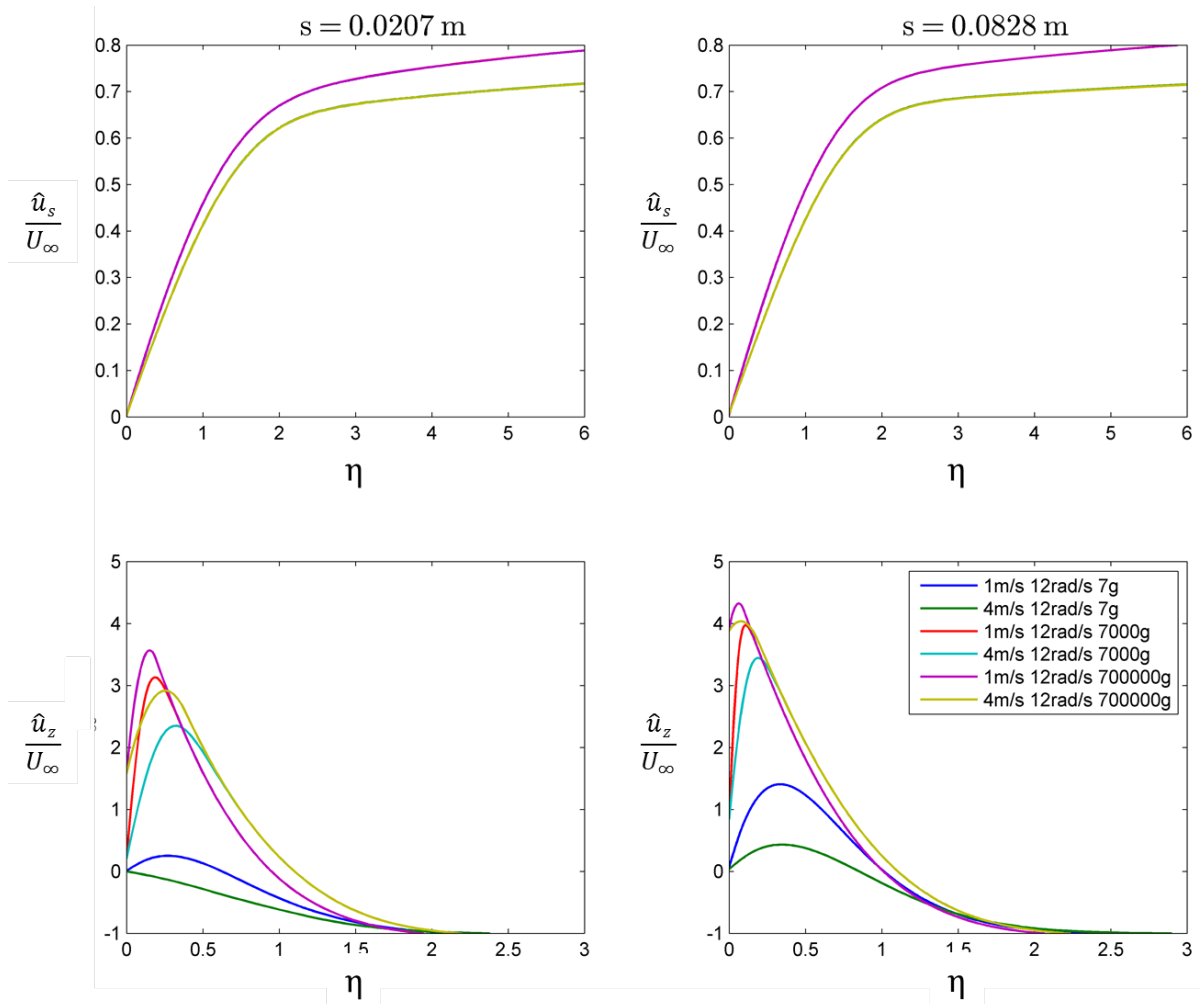
$$\begin{aligned}
& \hat{\rho} \left[ \frac{\partial \hat{V}_3}{\partial t} + \frac{\hat{V}_1}{h_1} \frac{\partial \hat{V}_3}{\partial \hat{u}_1} + \frac{\hat{V}_2}{h_2} \frac{\partial \hat{V}_3}{\partial \hat{u}_2} + \frac{\hat{V}_3}{h_3} \frac{\partial \hat{V}_3}{\partial \hat{u}_3} - \hat{V}_1 \left( \frac{\hat{V}_1}{h_1 h_3} \frac{\partial h_1}{\partial \hat{u}_3} - \frac{\hat{V}_3}{h_1 h_3} \frac{\partial h_3}{\partial \hat{u}_1} \right) + \hat{V}_2 \left( \frac{\hat{V}_3}{h_2 h_3} \frac{\partial h_2}{\partial \hat{u}_1} - \frac{\hat{V}_2}{h_2 h_3} \frac{\partial h_2}{\partial \hat{u}_3} \right) \right] \\
& = -\frac{1}{h_1} \frac{\partial \hat{p}}{\partial \hat{u}_3} + \frac{1}{h_2} \frac{\partial}{\partial \hat{u}_2} \hat{\mu} \frac{h_3}{h_2} \frac{\partial \hat{u}_2}{\partial \hat{u}_2} \frac{\hat{V}_3}{h_3} \\
& + \hat{\rho} \left[ \underbrace{2\hat{V}_1 \omega_2 - 2\hat{V}_2 \omega_1}_{\text{Coriolis}} + \underbrace{\hat{u}_3 (\omega_2^2 + \omega_1^2)}_{\text{Centrifugal}} + \underbrace{2V_{e1} \omega_2 - 2V_{e2} \omega_1}_{\text{Magnus}} \right]
\end{aligned} \tag{9.14}$$

CHAPTER 9. BOUNDARY LAYER RESPONSE IN COMBINED TRANSLATION AND ROTATION - ARBITRARY CONE FLOW

9.3.1.2 Steady Translation with Decelerating Rotation

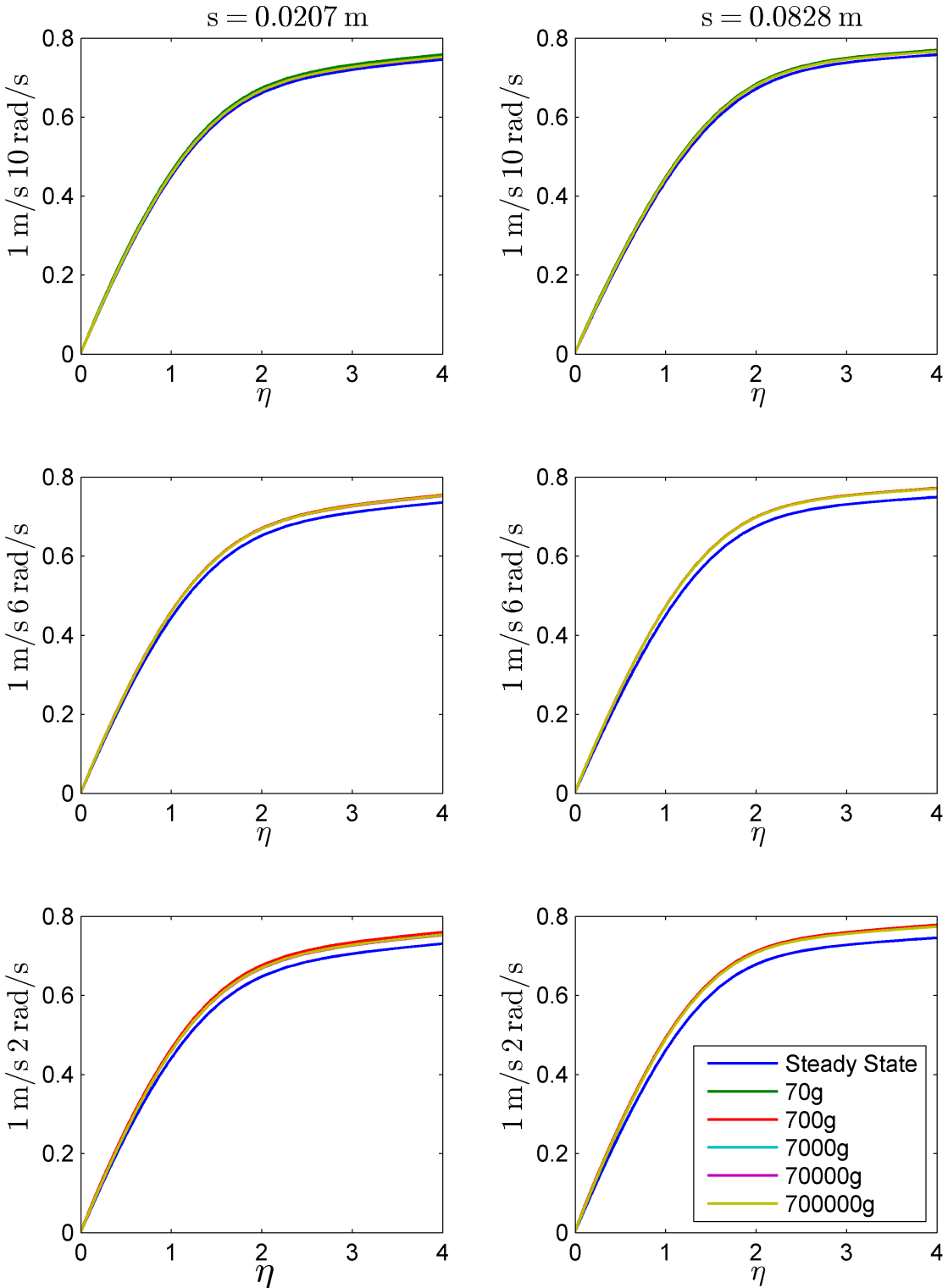
The deceleration of the rotational velocities was done in accordance with *Table 9.2*. The Group 4 and Group 5 results are indicated in *Figure 9.36* below. It is shown in these graphs that the  $s$ -direction velocity profiles are independent on rotational velocity and deceleration strength. Furthermore, the rotational velocity profiles, in the  $z$ -direction, are affected by the axial velocity. At a lower axial velocity (1 m/s), the peak values of the separation is higher than for a compatible case (same rotational velocity and deceleration). Furthermore, at lower axial velocities the near-wall velocity gradient is steeper than in the case of higher axial velocities. Translation velocity dominates the flow, since it is higher than the rotational velocity, and has a stabilizing effect on the rotational flow in deceleration.

Figure 9.36: Comparison between Group 4 and Group 5 Simulation Results for Deceleration



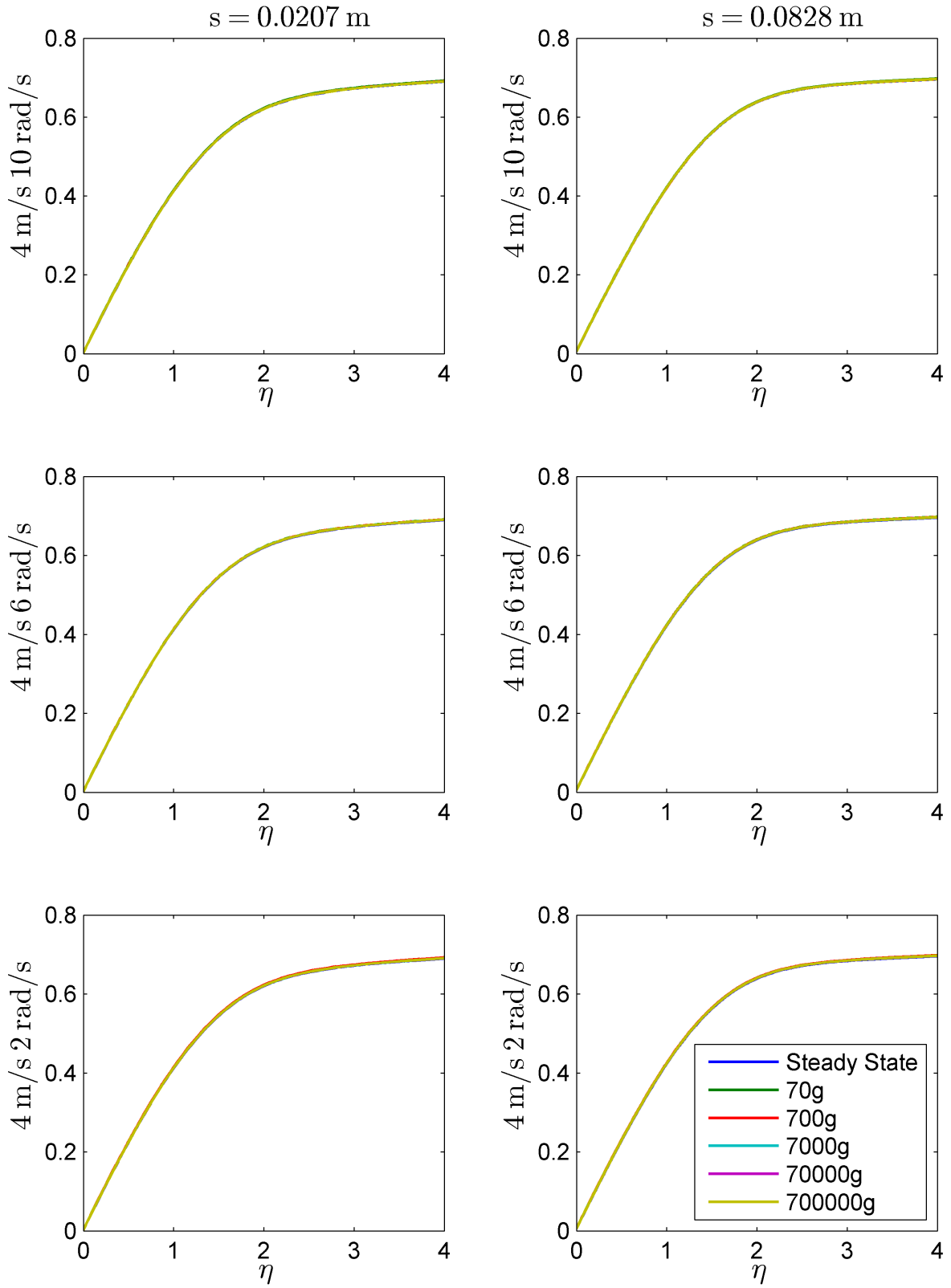
In Figures 9.37 and 9.38 the  $s$ -direction velocities for the Group 4 and Group 5 results are shown.

Figure 9.37: Non-Dimensional  $s$ -Direction Velocity Profiles: Group 4 Decelerating Cone



CHAPTER 9. BOUNDARY LAYER RESPONSE IN COMBINED TRANSLATION AND ROTATION - ARBITRARY CONE FLOW

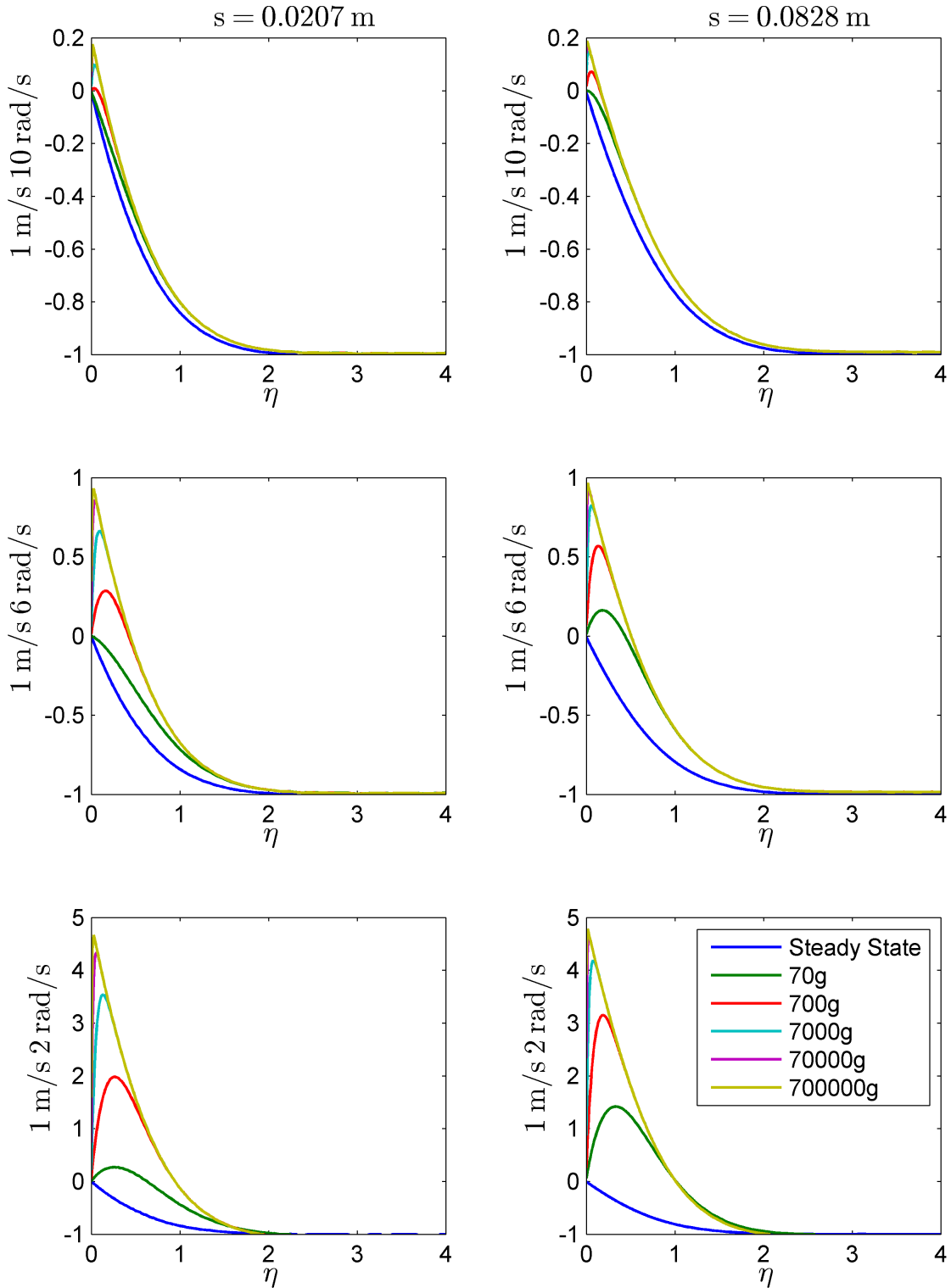
Figure 9.38: Non-Dimensional  $s$ -Direction Velocity Profiles: Group 5 Decelerating Cone



9.3. RESULTS AND DISCUSSION - DECELERATION

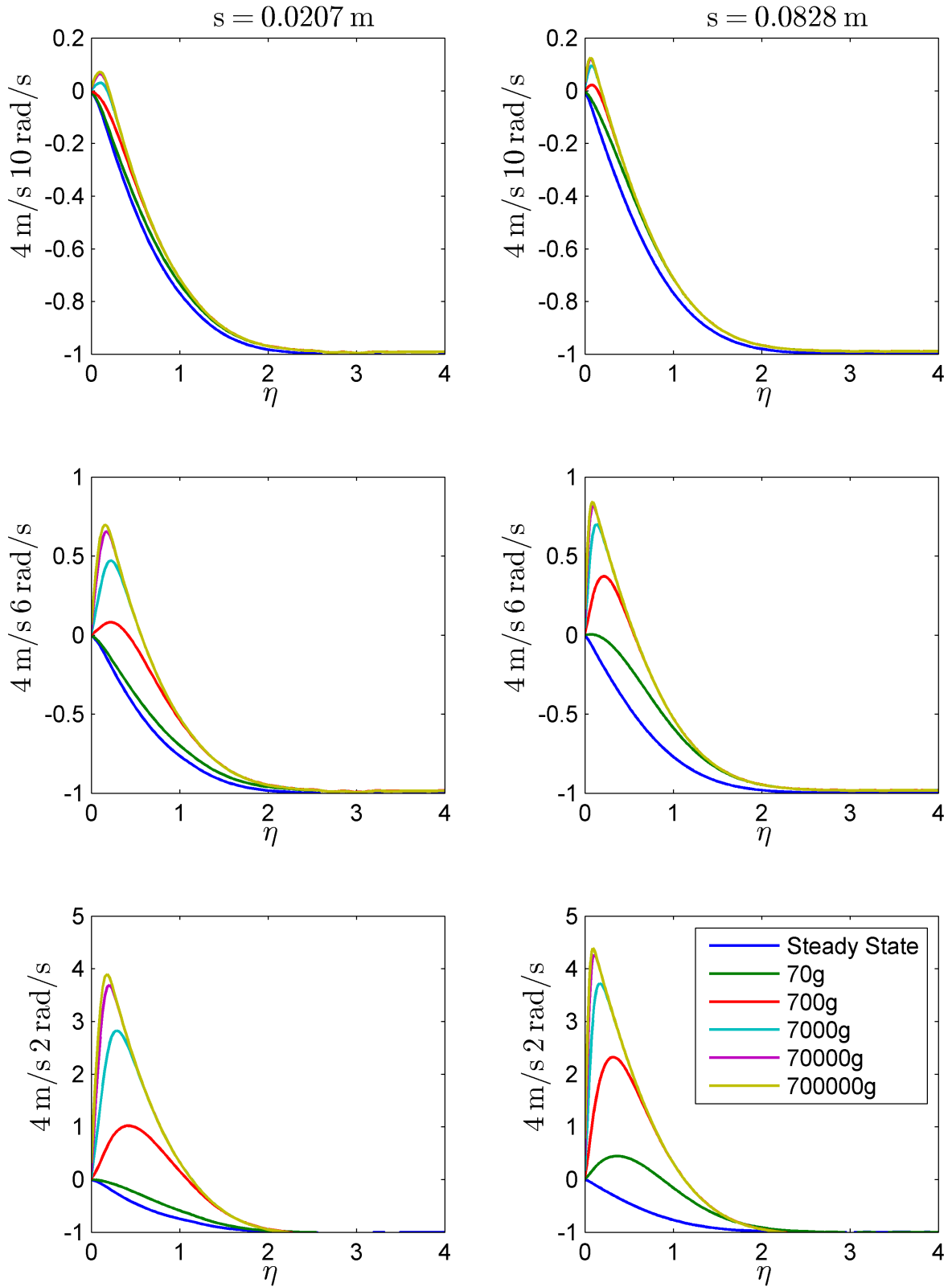
In Figures 9.39 and 9.40 the tangential velocities (itz-direction) for the Group 4 and Group 5 results are shown.

Figure 9.39: Non-Dimensional  $z$ -Direction Velocity Profiles: Group 4 Decelerating Cone



CHAPTER 9. BOUNDARY LAYER RESPONSE IN COMBINED TRANSLATION AND ROTATION - ARBITRARY CONE FLOW

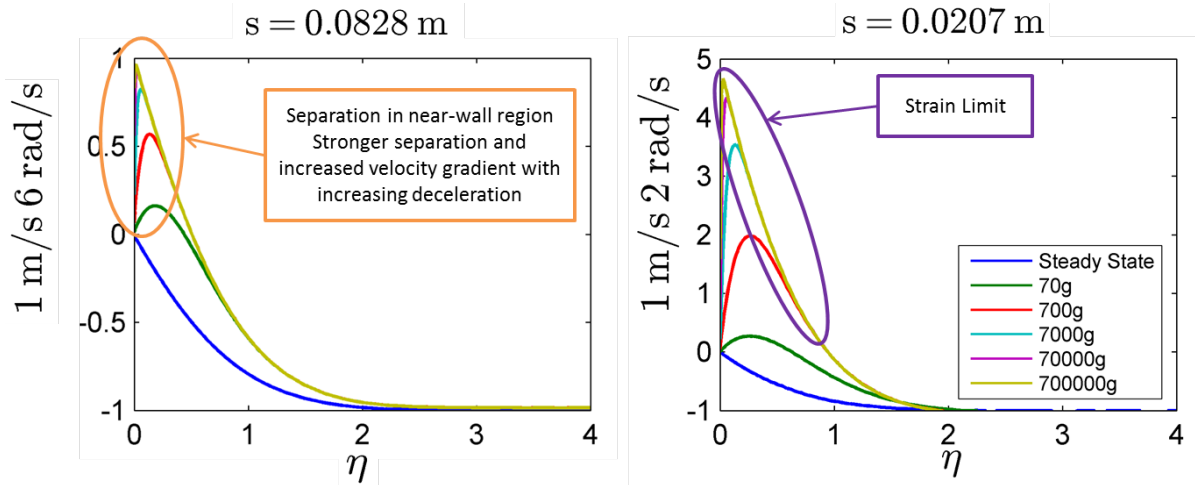
Figure 9.40: Non-Dimensional z-Direction Velocity Profiles: Group 5 Decelerating Cone



9.3. RESULTS AND DISCUSSION - DECELERATION

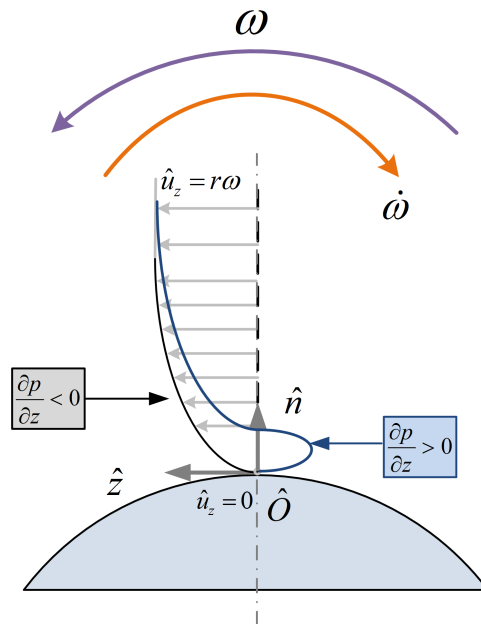
The decelerating rotational flow on the cone, in the tangential direction, has similarities with the flat plate and rotating disk in deceleration (*Figure 9.41*). In the near-wall region the flow separates. This separation is directly proportional to the deceleration strength. Stronger separation is associated with an increased velocity gradient at the wall. The strain limit, as explained in *Section 9.2.1* as also seen here. The flow responses are of **Type III** and is momentum dominant.

Figure 9.41: Responses of the Boundary Layer on the Cone to Deceleration in Rotation



The mechanism that leads to the responses as shown above is similar to the flat plate and rotating disk in deceleration (*Figure 9.42*).

Figure 9.42: Decelerating Velocity Profile in the z-Direction on the Cone



In *Equation 5.164* the general equation for an object in general arbitrary acceleration was deter-

CHAPTER 9. BOUNDARY LAYER RESPONSE IN COMBINED TRANSLATION AND ROTATION - ARBITRARY CONE FLOW

mined. This equation can be reduced, by exclusion on the terms that are not relevant, to obtain an expression for the boundary layer in this case.

$$\begin{aligned}
& \hat{\rho} \left[ \frac{\partial \hat{V}_3}{\partial t} + \frac{\hat{V}_1}{h_1} \frac{\partial \hat{V}_3}{\partial \hat{u}_1} + \frac{\hat{V}_2}{h_2} \frac{\partial \hat{V}_3}{\partial \hat{u}_2} + \frac{\hat{V}_3}{h_3} \frac{\partial \hat{V}_3}{\partial \hat{u}_3} - \hat{V}_1 \left( \frac{\hat{V}_1}{h_1 h_3} \frac{\partial h_1}{\partial \hat{u}_3} - \frac{\hat{V}_3}{h_1 h_3} \frac{\partial h_3}{\partial \hat{u}_1} \right) + \hat{V}_2 \left( \frac{\hat{V}_3}{h_2 h_3} \frac{\partial h_2}{\partial \hat{u}_1} - \frac{\hat{V}_2}{h_2 h_3} \frac{\partial h_2}{\partial \hat{u}_3} \right) \right] \\
& = -\frac{1}{h_1} \frac{\partial \hat{p}}{\partial \hat{u}_3} + \frac{1}{h_2} \frac{\partial}{\partial \hat{u}_2} \hat{\mu} \frac{h_3}{h_2} \frac{\partial \hat{u}_2}{h_2} \frac{\hat{V}_3}{h_3} \\
& + \hat{\rho} \left[ \underbrace{2\hat{V}_1 \omega_2 - 2\hat{V}_2 \omega_1}_{\text{Coriolis}} + \underbrace{\hat{u}_3 (\omega_2^2 + \omega_1^2)}_{\text{Centrifugal}} + \underbrace{\hat{u}_1 \omega_2 - \hat{u}_2 \omega_1}_{\text{Euler}} + \underbrace{2V_{e_1} \omega_2 - 2V_{e_2} \omega_1}_{\text{Magnus}} \right]
\end{aligned} \tag{9.15}$$

During deceleration, the non-inertial terms on the right hand side of the equation become a momentum sink. These reduce the terms on the right hand side. In response, to keep the equation balance, the momentum terms on the left hand side decrease. This results in a decrease of the velocity component  $\hat{V}_3$ . Subsequently the velocity gradient in the near-wall region decreases. If the gradient is low enough, it results in a positive pressure gradient which induces an adverse pressure gradient and flow reversal.

$$\begin{aligned}
& \hat{\rho} \left[ \frac{\partial \hat{V}_3}{\partial t} + \frac{\hat{V}_1}{h_1} \frac{\partial \hat{V}_3}{\partial \hat{u}_1} + \frac{\hat{V}_2}{h_2} \frac{\partial \hat{V}_3}{\partial \hat{u}_2} + \frac{\hat{V}_3}{h_3} \frac{\partial \hat{V}_3}{\partial \hat{u}_3} - \hat{V}_1 \left( \frac{\hat{V}_1}{h_1 h_3} \frac{\partial h_1}{\partial \hat{u}_3} - \frac{\hat{V}_3}{h_1 h_3} \frac{\partial h_3}{\partial \hat{u}_1} \right) + \hat{V}_2 \left( \frac{\hat{V}_3}{h_2 h_3} \frac{\partial h_2}{\partial \hat{u}_1} - \frac{\hat{V}_2}{h_2 h_3} \frac{\partial h_2}{\partial \hat{u}_3} \right) \right] \\
& = -\frac{1}{h_1} \frac{\partial \hat{p}}{\partial \hat{u}_3} + \frac{1}{h_2} \frac{\partial}{\partial \hat{u}_2} \hat{\mu} \frac{h_3}{h_2} \frac{\partial \hat{u}_2}{h_2} \frac{\hat{V}_3}{h_3} \\
& + \hat{\rho} \left[ \underbrace{2\hat{V}_1 \omega_2 - 2\hat{V}_2 \omega_1}_{\text{Coriolis}} + \underbrace{\hat{u}_3 (\omega_2^2 + \omega_1^2)}_{\text{Centrifugal}} + \underbrace{\hat{u}_1 \omega_2 - \hat{u}_2 \omega_1}_{\text{Euler}} + \underbrace{2V_{e_1} \omega_2 - 2V_{e_2} \omega_1}_{\text{Magnus}} \right]
\end{aligned} \tag{9.16}$$

The flow in the axial direction,  $s$ -direction is governed by the reduced form of *Equation 5.162*. At lower axial velocities, i.e. Group 4, the axial velocity profiles are only slightly affected by the deceleration in the tangential direction. The Group 5 results, at a higher axial velocity of 4 m/s, are unaffected by the changes in rotational velocity - the higher axial flow dominates the effects of rotational deceleration.

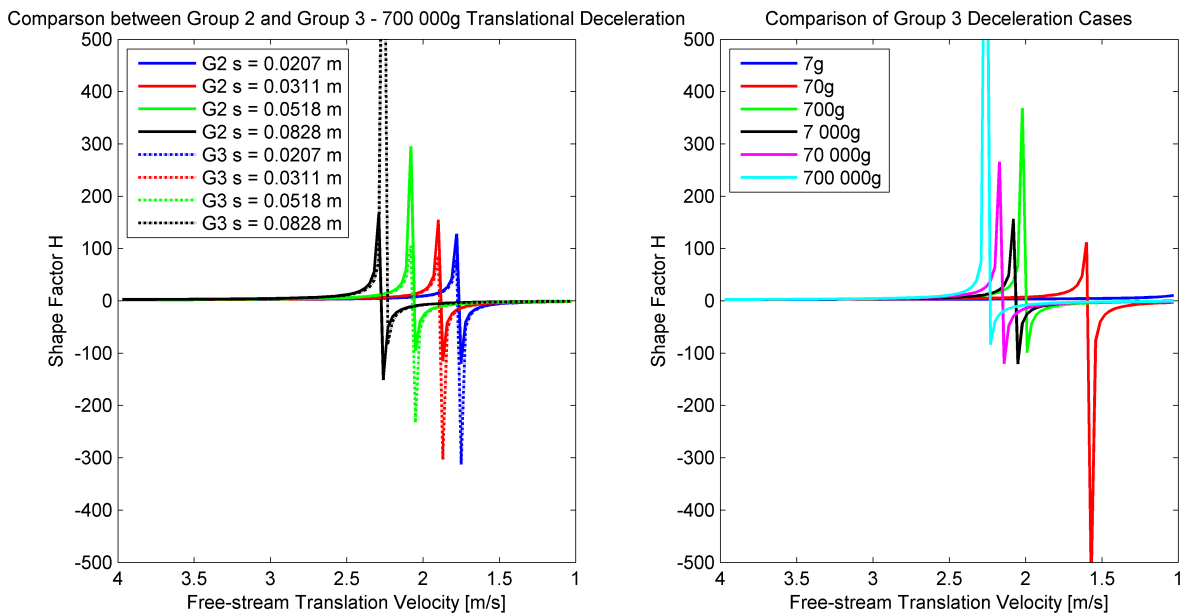
$$\begin{aligned}
& \hat{\rho} \left[ \frac{\partial \hat{V}_1}{\partial t} + \frac{\hat{V}_1}{h_1} \frac{\partial \hat{V}_1}{\partial \hat{u}_1} + \frac{\hat{V}_2}{h_2} \frac{\partial \hat{V}_1}{\partial \hat{u}_2} + \frac{\hat{V}_3}{h_3} \frac{\partial \hat{V}_1}{\partial \hat{u}_3} - \hat{V}_2 \left( \frac{\hat{V}_2}{h_1 h_2} \frac{\partial h_2}{\partial \hat{u}_1} - \frac{\hat{V}_1}{h_1 h_2} \frac{\partial h_1}{\partial \hat{u}_2} \right) + \hat{V}_3 \left( \frac{\hat{V}_1}{h_1 h_3} \frac{\partial h_1}{\partial \hat{u}_3} - \frac{\hat{V}_3}{h_1 h_3} \frac{\partial h_3}{\partial \hat{u}_1} \right) \right] \\
& = -\frac{1}{h_1} \frac{\partial \hat{p}}{\partial \hat{u}_1} + \frac{1}{h_2} \frac{\partial}{\partial \hat{u}_2} \hat{\mu} \frac{h_1}{h_2} \frac{\partial \hat{u}_2}{h_2} \frac{\hat{V}_1}{h_1} \\
& + \hat{\rho} \left[ \underbrace{\hat{u}_1 \omega_2^2 - \hat{u}_2 \omega_1 \omega_2}_{\text{Centrifugal}} \right] - \hat{u}_3 \omega_2
\end{aligned} \tag{9.17}$$



### 9.3.2 Boundary Layer Parameters

The shape factor related to the cone in decelerating translation displays the same tendencies as for the flat plate in deceleration. A discontinuity is approached in the shape factor that is dependant both on position on the plate and deceleration strength (*Figure 9.43*). Positions further away from the cone front end reach the discontinuity first. It is further seen that higher decelerations also reach the discontinuity before lower decelerations.

Figure 9.43: Shape Factor in  $s$ -Direction for Translational Deceleration

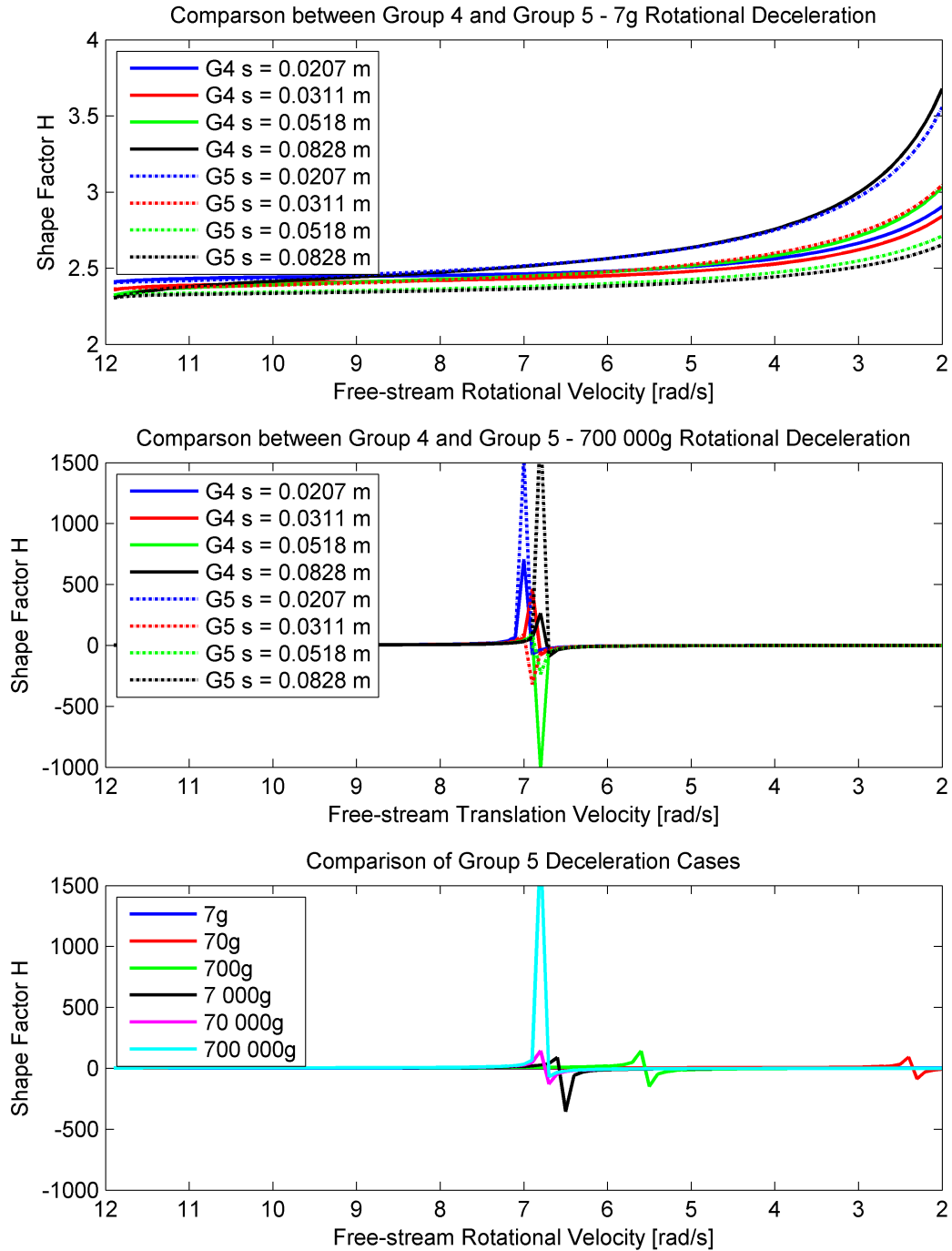


Similar effects is seen for the cone in decelerating rotation (*Figure 9.44*) with the exception of dependence on position. All points on the cone surface reach the discontinuity at approximately the same time. The discontinuity position is however also dependant on deceleration strength here - higher decelerations reach the discontinuity first.

As discussed in *Chapters 7* and *8* the presence of the discontinuity is a sign of regime change. Before the discontinuity the flow can be assumed to be fully laminar. After the discontinuity the flow no longer falls within the laminar regime. A negative shape factor is not physically possible since it means that the momentum thickness assumes a negative value. This is not just an indication that the flow has separated from the wall, but also indicates a change in the flow regime. The flow is most likely in transition or turbulent after this point.

CHAPTER 9. BOUNDARY LAYER RESPONSE IN COMBINED TRANSLATION AND ROTATION - ARBITRARY CONE FLOW

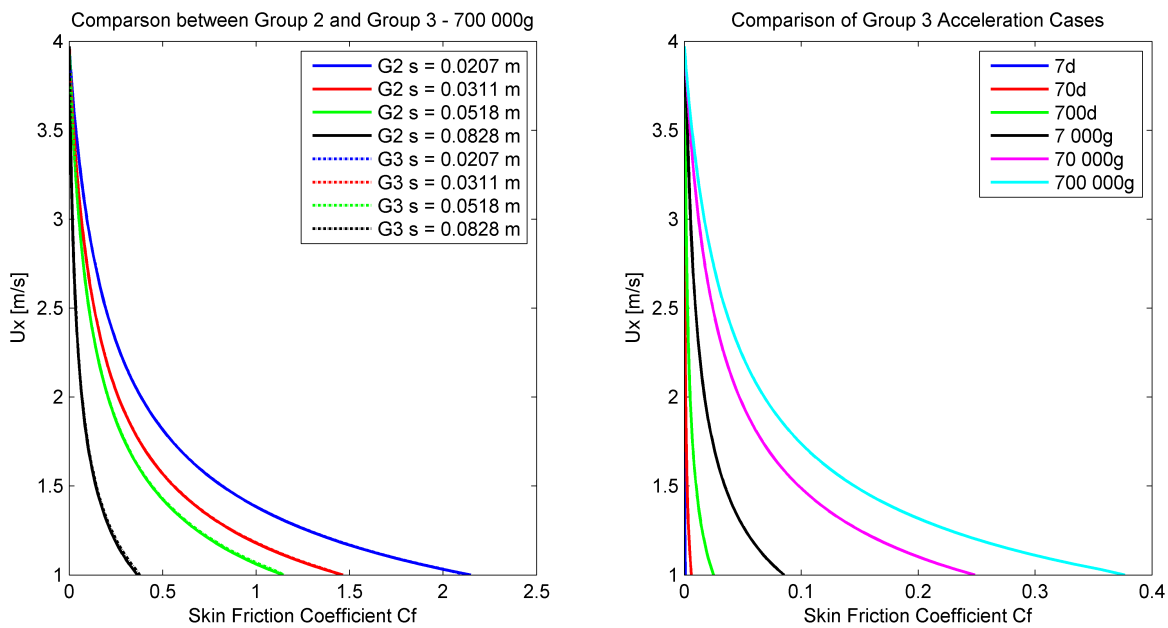
Figure 9.44: Shape Factor in z-Direction for Rotational Deceleration



### 9.3.3 Skin Friction Coefficients

The skin friction values for the rotating cone in translational deceleration, as shown in *Figure 9.45*, behaves in a similar manner as the flat plate in deceleration. Deceleration takes place from 4 m/s to 1 m/s. The skin friction coefficient is dependant on position and deceleration strength. The highest values is displayed at positions closest to the tip of the cone for stronger decelerations. The values are divergent, since the first and second derivatives are divergent (*Figure 9.46*). In this case the values are independent on the rotational velocity. The axial velocity dominates and is much larger than the rotational velocity.

Figure 9.45: Skin Friction Coefficient in *s*-Direction for Translational Deceleration



The skin friction coefficients for the cone in axial flow with deceleration in rotation (*Figure 9.47*) has a similar response as the cone in acceleration (*Figure 9.27*). The results are influences by the axial velocity, as can be seen in the differences between the Group 4 and 5 results. Higher axial velocities render lower skin friction coefficients. Results are also dependant on deceleration strength where higher decelerations cause larger skin friction coefficients.

CHAPTER 9. BOUNDARY LAYER RESPONSE IN COMBINED TRANSLATION AND ROTATION - ARBITRARY CONE FLOW

Figure 9.46: Derivatives of Skin Friction Coefficient in  $s$ -Direction for Translational Deceleration

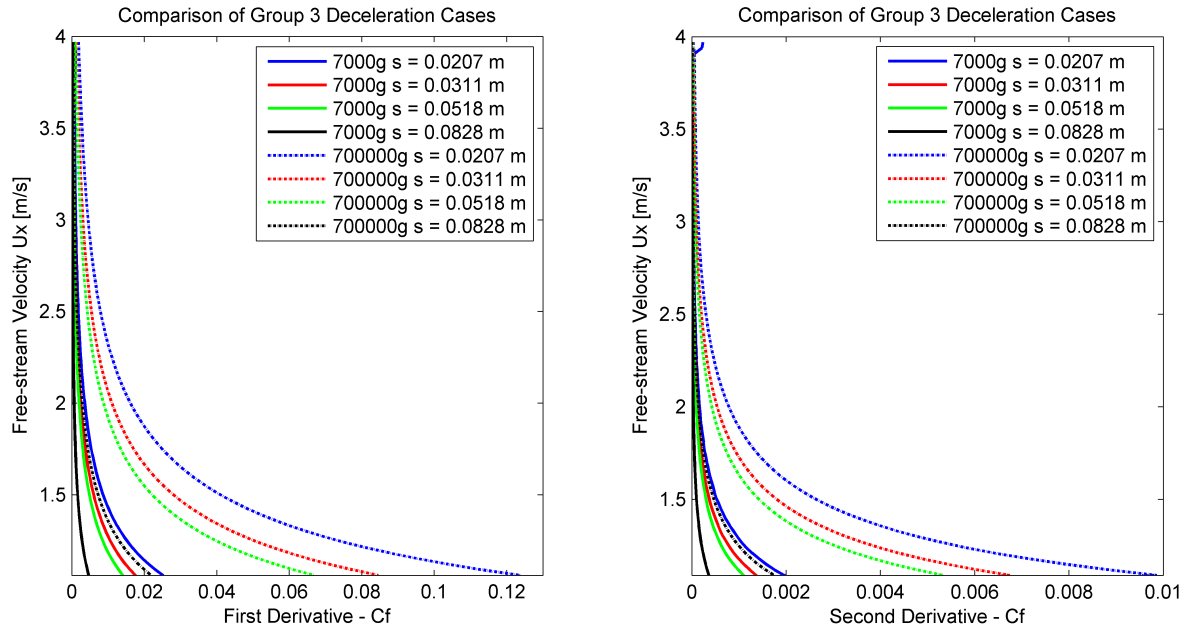
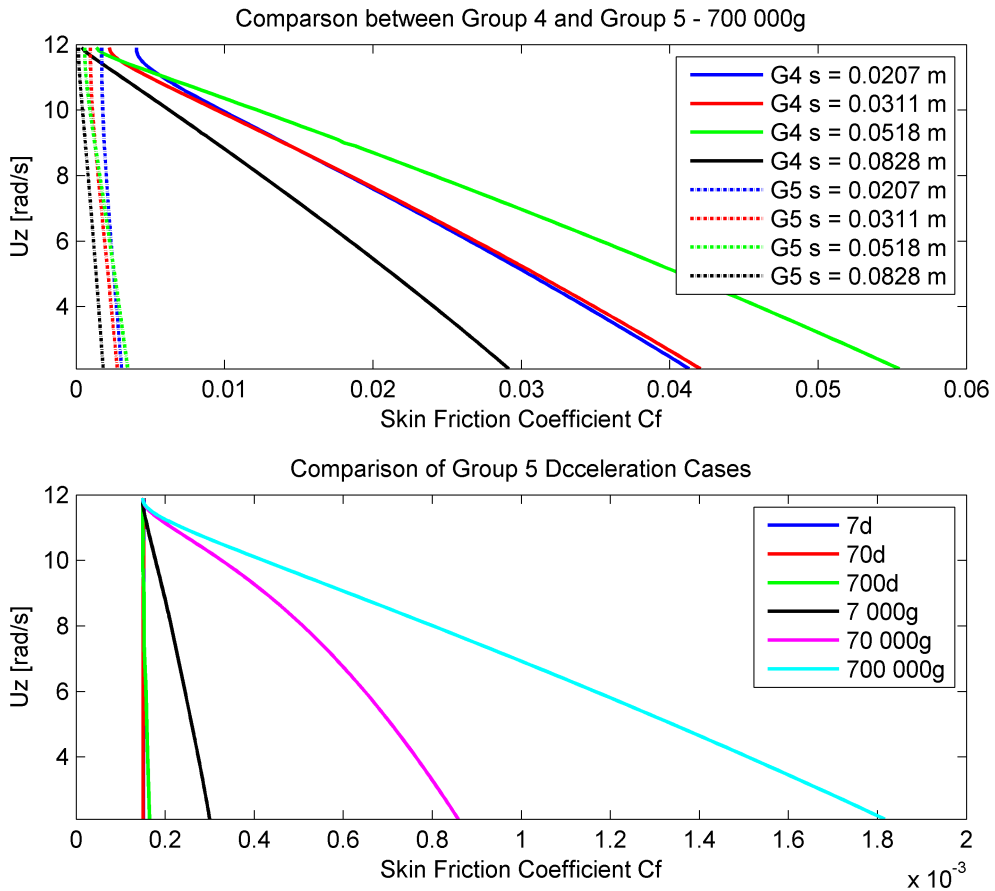


Figure 9.47: Skin Friction Coefficient in  $z$ -Direction for Rotational Deceleration



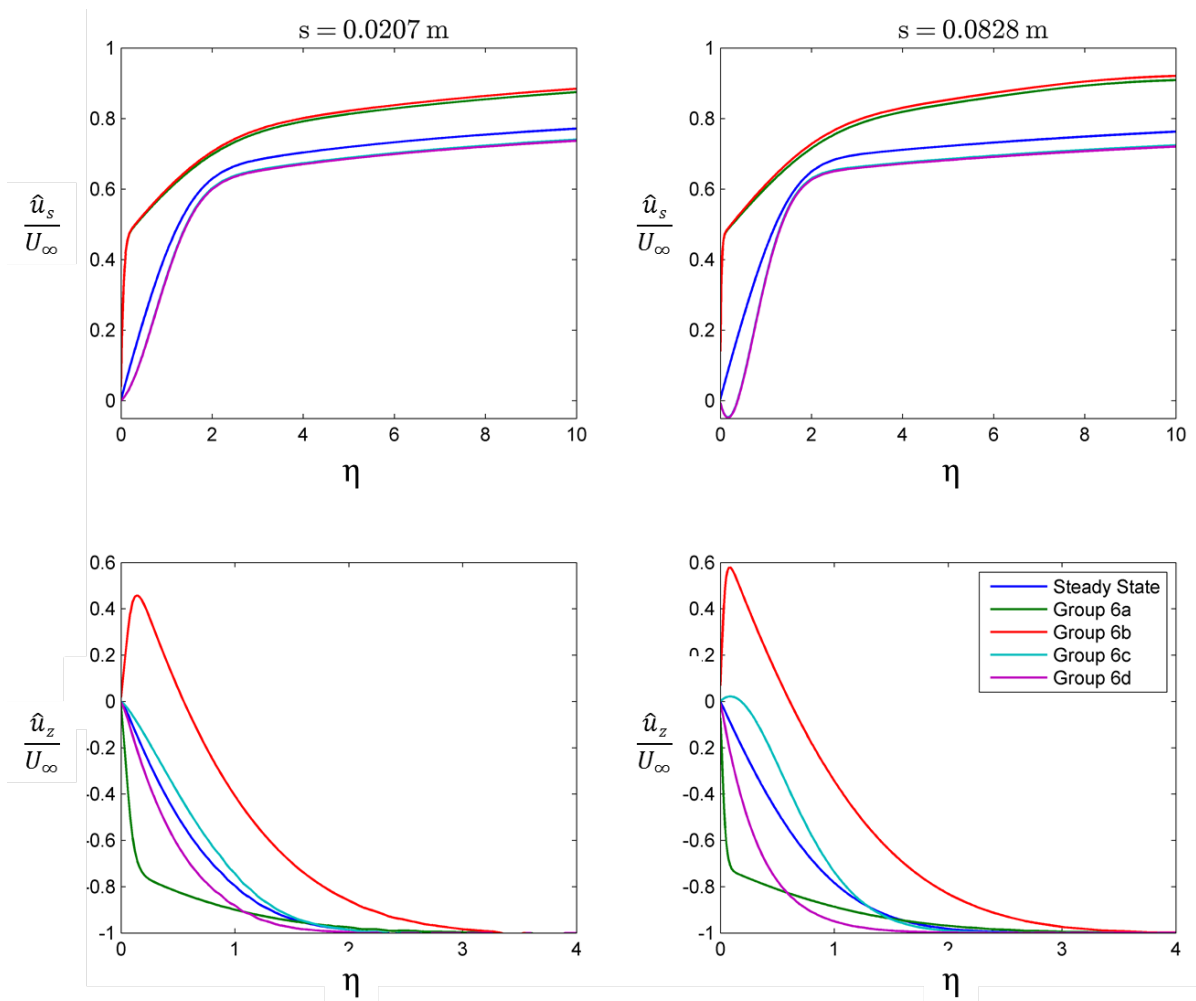
## 9.4 Results and Discussion - Arbitrary Motion

### 9.4.1 Velocity Profiles

The cone in arbitrary motion simulations were conducted in accordance with *Table 9.3*.

In all the cases analysed an immediate response to the changing conditions can be observed. The  $s$ -direction and normal profiles react similar to the flat plate under accelerating conditions, while similarities can be drawn between the tangential direction ( $z$ ) profiles and the rotating disk results (*Figure 9.48*). The boundary layer responses is all classified as **Type III**.

Figure 9.48: Comparison between Group 6a,b,c and d at a Condition 2.5 m/s 7 rad/s

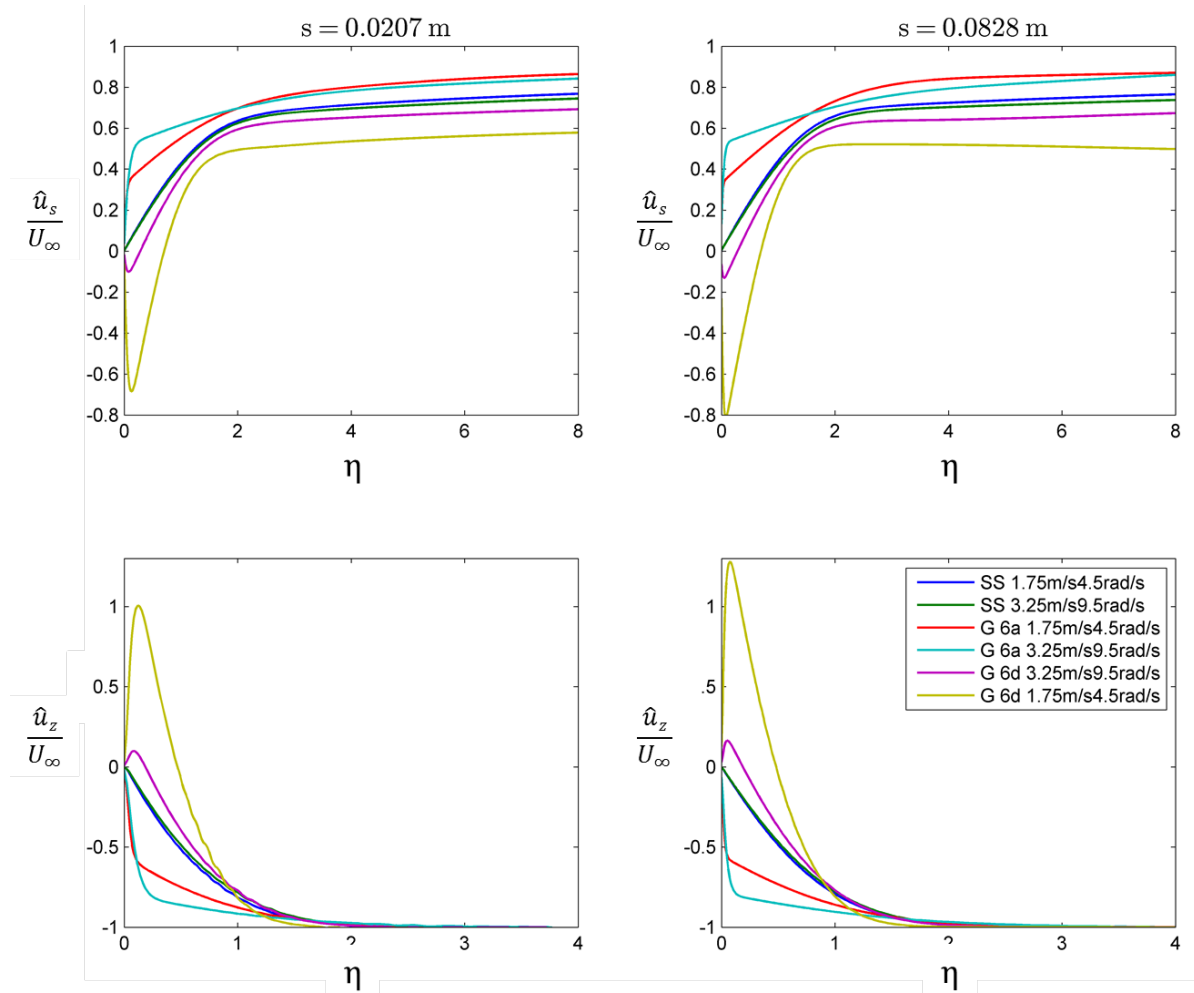


The  $s$ -direction and normal profiles in acceleration shown a thinning of the boundary layer in comparison with the steady state result. In the near-wall region the profile slope responds proportionally to the acceleration parameter. In deceleration low reversal is observed that is also proportional to the deceleration parameter. The flow is slightly influenced by the changes in rotation, but since the axial flow is large that the rotational flow, it dominates the responses of the boundary layer.

CHAPTER 9. BOUNDARY LAYER RESPONSE IN COMBINED TRANSLATION AND ROTATION - ARBITRARY CONE FLOW

The rotational flow profiles are affected significantly by the changes in the axial flow. This is further shown in *Figures 9.49* and *9.50*.

Figure 9.49: Comparison between Group 6a and Group 6c



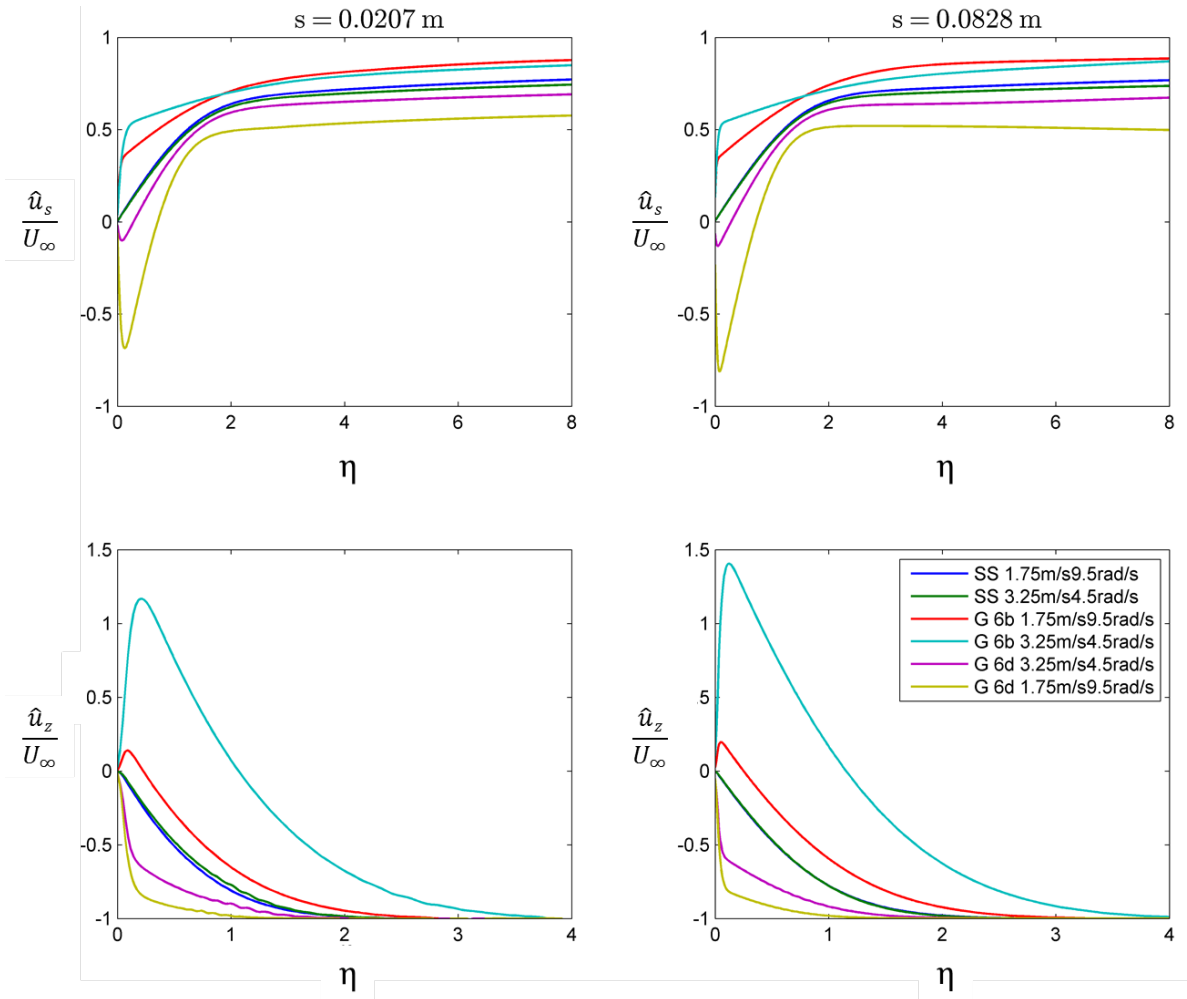
The tangential boundary in accelerating conditions mimics the behaviour of the rotating disk; the profile becomes steeper in the near wall region in a manner directly proportional to the acceleration. However, in accelerating axial flow the near-wall profile is steeper and the boundary layer thicker than in decelerating axial flow. The decelerating axial flow retards the effect of the rotational acceleration while accelerating axial flow enhances the effect.

In rotational deceleration the axial flow has a similar effect on the rotational boundary profile. In axial acceleration the rotational profile displays a greater reversal and a thicker boundary layer than for the same case but with axial deceleration. The flow is dominated by the axial flow in these cases since the axial flow affects the rotational profiles, but the  $s$ -direction and normal profiles are only minimally affected by the changes in rotation. A tabular summation of the general behaviour is shown in *Table 9.4*.

Based on the previous two sections, a summation can be derived for the mechanisms involved in the

9.4. RESULTS AND DISCUSSION - ARBITRARY MOTION

Figure 9.50: Comparison between Group 6b and Group 6d



boundary layer flow (Figures 9.51-9.54). In general the following apply in both the  $s$ - and  $z$ -directions:

- **Acceleration.** The non-inertial terms becomes a momentum source. This leads to an increase in the near-wall velocity gradient which influences the velocity profile,  $\frac{1}{h_2} \frac{\partial}{\partial \hat{u}_2} \hat{\mu} \frac{h_1}{h_2} \partial \hat{u}_2 \frac{\hat{V}_1}{h_1}$ .
- **Deceleration.** The non-inertial terms becomes a momentum sink. This lead to a decrease in the near-wall velocity gradient. In turn the pressure gradient becomes positive and forces an adverse pressure gradient,  $-\frac{1}{h_1} \frac{\partial \hat{p}}{\partial \hat{u}_1}$ . The flow separates.

CHAPTER 9. BOUNDARY LAYER RESPONSE IN COMBINED TRANSLATION AND ROTATION - ARBITRARY CONE FLOW

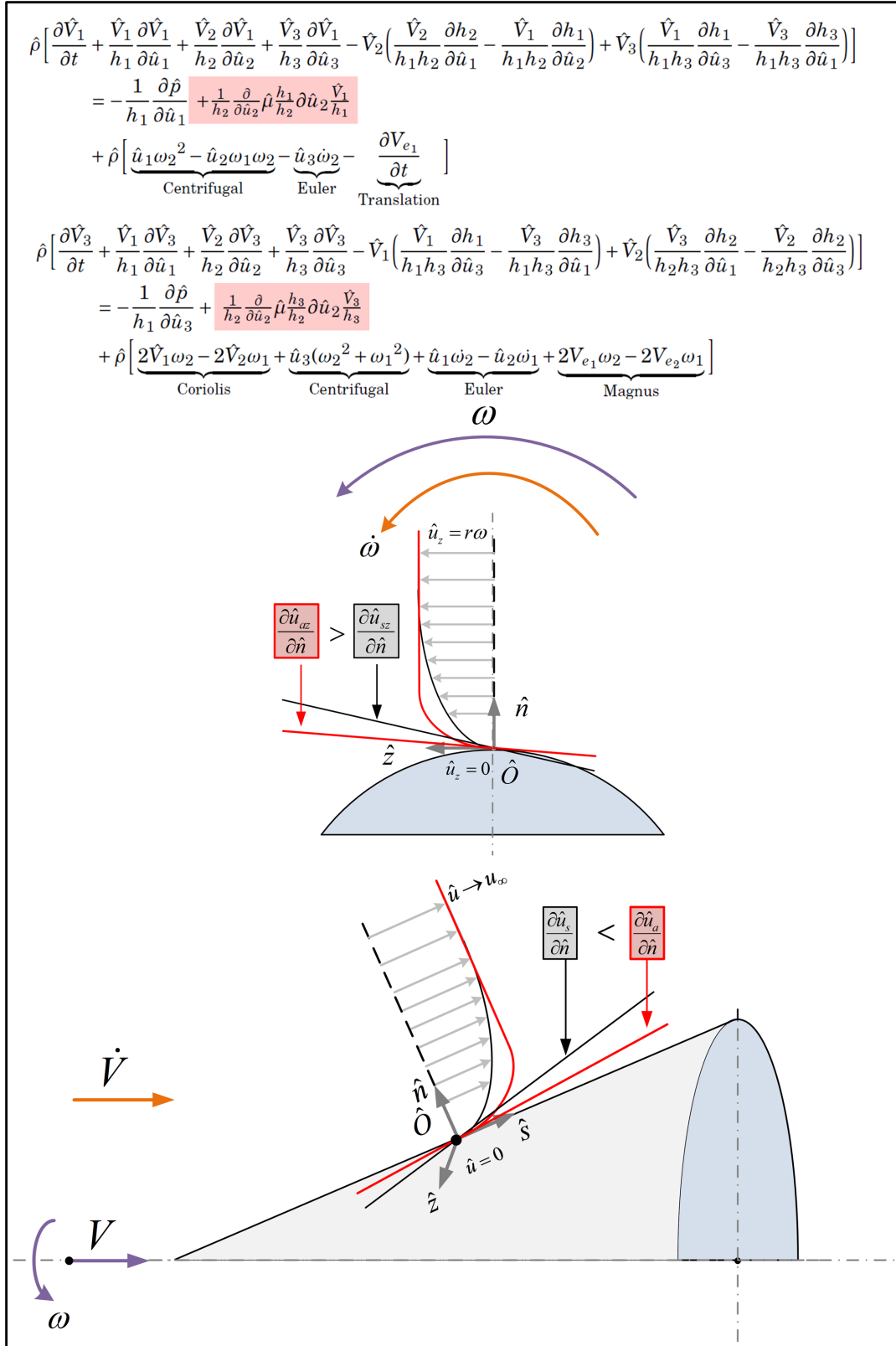
Table 9.4: Cone Arbitrary Motion Results Matrix

Group 6a		Group 6b	
1 - 4 m/s 2 - 12 rad/s		1 - 4 m/s 12 - 2 rad/s	
s-direction	Boundary layer thinner Profile similar to steady state Steeper gradient with increased acceleration	s-direction	Boundary layer thinner Profile similar to steady state Steeper gradient with increased acceleration
n-direction	Similar reaction as s-direction	n-direction	Similar reaction as s-direction
z-direction	Boundary layer slightly thicker Profile similar to steady state Steeper gradient with increased acceleration	z-direction	Boundary layer significantly thicker Flow reversal observed Reversal proportional to deceleration
Group 6c		Group 6d	
4 - 1 m/s 12 - 2 rad/s		4 - 1 m/s 2 - 12 rad/s	
s-direction	Boundary layer thicker Flow reversal observed Near-wall gradient proportional to deceleration	s-direction	Boundary layer thicker Flow reversal observed Near-wall gradient proportional to deceleration
n-direction	Similar reaction as s-direction	n-direction	Similar reaction as s-direction
z-direction	Boundary layer thinner Flow reversal observed Reversal proportional to deceleration	z-direction	Boundary layer significantly thinner Profiles similar to steady state Curve slopes proportional to acceleration



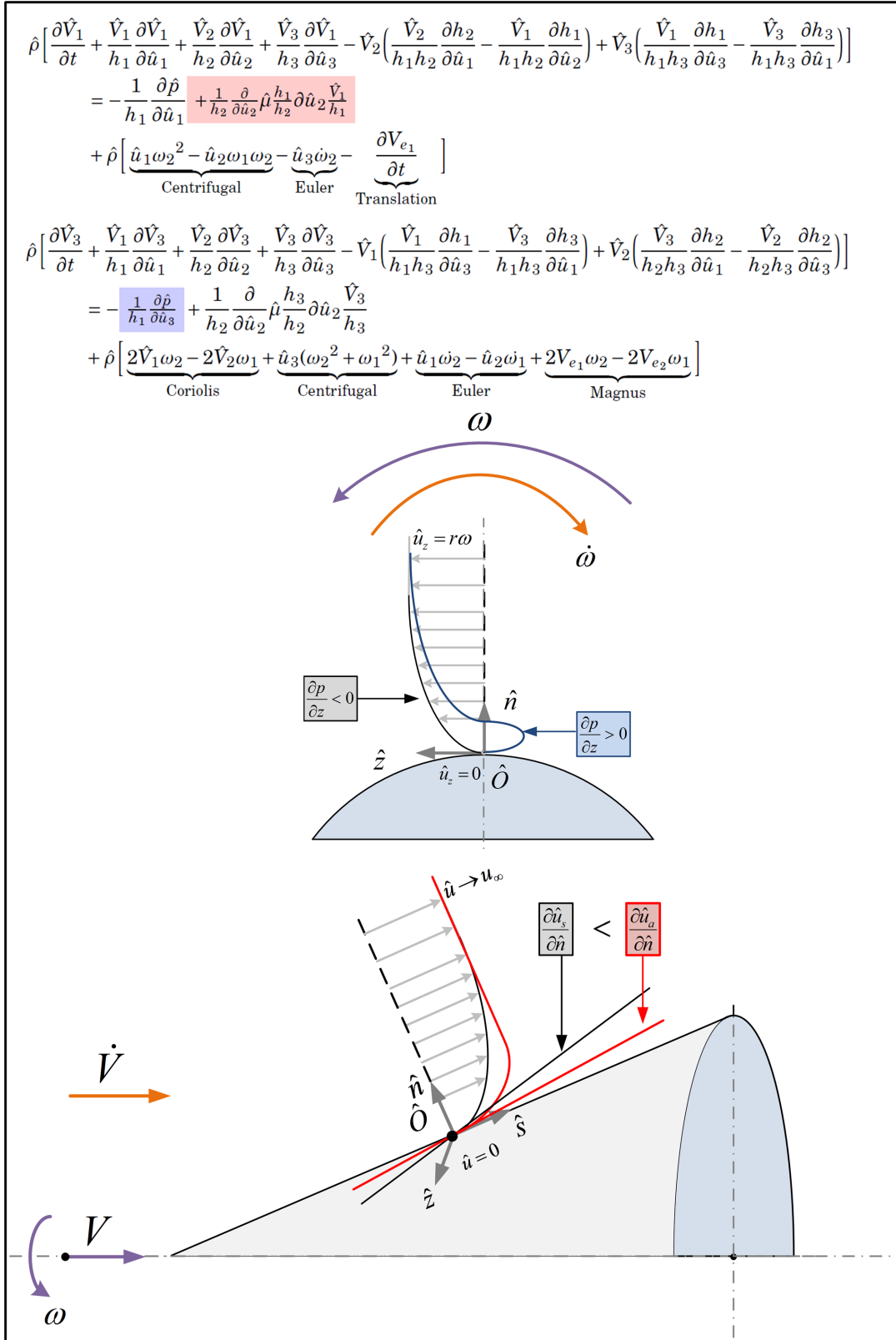
## 9.4. RESULTS AND DISCUSSION - ARBITRARY MOTION

Figure 9.51: Mechanisms Associated with Case 6a of the Cone



CHAPTER 9. BOUNDARY LAYER RESPONSE IN COMBINED TRANSLATION AND ROTATION - ARBITRARY CONE FLOW

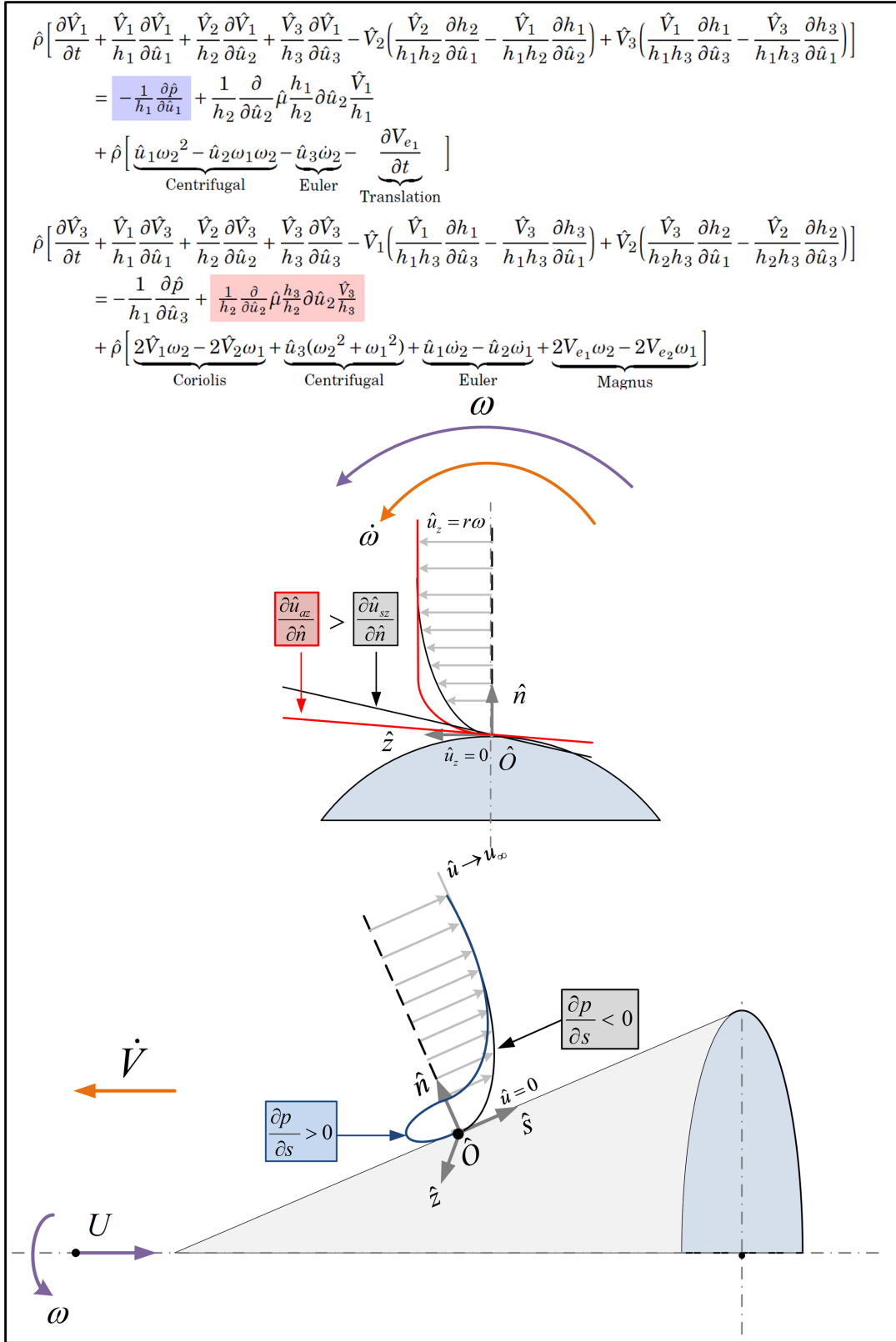
Figure 9.52: Mechanisms Associated with Case 6a of the Cone





CHAPTER 9. BOUNDARY LAYER RESPONSE IN COMBINED TRANSLATION AND ROTATION - ARBITRARY CONE FLOW

Figure 9.54: Mechanisms Associated with Case 6a of the Cone



### 9.4.2 Boundary Layer Parameters

Figures 9.55 and 9.56 show the shape factor in the  $s$ -direction. In both cases the flow in translation is accelerating. Group 6a are accelerating in rotation while Group 6b are decelerating in rotation. The shape factor in the  $s$ -direction is affected by the rotation as can be seen in the slightly lower results of Group 6b. The general tendencies in the results are similar to the shape factors of the flat plate in accelerating translation.

Figure 9.55: Group 6a Shape Factor in the  $s$ -Direction

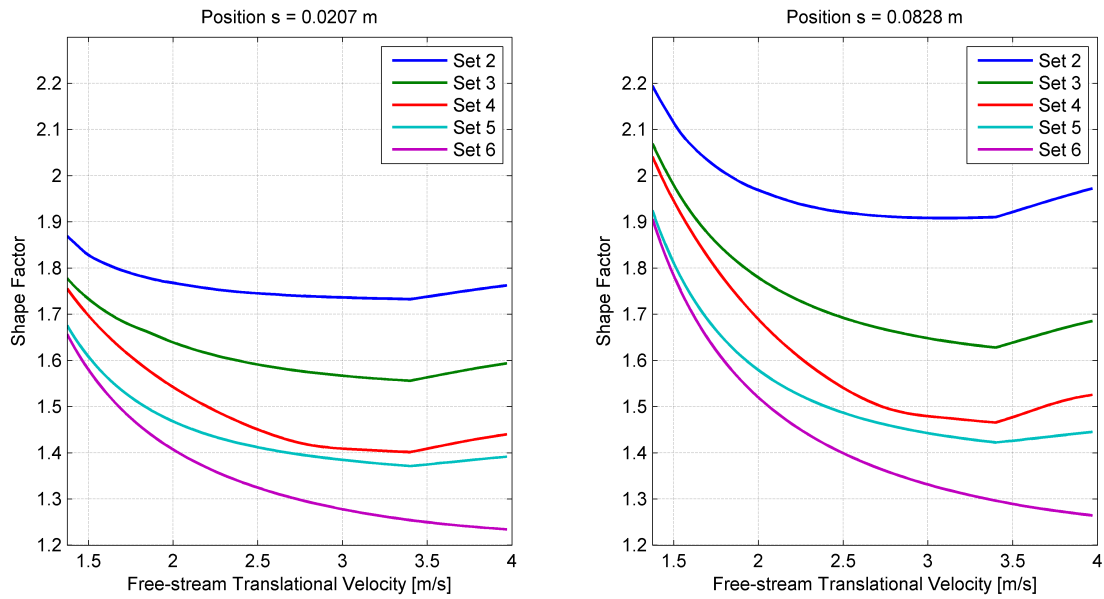
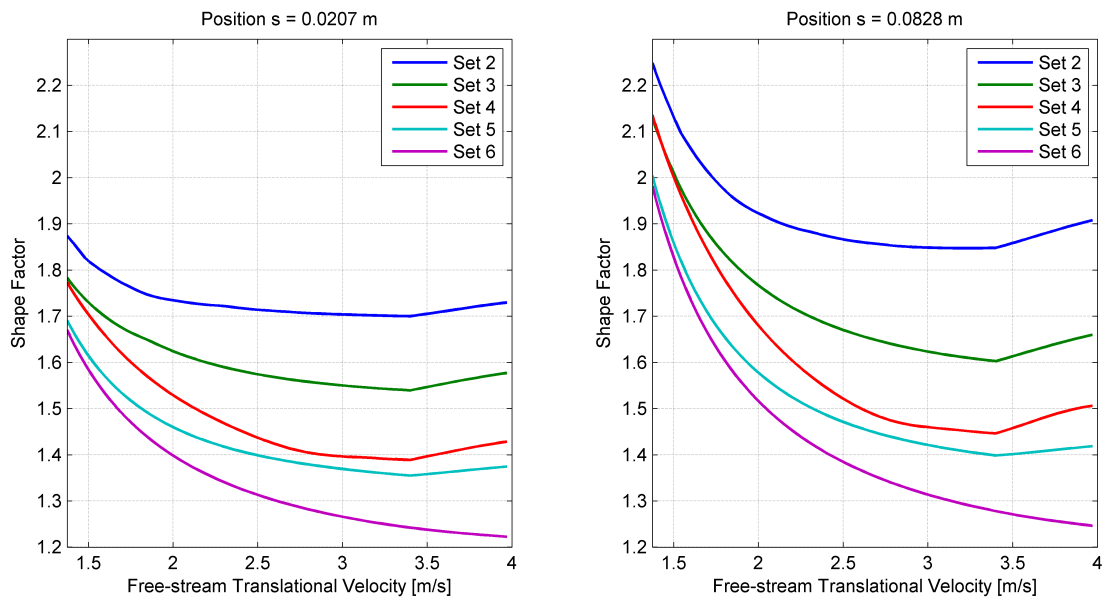


Figure 9.56: Group 6b Shape Factor in the  $s$ -Direction



CHAPTER 9. BOUNDARY LAYER RESPONSE IN COMBINED TRANSLATION AND ROTATION - ARBITRARY CONE FLOW

Figures 9.57 and 9.58 show the shape factor in the  $z$ -direction for Groups 6a and 6d respectively. Both cases are accelerating in rotation. Deceleration in translation causes the shape factor to start at higher values and end at lower values than if there had been acceleration in translation. This is due to residual flow effects from starting at a higher free-stream velocity. The profiles of the shape factor are comparable to the tangential profiles of a rotating disk in acceleration.

Figure 9.57: Group 6a Shape Factor in the  $z$ -Direction

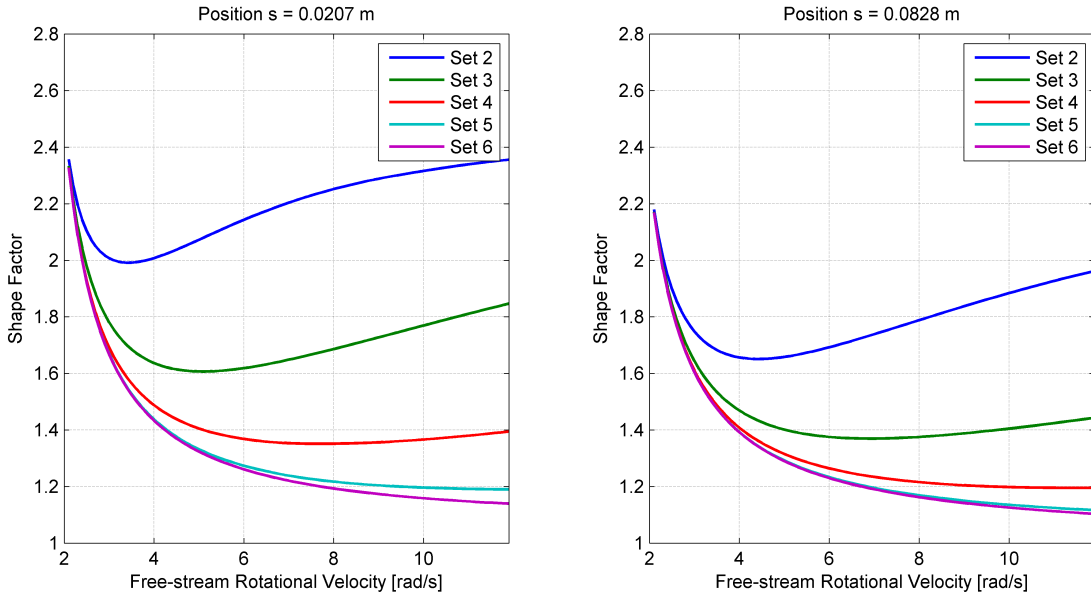
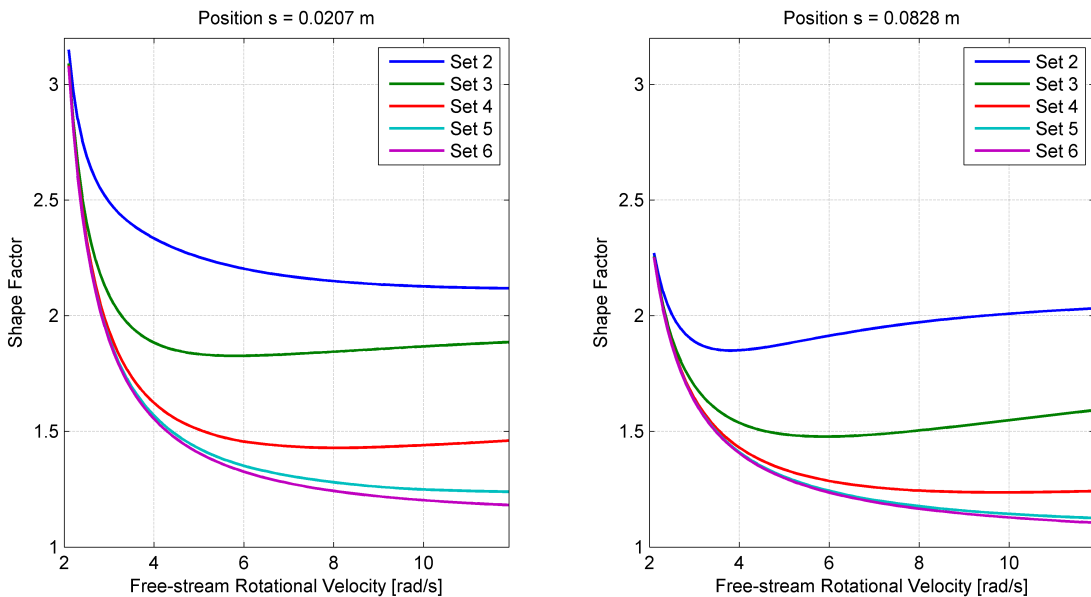


Figure 9.58: Group 6d Shape Factor in the  $z$ -Direction



9.4. RESULTS AND DISCUSSION - ARBITRARY MOTION

Figures 9.59 and 9.60 show the shape factor in the  $z$ -direction for Group 6b and 6c respectively. The rotational flow is in deceleration. The profiles are similar to the tangential profiles of a rotating disk in deceleration. The same discontinuity in the shape factor is observed. Acceleration in the axial flow has a destabilizing effect on the boundary layer since it causes the discontinuity to occur earlier than in the case of decelerating axial flow. Higher rotational deceleration cases are less affected by changes in translation since Sets 5 and 6 do not indicate earlier onset of discontinuity.

Figure 9.59: Group 6b Shape Factor in the  $z$ -Direction

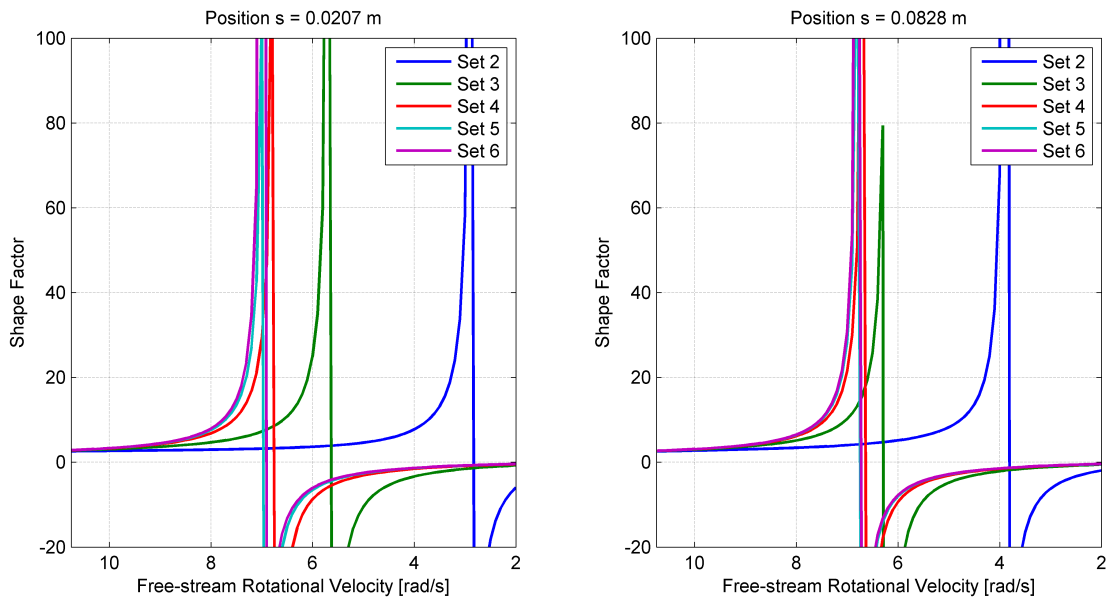
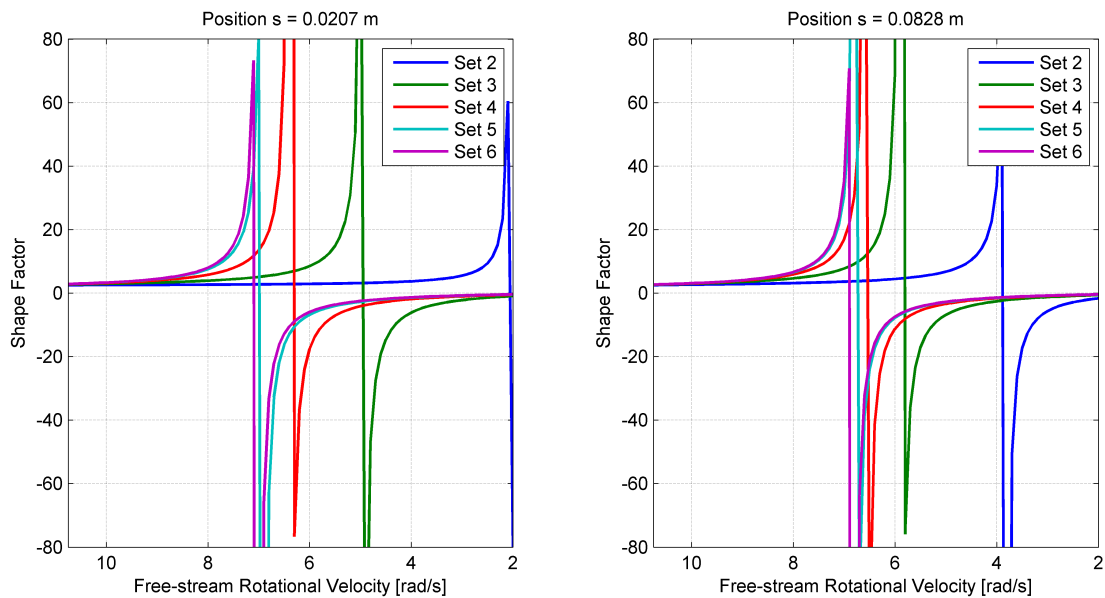


Figure 9.60: Group 6c Shape Factor in the  $z$ -Direction



CHAPTER 9. BOUNDARY LAYER RESPONSE IN COMBINED TRANSLATION AND ROTATION - ARBITRARY CONE FLOW

Figures 9.61 and 9.62 show the shape factor in the  $z$ -direction for Group 6c and 6d respectively. Translational velocities are in deceleration. Since the flow is dominated by the higher translation, it dominates the shape factor behaviour. The profiles are similar to a flat plate in deceleration as indicated by the presence of the discontinuity in the shape factor.

Figure 9.61: Group 6c Shape Factor in the  $s$ -Direction

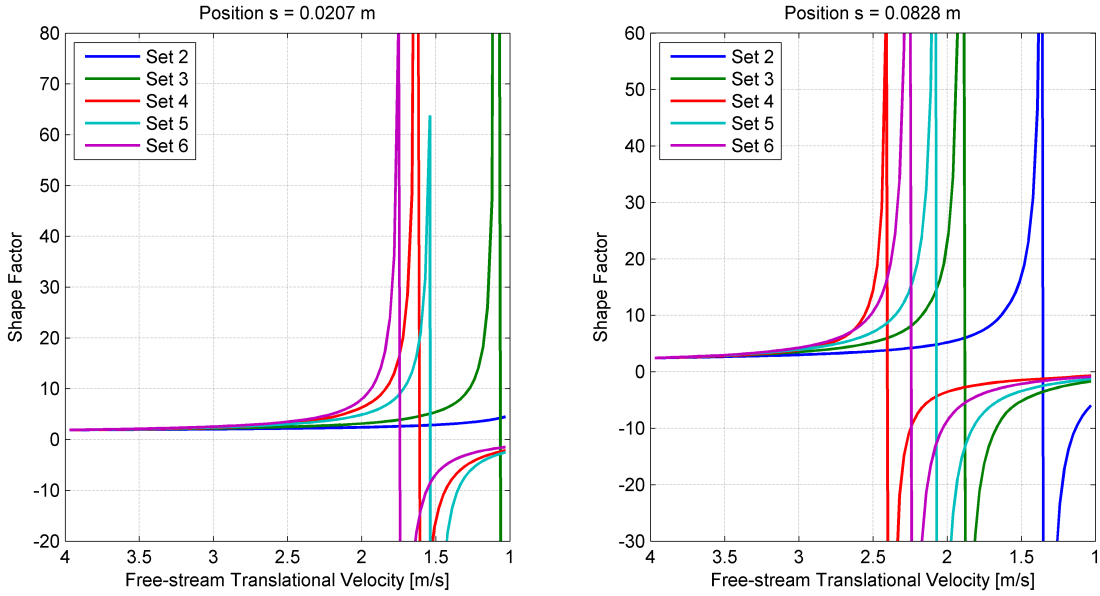
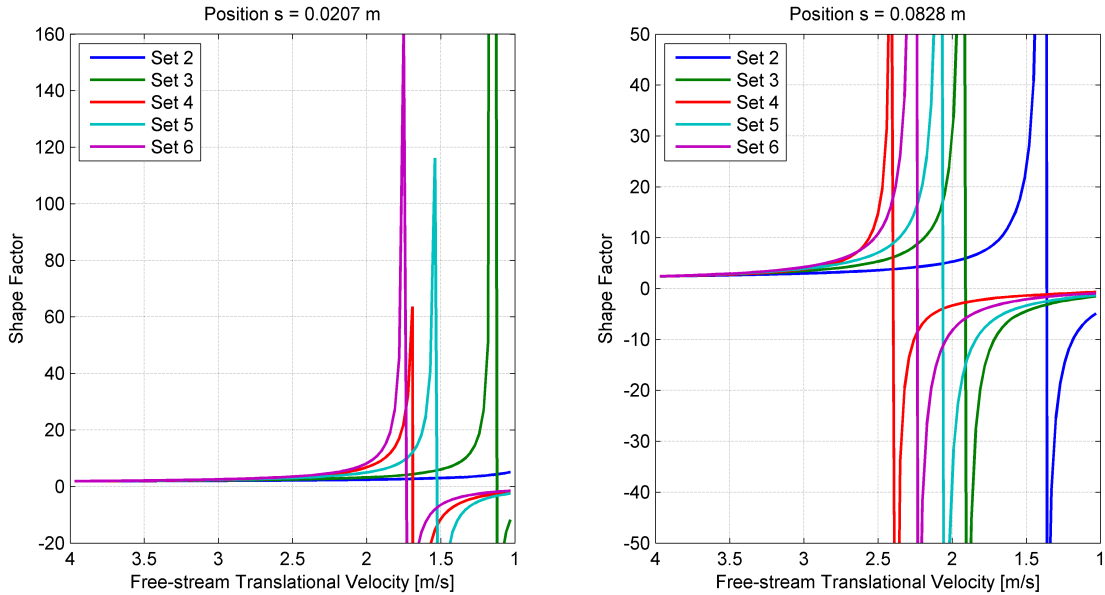


Figure 9.62: Group 6d Shape Factor in the  $s$ -Direction





### 9.4.3 Skin Friction Coefficients

In *Figures 9.63* and *9.64* the skin friction coefficient results for Group 6a and 6b are given respectively. In both cases the translational flow is in acceleration and dominates the flow. The skin friction coefficients display similar patterns than the flat plate and the rotating disk in acceleration. The values are increasing during the beginning stages of the acceleration event. It reaches a maximum after which it decreases to approach an asymptotic value.

Figure 9.63: Group 6a Skin Friction Coefficient

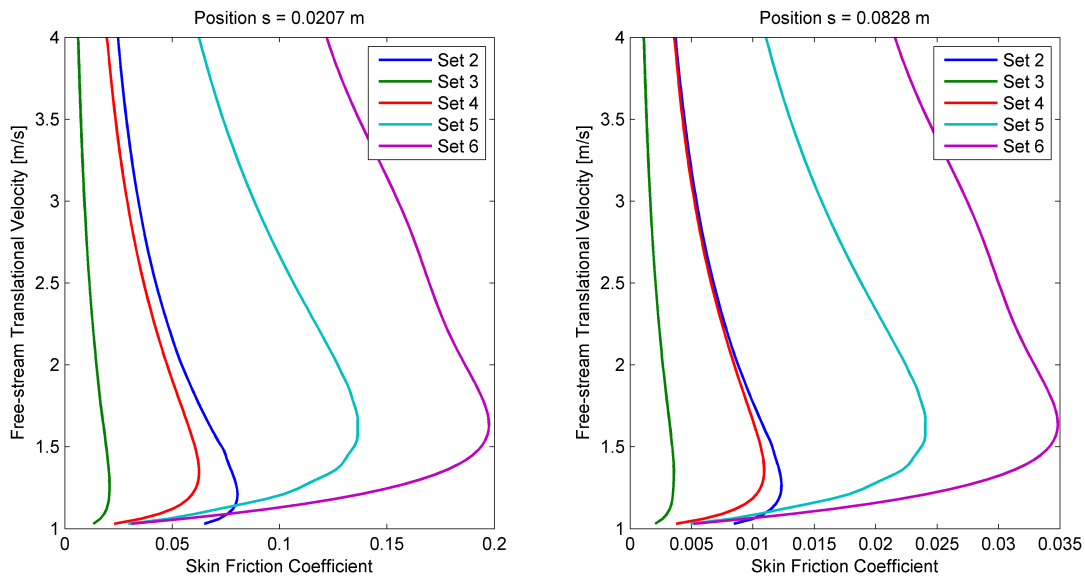
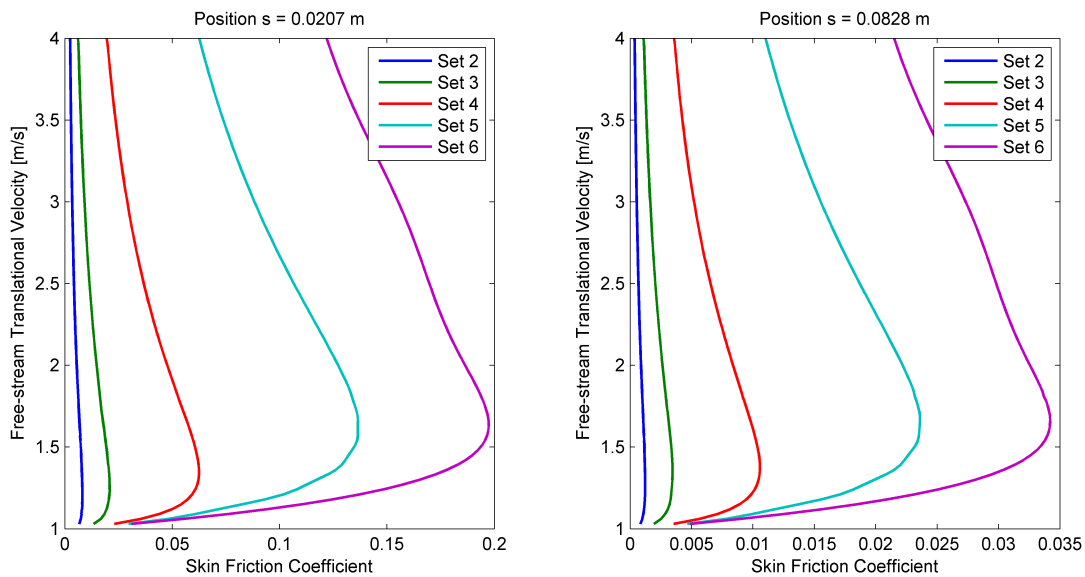


Figure 9.64: Group 6b Skin Friction Coefficient



CHAPTER 9. BOUNDARY LAYER RESPONSE IN COMBINED TRANSLATION AND ROTATION - ARBITRARY CONE FLOW

Figures 9.65 and 9.66 show the skin friction coefficient for the Group 6c and 6d respectively. In both these cases the flow is in translational deceleration. Translation dominates the flow. The behaviour of the skin friction coefficient is similar to the flat plate and rotating disk in deceleration. The values increase with deceleration and is divergent. Stronger decelerations causes higher skin friction coefficient values.

Figure 9.65: Group 6c Skin Friction Coefficient

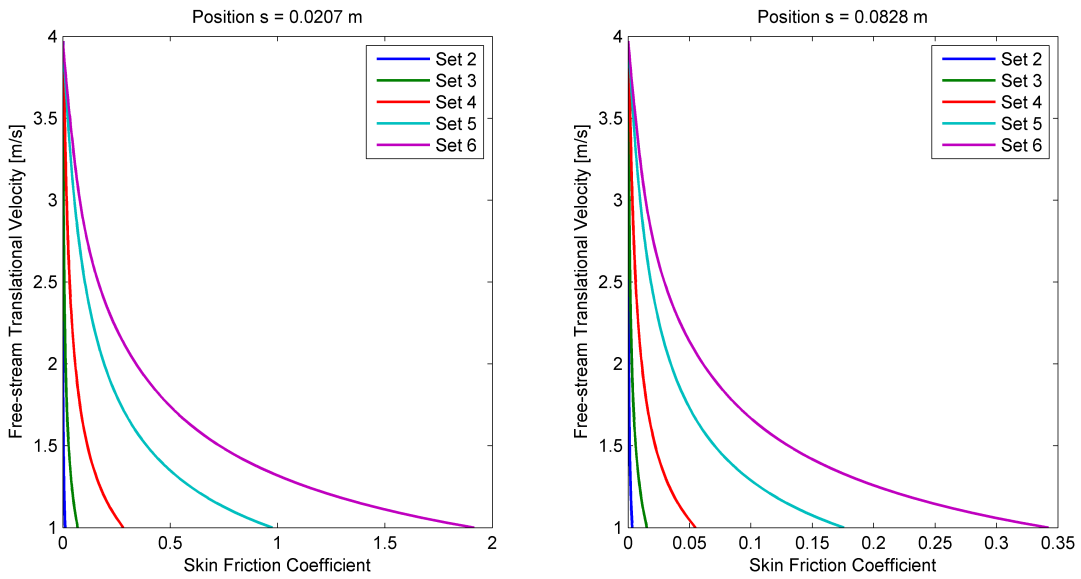
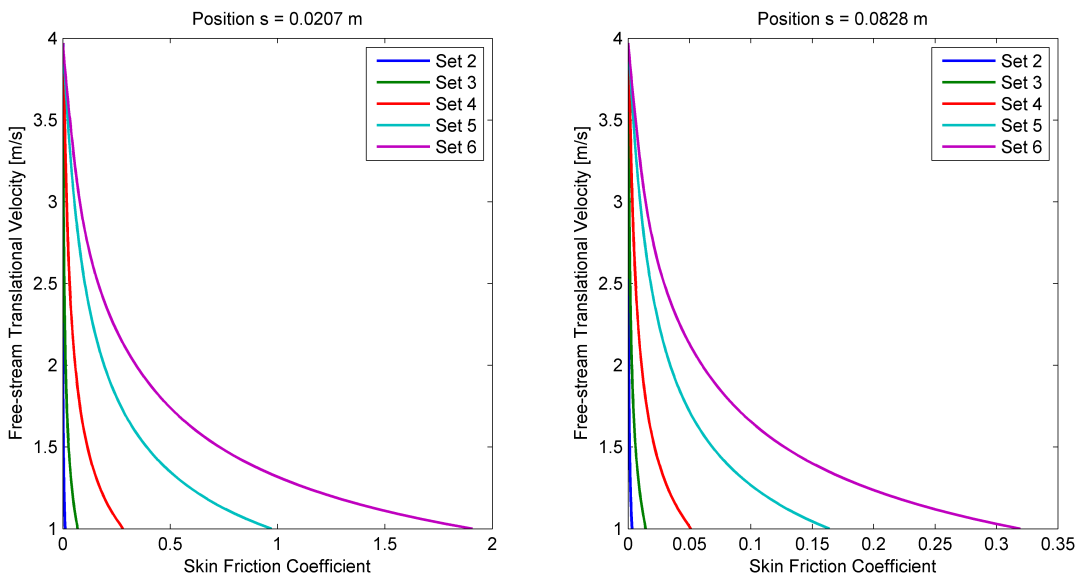


Figure 9.66: Group 6d Skin Friction Coefficient



## 9.5 Closure

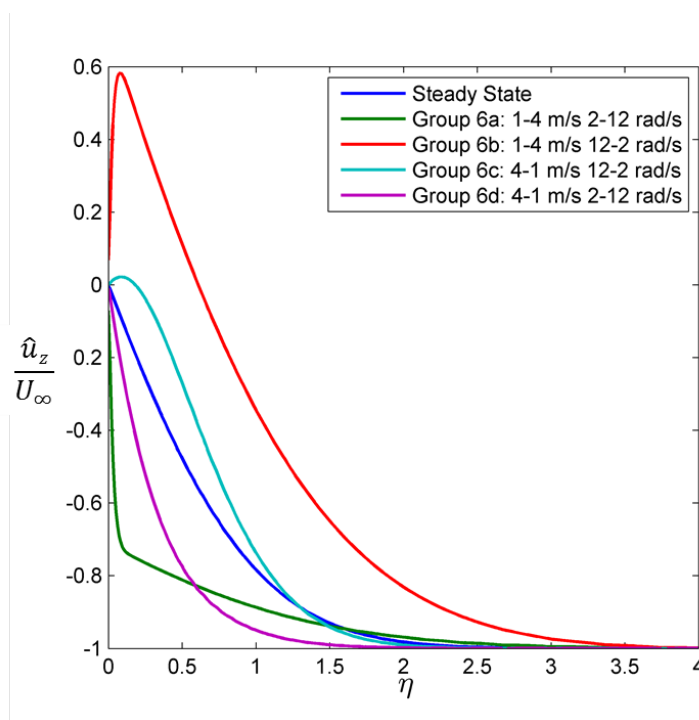
In this chapter the response of the boundary layer to arbitrary acceleration of rotating cone in axial flow have been investigated. The specific contribution of this chapter is summarized as:

- 1) Characterization of the boundary layer behaviour for a cone in
  - i) variable translation with steady rotation,
  - ii) steady translation with variable rotation and
  - iii) variable translation with variable rotation.
- 2) Definition of a mechanism that explains the behaviour of the boundary layer for each case.
- 3) The characterisation of the response of the shape factor to arbitrary motion.
- 4) The characterisation of the response of the skin friction coefficient to arbitrary motion.

The rotating cone in axial flow was subjected to various cases of acceleration and deceleration. Similarities can be drawn between the response of the cone in the  $s$ -direction and the flat plate in variable translation. The responses in the  $z$ -direction are comparable to the rotating disk. In all cases **Type III** response were observed. The cone case is therefore dominated by momentum effects in the boundary layer.

The unsteady rotation is affected by the axial velocities as indicated in *Figure 9.67* below. This figure illustrates the importance of taking flow history into account when conducting analysis in arbitrary motion.

Figure 9.67: Comparison of Various Profile at a Free-Stream of 2 m/s 7.5 rad/s



CHAPTER 9. BOUNDARY LAYER RESPONSE IN COMBINED TRANSLATION AND ROTATION - ARBITRARY CONE FLOW

In acceleration the near-wall velocity profile becomes steeper in comparison to the steady state case, while in deceleration flow reversal is observed. The profiles are dependant on the strength of the velocity change rate. Higher accelerations cause greater velocity gradients in the near-wall region, while higher decelerations result in stronger separation of the flow.

The profiles in the  $s$ -direction are influenced by the Centrifugal effects in the far-fields of the boundary layer. A decrease was observed in the centrifugal effect with increasing acceleration and an increase with increasing deceleration. The profiles are also subjected to a strain limit where the gradient of the velocity profile is independent from the arbitrary motion.

The boundary layer responses are explained using the same mechanisms of the flat plate and rotating disk in acceleration and deceleration. This is depicted in *Figures 9.68* and *9.69* for translation and rotation respectively.

Figure 9.68: Flow Mechanisms for Translation

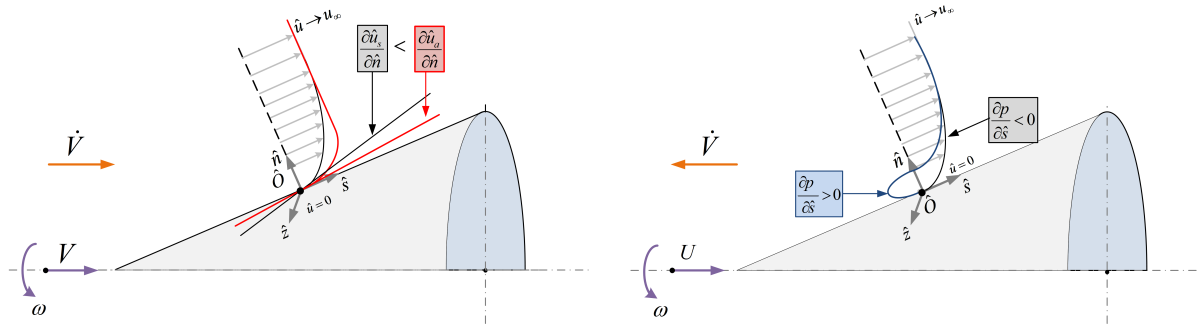
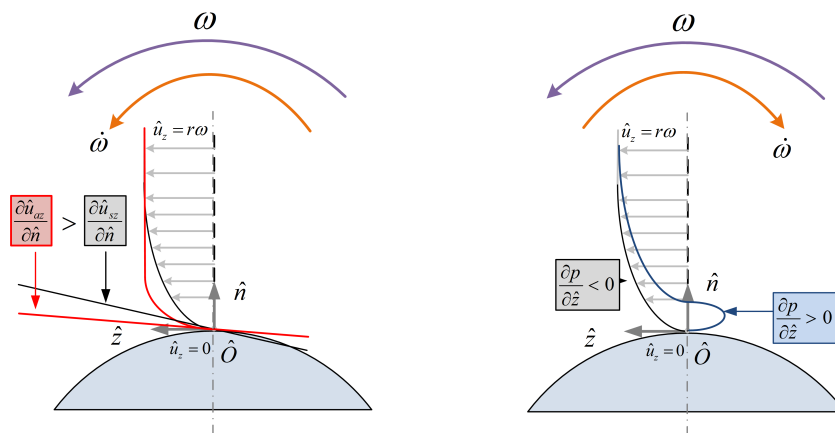


Figure 9.69: Flow Mechanisms for Rotation



In acceleration the non-inertial terms becomes a momentum source. This leads to an increase in the near-wall velocity gradient which influences the velocity profile. In deceleration the non-inertial terms becomes a momentum sink. This lead to a decrease in the near-wall velocity gradient. In turn the pressure gradient becomes positive and forces an adverse pressure gradient. The flow separates in response to the adverse pressure gradient.

Shape factor results are comparable with the shape factor results of the flat plate. Since translation dominates, the shape factor reacts according to the conditions of the axial flow as indicated in

In a similar manner where the shape factor are dependant on the conditions of the axial flow, so does the skin friction coefficient respond to acceleration or deceleration in translation.

Figure 9.70: Skin Friction Coefficient Comparisons with respect to Arbitrary Motion in Translation

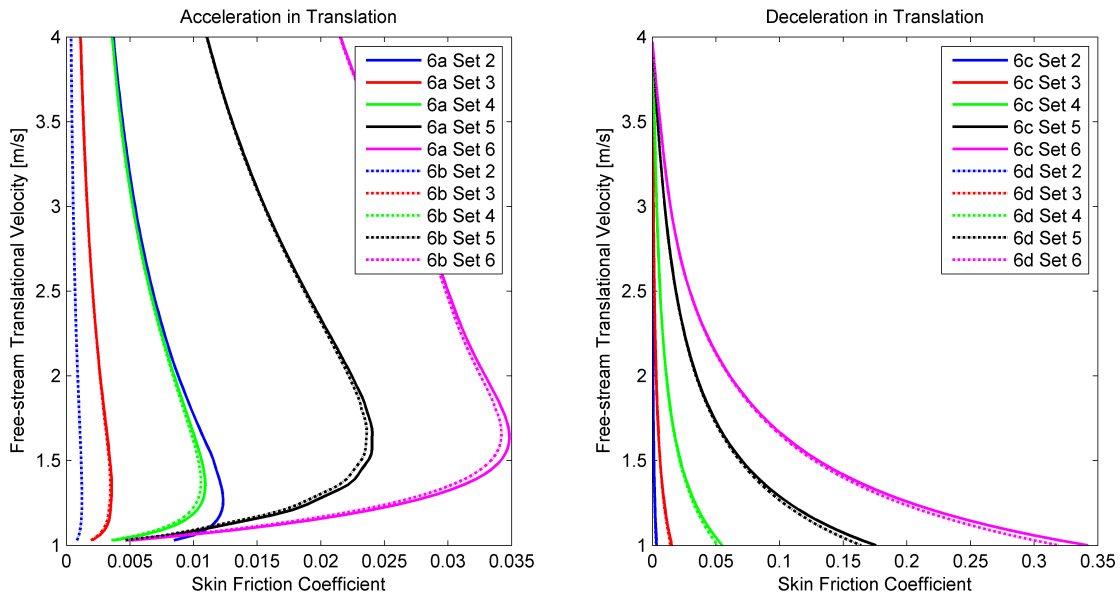
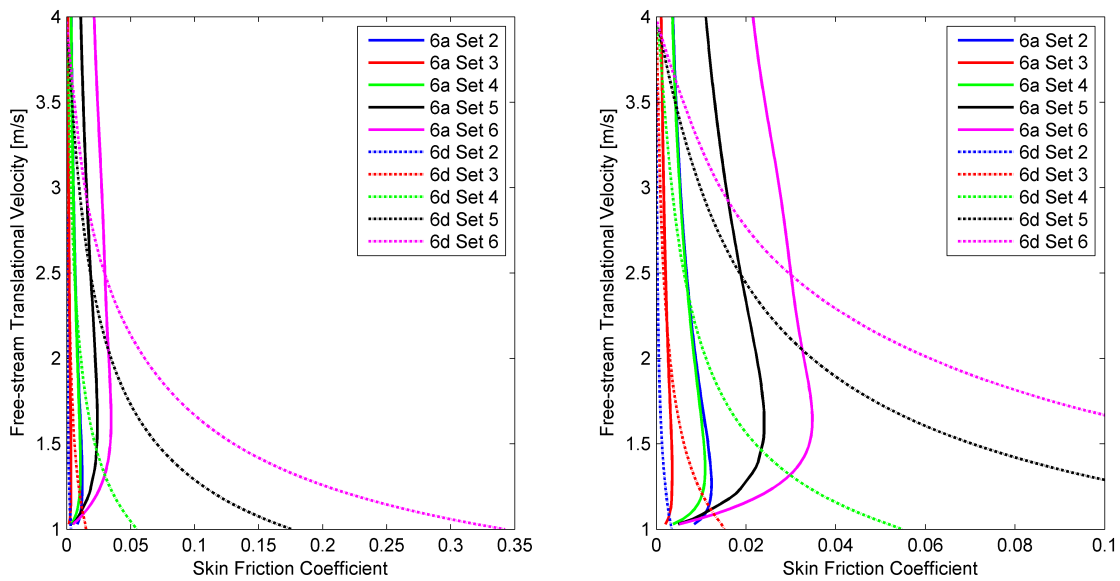


Figure 9.71: Skin Friction Coefficient Comparisons for Arbitrary Motion





UNIVERSITEIT VAN PRETORIA  
UNIVERSITY OF PRETORIA  
YUNIBESITHI YA PRETORIA

## Conclusion

This thesis was aimed at characterizing the response of the boundary layer to arbitrary motion. The task was approached by addressing the identified gaps in the body of knowledge. The objectives that followed from the literature survey were related to boundary layers of objects in unsteady six-degree-of-freedom motion. The formalized research question, objectives and outcomes are as follow:

### **Research Question**

How does the boundary layer on an airframe in arbitrary motion respond the unsteady flow conditions?

### **Objective 1**

Derive the non-inertial Navier-Stokes bulk flow and boundary layer equations.

### **Outcome 1**

Mathematical formulations for the bulk flow and boundary layer equations in arbitrary motion.

### **Objective 2**

Implement the non-inertial Navier-Stokes equations in a solver in OpenFOAM.

### **Outcome 2**

Solver, for prescribed, arbitrary motion in the non-inertial reference frame, implemented in OpenFOAM.

### **Objective 3**

Conduct numerical simulations to determine the response of the boundary layer to arbitrary motion.

### **Outcome 3**

Insight into the response of the boundary layer to arbitrary motion.

## 10.1 Contributions

The contributions made during the course of this research is grouped per objective below.

### Objective 1

1 Derive the non-inertial Navier-Stokes bulk flow and boundary layer equations.

It was shown through derivation that both the **continuity and conservation of energy equations** remains **invariant** under transformation - no additional terms are added to these equations:

$$\frac{\partial \hat{\rho}}{\partial t} + \hat{\nabla} \cdot \hat{\rho} \hat{\mathbf{u}} = 0 \quad (10.1)$$

$$\frac{\partial \hat{\rho} \hat{\mathbf{e}}}{\partial t} + (\hat{\nabla} \cdot \hat{\rho} \hat{\mathbf{e}} \hat{\mathbf{u}}) = -\hat{p}(\hat{\nabla} \cdot \hat{\mathbf{u}}) + \hat{\nabla} \cdot (\hat{k} \hat{\nabla} \hat{T}) + \hat{\varphi} \quad (10.2)$$

The conservation of **momentum equation** for full arbitrary acceleration below, indicated that there are **six fictitious terms** in the non-inertial equation. These are the only terms that are present during arbitrary acceleration. The higher order terms become negligible or cancel out during the derivation.

$$\begin{aligned} \frac{\partial \hat{\rho} \hat{\mathbf{u}}}{\partial t} + \hat{\nabla} \cdot (\hat{\rho} \hat{\mathbf{u}} \otimes \hat{\mathbf{u}}) = & -\hat{\nabla} \hat{p} + \hat{\nabla} \cdot [\hat{\mu}(\hat{\nabla} \hat{\mathbf{u}} + \hat{\nabla} \hat{\mathbf{u}}^T) + \hat{\lambda}(\hat{\nabla} \cdot \hat{\mathbf{u}}) \hat{\mathbf{I}}] \\ & - \underbrace{\frac{\partial}{\partial t}(\rho \mathbf{V}(t))}_{\text{Translation}} + \underbrace{\rho \hat{\mathbf{x}} \wedge \boldsymbol{\Omega} + \rho \hat{\mathbf{x}} \wedge \dot{\boldsymbol{\Omega}}}_{\text{Unsteady motion}} + \underbrace{2\rho \hat{\mathbf{u}} \wedge \boldsymbol{\Omega}}_{\text{Coriolis}} - \underbrace{\rho \hat{\mathbf{x}} \wedge \boldsymbol{\Omega} \wedge \boldsymbol{\Omega}}_{\text{Centrifugal}} + \underbrace{2\rho \mathbf{V}(t) \wedge \boldsymbol{\Omega}}_{\text{Magnus}} \end{aligned} \quad (10.3)$$

Clarification were obtained on the **mathematical origin** of the **fictitious forces** through the derivations. This indicated that the fictitious forces stem from the transformation of the temporal and advection terms. The presence of fictitious forces is case dependant and is a function of the motion of the relative frame. The diffusion terms and pressure gradient terms remain invariant under transformation.

The **continuity equation** in the **boundary layer** for both compressible and incompressible flows were obtained. No terms are neglected from the continuity equation. Therefore, the form remains the same as in the bulk flow. Here it is indicated in the curvilinear form.

$$\frac{\partial \hat{\rho}}{\partial t} + \frac{1}{h_1 h_2 h_3} \left[ \frac{\partial}{\partial \hat{u}_1} (h_2 h_3 \hat{\rho} \hat{V}_1) + \frac{\partial}{\partial \hat{u}_2} (h_1 h_3 \hat{\rho} \hat{V}_2) + \frac{\partial}{\partial \hat{u}_3} (h_1 h_2 \hat{\rho} \hat{V}_3) \right] = 0 \quad (10.4)$$

The momentum equation in the boundary layer for compressible and incompressible flow were determined for Cartesian, Cylindrical and Curvilinear co-ordinate systems.

#### x-momentum

$$\begin{aligned} \frac{\partial \hat{\rho} \hat{u}}{\partial t} + \hat{u} \frac{\partial \hat{\rho} \hat{u}}{\partial \hat{x}} + \hat{v} \frac{\partial \hat{\rho} \hat{u}}{\partial \hat{y}} + \hat{w} \frac{\partial \hat{\rho} \hat{u}}{\partial \hat{z}} = & -\frac{\partial \hat{p}}{\partial \hat{x}} + \frac{\partial}{\partial \hat{y}} \hat{\mu} \frac{\partial \hat{u}}{\partial \hat{y}} + 2\hat{\rho} \hat{v} \omega_3 - 2\hat{\rho} \hat{w} \omega_2 + \hat{\rho} \hat{x} (\omega_3^2 + \omega_2^2) \\ & - \hat{\rho} \hat{y} \omega_1 \omega_2 - \hat{\rho} \hat{z} \omega_1 \omega_3 + \hat{\rho} \hat{y} \hat{\omega}_3 - \hat{\rho} \hat{z} \hat{\omega}_2 + \hat{\rho} \hat{y} \omega_3 - \hat{\rho} \hat{z} \omega_2 + 2\hat{\rho} V_y \omega_3 - 2\hat{\rho} V_z \omega_2 - \frac{\partial \hat{\rho} V_x}{\partial t} \end{aligned} \quad (10.5)$$



**r-momentum**

$$\begin{aligned} \frac{\partial \hat{\rho} \hat{u}_r}{\partial t} + \hat{u}_r \frac{\partial \hat{\rho} \hat{u}_r}{\partial \hat{r}} + \frac{\hat{u}_\theta}{\hat{r}} \frac{\partial \hat{\rho} \hat{u}_r}{\partial \hat{\theta}} - \frac{\hat{\rho} \hat{u}_\theta^2}{\hat{r}} + \hat{u}_y \frac{\partial \hat{\rho} \hat{u}_r}{\partial \hat{y}} = -\frac{\partial \hat{p}}{\partial \hat{r}} + \frac{\partial}{\partial \hat{y}} \hat{\mu} \frac{\partial \hat{u}_r}{\partial \hat{y}} - 2\hat{\rho} \hat{u}_\theta \omega_y + 2\hat{\rho} \hat{u}_y \omega_\theta \\ - \hat{\rho} \hat{y} \omega_r \omega_y + \hat{\rho} \hat{r} \omega_y^2 + \hat{\rho} \hat{r} \omega_\theta^2 + \hat{\rho} \hat{y} \dot{\omega}_\theta - \hat{\rho} \hat{u}_\theta \omega_y + \hat{\rho} \hat{u}_y \omega_\theta - 2\hat{\rho} V_\theta \omega_y + 2\hat{\rho} V_y \omega_\theta - \frac{\partial \hat{\rho} V_r}{\partial t} \end{aligned} \quad (10.6)$$

**u<sub>1</sub>-momentum:**

$$\begin{aligned} \hat{\rho} \left[ \frac{\partial \hat{V}_1}{\partial t} + \frac{\hat{V}_1}{h_1} \frac{\partial \hat{V}_1}{\partial \hat{u}_1} + \frac{\hat{V}_2}{h_2} \frac{\partial \hat{V}_1}{\partial \hat{u}_2} + \frac{\hat{V}_3}{h_3} \frac{\partial \hat{V}_1}{\partial \hat{u}_3} - \hat{V}_2 \left( \frac{\hat{V}_2}{h_1 h_2} \frac{\partial h_2}{\partial \hat{u}_1} - \frac{\hat{V}_1}{h_1 h_2} \frac{\partial h_1}{\partial \hat{u}_2} \right) + \hat{V}_3 \left( \frac{\hat{V}_1}{h_1 h_3} \frac{\partial h_1}{\partial \hat{u}_3} - \frac{\hat{V}_3}{h_1 h_3} \frac{\partial h_3}{\partial \hat{u}_1} \right) \right] \\ = -\frac{1}{h_1} \frac{\partial \hat{p}}{\partial \hat{u}_1} + \frac{1}{h_2} \frac{\partial}{\partial \hat{u}_2} \hat{\mu} \frac{h_1}{h_2} \frac{\partial \hat{u}_2}{\partial \hat{u}_1} \frac{\hat{V}_1}{h_1} + \hat{\rho} \left[ 2\hat{V}_2 \omega_3 - 2\hat{V}_3 \omega_2 + \hat{u}_1 (\omega_3^2 + \omega_2^2) - \hat{u}_2 \omega_1 \omega_2 - \hat{u}_3 \omega_1 \omega_3 \right. \\ \left. + \hat{u}_2 \dot{\omega}_3 - \hat{u}_3 \dot{\omega}_2 + \hat{u}_2 \omega_3 - \hat{u}_3 \omega_2 + 2V_{e2} \omega_3 - 2V_{e3} \omega_2 - \frac{\partial V_{e1}}{\partial t} \right] \end{aligned} \quad (10.7)$$

It was shown that the **compressible and incompressible equations** have the same terms. The only difference between the two forms is that in the incompressible case the density parameter,  $\rho$ , can be divided through out the equation.

The following **similarities** in boundary layer equations were observed for all **co-ordinate systems**:

- The fictitious terms can not be neglected from the boundary layer equations. Therefore all the terms have an influence on the boundary layer velocity profile during acceleration and deceleration of the object.
- The material derivative (left hand side of the Navier-Stokes equation) are unchanged in the longitudinal and transversal directions. However, all left hand side terms are neglected in the direction normal to the surface.

$$0 = -\frac{\partial \hat{\psi}}{\partial \hat{y}} - 2\hat{u}_r \omega_\theta + 2\hat{u}_\theta \omega_r - \hat{r} \omega_r \omega_y + \hat{y} \omega_r^2 + \hat{y} \omega_\theta^2 - \hat{r} \dot{\omega}_\theta \quad (10.8)$$

- The pressure gradient terms are present in all directions.
- The diffusion terms in the boundary layer originate from specific components in the stress tensor of the  $\tau_{12}$  and  $\tau_{32}$  terms.

$$\hat{\tau}_{12} = \hat{\mu} \left[ \frac{h_2}{h_1} \frac{\partial}{\partial \hat{u}_1} \left( \frac{\hat{V}_2}{h_2} \right) + \frac{h_1}{h_2} \frac{\partial}{\partial \hat{u}_2} \left( \frac{\hat{V}_1}{h_1} \right) \right] \quad \& \quad \hat{\tau}_{32} = \hat{\mu} \left[ \frac{h_3}{h_2} \frac{\partial}{\partial \hat{u}_2} \left( \frac{\hat{V}_3}{h_3} \right) + \frac{h_2}{h_3} \frac{\partial}{\partial \hat{u}_3} \left( \frac{\hat{V}_2}{h_2} \right) \right] \quad (10.9)$$



**Outcome 1**

Mathematical formulations for the bulk flow and boundary layer equations in arbitrary motion.

### Objective 2

Implement the non-inertial Navier-Stokes equations in a solver in OpenFOAM.

The non-inertial formulations for the Navier-Stokes equations developed in addressing **Objective 1**, a non-inertial solver was developed. The resulting code, **ARFrhoPimpleFoam** have the following properties:

- Non-inertial momentum equation implementation,
- Prescribed motion definitions required,
- Operating on a stationary mesh,
- Using specialized boundary conditions and
- Capability of resolving compressible flow.

The governing equations that were implemented are the conservation of mass, momentum and energy equations respectively:

$$\frac{\partial \hat{\rho}}{\partial t} + \hat{\nabla} \cdot \hat{\rho} \hat{\mathbf{u}} = 0$$

$$\frac{\partial \hat{\rho} \hat{\mathbf{u}}}{\partial t} + \hat{\nabla} \cdot (\hat{\rho} \hat{\mathbf{u}} \otimes \hat{\mathbf{u}}) - \hat{\nabla} \cdot [\hat{\mu} (\hat{\nabla} \hat{\mathbf{u}} + \hat{\nabla} \hat{\mathbf{u}}^T) + \hat{\lambda} (\hat{\nabla} \cdot \hat{\mathbf{u}}) \hat{\mathbf{I}}]$$

$$+ \underbrace{\frac{\partial}{\partial t} (\rho \mathbf{V}(t))}_{\text{Translation}} - \underbrace{\rho \hat{\mathbf{x}} \wedge \hat{\boldsymbol{\Omega}}}_{\text{Euler}} - \underbrace{2\rho \hat{\mathbf{u}} \wedge \hat{\boldsymbol{\Omega}}}_{\text{Coriolis}} + \underbrace{\rho \hat{\mathbf{x}} \wedge \hat{\boldsymbol{\Omega}} \wedge \hat{\boldsymbol{\Omega}}}_{\text{Centrifugal}} - \underbrace{2\rho \mathbf{V}(t) \wedge \hat{\boldsymbol{\Omega}}}_{\text{Magnus}} = -\hat{\nabla} \hat{p}$$

$$\frac{\partial \hat{\rho} \hat{h}_s}{\partial t} + (\hat{\nabla} \cdot \hat{\rho} \hat{h}_s \hat{\mathbf{u}}) + \frac{\partial \hat{\rho} \hat{K}}{\partial t} + (\hat{\nabla} \cdot \hat{\rho} \hat{K} \hat{\mathbf{u}}) - \frac{\partial \hat{p}}{\partial t} - \hat{\nabla} \cdot (\hat{k} \hat{\nabla} \hat{T}) = 0$$

A special boundary condition, **ARFFreeStreamVelocity**, was developed that allows for defining the free stream velocity conditions in the inertial frame. It is a simplified manner of describing the flow boundaries where the inertial velocity is stationary. The code transforms the boundary values to the non-inertial frame using the prescribed motion definitions.

Two validation cases were conducted to assess the functionality of the solver; a flat plate and a rotating cone. Numerical results from these analyses were compared with analytical results from Blasius [37], Monaghan [87] and von Karman [41] respectively. The simulated results compared well with the analytical results. It was subsequently used to analyse the behaviour of the boundary layer under various arbitrary flow conditions.

### Outcome 2

Solver, for prescribed, arbitrary motion in the non-inertial reference frame, implemented in OpenFOAM.

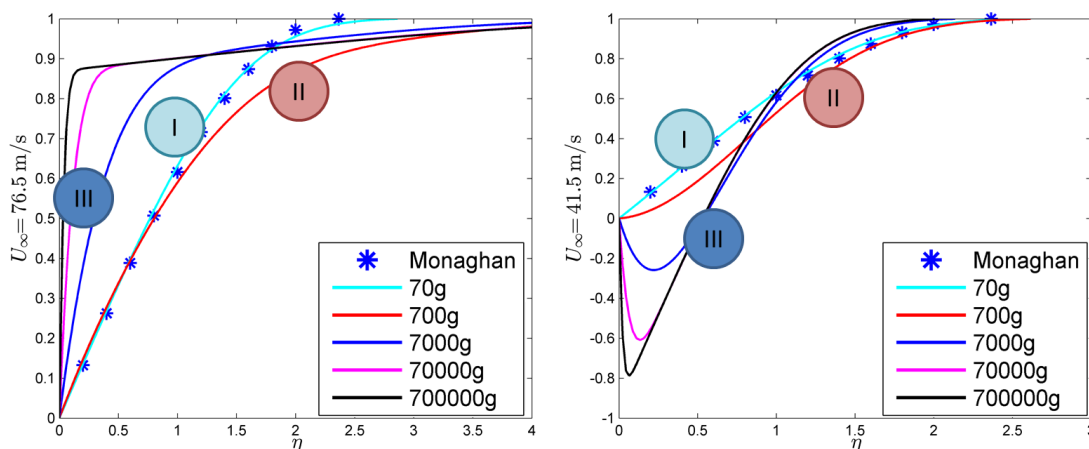
**Objective 3**

Conduct numerical simulations to determine the response of the boundary layer to arbitrary motion.

The numerical simulations were done for a translating flat plate, a rotating disk and a rotating cone in axial flow. Test matrices were constructed to obtain sample results of various accelerating and decelerating conditions. In all the cases simulated, three types of behaviour to arbitrary motion were observed. The three type were defined in this thesis as **Response Types I, II and III**. This is illustrated in *Figure 10.1*.

- **Response Type I**, which is viscous dominant. The time scale at which the event occurs is low enough to allow time for the viscous forces in the boundary layer to adjust to the changes and keep the steady state profile.
- **Response Type II**, where the time scales of the viscous and momentum forces are of the same order. Certain regions of the boundary layer are dominated by viscosity and others by momentum. In acceleration the viscosity dominates in the near-wall region and momentum in the far field regions. In deceleration momentum dominates in the near-wall region and viscosity in the far field.
- **Response Type III**, which is dominated by momentum. The time scale at which the event occurs is too high for viscous forces in the boundary layer to adjust to the changes and keep the steady state profile. In acceleration the near-wall velocity profile increases with increasing acceleration. In deceleration separation occurs at a result of momentum changes in the flow.

Figure 10.1: Response Types for Accelerating and Decelerating Conditions on a Flat Plate



CHAPTER 10. CONCLUSION

The mechanisms that cause changes in the boundary layer due to arbitrary motion were identified. This is similar for all test cases and was explained using the boundary layer equations previously derived. There are similarities in behaviour of the translating plate profiles and the longitudinal velocity profiles of the rotating cone in axial flow. More similarities are observed in the rotating cone and the tangential velocity profile of the cone. This is depicted in *Figures 10.2* and *10.3* respectively.

Figure 10.2: Comparison between the Arbitrary Flow Mechanisms for the Translating Plate (left) and the Longitudinal Velocity Component of the Rotating Cone in Axial Flow (right)

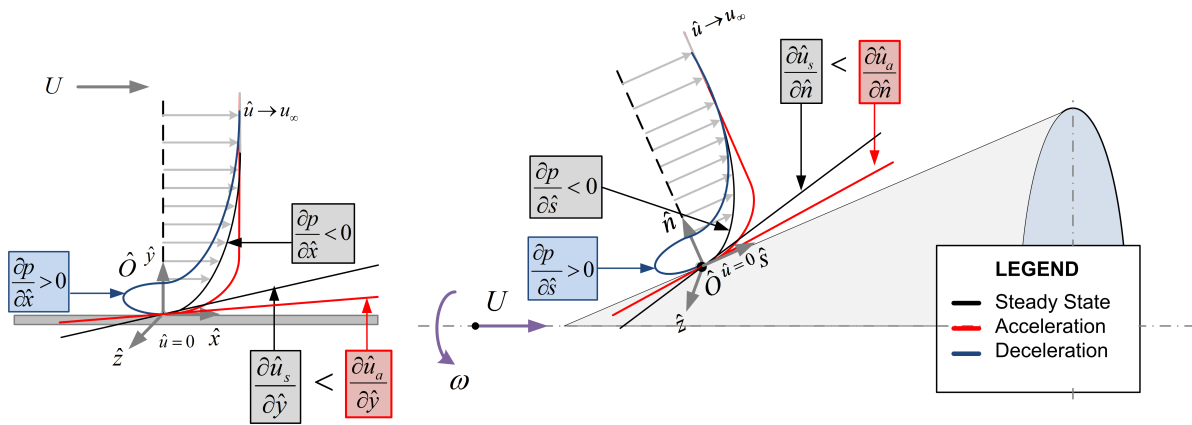
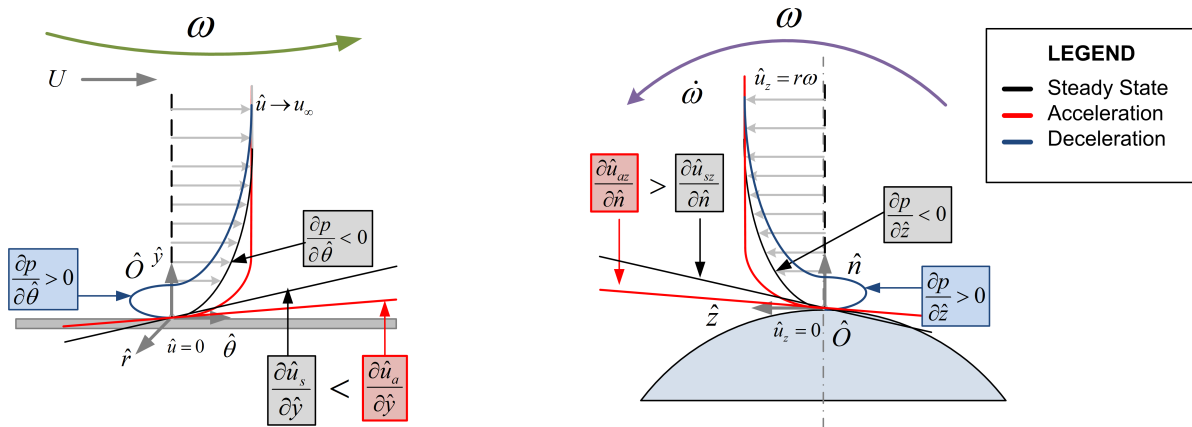


Figure 10.3: Comparison between the Arbitrary Flow Mechanisms for the Rotating Disk (left) and the Tangential Velocity Component of the Rotating Cone in Axial Flow (right)



In acceleration the relative frame fictitious terms become a momentum source. An increase in momentum on the right hand side of the equation leads to an increase in the material derivative on the left hand side of the equation. This increase results in a velocity increase in the boundary layer near-wall region. In turn it causes the velocity gradient at the wall to increase. This is the effect observed in the simulation results for accelerating cases.

The opposite occurs in deceleration where the relative frame fictitious terms become a momentum sink. A decrease in momentum on the right hand side of the equation leads to a decrease in the material

derivative on the left hand side of the equation. This decrease results in a velocity decrease in the boundary layer near wall region. In turn it causes the velocity gradient at the wall to decrease. The pressure gradient has an opposite sign to the diffusion term and increases to such an extent that an adverse pressure gradient form. This results in flow separation as observed in the simulation results.

These mechanisms are depicted in the equations below. It corresponds with the figures above. The red terms cause the velocity gradient increase during acceleration. The blue terms are responsible for flow separation during decelerating.

The equation below is the boundary layer equation for the translating plate.

$$\frac{\partial \hat{\rho} \hat{u}}{\partial t} + \hat{u} \frac{\partial \hat{\rho} \hat{u}}{\partial \hat{x}} + \hat{v} \frac{\partial \hat{\rho} \hat{u}}{\partial \hat{y}} = - \left( \frac{\partial \hat{p}}{\partial \hat{x}} \right) + \frac{\partial}{\partial \hat{y}} \left( \hat{\mu} \frac{\partial \hat{u}}{\partial \hat{y}} \right) - \frac{\partial \hat{\rho} V_x}{\partial t}$$

The equation below is the boundary layer equation for the longitudinal velocity component of the rotating cone in axial flow. It has similarities with the equation for the translating plate.

$$\hat{\rho} \left[ \frac{\partial \hat{V}_1}{\partial t} + \frac{\hat{V}_1}{h_1} \frac{\partial \hat{V}_1}{\partial \hat{u}_1} + \frac{\hat{V}_2}{h_2} \frac{\partial \hat{V}_1}{\partial \hat{u}_2} + \frac{\hat{V}_3}{h_3} \frac{\partial \hat{V}_1}{\partial \hat{u}_3} - \hat{V}_2 \left( \frac{\hat{V}_2}{h_1 h_2} \frac{\partial h_2}{\partial \hat{u}_1} - \frac{\hat{V}_1}{h_1 h_2} \frac{\partial h_1}{\partial \hat{u}_2} \right) + \hat{V}_3 \left( \frac{\hat{V}_1}{h_1 h_3} \frac{\partial h_1}{\partial \hat{u}_3} - \frac{\hat{V}_3}{h_1 h_3} \frac{\partial h_3}{\partial \hat{u}_1} \right) \right]$$

$$= - \left( \frac{1}{h_1} \frac{\partial \hat{p}}{\partial \hat{u}_1} \right) + \left[ \frac{1}{h_2} \frac{\partial}{\partial \hat{u}_2} \hat{\mu} \frac{h_1}{h_2} \frac{\partial \hat{u}_2}{\partial \hat{u}_1} \frac{\hat{V}_1}{h_1} \right] + \hat{\rho} \left[ \hat{u}_1 \omega_2^2 - \hat{u}_2 \omega_1 \omega_2 - \frac{\partial V_{e1}}{\partial t} \right]$$

The equation below is the boundary layer equation for the rotating disk.

$$\frac{\partial \hat{\rho} \hat{u}_\theta}{\partial t} + \hat{u}_r \frac{\partial \hat{\rho} \hat{u}_\theta}{\partial \hat{r}} + \frac{\hat{u}_\theta}{\hat{r}} \frac{\partial \hat{\rho} \hat{u}_\theta}{\partial \hat{\theta}} + \frac{\hat{\rho} \hat{u}_\theta \hat{u}_r}{\hat{r}} + \hat{u}_y \frac{\partial \hat{\rho} \hat{u}_\theta}{\partial \hat{y}} = - \left( \frac{1}{\hat{r}} \frac{\partial \hat{p}}{\partial \hat{\theta}} \right) + \left( \frac{\partial}{\partial \hat{y}} \left( \hat{\mu} \frac{\partial \hat{u}_\theta}{\partial \hat{y}} \right) \right) + 2 \hat{\rho} \hat{u}_r \omega_y + \hat{\rho} \hat{r} \dot{\omega}_y$$

The equation below is the boundary layer equation for the tangential velocity component of the rotating cone in axial flow. It has similarities with the equation for the translating plate.

$$\hat{\rho} \left[ \frac{\partial \hat{V}_3}{\partial t} + \frac{\hat{V}_1}{h_1} \frac{\partial \hat{V}_3}{\partial \hat{u}_1} + \frac{\hat{V}_2}{h_2} \frac{\partial \hat{V}_3}{\partial \hat{u}_2} + \frac{\hat{V}_3}{h_3} \frac{\partial \hat{V}_3}{\partial \hat{u}_3} - \hat{V}_1 \left( \frac{\hat{V}_1}{h_1 h_3} \frac{\partial h_1}{\partial \hat{u}_3} - \frac{\hat{V}_3}{h_1 h_3} \frac{\partial h_3}{\partial \hat{u}_1} \right) + \hat{V}_2 \left( \frac{\hat{V}_3}{h_2 h_3} \frac{\partial h_2}{\partial \hat{u}_1} - \frac{\hat{V}_2}{h_2 h_3} \frac{\partial h_2}{\partial \hat{u}_3} \right) \right]$$

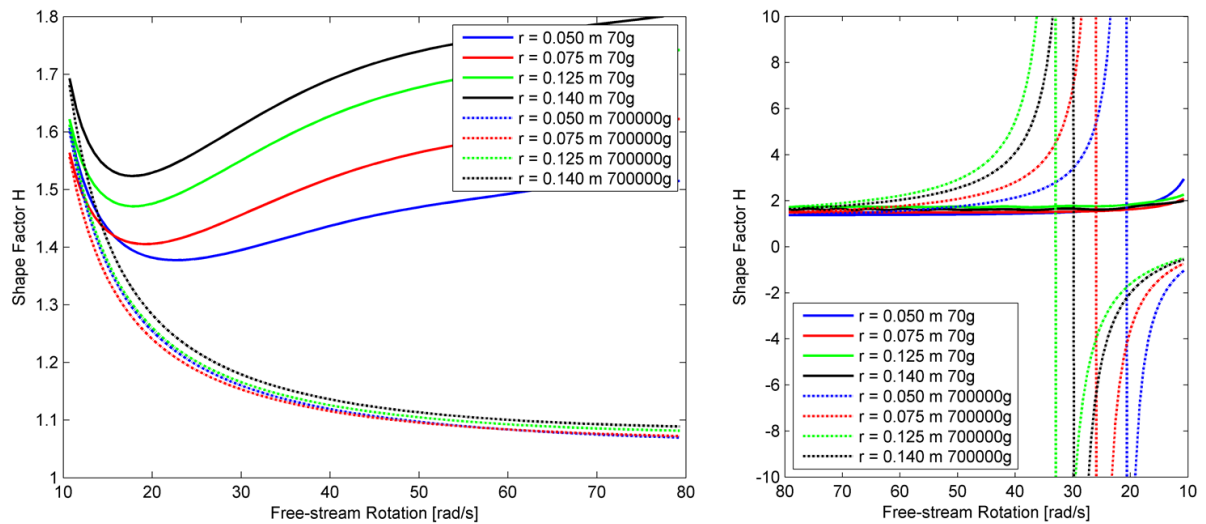
$$= - \left( \frac{1}{h_1} \frac{\partial \hat{p}}{\partial \hat{u}_3} \right) + \left[ \frac{1}{h_2} \frac{\partial}{\partial \hat{u}_2} \hat{\mu} \frac{h_3}{h_2} \frac{\partial \hat{u}_2}{\partial \hat{u}_3} \frac{\hat{V}_3}{h_3} \right]$$

$$+ \hat{\rho} \left[ 2 \hat{V}_1 \omega_2 - 2 \hat{V}_2 \omega_1 + \hat{u}_3 (\omega_2^2 + \omega_1^2) + \hat{u}_1 \omega_2 - \hat{u}_2 \omega_1 + 2 V_{e1} \omega_2 - 2 V_{e2} \omega_1 \right]$$

The shape factor behaves in a similar manner for all cases. An example set is shown in *Figure 10.4* for accelerating and decelerating conditions.

CHAPTER 10. CONCLUSION

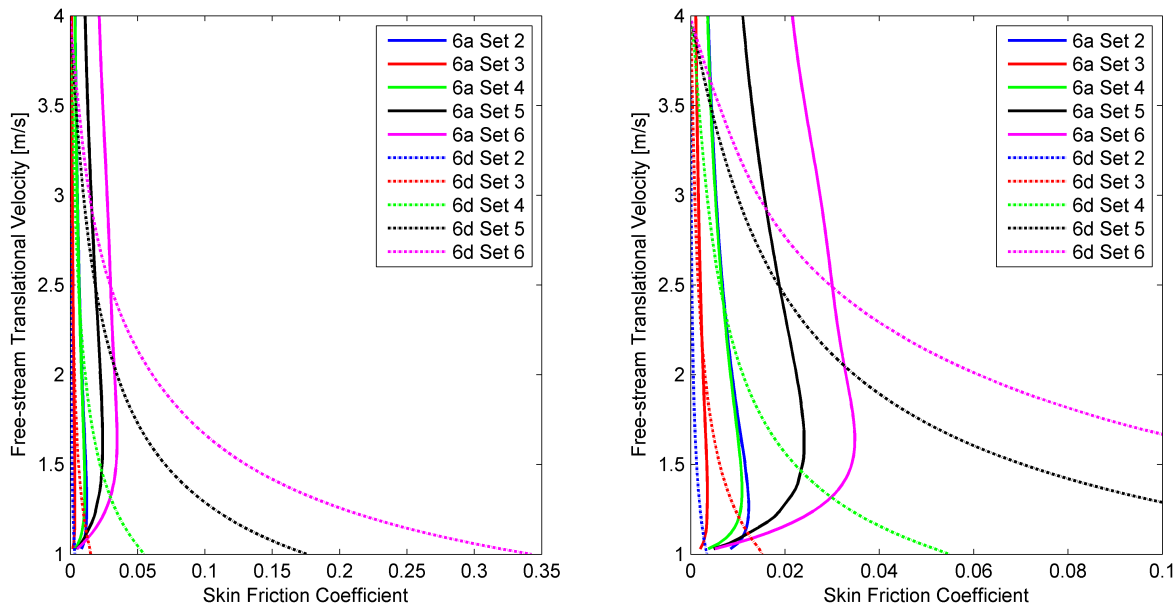
Figure 10.4: Results of the tangential shape factor response for acceleration (left) and deceleration (right) events on a rotating disk



The higher acceleration cases is monotonically decreasing and approximates a minimum value. In contrast, the lower acceleration cases reach a minimum value very early in the event. It then recovers the initial value and approaches an asymptotic shape factor value. In deceleration the shape factor displays a discontinuity. The shape factor approaches positive infinity at this point. A discontinuity in the mathematics is an indication that the flow regime has changed. It is therefore postulated that the discontinuity is the point where the flow becomes turbulent.

The skin friction coefficient behaviour is the same for all cases analysed. A sample of the behaviour is shown in (*Figure 10.5*). In acceleration the skin friction coefficient value first increase. It reach a maximum after which it is reduced. An asymptote is approximated as the acceleration event continues. Boundary layers in acceleration has a cooling effect on the wall due to a lower skin friction which results in a lower skin drag value. The skin friction coefficient in deceleration is divergent and continues to increase. The higher skin drag is responsible for the heating effect on the wall of objects in deceleration.

Figure 10.5: Skin Friction Coefficient Comparisons for Arbitrary Motion on the Cone

 **Outcome 3**

Insight into the response of the boundary layer to arbitrary motion.

## 10.2 Suggested Further Work

This research provides a basis for further work in the field of boundary layers of objects in arbitrary motion. Additional commended research are divided into three categories; Mathematical Research, Code Improvements and Numerical Research.

### 10.2.1 Mathematical Research

Continuation of this research will greatly benefit from analysis of the boundary layer equations using asymptotic methods (Cathalifaud et al. [98], Hamouda [99], Lundgreny [100]). The aim will be to obtain a semi-analytical solution for boundary layers in arbitrary motion against which the numerical results can be compared. This will further assist in defining an acceleration parameter to characterize the similarities in the flow for different response types. The acceleration limits that divide the behaviour according to response types can hence be determined. Asymptotic analysis is also a method to study disturbance propagation in the boundary layer. Examples include, transition of the boundary layer due to Tollmien-Schlichting waves, Taylor-Görtler vortices and the Kelvin-Helmholtz instability in separated flows (Dovgal et al. [101, 102]). Studies could not be found where the effect of arbitrary motion on these disturbances are analytically investigated. To investigate the shock wave boundary layer interaction of supersonic and hypersonic flows analytically, it is suggested that the method of characteristics be augmented to account for arbitrary motion.

### 10.2.2 Improvements to the Code

There are a number of ways in which the current solver can be improved upon. The solver does not make provision for flow with a moving axis. Implementing the additional term is simple. It involves inclusion of the additional unsteady term in the source terms and accounting for the movable axis by specifying a centre of gravity on the object under analysis. However, in external ballistic applications the Magnus force acts through the centre of pressure. Implementing a movable axis might influence the manner in which the Magnus source term is implemented. A pressure-based solver was used in this study. Pressure-based solvers were not created for the resolution of supersonic and hypersonic flows (Ferziger and Peric [92], Versteeg and Malalasekera [69]). Although, it has been augmented in recent years and applied to the higher flow regime (Menter et al. [103]). It is advisable that a density based solver be developed for the analysis of high velocity flows (Xisto et al. [104]). These types of solvers are able to capture the shock wave propagation more accurately with fewer computational nodes than other methods. A study with the aim to numerically investigate disturbance propagation in turbulent boundary layers will benefit from alternative simulation techniques such as Large Eddy Simulation (LES) or Direct Numerical Simulation (DNS) (Hattori et al. [105], Spalart et al. [106], Orellano and Wengle [107]). The Reynolds Average Navier-Stokes (RANS) methodology currently employed can easily be extended to include reacting flows, two-phase flows and porous flows. These have specific application in the defence environment for air-breathing engines and internal ballistic analysis.

### 10.2.3 Numerical Research

Further investigation can be done to numerically define the limits of the response types as proposed in this research. Accelerations and decelerations of 70g to 700 000g were imposed on the flow field. The exact limits of transition from one response to the other were not defined explicitly. Furthermore, Response Type I was not invoked for the disk case and the cone only displayed a Type III response. More simulations are required to predict the onset of response types.

The solver was validated in this case for laminar boundary layers. The modularity of OpenFOAM allows for the immediate inclusion of turbulence models and the subsequent validation of low velocity turbulent cases. One equations models, such as a Spalart-Almaras, and two equations models, such as the  $\kappa - \epsilon$ -model and the  $\kappa - \omega$ -model can be directly implemented without changes to the source code (Ferziger and Peric [92], Versteeg and Malalasekera [69]). The parameters in these turbulence models are scalar values and therefore invariant under transformation.

Improvements to the code suggested in the previous section will allow for more complex simulations. The cases can be extended to the supersonic and hypersonic regimes. Disturbance formation and propagation can be studied with slight alterations to the code. More complex flows, such as turbulent combustion in air breathing engines, porous flow inside large calibre gun chambers and two-phase flow in rocket engines can be studied using this methodology.

The graph of Wazzan et al. [78] were generated for steady conditions. The analytical and numerical studies can be used to generate a similar graph for unsteady conditions. This will assist in the



classification of flow regimes for arbitrary motion.

### 10.3 Alternative Applications

The methods used in this research, were developed to study the behaviour of the boundary layer to arbitrary motion. There are however a number of unforeseen alternative applications where it can be used.

The down-wash of a helicopter hovering above a ship's flight deck has been widely studied (Schau et al. [108], Scott et al. [109]). The computational requirement of such a study is very expensive since a movable mesh is required. Constant re-meshing of the grid does not allow for accurate resolution of the boundary layer on the helicopter blades. The code developed in this study is capable resolving such a domain with a stationary grid. Not only does this significantly reduce the computational time required, but it also allows for proper resolution of the boundary layer around the blades. Similarly, studying the effect of the helicopter blades on each other, specifically the disturbances generated by each blade, can be done with relative ease. This can also be employed in studies where the effect of a ship's body on the propeller is investigated (Martin et al. [110], Shin et al. [111]). In military applications the ship's propeller must be optimized to generate as little cavitation as possible. Cavitation damages the propeller blades and generates noise which an opposing force can use to track the ship. Again, as in the case of the helicopter, a manoeuvring ship can be studied with a stationary grid and fine resolution of the boundary layer on the propeller. The research methods can be used for unsteady solutions of the start-up or shut-down of turbo-machines (Rainbird et al. [112], C.Trivedi et al. [113]). The majority of computational studies in turbo-machines only considers steady conditions. It was seen in the body of this thesis that the flow history plays an important part in the unsteady boundary layer of an object. The velocity profiles for unsteady condition on turbine blades, wind turbines and other rotating machines can be determined.

Advanced boundary layer research can be conducted with the methods developed in this thesis. Since the behaviour of the boundary layer can be predicted, it is of use in flow control studies. Stability analysis, disturbance propagation and transition studies can also be done.

Fluid structure interaction studies requires input from the fluid flow and more specifically the boundary layer. More realistic prediction of the boundary layer flow will result in enhanced simulations for structural response. This is applicable in flutter analysis and development of intelligent materials.



UNIVERSITEIT VAN PRETORIA  
UNIVERSITY OF PRETORIA  
YUNIBESITHI YA PRETORIA

## Bibliography

- [1] R.T. Biedron and J.L. Thomas.  
Recent enhancements to the fun3d flow solver for moving mesh applications.  
*AIAA Paper 1360*, 2009.
- [2] A. Gardi.  
*Moving Reference Frame and Arbitrary Lagrangian Eulerian Approaches for the Study of Moving Domains in Typhon*.  
PhD thesis, Politecnico di Milano, Spain, 2011.
- [3] Alejandro Cesar Limache.  
*Aerodynamic Modeling using Computational Fluid Dynamics and Sensitivity Equations*.  
PhD thesis, Virginia Polytechnic Institute and State University, 2000.  
URL <http://scholar.lib.vt.edu/theses/available/etd-04202000-14540007/>.
- [4] O. Inoue, T. Sakari, and M. Nishida.  
Focusing shock waves generated by an accelerating projectile.  
*Fluid Dynamics Research*, 21:403--416, 1997.
- [5] H. Roohani and B.W Skews.  
Unsteady aerodynamic effects experienced by aerofoils during acceleration and retardation.  
*Proceedings of the Institution of Mechanical Engineers, Part G: Journal of Aerospace Engineering* 222, 631–636, 2008.
- [6] G.K. Batchelor.  
*An Introduction to Fluid Dynamics*.  
Cambridge University Press, 1st edition, 1967.
- [7] H.P. Greenspan.  
*The Theory of Rotating Fluids*.  
Cambridge University Press, 1st edition, 1968.
- [8] J.L. Meriam and L.G. Kraige.  
*Engineering Mechanics Dynamics*.  
John Wiley and Sons Inc, 5th edition, 2003.

## BIBLIOGRAPHY

---

- [9] F.M. White.  
*Viscous Fluid Flow*.  
McGraw-Hill, 3rd edition, 2006.
- [10] J.B. Hart, R.E. Miller, and R.L. Mills.  
A simple geometric model for visualizing the motion of a Foucault pendulum.  
*American Journal of Physics*, 55:67--70, 1987.
- [11] W.B. Somerville.  
The description of Foucault's pendulum.  
*Quarterly Journal of the Royal Astronomical Society*, 13:40--62, 1972.
- [12] A.O. Persson.  
The Coriolis effect: Four centuries of conflict between common sense and mathematics, part I: A history to 1885.  
Department of Research and Development, Swedish Meteorological and Hydrological Institute, Norrköping, Sweden, Lecture Notes on History of Meteorology, 2005.
- [13] G. Magnus.  
On the deviation of projectile and on a sinking phenomenon among rotating bodies.  
*Annalen der Physik*, 164(1):1--29, 1853.
- [14] M. Costello and J. Sahu.  
Using computational fluid dynamic/rigid body dynamic results to generate aerodynamic models for projectile flight simulation.  
*Journal of Aerospace Engineering*, 222:1067--1079, 2008.
- [15] J. DeSpirito and K. Heavy.  
CFD computation of Magnus moment and roll damping moment of a spinning projectile.  
*Proceedings of the AIAA Atmospheric Flight Mechanics Conference and Exhibit*, 2004.
- [16] J. Sahu.  
Time-accurate numerical prediction of free-flight aerodynamics of a finned projectile.  
*Journal of Spacecraft and Rockets*, 45(5):946--954, 2008.
- [17] J. Sahu.  
Numerical computations of dynamic derivatives of a finned projectile using a time-accurate CFD method.  
*Proceedings of the AIAA Atmospheric Flight Mechanics Conference and Exhibit*, 2007.
- [18] S.I. Siltou.  
Navier-Stokes computations for a spinning projectile from subsonic to supersonic speeds.  
*Journal of Spacecraft and Rockets*, 42(2):223--231, 2005.

- [19] B.S. Davis, B.J. Guidos, and T.E. Harkins.  
Complementary roles of spark range and onboard free-flight measurements of projectile development.  
*ARL Technical Report ARL-TR-4910*, 2009.
- [20] T. Pettersson, R. Buretta, and D. Cook.  
Aerodynamics and flight stability for a course corrected artillery round.  
*Proceedings of the 23rd International Symposium on Ballistics*, 2007.
- [21] P. Wernert, F. Leopold, L. Lehmann, K. Baer, A. Reindler, D. Bidino, and J. Juncker.  
Wind tunnel tests and open-loop trajectory simulations for a 155 mm canards guided spin stabilized projectile.  
*Proceedings of the AIAA Atmospheric Flight Mechanics Conference and Exhibit*, 2008.
- [22] I.M.A. Gledhill, K. Forsberg, P. Eliasson, J.J. Baloyi, and J. Nordström.  
Investigation of acceleration effects on missile aerodynamics using computational fluid dynamics.  
*Aerospace Science and Technology*, 13:197--203, 2009.
- [23] A. Kageyama and M. Hyodo.  
Eulerian derivation of the coriolis force.  
*Geochemistry, Geophysics and Geosystems*, 7(2):1--5, 2006.
- [24] J. Garibaldi, M. Storti, L. Battaglia, and J. D'Elia.  
Numerical simulations of the flow around a spinning projectile in subsonic regime.  
*Latin American Applied Research*, 38:241--247, 2008.
- [25] K. Forsberg.  
Treatment of a moving reference frame for discretised ns equations.  
*The Swedish Aeronautical Institute, Flygtekniska Försöksanstalten*, 2000.
- [26] P.F. Brinich and H.E. Neumann.  
Some characteristics of turbulent boundary layers in rapidly accelerated flows.  
*NASA Technical Note D-6587*, 1971.
- [27] J. Yuan and U. Piomelli.  
Large-eddy simulation of accelerating boundary layers over rough surfaces.  
*Proceedings of the International Symposium of Turbulence and shear Flow Phenomena*, 2011.
- [28] L.H. Back.  
Accelerating and cooling effects in laminar boundary layers - subsonic, transonic and supersonic speeds.  
*AIAA Journal*, 8(4):974--802, 1970.

## BIBLIOGRAPHY

---

- [29] M. Escudier, A. Abdel-Hameed, M. Johnson, and C. Sutcliffe.  
Laminarisation and re-transition of a turbulent boundary layer subjected to favourable pressure gradient.  
*Experiments in Fluids*, 25:491--502, 1998.
- [30] D.R. Webster and J.K. Eaton.  
The effect of three-dimensionality on a laminarizing boundary layer.  
*Physics of Fluids*, 7:1782--1784, 1995.
- [31] S. Pirozzoli, J. Larsson, W. W. Nichols, M. Bernardini, B.E. Morgan, and S.K. Lele.  
Analysis of unsteady effects in shock/boundary layer interactions.  
*Proceedings of the Summer Program 2010, Centre for Turbulence Research, Stanford University*, 2010.
- [32] F.K. Moore.  
Unsteady laminar boundary-layer flow.  
*NACA Technical Note 2471*, 1951.
- [33] J. Vlegaar.  
Laminar boundary-layer behaviour on continuous, accelerating surfaces.  
*Chemical Engineering Science*, 32:1517--1525, 1977.
- [34] L. Back and R. Cuffel.  
Compressible laminar boundary layers with large acceleration and cooling.  
*AIAA Journal*, 14:968--971, 1976.
- [35] V.V. Bogolepov and I.I. Lipatov.  
Effect of compressibility on the development of Taylor-Görtler vortices at high Reynolds numbers.  
*Journal of Fluid Dynamics*, 32:28--37, 1997.
- [36] L.N. Dala and I.I. Lipatov.  
Görtler vortices development in compressible flow with streamline curvature.  
*Proceedings of EUROMECH 403*, 1999.
- [37] H. Blasius.  
Grenzschichten in Flüssigkeiten mit kleiner Reibung.  
*Z. Angew. Math. Phys.*, 56:1--37, 1908.
- [38] J. Kay.  
The transient temperature distribution in a wing flying at supersonic speeds.  
*Journal of Aeronautical Science*, 17(12):787--807, 1950.
- [39] A. Samad and S.J. Garrett.

- On the laminar boundary-layer flow over rotating spheroids.  
*International Journal of Engineering Science*, 48:2015--2027, 2010.
- [40] Y.P. Kohama.  
Three-dimensional boundary layer transition study.  
*Current Science*, 79(6):800--807, 2000.
- [41] T. von Karman.  
Über laminare und turbulente reibung.  
*Z. Angew. Math. Phys.*, 1:233--252, 1921.
- [42] H. Schlichting.  
*Boundary-Layer Theory*.  
McGraw-Hill, 3rd edition, 1968.
- [43] S. Imayama.  
Studies of the rotating-disk boundary-layer flow.  
Technical Reports from the Royal Institute of Technology, Stockholm, Sweden,  
[urlhttps://www.diva-portal.org/smash/get/diva2:781517/SUMMARY01.pdf](https://www.diva-portal.org/smash/get/diva2:781517/SUMMARY01.pdf), 2014.
- [44] P.J. Schmid and D.S. Henningson.  
*Stability and Transition in Shear Flows*.  
Springer, 1st edition, 2001.
- [45] P. Ram.  
Revolving ferrofluid flow under the influence of mfd viscosity and porosity with rotating disk.  
*Journal of Electromagnetic Analysis and Applications*, 3(9):378--386, 2011.
- [46] R. Kobayashi, Y. Kohama, and C. Takamadate.  
Spiral vortices in boundary layer transition regime on a rotating disk.  
*Acta Mechanica*, 35(1):71--82, 1980.
- [47] F.Y. Moulin and J.B. Flór.  
On the spin-up by a rotating disk in a rotating stratified fluid.  
*Journal of Fluid Mechanics*, 516:155--180, 2004.
- [48] F. Zoueshtiagh, R. Ali, A.J. Colley, P.J. Thomas, and P.W. Carpenter.  
Laminar-turbulent boundary-layer transition over a rough rotating disk.  
*Journal of Fluid Mechanics*, 15(8):2441--2444, 2003.
- [49] H.A. Attia.  
Steady flow over a rotating disk in porous medium with heat transfer.  
*Nonlinear Analysis: Modelling and Control*, 14(1):21--26, 2009.

## BIBLIOGRAPHY

---

- [50] J.H. Harris, P.J. Thomas, and S.J. Garret.  
On the stability of flows over rough rotating disks.  
*Proceedings of the 42nd AIAA Fluid Dynamics Conference and Exhibit*, 2012.
- [51] M.E. Siddiqui.  
*Experimental Study of Natural and Forced Instabilities and Transition of a Rotating-Disk Boundary-Layer Flow*.  
PhD thesis, L'Ecole Centrale de Lyon, France, 2011.
- [52] S.J. Garret and N. Peake.  
The absolute instability of the boundary layer on a rotating cone.  
*European Journal of Mechanics B/Fluids*, 26:344--353, 2007.
- [53] Z. Hussain, S.J. Garrett, and S.O. Stephen.  
Centrifugal instability over a rotating cone.  
*Proceedings of the 19th Australasian Fluid Mechanics Conference*, 2014.
- [54] A. Kargar and K. Mansour.  
Experimental investigation of boundary layer transition of rotating cones in axial flow in 0 and 35 degrees angle of attack.  
*Proceedings of the 10th Symposium on Flow Visualization and Image Processing*, 2015.
- [55] R. Kobayashi, Y. Kohama, and M. Kurosawa.  
Boundary-layer transition on a rotating cone in axial flow.  
*Journal of Fluid Mechanics*, 127:341--352, 1983.
- [56] P.D. Towers and S.J. Garrett.  
Similarity solutions of compressible flow over a rotating cone with surface suction.  
*Thermal Science*, 20(2):516--528, 2016.
- [57] K. Mansour and A. Kargar.  
An experimental investigation on rotating cones in axial flow by hot wire anemometer and smoke visualization.  
*Proceedings of the 11th International Conference of Fluid Dynamics*, 2013.
- [58] J.D. Anderson.  
*Fundamentals of Aerodynamics*.  
McGraw-Hill, 3rd edition, 2001.
- [59] J.C. Tannehill, D..A. Anderson, and R.H. Pletcher.  
*Computational Fluid Mechanics and Heat Transfer*.  
Taylor and Francis Publishers, 2nd edition, 1997.



- [60] D. Kleppner and R.J. Kolenkow.  
*An Introduction to Mechanics.*  
Cambridge University Press, 1st edition, 2010.
- [61] J.L. McCauley.  
*Classic Mechanics, Transformations, Flows, Integrable and Chaotic Dynamics.*  
Cambridge University Press, 1st edition, 1997.
- [62] R.A. Diaz, W.J. Herrera, and D.A. Manjarres.  
Work and energy in inertial and non inertial reference frames.  
*American Journal of Physics*, 77(3):270, 2009.
- [63] A.T. Dolovich, e.J. Llewellyn, G.J. Sofko, and Y.P. Wang.  
The coriolis effect - what's going on?  
*Proceedings of the Canadian Engineering Education Association Conference*, 2012.
- [64] S.T. Thornton and J.B. Marion.  
*Classical Dynamics of Particles and Systems.*  
Thomson, Brooks and Cole Publishers, 5th edition, 2004.
- [65] R. Cayzac, E. Carette, P. Denis, and P. Guillen.  
Magnus effect: Physical origins and numerical prediction.  
*Proceedings of the 26th International Symposium on Ballistics*, 2011.
- [66] S.I. Siltou.  
Navier-stokes predictions of aerodynamic coefficients and dynamic derivatives of a 0.5 cal projectile.  
*Proceedings of the 29th AIAA Applied Aerodynamics Conference*, 2011.
- [67] P. Weinacht, W.B. Sturek, and L.B. Schiff.  
Navier-stokes predictions of pitch-damping for axisymmetric shell using steady coning motion.  
*Army Research Laboratory Report ARL-TR-575*, 1994.
- [68] J. Steward.  
*Calculus.*  
Brooks/Cole Publishing Company, 4th edition, 1999.
- [69] H.K. Versteeg and W. Malalasekera.  
*An Introduction to Computational Fluid Mechanics.*  
Longman Scientific and Technical, 1st edition, 1995.
- [70] R. Aris.  
*Vectors, Tensors and the Basic Equations of Fluid Mechanics.*  
Dover Publications Inc, 1st edition, 1962.

## BIBLIOGRAPHY

---

- [71] K.A. Hoffmann and S.T. Chiang.  
*Computational Fluid Dynamics Volume I.*  
Engineering Education System, 4th edition, 2000.
- [72] D.J. Griffiths.  
*An Introduction to Electrodynamics.*  
Prentice Hall, 3rd edition, 1999.
- [73] C.D.H. Williams.  
Curvilinear coordinate systems.  
University of Exeter, School of Engineering, Mathematics and Physical Sciences, Course Notes PHY2206, url<https://newton.ex.ac.uk/teaching/CDHW/EM/CW970129-3.pdf>, 1995.
- [74] R. Marskar.  
Vector calculus and continuum conservation equations in curvilinear orthogonal coordinates.  
Norwegian University of Science and Technology, Department of Physics, Course Notes TEP4105, url<http://www.ivt.ntnu.no/ept/fag/tep4105/pensum/pensum/curv.pdf>, 2008.
- [75] Anon.  
Orthogonal curvilinear coordinates.  
University of California Santa Barbara, School of Engineering, Course Notes ChE230A, url-<http://www.engineering.ucsb.edu/baronp/ChE230A/ortho-curvilinear-coords.pdf>, 2011.
- [76] X. Liu, Y. Ji, and Q. Liang.  
Expression of strain tensor in orthogonal curvilinear coordinates.  
*Geodesy and Geodynamics*, 1(1):48--56, 2010.
- [77] J.R. Kee, M.E. Coltrin Ji, and P. Glarborg.  
*Chemically Reacting Flow: Theory and Practice.*  
Wiley and Sons Ltd, 1st edition, 2003.
- [78] A.R. Wazzan, C. Gasley, and A.M.O. Smith.  
H-rx method for prediction transition.  
*AIAA Journal*, 19(6):810--812, 1981.
- [79] S.V. Patankar.  
*Numerical Heat Transfer and Fluid Flow.*  
Hemisphere Publishing Corporantion, 1st edition, 1980.
- [80] D.F. Rogers.  
*Laminar Flow Analysis.*  
Cambridge University Press, 1st edition, 1992.

- [81] A. Mager.  
*Laminar Boundary Layer Problems Associated with Flow Through Turbomachines.*  
PhD thesis, California Institute of Technology, California, 1953.
- [82] V.V. Bogdanova.  
Universal equations of the laminar boundary layer on a rotating blade.  
*Fluid Dynamics*, 6(2):251--259, 1971.
- [83] H.A. Dwyer.  
Calculation of unsteady and three dimensional boundary layer flows.  
*AIAA Journal*, 11(6):773--774, 1973.
- [84] Anon.  
Navier-stokes equations presentation.  
Indian Institute of Technology Madras, CH2030 Momentum Transfer, Lecture Series url-  
<http://www.che.iitm.ac.in/srinivar/FM/>, 2005.
- [85] H. Dumitrescu, V. Cardos, and Dumitrache A.  
Modelling of inboard stall delay due to rotation.  
*Journal of Physics: Conference Series*, 75, 2007.
- [86] G.G. Martinez, J.N. Sorensen, and Shen W.Z.  
Three-dimensional laminar boundary layer study on a rotating wind turbine blade.  
*Journal of Physics: Conference Series*, 75, 2007.
- [87] R.J. Monaghan.  
*An Approximate Solution of the Compressible, Laminar Boundary Layer on a Flat Plate.*  
Her Majesty's Stationary Office, London, 1953.
- [88] OpenFOAM.  
Official website.  
OpenFOAM, url<http://www.openfoam.com/>, 2016.
- [89] GNU.  
Official website.  
GNU General Public License, url<http://www.gnu.org/licenses/gpl-3.0.en.html>, 2016.
- [90] CD-adapco.  
Official website.  
Star-CD, url<http://www.cd-adapco.com/products/star-cd>, 2016.
- [91] ANSYS.  
Official website.  
Fluent, url<http://www.ansys.com/Products/Fluids/ANSYS-Fluent>, 2016.

BIBLIOGRAPHY

---

- [92] J.H. Ferziger and M. Peric.  
*Computational Methods for Fluid Dynamics*.  
Springer, 3rd edition, 2001.
- [93] R.E. Sonntag and C. Borgnakke.  
*Fundamentals of Thermodynamics*.  
Wiley and Sons Inc, 1st edition, 2001.
- [94] C.T. Crowe, D.F. Elger, and J.A. Roberson.  
*Engineering Fluid Mechanics*.  
Wiley and Sons, 7th edition, 2001.
- [95] R. Kobayashi and Y. Kohama.  
Boundary-layer transition on a rotating cone in axial flow.  
*Journal of Fluid Mechanics*, 127:341--352, 1983.
- [96] S.G. Chefranov.  
Linear eckman friction in the mechanism of the cyclone-anticyclone vortex asymmetry and in a new theory of rotating superfluid.  
A. M. Obukhov Institute of Atmospheric Physics RAS, Moscow, Russia,  
[urlhttp://www.cardiometry.net/issues/no4-may-2014/new-theory-of-rotating-superfluid](http://www.cardiometry.net/issues/no4-may-2014/new-theory-of-rotating-superfluid), 2014.
- [97] A. Mager.  
Three-dimensional laminar boundary layer with small cross flow.  
*Journal of the Aeronautical Sciences*, 21(12):1, 1954.
- [98] P. Cathalifaud, J. Mauss, and J. Cousteix.  
Nonlinear aspects of high reynolds number channel flows.  
*European Journal of Mechanics - B/Fluids*, 29(4):0997--7546, 2010.
- [99] M. Hamouda.  
Boundary layers for the navier-stokes equations : Asymptotic analysis.  
*International Conference on Boundary and Interior Layers*, 2006.
- [100] T. S. Lundgreny.  
Asymptotic analysis of the constant pressure turbulent boundary layer.  
*Center for Turbulence Research Annual Research Briefs*, 2006.
- [101] A.V. Dovgal, V.V. Kozlov, and A. Michalke.  
Laminar boundary layer separation: Instability and associated phenomena.  
*Progress in Aerospace Sciences*, 30(1):61--94, 1994.
- [102] A.V. Dovgal, V.V. Kozlov, and A. Michalke.

- On the origins of unsteadiness and three-dimensionality in a laminar separation bubble.  
*Philosophical Transactions of the Royal Society A*, 385:3229--3246, 2000.
- [103] F. Menter, P.F. Galpin, T. Esch, M. Kuntz, and C. Berner.  
Cfd simulations of aerodynamics flows with a pressure-based method.  
*Proceedings of the 24th International Congress of the Aeronautical Sciences*, 2004.
- [104] C.M. Xisto, J.C. Pascoa, P.J. Oliveira, and D.A. Nicolini.  
A hybrid pressure-density-based algorithm for the euler equations at all mach number regimes.  
*International Journal for Numerical Methods in Fluids*, 70(8):961--976, 2012.
- [105] H. Hattori, S. Yamada, M. Tanaka, T. Houra, and Y. Nagano.  
Dns, les and rans of turbulent heat transfer in boundary layer with suddenly changing wall thermal conditions.  
*International Journal of Heat and Fluid Flow*, 41:34--44, 2013.
- [106] P.R. Spalart, W.H. Jou, M. Strelets, and S.R. Allmaras.  
Comments of the feasibility of les for wings, and on a hybrid rans/les approach.  
*International Conference of DNS/LES*, 1997.
- [107] A. Orellano and H. Wengle.  
Numerical simulation (dns ad les) of manipulated turbulent boundary layer over a surface-mounted fence.  
*European Journal of Mechanics - B/Fluids*, 19(5):765--788, 2000.
- [108] K.A. Schau, G. Gaonkar, and S. Polsky.  
Rotorcraft downwash impact on ship airwake: Statistics, modelling and simulation.  
*The Aeronautical Journal*, 120(1229):765--788, 2016.
- [109] P. Scott, M. White, and I. Owen.  
Unsteady cfd modelling of ship engine exhaust gases and over-deck air temperature and the implications for maritime helicopter operations.  
*Proceedings of the AHS 71st Annual Forum*, 2015.
- [110] J. Martin, M Thad, and P.M. Pablo.  
Submarine manoeuvres using direct overset simulation of appendages and propeller and coupled cfd/potential flow propeller solver.  
*Journal of Ship Research*, 59(1):31--48, 2015.
- [111] K.W. Shin, P.B. Pelle, and P. Andersen.  
Methods for cavitation prediction on tip-modified propellers in ship wake fields.  
*Proceedings of the 4th International Symposium on Marine Propulsors*, 2015.

## BIBLIOGRAPHY

---

- [112] J.M. Rainbird, E. Ferrer, J. Peiro, and J.M.R. Graham.  
Vertical-axis wind turbine start-up modelled with a high-order numerical solver.  
*CFD for Wind and Tidal Offshore Turbines, Springer Tracts in Mechanical Engineering*, 2015.
- [113] C.Trivedi, M.J. Cervantes, B.K. Gandhi, and G.O. Dahlhaug.  
Experimental investigation of transient pressure variations in a high head model francis turbine during start-up and shutdown.  
*Journal of Hydrodynamics*, 26(2):277--290, 2014.



## Proof of Identities

The identities below are referred to in the main text of this thesis.

### Identity 1

$$\begin{aligned}
 & \nabla \cdot (\mathbf{x} \wedge \Omega) \\
 &= \frac{\partial}{\partial x_i} [x_j \Omega_k - x_k \Omega_j] \mathbf{i} \\
 & \quad - \frac{\partial}{\partial x_j} [x_i \Omega_k - x_k \Omega_i] \mathbf{j} \\
 & \quad + \frac{\partial}{\partial x_k} [x_i \Omega_j - x_j \Omega_i] \mathbf{k} \\
 &= 0
 \end{aligned}$$

### Identity 2

$$\begin{aligned}
 & \nabla \cdot (\mathbf{x} \wedge \dot{\Omega}) \\
 &= \frac{\partial}{\partial x_i} [x_j \dot{\Omega}_k - x_k \dot{\Omega}_j] \mathbf{i} \\
 & \quad - \frac{\partial}{\partial x_j} [x_i \dot{\Omega}_k - x_k \dot{\Omega}_i] \mathbf{j} \\
 & \quad + \frac{\partial}{\partial x_k} [x_i \dot{\Omega}_j - x_j \dot{\Omega}_i] \mathbf{k} \\
 &= 0
 \end{aligned}$$

APPENDIX A. PROOF OF IDENTITIES

---

**Identity 3**

$$\begin{aligned}
 & \nabla^2(\mathbf{x} \wedge \Omega) \\
 &= \left( \frac{\partial^2}{\partial x_i^2} + \frac{\partial^2}{\partial x_j^2} + \frac{\partial^2}{\partial x_k^2} \right) [x_j \Omega_k - x_k \Omega_j] \mathbf{i} \\
 & - \left( \frac{\partial^2}{\partial x_i^2} + \frac{\partial^2}{\partial x_j^2} + \frac{\partial^2}{\partial x_k^2} \right) [x_i \Omega_k - x_k \Omega_i] \mathbf{j} \\
 & + \left( \frac{\partial^2}{\partial x_i^2} + \frac{\partial^2}{\partial x_j^2} + \frac{\partial^2}{\partial x_k^2} \right) [x_i \Omega_j - x_j \Omega_i] \mathbf{k} \\
 &= 0
 \end{aligned}$$

**Identity 4**

$$\begin{aligned}
 & \nabla^2(\mathbf{x} \wedge \dot{\Omega}) \\
 &= \left( \frac{\partial^2}{\partial x_i^2} + \frac{\partial^2}{\partial x_j^2} + \frac{\partial^2}{\partial x_k^2} \right) [x_j \dot{\Omega}_k - x_k \dot{\Omega}_j] \mathbf{i} \\
 & - \left( \frac{\partial^2}{\partial x_i^2} + \frac{\partial^2}{\partial x_j^2} + \frac{\partial^2}{\partial x_k^2} \right) [x_i \dot{\Omega}_k - x_k \dot{\Omega}_i] \mathbf{j} \\
 & + \left( \frac{\partial^2}{\partial x_i^2} + \frac{\partial^2}{\partial x_j^2} + \frac{\partial^2}{\partial x_k^2} \right) [x_i \dot{\Omega}_j - x_j \dot{\Omega}_i] \mathbf{k} \\
 &= 0
 \end{aligned}$$



### Identity 5

$$(\mathbf{c} \cdot \nabla)(\mathbf{x} \wedge \Omega) = \mathbf{c} \wedge \Omega$$

$$\begin{aligned} LH &= (\mathbf{c} \cdot \nabla)(\mathbf{x} \wedge \Omega) \\ &= (c_i \frac{\partial}{\partial x_i} + c_j \frac{\partial}{\partial x_j} + c_k \frac{\partial}{\partial x_k})[(x_j \Omega_k - x_k \Omega_j)\mathbf{i} \\ &\quad - (x_i \Omega_k - x_k \Omega_i)\mathbf{j} + (x_i \Omega_j - x_j \Omega_i)\mathbf{k}] \\ &= (c_j \Omega_k - c_k \Omega_j)\mathbf{i} - (c_i \Omega_k - c_k \Omega_i)\mathbf{j} \\ &\quad + (c_i \Omega_j - c_j \Omega_i)\mathbf{k} \end{aligned}$$

$$(\mathbf{c} \cdot \nabla)(\mathbf{x} \wedge \Omega) = \mathbf{c} \wedge \Omega$$

$$\begin{aligned} RH &= \mathbf{c} \wedge \Omega \\ &= (c_j \Omega_k - c_k \Omega_j)\mathbf{i} - (c_i \Omega_k - c_k \Omega_i)\mathbf{j} \\ &\quad + (c_i \Omega_j - c_j \Omega_i)\mathbf{k} \end{aligned}$$

$$LH = RH$$

### Identity 6

$$(\mathbf{c} \cdot \nabla)(\mathbf{x} \wedge \dot{\Omega}) = \mathbf{c} \wedge \dot{\Omega}$$

$$\begin{aligned} LH &= (\mathbf{c} \cdot \nabla)(\mathbf{x} \wedge \dot{\Omega}) \\ &= (c_i \frac{\partial}{\partial x_i} + c_j \frac{\partial}{\partial x_j} + c_k \frac{\partial}{\partial x_k})[(x_j \dot{\Omega}_k - x_k \dot{\Omega}_j)\mathbf{i} \\ &\quad - (x_i \dot{\Omega}_k - x_k \dot{\Omega}_i)\mathbf{j} + (x_i \dot{\Omega}_j - x_j \dot{\Omega}_i)\mathbf{k}] \\ &= (c_j \dot{\Omega}_k - c_k \dot{\Omega}_j)\mathbf{i} - (c_i \dot{\Omega}_k - c_k \dot{\Omega}_i)\mathbf{j} \\ &\quad + (c_i \dot{\Omega}_j - c_j \dot{\Omega}_i)\mathbf{k} \end{aligned}$$

$$\begin{aligned} RH &= \mathbf{c} \wedge \dot{\Omega} \\ &= (c_j \dot{\Omega}_k - c_k \dot{\Omega}_j)\mathbf{i} - (c_i \dot{\Omega}_k - c_k \dot{\Omega}_i)\mathbf{j} \\ &\quad + (c_i \dot{\Omega}_j - c_j \dot{\Omega}_i)\mathbf{k} \end{aligned}$$

$$LH = RH$$

APPENDIX A. PROOF OF IDENTITIES

---

**Identity 7**

$$\nabla(\mathbf{x} \wedge \Omega) + \nabla(\mathbf{x} \wedge \Omega)^T = 0$$

$$\nabla(\mathbf{x} \wedge \Omega) =$$

$$\begin{aligned} & \left\{ \begin{array}{ccc} \frac{\partial}{\partial x_i}(x_j \Omega_k - x_k \Omega_j) & \dots & \frac{\partial}{\partial x_k}(x_j \Omega_k - x_k \Omega_j) \\ \frac{\partial}{\partial x_i}(-x_i \Omega_k + x_k \Omega_i) & \dots & \frac{\partial}{\partial x_k}(-x_i \Omega_k + x_k \Omega_i) \\ \frac{\partial}{\partial x_i}(x_i \Omega_j - x_j \Omega_i) & \dots & \frac{\partial}{\partial x_k}(x_i \Omega_j - x_j \Omega_i) \end{array} \right\} \\ & = \begin{Bmatrix} 0 & \Omega_k & -\Omega_j \\ -\Omega_k & 0 & \Omega_i \\ \Omega_j & -\Omega_i & 0 \end{Bmatrix} \end{aligned}$$

$$\nabla(\mathbf{x} \wedge \Omega) + \nabla(\mathbf{x} \wedge \Omega)^T = 0$$

$$\begin{Bmatrix} 0 & \Omega_k & -\Omega_j \\ -\Omega_k & 0 & \Omega_i \\ \Omega_j & -\Omega_i & 0 \end{Bmatrix} + \begin{Bmatrix} 0 & -\Omega_k & \Omega_j \\ \Omega_k & 0 & -\Omega_i \\ -\Omega_j & \Omega_i & 0 \end{Bmatrix} = 0$$

**Identity 8**

$$\mathbf{x} \wedge \Omega = -\Omega \wedge \mathbf{x}$$

$$LH = \mathbf{x} \wedge \Omega$$

$$\begin{aligned} & = (x_j \Omega_k - x_k \Omega_j)\mathbf{i} - (x_i \Omega_k - x_k \Omega_i)\mathbf{j} \\ & + (x_i \Omega_j - x_j \Omega_i)\mathbf{k} \end{aligned}$$

$$RH = -\Omega \wedge \mathbf{x}$$

$$\begin{aligned} & = -[(x_k \Omega_j - x_j \Omega_k)\mathbf{i} - (x_k \Omega_i - x_i \Omega_k)\mathbf{j} \\ & + (x_j \Omega_i - x_i \Omega_j)\mathbf{k}] \\ & = (x_j \Omega_k - x_k \Omega_j)\mathbf{i} - (x_i \Omega_k - x_k \Omega_i)\mathbf{j} \\ & + (x_i \Omega_j - x_j \Omega_i)\mathbf{k} \end{aligned}$$

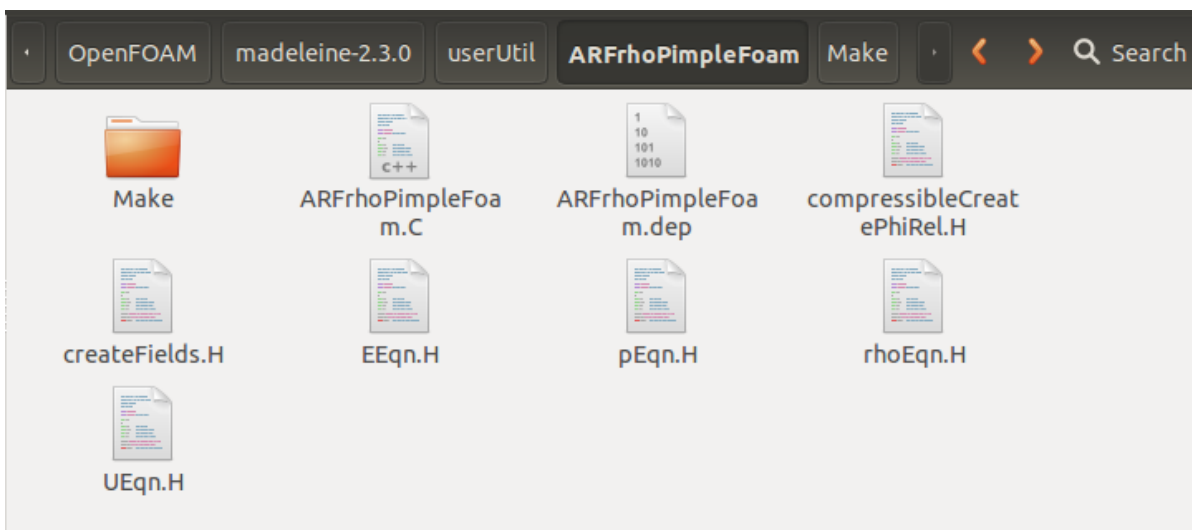
$$LH = RH$$

## Code Formulations for the Accelerating Reference Frame Solving Utility

In this appendix the code formulations for the Accelerating Reference Frame Solver, designated **ARFrhoPimpleFoam**, are shown.

### B.1 ARFrhoPimpleFoam Code Formulation

Figure B.1: ARFrhoPimpleFoam Solver Root Folder



APPENDIX B. CODE FORMULATIONS FOR THE ACCELERATING REFERENCE FRAME SOLVING UTILITY

Figure B.2: ARFrhoPimpleFoam Solver Make Folder

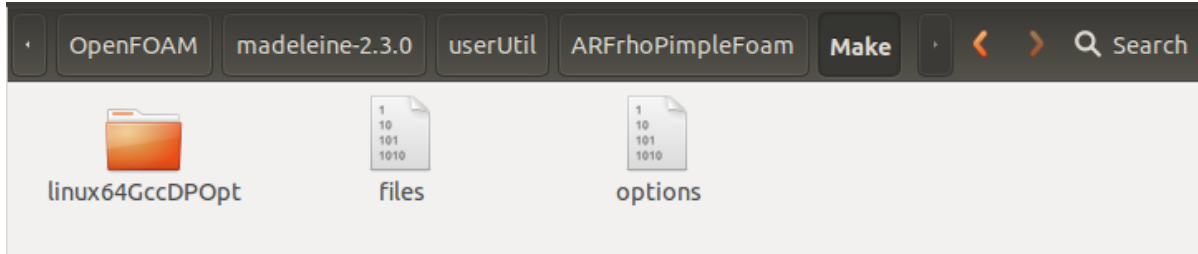


Figure B.3: ARFrhoPimpleFoam Solver Installation Location

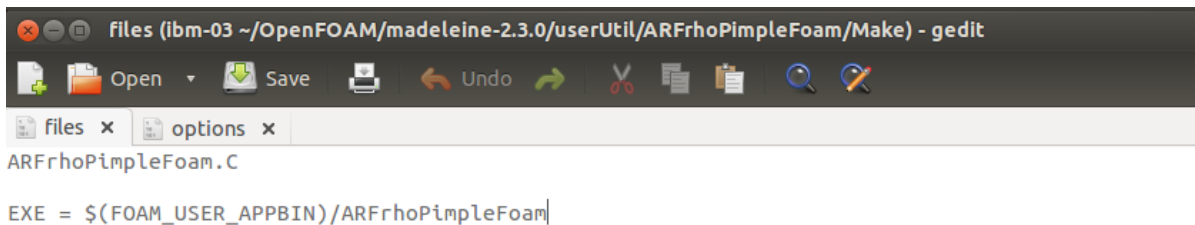
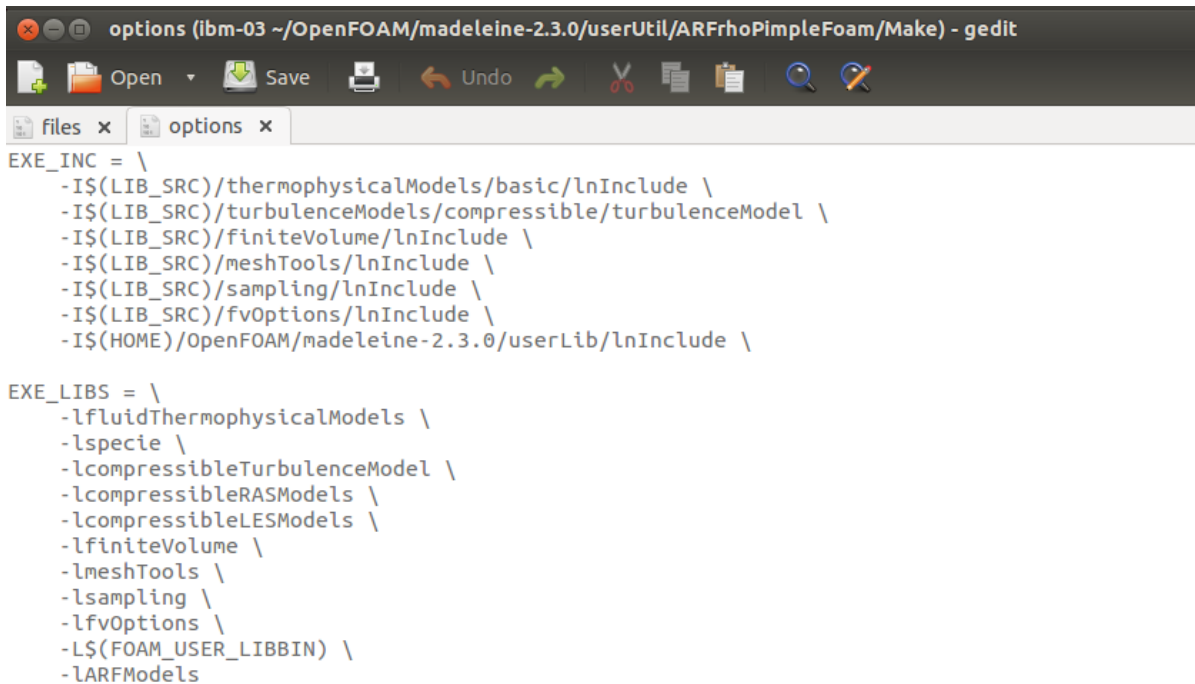


Figure B.4: ARFrhoPimpleFoam Solver Dependent Utilities



## B.1. ARFRHOPIMPLEFOAM CODE FORMULATION

Figure B.5: ARFrhoPimpleFoam C++ Main Code

```
ARFrhoPimpleFoam.C (ibm-03 ~/OpenFOAM/madeleine-2.3.0/userUtil/ARFrhoPimpleFoam) - gedit
Open Save Undo
ARFrhoPimpleFoam.C x
while (runTime.run())
{
    #include "readTimeControls.H"
    #include "compressibleCourantNo.H"
    #include "setDeltaT.H"

    runTime++;

    Info<< "Time = " << runTime.timeName() << nl << endl;

    if (pimple.nCorrPIMPLE() <= 1)
    {
        #include "rhoEqn.H"
    }

    // --- Pressure-velocity PIMPLE corrector loop
    while (pimple.loop())
    {
        #include "UEqn.H"
        #include "EEqn.H"

        // --- Pressure corrector loop
        while (pimple.correct())
        {
            #include "pEqn.H"
        }

        // Update the absolute velocity
        U = Urel + ARF->U();

        if (pimple.turbCorr())
        {
            turbulence->correct();
        }
    }

    runTime.write();

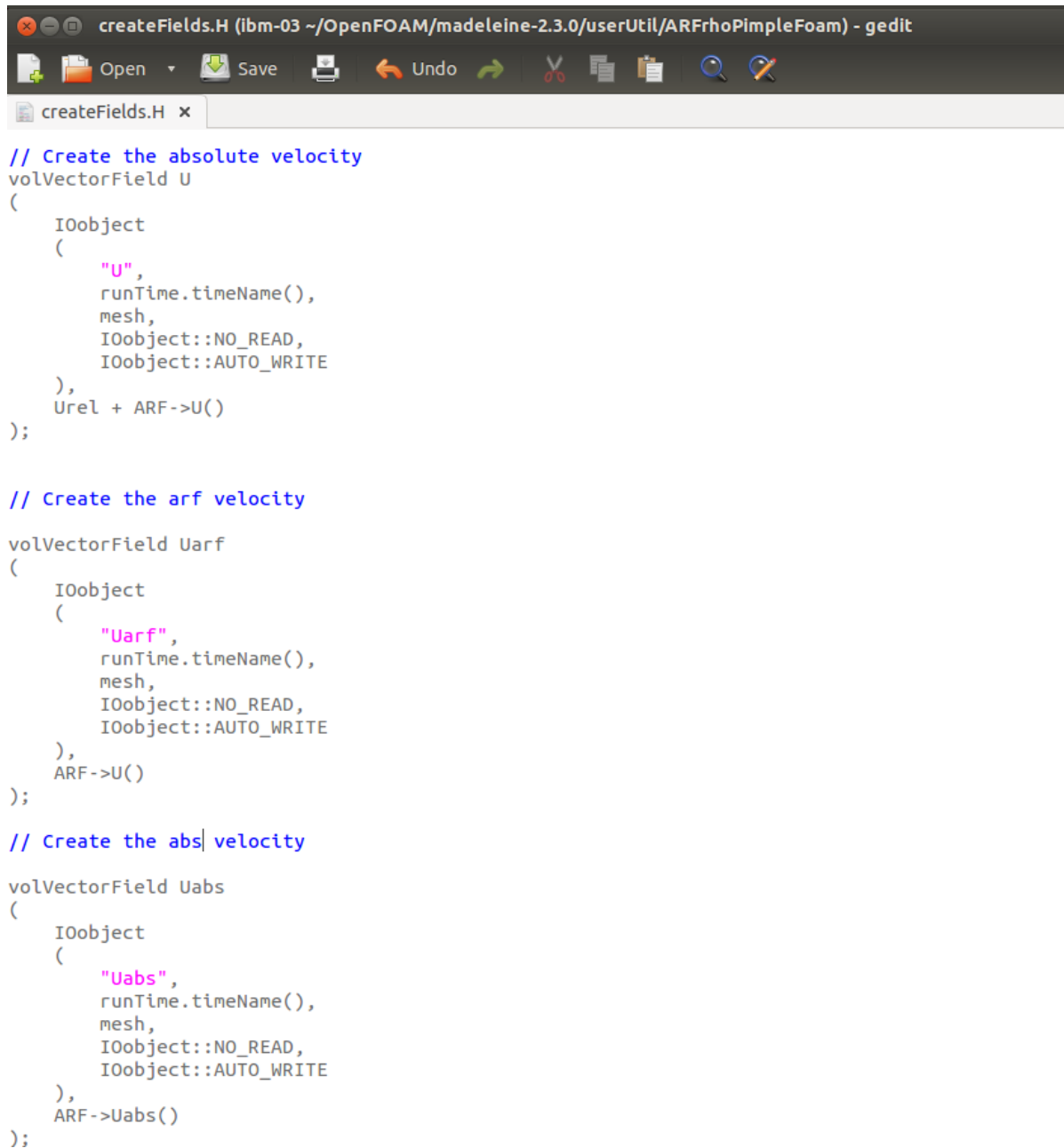
    Info<< "ExecutionTime = " << runTime.elapsedCpuTime() << " s"
        << " ClockTime = " << runTime.elapsedClockTime() << " s"
        << nl << endl;
}

Info<< "End\n" << endl;
```

APPENDIX B. CODE FORMULATIONS FOR THE ACCELERATING REFERENCE FRAME SOLVING UTILITY

---

Figure B.6: ARFrhoPimpleFoam C++ Create Fields Header File



```
// Create the absolute velocity
volVectorField U
(
    IOobject
    (
        "U",
        runtime.timeName(),
        mesh,
        IOobject::NO_READ,
        IOobject::AUTO_WRITE
    ),
    Urel + ARF->U()
);

// Create the arf velocity
volVectorField Uarf
(
    IOobject
    (
        "Uarf",
        runtime.timeName(),
        mesh,
        IOobject::NO_READ,
        IOobject::AUTO_WRITE
    ),
    ARF->U()
);

// Create the abs velocity
volVectorField Uabs
(
    IOobject
    (
        "Uabs",
        runtime.timeName(),
        mesh,
        IOobject::NO_READ,
        IOobject::AUTO_WRITE
    ),
    ARF->Uabs()
);
```

## B.1. ARFRHOPIMPLEFOAM CODE FORMULATION

Figure B.7: ARFrhoPimpleFoam C++ rhoEqn.H Code

```
rhoEqn.H (ibm-03 ~/OpenFOAM/madeleine-2.3.0/userUtil/ARFrhoPimpleFoam) - gedit
Open Save Undo
rhoEqn.H x
/*-----*/
=====
\ \ F i e l d           |   OpenFOAM: The Open Source CFD Toolbox
\ \ O p e r a t i o n  |
\ \ A n d              |   Copyright (C) 2011 OpenFOAM Foundation
\ \ M a n i p u l a t i o n |
-----
License
  This file is part of OpenFOAM.

  OpenFOAM is free software: you can redistribute it and/or modify it
  under the terms of the GNU General Public License as published by
  the Free Software Foundation, either version 3 of the License, or
  (at your option) any later version.

  OpenFOAM is distributed in the hope that it will be useful, but WITHOUT
  ANY WARRANTY; without even the implied warranty of MERCHANTABILITY or
  FITNESS FOR A PARTICULAR PURPOSE. See the GNU General Public License
  for more details.

  You should have received a copy of the GNU General Public License
  along with OpenFOAM. If not, see <http://www.gnu.org/licenses/>.

Global
  rhoEqn

Description|
  Solve the continuity for density.

/*-----*/

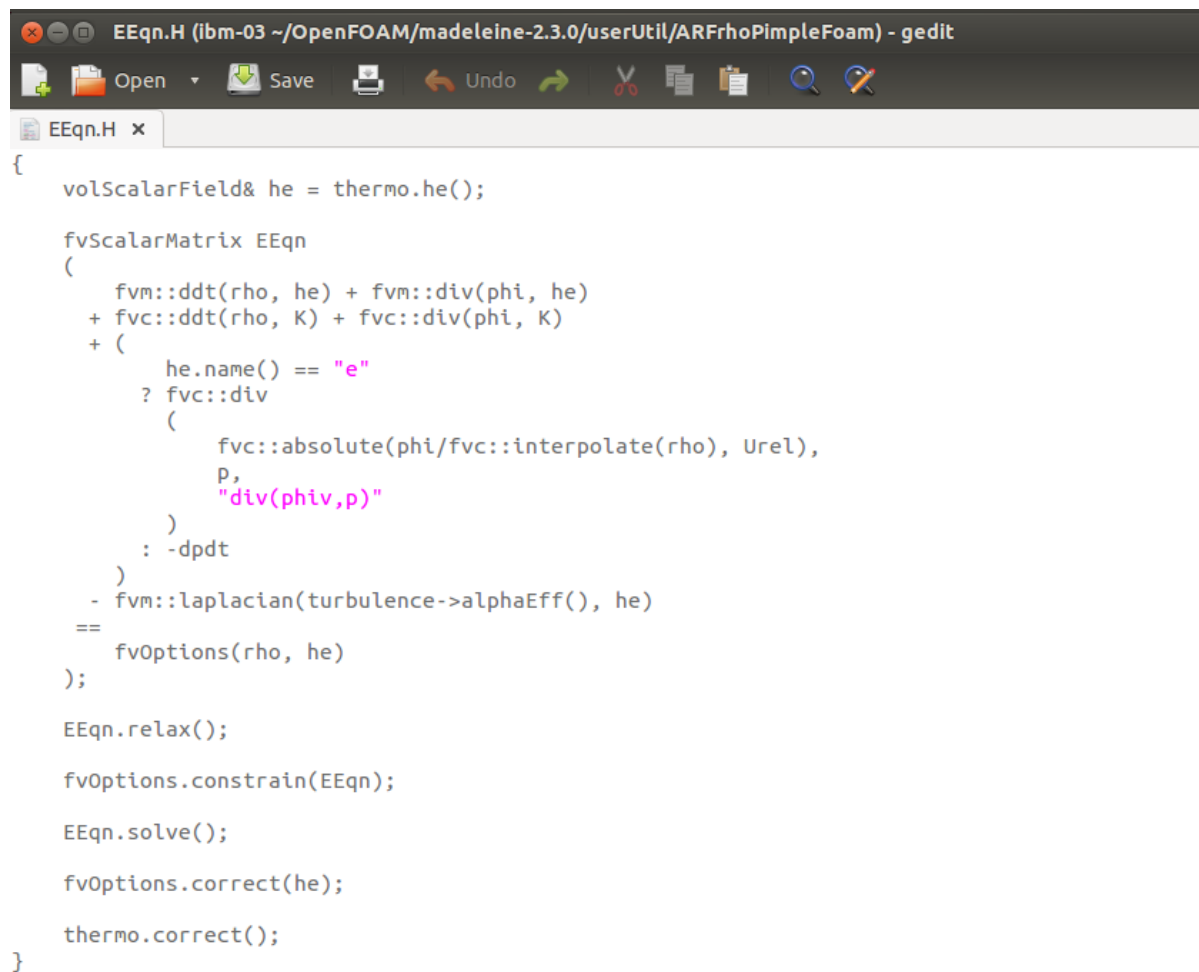
{
  solve(fvm::ddt(rho) + fvc::div(phi));
}

// ***** //
```

APPENDIX B. CODE FORMULATIONS FOR THE ACCELERATING REFERENCE FRAME SOLVING UTILITY

---

Figure B.8: ARFrhoPimpleFoam C++ EEqn.H Code



```

{
  volScalarField& he = thermo.he();

  fvScalarMatrix EEqn
  (
    fvm::ddt(rho, he) + fvm::div(phi, he)
    + fvc::ddt(rho, K) + fvc::div(phi, K)
    + (
        he.name() == "e"
        ? fvc::div
          (
            fvc::absolute(phi/fvc::interpolate(rho), Urel),
            p,
            "div(phi,v,p)"
          )
        : -dpdt
      )
    - fvm::laplacian(turbulence->alphaEff(), he)
    ==
    fvOptions(rho, he)
  );

  EEqn.relax();

  fvOptions.constrain(EEqn);

  EEqn.solve();

  fvOptions.correct(he);

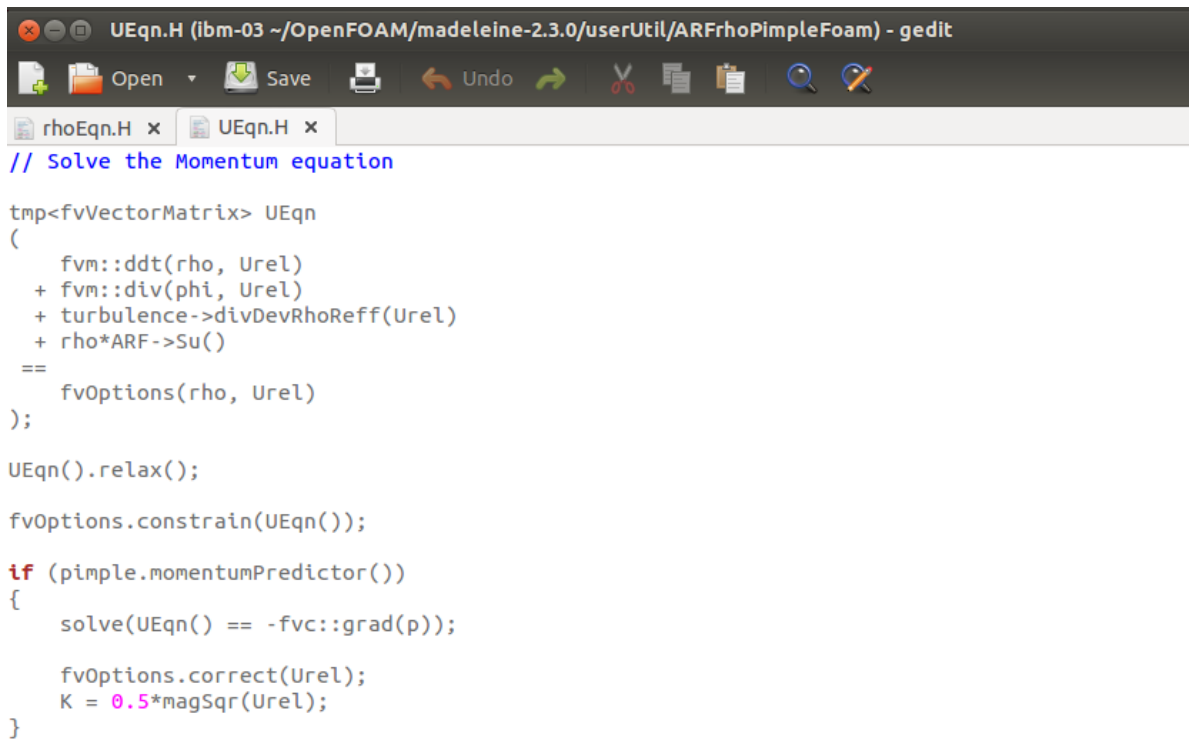
  thermo.correct();
}

```



## B.1. ARFRHOPIMPLEFOAM CODE FORMULATION

Figure B.9: ARFrhoPimpleFoam C++ UEqn.H Code



```
UEqn.H (ibm-03 ~/OpenFOAM/madeleine-2.3.0/userUtil/ARFrhoPimpleFoam) - gedit
// Solve the Momentum equation

tmp<fvVectorMatrix> UEqn
(
    fvm::ddt(rho, Urel)
  + fvm::div(phi, Urel)
  + turbulence->divDevRhoReff(Urel)
  + rho*ARF->Su()
  ==
    fvOptions(rho, Urel)
);

UEqn().relax();

fvOptions.constrain(UEqn());

if (pimple.momentumPredictor())
{
    solve(UEqn() == -fvc::grad(p));

    fvOptions.correct(Urel);
    K = 0.5*magSqr(Urel);
}
```

APPENDIX B. CODE FORMULATIONS FOR THE ACCELERATING REFERENCE FRAME SOLVING UTILITY

## B.2 ARFModel Code Formulation

Figure B.10: ARF Library Root Folder

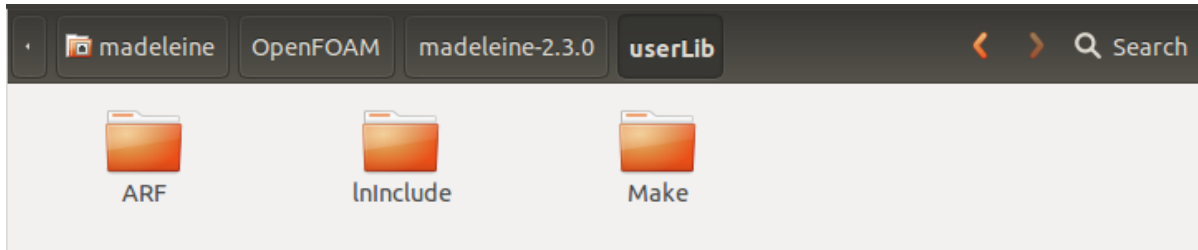


Figure B.11: ARFModel Library Root Folder

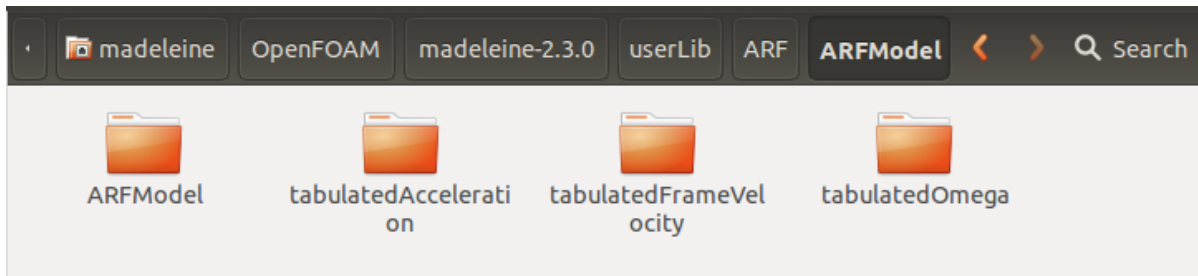


Figure B.12: ARFModel Library Sources

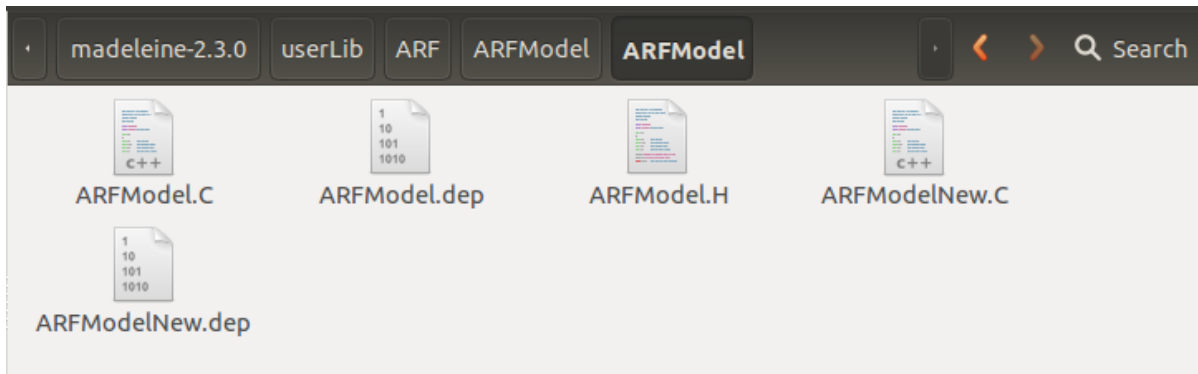


Figure B.13: ARFModel C++ Source Code ARFProperties Constructors

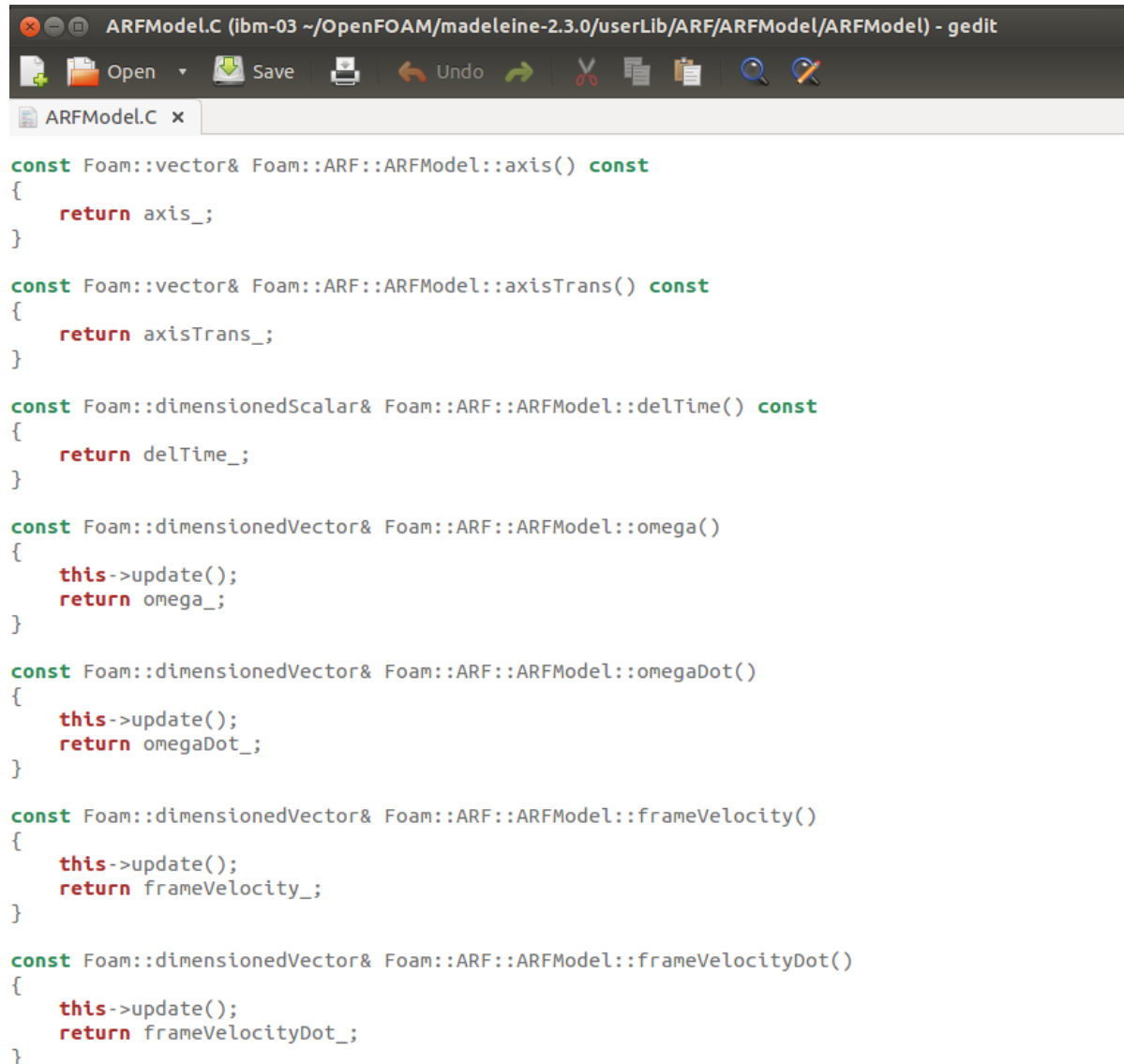
```
ARFModel.C (ibm-03 ~/OpenFOAM/madeleine-2.3.0/userLib/ARF/ARFModel/ARFModel) - gedit
Open Save Undo
ARFModel.C x

// * * * * * Constructors * * * * * //
Foam::ARF::ARFModel::ARFModel
(
    const word& type,
    const volVectorField& Urel
)
:
    IOdictionary
    (
        IOobject
        (
            "ARFProperties",
            Urel.time().constant(),
            Urel.db(),
            IOobject::MUST_READ_IF_MODIFIED,|
            IOobject::NO_WRITE
        )
    ),
    Urel_(Urel),
    mesh_(Urel_.mesh()),
    axis_(lookup("axis")),
    axisTrans_(lookup("axisTrans")),
    omegaModelCoeffs_(subDict("tabulatedOmegaCoeffs")),
    velocityModelCoeffs_(subDict("tabulatedFrameVelocityCoeffs")),
    delTime_(dimensionedScalar("delTime", dimTime, lookup("delTime"))),
    omega_(dimensionedVector("omega", dimless/dimTime, vector::zero)),
    omegaDot_(dimensionedVector("omegaDot", dimless/dimTime/dimTime, vector::zero)),
    frameVelocity_(dimensionedVector("frameVelocity", dimLength/dimTime, vector::zero)),
    frameVelocityDot_(dimensionedVector("frameVelocityDot", dimLength/dimTime/dimTime,
vector::zero))
```

APPENDIX B. CODE FORMULATIONS FOR THE ACCELERATING REFERENCE FRAME SOLVING UTILITY

---

Figure B.14: ARFModel C++ Source Code Vector Definitions



```

const Foam::vector& Foam::ARF::ARFModel::axis() const
{
    return axis_;
}

const Foam::vector& Foam::ARF::ARFModel::axisTrans() const
{
    return axisTrans_;
}

const Foam::dimensionedScalar& Foam::ARF::ARFModel::delTime() const
{
    return delTime_;
}

const Foam::dimensionedVector& Foam::ARF::ARFModel::omega()
{
    this->update();
    return omega_;
}

const Foam::dimensionedVector& Foam::ARF::ARFModel::omegaDot()
{
    this->update();
    return omegaDot_;
}

const Foam::dimensionedVector& Foam::ARF::ARFModel::frameVelocity()
{
    this->update();
    return frameVelocity_;
}

const Foam::dimensionedVector& Foam::ARF::ARFModel::frameVelocityDot()
{
    this->update();
    return frameVelocityDot_;
}

```

Figure B.15: ARFModel C++ Source Code - Coriolis and Centrifugal Source Calculation

```

Foam::tmp<Foam::DimensionedField<Foam::vector, Foam::volMesh> >
Foam::ARF::ARFModel::Fcoriolis()
{
    return tmp<DimensionedField<vector, volMesh> >
    (
        new DimensionedField<vector, volMesh>
        (
            IOobject
            (
                "Fcoriolis",
                mesh_.time().timeName(),
                mesh_,
                IOobject::NO_READ,
                IOobject::NO_WRITE
            ),
            2.0*omega_ ^ Urel_
        )
    );
}

Foam::tmp<Foam::DimensionedField<Foam::vector, Foam::volMesh> >
Foam::ARF::ARFModel::Fcentrifugal()
{
    return tmp<DimensionedField<vector, volMesh> >
    (
        new DimensionedField<vector, volMesh>
        (
            IOobject
            (
                "Fcentrifugal",
                mesh_.time().timeName(),
                mesh_,
                IOobject::NO_READ,
                IOobject::NO_WRITE
            ),
            omega() ^ (omega() ^ mesh_.C())
        )
    );
}

```

APPENDIX B. CODE FORMULATIONS FOR THE ACCELERATING REFERENCE FRAME SOLVING UTILITY

---

Figure B.16: ARFModel C++ Source Code - Euler and Rotation-Translation Interaction Source Calculation

```

)
);
}

Foam::tmp<Foam::DimensionedField<Foam::vector, Foam::volMesh> >
Foam::ARF::ARFModel::Feuler()
{
    return tmp<DimensionedField<vector, volMesh> >
    (
        new DimensionedField<vector, volMesh>
        (
            IObject
            (
                "Feuler",
                mesh_.time().timeName(),
                mesh_,
                IObject::NO_READ,
                IObject::NO_WRITE
            ),
            omegaDot() ^ mesh_.C()
        )
    );
}

Foam::tmp<Foam::DimensionedField<Foam::vector, Foam::volMesh> >
Foam::ARF::ARFModel::FinterframeCoriolis()
{
    return tmp<DimensionedField<vector, volMesh> >
    (
        new DimensionedField<vector, volMesh>
        (
            IObject
            (
                "FinterframeCoriolis",
                mesh_.time().timeName(),
                mesh_,
                IObject::NO_READ,
                IObject::NO_WRITE
            ),
            mesh_,
            2.0*omega() ^ frameVelocity()
        )
    );
}

```

Figure B.17: ARFModel C++ Source Code - Frame Acceleration and Source Summation Calculations

```
ARFModel.C (ibm-03 ~/OpenFOAM/madeleine-2.3.0/userLib/ARF/ARFModel/ARFModel) - gedit
Open Save Undo Cut Copy Paste Find
ARFModel.C x
    mesh_.time().timeName(),
    mesh_,
    IOobject::NO_READ,
    IOobject::NO_WRITE
),
mesh_,
2.0*omega() ^ frameVelocity()
);
}

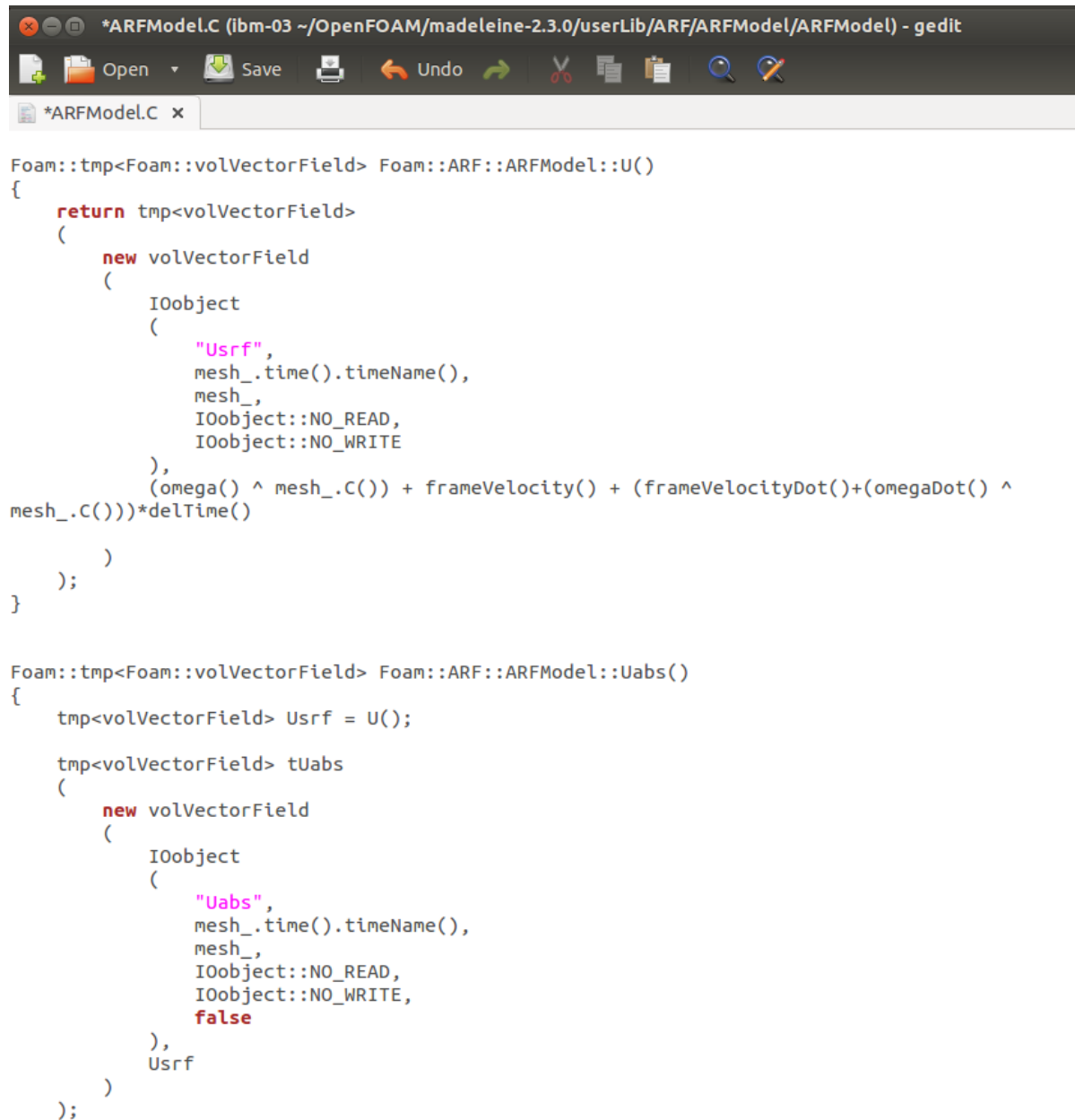
Foam::tmp<Foam::DimensionedField<Foam::vector, Foam::volMesh> >
Foam::ARF::ARFModel::FtranslationAccelleration()
{
    return tmp<DimensionedField<vector, volMesh> >
    (
        new DimensionedField<vector, volMesh>
        (
            IOobject
            (
                "FtranslationAccelleration",
                mesh_.time().timeName(),
                mesh_,
                IOobject::NO_READ,
                IOobject::NO_WRITE
            ),
            mesh_,
            frameVelocityDot_
        )
    );
}

Foam::tmp<Foam::DimensionedField<Foam::vector, Foam::volMesh> >
Foam::ARF::ARFModel::Su()
{
    return Fcoriolis() + Fcentrifugal() + Feuler() + FinterframeCoriolis() +
    FtranslationAccelleration();
}
```

APPENDIX B. CODE FORMULATIONS FOR THE ACCELERATING REFERENCE FRAME SOLVING UTILITY

---

Figure B.18: ARFModel C++ Source Code Velocity Calculation



```

Foam::tmp<Foam::volVectorField> Foam::ARF::ARFModel::U()
{
    return tmp<volVectorField>
    (
        new volVectorField
        (
            IObject
            (
                "Usrf",
                mesh_.time().timeName(),
                mesh_,
                IObject::NO_READ,
                IObject::NO_WRITE
            ),
            (omega() ^ mesh_.C()) + frameVelocity() + (frameVelocityDot()+omegaDot() ^
mesh_.C()))*delTime()
        )
    );
}

Foam::tmp<Foam::volVectorField> Foam::ARF::ARFModel::Uabs()
{
    tmp<volVectorField> Usrf = U();

    tmp<volVectorField> tUabs
    (
        new volVectorField
        (
            IObject
            (
                "Uabs",
                mesh_.time().timeName(),
                mesh_,
                IObject::NO_READ,
                IObject::NO_WRITE,
                false
            ),
            Usrf
        )
    );
}

```



Figure B.19: ARFModel C++ Source Code Internal Field and Boundary Layer Correction

```
*ARFModel.C (ibm-03 ~/OpenFOAM/madeleine-2.3.0/userLib/ARF/ARFModel/ARFModel) - gedit
Open Save Undo Cut Copy Paste Find
*ARFModel.C x
new volVectorField
(
    IOobject
    (
        "Uabs",
        mesh_.time().timeName(),
        mesh_,
        IOobject::NO_READ,
        IOobject::NO_WRITE,
        false
    ),
    Usrcf
);

// Add ARF contribution to internal field
tUabs().internalField() += Urel_.internalField();

// Add Urel boundary contributions
const volVectorField::GeometricBoundaryField& bvf = Urel_.boundaryField();

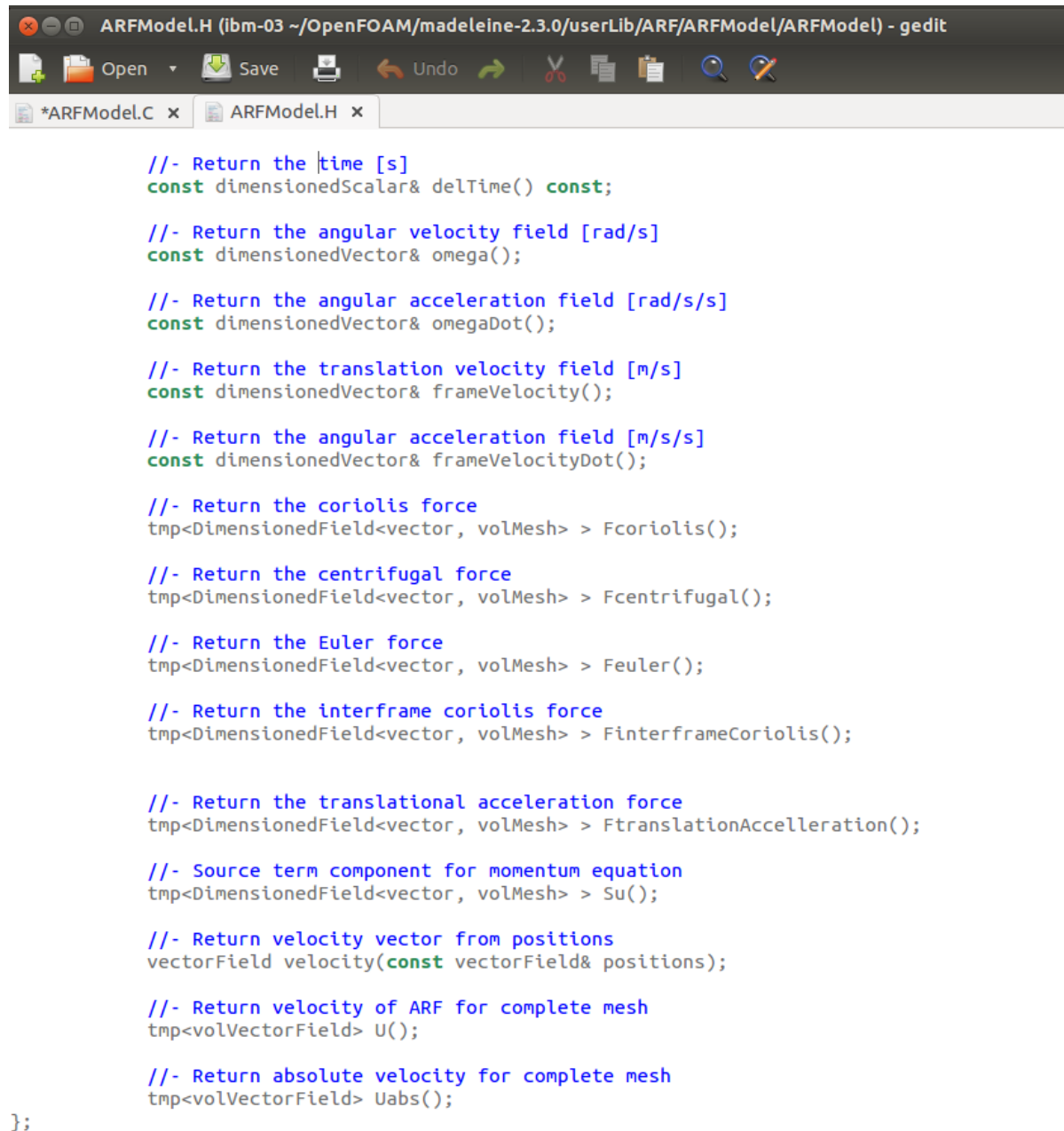
forAll(bvf, i)
{
    if (isA<ARFVelocityFvPatchVectorField>(bvf[i]))
    {
        // Only include relative contributions from
        // ARFVelocityFvPatchVectorField's
        const ARFVelocityFvPatchVectorField& UrelPatch =
            refCast<const ARFVelocityFvPatchVectorField>(bvf[i]);
        if (UrelPatch.relative())
        {
            tUabs().boundaryField()[i] += Urel_.boundaryField()[i];
        }
    }
    else
    {
        tUabs().boundaryField()[i] += Urel_.boundaryField()[i];
    }
}

return tUabs;
}
```

APPENDIX B. CODE FORMULATIONS FOR THE ACCELERATING REFERENCE FRAME SOLVING UTILITY

---

Figure B.20: ARFModel Header File Returned Parameters



```

//- Return the time [s]
const dimensionedScalar& delTime() const;

//- Return the angular velocity field [rad/s]
const dimensionedVector& omega();

//- Return the angular acceleration field [rad/s/s]
const dimensionedVector& omegaDot();

//- Return the translation velocity field [m/s]
const dimensionedVector& frameVelocity();

//- Return the angular acceleration field [m/s/s]
const dimensionedVector& frameVelocityDot();

//- Return the coriolis force
tmp<DimensionedField<vector, volMesh> > Fcoriolis();

//- Return the centrifugal force
tmp<DimensionedField<vector, volMesh> > Fcentrifugal();

//- Return the Euler force
tmp<DimensionedField<vector, volMesh> > Feuler();

//- Return the interframe coriolis force
tmp<DimensionedField<vector, volMesh> > FinterframeCoriolis();

//- Return the translational acceleration force
tmp<DimensionedField<vector, volMesh> > FtranslationAccelleration();

//- Source term component for momentum equation
tmp<DimensionedField<vector, volMesh> > Su();

//- Return velocity vector from positions
vectorField velocity(const vectorField& positions);

//- Return velocity of ARF for complete mesh
tmp<volVectorField> U();

//- Return absolute velocity for complete mesh
tmp<volVectorField> Uabs();
};

```

Figure B.21: tabulatedAcceleration Library Root Folder

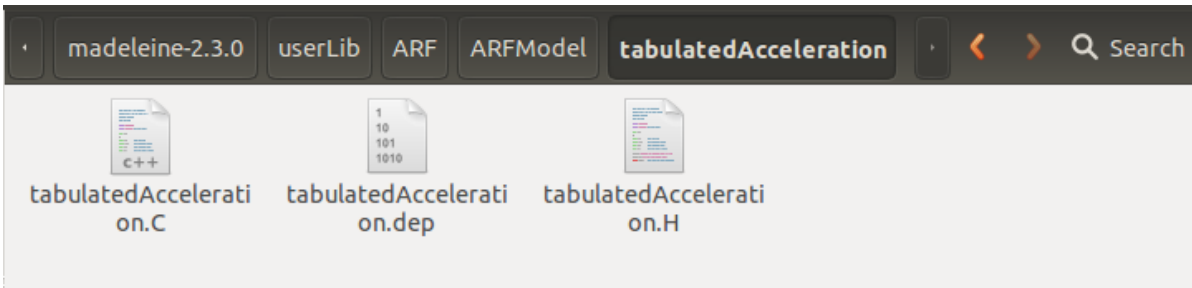


Figure B.22: tabulatedAcceleration C++ Source Constructors

```

tabulatedAcceleration.C (ibm-03 ~/OpenFOAM/madeleine-2.3.0/userLib/ARF/ARFModel/tabulatedAccele
Open Save Undo
tabulatedAcceleration.H x tabulatedAcceleration.C x
// ***** Static Data Members ***** //
namespace Foam
{
  namespace ARF
  {
    defineTypeNameAndDebug(tabulatedAcceleration, 0);

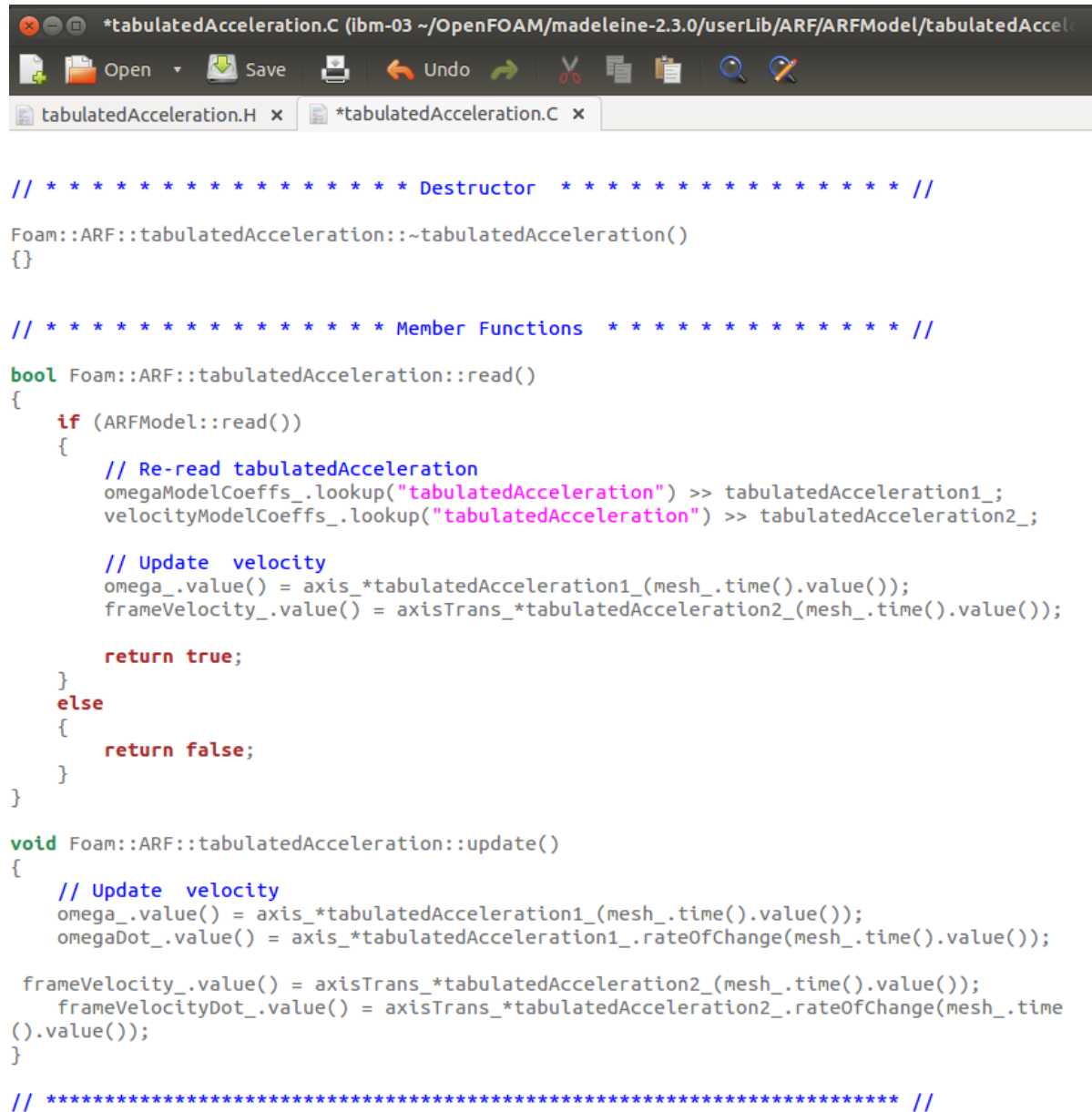
    addToRunTimeSelectionTable
    (
      ARFModel,
      tabulatedAcceleration,
      dictionary
    );
  }
}

// ***** Constructors ***** //
Foam::ARF::tabulatedAcceleration::tabulatedAcceleration
(
  const volVectorField& U
)
:
  ARFModel(typeName, U),
  tabulatedAcceleration1_(omegaModelCoeffs_),
  tabulatedAcceleration2_(velocityModelCoeffs_)
{
  // Initialise the angular velocity
  omega_.value() = axis_*tabulatedAcceleration1_(U.mesh().time().value());
  frameVelocity_.value() = axisTrans_*tabulatedAcceleration2_(U.mesh().time().value());
}
  
```

APPENDIX B. CODE FORMULATIONS FOR THE ACCELERATING REFERENCE FRAME SOLVING UTILITY

---

Figure B.23: tabulatedAcceleration C++ Source Member Functions



```

// ***** Destructor ***** //
Foam::ARF::tabulatedAcceleration::~tabulatedAcceleration()
{}

// ***** Member Functions ***** //
bool Foam::ARF::tabulatedAcceleration::read()
{
    if (ARFModel::read())
    {
        // Re-read tabulatedAcceleration
        omegaModelCoeffs_.lookup("tabulatedAcceleration") >> tabulatedAcceleration1_;
        velocityModelCoeffs_.lookup("tabulatedAcceleration") >> tabulatedAcceleration2_;

        // Update velocity
        omega_.value() = axis_*tabulatedAcceleration1_(mesh_.time().value());
        frameVelocity_.value() = axisTrans_*tabulatedAcceleration2_(mesh_.time().value());

        return true;
    }
    else
    {
        return false;
    }
}

void Foam::ARF::tabulatedAcceleration::update()
{
    // Update velocity
    omega_.value() = axis_*tabulatedAcceleration1_(mesh_.time().value());
    omegaDot_.value() = axis_*tabulatedAcceleration1_.rateOfChange(mesh_.time().value());

    frameVelocity_.value() = axisTrans_*tabulatedAcceleration2_(mesh_.time().value());
    frameVelocityDot_.value() = axisTrans_*tabulatedAcceleration2_.rateOfChange(mesh_.time().value());
}

// ***** //

```

## B.3 ARFFreeStreamVelocity Boundary Implementation

Figure B.24: ARF derivedFvPatchFields Root Folder

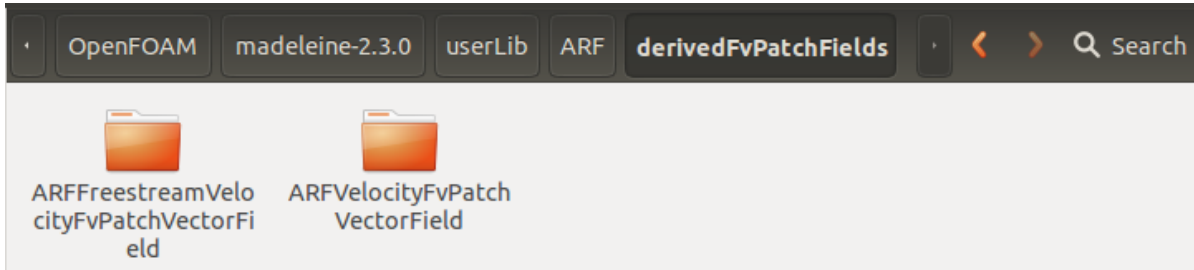
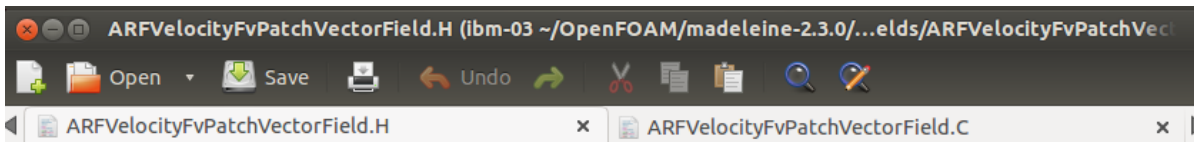


Figure B.25: ARFVelocity Boundary Condition Description



### Description

Velocity condition to be used in conjunction with the single rotating frame (ARF) model (see: ARFModel class)

Given the free stream velocity in the absolute frame, the condition applies the appropriate rotation transformation in time and space to determine the local velocity.

The optional `\c relative` flag switches the behaviour of the patch such that:

- `relative = yes`: inlet velocity applied 'as is':

```
\f[
  U_p = U_{in}
\f]
```

- `relative = no`: ARF velocity is subtracted from the inlet velocity:

```
\f[
  U_p = U_{in} - U_{p,srf}
\f]
```

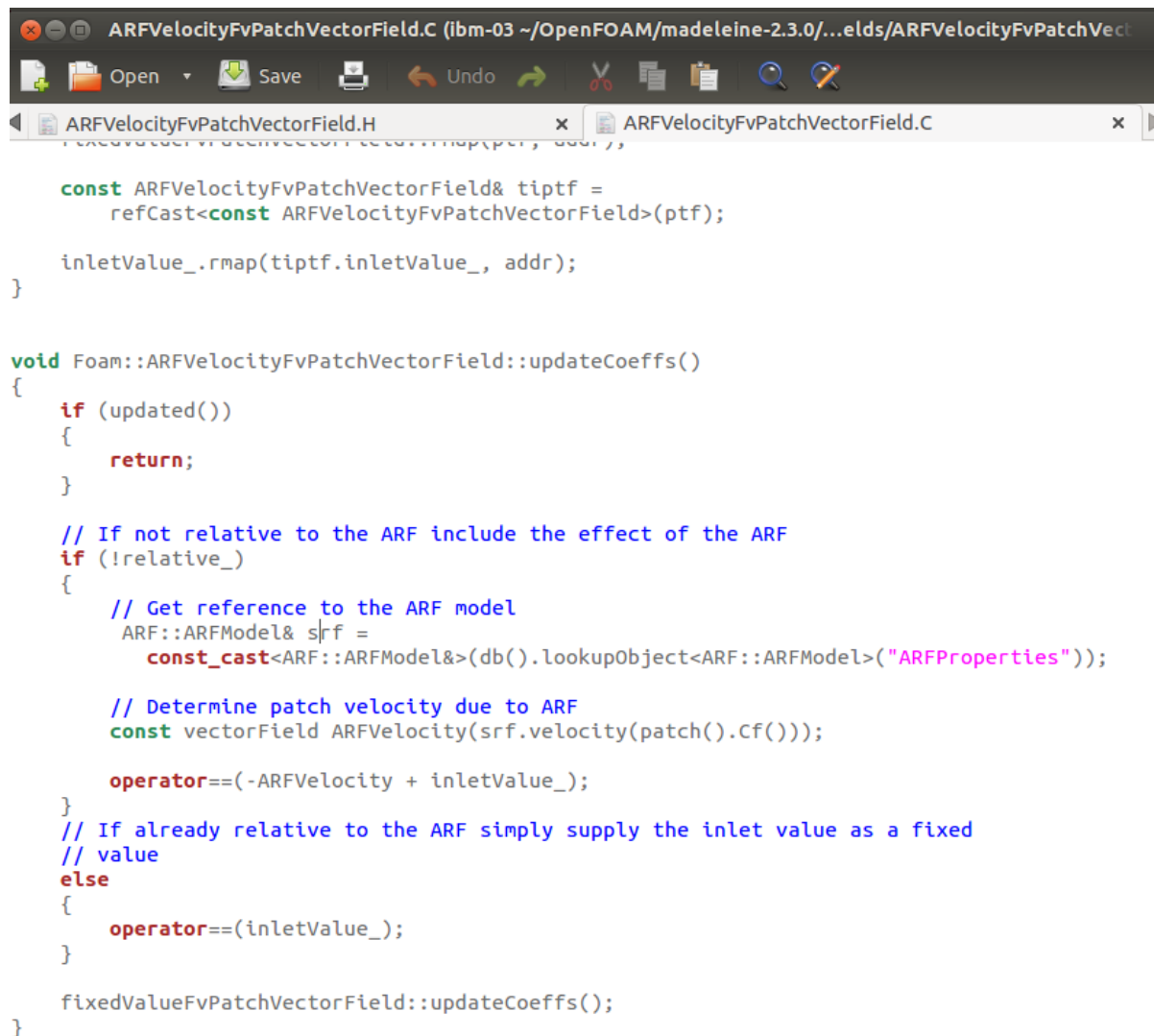
where

```
\variable
  U_p      = patch velocity [m/s]
  U_{in}   = user-specified inlet velocity
  U_{p,srf} = ARF velocity
\endvariable
```

APPENDIX B. CODE FORMULATIONS FOR THE ACCELERATING REFERENCE FRAME SOLVING UTILITY

---

Figure B.26: ARFVelocity Boundary Condition Source Code



```

const ARFVelocityFvPatchVectorField& tiptf =
    refCast<const ARFVelocityFvPatchVectorField>(ptf);

inletValue_.rmap(tiptf.inletValue_, addr);
}

void Foam::ARFVelocityFvPatchVectorField::updateCoeffs()
{
    if (updated())
    {
        return;
    }

    // If not relative to the ARF include the effect of the ARF
    if (!relative_)
    {
        // Get reference to the ARF model
        ARF::ARFModel& srf =
            const_cast<ARF::ARFModel>(db().lookupObject<ARF::ARFModel>("ARFProperties"));

        // Determine patch velocity due to ARF
        const vectorField ARFVelocity(srf.velocity(patch().Cf()));

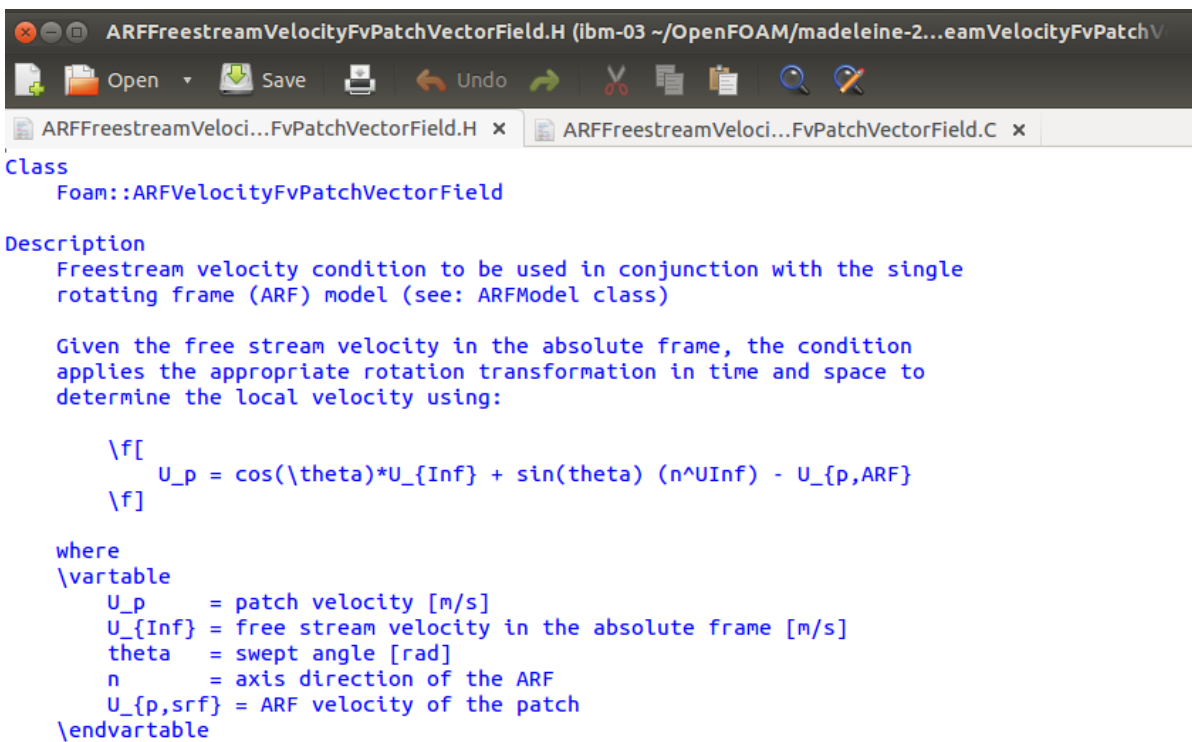
        operator==(-ARFVelocity + inletValue_);
    }
    // If already relative to the ARF simply supply the inlet value as a fixed
    // value
    else
    {
        operator==(inletValue_);
    }

    fixedValueFvPatchVectorField::updateCoeffs();
}

```

### B.3. ARFFREESTREAMVELOCITY BOUNDARY IMPLEMENTATION

Figure B.27: ARFFreestreamVelocity Boundary Condition Description



```

ARFFreestreamVelocityFvPatchVectorField.H (ibm-03 ~/OpenFOAM/madeleine-2...eamVelocityFvPatchV
Open Save Undo
ARFFreestreamVeloci...FvPatchVectorField.H x ARFFreestreamVeloci...FvPatchVectorField.C x
Class
Foam::ARFVelocityFvPatchVectorField
Description
Freestream velocity condition to be used in conjunction with the single
rotating frame (ARF) model (see: ARFModel class)

Given the free stream velocity in the absolute frame, the condition
applies the appropriate rotation transformation in time and space to
determine the local velocity using:

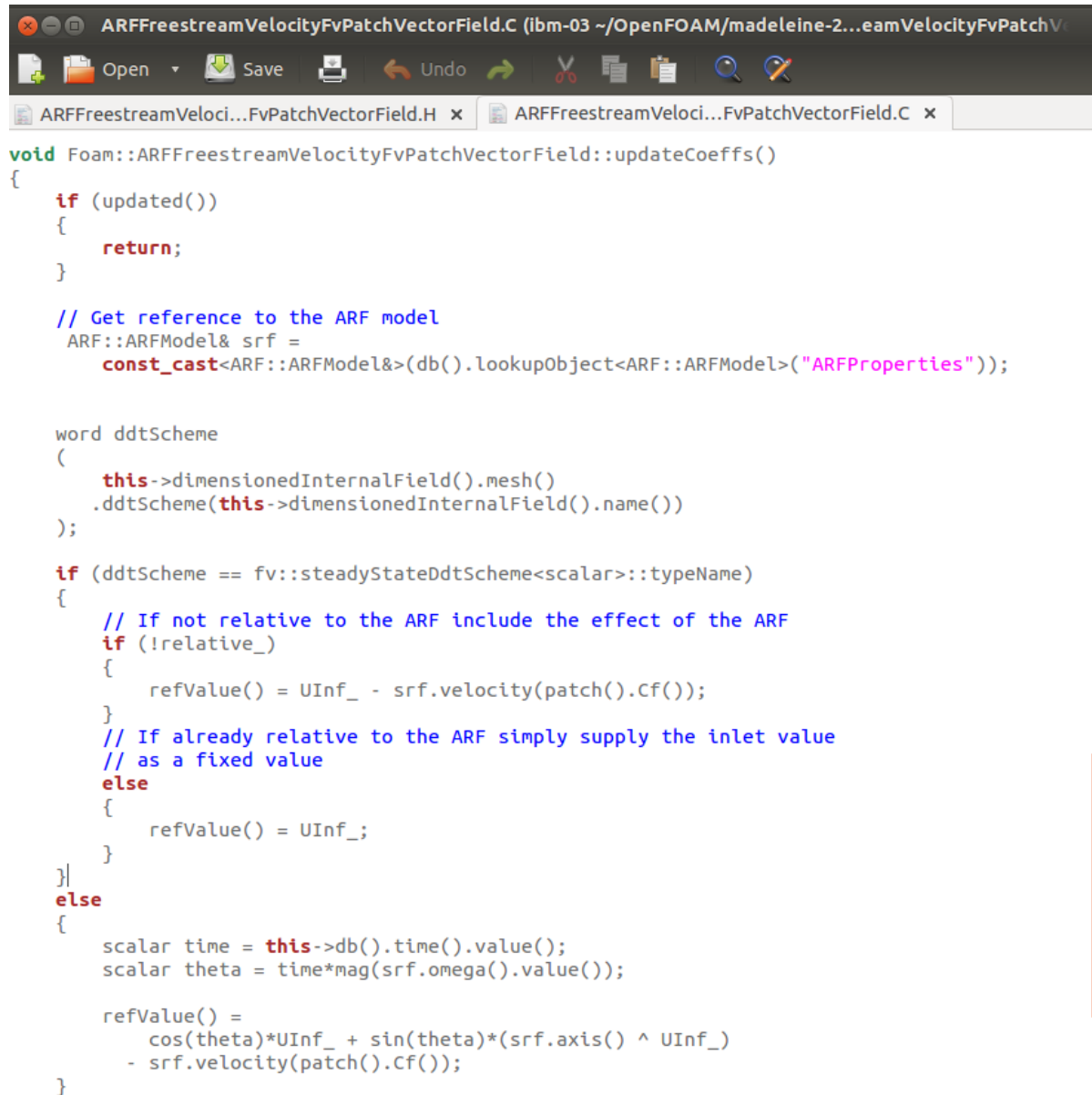
\[\
U_p = \cos(\theta)U_{Inf} + \sin(\theta) (n^{\wedge}U_{Inf}) - U_{\{p,ARF\}}
\]

where
\variable
U_p = patch velocity [m/s]
U_{Inf} = free stream velocity in the absolute frame [m/s]
theta = swept angle [rad]
n = axis direction of the ARF
U_{\{p,srf\}} = ARF velocity of the patch
\endvariable

```

## APPENDIX B. CODE FORMULATIONS FOR THE ACCELERATING REFERENCE FRAME SOLVING UTILITY

Figure B.28: ARFFreestreamVelocity Boundary Condition Source Code



```
void Foam::ARFFreestreamVelocityFvPatchVectorField::updateCoeffs()
{
    if (updated())
    {
        return;
    }

    // Get reference to the ARF model
    ARF::ARFModel& srf =
        const_cast<ARF::ARFModel&>(db().lookupObject<ARF::ARFModel>("ARFProperties"));

    word ddtScheme
    (
        this->dimensionedInternalField().mesh()
        .ddtScheme(this->dimensionedInternalField().name())
    );

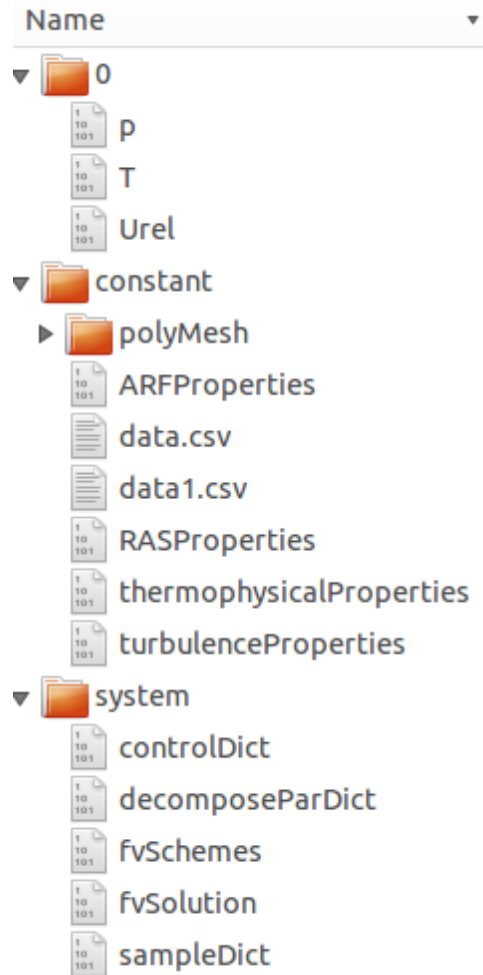
    if (ddtScheme == fv::steadyStateDdtScheme<scalar>::typeName)
    {
        // If not relative to the ARF include the effect of the ARF
        if (!relative_)
        {
            refValue() = UInf_ - srf.velocity(patch().Cf());
        }
        // If already relative to the ARF simply supply the inlet value
        // as a fixed value
        else
        {
            refValue() = UInf_;
        }
    }
    else
    {
        scalar time = this->db().time().value();
        scalar theta = time*mag(srf.omega().value());

        refValue() =
            cos(theta)*UInf_ + sin(theta)*(srf.axis() ^ UInf_)
            - srf.velocity(patch().Cf());
    }
}
```



## B.4 Case Structure

Figure B.29: OpenFOAM Case Initial Set-up



APPENDIX B. CODE FORMULATIONS FOR THE ACCELERATING REFERENCE FRAME SOLVING UTILITY

Figure B.30: OpenFOAM Root Case Folder

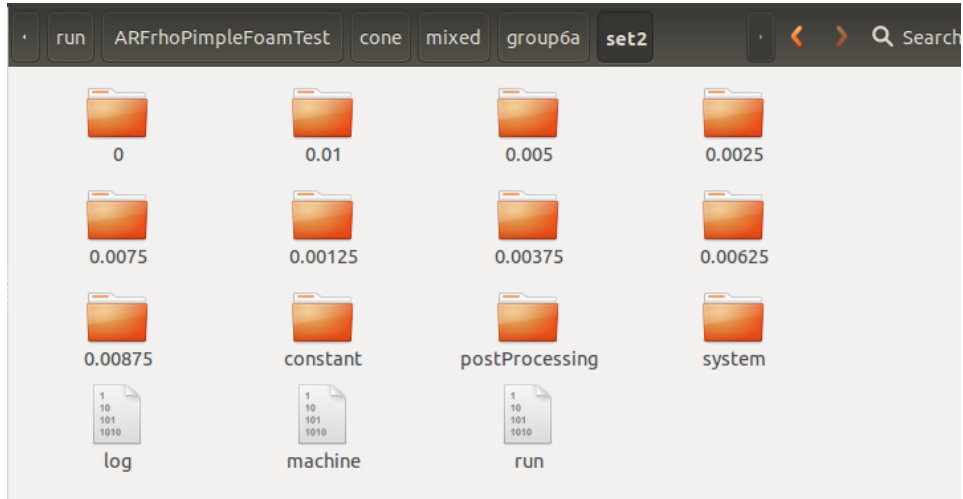


Figure B.31: OpenFOAM Mesh Description Files

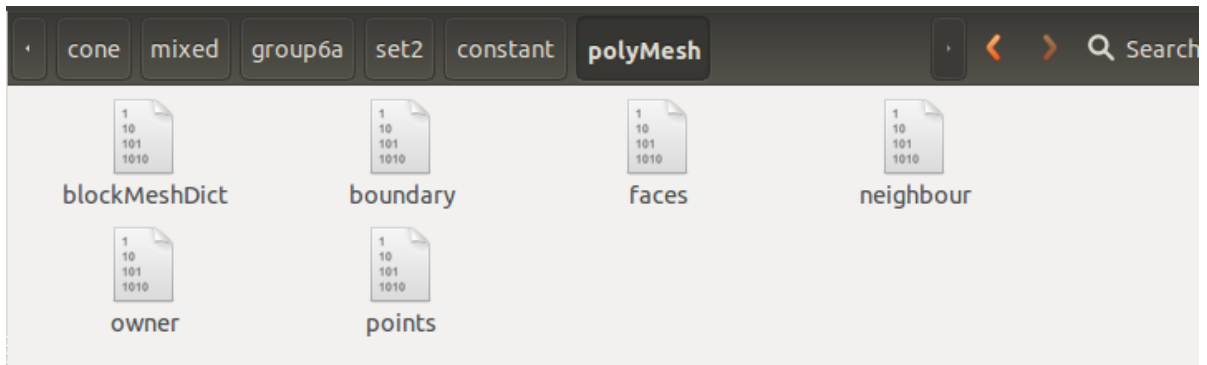


Figure B.32: OpenFOAM Case System Folder

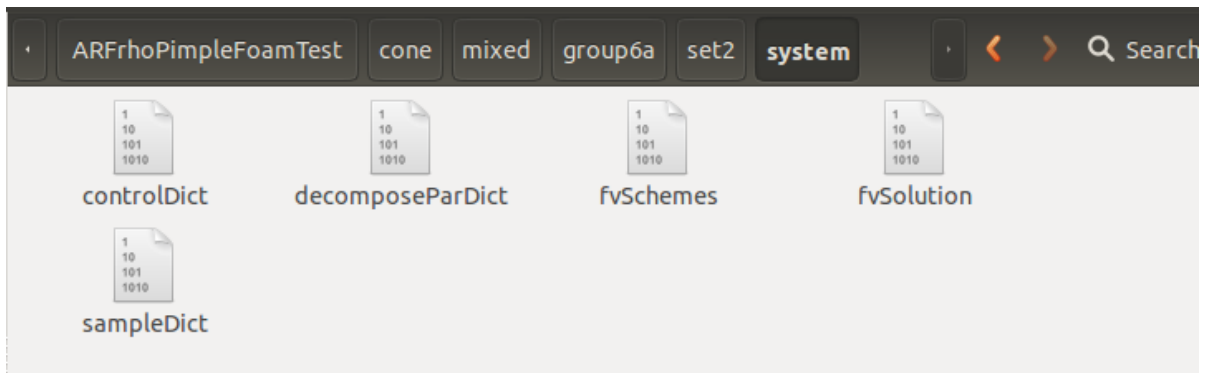


Figure B.33: OpenFOAM Case Initial Conditions Folder

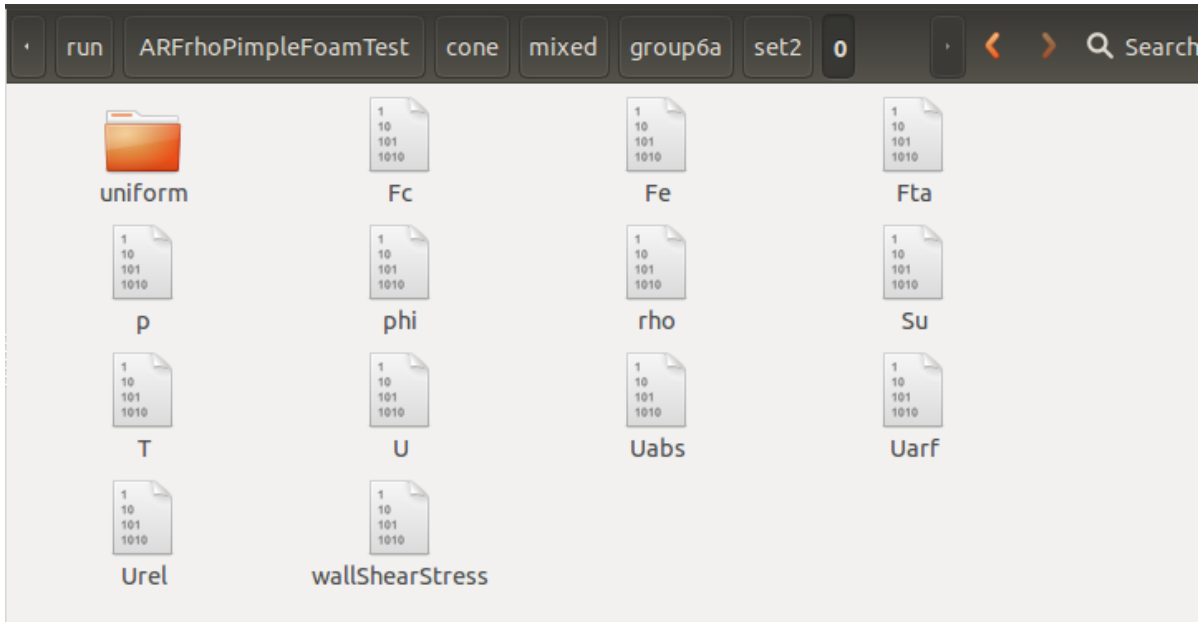


Figure B.34: OpenFOAM Case Constant Folder

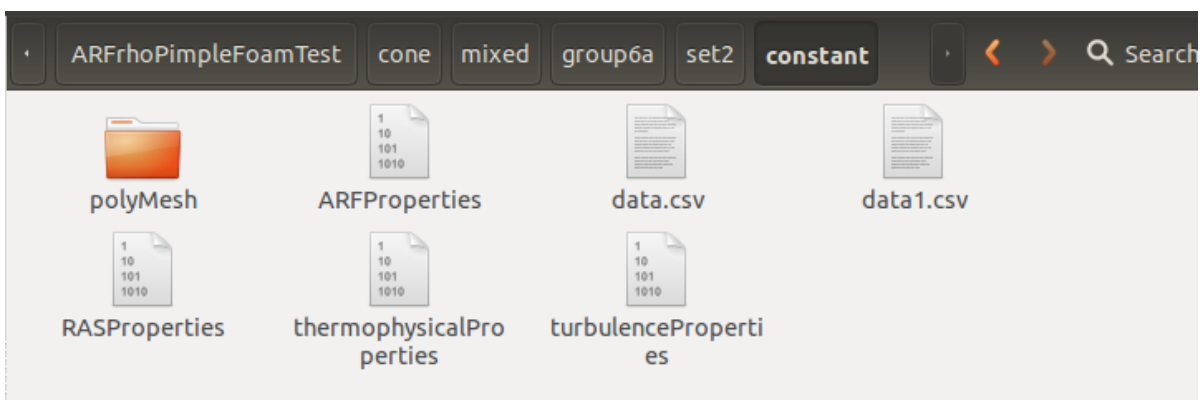
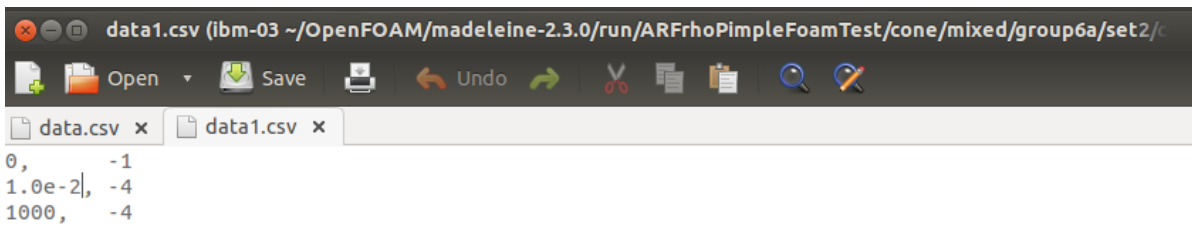




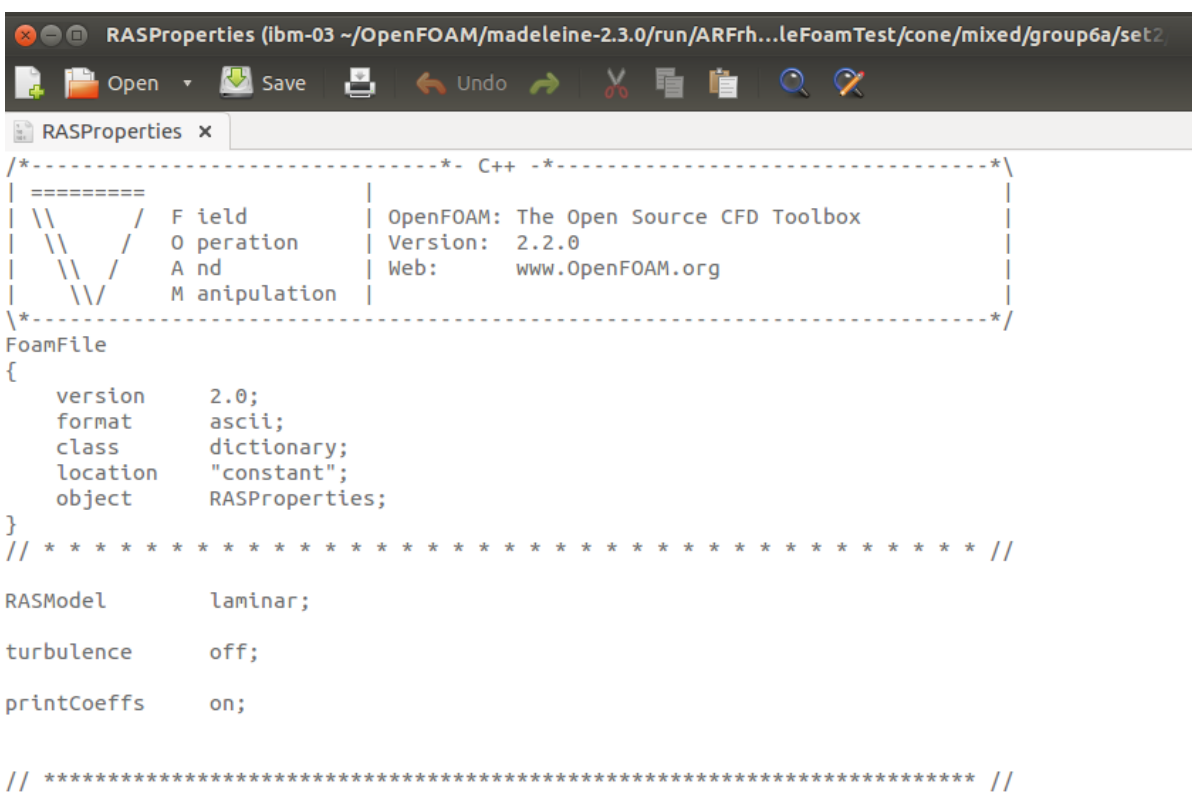
Figure B.36: Tabulated Frame Velocity at Specified Time



```

data1.csv (ibm-03 ~/OpenFOAM/madeleine-2.3.0/run/ARFrhoPimpleFoamTest/cone/mixed/group6a/set2/c
Open Save Undo
data.csv x data1.csv x
0, -1
1.0e-2, -4
1000, -4
  
```

Figure B.37: Turbulence Model Description



```

RASProperties (ibm-03 ~/OpenFOAM/madeleine-2.3.0/run/ARFrhoPimpleFoamTest/cone/mixed/group6a/set2/c
Open Save Undo
RASProperties x
/*-----* C++ */
|=====|
| \\ / | F i e l d | OpenFOAM: The Open Source CFD Toolbox
| \\ / | O p e r a t i o n | Version: 2.2.0
| \\ / | A n d | Web: www.OpenFOAM.org
| \\ / | M a n i p u l a t i o n |
/*-----*/
FoamFile
{
  version      2.0;
  format       ascii;
  class        dictionary;
  location     "constant";
  object       RASProperties;
}
// *****

RASModel      laminar;

turbulence    off;

printCoeffs   on;

// *****
  
```



Figure B.38: Thermo-Physical Property Specification

```
thermophysicalProperties (ibm-03 ~/OpenFOAM/madeleine-2.3.0/run...mTest/cone/mixed/group6a/set2/
Open Save Undo
thermophysicalProperties x
| \\ / A nd | Web: www.OpenFOAM.org |
| \\ / M anipulation |
|*-----*/
FoamFile
{
  version      2.0;
  format       ascii;
  class        dictionary;
  location     "constant";
  object       thermophysicalProperties;
}
// *****

thermoType
{
  type          hePsiThermo;
  mixture       pureMixture;
  transport     const;
  thermo        hConst;
  equationOfState perfectGas;
  specie        specie;
  energy        sensibleEnthalpy;
}

mixture
{
  specie
  {
    nMoles      1;
    molWeight    28.9;
  }
  thermodynamics
  {
    Cp          1007;
    Hf          0;
  }
  transport
  {
    mu          1e-04;
    Pr          0.7;
  }
}
}
```